NASA/CR—2005-213584/VOL2

Critical Propulsion Components
Volume 2: Combustor

Pratt & Whitney
West Palm Beach, Florida

General Electric Aircraft Engines
Cincinnati, Ohio

May 2005

The NASA STI Program Office . . . in Profile

Since its founding, NASA has been dedicated to the advancement of aeronautics and space science. The NASA Scientific and Technical Information (STI) Program Office plays a key part in helping NASA maintain this important role.

The NASA STI Program Office is operated by Langley Research Center, the Lead Center for NASA's scientific and technical information. The NASA STI Program Office provides access to the NASA STI Database, the largest collection of aeronautical and space science STI in the world. The Program Office is also NASA's institutional mechanism for disseminating the results of its research and development activities. These results are published by NASA in the NASA STI Report Series, which includes the following report types:

- TECHNICAL PUBLICATION. Reports of completed research or a major significant phase of research that present the results of NASA programs and include extensive data or theoretical analysis. Includes compilations of significant scientific and technical data and information deemed to be of continuing reference value. NASA's counterpart of peer-reviewed formal professional papers but has less stringent limitations on manuscript length and extent of graphic presentations.

- TECHNICAL MEMORANDUM. Scientific and technical findings that are preliminary or of specialized interest, e.g., quick release reports, working papers, and bibliographies that contain minimal annotation. Does not contain extensive analysis.

- CONTRACTOR REPORT. Scientific and technical findings by NASA-sponsored contractors and grantees.

- CONFERENCE PUBLICATION. Collected papers from scientific and technical conferences, symposia, seminars, or other meetings sponsored or cosponsored by NASA.

- SPECIAL PUBLICATION. Scientific, technical, or historical information from NASA programs, projects, and missions, often concerned with subjects having substantial public interest.

- TECHNICAL TRANSLATION. English-language translations of foreign scientific and technical material pertinent to NASA's mission.

Specialized services that complement the STI Program Office's diverse offerings include creating custom thesauri, building customized databases, organizing and publishing research results . . . even providing videos.

For more information about the NASA STI Program Office, see the following:

- Access the NASA STI Program Home Page at ***http://www.sti.nasa.gov***

- E-mail your question via the Internet to help@sti.nasa.gov

- Fax your question to the NASA Access Help Desk at 301–621–0134

- Telephone the NASA Access Help Desk at 301–621–0390

- Write to:
  NASA Access Help Desk
  NASA Center for AeroSpace Information
  7121 Standard Drive
  Hanover, MD 21076

NASA/CR—2005-213584/VOL2

Critical Propulsion Components

Volume 2: Combustor

Pratt & Whitney
West Palm Beach, Florida

General Electric Aircraft Engines
Cincinnati, Ohio

Prepared under Contract NAS3–27235

National Aeronautics and
Space Administration

Glenn Research Center

May 2005

Document History

This research was originally published internally in September 2000.

Available from

NASA Center for Aerospace Information
7121 Standard Drive
Hanover, MD 21076

National Technical Information Service
5285 Port Royal Road
Springfield, VA 22100

Available electronically at http://gltrs.grc.nasa.gov

Abstract

Several studies have concluded that a supersonic aircraft, if environmentally acceptable and economically viable, could successfully compete in the 21st century marketplace. However, before industry can commit to what is estimated as a 15-to-20 billion dollar investment, several barrier issues must be resolved. In an effort to address these barrier issues, NASA and Industry teamed to form the High-Speed Research (HSR) program. As part of this HSR program, the Critical Propulsion Components (CPC) element was created and assigned the task of developing those propulsion component technologies necessary to: (1) reduce cruise emissions by a factor of 10 and (2) meet the ever-increasing airport noise restrictions with an economically viable propulsion system. The CPC-identified critical components were ultra-low-emission combustors, low-noise/high-performance exhaust nozzles, low-noise fans, and stable/high-performance inlets. Propulsion cycle studies (coordinated with NASA–Langley sponsored airplane studies) were conducted throughout this CPC program to help evaluate candidate components and select the best concepts for the more complex and larger scale research efforts. The propulsion cycle and components ultimately selected were a mixed-flow turbofan (MFTF) engine employing a lean, premixed, prevaporized (LPP) combustor coupled to a two-dimensional mixed compression inlet and a two-dimensional mixer/ejector nozzle.

The CPC program began in 1994 and was planned for completion in 2002. Unfortunately, in 1999 NASA chose to prematurely end the HSR program. Although terminated early, the HSR program demonstrated that an economically viable and environmentally acceptable supersonic aircraft (and propulsion system) was achievable. The purpose of this document is to document the CPC findings in support of those visionaries in the future who have the courage to once again pursue a supersonic passenger airplane.

Due to the large amount of material presented in this report, it was prepared in four volumes:

Volume 1: Section 1 – Summary
Section 2 – Introduction
Section 3 – Propulsion System Studies

Volume 2: Section 4 – Combustor

Volume 3: Section 5 – Exhaust Nozzle

Volume 4: Section 6 – Inlet
Section 7 – Fan/Inlet Acoustic Team

Table of Contents

Table of Contents (Continued)

Table of Contents (Continued)

List of Illustrations

List of Illustrations (Continued)

List of Illustrations (Continued)

List of Illustrations (Continued)

List of Illustrations (Continued)

List of Illustrations (Continued)

List of Illustrations (Continued)

List of Illustrations (Continued)

List of Illustrations (Continued)

List of Illustrations (Continued)

List of Illustrations (Continued)

List of Illustrations (Continued)

List of Illustrations (Continued)

List of Illustrations (Concluded)

List of Tables

List of Tables (Concluded)

Lexicon

16TT	NASA–Langley 16-ft transonic wind tunnel
2D	Configuration similar to two back-to-back letter D's, also two dimensional
2DB	Two-dimensional bifurcated (inlet concept)
2DCD	Two-dimensional convergent/ divergent (exhaust nozzle)
2DFC	Two-dimensional fixed chute
2E	Two excitations per rotor revolution (vibration mode)
A_8	Exhaust nozzle throat area
A8CD	Exhaust nozzle effective jet area
A_9	Exhaust nozzle exit area
A16, A_{16}	Variable-area fan/core mixer duct-side area
A56	Mixer-exit area, core stream
AACE	Aeroacoustics collaborative effort
AAPL	Aeroacoustic Propulsion Laboratory
ACE	Axisymmetric coannular ejector (exhaust nozzle)
ADP	Aerodynamic design point
AE8, A_{E8}	Effective exhaust nozzle throat area
AEDC	Arnold Engineering Development Center
AFRL–MMD	Air Force Research Laboratory, Materials and Manufacturing Directorate
AIP	Aerodynamic interface plane (between inlet and engine)
AJ2	Exhaust nozzle suppressed throat area
ALMMC	Aluminum metal-matrix composite
AMEN	Axisymmetric mixer/ejector nozzle
AMT	Airframe Management Team
AN^2	Blade root stress parameter
ANSYS	GEAE design-analysis tool (software)
AR	Aspect ratio, also area ratio
ARP	Aerospace Recommended Practice
ASAR	Flowpath area aft of ejector mixer
ASME	American Society of Mechanical Engineers
AST	Advanced subsonic technology
A_t/A_{mix}	Ratio of acoustic treatment area to mixing area
ATC	Axi-tilt chute
ATCB	Axisymmetric translating centerbody (engine inlet)
AV	Arc valve
AVP	Active-volume parameter
BAC	Boeing Aircraft Company
BCAE	Boeing Commercial Aircraft Group
BDSM	"Best" downstream mixer (exhaust nozzle)
BLISK	Blade on disk (rotor type)
BOAS	Blade outer air seals
BPF	Blade-passing frequency
BPR	Bypass ratio
BS&D	Bearings, seals, and drives
BTSSI	Bifurcated two-stage supersonic inlet
C&A	Controls and accessories
CAFD	Circumferentially averaged flow determination (computer program)
CAM	Cold acoustic model, cold aerodynamic model
CASL	Chute aerodynamics with stereolithography
CB	Customer bleed
CBM	Computation-based method
CDA	Controlled-diffusion airfoil
CDP	Compressor-discharge plane
CER	Chute expansion ratio
CFD	Computational fluid dynamics
CFG, C_{FG}, C_{fg}	Coefficient of gross thrust
CFN, C_{FN}, C_{fn}	Coefficient of net thrust

CG	Center of gravity
CG1	Turbomachinery center of gravity
CG2	Exhaust nozzle center of gravity
CG3	Overall engine center of gravity
CM	Coordination memo
CMC	Ceramic-matrix composite
CMMR	Critical major milestone review
CMT	CPC management team
CO	Carbon monoxide
COTR	Contracting Officer's Technical Representative
CPC	Critical Propulsion Components
CPR	Compressor pressure ratio
CR	Contractor report
CRAFT	Combustion Research and Flow Technology Inc.
CTOL	Conventional takeoff and landing
dB	Decibels
DEN	Double-edge notch
$\Delta H/T$	Specific work
DOC	Direct operating cost
DOC+I	Direct operating cost + interest
DoD	Department of Defense
DOE	Design of experiments
DOSS	Design optimization synthesis system (Boeing)
DP	Pressure drop or differential
DPC	Circumferential pressure distortion
DPC/Pmx	Circumferential-distortion parameter (total pressure)
DPE	Perfluoroalkyldiphenylether
DPR	Radial pressure distortion
DPR/Pmx	Radial-distortion parameter (total pressure)
DR&O	Design requirements and objectives (Boeing document)
DRD	Documentation requirements document
DS	Directionally solidified
DSM	Downstream mixer (exhaust nozzle)
DTR	Diffuser test rig
DVM	Discrete-vortex method
EB	Electron beam
EDM	Electrical-discharge machining (or machined)
EFH	Engine flight hour(s)
EI	Emissions index: g of pollutant per kg of fuel burned; also, environmental impact
EICO	CO emissions index: g CO/kg fuel
EIHC	HC emissions index: g of unburned hydrocarbons per kg of fuel burned
EINOx	NOx emissions index: g of NOx/kg fuel
EPM	Enabling Propulsion Materials
EPNdB	Effective perceived noise decibels
EPNL	Effective perceived noise level
ER	Extraction ratio: P_{16}/P_{56}
ESF	Engine scale factor
ESP	Electronically scanned pressure
ETA (η)	Efficiency
f/a	Fuel/air ratio
F/C	Fan/core
FA&M	Florida Agricultural and Mechanical University
FADEC	Full-authority digital electronic control
FAR	Fuel/air ratio, also Federal Aviation Regulation
FC	Fixed chute (mixer/ejector nozzle)
FCG	Fatigue crack growth
FCM	Fixed-chute mixer
FCN	Fixed-chute nozzle
FEGV	Fan exit guide vane
FEM	Finite-element model
FENTD	Full-scale engine nozzle technology demonstration/demonstrator (more frequently called FSD)

FH	Flight hour(s)
FIAT	Fan inlet/acoustics team (ITD team)
FLABI	"FLADE" bypass injector valve
FLADE	Fan-on-blade HSCT engine concept
FN, F_N, F_n	Net thrust
FNAA	Fan average
FNDAB	Net thrust with afterbody drag removed
FNP	Fixed chute, no plug; unsuppressed primary (idle) thrust; uninstalled net thrust
FNS	Full Navier–Stokes
$F_{n\ sup}$	Net thrust with nozzle in noise-suppression mode
FOD	Foreign-object damage
FPR	Fan pressure ratio
FSD	Full-scale demonstrator
FSN	Fluid-shield nozzle
FSPSTD	Full-scale propulsion system technology demonstrator
FTR	Formal test report
γ	Gamma titanium aluminide (TiAl)
GC/MS	Gas chromatography/mass spectrometry
GE AE	GE Aircraft Engines
GFY	Government fiscal year
GI	Ground idle
GOCAP	Goals, objectives, challenges, approaches, and programs
GOTCHA	Goals, objectives, technical challenges, and approaches
GRA	Geared rotary actuator
GRC	Glenn Research Center
HAM	Hot acoustic model
HART	Hot acoustic rig test
HARW	High aspect ratio wing
HC	Hydrocarbons (unburned, in exhaust gas)
HCF	High-cycle fatigue
HEAT	High-lift engine aeroacoustic technology
HIN	HEAT isolated nacelle
HISCAT	Highly integrated supersonic cruise airplane technology
HMMRA	Highly mixed multistage radial/axial
HP	High pressure, also horsepower
HPC	High-pressure compressor
HPT	High-pressure turbine
HPX	Horsepower extraction
HPXH	Customer (aircraft) power extraction
HPX(2)	Customer (aircraft) power extraction plus engine parasitic requirements
HS	High speed; also, Hamilton Sundstrand
HSCT	High Speed Civil Transport
HSR	High Speed Research
HSS	HEAT semispan
IBR	Integrally bladed rotor
ICAO	International Civil Aviation Organization
ICD	Interface control document
ID	Inner diameter
IFV	Inverter flow valve
IGV	Inlet guide vane(s)
IHPTET	Integrated High Performance Turbine Engine Technology
ILT	Interlaminar tension
IMFH	Integrated mixer/flameholder
IML	Increased mixer length (exhaust nozzle)
IMT	Industry method test-bed
IR&D	Independent Research and Development
IRR	Internal rate of return
ITD	Integrated technology development
JBTS	Jet burner test stand (UTRC facility)
JER	Jet exit rig
JN8, Jn8B2	Jet-noise prediction models (P&W)

JNL	Jet Noise Laboratory (NASA–Langley
KCAS	Knots, calibrated air speed
KEAS	Knots, equivalent air speed
KIVA II	A multidimensional CFD code
KONA	NASA database Unix server
KTAS	Knots, true air speed
L/D	Lift/drag ratio, also length/diameter ratio
LAPIN	Large-amplitude perturbation inlet (model)
LaRC	Langley Research Center
LBO	Lean blowout
LCF	Low-cycle fatigue
LDI	Lean direct (fuel) injection
LDV	Laser doppler velocimeter
LE, Le	Leading edge
LeRC	Lewis Research Center
LET	Large Engine Technology
LF	Linked flap
LHV	Latent heat value
LOL, LoL	Lobe on lobe
LP	Low pressure
LPC	Low-pressure compressor (main engine fan)
LPP	Lean premixed/prevaporized
LPT	Low-pressure turbine
LSAF	Low-speed aeroacoustic facility (Boeing)
LSAWT	Low-speed aeroacoustic wind tunnel
LSM	Large-scale model
LSMS	LSM similitude
LSWT	Low-speed wind tunnel
LTO	Landing/takeoff
LV	Laser velocimeter
M	Mach number
M_∞	Ambient Mach number
M_0	Free-stream Mach number
M14	Mach number at bypass duct inlet
M15	Mach number at bypass duct average area
M155, $M_{15.5}$	Maximum Mach number in fan duct (bypass duct over rear frame)
M16, M_{16}	Mach number at fan duct mixing plane (fan/core mixer duct side)
M2	Mach number at engine inlet
M21ID	Mach number at fan discharge ID
M21OD	Mach number at fan discharge OD
M25	Mach number at compressor inlet
M3	Mach number at compressor discharge
M36	Mach number at combustor inlet
M4	Mach number at HPT vane inlet
M49	Mach number at LPT rotor 1 inlet
M5	Mach number at LPT exit
M54	Mach number at rear frame/diffuser average area
M55	Mach number at mixer entrance, core stream
M56	Mach number at mixer exit, core stream
M68	Mach number at miniaugmentor exit
MAR	Mixing area ratio (duct)
MCP	Modular component predictor
MCTCB	Mixed compression translating centerbody (inlet)
MDA	McDonnell Douglas Aircraft
MDC	McDonnell Douglas Corporation
MDO	Multidiscipline optimization
M–E, M/E	Mixer/ejector (exhaust nozzle)
MFTF	Mixed-flow turbofan
MIDIS	Mixer/ejector inlet distortion study
MIT	Massachusetts Institute of Technology
MITCFA	MIT compound flow analysis (computer program)
MMC	Metal-matrix composite
Mn	Mach number

MPC	Multiple-component predictor
MRA	Multistage radial/axial
M&S	Materials and structure
MTF	Mid-tandem fan
MTOGW	Maximum takeoff gross weight
MTOW	Maximum takeoff weight
N1	Low-pressure rotor speed
N1C2	Low-pressure rotor speed corrected to station 2
N2C2.5	High-pressure rotor speed corrected to station 25 (compressor inlet)
N4	HP spool speed
N5	LP spool speed
NASA	National Aeronautics and Space Administration
NASA LaRC	NASA Langley Research Center
NASA LeRC	NASA Lewis Research Center (now NASA Glenn)
NASTRAN	Computer modeling software
NATR	Nozzle acoustic test rig
Nc, N_c	Corrected engine (shaft) speed
NCP	National cycle program
NFM	Nearly fully mixed
NOx	Oxides of nitrogen
Noy	Acoustic annoyance parameter
NPD	Noise power distance
NPSS	Numerical propulsion-system simulation
NPR	Nozzle pressure ratio
NRA	NASA Research Announcement
OAC	Optimized aeroelastic concept
OD	Outer diameter
OEW	Operating empty weight (no fuel, oil, etc.)
OEW–PR	OEW minus propulsion-system weight
OGV	Outlet guide vane(s)
OML	Outer mold line
OPR	Overall pressure ratio
P_{16}	Pressure exiting bypass duct
P16Q56	Extraction ratio
P_{56}	Pressure exiting core engine
PAI	Propulsion/airframe integration
PAIT	Propulsion/airframe integration technology
PC	Power code
PCC	Precision Castparts Co.
PDF	Probability density function
PDPA	Phase Doppler particle analyzer
PDR	Preliminary design (or data) review
PFPAE	Perfluoropolyakylether
PH3	Tri-perfluoropolyalkylether-phenyl-phosphine
PIC	Pressure-infiltration casting
PLIF	Planar laser-induced fluoresence
PLR	Programmable lapse rate
PMT	Propulsion Management Team
PMC	Polymer-matrix composite
PNLT	Tone-controlled perceived noise level
P&O	Performance and operability
PSET	Propulsion System Evaluation Team
PSI	Propulsion system integration, also Pressure Systems Inc.
PST	Propulsion selection team
PT, P_T	Total pressure
PT8	Exhaust gas total pressure at nozzle throat
PT14	Total pressure at bypass duct inlet
PT15	Total pressure at bypass duct average area
PT155	Total pressure at bypass duct over turbines and rear frame (mixer entrance)
PT16	Total pressure at mixer exit, bypass stream side
PT21	Total pressure at fan discharge
PT21A	Average total pressure at fan discharge

PT21ID	Total pressure at fan discharge inner diameter
PT21ID	Total pressure at fan discharge outer diameter
PT25	Total pressure at compressor inlet
PT3	Total pressure at compressor discharge
PT36, P_{T36}	Total pressure at compressor inlet
PT4	Total pressure at HPT vane inlet
PT5	Total pressure at LPT exit
PT55	Total pressure at mixer entrance, core stream side
PT56	Total pressure at mixer exit, core stream side
PT68	Total pressure at miniaugmentor exit
PT7	Total pressure at convergent nozzle inlet
PT8	Total Pressure at nozzle throat
PTC	Preliminary technology configuration
Q	Dynamic pressure
R1	First-stage rotor
R2	Second-stage rotor
R3	Third-stage rotor
RAN	Reynolds-averaged Navier–Stokes
RC	Round convergent (exhaust nozzle)
RM	Relative “mixedness”
ROM	Rough order of magnitude
RPM	Revolutions per minute
RQL	Rich (burn), quick (quench), lean (burn)
RR	Rolls Royce
RSQ	Reduced-scale quench
RTI	Reversing through inlet
RTO	Refused takeoff
Rx4	HPT pitch reaction
S/MTD	STOL and maneuvering technology demonstratior
S1	First-stage stator
S2	Second-stage stator
S3	Third-stage stator
SAE	Society of Automotive Engineers
SAR	Suppressor area ratio
SAVE	Systematic approach to value engineering
SCC	Sizing-code calibration
SCID	Supersonic cruise integrated design
SCN	Sliding-chute nozzle
SD	Stepped dome
SDOF	Single degree of freedom
SERN	Single-expansion-ramp nozzle
SFC	Specific fuel consumption: lbm of fuel per hour per lbf
SFCDAB	SFC based on FNDAB
SI_{cp}	Stability index
SLA	Stereolithographic apparatus
SLS	Sea-level static
SLTO	Sea level takeoff
SMFAN	Stall margin, fan
SOAPP	State-of-the-art performance program (P&W)
SPFDB	Superplastic formed, diffusion bonded
SPL	Sound power level
SRP	Separate reverser port
SSC	Supersonic cruise
SST	Supersonic transport
STMT	System technology management team
STOL	Short takeoff and landing
SW	Sidewall
SWET	Substrate welding at elevated temperature
SW	Toal wing planform area
SwRI	Southwest Research Institute
SWT	Supersonic wind tunnel
T/b	Thickness-to-chord ratio
T/O	Takeoff

T_3	High-pressure compressor exit temperature
T_4	Combustor exit temperature
T_{41}, $T_{4.1}$	High-pressure turbine rotor inlet temperature
TAC	Total accumulated cycles
TBC	Thermal-barrier coating
TBE	Turbine bypass engine
TC	Technology configuration
TCA	Technology concept aircraft
TCB	Translating centerbody (inlet)
TCE	Technology concept engine
TCLA	Turbine cooling air
TCS	Turbulence control structure, also technology concept solution
TE	Trailing edge
TF	Turbofan
TF–IFV	Turbofan-inverter flow valve
TI	Technical integration (team)
TIC	Transient inlet/compressor (model)
TJ	Turbojet
TJ–IFV	Turbojet-inverter flow valve
TLID	Thrust-lapse parameter
TMT	Technology management team
TOBI	Tangential on-board bleed injection
TOC	Top of climb
TOGW	Takeoff gross weight
TP3	GEAE performance-analysis software
TPS	Thermal-protection system, also turbulence-prevention structure
TRF	Turbine rear frame
TRL	Technology readiness level
TSI	Triton Systems Inc.
TT, T_T	Total temperature
TT3	Compressor discharge total temperature
TT4	Total temperature at HPT vane inlet
TT4.1	High-pressure turbine rotor inlet total temperature
T_{T7}	Augmentor-exit total temperature
TT8	Exhaust gas total temperature at nozzle throat
TTC	Technology transition (or tracking) chart
TTR	Total-temperature ratio
UHB	Ultrahigh bypass
UHC	Unburned hydrocarbons
UPS	Universal propulsion simulator
UTRC	United Technology Research Center
VABI	Variable-area bypass injector
VAM	Variable-area mixer
VAMP	Variable-area mixing plane
VCE	Variable-cycle engine
VCF	Variable-capacity fan
VDC	Variable-diameter centerbody
VDVP	Variable-displacement vane pump
VEN	Variable exhaust nozzle
VFX	Variable-capacity fan, experimental
VG	Variable geometry
VJIP	Primary ideal jet velocity
VPI	Virginia Polytechnic Institute
W2AR	Engine corrected airflow
W5GR	LPT exit gas flow function
W_a	Airflow
WAE, W_{AE}	Engine airflow
WB3	Customer bleed
WBS	Work breakdown structure
W_c	Corrected airflow, also coolant flow
WG	Air (gas) flow
WG36	Airflow at combustor inlet
W_p	Primary flow, lbm/s
W_s	Secondary flow, lbm/s
XNH	Rotor speed (high-pressure spool)
XNL	Rotor speed (low-pressure spool)

4.0 Combustor

4.1 Overview

A key issue in the development of the High Speed Civil Transport (HSCT) was environmental acceptability. Of particular concern was the impact of combustion-generated nitrogen oxides (NOx) emissions on the stratospheric ozone layer. Thus, a significant portion of the development cycle focused on NOx reductions at supersonic cruise flight conditions. However, to maintain commercial viability, emissions at subsonic cruise had to be at least as good as current engines in the subsonic fleet. Additionally, increasingly stringent airport-vicinity emissions restrictions had to be addressed. Reliability, durability, cost, weight, and performance are also critical to commercial viability. These were the primary drivers of the technology development performed under this contract.

To meet these requirements, three fundamental combustor concepts were considered: lean direct injection (LDI), lean premixed prevaporized (LPP), and rich/quench/lean (RQL). NASA–Glenn (with GEAE assistance) would be the focal point of LDI development. GEAE and P&W would be the focal points for LPP and RQL development, respectively. Each would require a significant development effort to even have a chance of achieving the stringent requirements set forth in the contract. Each had advantages to be exploited and disadvantages to be overcome. Assessments would then have to be made regarding the designs that best optimize the tradeoffs necessary to produce a commercially viable engine. These assessments would be made through a series of "downselects" to reach the final combustor design.

In the end, the LPP design was selected for final development. After an intricate series of tests, the design demonstrated emissions and operability that met levels set forth in the contract. Although other concepts showed significant promise in some areas, they tended to fall short in meeting all the goals of the program. The development of each of the concepts will be discussed herein.

This portion of the report will detail the development of a combustor for the HSCT engine. LDI, LPP, and RQL concepts will be discussed, along with the results of a multitude of tests performed on each. The primary downselects along the development path will be discussed to demonstrate the complexity of the tradeoffs. Finally, the primary combustor design selected will be presented.

4.1.1 Combustor Goals, Objectives, Challenges, Approaches, and Programs

Initiation of the development program began with the issuance of the Goals, Objectives, Challenges, Approaches, and Programs (GOCAP) chart, Figure 1. This chart was created to ensure that all participants were striving for the same goals and understood the primary challenges of the program — and to help minimize straying from the primary development path. The chart is a high-level overview of the process used to meet the program goals for a combustor for an HSCT engine.

4.1.2 Combustor Logic

The HSCT combustor development logic is summarized in Figure 2. Ideally, single-cup and flame-tube tests would be used to evaluate a variety of subcomponent designs for the combustor. The best designs at a given point in time would then be put into a sector to study the impact of interactions between the subcomponents. As development continued at the subcomponent level and a better understanding of the interactions was achieved with sectors, improvements and new concepts would be developed. At specified intervals in the program, downselects would occur. These primarily

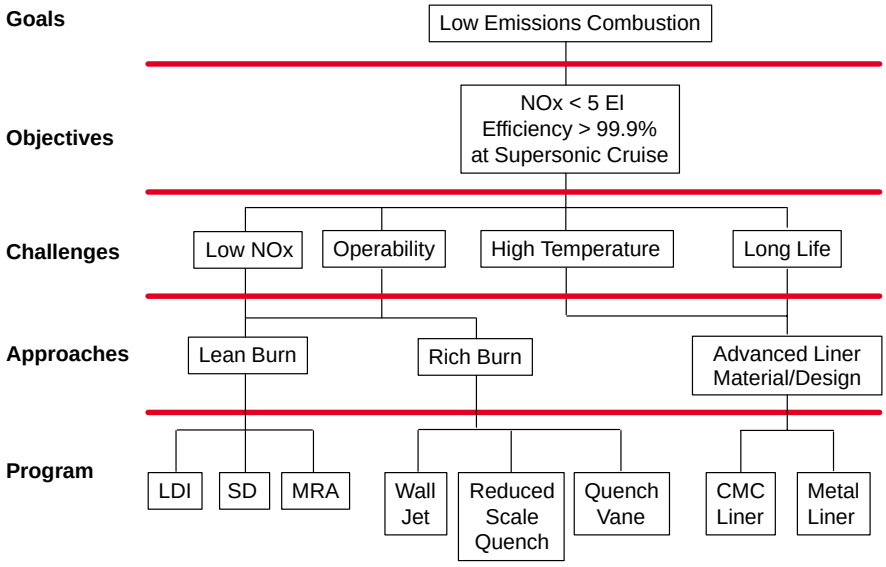

Figure 1. Combustor GOCAP Chart

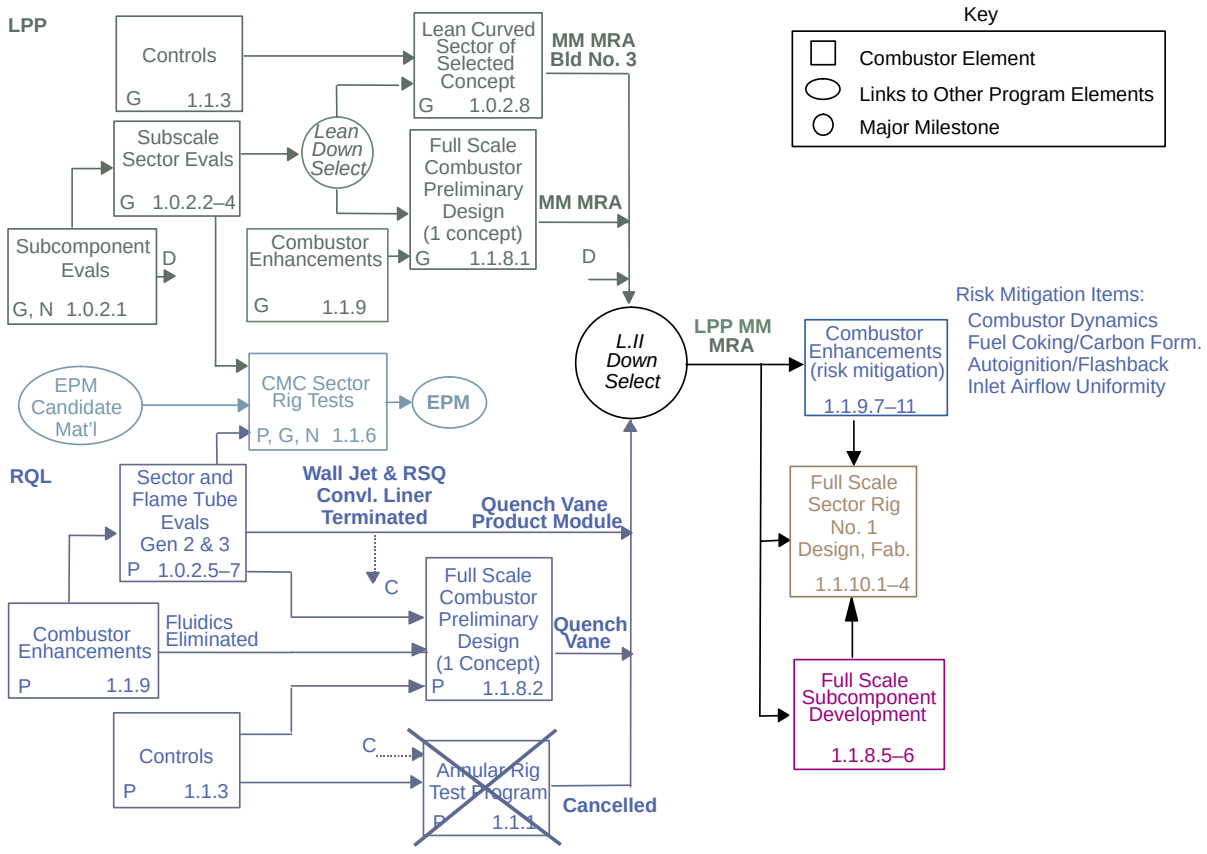

Figure 2. Combustor Development Logic Diagram

included a lean downselect between the stepped-dome and multistage radial/axial (MRA) concepts (described in detail later in this report) and a Level II downselect between the LPP and RQL concepts (also described in detail later in this report). Following downselect, design and fabrication of a full-scale LPP sector would complete the program.

4.1.3 Combustor Metrics

The metrics used to track the progress of the combustor program and to select the final design are listed in Table 1. Generally, the criteria cover emissions, performance, and product-viability issues critical to program success. These would be the primary selection criteria used in each of the intermediate downselects as well as the final LPP/RQL downselect.

Table 1. Combustor Downselect Criteria

Combustor Downselect Criteria			Requirement
Emissions and Performance	Supersonic Cruise	NOx	< 5 EI (g/kg Fuel)
		Combustion Efficiency	> 99.9%
	Subsonic Cruise	NOx	< 10 EI (Typical Subsonic Aircraft)
		Combustion Efficiency	> 99% (Typical Subsonic Aircraft)
	Airport Vicinity Landing/Takeoff (LTO) Emissions	NOx (Supersonic*)	< 5 lbm/klbm–°F–hr
		CO (Supersonic*)	< 7.8 lbm/klbm–°F–hr
		UHC (Supersonic*)	< 1 lbm/klbm–°F–hr
		NOx (Subsonic**)	< 64.3 g/kN
		CO (Subsonic**)	< 118 g/kN
		UHC (Subsonic**)	< 19.6 g/kN
	Particulates per cm^3 of Exhaust Gas		10^7 (Typical Subsonic Aircraft)
	Transient Stability (Autoignition, Flashbacks)		
	Combustor Blowout Margin		> 0.1 Equivalence Ratio Units
	Altitude Relight		
	Profile and Pattern Factor		< 5%
	Combustor Overall Pressure Loss		
	Fuel System Coking		
	Compressor Distortion		
Product Viability	Safety		
	Complexity		
	Combustor Dynamics		
	Controls Stability		
	Maintainability		
	Component Life		
	Reliability		
	Initial Cost and Producibility		
	Size and Weight		
	Repairability		

4.2 Historical Progression of Concepts Development

Lean and RQL systems have been studied for a number of years. The ability to produce low NOx at very lean and very rich equivalence ratios is clearly demonstrated in the classic bell-shaped curve of Figure 3. Traditional engines have operated with diffusion flames — burning essentially stoichiometrically. These were fairly simple, straightforward systems, but they produced high levels of NOx. With the strong push towards reduced pollutant emissions over the last few decades, alternative methods had to be considered. Although marine and ground-based industrial systems were able to use water injection or catalytic systems to reduce emissions, such techniques are not generally viable alternatives for use in jet engines. This led to the development of many of the lean- and rich-burning alternatives in use today.

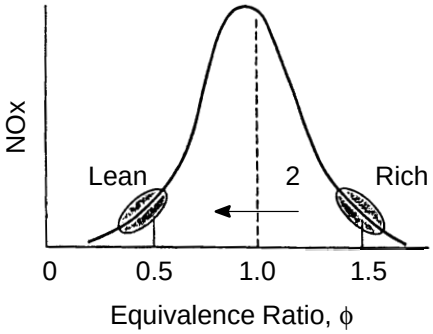

Figure 3. Variation of NOx With Equivalence Ratio

Low emissions are especially critical for the HSCT because supersonic flight would be at altitudes in which exhaust gases are discharged directly into the stratosphere. At the same time, airport landing/takeoff (LTO) emissions requirements continue to be made more stringent. Thus the engines must operate efficiently over the entire LTO cycle from low-power ground idle to full-power takeoff.

Three fundamentally different concepts were considered for low-emissions combustors. The first was a LDI system in which fuel is rapidly atomized and mixed with air at lean fuel/air ratios prior to burning. The lean mixture produces low NOx, as long as the mixture is well atomized and uniformly mixed. The second concept is a LPP system. It is similar to LDI in that fuel and air are mixed at lean fuel/air ratios, but it uses a long premixing chamber to allow the fuel and air mixture time to more fully vaporize and premix before entering the combustion zone. Finally, RQL concepts were considered. In these designs, fuel and air are initially mixed and burned at very rich fuel/air ratios. The gases are then rapidly mixed with additional air, in the quench zone, before burning again at very lean overall fuel/air ratios. A variety of designs were considered for each of the LDI, LPP, and RQL concepts, as summarized in the following subsections.

4.2.1 Lean Combustion Systems

Several combustor configurations were considered for the HSCT engine. Initial consideration was given to direct modifications of current combustor designs, but meeting stringent supersonic cruise emissions requirements under such severe operating conditions proved difficult. Significant advancements were clearly necessary, so LDI and LPP systems were considered.

Lean direct injectors tested under this contract were of “multiventuri” form. The designs consisted of an axial or radial swirler, a spray nozzle forming a centerbody within the cavity, a venturi throat, and a short expansion region feeding into the main combustor (Figures 4 and 5). The spray nozzle injects fuel near the venturi throat, where the high-swirl and high-velocity air rapidly atomize the fuel. The intent is to atomize the fuel as quickly and uniformly as possible prior to injecting it directly into the combustion zone. As long as the fuel/air mixture is lean, well-atomized, and uniformly mixed, emissions will behave similar to those of premixed systems; NOx levels should be low even at severe operating conditions. Unfortunately producing a well-atomized, uniform mixture in a very short distance is extremely difficult. This led to consideration of LPP systems as alternatives.

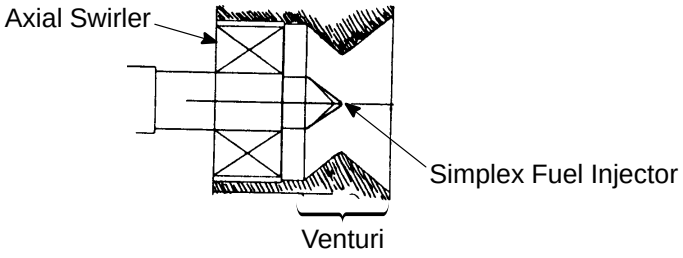

Figure 4. Axially Swirled LDI Concept

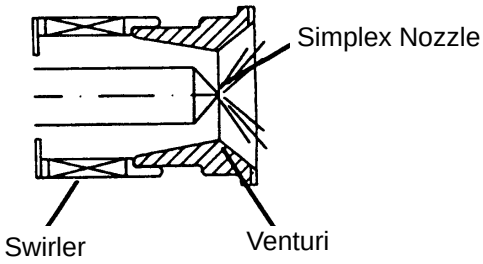

Figure 5. Radially Swirled LDI Concept

LPP systems can be designed in a variety of shapes and forms. Some tend to be similar to LDI injectors in that swirlers are used to improve mixing and stability. A venturi is generally not used, and overall length is often added to allow more time for fuel vaporization and premixing. This helps ensure that the fuel/air mixture is properly "prepared" prior to entering the combustion chamber, producing low emissions. However, the use of swirlers creates problems in physically trying to package the injectors into the dome. Because of the high blockage of the swirlers, they must be relatively large to pass sufficient air into the combustor. Thus, the LPP concepts studied under this contract did not use swirlers. Instead, a simple, long mixing tube was used to produce a prevaporized, uniform fuel/air mixture (Figure 6). The mixing length is limited by autoignition concerns, potentially limiting the completeness of the premixing and prevaporization. This is directly reflected in the emissions. These tubes were referred to as integrated mixer/flameholder (IMFH) designs.

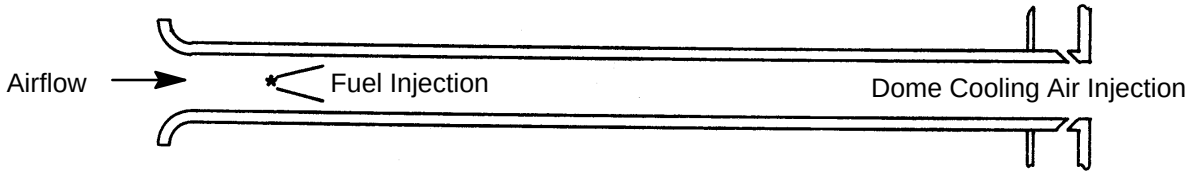

Figure 6. LPP Main Stage Integrated Mixer/Flameholder Concept

LDI systems have the advantage of being much shorter and inherently more stable than the LPP systems considered here. However, they can be costly and difficult to package because of complexity. Also, with the small passages in the LDI fuel nozzles, required to produce the finely atomized spray, coking becomes a concern (similar concerns exist for some of the LPP systems studied).

LDI and LPP systems tend to have relatively poor combustion efficiency at low power. This is an artifact of generally poor stability at low operating temperatures. Although LDI injectors are much more stable than the LPP and IMFH designs considered here, they really do not provide the required stability for practical use in an engine. Thus, in both systems the addition of a pilot stage was assessed. A cyclone pilot was chosen, since that concept provides extremely stable operation even at very low power. However, since it also had to produce low NOx at high power, significant development would be required to make the design feasible.

The cyclone pilots chosen were basically hybrids of the LDI and LPP concepts. As shown in Figure 7, the pilot consists of a radial swirler, a centerbody with a number of plain jet fuel injectors, a throat,

and a short diverging section feeding into the combustor. This is very much like the LDI concepts described above, except fuel is injected radially outward at the midheight of the swirler, rather than being injected through a spray nozzle at the throat. By injecting further upstream, more time is allowed for premixing and vaporization, along the lines of LPP concepts. A pilot stage was added to each LDI and LPP combustor concept under consideration.

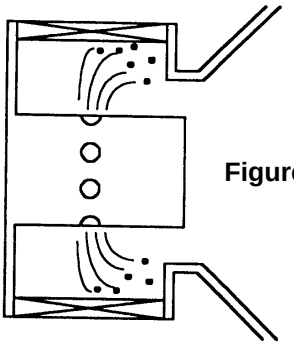

Figure 7. LPP Cyclone Pilot Concept

Three basic lean combustor systems were considered for advanced development: an LDI stepped dome, an LPP stepped dome, and an LPP multistage radial/axial configuration. Variations of each concept are described in the following paragraphs.

LDI Stepped Dome Concepts – Several LDI combustor concepts were considered for development, as shown in Figure 8. All were variations of what was referred to as a "stepped dome" concept, in which at least one of the annular sections of the dome was recessed relative to the others. Because the interactions between burning stages and "cold" air from unfired stages typically has adverse effects on low-power CO emission, the dome was recessed to help isolate the pilots from the other injectors. This is especially important at low power, where CO and unburned hydrocarbon emissions tend to be of greatest concern. The recessed dome typically contained the cyclone pilots, which were used for improved stability. In some cases, each stage of LDI injectors was isolated from the others by additional steps in the dome. As shown in Figure 8, LDI injectors in a variety of sizes and arrangements were considered.

LPP Stepped Dome Concepts – The LPP stepped-dome combustor concepts (Figures 9) were nearly identical to the LDI stepped-dome concepts. In general, the cyclone pilots were the same as those used in the LDI concepts, and the LDI injectors were simply replaced by IMFH tubes. Because the IMFH tubes are longer than the LDI injectors, the overall length of the combustor also increased. This was undesirable but was a tradeoff that had to be considered in order to address the high-power NOx requirements. Each of the LPP concepts used essentially the same internal components (IMFH tubes and cyclone pilots) but arranged in different quantities and patterns within the combustor.

LPP Multistage Radial/Axial Concepts – The LPP MRA combustor concepts were really variations of the LPP stepped-dome designs, except that the cyclone pilot stage was moved from the main dome to an outboard position. Multiple concepts were considered, as shown in Figures 10 and 11. Early designs attempted to maintain staging isolation by angling the main dome to effectively introduce "steps" between each row of IMFH tubes, and to angle the pilot stage relative to the main dome. From a mechanical standpoint, this was undesirable, and the simpler vertical dome with pilots pointing radially inward was introduced (Concept 4 in Figure 10). The main concern with this simplified design was that all staging isolation was lost; low-power CO was expected to be higher than with the alternative designs because the burning pilot gases were directly interacting with the unfired IMFH air (such as at ground idle). Additionally, because of the outboard pilot, exit temperature profiles at partially staged conditions were expected to be outer-peaked. This was very undesirable for turbine efficiency. Conversely, this was one of the advantages of the stepped-dome designs: at low power, exit profiles would be essentially center-peaked, the preferred result. However, by locating the pilots perpendicular to the main dome, it was felt that the IMFH stages could burn more

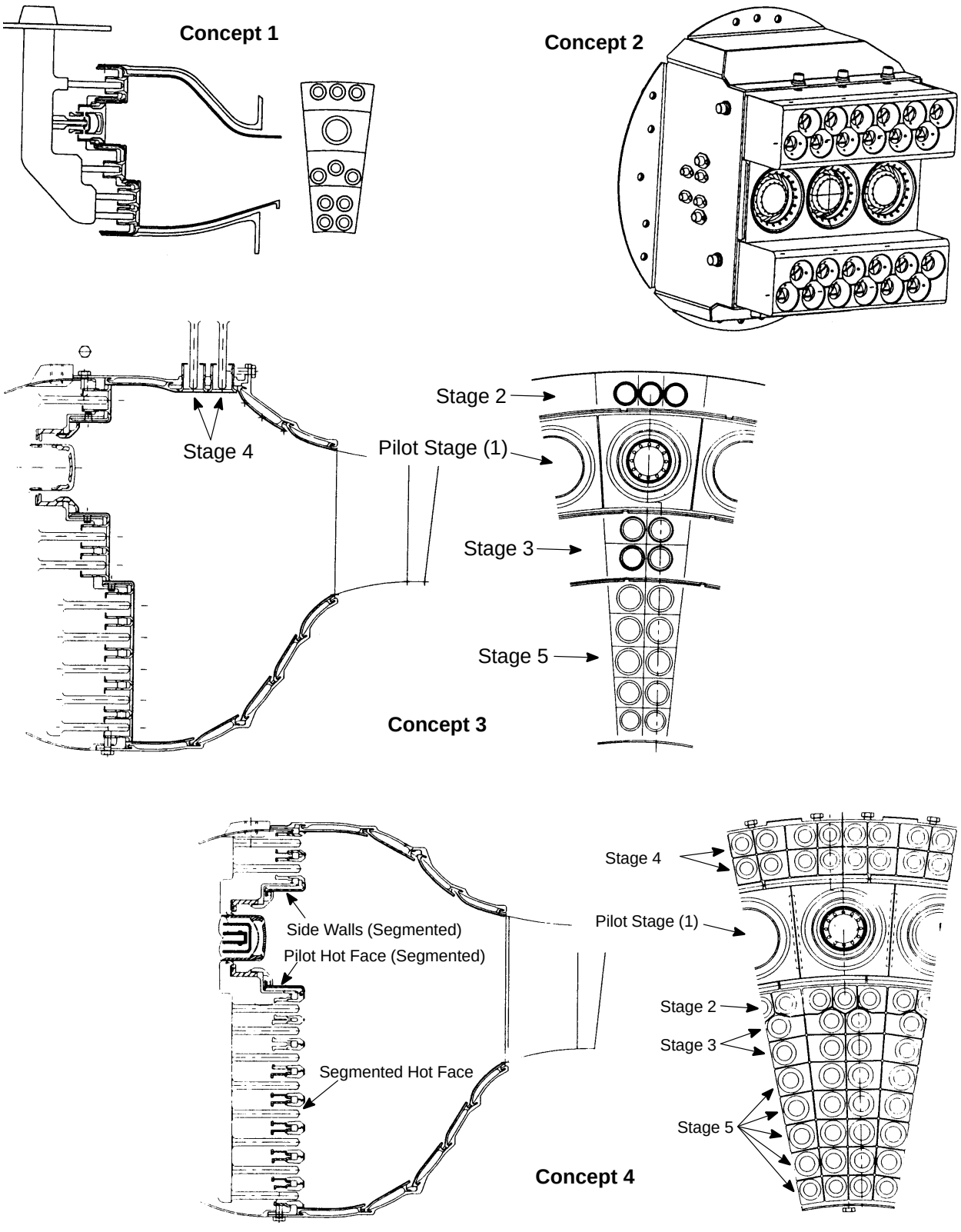

Figure 8. LDI Combustor Concepts

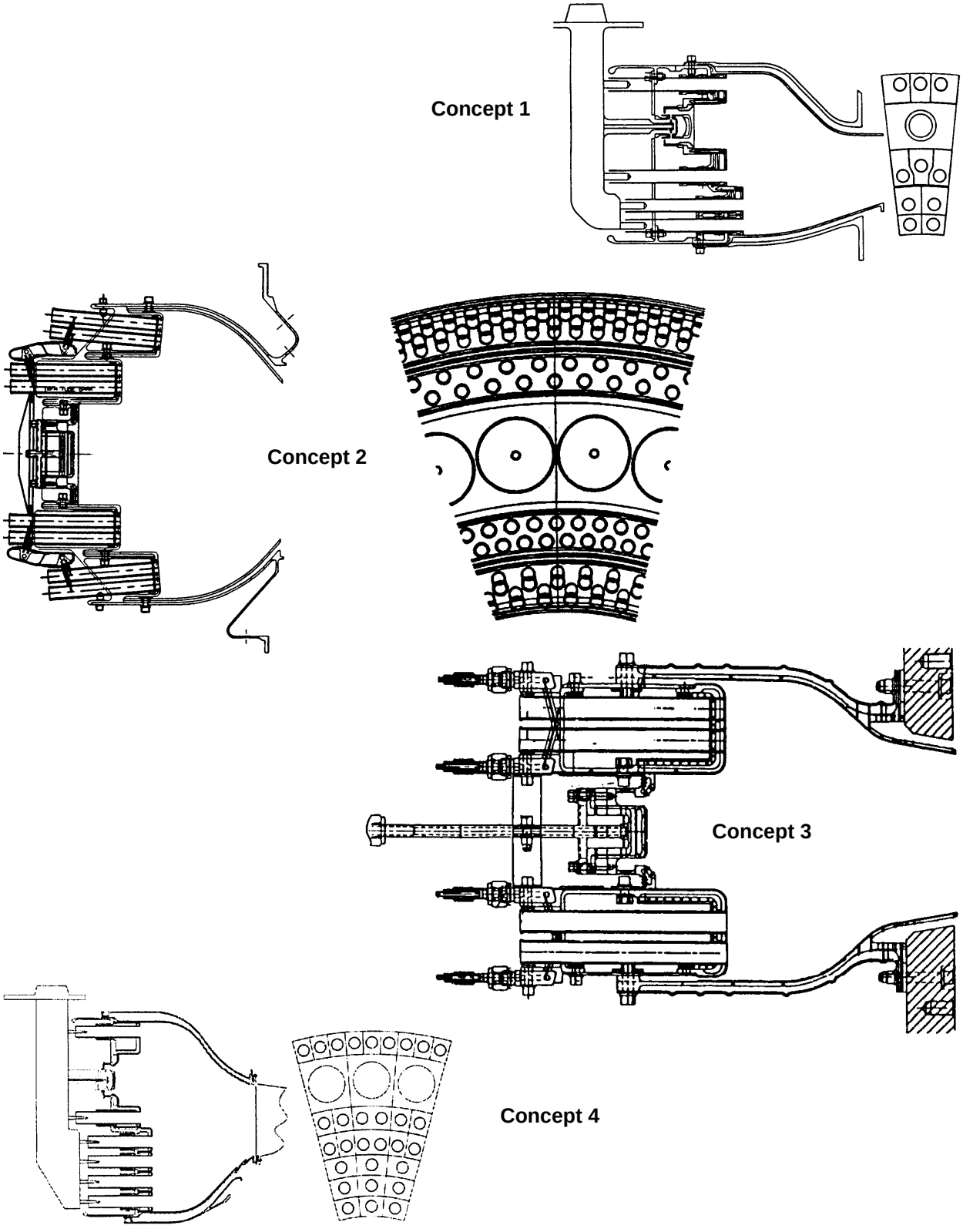

Figure 9. LPP Combustor Concepts

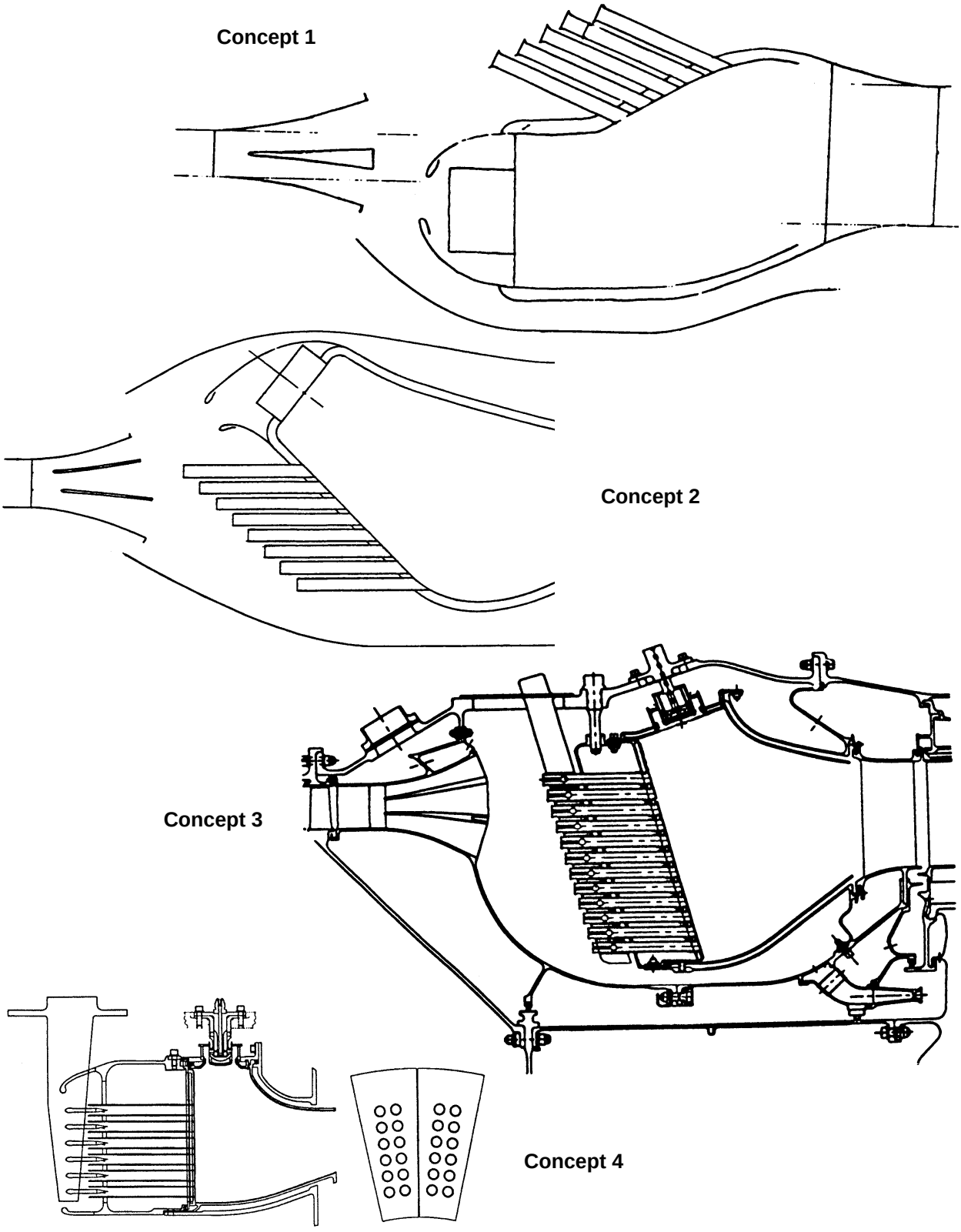

Figure 10. LPP MRA Combustor Concepts 1–4

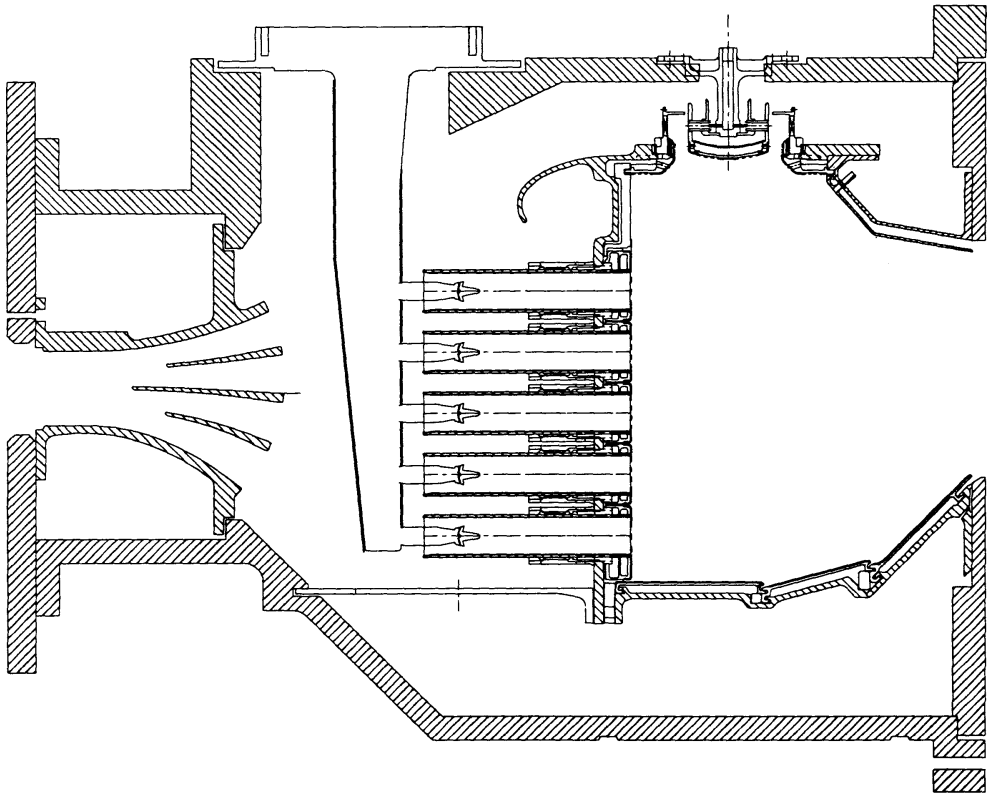

Figure 11. LPP MRA Combustor Concept 5

efficiently at low to moderate power, as the pilots would essentially act as a constant ignition source. Additionally, at high power, with all stages fired, the intense interactions between the burning gases from the pilots and main stages could very well help ensure maximum efficiency and low emissions. MRA Concept 4 was tested heavily and met supersonic cruise emissions requirements. This was the concept chosen in the LPP/RQL downselect. The design shown in Figure 11 was eventually selected for final full-scale development.

4.2.2 Rich-Quench, Lean-Combustion Systems

Development of the RQL combustion system was considered a natural progression from state-of-the-art aircraft gas turbine combustors. Historically, many combustors use a rich-front-end approach to provide good operability and efficiency at low-power conditions while remaining operable with simple or no control requirements over a wide range of conditions required for safe, dependable aircraft operation. However, significant optimization would be required to meet the emissions requirements for this advanced application.

Optimization towards reduced emissions drives combustor design to a single zone of combustion air addition to minimize or eliminate the time spent at or near stoichiometric burning conditions. The intent is to form a rich zone of combustion in the front end to provide flame stability while accomplishing approximately 50% of the energy release from partially burning the fuel in an oxygen-starved environment — without creating any NOx emissions. Because of the nature of the chemical kinetics of rich reactions, the inherent lack of oxygen yields combustion products primarily consisting of CO with essentially no NOx formed. Then the remaining combustion air is added, as rapidly

as possible, in the quench zone to enable the reactions to complete to CO_2, thereby providing the remaining energy release. This air is added as rapidly as possible to minimize combustion residence time near stoichiometric conditions and thus minimize the formation of NOx that occurs at the high temperatures commensurate with stoichiometric burning in an environment that has nitrogen (N_2) and excess oxygen (O_2).

The air addition or quench zone progressed in development to configurations that could allow more rapid air addition and mixing. Initial configurations of the RQL combustor were categorized as "wall-jet." They featured relatively large combustion air jets that penetrate to the center region of the combustor from the walls. These wall-jet configurations could be embodied in annular or "can" combustor configurations. It is noteworthy that, at the region of wall-jet air addition, the combustor walls would typically be necked down into a "wasp waist" to aid penetration and mixing of the combustion air jet and reduce the jet penetration and mixing time.

Further development and optimization of the quench air addition zone led to the introduction of reduced-scale quench (RSQ). In these configurations, the rich combustion effluent would be exhausted in smaller, channel-like regions, and the quench air would be directed into the flowpath through an increased number of combustion holes, smaller relative to the typical size of a wall-jet combustion hole. The smaller, narrower, channel-like quench regions and smaller combustion quench hole sizes would improve mixing and reduce residence time at stoichiometric conditions, thereby further reducing NOx emissions. Two forms of combustion systems were developed: (1) a convoluted liner approach and (2) a quench vane approach. In the convoluted liner approach, the walls of the combustor would convolute the rich-zone air into small channels while the quench air would convectively cool the convoluted surfaces that would essentially protrude into the hot-gas path. In the quench vane approach, a vane, similar to a turbine vane, would protrude into the flowpath, segregating the rich effluent into narrow, radially oriented channels while enabling the quench air to be injected from the side wall of the vane.

All RQL configurations used traditional fuel injector designs, either air-blast or radial jet injection, to provide shear layer mixing in swirl-stabilized, front-end flow fields. The three basic rich combustion systems are described in greater detail in the following subsections.

4.2.2.1 Wall-Jet Combustion Systems

Wall-jet configurations were considered for development as both annular and modular front-end regions. Initially, weight considerations and flame propagation during an ignition sequence drove the design process towards an annular front-end approach (Figure 12). However, early sector rig tests, conducted as precursors to this particular program, showed that a modular approach to wall-jet RQL combustors had a higher potential for achieving the low-emissions goals. This modular approach had the added advantage of eliminating injector-to-injector interactions that could have been the cause of the poorer emissions performance of these early configurations (Figures 13 through 16). Furthermore, concept development could be conducted in single module test vehicles since emissions results would be independent of module-to-module interactions.

4.2.2.2 Reduced-Scale Quench, Convoluted Liner

To meet the stringent NOx emissions for the HSCT application, it became apparent that a modular wall-jet configuration in a product-like design would not be practical. It was necessary to reduce the

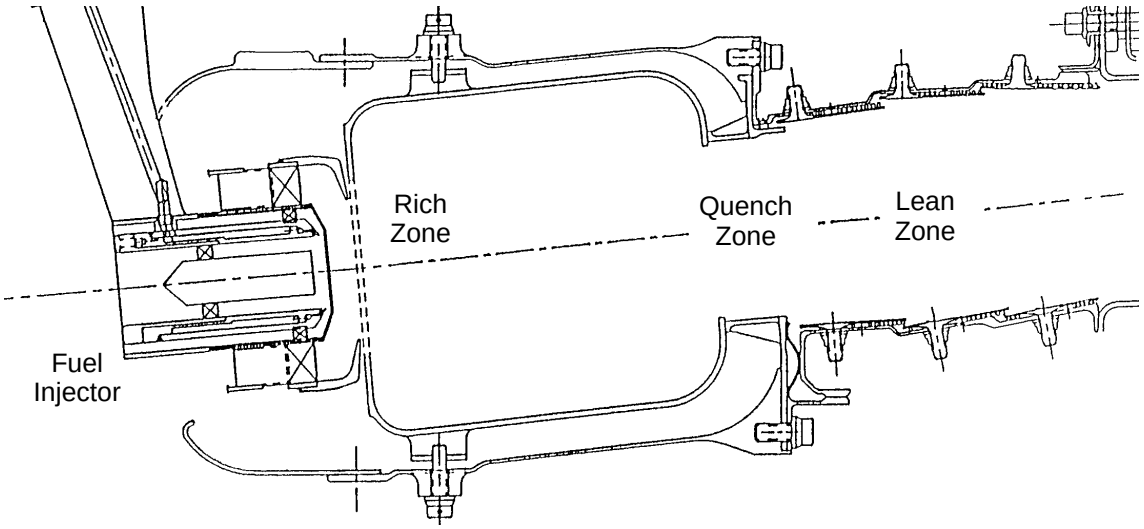

Figure 12. Wall-Jet RQL Combustor with an Annular Front-End Rich/Quench Zone

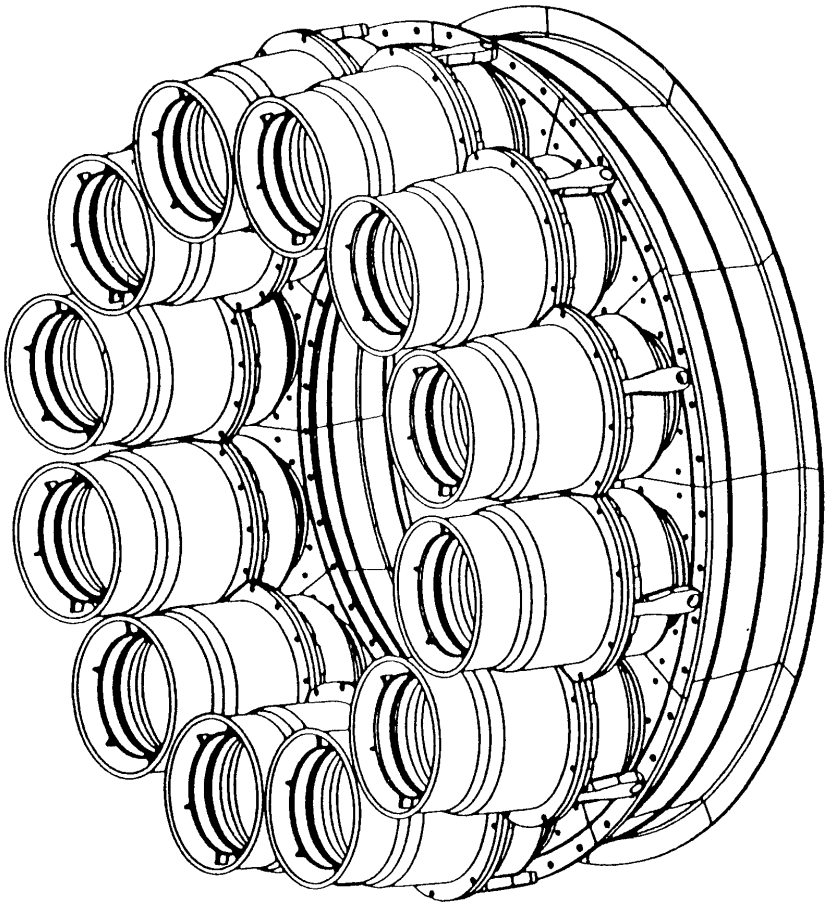

Figure 13. RQL Combustor with Modular Front-End Rich/Quench Zone

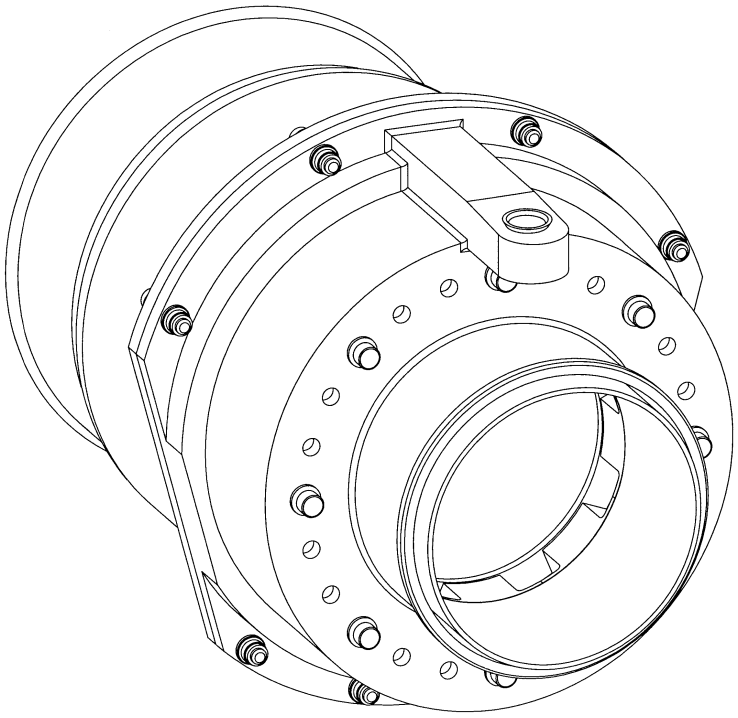

Figure 14. RQL Wall-Jet Front-End Rich/Quench Zone Module, Aft Looking Forward

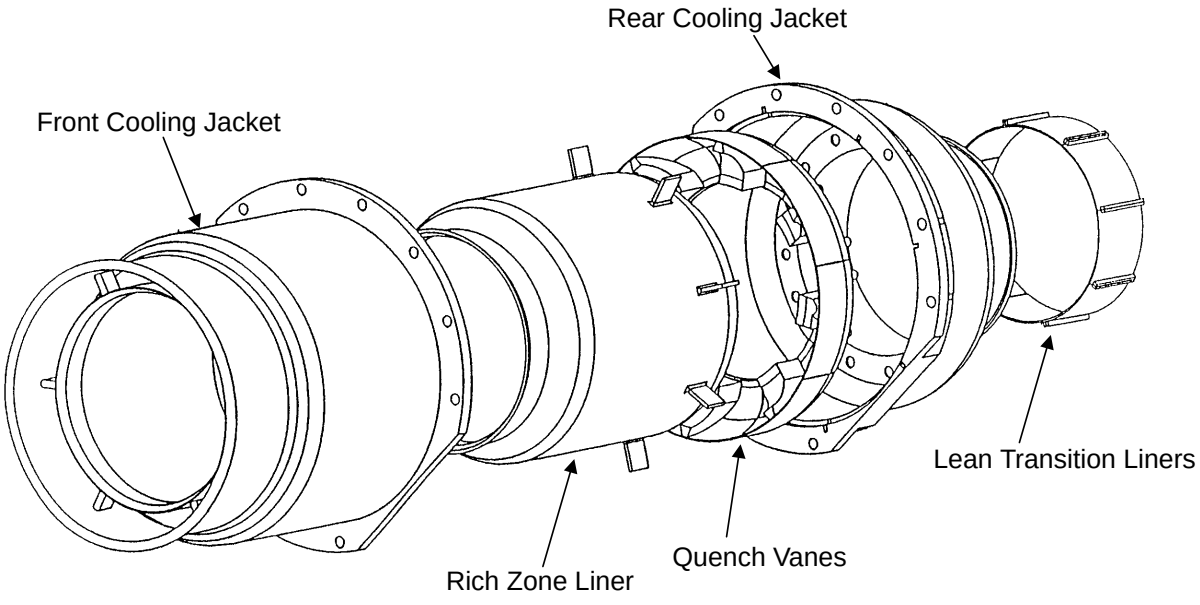

Figure 15. Rich/Quench Module Assembly, Wall-Jet Configuration

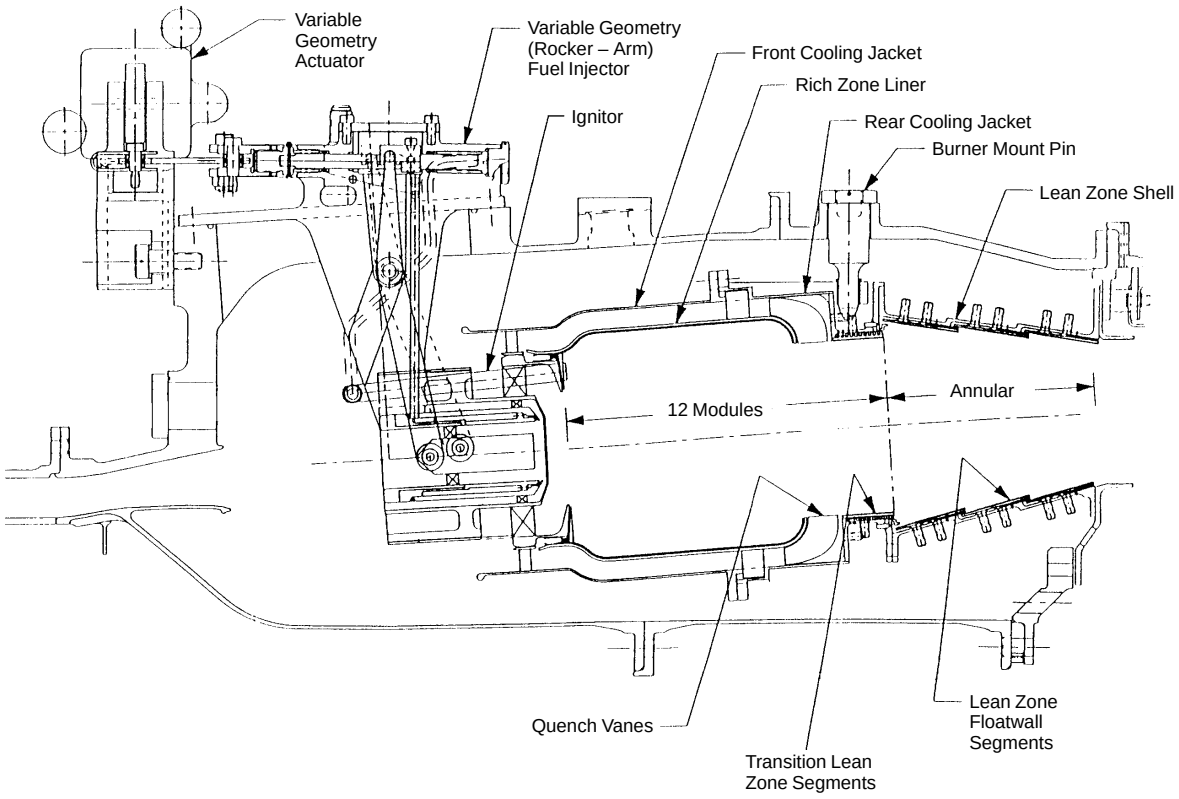

Figure 16. RQL Wall-Jet Combustor with Modular Front-End Rich/Quench Zone

size of the combustion jets to improving mixing and shorten the time required to add and mix the quench air to the combustion process to further reduce the emissions of the rich combustion systems. Because of the modular design that evolved for the RQL combustion systems, implementation of an RSQ approach resulted in convoluting the aft end of the rich-zone liner to provide more perimeter/surface area in which to add the quench air — in what would now be an increased number of smaller combustion jets.

As the number of quench orifices increased, it became apparent that individual, mechanically attached, quench/turning vanes such as those used in the wall-jet configuration would not be feasible. The small-scale turning features were cast into a single quench plate structure but essentially performed the same process; to turn the quench air that was convectively cooling the rich zone liner into discreet jets that would penetrate the rich effluent. A typical module geometry is shown in Figures 17 and 18. As this concept evolved, it was found that significant tailoring of the quench air addition orifices was necessary to enforce uniformity at the quench plane region. It also became necessary to consider narrower quench channel regions. Application of thermal-barrier coating to the flowpath surfaces of the convoluted rich zone liner became a challenge as the convolutions narrowed. This challenge was best addressed through the use of quench vanes that could be individually manufactured (including application of thermal-barrier coatings to the external vane flowpath surfaces). It was also presumed that the flowfield approaching the quench plane region could be made more uniform as the flow was channeled between quench vanes.

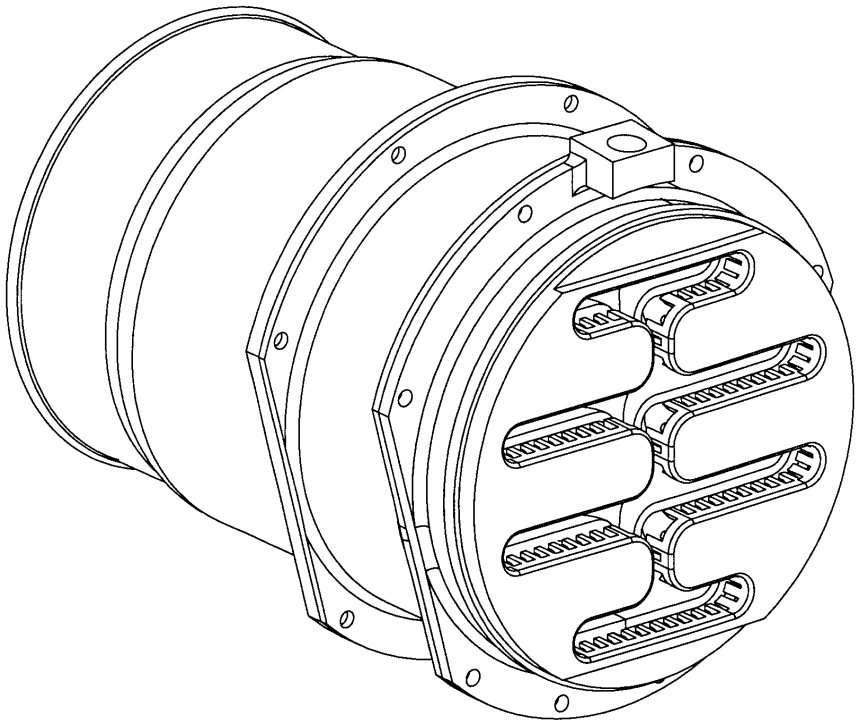

Figure 17. RQL RSQ/Convoluted Liner Front-End Rich/Quench Zone Module, Aft Looking Forward

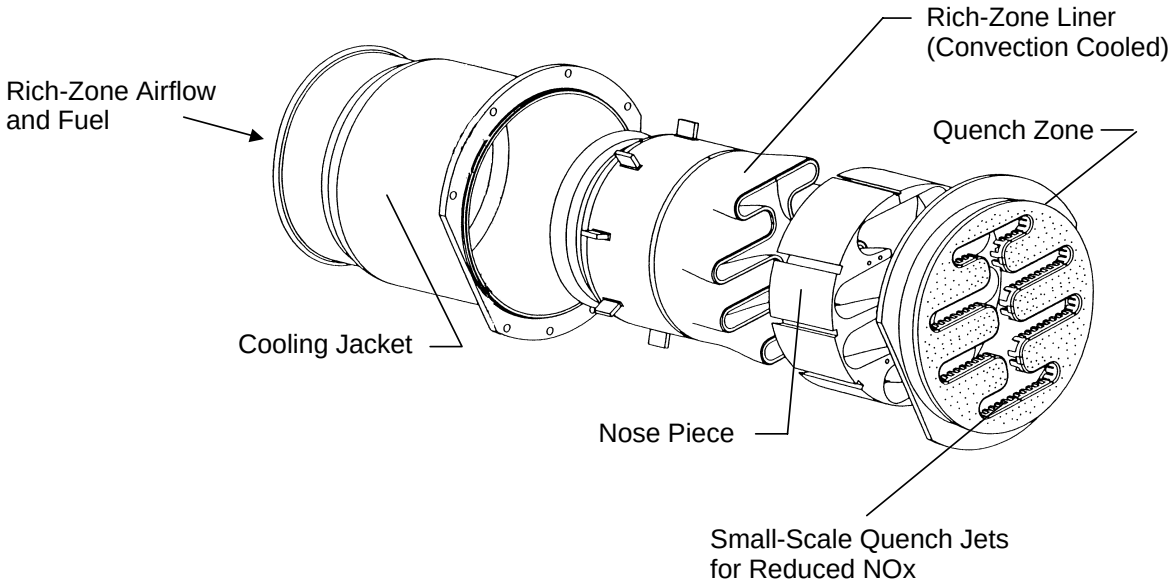

Figure 18. Rich/Quench Module Assembly – RSQ/Convoluted Liner Configuration

4.2.2.3 Reduced-Scale Quench, Quench Vane

Implementation of quench vanes into an RQL combustion system enabled reconsideration of an annular front-end rich zone because the quench vanes are inserted into the flowpath and, at the same time, the use of a vane structure would isolate the quench region processes from any potential interactions with the front-end flowfields. At approximately the same time in the development process, the concept of fuel shifting was evolved and eliminated the need to incorporate a higher risk air-management system such as a variable-geometry fuel injector. Instead, a low-risk fuel-management approach, fuel shifting between two radially positioned front end regions, could achieve the same goals of enabling low-emissions operation throughout the flight cycle and avoiding local flame conditions that would impact the durability of the combustor liners. The resultant full-scale combustor configuration for the 3770.54 engine cycle that incorporates dual-radial, annular, rich front ends with RSQ/quench vanes is shown in Figure 19. This became the ultimate embodiment of the RQL combustion system for HSCT application.

4.3 Design and Analysis Methods and Tools

Every development process goes through a series of design iterations. The iterations often result from tradeoffs that arise among aerodynamic, thermodynamic, heat transfer, and mechanical issues. An acceptable balance must must satisfy the often conflicting needs to meet emissions requirements, efficiently operate the engine, meet hardware life and reliability requirements, and hold weight and costs to acceptable levels. The concepts discussed in the previous subsections had to be analyzed to determine which should be considered for physical testing and final development. Many design methods and analysis tools were required, not only because both aerothermal and mechanical issues had to be addressed but also because multiple lean and RQL concepts were under consideration.

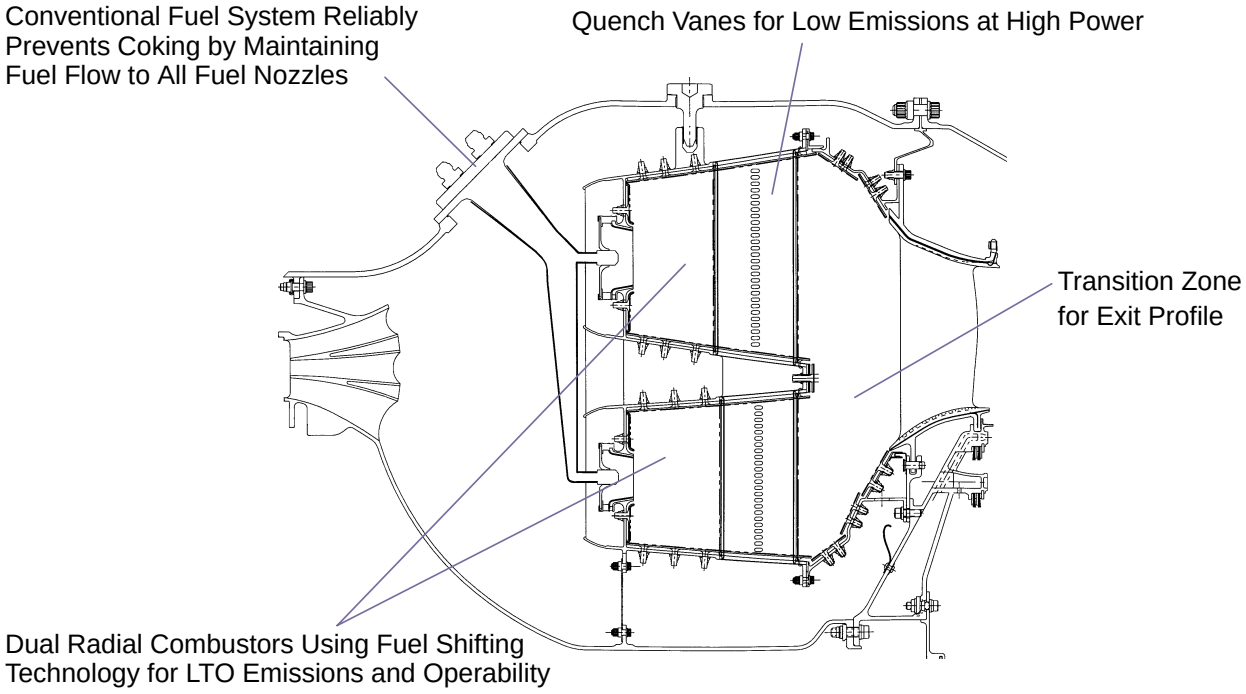

Figure 19. RQL Combustor with RSQ/Quench-Vane Configuration

4.3.1 Lean Premixed/Prevaporized Concepts

Multiple design tools were used in the development of the LPP combustor concepts. These included off-the-shelf and in-house programs. The latter were usually required because of the specialized nature of many of the design features. Wherever possible, off-the-shelf tools were used because they generally offer lower cost and more universal acceptance.

4.3.1.1 Combustor Definition

The primary flow parameters and thermodynamic requirements of the combustor were defined using complex industry computational tools that ensure all components of the engine are matched appropriately to provide the desired engine thrust characteristics. The internal flow distribution and resulting geometric requirements for the combustor itself were determined by developing a specialized program in *MathCad*. Using in-house design practices as a guide, the appropriate estimates, limitations, requirements, and prediction capabilities were added to the program. In this phase, simple empirical correlations were used for emissions predictions. Arrays were used such that calculations could be made at all of the key cycle points in the flight envelope. The program was set up to allow various geometric features and internal flows to be altered in order to minimize emissions. This was also accomplished by changing the number of fuel stages and the staging points. Staging was limited on the low end by lean blowout (or high CO and HC and the related poor combustion efficiency) and at the high end by hardware temperature limitations and high NOx (potentially by high CO as well, if flame temperatures were moving up the equilibrium line). A higher number of stages improves emissions but clearly adds engine complexity, weight, and cost.

Once defined, an in-house computational fluid dynamics (CFD) code was used to predict emissions and exit profiles. This was a complex 3D code capable of providing detailed insight into subcomponent interactions and overall combustor flow characteristics that simple empirical correlations cannot predict. These predictions were still limited, however, since some inputs and boundary conditions are uncertain, or even subjective. Thus, once a concept had been developed which appeared to meet the desired emissions and operability targets, hardware had to be fabricated and tested. The initial and boundary conditions of the CFD code were then modified such that the predicted emissions matched measurements. Once anchored, the code could be used to predict emissions and profiles at other operating conditions, and for similar conceptual designs, with higher confidence.

4.3.1.2 Subcomponent Development

The *MathCad* program described above provided the internal flow distribution, effective flow areas, and staging requirements for the combustor. It did not, however, design each of the subcomponents in fine detail. Primary features were the inner and outer liners, sidewalls (for sectors), the main dome and IMFH tubes, cyclone pilots, and the main fuel nozzle and injectors. They would have to be designed for proper air and fuel flows, resistance to autoignition and flashback, proper cooling to maintain hardware temperature limitations, and geometric features to minimize internal stresses.

Most features of the combustor were simply sized to meet the geometric requirements of the system. In many cases, a flow coefficient could be estimated to increase the physical dimensions such that the proper effective area resulted. In other cases, a more complex in-house computational code was used that not only empirically calculated flow coefficients but also linked the subcomponents in a network and calculated the resulting internal pressure distribution. The final results of the model

provided the designer with physical areas needed to properly size each subcomponent. This method was used for all features except the cyclone pilot, which required a more specialized design tool.

For detailed design of the cyclone pilot, another in-house *MathCad* program was used. Knowing the effective area required, and providing initial sizing inputs on specific features, the program will output all remaining sizing information. Fuel/air residence time and the cyclone swirl number are two of the main parameters that are monitored since they relate to autoignition and stability. Geometric results are also monitored for interferences, flow limitations, and general desirability. Initial inputs to the program are manually changed until residence times, swirl numbers, and geometric features all meet design preferences.

Design of the main fuel nozzle also required special techniques. Because of concerns over fuel coking in the passages, 1D bulk heat pickup analyses were performed to monitor fuel temperatures. Passages were sized and cooling methods implemented to keep heat pickup to a minimum while passing through the nozzle. Stress and vibration analyses were also performed to ensure that vibrational modes did not correspond with acoustic frequencies anticipated for the combustor. ANSYS was the primary tool used for the vibration and stress analyses.

Once all the physical sizes of the internal features had been determined, stress and thermal analyses were performed. The in-house CFD code and off-the-shelf *P/Thermal* and ANSYS software were the primary tools used in this phase. The CFD model was used to predict worst case temperatures and heat transfer coefficients in the combustor hot section. This information was then used for boundary conditions in *P/Thermal* and ANSYS to produce stress fields in each part. If the resulting stresses and temperatures were unacceptable, cooling and hardware designs were modified. The process was iterative until the parts met the necessary life requirements.

4.3.1.3 Controls

The fundamental control system was to be a straightforward design. In general, it would be very similar to the *MathCad* program used to design the combustor itself. The primary functions would be to control total fuel flow rates and to turn fuel flow on and off to specific portions of the combustor at the appropriate staging points in the engine cycle. This would provide the engine with the proper fuel flow to produce the required T_4 into the turbine. Staging would allow the combustor to provide the needed T_4 while minimizing emissions and ensuring stability. Total fuel flow would be set using a standard fuel pump and feedback control system. Fuel staging would be accomplished with a staging valve located on top of each of the fuel nozzles. The valve would isolate the stages and would be hydraulically actuated to open or close as necessary to fuel the appropriate number of stages.

4.3.1.4 Supporting Technology

Though not a part of the combustor itself, the inlet diffuser (located just aft of Plane 3.0) was also an important component of the engine. This feature was used to reduce the flow velocity entering the combustor without inducing the significant pressure losses associated with a simple dump design (a sudden expansion with no divergent transition ahead of it). The diffuser was designed using in-house correlations and models to meet specified pressure loss limitations for the given engine flows. The resulting multipassage diffuser was relatively complex from a manufacturing standpoint, but aerodynamically it performed up to expectations in multiple tests.

Finally, analytical tools were developed to help predict acoustics in the combustor. The design program is FORTRAN based, into which geometric features and thermodynamic inputs are placed.

The program predicts mode shape, amplitude, and frequency. Unsteady heat release and impedance (boundary condition) models are included. The model was anchored to acoustic data from one of the LPP sector tests in order to predict acoustics in future sectors and full-annular systems.

4.3.2 Rich-Quench, Lean-Combustion Concepts

4.3.2.1 Combustor Definition

Combustor effort at P&W focused on the RQL concept, Figures 13 and 16 (pages 12 and 14). This concept incorporates separated zones of combustion to preserve stability while controlling emissions. The combustion process is initiated in a fuel-rich zone and completed in a fuel-lean zone, with a rapid transition between. All of the fuel is introduced in the rich zone but with only a fraction of the air required for complete combustion. The rich-combustion process provides stability and, being deficient in oxygen, completes a significant portion of the overall energy release without forming oxides of nitrogen. The combustion products proceed to a quench section where the remainder of the combustion air is introduced in a rapid, intense, mixing process. The downstream lean zone is used to complete CO and soot burn-off. NOx emissions will be low only if the quench or transition process between the zones is sufficiently vigorous to avoid significant flow residence time near stoichiometric mixture proportions. Subscale testing of a single injector or modular version of the RQL combustor at the HSCT engine supersonic cruise operating conditions has demonstrated the low-emissions potential of this concept and generated a significant design database. As shown in Figures 13 and 16, the initially preferred configuration of the combustor incorporated circumferentially spaced modules composing the rich and quench zones followed by an annular lean zone.

For the HSCT engine application, the aerothermal design point of the RQL combustor is the supersonic cruise condition. Evaluations performed in prior flametube tests indicate that the equivalence ratio in the rich zone should be between 1.6 to 2.0, which is sufficiently high to preclude NOx emissions at the exit of the rich zone while minimizing the proclivity for smoke formation. To minimize NOx production in the quench and lean zones, liner cooling airflow to the lean zone is minimized and the remainder of the combustor air enters through the quench air system. This air serves a dual function; it provides convective cooling of the rich-zone liner while being directed to the quench section by an enclosing hood. Based on an overall fuel/air ratio of 0.030 at nominal supersonic cruise, these considerations lead to a combustor airflow distribution of about 22% to 24% in the rich zone, 71% to 73% through the quench system, and 5% for lean-zone liner cooling.

4.3.2.2 Control Modes

Two control modes for the RQL combustor were evaluated fuel injectors with variable-geometry airflow paths and fuel shifting; the latter was ultimately selected.

Variable Geometry

While the airflow distribution cited above is optimized from the point of view of supersonic cruise operation, as the engine is operated at fuel/air ratios less than supersonic cruise, the mixture strength in the rich zone would approach and eventually pass through stoichiometric proportions. Since the highest gas temperatures occur in the products of stoichiometric or near-stoichiometric combustion, steady-state operation at points in this regime could have adverse effects on durability of the rich-zone liner and on the emissions output at some intermediate power levels.

A second prohibited region occurs at low overall engine fuel/air ratios and high rich-zone equivalence ratios. This regime indicates the operation of the rich zone at above stoichiometric conditions that will generate large quantities of CO and smoke but for which there is inadequate temperature levels in the quench and lean zones to oxidize these products. Consequently, the so-called "rich" zone (at high power) can only be operated at lean, or below stoichiometric, proportions at low power to preclude large quantities of CO and smoke in the exhaust.

With the constraints of avoiding steady-state operation in the prohibited near-stoichiometric zone while still achieving the operational capability of a flight engine, variable-geometry approaches to manipulate combustor airflow distribution were considered an enabling technology. Design issues associated with a variable-geometry combustor were addressed. The findings from that effort were applied in the development of the integrated module rig that extensively used a variable-geometry fuel injector during this combustor development activity. A representative stoichiometry diagram for a variable-geometry RQL combustor and a fuel-shifted RQL combustor are shown in Figure 20.

Fuel Shifting

The fuel-shifting approach involves designing the combustor with both an inner and an outer bank of rich-quench zone modules as shown on Figure 21. Shifting the split of fuel between banks according to a schedule like that shown on Figure 20 accomplishes the control function. Once the combustor is started and brought to idle, fuel flow to a terminal is never interrupted. This is a decided advantage over more conventional staged systems. As evident from Figure 20, fuel-shifting control technology is intended primarily to improve emissions and performance at moderate power levels from above idle to just below subsonic cruise power. It also must function to avoid liner durability problems at some regimes of the high-power portion of the operating envelope, primarily the descent from supersonic cruise.

To provide for the operational capability of a flight engine while avoiding the constraint of avoiding steady-state operation in the prohibited zones of rich-zone stoichiometry, the airflow split between the inner and outer banks is established at 63% to the inner while 37% is delivered to the outer bank.

The descent and approach conditions are within the regime where the combustor must be operated in the unequal inner-to-outer fuel/air ratios or the so-called fuel-shifted mode. At the descent condition the inner-bank front end is operating above stoichiometric while the front end of the outer bank is lean. As power level is increased to approach, the mode-shifting behavior is reversed so that the OD bank is rich while the ID bank is lean. Studies and combustor tests indicate that the combustor exit gas temperature profiles are maintained within limits acceptable to turbine durability. At power levels where the combustor would operate with both banks producing the same gas temperature levels (that is, idle and high-thrust conditions), the combustor exit radial temperature profile will be very flat and uniform commensurate with a low-emissions RQL combustor.

4.3.2.3 Subcomponent Development

Evolution of the RQL combustor involved a multistep engineering process in which preliminary and supporting development activities provided a major contribution. In following sections of this report, particularly Section 4.4.2 , these supporting activities are associated with the subcomponents and evolving technology base for the the RQL combustor.

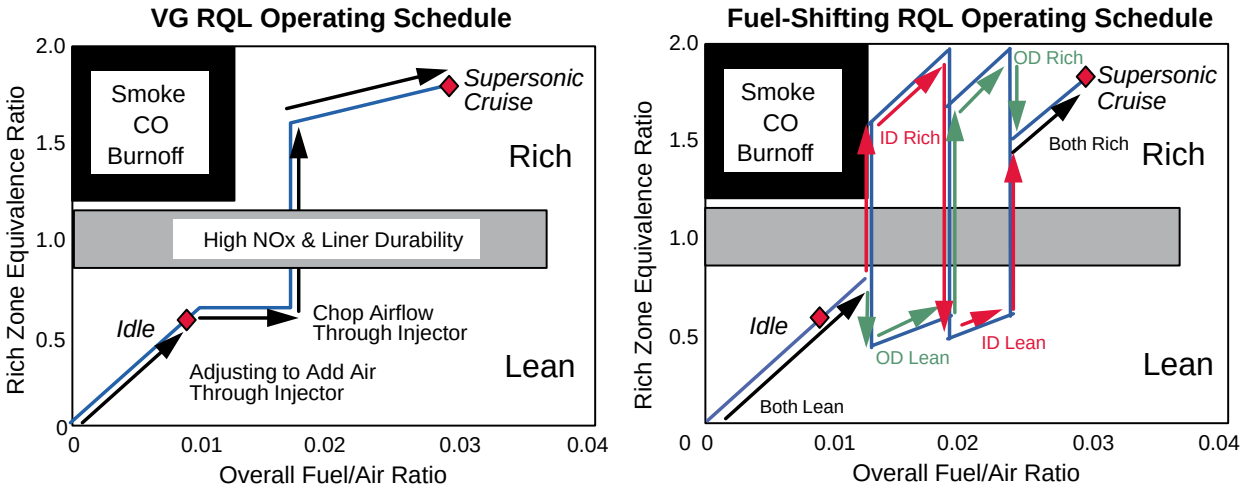

Figure 20. Rich-Zone Stoichiometry of a Variable-Geometry RQL Combustor (Left) and a Fuel-Shifted RQL Combustor (Right)

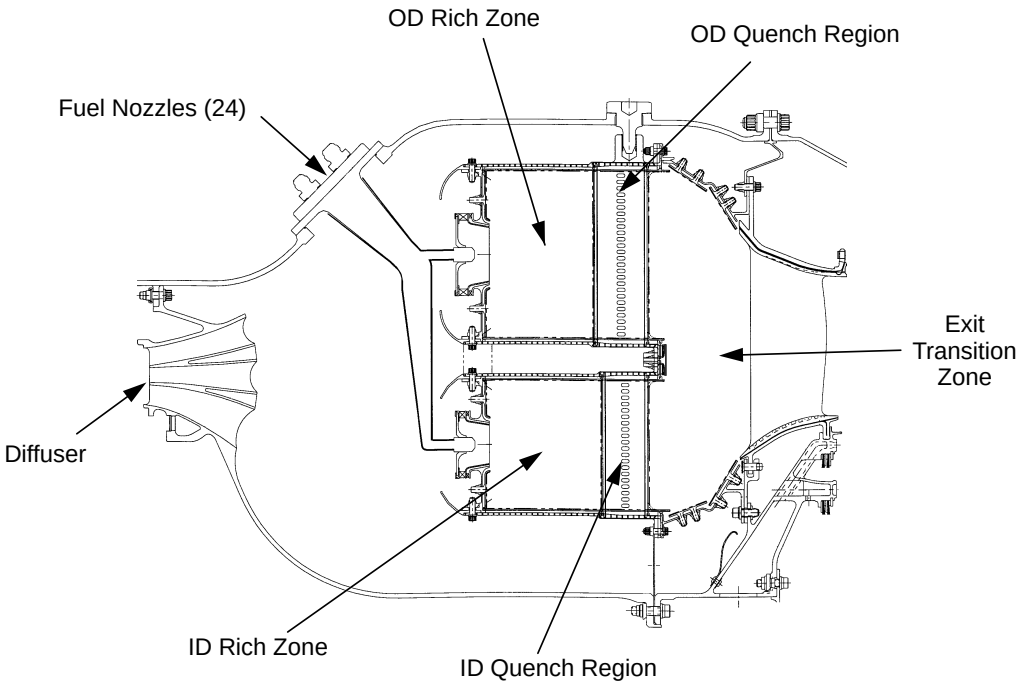

Figure 21. Rich/Quench/Lean HSCT Combustor

For reference, the activities are numbered:

1. The preliminary definition of the characteristics of the RQL combustor was derived from a flametube combustor constructed at Uniter Technologies Research Center (UTRC). The rig consisted of cylindrical and conical segments of a ceramic, ply-cast construction. These exploratory tests included more than 50 configurations and provided bases for defining zone sizing and other design parameter values as well as evaluation of the effect of number and shape of wall-jet-type quench orifices.

2. Flow-visualization tests were concentrated in fuel injector/rich-zone flow interactions and, to a larger degree, qualitative assessment of quench-zone performance and mixing. Both included water-tunnel testing, but most of the quench-zone assment was conducted on air/air models. Mie scattering of laser illumination from the air in the quench jets — seeded with a fine mist of oil droplets — was used extensively to generate instantaneous and time-averaged profiles of quench jet penetration and mixing at selected downstream planes..

3. A supporting effort to define and develop a cast PW1422 liner for the rich zone of a modular RQL combustor was conducted to address and resolve the design and fabrication issues. Variations in outer surface texture — smooth versus augmenting ridges — were evaluated in hot-flow, combusting-rich-zone test rigs. The task also addressed aerothermal integration of the quench air delivery system with the downstream end of the liner and established the rich-zone liner construction base for the duration of the program.

4. A supporting investigation was conducted to define and optimize a fuel injector with a variable-geometry, atomizing, airflow path for the RQL combustor. Models were built of several candidate configurations and variations. These were evaluated in flow-visualization and qualitative fuel spray characterization over the entire operating range. The best configuration was selected and, when fabricated in metal, served the remainder of tested variable-geometry-type combustor module tests.

5. When the characteristic dimensions of wall jets and penetration distances were found to be excessive for NOx control, design studies were addressed at the RSQ concept. Again, extensive computational and flow-visualization experiments were conducted to define the convoluted rich-zone liner approach in which quench air jets were discharged from numerous small orifices, with characteristic dimensions of 0.10 to 015 inches into gas-path convolutions of nominal depths of 0.5 inches or less. The cast rich-zone liner technology cited above was readily extended to these constructions.

6. RSQ was extended further by installing quench orifices on both sides of vanes that spanned the RQL combustor gas path in the radial direction. The definition of the vanes required aerodynamic testing and flow visualization of larger size plexiglass models as well as numerical analyses to optimize the flow of quench air into the vanes from each end and equalize the flow distribution to each orifice.

4.4 Precursor Subcomponent Development

Subcomponent development generally focused on the design and test of a variety of fuel injectors and fuel/air mixing techniques. In the lean systems, the subject subcomponents were the LDI injectors, IMFH premixers, and cyclone pilots. In the RQL systems, development focused on the rich-zone fuel injection, the quench-zone air injection and mixing, and the lean-zone uniformity.

4.4.1 Lean System

Subcomponents developed for lean systems include injectors/mixers for LDI systems as well as an array of IMFH premixers and cyclone pilots for LPP systems. These were tested as either single entities or in small bundles, usually firing into a ceramic-lined tube. Subscale hardware was used as a method of relatively quickly filtering a large number of potential design concepts. The best designs could then be implemented into sectors for studying the overall impact of interactions among subcomponents. Fixed rakes as well as traversing probes were used for emissions sampling.

4.4.1.1 Lean Direct Injection

In most low-emissions systems, the combinations of fuel injection, atomization, vaporization, and premixing are the keys to meeting stringent emissions requirements. This becomes especially difficult in LDI systems, which rely almost entirely on atomization to quickly distribute the fuel as uniformly as possible in a lean mixture of fuel and air, with minimal time available for vaporization and premixing. For poorly atomized fuel and/or highly nonuniform fuel/air mixtures, poor emissions are readily observed. Thus, LDI development focused on fuel injection methods and rapid atomization mechanisms that could provide the best atomization and most uniform fuel/air mixtures to the combustor.

Three primary multiventuri injection configurations were tested in support of the LDI combustor concepts described in Section 4.2.1. Tests were performed on axial swirler designs with 45° helical vanes and radial swirler designs with 30° and 60° vanes (Figures 22 and 23). Key dimensions and flow areas are summarized in Table 2. The injectors were sized to have approximately the same effective flow area as the half-inch IMFH tubes, which were under simultaneous development. A Textron simplex air-blast nozzle located along the axial centerline was used for fuel injection. These injectors create finely atomized sprays at the throat of the venturi, rapidly mixing with the highly swirled air. For improved stability, and to better simulate side-by-side operation in an engine, each of the axial and radial swirler designs was tested in 3×3 arrays rather than as individual entities. In one test, an alternating mixture of 30° and 60° radial swirler designs was tested (30°/60°/30° on the top and bottom; 60°/30°/60° for the middle row). Note that in all cases the injectors were located on one-inch centers from each other.

LDI testing under this contract was performed at NASA–Glenn. Data were acquired over a range of operating conditions. Variables included inlet air temperature, pressure, pressure drop, and fuel/air ratio. The best results came from the 45° axial swirler design and are summarized in Table 3 and Figure 24. Unfortunately, high-power NOx was higher than desired, with NOx at 1075°F, 155 psia, 3.8% ΔP, and 3410°R flame temperature coming in just above 8 EI. This was projected to extrapolate to 9 to 10 NOx EI at nominal supersonic cruise conditions (1200°F, 150 psia). Combustion efficiency was extremely good, coming in above 99.9% at most flame temperatures tested.

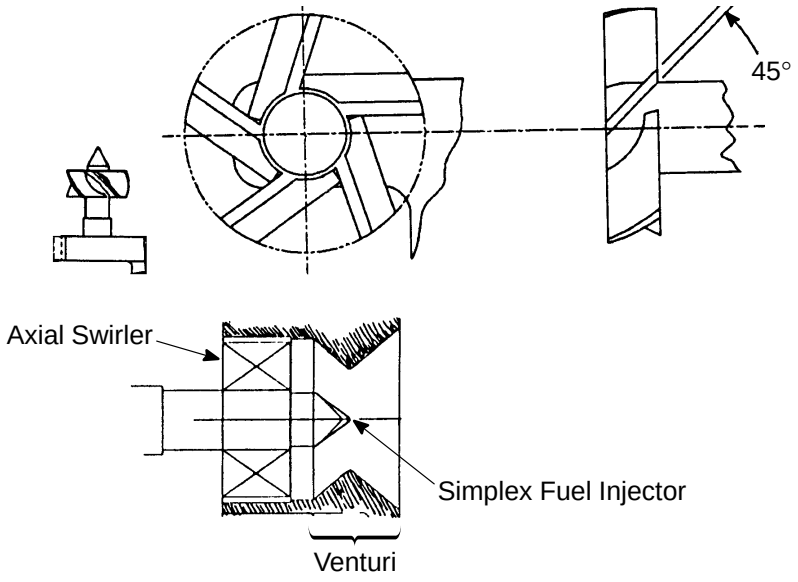

Figure 22. Axially Swirled LDI Injector

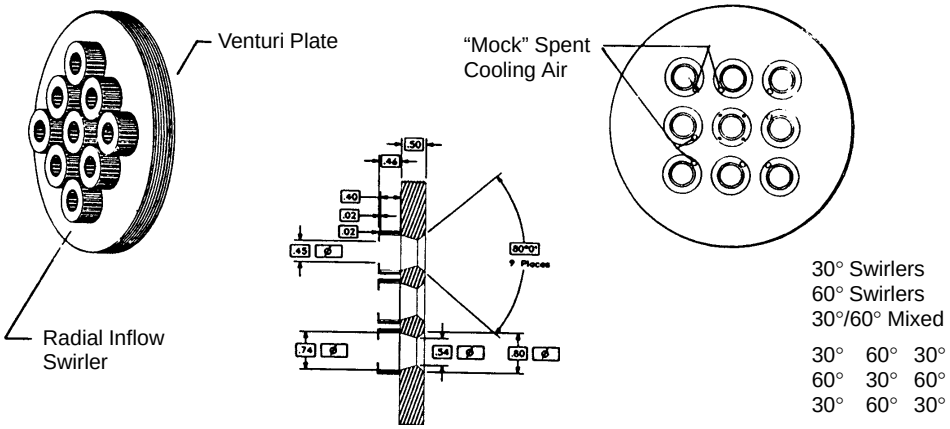

Figure 23. Radially Swirled LDI Injector Array

Table 2. LDI Design Summary Table

Parameter	LDI Injector Configuration		
	Axial 45	**Radial 30**	**Radial 60**
Swirler Vane Type	Axial	Radial	Radial
Swirler Vane Angle (Degrees)	45	30	60
Number of Swirler Vanes	5	30	24
Swirler Vane Thickness (Inches)	0.033	N/A	N/A
Axial Component of Swirler Vane Length (Inches)	0.373	N/A	N/A
Swirler Slot Height (Inches)	N/A	0.400	0.400
Swirler Slot Width (Inches)	N/A	0.042	0.030
Swirler Outer Diameter (Inches)	0.848	0.900	0.900
Swirler Inner Diameter (Inches)	0.320	0.740	0.740
Centerbody (Spray Nozzle) Diameter (Inches)	0.29	0.29 (?)	0.29 (?)
Venturi Throat Diameter (Inches)	0.50	0.54	0.54
Diverging Cone Angle (Downstream of Throat, Degrees)	80	80	80
Effective Flow Area (Square Inches)	0.172	0.172	0.175
Swirl Number	(?)	0.23	0.56

Table 3. LDI Injector Emissions Summary: 45º Axially Swirled

T_3 (ºF)	P_3 (psia)	ΔP/P (%)	Sampled Equivalence Ratio	T_{flame} (ºR)	Combustion Efficiency (%)	NOx EI (g/kg Fuel)
1069	153	3.80	0.395	3163	99.94	4.7
1075	158	3.85	0.442	3344	99.94	7.2
1082	154	3.83	0.470	3452	99.95	9.1
1094	150	5.99	0.531	3683	99.94	4.0
1072	158	4.50	0.519	3630	99.92	7.3
1080	154	4.21	0.540	3710	99.92	4.5
1080	155	3.61	0.540	3711	99.93	4.4
1100	202	4.60	0.437	3364	99.51	2.2
1099	200	4.85	0.486	3555	99.97	4.6
1101	201	4.83	0.515	3670	99.98	5.9
1099	200	4.85	0.550	3802	99.97	7.3

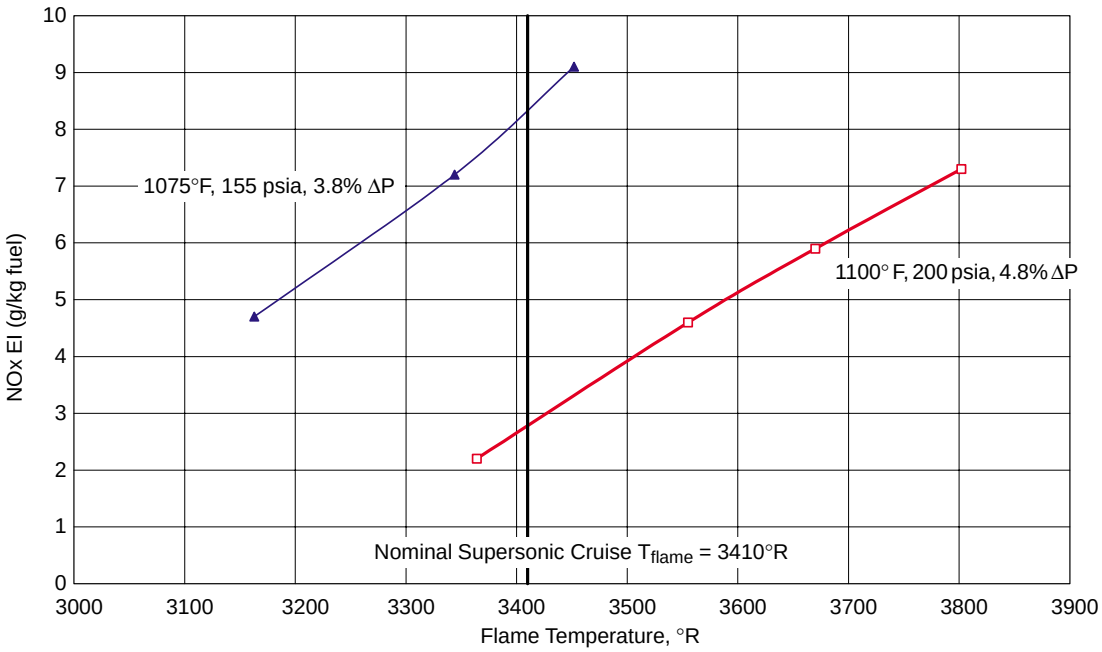

Figure 24. NOx Emissions for the 45º Axial Swirler LDI Configuration

The most surprising result of the test was the significant decrease in NOx when the pressure increased (at high temperatures, holding temperature constant). Although pressure drop was slightly different between the two cases, other data suggest the impact of pressure drop accounts for less than 1 EI of the nearly 5.5 EI NOx reduction (see Table 3 and Figure 25). A typical equation used to estimate NOx is:

$$EINOx = C \times t \times \exp[(-72.28) + 2.087(T_{flame}^{0.5}) - 0.014611T_{flame}]$$

for $T_3 > 650$°F, where C is a constant, t is the residence time in the primary zone of the combustor, and T_{flame} is the flame temperature (°R). The operating pressure impacts the residence time, t (holding flame temperature constant). Thus, in theory, NOx in premixed flames will increase with the square root of pressure. The observed NOx decrease was therefore highly unexpected. The only explanation at this time is that there was a substantial improvement in atomization and mixing when the pressure was increased at these elevated temperatures. Surprisingly (or maybe consistently), similar NOx reductions at high temperatures with increasing pressure were observed in IMFH and cyclone development as well.

From the subcomponent LDI development tests, the 45° axial swirler design proved to be the best. This design was eventually selected for use in the rectangular three-cup LDI sector (described later).

4.4.1.2 Integrated Mixer/Flameholder Development

LDI systems have great potential because they offer relatively short axial length. This helps keep the combustor as short as possible, directly impacting overall engine length and weight. However, the brief vaporization and premixing time makes stringent emissions requirements difficult to meet. Although the combustor is short, the LDI mixers tend to be difficult to package in the dome area available and are fairly complex devices to manufacture. Thus LPP systems were considered to help

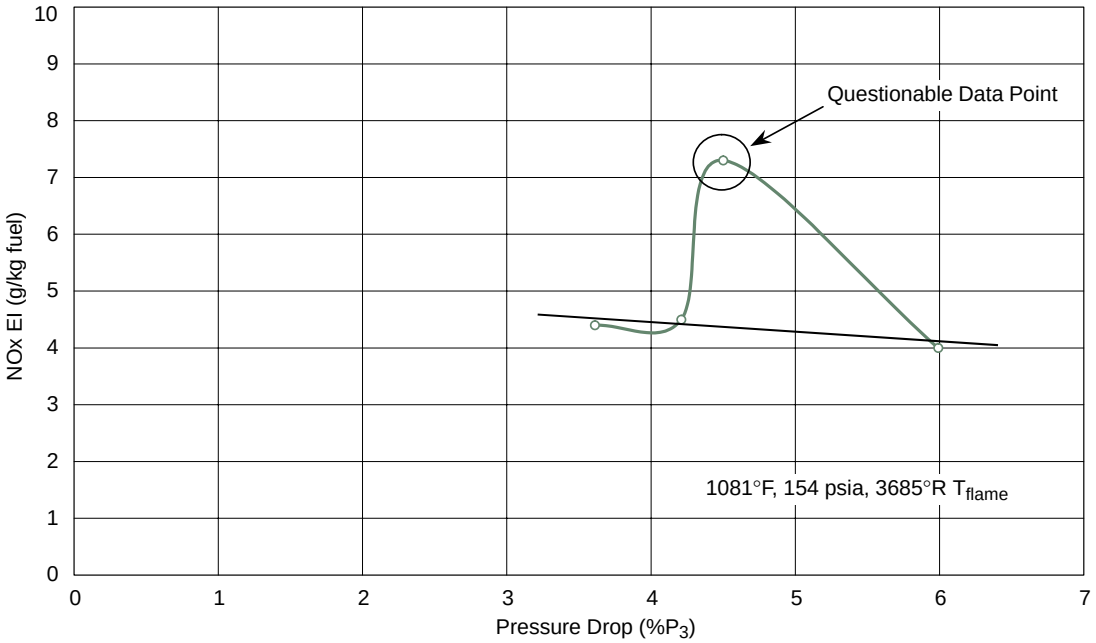

Figure 25. Impact of Pressure Drop on NOx Emissions for the 45º Axial Swirler LDI Configuration *The data suggest pressure drop has only a small impact on NOx emissions at elevated temperatures and pressures.*

meet the emissions targets. The eventual tradeoff is a common one that must be made in engine design: cost, weight, and complexity against emissions.

Like the LDI injectors, IMFH development was given considerable attention because of significant concerns early in the program about meeting supersonic cruise NOx emissions requirements. Because an IMFH burns 75 to 80% of consumed fuel at cruise (in the latest design), it is extremely important that very low NOx be generated at these conditions. Although the cyclone pilots only burn 20 to 25% of the fuel at cruise, it was anticipated (and later demonstrated) that supersonic cruise NOx emissions would be much higher than with the IMFH premixers. Thus, it was a key driver for the IMFH to demonstrate EI NOx well below 5 to enable meeting the overall engine supersonic cruise emissions requirement of 5 EI NOx.

Over the course of the contract, dozens of design variations of the IMFH premixer were tested (see Tables 4 and 5). Of these, 26 were subscale (Configurations 12–37), and 14 were full-scale (Configurations 38–51) variations developed prior to the LPP/RQL downselect. Most were tested at low pressure (60 psia or less), although several of the later designs were tested up to 150 psia. Primary changes were to the method of fuel injection. This started as a simple 0.020-in ID by 0.040-in OD hypo tube and progressed to the more advanced “stinger” designs (Figure 26). Note that some of the variations were simply changes to the radial location, or immersion, of the point of fuel injection within the tube (such as Configurations 28–30 and 31–33, Figure 27). In these cases, the design of the fuel injector itself was not changed. In other cases, mixing length (the distance from the point of fuel injection to the aft end of the IMFH tube) and/or the total tube length were changed. The IMFH tube diameter was also a variable. IMFH testing was performed at GEAE.

Table 4. Summary of IMFH Configurations

Configuration Number	Tube Dimensions (in)			Dome Cooling Air		Flange	Hot-Section [1]		Test Date [2]	Comments
	Tube ID	Total Length	Mixing Length	No. of Holes	Hole Dia. (in)	Mixer Tubes	Liner ID (in)	Dist. to Sample Probe (in)		
12	0.65	5.50	4.50	6	0.121	7	3.70	7.4	10/94	
13	0.65	5.50	4.50	6	0.121	7	3.70	7.4	10/94	
14	0.65	5.50	4.50	6	0.121	7	3.70	7.4	11/94	
15	0.50	5.50	4.50	6	0.090	7	2.80	7.4	12/94	
16	0.50	5.50	4.50	6	0.090	7	2.80	7.4	12/94	
17	0.50	5.50	4.50	6	0.090	7	2.80	7.4	02/95	Slotted inlet
18	0.50	5.50	4.50	6	0.090	7	2.80	7.4	02/95	0.4-in patch on inlet slot
19	0.71	4.00	2.80	6	0.100	5	3.70	7.4	NT	20° inlet swirler, 0.84-in inlet diameter
20	0.50	5.50	4.50	6	0.090	7	2.80	7.4	03/95	Long slot cover on inlet
21	0.50	5.50	4.50	6	0.090	7	2.80	7.4	04/95	Covered slot inlet
22	0.50	5.50	4.50	6	0.090	7	2.80	7.4	05/95	
23	0.71	4.00	2.80	10	0.100	5	3.70	7.4	06/95	10° inlet swirler, 0.84-in inlet diameter
24	0.50	5.50	4.50	6	0.090	7	2.80	7.4	06/95	
25	0.50	5.50	4.50	6	0.090	7	2.80	7.4	06/95	
26	0.50	5.50	4.50	6	0.090	7	2.80	7.4	08/95	Long slot cover on inlet
27	0.50	5.50	4.50	6	0.090	7	2.80	7.4	NT	Long slot cover on inlet
28	Oval	5.50	4.50	10	0.080	6	3.20	7.4	08/95	0.839x0.25-in oval mixer tube with conformal injector body
29	Oval	5.50	4.50	10	0.080	6	3.20	7.4	09/95	
30	Oval	5.50	4.50	10	0.080	6	3.20	7.4	09/95	
31	0.50	5.50	4.50	6	0.090	7	2.80	7.4	10/95	
31	0.50	5.50	4.50	6	0.090	7	2.80	7.4	01/98	Retested in another cell
32	0.50	5.50	4.50	6	0.090	7	2.80	7.4	11/95	
33	0.50	5.50	4.50	6	0.090	7	2.80	7.4	11/95	
34	0.71	4.00	2.80	10	0.100	5	3.70	7.4	11/95	0.843-in diameter inlet, 0.710-in exit
35	0.65	5.50	4.50	6	0.121	7	3.70	7.4	12/95	
36	0.83	5.50	4.50	6	0.152	7	4.90	7.4	12/95	
37	0.65	5.50	4.50	6	0.121	7	3.70	7.4	12/95	
38	1.00	5.50	4.50	12	0.149	4	4.50	7.4	08/96	
39	1.00	5.50	4.50	12	0.149	4	4.50	7.4	09/96	
40	1.00	5.50	4.50	12	0.149	4	4.50	7.4	09/96	
41	1.00	5.50	4.50	12	0.149	4	4.50	9.3	05/97	
41	1.00	5.50	4.50	12	0.149	4	4.50	9.3	09/97	Retested in another cell
42	1.00	5.50	4.50	12	0.149	4	4.50	9.5	09/97	
43	1.00	5.50	4.50	12	0.149	4	4.50	9.5	10/97	
44	1.00	5.50	4.50	12	0.149	4	4.50	9.5	10/97	
45	1.00	5.50	4.50	12	0.149	4	4.50	9.5	11/97	
46	1.00	5.50	4.50	12	0.149	4	4.50	9.5	02/98	
47	1.00	5.50	4.50	12	0.149	4	4.50	9.5	03/98	
48	1.00	5.50	4.50	12	0.149	4	4.50	9.5	03/98	
49	1.00	5.50	4.50	12	0.149	4	4.50	9.5	03/98	Dome cooling-air holes introduce 30° swirl
50	1.00	5.50	4.00	12	0.149	4	4.50	9.5	03/98	
51	1.00	5.50	4.50	12	0.149	4	4.50	9.5	04/98	

Notes: 1. Hot section had cast ceramic liner.
2. NT = Not tested

Table 5. Summary of IMFH Configurations Fuel Injector Information

Fuel Injector Type	Configuration Number	Fuel Injector Discharge				Test Date [1]
		No. of Ports	ID (in)	OD (in)	Immersion (%)	
Hypo tube angled 15°	12	1	0.020	0.040	25	10/94
Fan spray tube angled 15°	13	1	Oval		25	10/94
Beveled hypo tube angled 15°	14	1	0.020	0.040	25	11/94
	15	1	0.020	0.040	50	12/94
	16	1	0.020	0.040	20	12/94
	17	1	0.020	0.040	50	02/95
	18	1	0.020	0.040	50	02/95
90° conical spray injectors	19	1	90° Spray		50	NT
Beveled hypo tube angled 15°	20	1	0.020	0.040	50	03/95
	21	1	0.020	0.040	50	04/95
Thick wall, beveled hypo tube angled 15°	22	1	0.020	0.063	50	05/95
90° conical spray injectors	23	1	90° Spray		50	06/95
Thick wall, beveled hypo tube angled 15°	24	1	0.020	0.063	50	06/95
	25	1	0.020	0.063	9	06/95
Conning tower, beveled, angled 15°	26	1	0.020	0.052[2]	50	08/95
	27	1	0.020	0.052[2]	9	NT
Hypo tube angled 15°	28	1	0.020	0.040	30	08/95
	29	1	0.020	0.040	6	09/95
	30	1	0.020	0.040	72	09/95
0.188-in OD single-port stinger, discharge at centerline	31	1	0.020	0.056[2]	50	10/95
	31	1	0.020	0.056[2]	50	01/98
0.188-in OD single-port stinger, reduced-immersion discharge	32	1	0.020	0.056[2]	40	11/95
0.188-in OD single-port stinger, increased-immersion discharge	33	1	0.020	0.056[2]	70	11/95
0.375-in OD four-port stinger, injector body at centerline	34	4	0.014	0.056[2]	38.8[3]	11/95
	35	4	0.014	0.056[2]	38.8[3]	12/95
	36	4	0.014	0.056[2]	39.7[3]	12/95
0.188-in OD single-port stinger, reduced-immersion discharge	37	1	0.020	0.056[2]	63.5[3]	12/95
0.400-in OD single-port stinger, injector body at centerline	38	1	0.020	0.056[2]		08/96
0.400-in OD four-port stinger, injector body at centerline	39	4	0.020	0.056[2]		09/96
0.400-in OD three-port stinger, injector body at centerline	40	3	0.020	0.056[2]		09/96
0.56-in OD base four-port stinger, injector body at centerline	41	4	0.020	0.056[2]	0.11[3]	05/97
	41	4	0.020	0.056[2]	0.11[3]	09/97
	42	4	0.020	0.056[2]	0.055[3]	09/97
0.56-in OD base four-port stinger, 0.030-in tip radius	43	4	0.020	0.056[2]	0.11[3]	10/97
0.56-in OD base four-port stinger, 0.060-in tip radius	44	4	0.020	0.056[2]	0.11[3]	10/97
0.56-in OD base four-port stinger, short tower, 0.060-in tip radius	45	4	0.020	0.056[2]	0.19[3]	11/97
0.48-in OD advanced four-port stinger, 0.060-in tip radius	46	4	0.020	0.056[2]	0.26[3]	02/98
0.48-in OD advanced four-port stinger, 0.125-in tip radius	47	4	0.020	0.056[2]	0.26[3]	03/98
0.48-in OD advanced five-port stinger, 0.060-in tip radius	48	5	0.020	0.056[2]	0.26[3]	03/98
0.48-in OD advanced four-port stinger, 0.125-in tip radius	49	4	0.020	0.056[2]	0.26[3]	03/98
	50	4	0.020	0.056[2]	0.26[3]	03/98
	51	4	0.020	0.056[2]	0.26[3]	04/98

Notes: 1. NT = Not tested 2. Width of conning tower strut 3. Inches from discharge to mixer wall

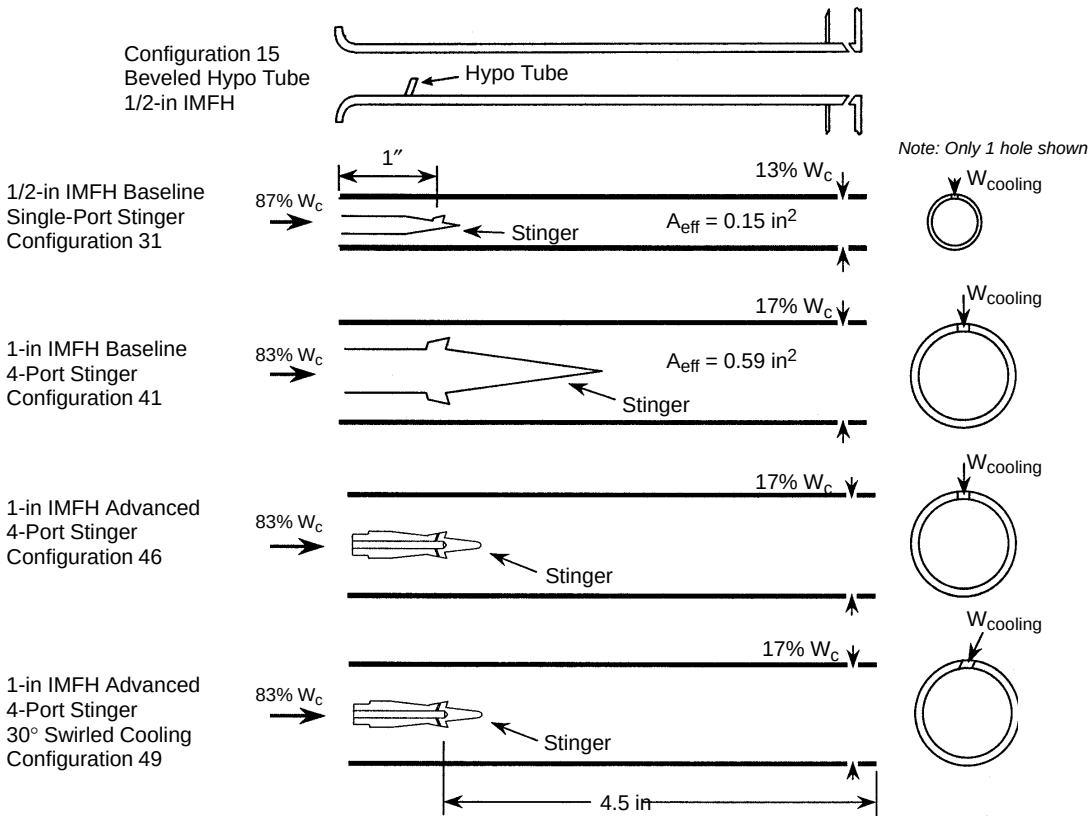

Figure 26. Primary LPP Main Stage IMFH Configurations

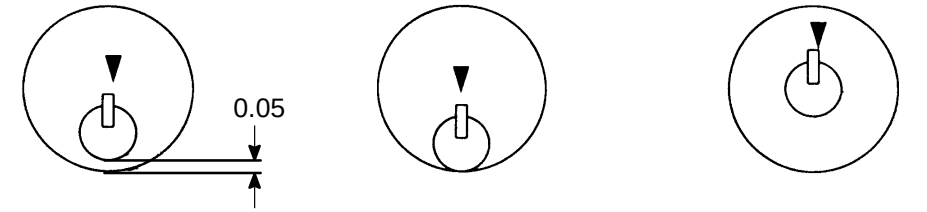

Figure 27. Variation of Injector Positioning Within the IMFH Tube

Reintroduction of postimpingement main dome cooling air into the IMFH premixer prior to entering the combustor was considered an important factor in improving emissions and stability. This air was introduced through a series of holes around the circumference of the tube just upstream of the aft end of the IMFH, prior to dumping into the combustor (Figure 26). In subscale designs, 13% of the total air flow exiting the IMFH tube would enter the tube through these aft holes. In the full-scale designs, this was increased to 17%. After downselect, full-scale development would test the impact of varying the amount of dump cooling air on emissions in more detail (described later).

Because of the inherent lack of stability in the IMFH design at low power, testing was normally done with an assembly containing four to seven bundled IMFH tubes simultaneously (Figure 28). This made it easier to light off and maintain flame at lower fuel/air ratios than would have been possible with a single-tube arrangement. Whenever possible, attempts were made to use tube-to-tube separations that were typical of what would be used in a sector or an engine to simulate any interactions that may be taking place. A ceramic liner 2.8 to 4.9 inches in diameter (Table 4) was placed downstream of the domes shown in Figure 28 to protect the test rig from hot combustion gases. Gas-sampling probes were located 7.4 to 9.5 inches downstream of the dome face.

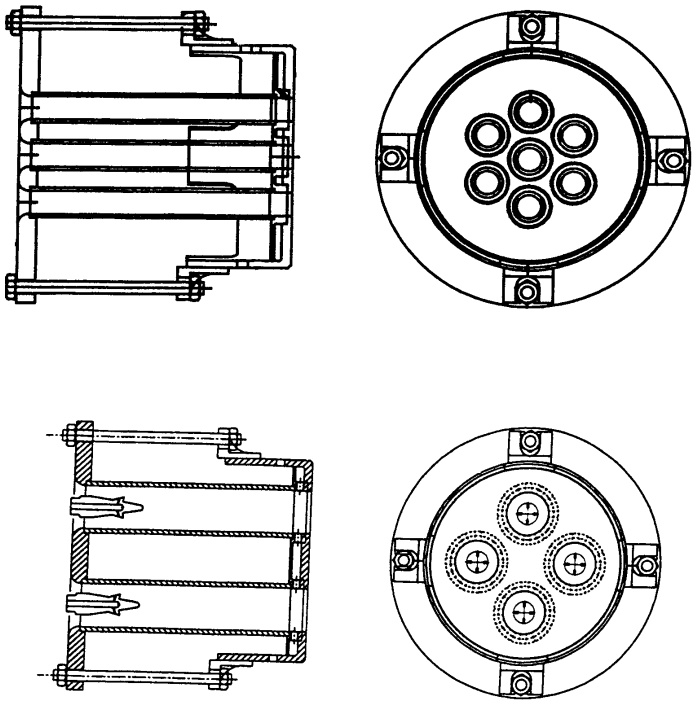

Figure 28. Subscale and Full-Scale IMFH Flametube Assemblies

Although inlet temperatures as high as 1050°F were tested, most of the subscale tests performed at this time were at low pressure (1 to 4 atmospheres). A few of the subscale designs and most of the full-scale designs were tested to as high as 17 atmospheres, but most data were acquired at 4 and 10 atmospheres.

This report will focus on five primary designs (Figure 26). Configuration 15 was a subscale design using a beveled hypo tube with centerline injection. Configuration 31 was a subscale design with a single-port stinger for fuel injection. Configuration 41 was the full-scale, four-port stinger —

which became the baseline for full-scale development. Configuration 46 was the advanced four-port stinger — which was significantly smaller than the baseline. Finally, Configuration 49 was the same as Configuration 46 (the advanced four-port stinger) but with swirled dump cooling air instead of radial injection at the aft end of the IMFH tube. Additional full-scale designs were tested after the LPP/RQL downselect and are described later in the report.

Subscale Concepts

The subscale concepts were summarized in Tables 4 and 5, Configurations 12–37. Half-inch diameter tubes were used in most cases. The length of the tubes was set to maximize the amount of time for fuel atomization, vaporization, and mixing, but length was limited by autoignition considerations. It was also desired that the point of fuel injection be placed a "safe" distance downstream of the tube inlet to avoid any undesirable flashback or autoignition events in regions that may separate near the inlet. The fuel-injection point was normally set to be one inch downstream of the inlet. In most cases, a total tube length of 5.5 inches was used, providing 4.5 inches for fuel vaporization and premixing.

Three main types of fuel injectors were used to introduce fuel into the IMFH tubes (Figure 29). Initially, a simple hypo tube penetrating the IMFH wall and perpendicular to the air flow was used. This would later be placed at an angle to the flow, and the tip of the tube would be beveled. The second basic configuration was a "conning tower" design. Although conceptually similar to the hypo tube, this was an attempt to reduce wakes behind the fuel injection device by making it more aerodynamic. The third design was referred to as a stinger. This was a small tube with a conical tip that protrudes axially down the centerline of the IMFH tube. A much smaller conning tower — essentially a fin — was located on the cone, which transversely injected the fuel into the air crossflow. Later designs (full scale) would test multiple fuel-injection ports on a single stinger. The stingers were attached to a main fuel injector that controlled the fuel staging to the combustor. Each of these concepts and the test results are described in more detail in the following paragraphs.

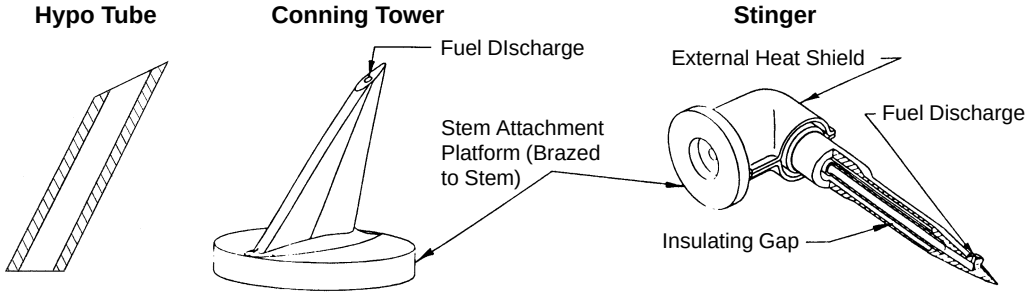

Figure 29. Main LPP Fuel Injector Tip Concepts

Hypo Tube Fuel Injection – Much of the early hypo tube testing focused on simple 0.020-in ID by 0.040-in OD tubes placed either perpendicular to, or angled 15° (aft) from, the air flow (Figure 29). Originally, the tip at the point of fuel injection was flat. Later the tip was beveled at 45°. With the tube angled at 15°, this placed the top surface at a 30° upward angle relative to the IMFH tube centerline. The beveled feature appeared to help prevent fuel from clinging to the tube surface and

running down the back side of the tube. The point of fuel injection was located at the IMFH tube centerline. This was Configuration 15, the most successful of the hypo tube designs.

Results of the Configuration 15 tests are summarized in Table 6. Figures 30 and 31 show NOx and combustion efficiency as functions of flame temperature. NOx is extremely low at only 2 EI at 3410°R flame temperature. Clearly the 150°F increase in T_3 did not have significant impact on the NOx, although combustion efficiency showed a noticeable improvement: nearly 1.5%.

Table 6. IMFH Configuration 15 Emissions Summary

T_3 (ºF)	P_3 (psia)	ΔP/P (%)	T_{flame} (ºR)	Combustion Efficiency (%)	NOx EI (g/kg Fuel)
807	60	4.40	3219	95.74	1.27
804	60	4.23	3370	97.9	1.84
816	60	4.48	3518	99.19	3.09
819	60	4.32	3627	999.45	4.07
810	60	4.74	3761	99.42	4.58
824	60	4.43	3991	98.99	6.86
961	60	4.38	2999	93.65	0.49
963	60	4.34	3261	98.77	1.15
964	60	4.54	3405	99.59	2.03
966	60	4.23	3458	99.64	2.38
957	60	4.05	3561	99.76	3.41
961	60	4.69	3665	99.69	4.5
959	60	4.41	3808	99.57	6.6

A beveled hypo tube fuel injection system, similar to Configuration 15, would be selected for use in all of the LPP stepped-dome sectors and the highly mixed MRA sector. The results of these tests will be described later in this report.

Conning Tower Fuel Injection – The conning tower design (Figure 29) was primarily an off-shoot of the knowledge gained from the hypo tube tests. An aerodynamic profile was introduced in an attempt to reduce or eliminate the wakes created by the hypo tube design. It was feared that these wakes posed potential autoignition hazards, although such an event was never observed during many hours of subcomponent and sector testing. Similar to the hypo tube injector, the conning tower protruded through the sidewall of the IMFH tube, injecting fuel perpendicular to the air flow. The top surface was tapered similar to the beveled hypo tubes, and the angle of injection was 15° aft of perpendicular. As with Configuration 15, the point of fuel injection was located at the centerline of the IMFH tube.

Configuration 26 was the only conning tower design tested. The results are summarized in Figures 32 and 33 and Table 7. NOx was about 1 EI higher than the Configuration 15 hypo tube design, coming in at slightly more than 3 EI at 3410°R flame temperature. However, combustion efficiency showed tremendous improvement over the hypo tubes, with efficiencies above 99.5% even at 650°F. In contrast, the efficiency of the hypo tubes had fallen off to less than 98.5% at 815°F.

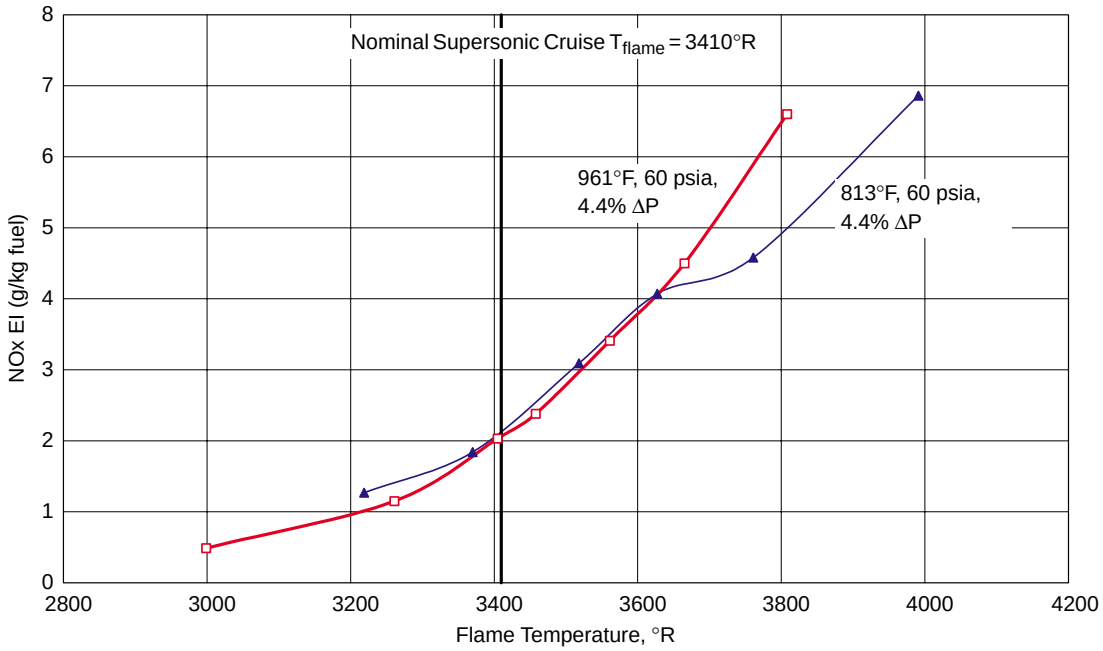

Figure 30. NOx Emissions for IMFH Configuration 15

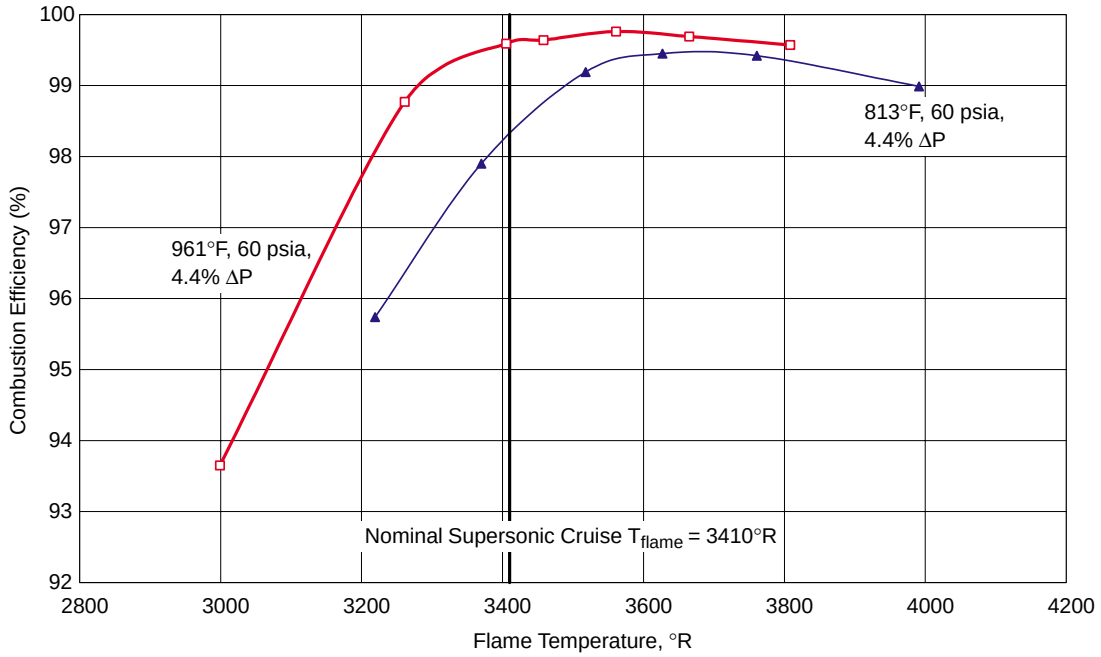

Figure 31. Combustion Efficiency for IMFH Configuration 15

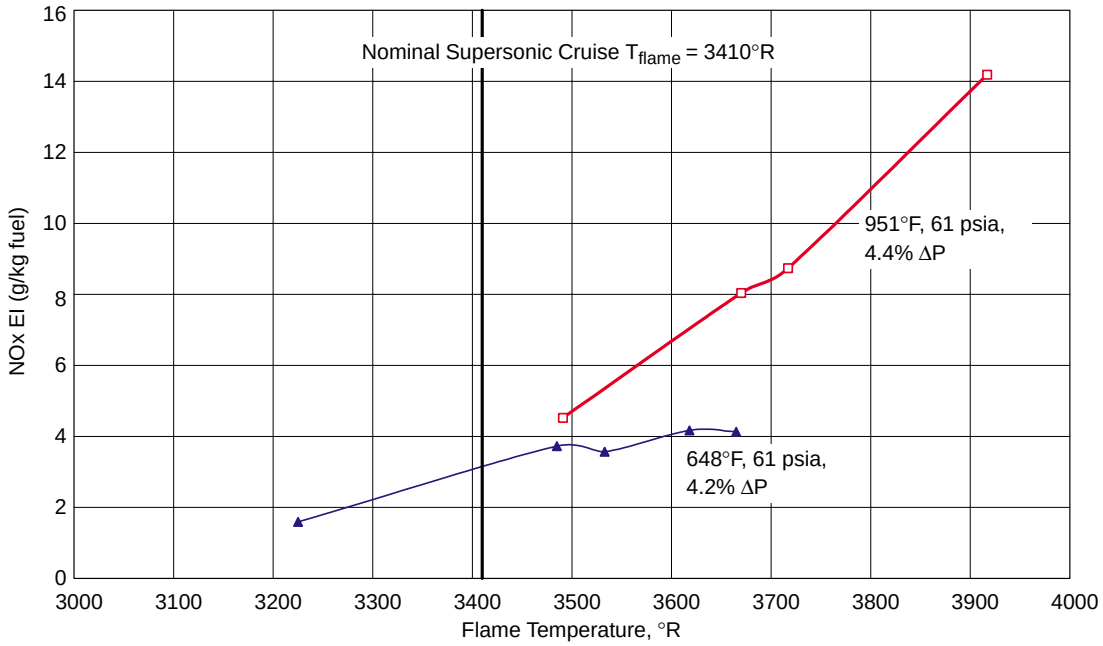

Figure 32. NOx Emissions for IMFH Configuration 26

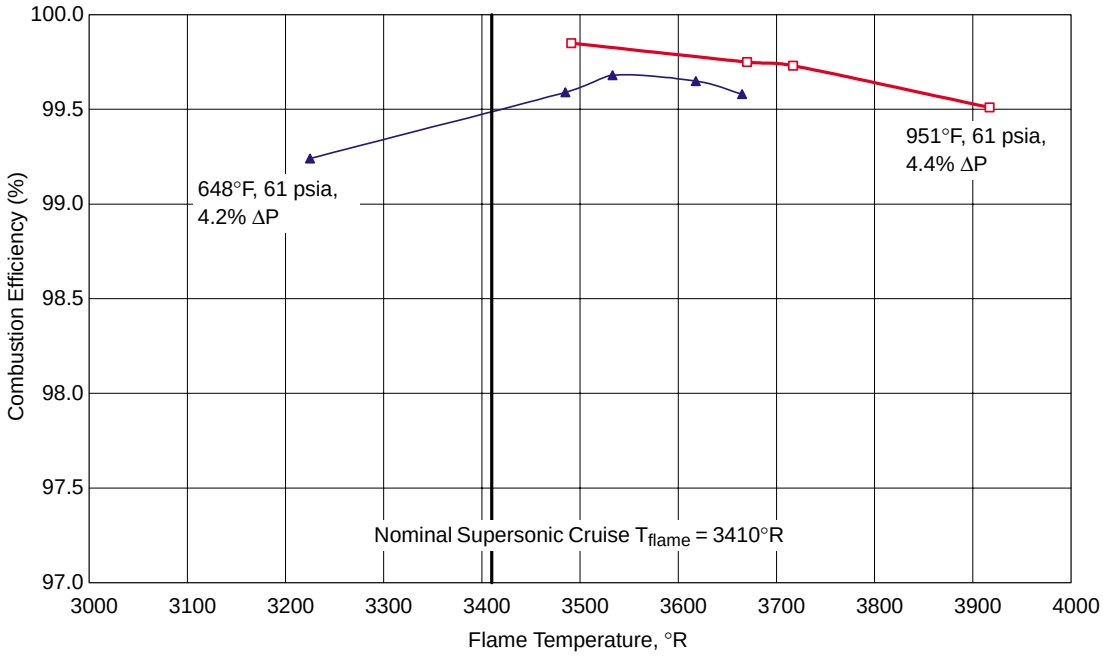

Figure 33. Combustion Efficiency for IMFH Configuration 26

Table 7. IMFH Configuration 26 Emissions Summary

T_3 (ºF)	P_3 (psia)	ΔP/P (%)	T_{flame} (ºR)	Combustion Efficiency (%)	NOx EI (g/kg Fuel)
648	60	4.38	3225	99.24	1.59
632	61	4.04	3485	99.59	3.73
648	60	4.12	3533	99.68	3.57
657	61	4.34	3618	99.65	4.17
651	61	4.17	3665	99.58	4.13
950	60	4.04	3491	99.85	4.52
950	61	4.28	3670	99.75	8.04
956	61	4.61	3717	99.73	8.74
949	60	4.71	3917	99.51	14.19

Despite these results, the anticipated cost of manufacturing and difficulties in integrating the conning tower into a commercially viable fuel nozzle made it impractical to use in a sector or engine.

Stinger Fuel Injection – Stingers (Figure 29) eventually replaced hypo tubes for several reasons. First, it was felt that the more advanced design could provide better emissions through improved atomization and mixing. Second, although no problems had occurred, concerns over the possibility of coking of the simple hypo tube led to a more advanced cooling/protection scheme. This required a much larger diameter than the hypo tubes, making it difficult to use the same method of injection (protruding through the IMFH tube sidewall). Finally, to make the fuel injectors commercially viable, they should be easily removable for inspection and replacement. Thus, a system other than that devised for the hypo tubes was necessary.

Configuration 31 was the primary stinger design tested (Figure 34). In this design, a small conning tower (fin) was located on a cone attached to a 0.188-in diameter centerbody. The centerbody was parallel to the IMFH tube centerline but was radially off-center such that the point of fuel injection

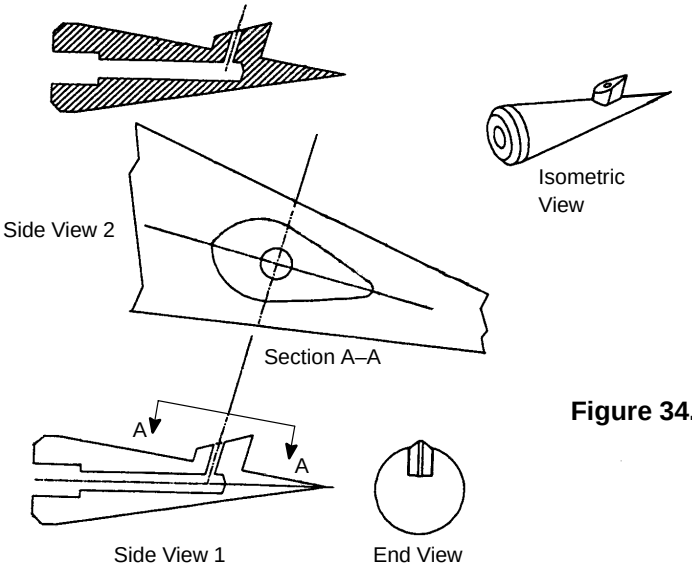

Figure 34. IMFH Configuration 31 Fuel Injector Tip

was at the centerline. Four-port designs with 0.375-in diameter centerbodies were also tested (0.65, 0.71, and 0.83-in ID IMFH tubes) but demonstrated higher emissions.

Configuration 31 results are summarized in Table 8 and Figures 35 and 36. NOx was similar to the conning tower design (Configuration 26) at a little over 3 EI. Combustion efficiencies were lower than the conning tower, and in fact were quite similar to the hypo tube of Configuration 15.

Table 8. IMFH Configuration 31 Emissions Summary

T_3 (ºF)	P_3 (psia)	ΔP/P (%)	T_{flame} (ºR)	Combustion Efficiency (%)	NOx EI (g/kg Fuel)
644	60	4.68	3060	95.72	2.47
657	59	4.73	3398	96.64	3.24
649	61	4.61	3735	99.01	4.94
648	59	4.27	3916	98.40	5.67
651	60	4.68	3967	98.03	6.49
916	60	4.45	3202	97.99	1.81
905	59	5.38	3396	99.68	3.32
908	61	3.56	3488	99.56	5.27
908	61	3.32	3626	99.61	5.99
903	60	3.72	3930	98.96	10.79

The Configuration 31 single-port stinger design would eventually be used in the highly successful moderately mixed MRA sector that demonstrated EINOx below 5 at supersonic cruise (described later).

Full-Scale Concepts

Subscale tests were quite successful, but use of the half-inch IMFH designs in a full-scale engine was not feasible. Figure 37 shows that continued use of the smaller tubes would require 1056 tubes per engine! This led to the development of one-inch designs, reducing the number to a more manageable 300 tubes per engine. However, this also raised significant concerns over meeting emissions requirements and the potential for flashback. As the following paragraphs will describe, the one-inch designs overall performed as well as the subscale designs.

Fourteen full-scale variations were tested, as listed in Tables 4 and 5 (Configurations 38–51). Because of the successes of flametube tests and the moderately mixed MRA sector (described later), the single-port stinger concept was carried forward as a starting point in full-scale development. Because of the larger diameter of the full-scale IMFH tubes under consideration, a stinger design with multiple fuel ports was considered as a prime candidate (Configuration 41, Figure 38). The centerbody was enlarged to simulate blockage of the IMFH tube comparable to that of the subscale design. Enlarging the centerbody also allowed more advanced cooling methods to be used to minimize fuel coking. Later tests varied the centerbody diameter and the design of the conical tip at the end of the stinger (Configuration 46, Figure 39). Finally, introduction of swirl to the postim-

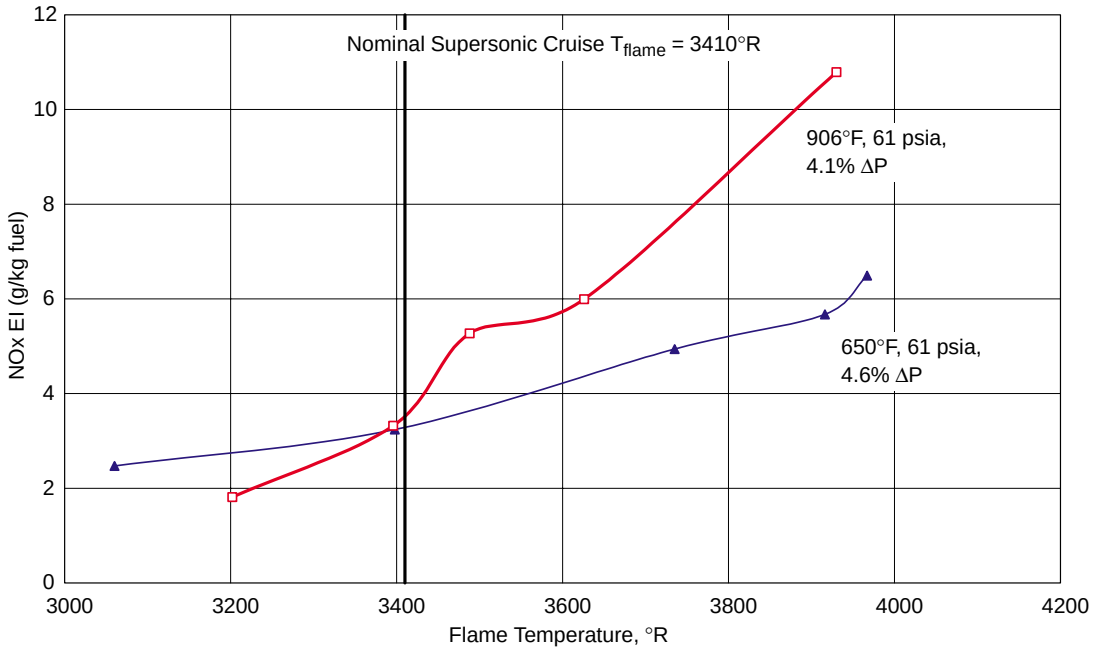

Figure 35. NOx Emissions for IMFH Configuration 31

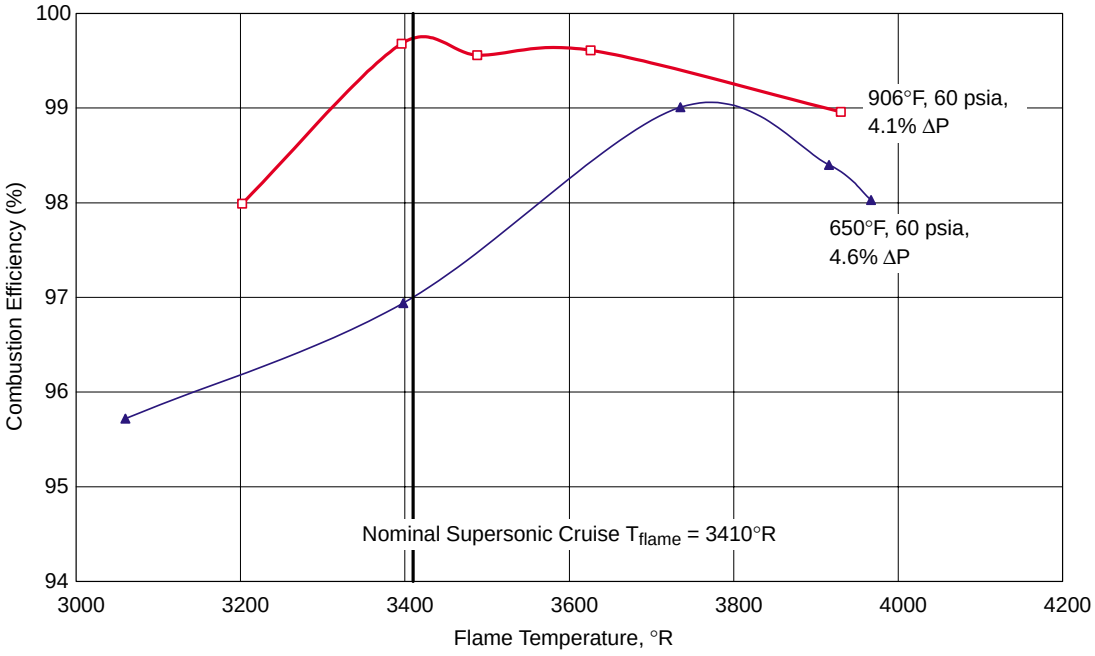

Figure 36. Combustion Efficiency for IMFH Configuration 31

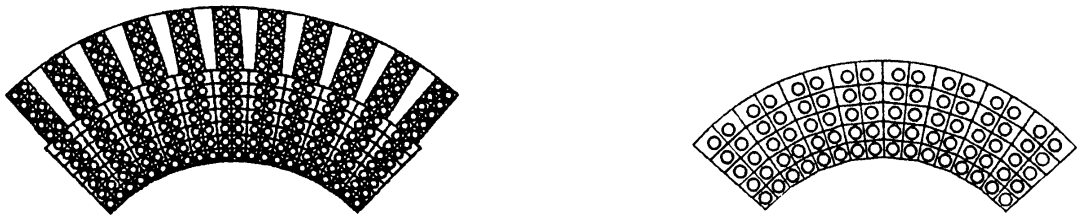

Figure 37. Significant Simplification Results from Increasing the IMFH Tube Diameter

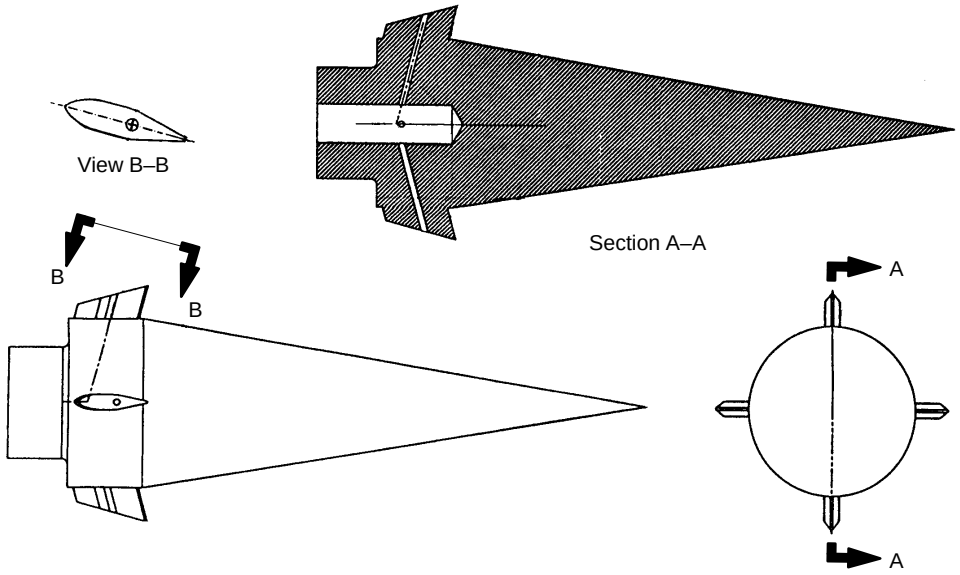

Figure 38. Schematic of IMFH Configuration 41 Fuel Injector Tip

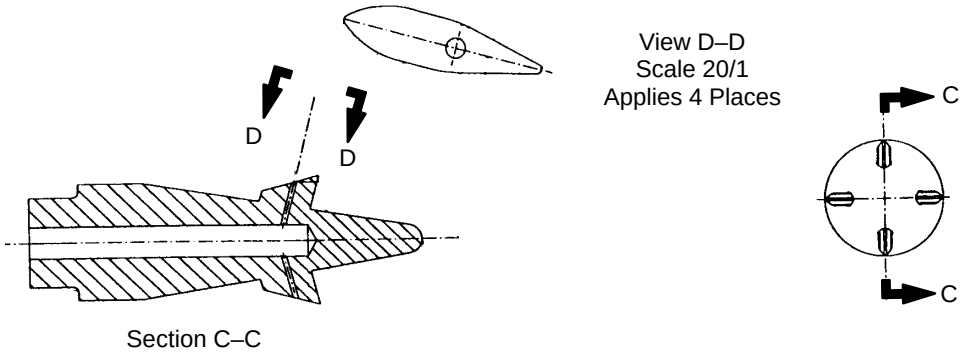

Figure 39. Schematic of IMFH Configuration 46 Fuel Injector Tip

pingement main dome cooling air as it is dumped into the aft end of the IMFH tube was tested (Configuration 49, Figure 40).

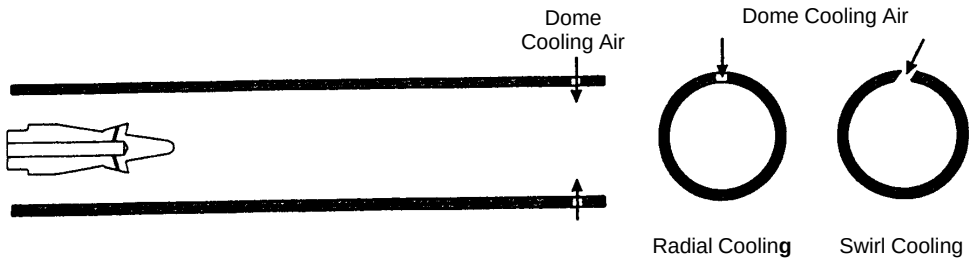

Figure 40. IMFH Configurations 46 (Radial Cooling) and 49 (Swirled Cooling)

The Configuration 41 results are summarized in Table 9 and Figures 41 and 42. The design was highly successful. Configuration 31 NOx EI was about 3.5 at 900°F, 60 psia; Configuration 41 was about the same but at 900°F, 150 psia. Normally the increase in pressure would increase NOx. Thus, NOx was shown to be at least as good as Configuration 31 and may actually be somewhat better. Combustion efficiency was slightly worse than Configuration 31 at 650°F, 60 psia but was well above 99.5% at 1100°F, 150 psia. Comparisons are being made to Configuration 31 because it was successfully used in the moderately mixed MRA sector (described later), demonstrating NOx EI of only 3.8 at nominal supersonic cruise conditions (1200°F, 150 psia) as part of an integrated sector. Thus, Configuration 41 was the first design to demonstrate viability for use in a full-scale sector or engine.

Table 9. IMFH Configuration 41 Emissions Summary

T_3 (°F)	P_3 (psia)	ΔP/P (%)	T_{flame} (°R)	Combustion Efficiency (%)	NOx EI (g/kg Fuel)
665	60	4.33	3169	95.45	1.31
656	60	4.49	3249	95.95	1.81
662	60	4.51	3471	97.00	3.45
657	60	4.33	3709	98.18	4.97
914	150	4.67	3135	98.69	1.06
905	150	4.46	3283	98.90	1.96
906	150	4.53	3488	99.34	4.76
900	150	4.47	3676	99.47	9.72
1106	150	4.40	3093	99.47	1.20
1092	150	4.54	3268	99.68	2.79
1098	150	4.41	3462	99.79	6.24
1099	150	4.53	3658	99.80	13.32

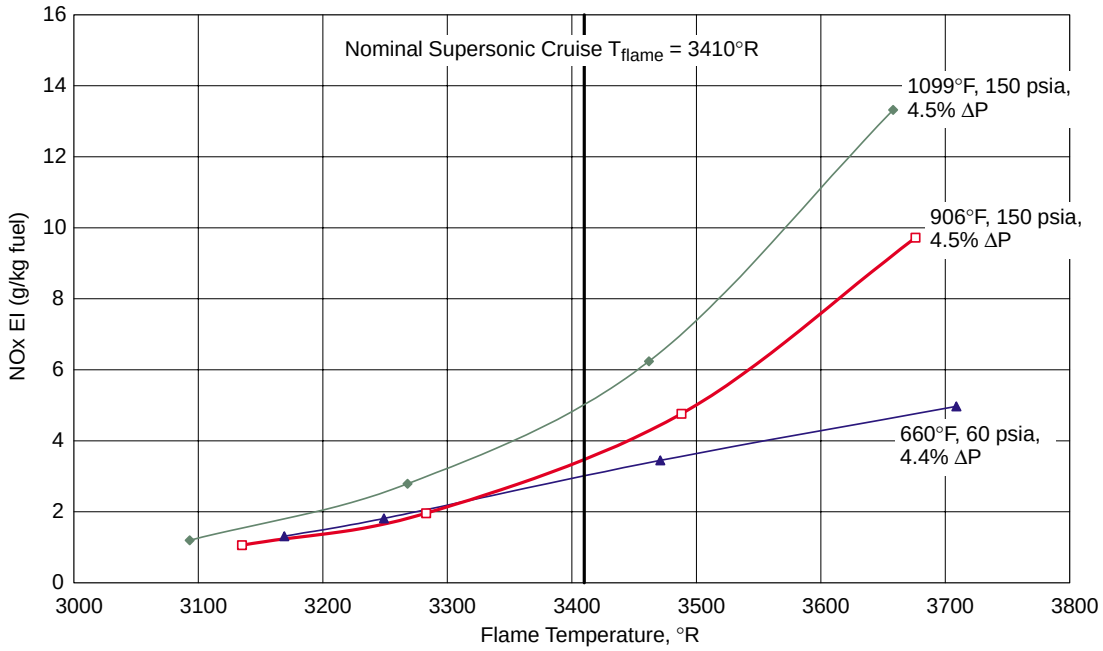

Figure 41. NOx Emissions for IMFH Configuration 41

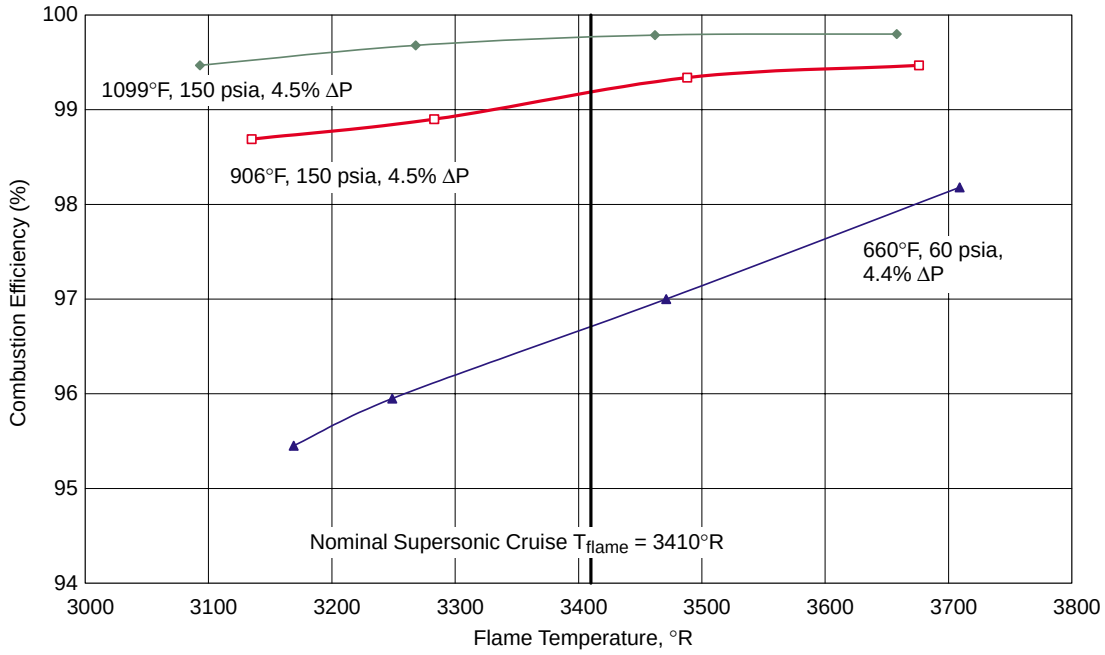

Figure 42. Combustion Efficiency for IMFH Configuration 41

The Configuration 46 results are summarized in Table 10 and Figures 43 and 44. Surprisingly, the design showed significant improvement over Configuration 41. At 900°F, 150 psia, NOx EI was reduced from about 3.5 to 2.5. Even at 1100°F, 150 psia, NOx EI was reduced from about 5 to 4. Combustion efficiencies at the elevated temperatures were above 99.9%. This was the configuration recommended for use in the full-scale sector at the time of the LPP/RQL downselect.

Table 10. IMFH Configuration 46 Emissions Summary

T_3 (ºF)	P_3 (psia)	ΔP/P (%)	T_{flame} (ºR)	Combustion Efficiency (%)	NOx EI (g/kg Fuel)
644	61	4.28	3523	97.89	2.27
642	61	4.45	3687	99.03	3.05
645	61	4.45	3840	98.28	3.92
902	150	4.50	3263	99.27	1.43
903	150	4.71	3337	98.99	1.68
905	150	4.50	3512	99.77	3.57
907	150	4.75	3703	99.92	5.77
1107	151	4.12	3229	99.88	1.40
1101	151	4.22	3450	99.97	4.89
1103	150	4.36	3615	99.98	8.7
1112	150	4.36	3747	99.98	12.59

Configuration 49 results are summarized in Figures 45 and 46 and Table 11. This design showed tremendous improvement over the highly successful Configuration 46. Tests showed that the swirled cooling air injected at the aft end of the IMFH tube was actually capable of reducing the worst case (tested) NOx EI to only 2 (at 1100°F, 150 psia, 3410°R flame temperature). This was an astonishing 50% reduction from the 4 EI demonstrated by Configuration 46! Unfortunately, the swirled feature was difficult to implement. Because the IMFH tube walls are quite thin, the cooling holes either have to be made quite small or the tube has to be made locally thicker to produce the necessary hole-length/diameter ratio for swirled injection. This was the only real drawback of the design.

It can be concluded that all of the full-scale four-port stingers tested had the potential for use in a sector. Although Configuration 49 demonstrated the lowest NOx, difficulty in adding the swirled cooling features prevented use in the full-scale sector. Although higher than Configuration 49, the success of Configuration 46 in demonstrating emissions at least as good as previous designs led to selection of that design for use in the full-scale sector (described later).

4.4.1.3 Main Fuel Injector Development

The main fuel injectors had four primary functions. First, they had to provide structural support to position the stingers (or hypo tubes) within the IMFH tube inlet. Acoustics in the 400–600 Hz range are commonly observed in sector tests, so injectors must be designed to have natural frequencies well outside this band.

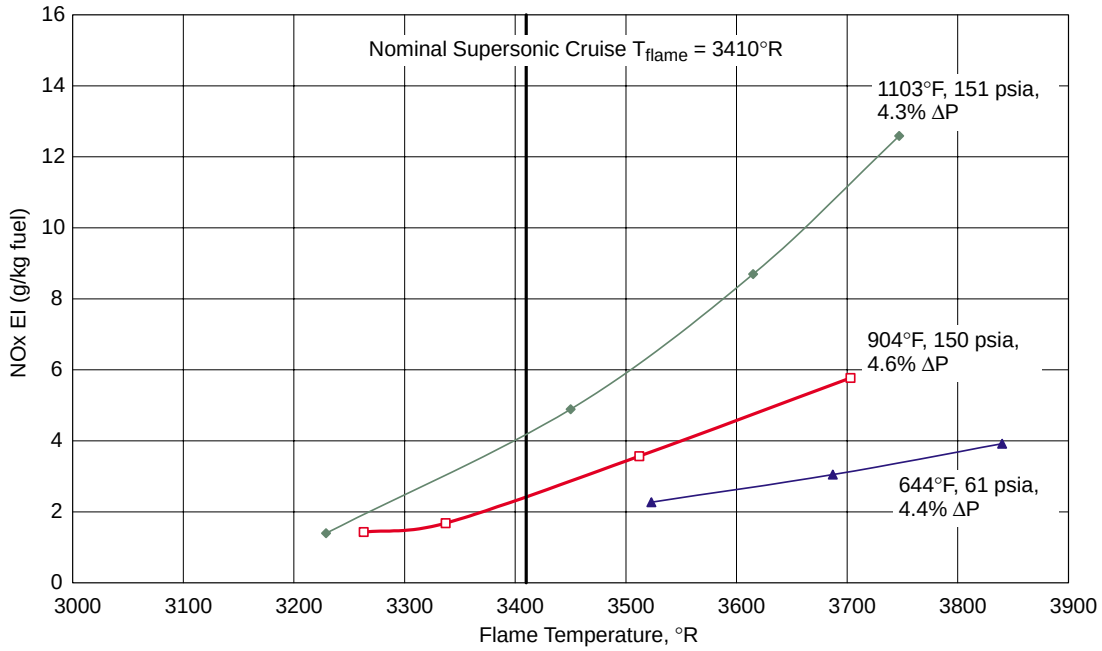

Figure 43. NOx Emissions for IMFH Configuration 46

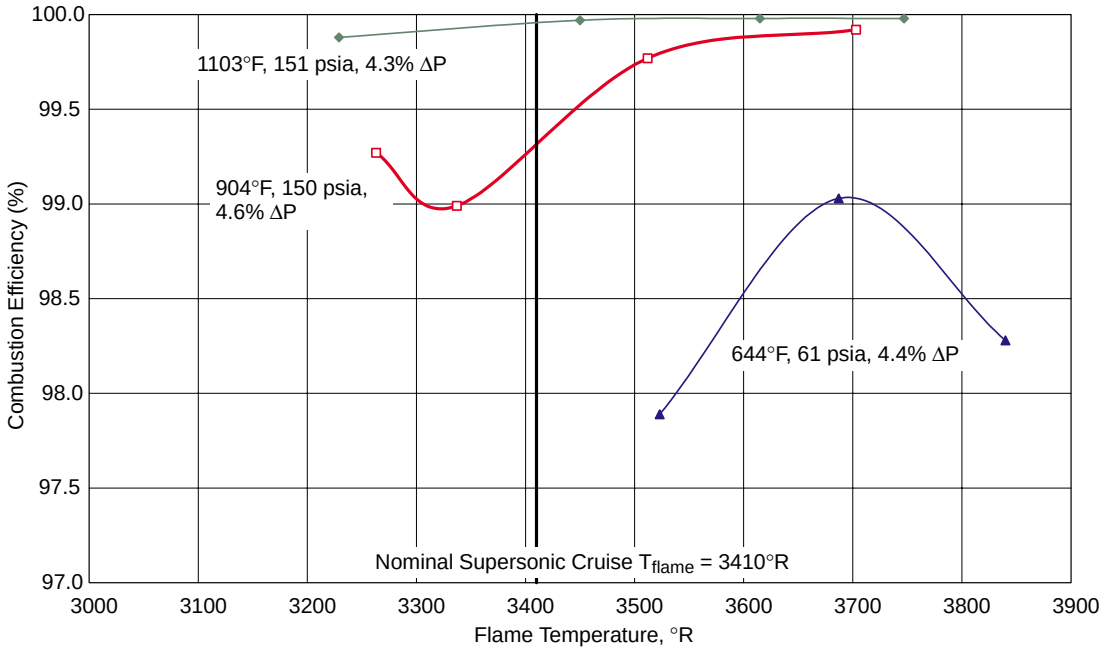

Figure 44. Combustion Efficiency for IMFH Configuration 46

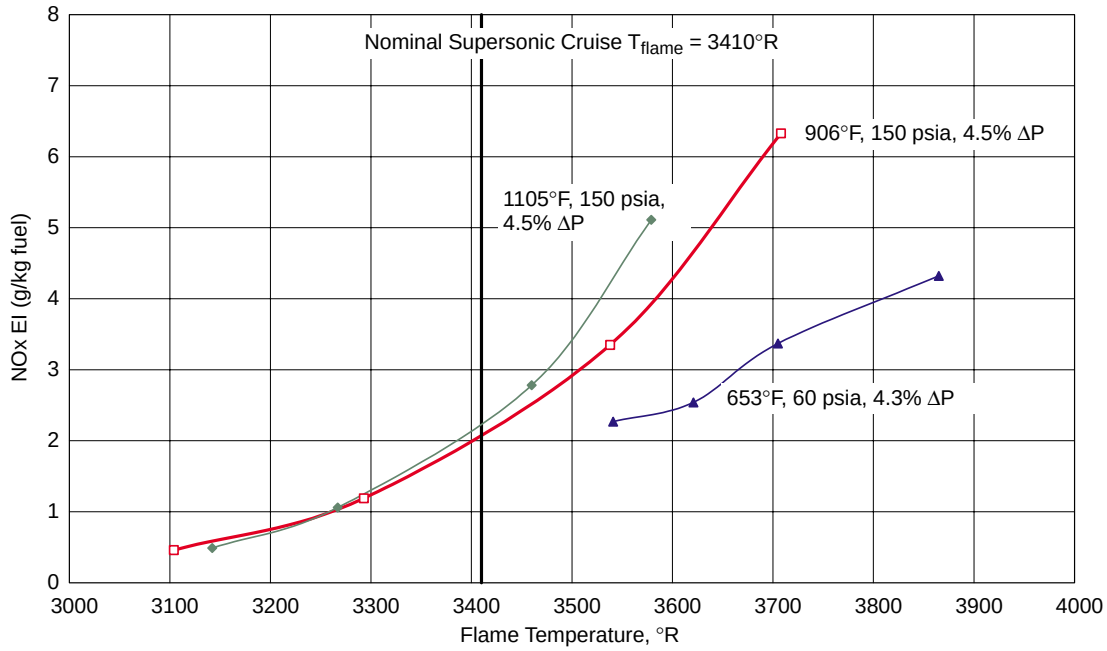

Figure 45. NOx Emissions for IMFH Configuration 49

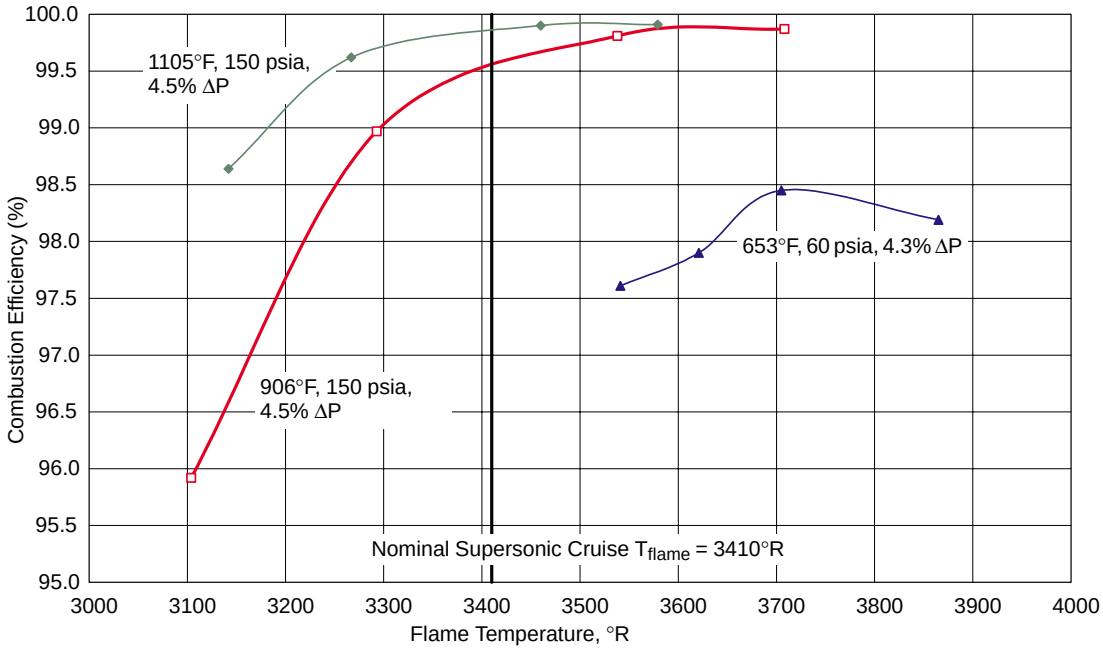

Figure 46. Combustion Efficiency for IMFH Configuration 49

Table 11. IMFH Configuration 49 Emissions Summary

T_3 (ºF)	P_3 (psia)	ΔP/P (%)	T_{flame} (ºR)	Combustion Efficiency (%)	NOx EI (g/kg Fuel)
659	60	4.41	3541	97.61	2.27
649	60	4.40	3621	97.9	2.54
654	60	4.32	3705	98.45	3.37
649	60	4.24	3865	98.19	4.32
915	150	4.49	3104	95.92	0.46
912	150	4.43	3293	98.97	1.19
906	150	4.46	3588	99.81	3.35
905	150	4.56	3708	99.87	6.33
1107	150	4.39	3142	98.64	0.49
1103	150	4.53	3267	99.62	1.06
1108	150	4.52	3460	99.90	2.78
1112	150	4.66	3579	99.91	5.11

Second, they had to accommodate fuel staging, such that stingers could be selectively fueled. Third, they had to control the fuel flow rate to each stage. Servovalves near the inlet of the injector normally serve this function. Finally, they had to thermally protect the fuel from the severe T_3 air environment to preclude coking and vaporization in the fuel passages, not only as the fuel was flowing to the stingers but also as stages were shut-off.

In addition to these primary functions, two significant design requirements had to be considered. First, the fuel injectors needed to be accessible and easily removable so that they could be replaced if problems arose or simply checked out during routine engine maintenance intervals. This requirement tends to preclude the use of fuel systems integral with the combustor dome. Second, differential thermal growth between the “cold” internal parts in contact with fuel and the “hot” adjacent parts exposed to the T_3 air can quickly lead to fuel leaks if cracks develop. This obviously places additional severe demands on the design of the main injectors.

Subscale Concepts

Several subscale concepts were considered. Ordinary tubing connected to a fuel manifold is the simplest and cheapest method of fuel delivery, but it does not provide the necessary thermal protection. Double- or triple-walled tubing provides better thermal protection but can make it difficult to implement the necessary staging characteristics. More advanced concepts focused on a solid stem containing separate fuel passages to allow staging, active cooling, and structural rigidity for accurate positioning of the stingers in the IMFH tubes. Such designs are obviously heavier and more expensive than simple tubing designs, but they provide the required combination of structural integrity, thermal protection, staging capabilities, and accessibility needed for commercial viability.

For the stepped-dome sectors (described later), simple tube-and-manifold systems were sufficient (Figure 47). They were acceptable because each “stage” was its own manifold and tube system,

which was either flowing fuel or being purged. This could be used in a test environment but was not really viable for an engine because purge systems are normally too heavy and expensive to use in an engine. Alternative removable fuel nozzle concepts were devised for both LDI and LPP stepped-dome systems, but they were never implemented (Figures 48 and 49).

For the highly mixed MRA sector (described later), the simple tube and manifold was modified such that the tubes passed through a more typical fuel nozzle design prior to feeding each stage of hypo tubes (Figure 50). This design allowed addition of a heat shield around the fuel lines to provid better thermal protection. The design was also removable and had more structural integrity for positioning the hypo tubes in the IMFH premixers.

For the moderately mixed MRA sector (described later), systems with and without heat shielding and with passive and active fuel cooling systems were considered. The need for heat shielding of the fuel stem was quickly identified using simple, one-dimensional heat transfer analyses, as high bulk fuel temperature rises were estimated in unprotected systems. The solid-stem design was selected (Figure 51). The body was a solid block, with line-drilled fuel passages. A cooling passage was included to help remove heat from the stem. In practice the pilot fuel line would have been used, since it is always flowing. For the sector test, water was used to ensure that the test would not be impeded by the cooling effectiveness. The stingers were attached to the sides and used a heat shield and passive cooling (Figure 52). The cooling was such that a small annular passage surrounded the bulk fuel passage. Active cooling was considered, but the added complexity of the passages and the small diameter of the stinger body precluded its use. Based on the moderately mixed MRA sector tests (described later), the passive system worked well overall. However, because fuel lines were purged as they were shut-off, it is not clear whether or not the system would sufficiently protect the fuel in an unpurged system. Active cooling would be reconsidered for the full-scale designs because the larger stinger centerbody provides more room to implement such a system.

Full-Scale Concepts

Four primary concepts were considered for full-scale development. All used the advanced four-port stinger (Configuration 46, with modified internal flow passages) that demonstrated low emissions in subcomponent development.

The first concept was the “solid stem” (Figure 53). It was fundamentally the same as the subscale design used in the moderately mixed MRA sector. Because of the successful demonstration in that test, a scaled-up version made sense for the full-scale system. However, because of the increase in total length of the fuel stem and the limited space available, line drilling was nearly impossible. The stem could have been made in sections, but getting passages to line up and the increased chances for fuel leaks made this alternative unappealing. This concept also tends to be expensive to fabricate and is quite heavy.

The second concept was the “T stem” (Figure 54). This design used a T-shaped structural member surrounded by a heat shield similar in shape to the solid stem. Each fuel stage had a fuel supply tube that ran through the open areas between the internal structure and the heat shield. Cooling flow passed through passages in the T-structure for heat removal. Internal brazements were the primary concern in this particular design.

The third concept was a “U stem” (Figure 55). This design was essentially the same as the T-stem, but the structural member was located just inside the heat shield, with the staging fuel tubes contained within this shell. Cooling flow passed through passages in the structural shell.

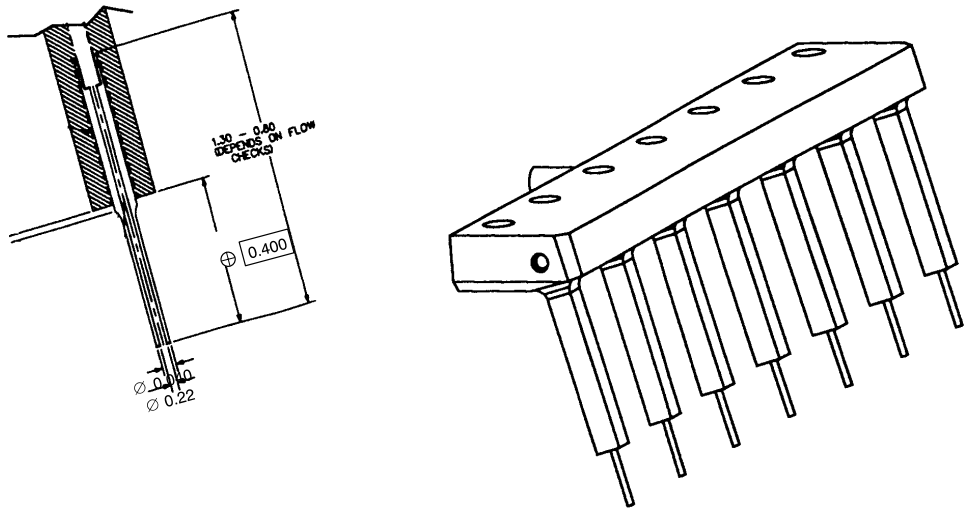

Figure 47. Hypo Tube Fuel Injectors used in the Stepped-Dome Sectors

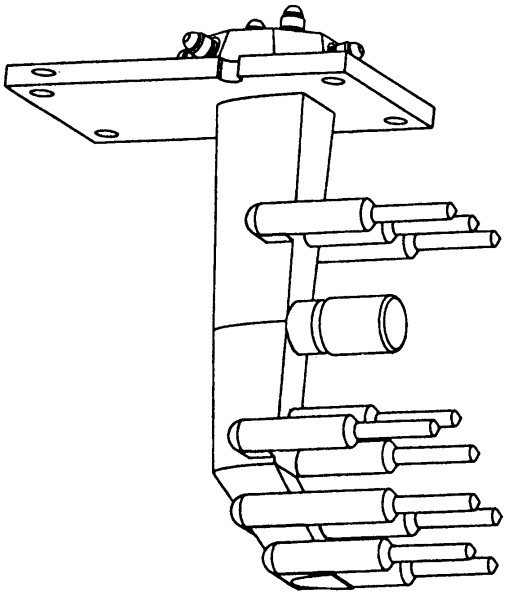

Figure 48. LDI Stepped-Dome Fuel Nozzle Concept

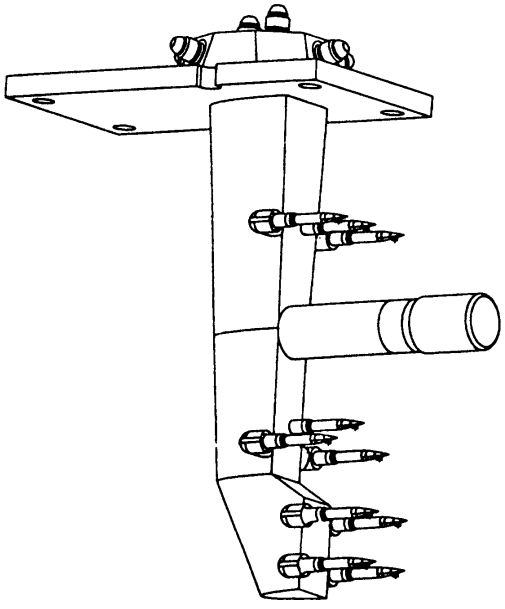

Figure 49. LPP Stepped-Dome Fuel Nozzle Concept

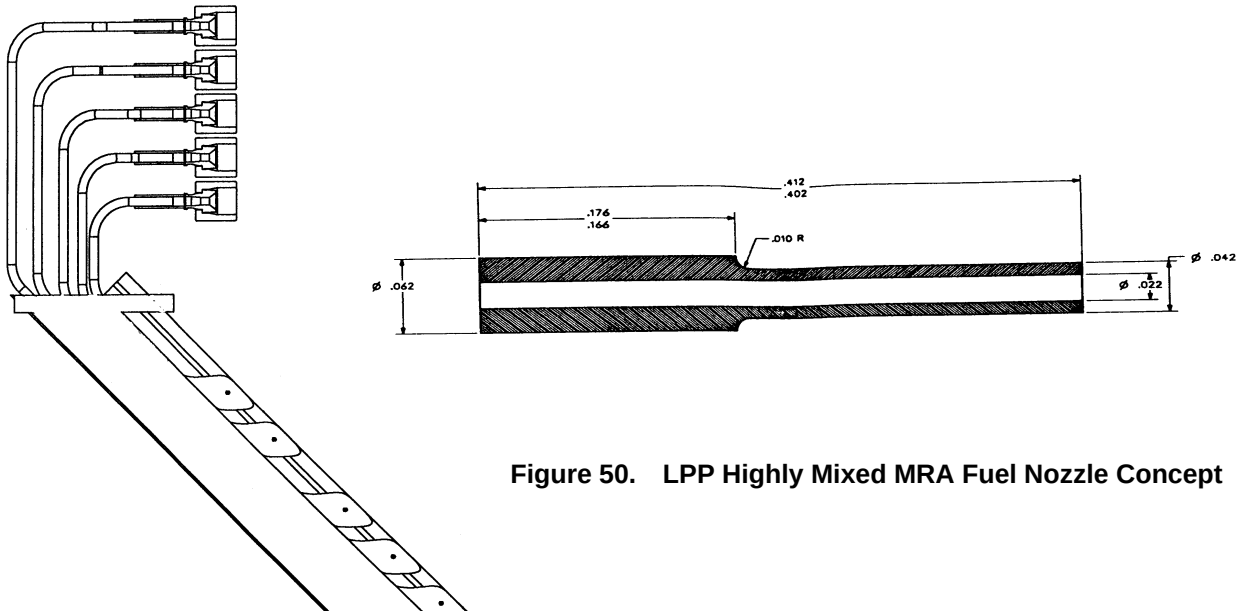

Figure 50. LPP Highly Mixed MRA Fuel Nozzle Concept

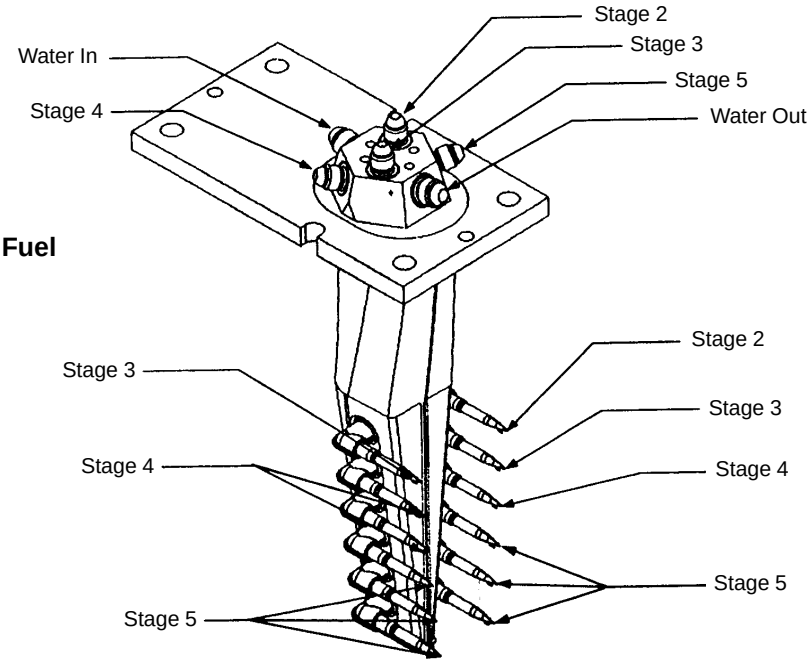

Figure 51. Subscale LPP MRA Fuel Nozzle Concept

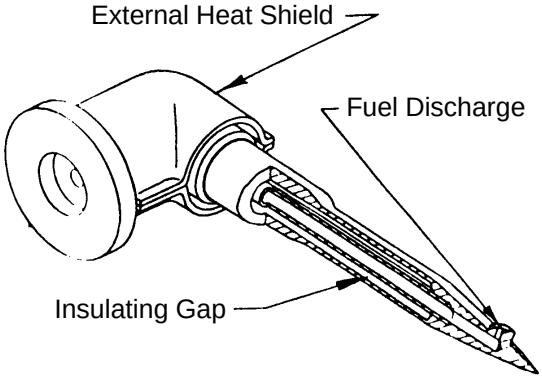

Figure 52. Subscale Stinger Injector Tip for LPP MRA Fuel Nozzle

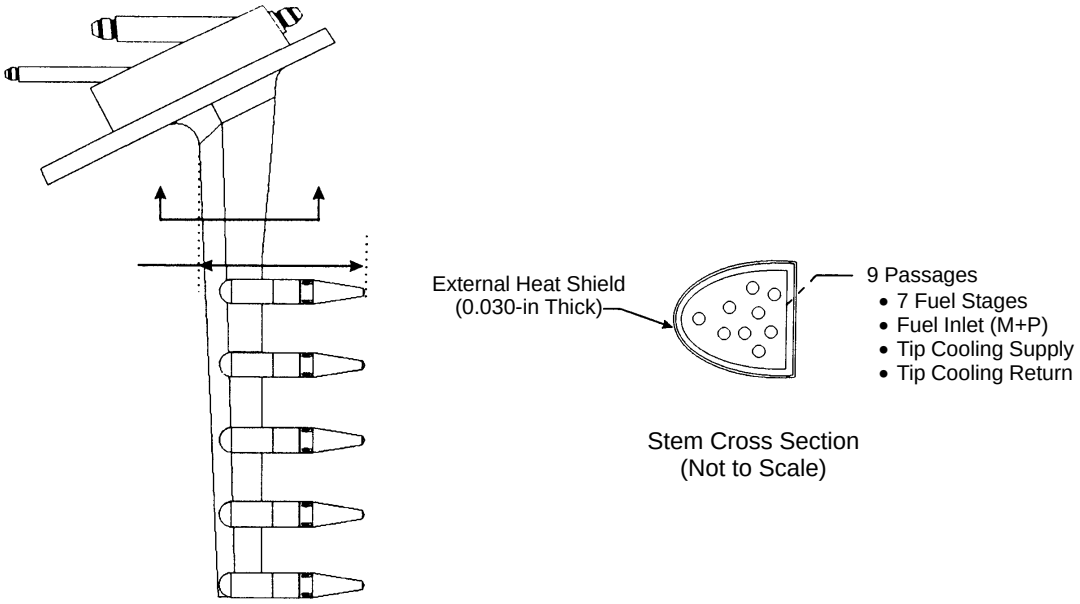

Figure 53. Full-Scale LPP Fuel Nozzle Concept 1 (Solid Stem)

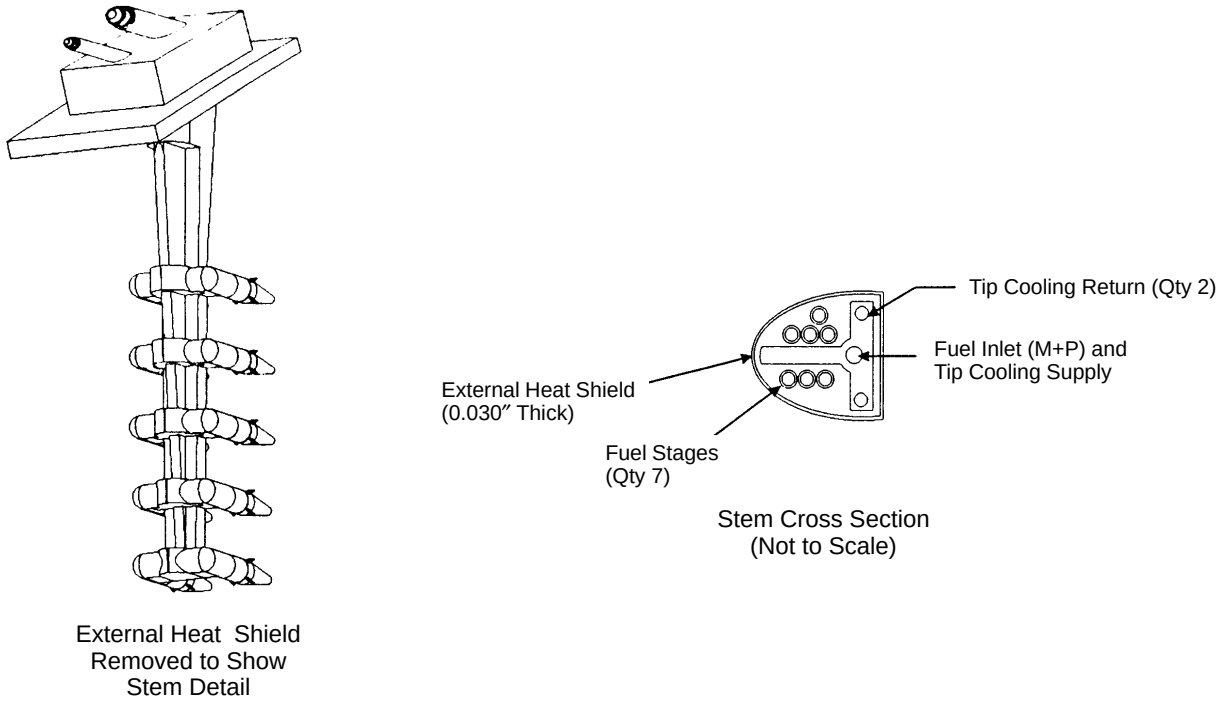

Figure 54. Full-Scale LPP Fuel Nozzle Concept 2 (T Stem)

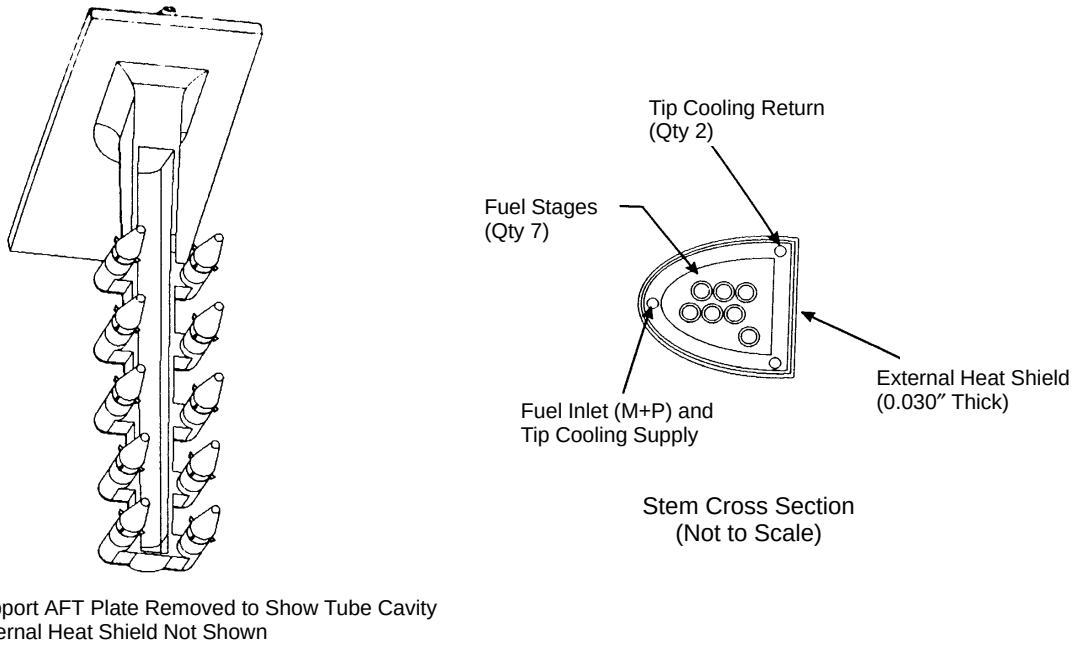

Figure 55. Full-Scale LPP Fuel Nozzle Concept 3 (U Stem)

The T- and U-stem concepts are fundamentally similar. The final concept, however, tends to separate itself from these designs. It was called the "double spraybar" (Figure 56) and used triple-concentric tubes that connect directly to each stinger. The design had the advantage of having the fuel tubes directly in line with the stingers, rather than having to make two 90° turns as in the other designs. This alignment did, however, introduce questions about the wakes coming off the tubes, which may impact air flow through the IMFH tubes. Additionally, because each of the five tubes is aligned

Figure 56. Full-Scale LPP Fuel Nozzle Concept 4 (Double Spraybar)

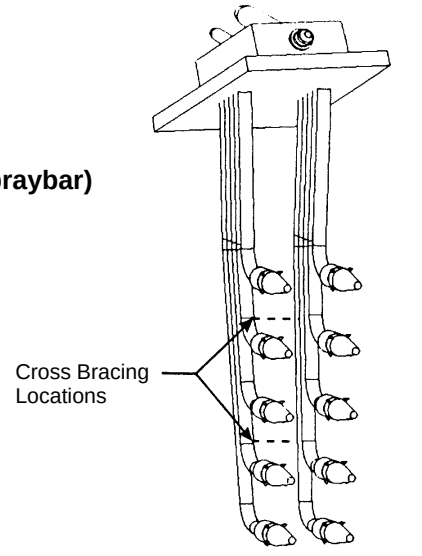

axially (in an engine axis system), the double spraybar increased the length of the hole in the engine case by about a half an inch. This was necessary to enable removal of the injectors for maintenance and replacement. However, because this design had the lowest weight of the designs considered and a relatively small part count, it appeared promising. The potential weight increase from extending the combustor length (if necessary to allow for a large enough case hole to remove the injectors) must be considered against the weight savings from the fuel stems.

The double-spraybar concept was selected as the primary design for full-scale use going into the LPP/RQL downselect, with the T-stem concept chosen as a backup. After downselect, additional development led to a modified design for use in the full-scale sector (described later).

Endurance/Coking Test

Throughout the flight envelope, fuel staging will be used to control engine emissions. As power is increased more stages will be fired, and as power is reduced, stages will be turned off. The latter scenario introduces potential for coking as stagnant fuel in the stinger tip continues to be exposed to high air temperatures (coke formation can also occur in flowing passages). From a coking standpoint, the most severe conditions occur at the point of initial deceleration from supersonic cruise, in which air temperatures are still very high (over 1000°F), but many of the main fuel stages have been shut off. Significant coking is detrimental to engine performance and emissions. It also leads to shorter required maintenance intervals and unscheduled maintenance, which adds significant operating cost.

To address these concerns, an endurance/coking test was performed at GEAE from February 19 through March 5, 1998. A full-scale, four-port, actively cooled stinger tip (Configuration 46 with the addition of active fuel cooling internally; see Figure 57) was attached to a mounting flange in a test rig. For environmental reasons, water was used in place of fuel in the cooling circuit surrounding the tip fuel supply. The water flow was set to match tip thermocouple readings with analytical predictions. The test was set-up to simulate a single flight cycle representative of stagnant coke

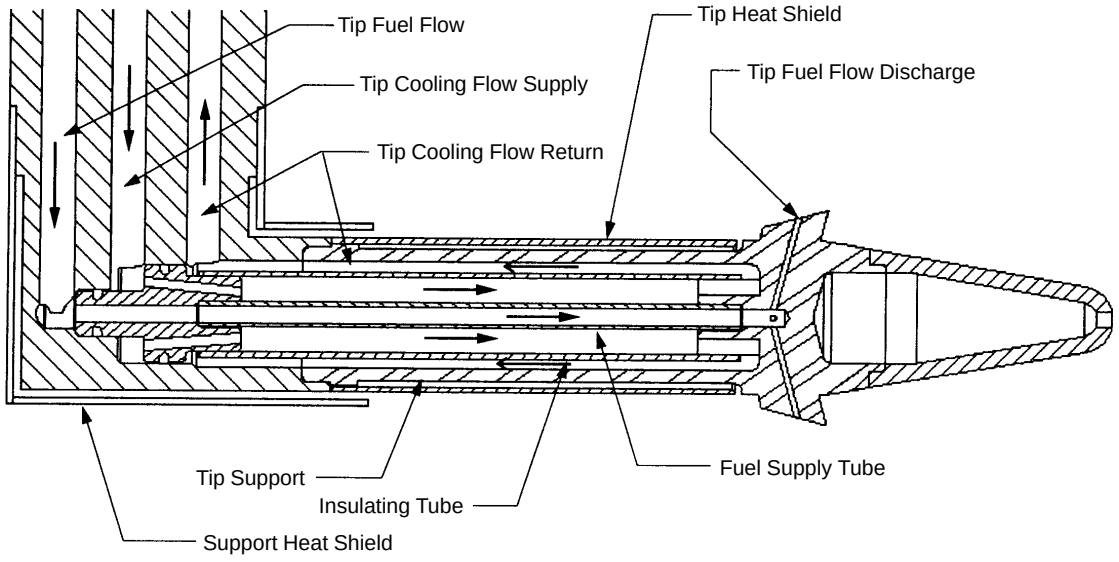

Figure 57. LPP Stinger Fuel Injector Tip Internal Cooling Concept

buildup. Air at 1029°F continuously flowed over the stinger while fuel (Jet A) was cycled on for one minute and off for three minutes. These times were deemed sufficient for thermal stabilization and to enable coke to "bake" onto the fuel passage surfaces. Fuel flow number was monitored during the test for changes and was physically measured on a separate calibrated fuel-flow stand before and after the test.

Although the test was originally planned for 2250 cycles or a 30% reduction in fuel flow number, whichever came first, by the end of the test the hardware had actually been cycled more than 2800 times over nearly 200 hours of testing (48 hours with fuel flowing), with no noticeable reduction in flow number. This included a period from March 1 (7:45 p.m.) through March 5 (7:30 a.m.) of continuous 24-hour-per-day operation. Several chronological readings are presented in Table 12. Note that, because of variability in the measured fuel flows and pressure drops, the flow numbers reported here (as measured while testing) show relatively high variability. The more telling measurements were taken before and after the test on a calibrated flow stand, which showed almost no change (10.5 pretest, 10.1 posttest).

The results of this test are strong evidence that the active cooling system is sufficient for preventing coke formation in stagnant fuel lines. This is significant because one of the primary alternatives was to require purging of stages with an inert gas as they were shut off. Such a system adds significant weight, complexity, and cost to the engine and requires the addition of onboard tanks for the inert gas, which must constantly be replenished. The actively cooled stinger, although also complex, is preferred over an inert gas system; however, more comprehensive tests are needed to ensure that coke formation is not a problem in other regions of the fuel-delivery system. The tests should cover complete flight cycles and ought to be performed before any fuel-delivery system is implemented in an engine.

4.4.1.4 Cyclone Pilot Development

Most of the combustor concepts contained cyclone pilots in addition to the IMFH premixers or LDI injectors. The IMFH premixers and LDI injectors were critical components of the combustor. They produce low NOx over a wide range of operating conditions and eventually made it possible to meet supersonic cruise emissions requirements. However, inherent lack of stability and relatively poor (high) low-power emissions of CO and unburned hydrocarbons had to be overcome. Thus, the cyclone pilots were added to improve low-power performance. Since the cyclone would be operated throughout the entire flight envelope, it also had to provide low emissions — especially NOx — at high power. Thus, while IMFH development focused mainly on high-power NOx, the cyclone pilot tests covered the entire flight envelope. After good moderate- and high-power emissions were demonstrated by the cyclone, the focus shifted towards low-power lean blowout, CO, and hydrocarbons. Low ground idle CO and hydrocarbons (that is, high combustion efficiency) were keys to meeting anticipated LTO cycle requirements.

Single-cup tests were used for development of the cyclones. Typical cross section and cutaway views are shown in Figure 58. The design consists of a swirler attached to an outer dome that houses the throat and dump cooling air holes. The outer dome also acts to mount the pilot in the facility. A centerbody houses the fuel injection system. The fuel injector is simply a main-supply tube with several small tubes (0.063-in OD by 0.020-in ID) added for fuel injection. Air is allowed to enter the centerbody; most is used for cooling the centerbody face, the remainder for "air assist" around the fuel tubes. The centerbody contains dump cooling air holes to reintroduce the air into the system

Table 12. IMFH Stinger Tip Endurance/Coking Test Results Summary

Rdg	Time	Total Hrs	Total Cycles	Wf (pph)	FN
0	2/19/98 2:30 PM	000:00	0	26.4	10.5
22	2/22/98 9:32 PM	004:14	64	25.5	9.7
90	2/23/98 1:15 PM	019:57	299	29.8	10.6
170	2/24/98 7:55 AM	038:37	579	26.8	9.9
175	2/24/98 9:03 AM	039:45	596	25.5	9.7
194	2/24/98 1:07 PM	043:49	657	27.8	10.8
214	2/24/98 5:42 PM	048:24	726	25.9	10.5
237	2/24/98 10:39 PM	053:20	800	26.2	10.6
241	2/24/98 11:11 PM	053:52	808	26.2	8.8
282	2/25/98 7:42 AM	062:24	936	26.2	9.8
283	2/25/98 7:46 AM	062:28	937	25.7	9.4
285	2/25/98 8:10 AM	062:52	943	25.7	9.6
303	2/25/98 12:04 PM	065:54	989	26.4	10.6
318	2/25/98 3:16 PM	069:06	1037	25	10.3
331	2/25/98 6:04 PM	071:54	1079	25.7	11.2
342	2/25/98 8:24 PM	074:14	1114	25	9.9
403	2/26/98 9:32 AM	087:21	1310	27.1	9.4
416	2/26/98 12:12 PM	090:01	1350	25.5	9.3
434	2/26/98 4:20 PM	094:09	1412	26.6	10.4
453	2/26/98 8:19 PM	098:07	1472	26.2	11.1
456	2/26/98 8:47 PM	098:35	1479	26.4	11.7
462	2/26/98 9:55 PM	099:43	1496	25.9	12.0
487	2/27/98 3:31 AM	105:20	1580	25.7	11.7
492	2/27/98 3:59 AM	105:47	1587	25.2	11.2
503	2/27/98 5:55 AM	107:43	1616	26.2	10.8
551	3/2/98 1:21 AM	114:03	1711	29.2	9.8
559	3/2/98 2:49 AM	115:31	1733	29.4	11.0
575	3/2/98 5:49 AM	118:31	1778	28.9	10.4
589	3/2/98 8:45 AM	121:27	1822	31.5	11.1
595	3/2/98 9:56 AM	122:39	1840	31.5	12.1
602	3/2/98 11:01 AM	123:43	1856	26.4	10.9
607	3/2/98 12:04 PM	124:46	1872	27	10.7
616	3/2/98 1:44 PM	126:26	1897	26.3	10.5
627	3/2/98 4:16 PM	128:58	1935	26.8	10.6
637	3/2/98 6:17 PM	131:00	1965	26.6	10.2
648	3/2/98 8:29 PM	133:11	1998	27.3	10.4
653	3/2/98 9:33 PM	134:15	2014	26.7	9.9
661	3/2/98 11:04 PM	135:46	2037	27	11.1
670	3/3/98 12:56 AM	137:38	2065	26.6	11.2
682	3/3/98 3:15 AM	139:57	2099	27.2	10.5
691	3/3/98 4:59 AM	141:41	2125	27	10.1
702	3/3/98 7:02 AM	143:44	2156	26.8	11.6
710	3/3/98 8:41 AM	145:23	2181	25.7	10.5
727	3/3/98 12:20 PM	149:03	2236	26.8	11.3
740	3/3/98 3:11 PM	151:54	2279	26.6	10.9
752	3/3/98 5:50 PM	154:32	2318	27	11.5
765	3/3/98 8:30 PM	157:12	2358	26.8	11.6
802	3/4/98 3:50 AM	164:33	2468	27	10.7
810	3/4/98 5:29 AM	166:12	2493	27.4	11.4
836	3/4/98 11:01 AM	171:43	2576	26.1	10.8
848	3/4/98 1:41 PM	174:23	2616	26.4	11.2
856	3/4/98 3:21 PM	176:03	2641	26.4	10.3
867	3/4/98 5:32 PM	178:15	2674	25.2	11.8
901	3/5/98 1:08 AM	185:50	2788	26.6	11.1
919	3/5/98 4:28 AM	189:10	2838	26.2	10.1
932	3/5/98 7:28 AM	192:10	2883	26.8	10.1

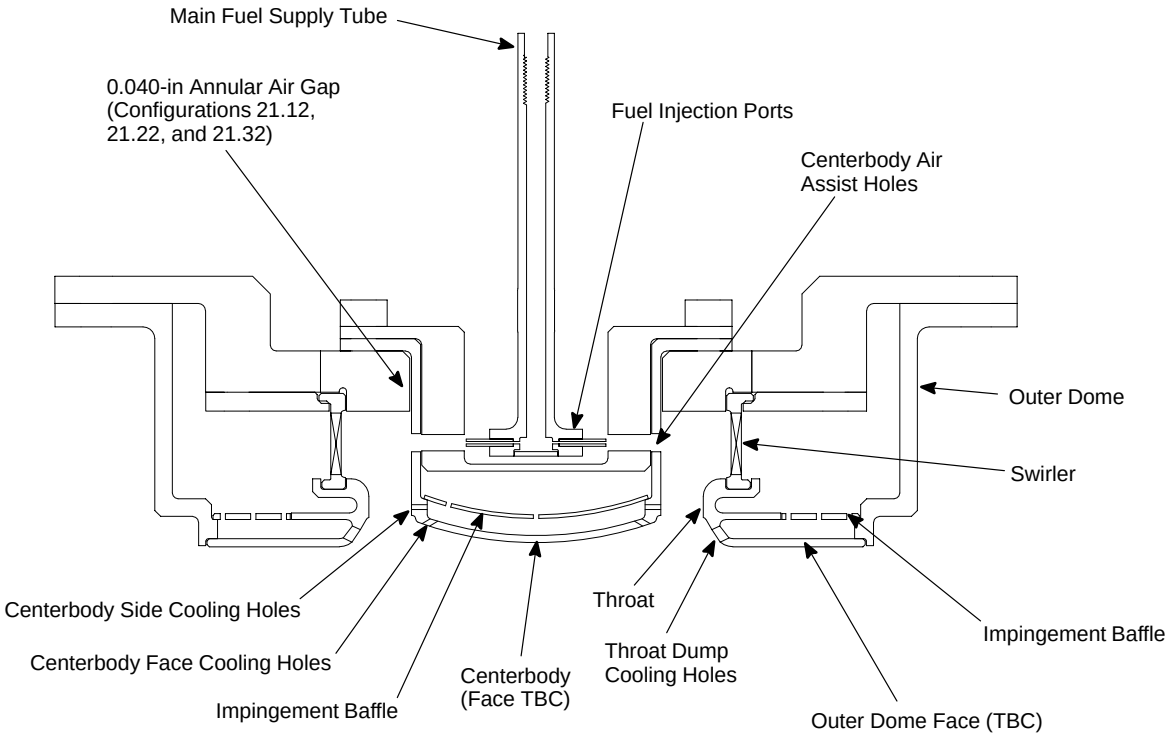

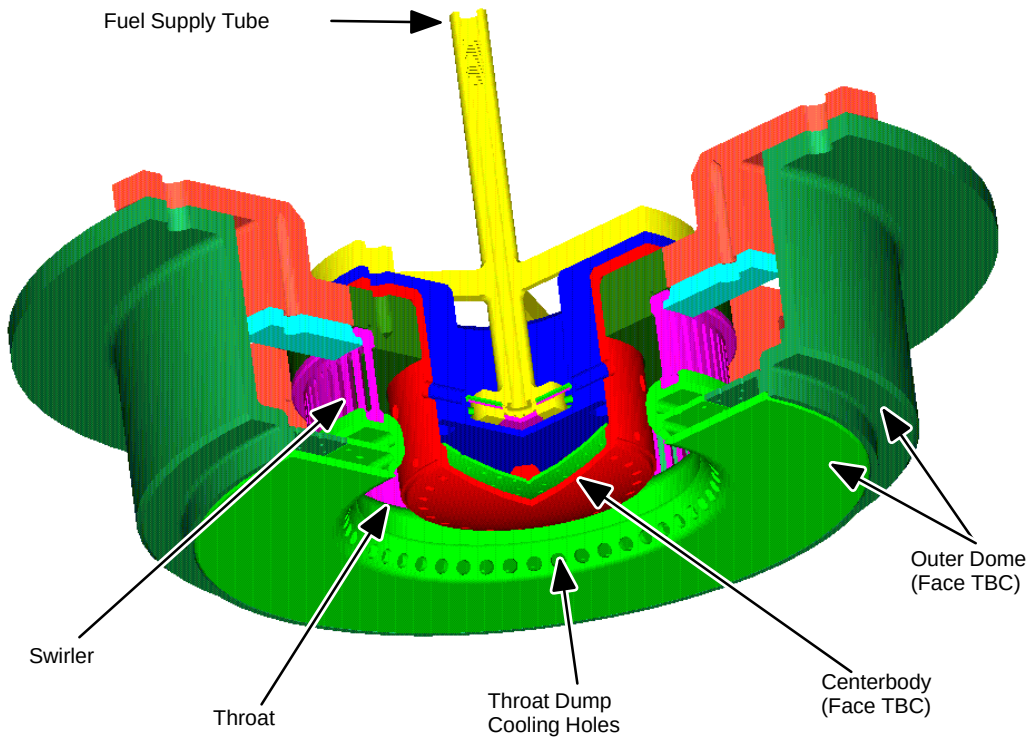

Figure 58. Typical LPP Cyclone Pilot

prior to combustion. The centerbody face and outer dome face both have thermal-barrier coating (TBC) to protect the metal from the high heat load of the flame. All of the configurations tested, both subscale and full scale, had features similar to those shown in Figure .

The cyclone pilots were tested at the Southwest Research Institute (SwRI) in San Antonio, Texas. Dr. Cliff Moses was the Principle Investigator on the project. The cyclones were mounted to a flange and placed in a horizontal flow tube (Figure 59; dimensions shown are for full-scale tests). The downstream hot section contained a ceramic liner to protect the metal pressure casing. Emissions samples were taken seven inches downstream of the dome face using five fixed probes arranged to sample approximately equiarea regions of the exit plane.

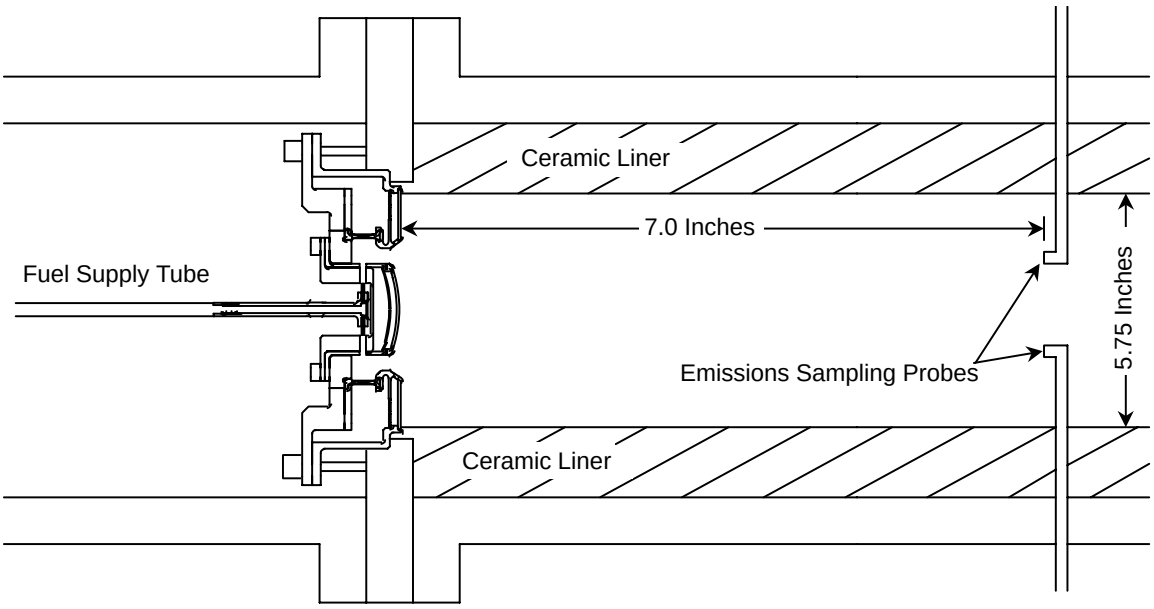

Figure 59. SwRI Test Rig Schematic

Several cyclone design parameters were varied and tested. In terms of fuel injection, this was accomplished by changing the number of injection ports. Most of the changes, however, were related to the cyclone air flow. Changes to the swirler included vane angle, number of vanes, slot height and width, and swirler diameter. All of these changes impacted the swirl number of the cyclone (and effective area, unless varied in the necessary proportions to maintain constant area). The centerbody and throat diameters and dump cooling hole patterns were also primary variables that were changed. In the subscale designs, the internal air flow distribution was held relatively constant (that is, the flow splits between the air through swirler, air assist ports, centerbody cooling, and outer dome cooling were nearly constant). The internal flow splits would be varied to some extent in full-scale designs.

Three subscale and two full-scale configurations were tested prior to the LPP/RQL downselect. Key features of these designs are listed in Table 13. The features of the subscale designs were drawn from previous development experience. The full-scale designs were developed from the subscale test experience. Note that the required full-scale flow area is more than three times that of the subscale designs, making the full-scale configurations much larger geometrically.

Table 13. LPP Cyclone Pilot Design Summary (Configurations 15–18, 20.3)

Parameter		Subscale Config 16	Subscale Config 17	Subscale Config 18	"Full Scale" Config 15	"Full Scale" Config 20.3
General	Overall Effective Flow Area, in^2	0.6	0.6	0.6	1.01	1.70
	Swirl Number	0.85	0.85	0.85	0.70	1.16
	Air Gap Around Centerbody, in	0.15	0.15 (Off Center)	0.013 (Ferrule)	None	None
Swirler	Inner Diameter, in	1.736	1.736	1.736	2.400	3.800
	Outer Diameter, in	1.975	1.975	1.975	2.600	4.050
	Number of Slots	48	48	48	80	80
	Slot Angle, °	45	45	45	30	50
	Slot Height, in	0.504	0.504	0.504	0.800	0.450
	Slot Width, in	0.025	0.025	0.025	0.025	0.050
Centerbody	Outer Diameter, in	1.181	1.181	1.181	1.350	2.750
	Fuel Injection Air-Assist Hole Dia, in	0.110	0.110	0.110	0.150	0.130
	Number of Holes	6	6	6	8	15
Throat	Diameter, in	1.592	1.592	1.592	2.000	3.400
	Side Cooling Hole Diameter, in	0.145	0.145	0.145	0.125	0.135
	Number of Holes	20	20	20	30	30
Fuel Injector	Number of Injection Ports	6	6	6	8	15
	Tube OD, in	0.065	0.065	0.065	0.065	0.0625
	Tube ID, in	0.020	0.020	0.020	0.020	0.020

Subscale Concepts

The three subscale concepts tested were actually simple variations of the same design. The primary design was Configuration 16, which was to be used in the moderately mixed MRA sector (described later). The intent of testing the other two was to assess the impact of centerbody centering and air leakage around the centerbody on emissions, lean blowout, autoignition, and flashback.

Configuration 16 featured a 0.15-in nominal gap around the centerbody, allowing additional air to enter the premixing cavity. The centerbody was centered such that the gap was essentially equal all the way around. This was the preferred design by the mechanical designers for manufacturing, assembly, cost, and weight reasons.

Configuration 17 was the same except that the centerbody was moved off-center. This was done to verify that misalignment, mainly as a result of differential thermal growth at different points in the flight envelope, did not impact performance.

Finally, Configuration 18 placed a ferrule around the centerbody to essentially eliminate the gap (to 0.013 inch nominally). This was tested in case the air gap proved to adversely impact emissions. If the presence of an air gap or the centerbody centering within the gap had proven to be a significant problem, the ferruled design would have been used in the sector.

The tests were very successful. No autoignition or flashback events were observed while testing any of the designs. No measurable differences in lean blowout were detected, although data scatter makes it difficult to compare the results with confidence (Figure 60). Key emissions plots are

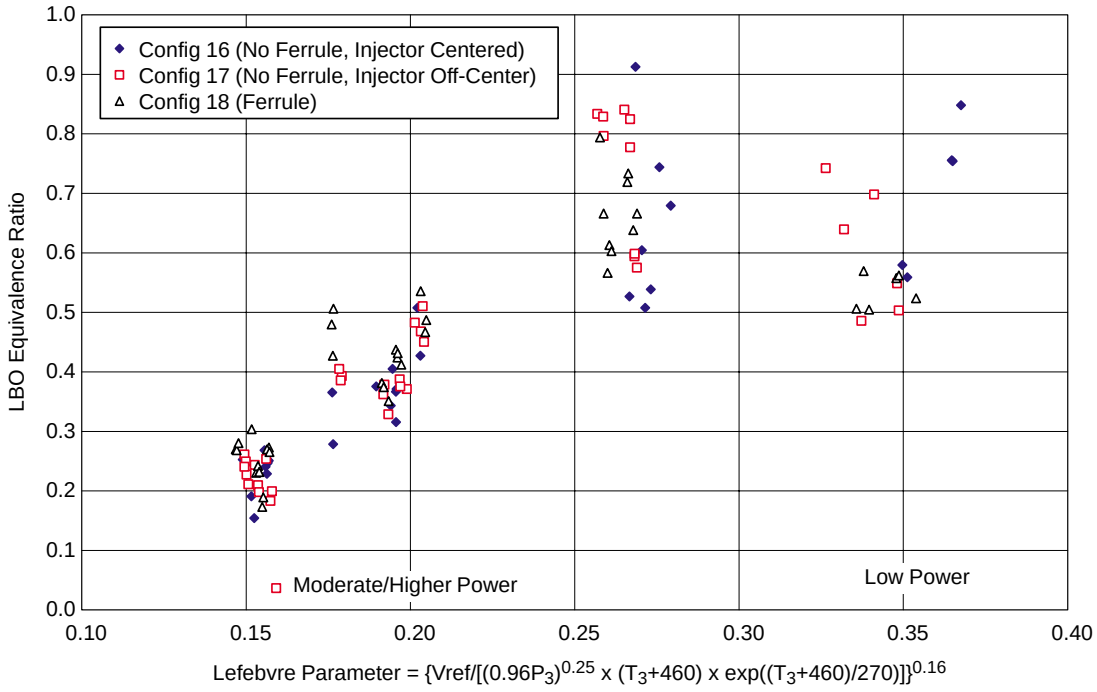

Figure 60. Impact of Injector Positioning on LPP Cyclone Lean Blowout

presented in Figures 61 through 64. These results suggest that NOx emissions were not impacted by the air leakage and centering. Combustion efficiencies showed some divergence but remained quite acceptable at the conditions tested. The results suggested there was no need to add a ferrule to the cyclone and that misalignment of the centerbody did not greatly impact operation.

The Configuration 16 cyclone was selected for use in the highly successful moderately mixed MRA sector that demonstrated supersonic cruise NOx EI below 5 (described later).

Full-Scale Concepts

Because of successful demonstration in the moderately mixed MRA sector, Configuration 16 became the baseline for development of full-scale designs. Ideally, the features of Configuration 16 could be scaled-up directly to the desired flow area for a full-scale design. However, this was not possible for several reasons. First and foremost, direct scale-up would greatly increase bulk residence times in the premixer and consequently raise significant autoignition concerns. Other reasons relate to a range of geometric limitations.

One is that direct scale-up would result in 18 to 24 fuel injection ports, much more than the original 6. So many ports are physically impossible to implement because cooling air flow area requirements internal to the centerbody limit the space available for injectors.

There are also diametrical limits to the swirler. Without increasing the diameter of the pilot dome (and therefore the outer casing) to increase the circumferential length available, the pilots were limited to a specific maximum outer diameter to avoid interferences. Although the number of pilots used in the engine could be varied to adjust the necessary flow area and size of each, that would simultaneously change the number of IMFH tube banks in the engine.

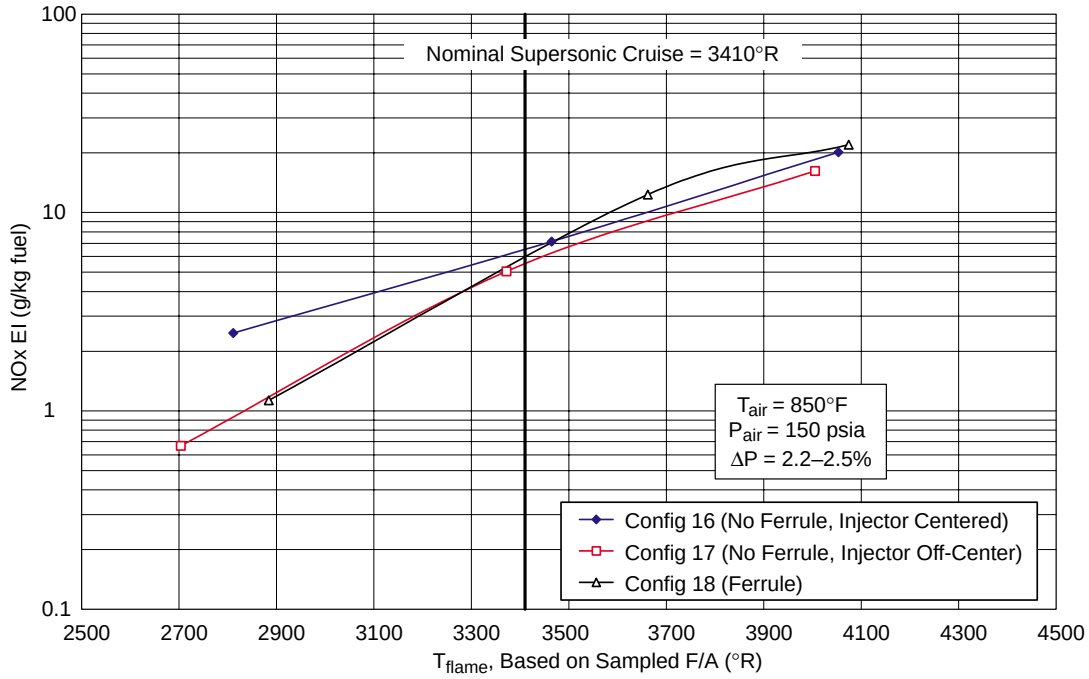

Figure 61. Impact of Injector Positioning on LPP Cyclone NOx at 850ºF, 150 psia

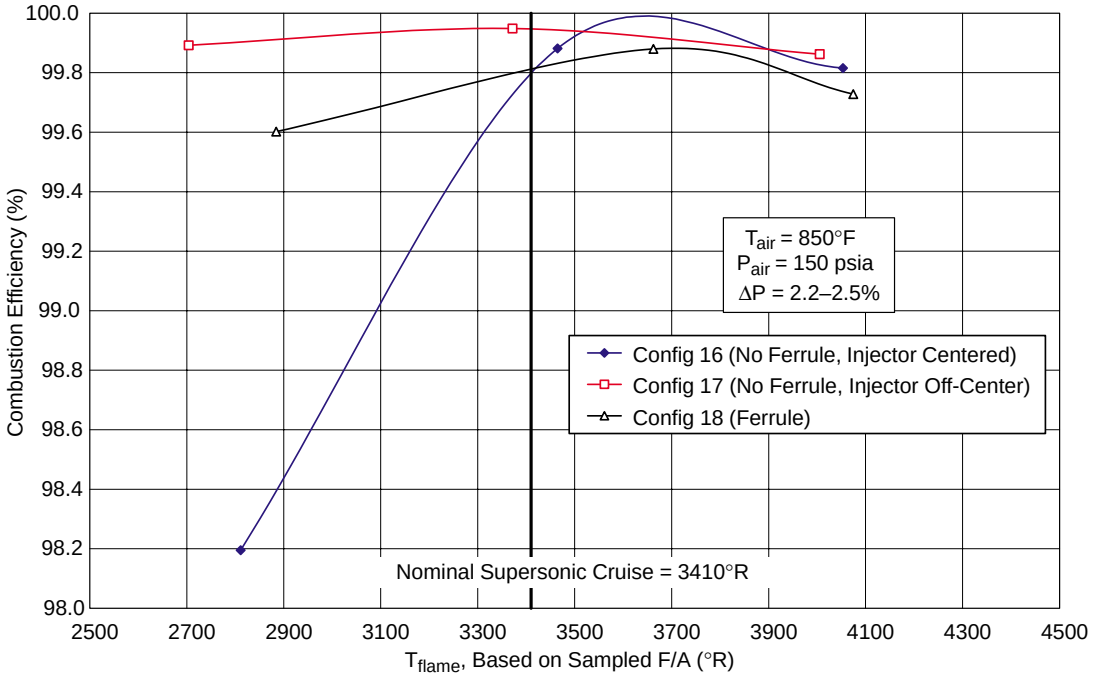

Figure 62. Impact of Injector Positioning on LPP Cyclone Combustion Efficiency at 850ºF, 150 psia

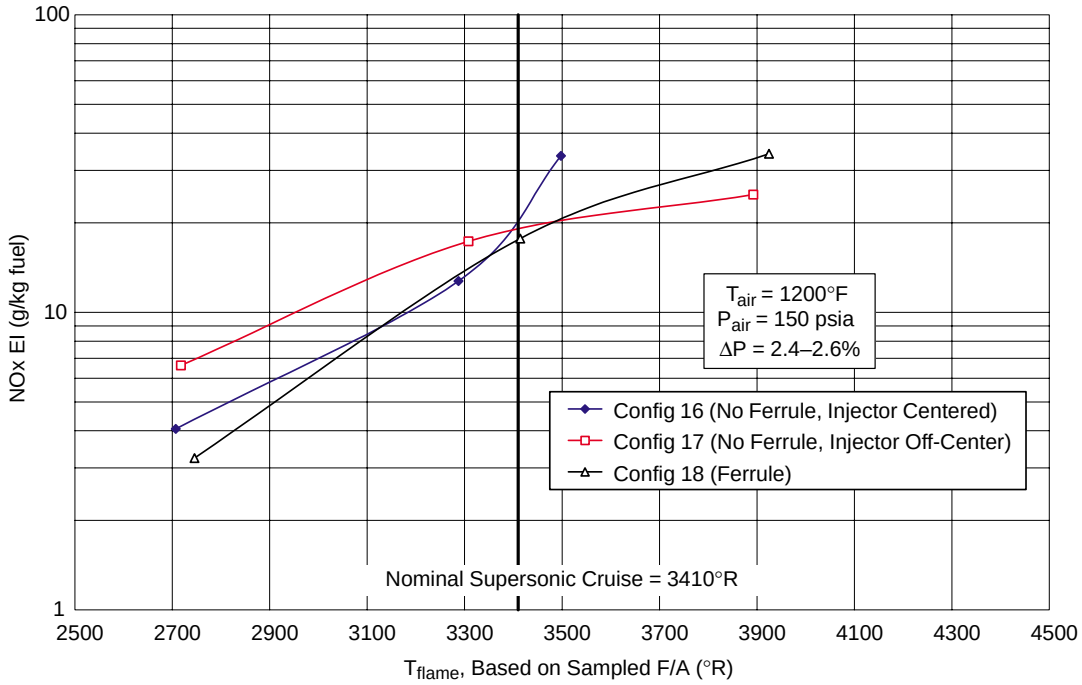

Figure 63. Impact of Injector Positioning on LPP Cyclone NOx at 1200ºF, 150 psia

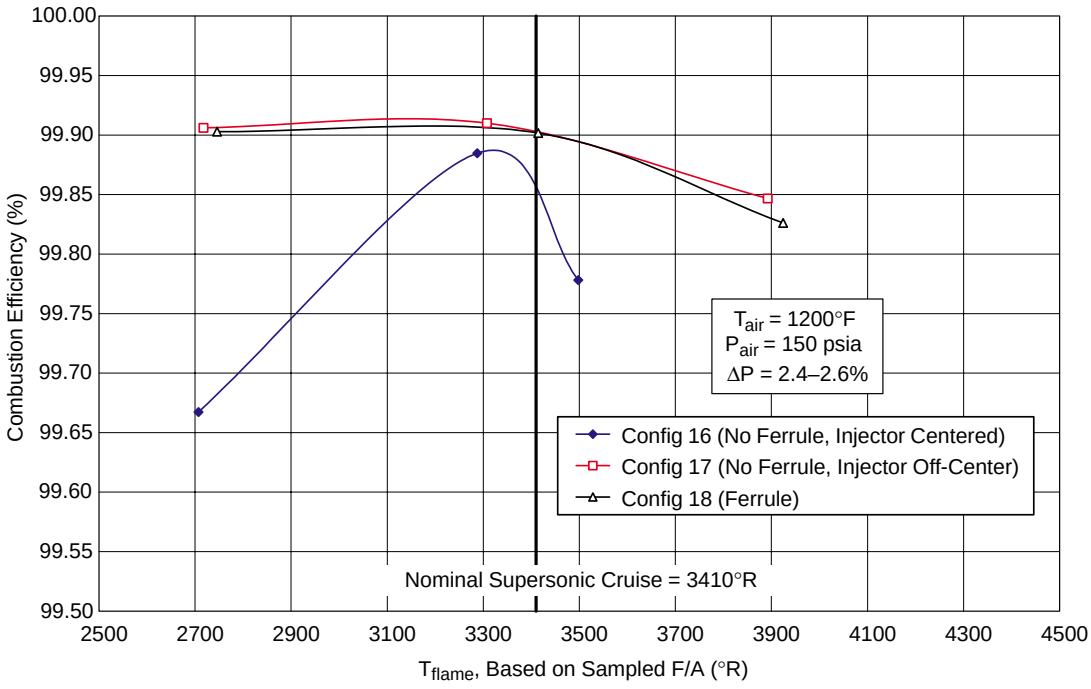

Figure 64. Impact of Injector Positioning on LPP Cyclone Combustion Efficiency at 1200ºF, 150 psia

Only two full-scale cyclones were tested prior to the LPP/RQL downselect. The first, designated Configuration 15, was designed to have much longer bulk residence times than the previous subscale configurations. This was done in an attempt to improve premixing and vaporization to reduce NOx, an early analytical concern as the size of the cyclone increased. Unfortunately, residence time appears to have been too long, as the bottom surface of the centerbody heat shield was completely burned off in the test. It is not clear when the damage occurred, but the final set of data acquired was at nominal supersonic cruise conditions (low pressure drop). It is also possible that a fuel leak was involved, but no proof exists to substantiate this. To the contrary, because the damage was mostly to the centerbody (with some spreading across to the throat), with no upstream damage, it was probably not the result of a fuel leak.

Emissions overall were reasonably low (Figures 65 through 68), but the design obviously could not be used. Combustion efficiencies were not quite as good as the baseline subscale design but remained quite high. It is interesting that the cyclone appeared to be operating as a diffusion burner at supersonic cruise. This is evident in the flatness of the NOx versus flame temperature curve. Unlike diffusion flames, premixed flames normally show patterns similar to the Configuration 16 data, or to the full-scale data shown at 850°F. Because of the hardware damage, no lean-blowout data were acquired.

To reduce the chances of additional hardware damage, all new full-scale cyclone configurations were designed with bulk residence times in the premixing chamber closer to those of the subscale designs (on the order of 0.3 ms).

The other full-scale design tested prior to downselect was Configuration 20.3. This configuration was designed to have a higher swirl number (1.15 versus 0.85 for Configuration 16) in an attempt

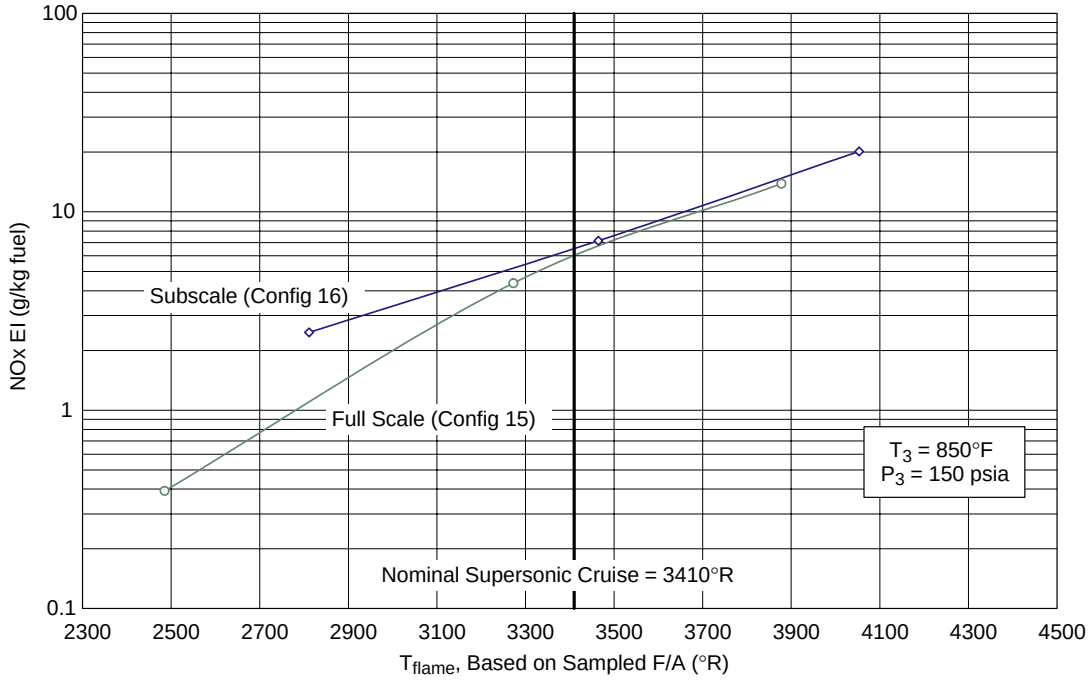

Figure 65. Subscale and First Full-Scale LPP Cyclone NOx Emissions at 850ºF, 150 psia

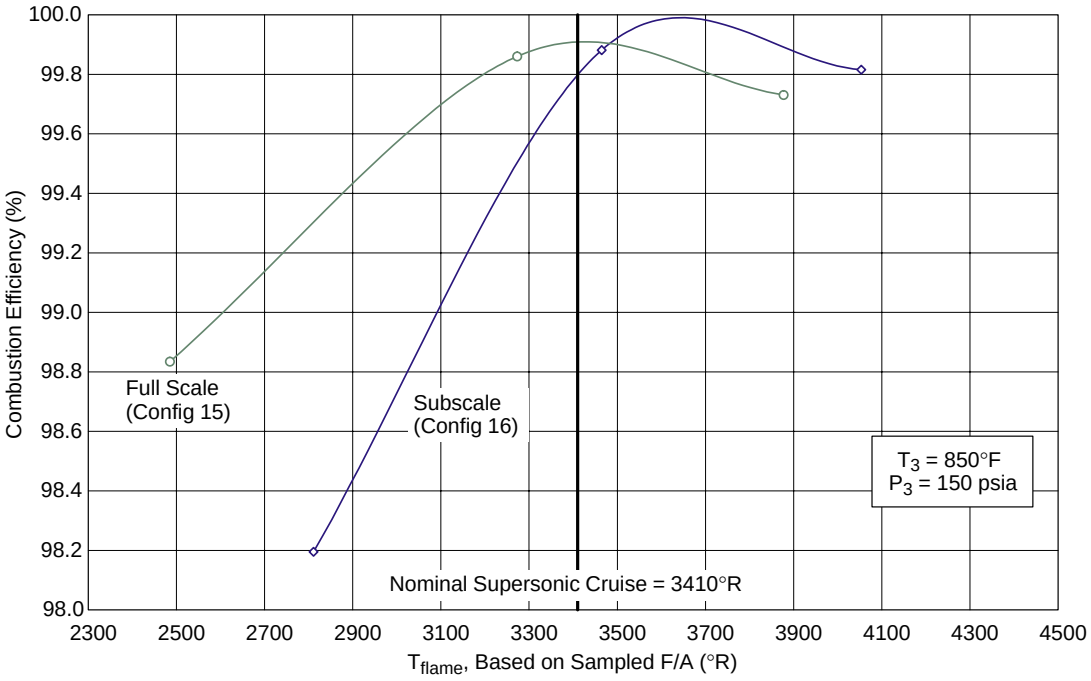

Figure 66. Subscale and First Full-Scale LPP Cyclone Combustion Efficiency at 850ºF, 150 psia

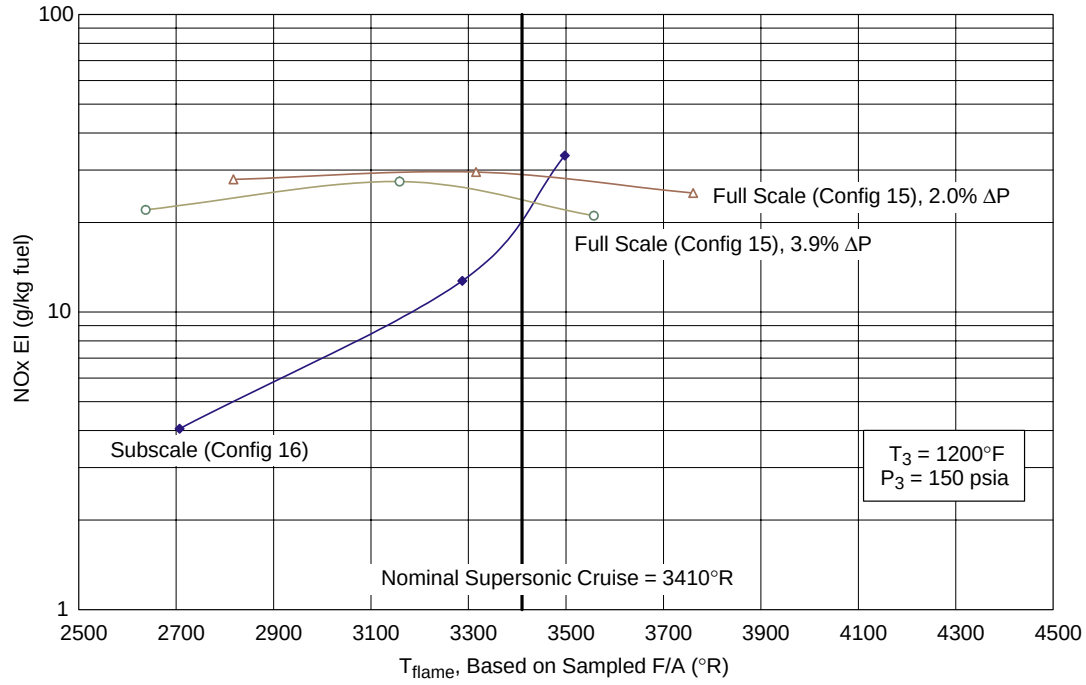

Figure 67. Subscale and First Full-Scale LPP Cyclone NOx Emissions at 1200ºF, 150 psia

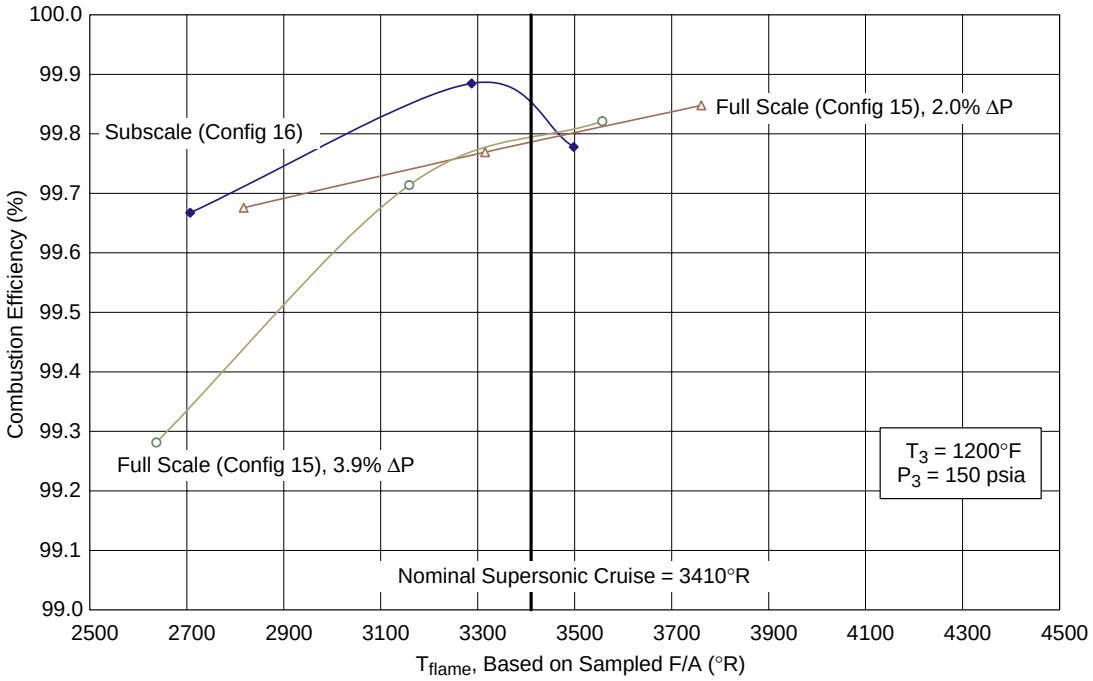

Figure 68. Subscale and First Full-Scale LPP Cyclone Combustion Efficiency at 1200ºF, 150 psia

to improve mixing and lean blowout. It was also quite large (4.05-in OD) with a large number of fuel injection ports (15), although still fewer than a true scale-up of subscale concepts. Some testing was performed at SwRI, but time limits necessitated shipment for completion of the testing at NASA–Glenn.

The results were quite promising. Lean blowout was significantly improved over Configuration 16 (Figure 69), which had already demonstrated acceptable lean blowout levels in a sector. Emissions were also similar to those demonstrated by the baseline subscale design (Figures 70 and 71). Configuration 16 was never tested at true ground idle conditions, but other data at low power suggest that CO EI was somewhere around 25, so the goal was to at least match this level with the new full-scale designs. Unfortunately, ground idle CO came in higher, at about 36 EI (Figure 72). Other ground idle data were acceptable, although combustion efficiency remained a bit lower than desired (Figures 73 and 74).

The data show that the full-scale designs are capable of providing emissions levels similar to those produced by the subscale designs. Although ground idle CO remained a little high, lean blowout showed measurable improvement. The significance of demonstrating reasonable emissions levels at full scale was tremendous, since scale-up for a sector or an engine would not have been possible if the performance had drastically changed. Several additional full-scale designs were tested after the LPP/RQL downselect and will be described later in this report.

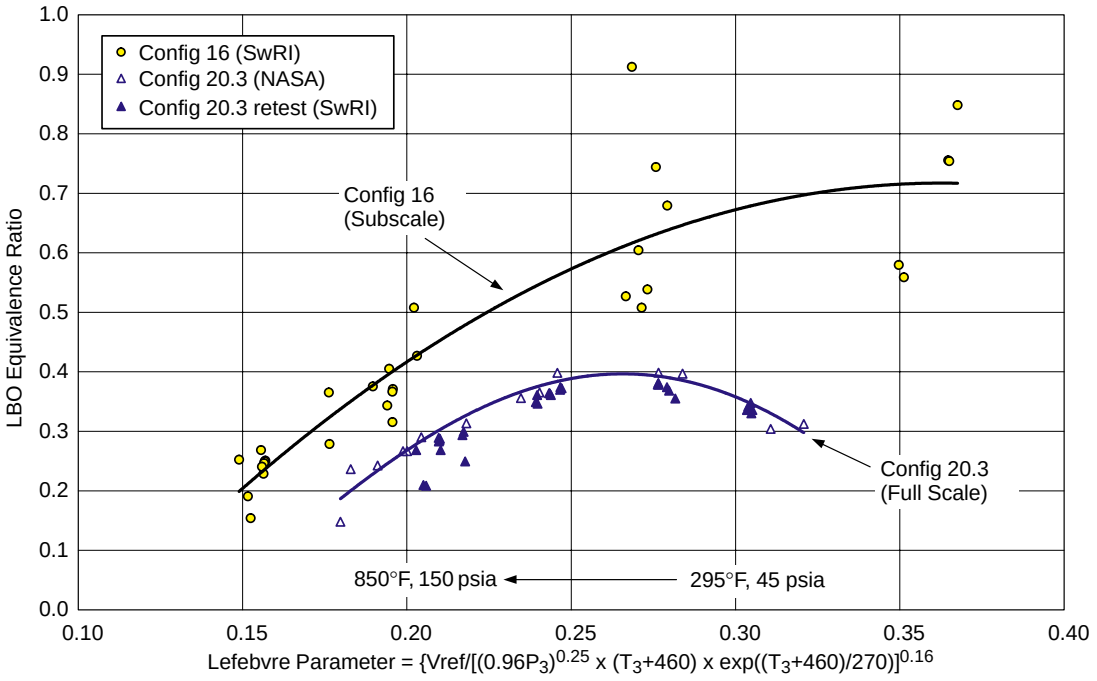

Figure 69. Subscale and Larger Full-Scale LPP Cyclone Lean Blowout Comparisons

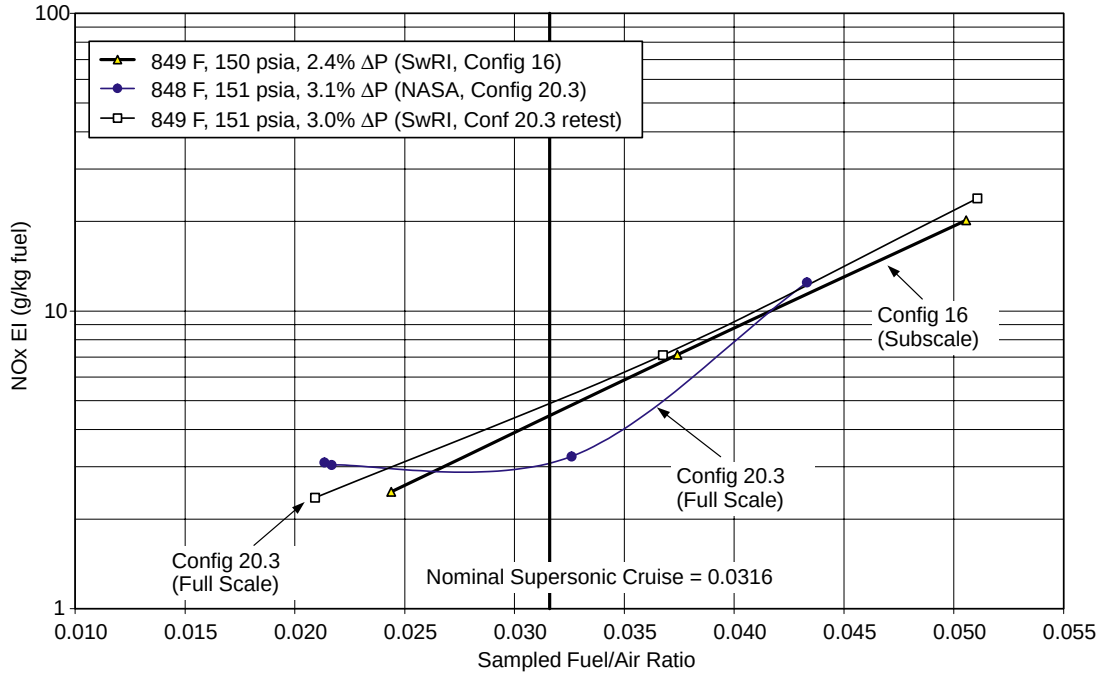

Figure 70. Subscale and Larger Full-Scale LPP Cyclone NOx at 850ºF, 150 psia

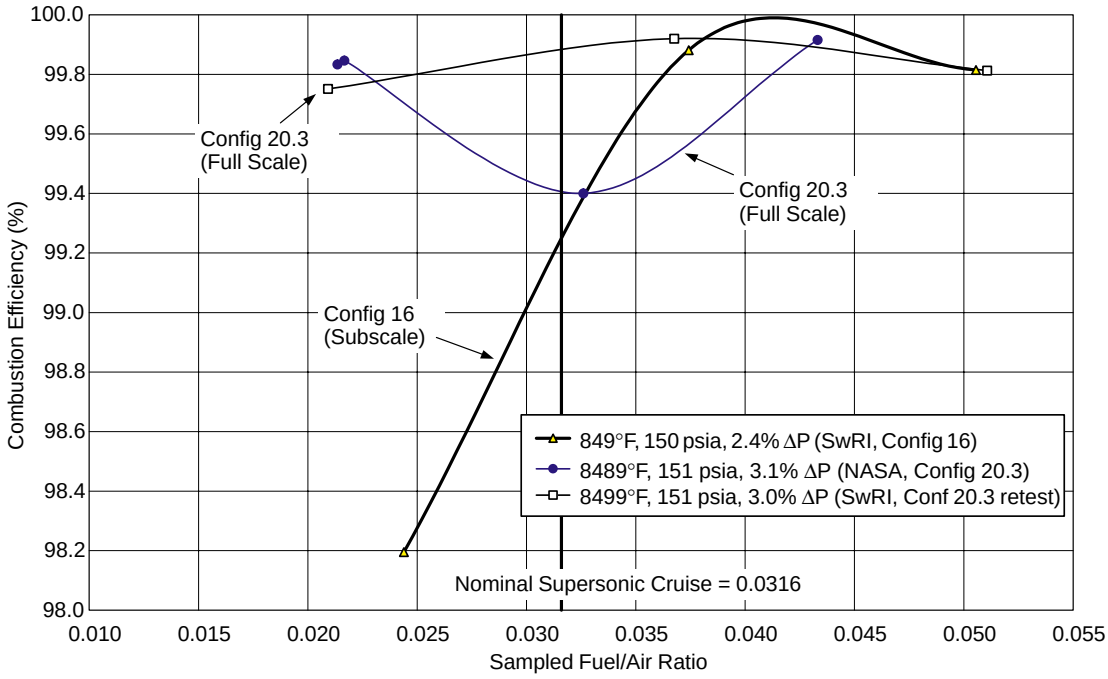

Figure 71. Subscale and Larger Full-Scale LPP Cyclone Combustion Efficiency at 850ºF, 150 psia

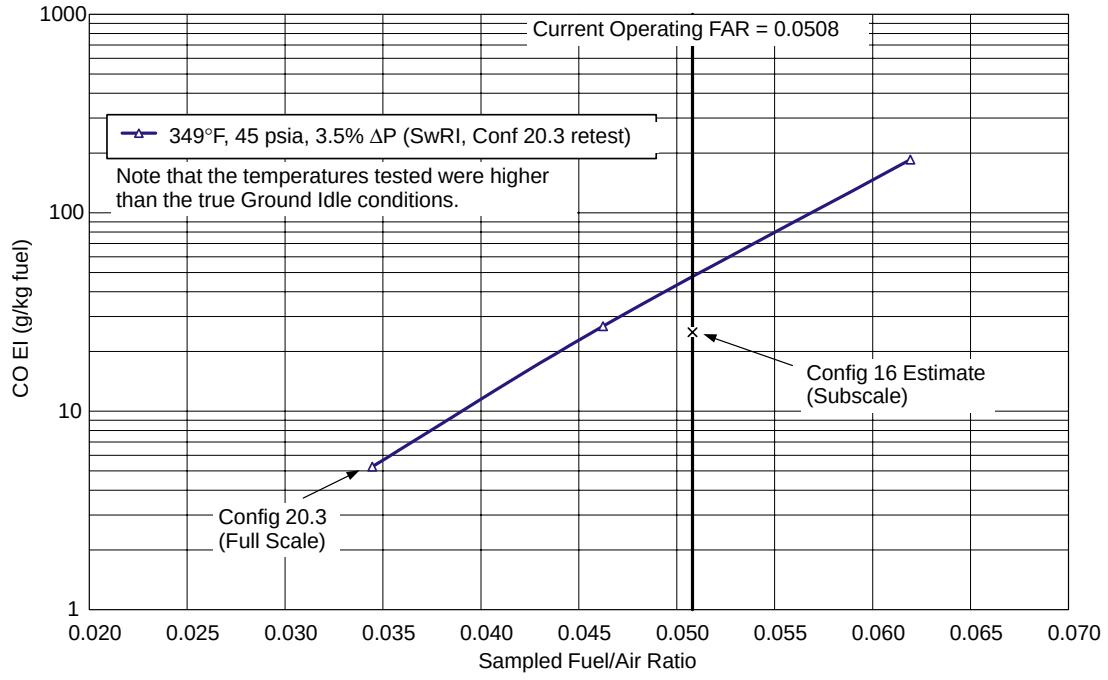

Figure 72. LPP Configuration 20.3 Cyclone Ground Idle CO (295ºF, 45 psia)

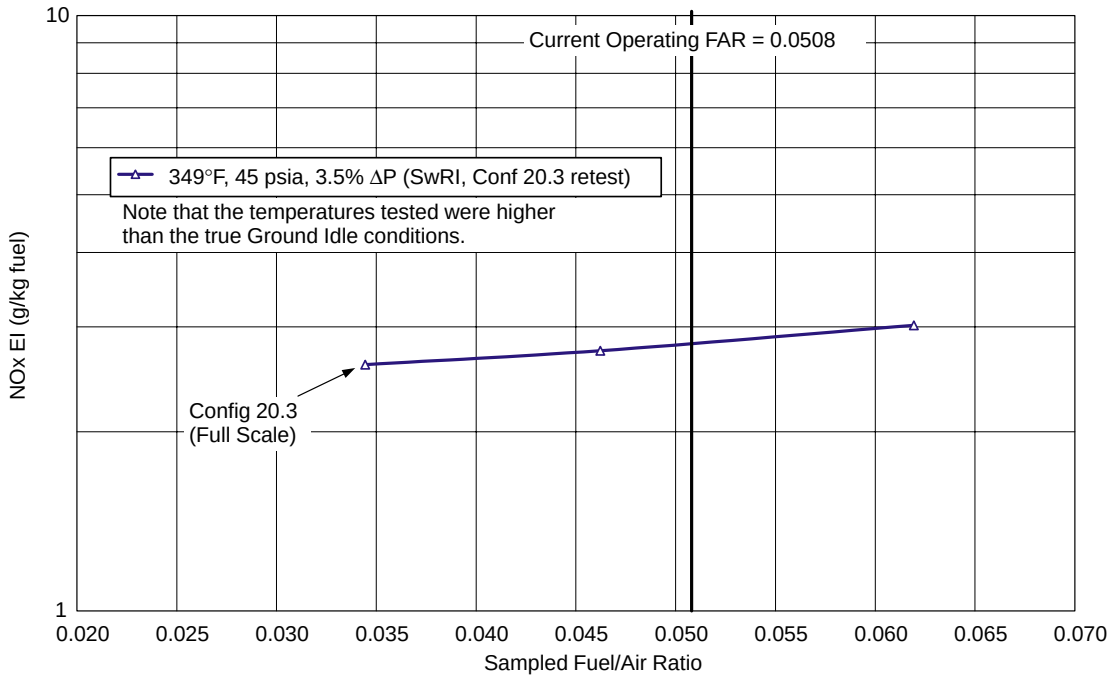

Figure 73. LPP Configuration 20.3 Cyclone Ground Idle NOx (295ºF, 45 psia)

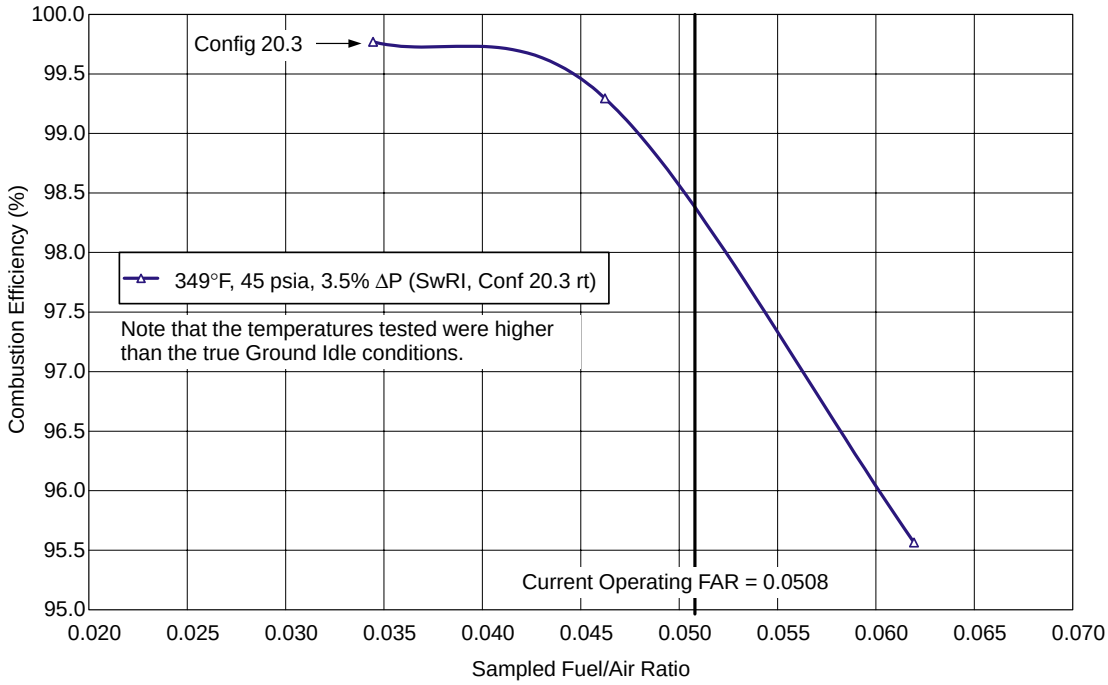

Figure 74. LPP Configuration 20.3 Cyclone Ground Idle Combustion Efficiency (295ºF, 45 psia)

4.4.2 RQL Combustor Development

4.4.2.1 Initial Wall-Jet Type RQL Combustor Rig

The earliest RQL investigations under this task used the single-nozzle, modular rig from the fundamental validation and design base data acquisition effort of Item 1 of Section 4.3.2.3. This and most subsequent RQL-type combustor rigs were evaluated in Cell 1 at the Jet Burner Test Stand at UTRC. The rig incorporated independent control of the airflow to the rich and quench zones of the combustor. The quench airstream was directed into the gas path from a manifold around the quench section of the rig. The rich combustion zone consisted of a cylindrical section followed by a conical convergent section to the quench entrance. Cylindrical spools of varying lengths were available to implement different residence times in the rich zone. The convergent section was 1.6-in long, transitioning from the 5-in diameter combustor to the 3-in diameter quench section at an included angle of 64°. The lean zone consisted of a divergent section at the quench exit followed by a separate cylindrical section. The 3.2-in long divergent section transitioned from the 3-in diameter quench to the 5-in diameter cylindrical section at an included angle of 34°. Cylindrical spools of various lengths were also available to implement alternative lean-zone lengths. All of these sections incorporated double-wall construction with an internal water jacket. The 8-in nominal pipe size spools contained a 1.25-in thick ceramic liner to provide thermal insulation and achieve the gas-path diameters mentioned above. The insulating liners were cast in place in the spools from Plibrico Plicast 40, a commercial ceramic consisting of mostly alumina. This material was selected because it offers favorable thermal shock properties and the ability to withstand combustor temperatures up to 3400°F.

While this rig provided significant sizing, performance, and emissions databases from which design criteria were developed, the performance of the quench jet penetration/mixing/dispersion was discovered to be a critical NOx generation mechanism. A number of candidate quench-zone configurations, having different numbers and sizes of quench air orifices, were evaluated in the initial program. These included oval or slotted orifices aligned at off-axial directions, circular and square orifices, and variations in the number of orifices, including a multiorifice sized configuration. In the final configuration, which provided the best NOx and CO emissions characteristics, the quench airflow was injected into the gas path through eight, 0.719-in-diameter, equally spaced, circular orifices. The quench section length and inner diameter was 3.375 and 3 inches, respectively, and the axial plane of the hole centerlines was equidistant from the quench entrance and exit. The eight-hole quench section design had one air inlet and was fabricated from 316 stainless steel. Again, heat loss to the cooled surface was minimized with use of a 0.03-in-thick, flame-sprayed coating of zirconia oxide. The design included two, 0.10-in-high, annular passages in a 0.75-in-thick-wall, quench-jet metal cylinder. Each annulus was 1.10-in wide and located to provide a 0.75-in-wide uncooled band at the center for the quench air orifices.

4.4.2.2 Integrated Module Rig, Further Wall-Jet Quench Development

At this point in the program, many of the initial subcomponent development efforts of Subsection 4.3.2.3 — such as Items 2, 3, and 4 — were coming to fruition and offered potential for incorporation into the next-generation RQL combustor rig. These offered an opportunity to break with the earlier cast-ceramic-type construction and use much more realistic design concepts including a variable-geometry airpath fuel injector, a cast metallic liner for the rich zone, a wall-jet-type quench zone

consistent with the metallic liner, and flow splits driven by local pressure distribution rather than a piping-valve control system.

In the integrated module rig, combustor airflow was delivered to the test section spool that housed the fuel injector as well as the combustor module, including the rich zone and quench sections, as shown in Figure 75. The aerating fuel injector shown on Figure 76 combines a small-airflow, two–passage injector with a variable-geometry airflow component located coaxially with the core two-passage injector. The two-passage aerating injector was sized consistent with minimum rich-zone air loading and was surrounded by a variable-geometry, annular swirler that can open to meet the entire range of airflow demand. This design approach offers the decided advantage of divorcing the fuel-atomization process from the modulated-airflow feature and was the preferred mechanical approach for the aerating injector.

The rich-zone liner was constructed from PWA1422, a directionally solidified nickel alloy. The liners were fabricated using the quick-cast process that employs a stereolithographic model as the pattern in the investment casting process. The liner was approximately 6.3 inches long and cylindrical, with approximately a 5-in ID. As the rich-zone flowfield progresses towards the quench plane, the liner shape is curved radially inward to create the quench throat diameter, a key parametric variable assessed during the combustion tests The liner was held in position by eight tabs spaced uniformly about the circumference of the outer surface of the liner. These tabs were engaged by a tab-holder mechanism that protruded from the test section spool to grab the tabs on the liner. The

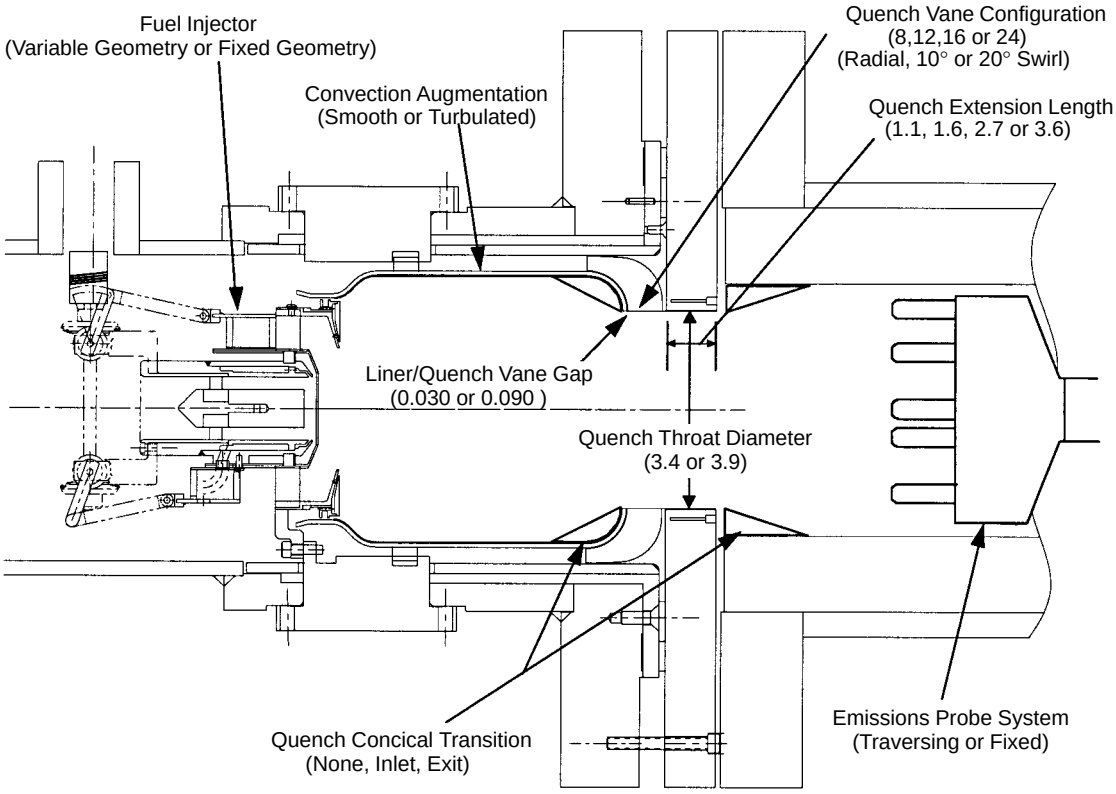

Figure 75. Key Configuration Variables Evaluated During Integrated Module Rig Testing of the Wall-Jet Combustor Configuration

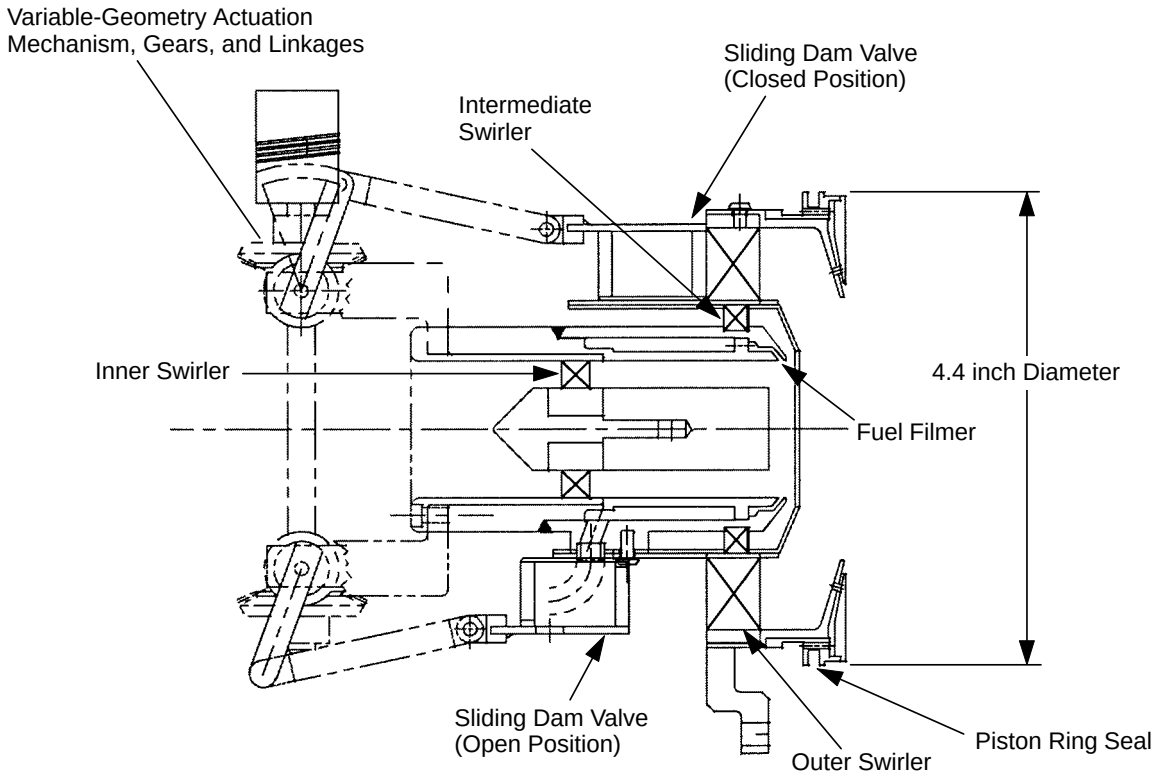

Figure 76. Variable-Geometry Fuel Injector Cross Section

surfaces of the rich-zone liner exposed to the combusting gases had a TBC, applied with a plasma-spray process. The rich-zone liner was convectively cooled with the quench air that flowed through an outer-shroud annulus.

The objective of the quench vane design was to achieve rapid mixing of the rich-zone flow with the quench air, so that minimal NOx is formed as the local conditions in the quench zone pass through an equivalence ratio of 1 and regions of hot mixed gas. The quench vanes were constructed from PWA1480, a single-crystal nickel alloy. A stereolithography pattern and the resulting quench vanes are shown in Figures 77 and 78 respectively.

The quench vanes were designed to take the rich-zone liner convective cooling air, turn it 90°, and divide it into discrete quench jets. To minimize pressure losses associate with this process, the air passage was designed to be continuously convergent as the vane transitioned flow from the cooling annulus into the quench jet. Many quench vane designs were committed to fabrication in addition to the 8- and 12-vane configurations of Figures 79 and 80. Others included 16- and 24-vane configurations, vanes with the flowpath canted relative to radial to induce a swirling component in the jets, and vanes compatible with different quench throat diameters.

The quench extension section consisted of a water-cooled spool piece with a diameter that matched the quench throat diameter and extended an axial distance to confine a region for the quench mixing process prior to expansion or dump of the flow into the lean zone. Various quench extension lengths were evaluated in this program, including 1.1, 1.6, 2.7, and 3.2 in. The lean-zone section was cylindrical in shape, 5-in diameter, and had a total spool section length of 9 in. The exit plane of the

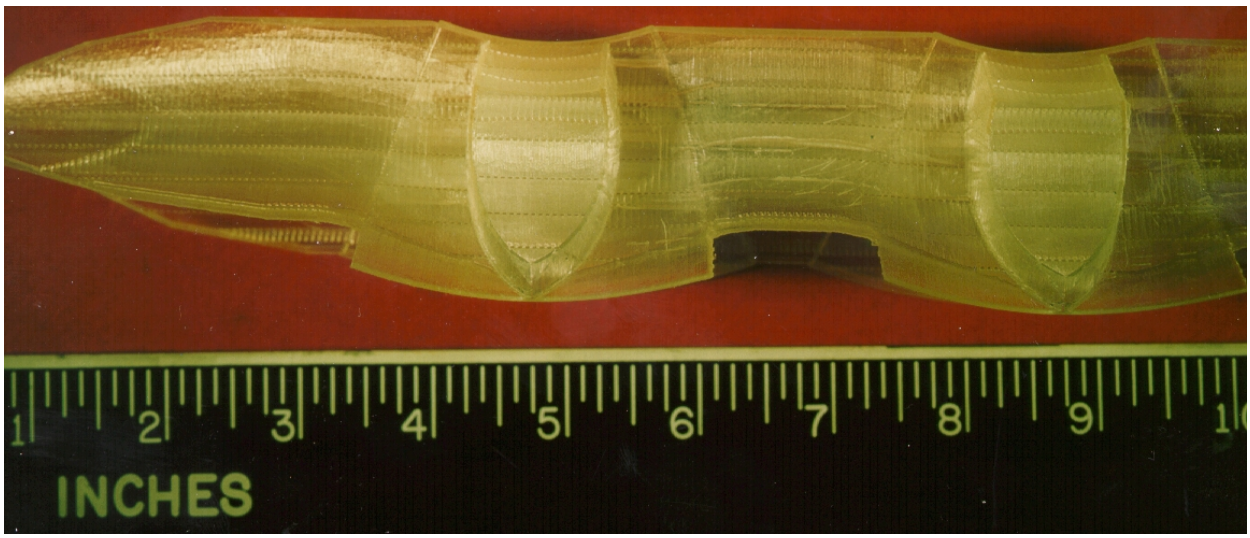

Figure 77. Stereolithography Pattern for Casting Quench Vanes for the Integrated Module Rig

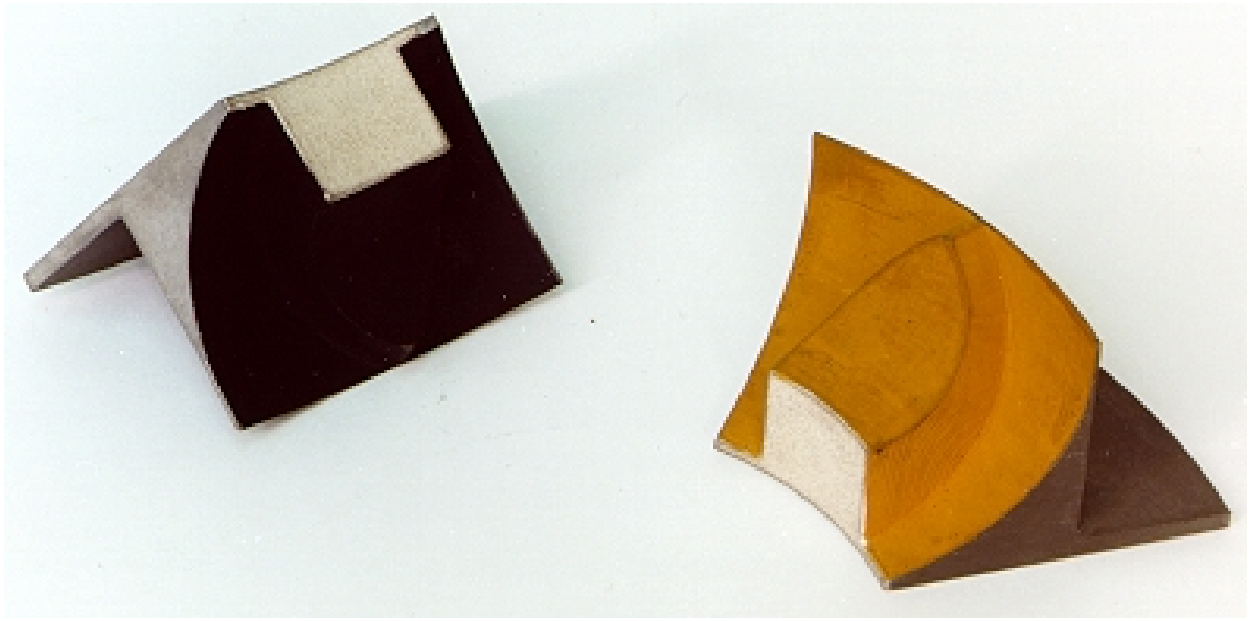

Figure 78. Quench Vanes with Thermal Paint Applied to Surface for Heat Transfer Evaluation

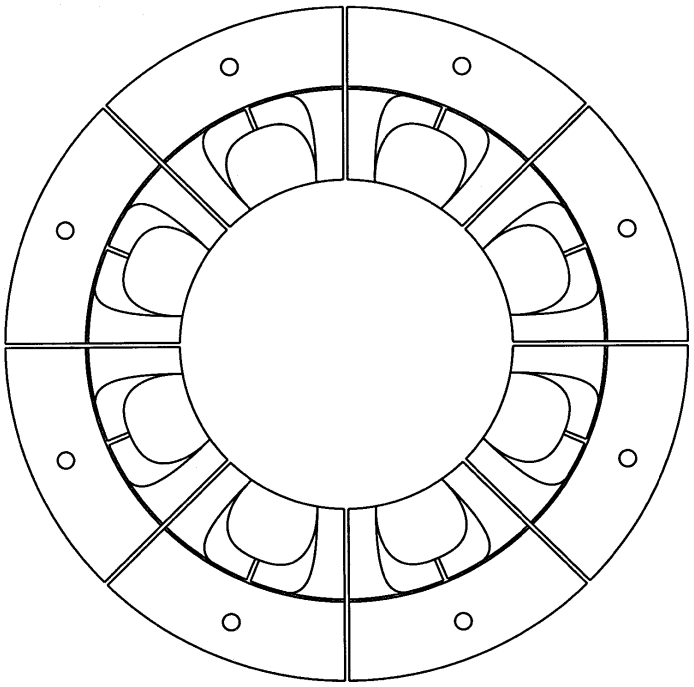

Figure 79. Eight-Quench-Vane Configuration

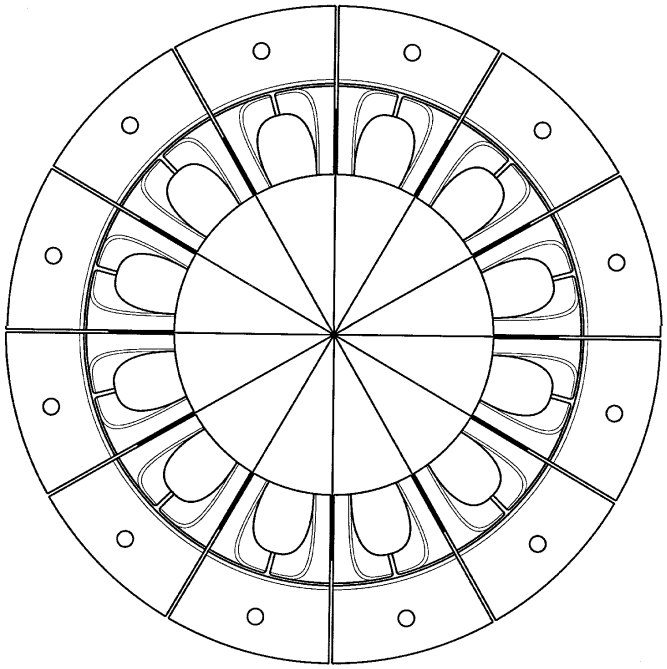

Figure 80. Twelve-Quench-Vane Configuration

combustor was defined by the location of the probe tips of the axially traversable emissions-probe system, making lean-zone residence time a primary focus in the combustion test program.

The results of combustion testing of this rig, presented in Section 4.6.3.1, will indicate a trend of nearly consistent NOx emissions — suggesting that NOx formation is a more global characteristic. CO residue trends indicate that geometries having more but smaller wall-jet orifices are more effective at consuming CO. Overall, it is concluded that a RQL combustor, using the more conventional wall-jet technology, demonstrated the capability of achieving an EINOx of 13.6 g/kg fuel at the supersonic flight condition (relative to the program goal of 5 g/kg fuel). This RQL combustor, with wall-jet technology, also demonstrated the capability of achieving the program goal of 99.9% efficiency at supersonic cruise conditions. However, this wall-jet RQL combustor was operated at an elevated combustor pressure drop, approximately 8.5% (relative to a design target combustor pressure drop of 5%), to achieve this NOx and CO emissions performance.

4.4.2.3 Reduced-Scale Quench, Convoluted Liner/Quench Plate Configuration

What is reduced scale quench? In the wall-jet configurations the characteristic diameter or dimension of the quench air jets was of the order of 0.7 inches, and these jets penetrated over a radial distance from wall to centerline of typically 1.5 inches. The testing of many wall-jet configurations indicated an insensitivity of NOx output — implying that the formation of NOx was rate sensitive. To counter this limitation, means were pursued to reduce the size or dimension associated with the wall jets while increasing the number of jets. Extensive computational and flow-visualization experiments were conducted to define means in which quench air jets could be discharged from numerous small orifices, with characteristic dimensions of 0.10 to 0.2 inches, into gas paths of nominal depths of 0.5 inches or less; that is, a three to sixfold reduction in scale. Per Item 5 of Subsection 4.3.2.3, the convoluted liner concept incorporates this technology, as described below.

The integrated module rig RSQ/convoluted-liner combustor configuration consisted of the variable-geometry fuel injector described in Subsection 4.4.2.2, a convoluted rich-zone liner, an insert “nose piece” to guide the convective cooling air around the outside of the convoluted liner, a quench plate, and a lean zone as shown in Figure 81 and the exploded view of the assembly in Figure 82 Details of each section are described in the following paragraphs.

The rich-quench module consisted of a rich-zone liner (Figure 83) constructed from PWA1422, a directionally solidified nickel alloy, following the same fabrication processes as the symmetric cast liners for the wall-jet type rig. The liner was 6.715 inches long and cylindrical with a 5-in ID for most of the rich-zone length. As the rich-zone flowfield progresses towards the exit or quench plane, the liner shape is convoluted to divide the rich-zone flow into four channels. The eight lobes formed become the majority of the flowpath for the rich zone, and the ½-in width and channel height become the characteristic dimensions for that flowpath. The two outermost channels extended 2.85 inches in vertical length; the inner two channels extended 5.15 inches in vertical length. These channels resulted in a flow area of 9.573 in^2 for the Gen I liner or 8.86 in^2 for the Gen II liner, approaching the quench air introduction plane.

The liner was held in position by eight tabs spaced uniformly about the circumference of the outer surface of the liner. These tabs were engaged by a tab-holder mechanism that protruded from the test section spool to grab the tabs on the liner. The surfaces of the rich-zone bulkhead and the convoluted liner exposed to the combusting gases had TBC applied with a plasma-spray process. The rich-zone

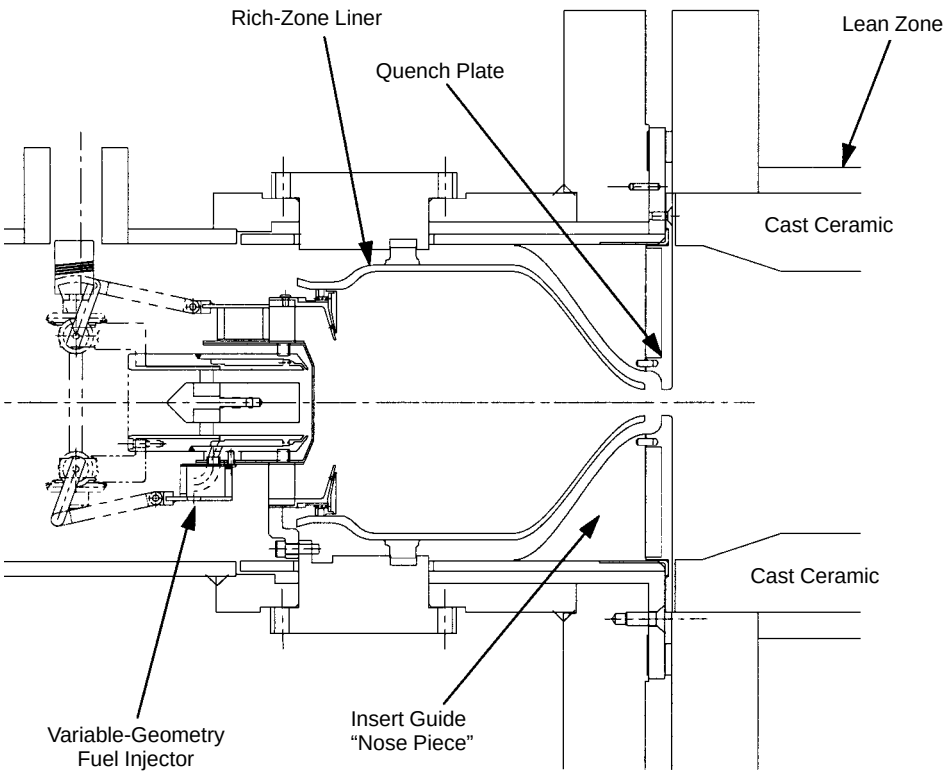

Figure 81. Integrated Module Rig Layout with RSQ Convoluted Liner/Quench Plate Combustor Configuration

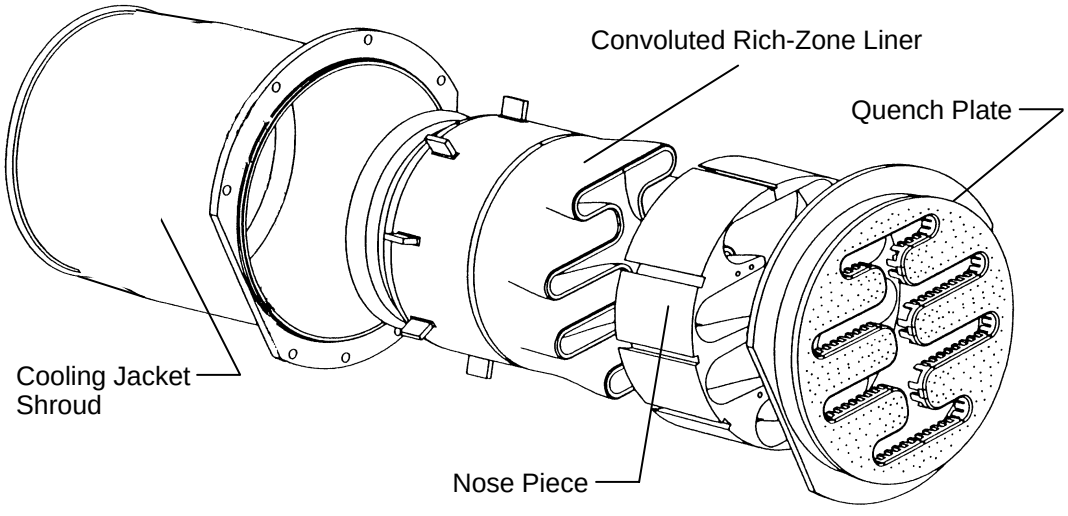

Figure 82. Rich-Quench Module Assembly (Bulkhead Subassembly Not Shown)

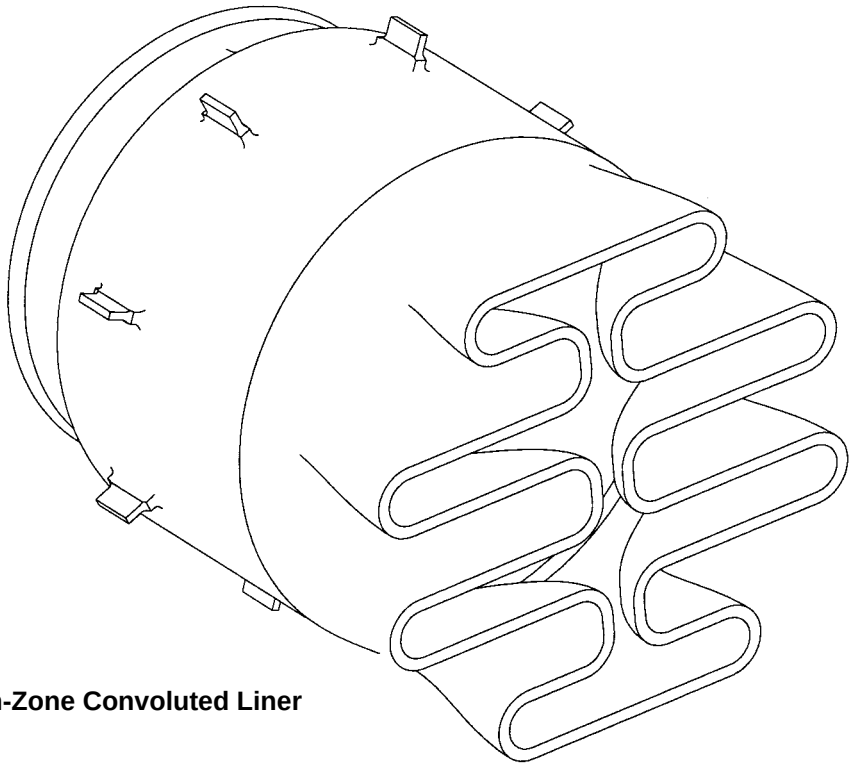

Figure 83. Rich-Zone Convoluted Liner

liner was convectively cooled with quench air. Towards the aft end of the rich-zone section, the convective cooling air was guided, to air maintain contact with the rich-zone liner, through the use of an insert “nose piece” that acts as a filler or an aerodynamic guide so that the convective air maintains velocity and, hence, cooling effectiveness as it is channeled between the convoluted regions. The liner/nose piece assemblies were suspended inside a Hastelloy X tubular shroud that forced the quench air across the upstream cylindrical surface of the rich liner for convective cooling of that region.

Beyond directing the cooling/quench air along the back-side surface of the convoluted liner, the insert “nose piece” also distributed the quench air to the downstream edge of the liner. There it was injected into the rich-zone gas from small orifices in a toothed quench plate to produce the RSQ mixing. This quench plate was the focus of development and optimization efforts.

One of several quench plate geometries designed, fabricated, and tested in the combustion rig is shown in Figure 84; details of the quench orifices are shown in Figure 85. The quench plate serves to collect the shroud or quench air, turn it in the radial direction perpendicular to the faces of the liner lobes, and discharge it as numerous RSQ air jets The quench orifices were sized to control the pressure drop and, in combination with the rich-zone swirler effective flow area, provide the appropriate quantity of quench air to maintain the desired split of approximately 23% air into the rich zone of the combustor. The quench orifices were slots 0.300 or 0.325 inches in axial length. The width of each slot varied throughout the channel lengths and was determined to provide optimum mixing for minimizing NOx emissions. The quench channels in the quench plate were designed to the same dimensions as the exhaust of the convoluted rich-zone liner, 0.5 inches in channel height. In the Configuration 15 quench plate shown in Figure 85, there are 100 quench-air jet orifices. These

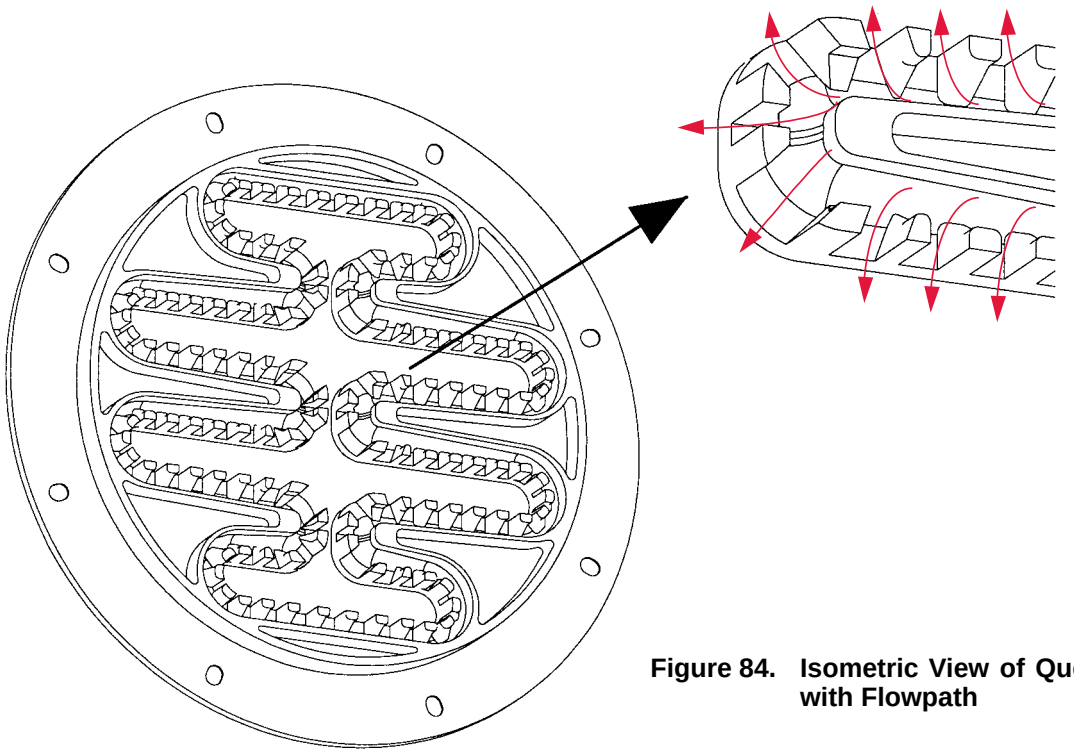

Figure 84. Isometric View of Quench Plate with Flowpath

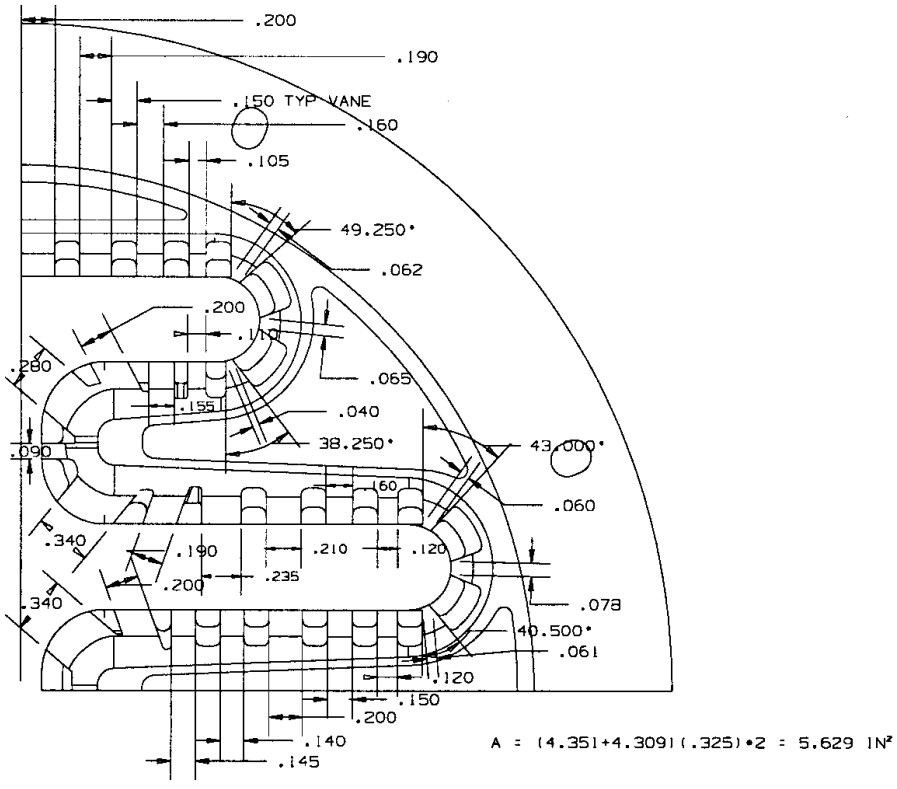

Figure 85. Reduced-Scale Quench Plate Configuration 15

quench plates were fabricated from PWA1422, using the quick-cast process. A small fraction of the quench air (4% of total combustor air) was bled through 274 small effusion holes, 0.030 inches in diameter, on the downstream face of the plate as cooling air for the aft face of the quench plate as shown in Figure 86. This aft face and the convoluted surface extending just downstream of the quench orifices had plasma-sprayed TBC for thermal protection.

The lean-zone section was cylindrical and fabricated by the same cast ceramic in a steel pipe approach used for this section of earlier rigs; section length was 9 inches. The gas-side diameter of the inlet region of the lean-zone section, as defined by the hot surface of the castable ceramic liner exposed to the combustion gases, was 6 inches so that none of the quench channels would be blocked. This flow area was quickly converged, over a 1-in length, to a 5-in diameter for the remaining 8 inches of the spool section.

The exit plane of the combustor was defined by the location of the axially and circumferentially traversable, five-probe-head, emissions rake system. In the furthest downstream position, the probe tips penetrated 3 inches into the lean-zone cylindrical section. Thus, the maximum effective axial length of the lean zone was 6 inches. However, this length could be shortened by traversing the probe system forward, hence making lean-zone residence time a primary focus in the combustion test.

Supporting technology activities provided a major effort toward definition and refinement of the convoluted liner RSQ approach. These drew from Item 5 of Subection 4.3.2.3. as well as the related technology of Items 3 and 4 of that section. Aerodynamic tests with probing and flow visualization were used in defining realistic convoluted liner shapes and “nose piece” contours These involved

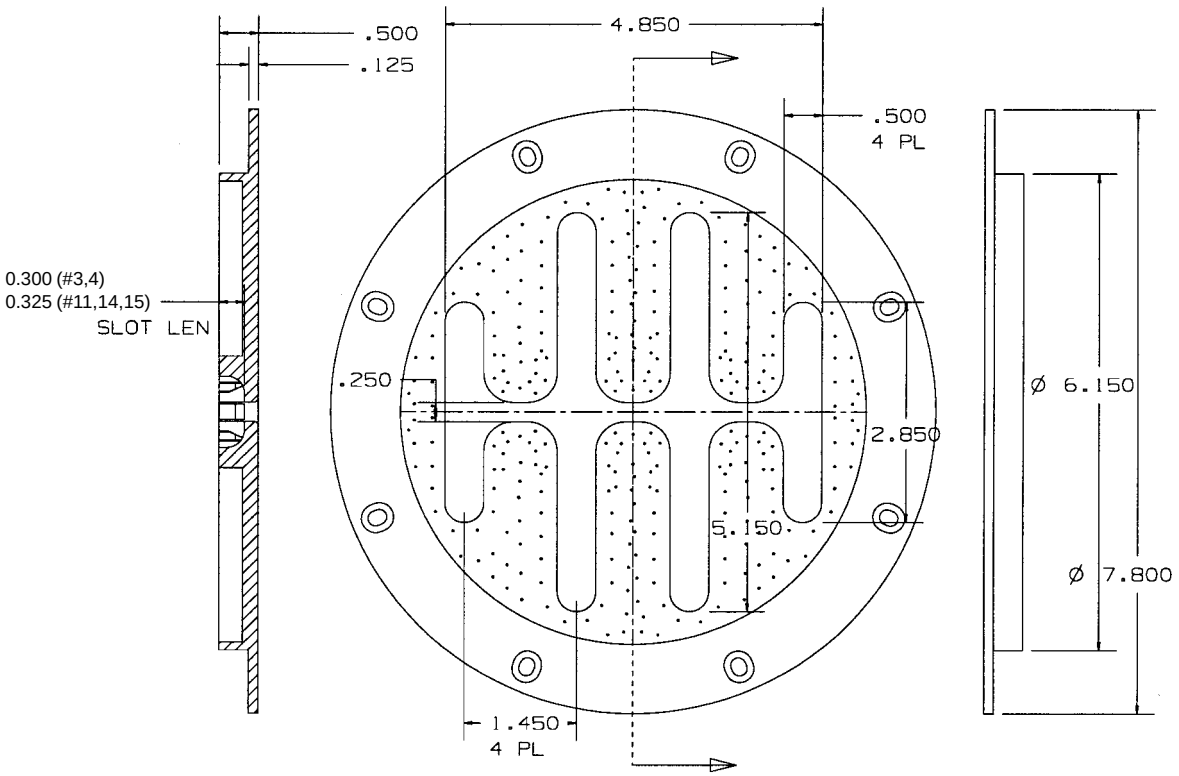

Figure 86. Reduced-Scale Quench Plate Design

oversize plexiglass models of the components. Similarly, a substantial number of different quench air orifice distributions were evaluated in cold-flow visualization tests on oversize plexiglass models of the quench plates.

The aerodynamic tests focused on (1) jet-to-jet measurements of airflow and (2) tracer-gas testing to assess uniformity of distribution among jets. The most successful configurations in these tests proceeded to fabrication of metal quench plates for ultimate testing in the combustor rig, and the results of these tests are reported in Subsection 4.6.3.2, where it will be shown that a RQL combustor, using RSQ technology implemented in a convoluted liner/quench plate configuration, demonstrated the capability of achieving an EINOx of 9.2 at the supersonic flight condition (relative to the program goal of 5 g/kg fuel). The RSQ configurations demonstrated exceptional efficiencies at supersonic cruise conditions. Uniformity was also found to play an important role in determining the emissions performance of the RSQ convoluted liner/quench plate combustor configuration.

4.4.2.4 RSQ Vane Development

The objective of the RSQ vane design was to achieve the most rapid mixing of the rich-zone flow with the quench air, so that minimal NOx is produced as the local conditions in the quench zone pass through an equivalence ratio of 1 and regions of hot mixed ga. Optimum mixing is generally taken to mean mixing to nearly a homogeneous flow within the minimum time (flow distance). A number of studies have been directed at determining flow geometries and parameters that lead to optimum mixing. Of particular relevance to this investigation are those studying normal jets in confined flows. While it could be argued that RSQ vanes (typically nonaerodynamically shaped) have flow expansion and the potential for some downstream recirculation, mixing should be completed within the confined-jet region of the quench zone in order to achieve low NOx emissions; therefore, the confined-jet flow studies have relevance for supporting this design.

To assess the impact of the many design variables associated with quench air introduction, many RSQ designs were committed to fabrication prior to the initiation of the single-module rig testing so that rapid changes in hardware could be accomplished, in most cases overnight, to facilitate efficient use of the combustion test facility. Consequently, feedback of test results to evolution of the design was not extensive, but a broader range of parameters was assessed. Nevertheless, several considerations can be described that were important in the RSQ vane design, such as jet-penetration analysis and mixing optimization.

Mixing studies of jets in crossflow found that the most significant flow variables are the momentum flux ratio, J, and the ratio of the orifice spacing to the channel height, S/H. Ultimately, these variables determine jet penetration, which has been identified as an important variable for mixing performance. If the jets do not penetrate, then quench air is confined to the boundary layer next to the RSQ vane. If the jets overpenetrate, a stratified region of quench air is formed on the centerline where the opposed jets meet. Therefore, for a given geometry an optimum J is expected. Optimum mixing is generally assumed to mean leading to a uniform distribution of conserved scalar quantities in a minimum downstream distance. It is presumed that achieving this degree of mixing should also result in the lowest NOx emissions because most NOx is formed in the quench mixing zone of a RQL combustor.

Studies of the penetration of a circular jet normal to an unconfined flow generally correlate the coordinates of the jet as a power law function in the normalized axial direction and have been extended here for noncircular jet shapes:

$$\frac{y_0}{d_h} = K\sqrt{J}(x/d_h)^{0.33}$$

where: y_0 = jet penetration in the unconfined flow,
d_h = jet orifice hydraulic diameter,
J = jet-to-crossflow momentum flux ratio in the unconfined flow, and
x = distance downstream of injection location.

The constant K depends on the point within the jet that is being followed: centerline or the inner or outer boundaries. A recommend value of $K = 0.56$ is used to track the penetration of the centerline of the jet.

A jet injected into a confined flow, as found in the quench zone, locally accelerates the crossflow, which in turn reduces the penetration. Ultimately the jet mixes with the crossflow, and a general flow acceleration results from the jet mass addition. Near the plane of injection, the jets are coherent and represent a blockage to the crossflow. Downstream the jets spread and mix, so the blockage effects change as the flow develops.

A model was developed in the early phases of the RQL development to estimate blockage effects of penetrating jets in a confined flow. In this model, a correction is applied to the jet-crossflow momentum flux ratio to compensate for blockage, and the penetration is defined as before:

$$\frac{y_0}{d_h} = K\sqrt{J_b}(x/d_h)^{0.33}$$

where: $$J_b = J\left(\frac{A_Q - N \cdot w \cdot y}{A_Q}\right)^2,$$

A_Q is the crossflow area with no jet blockage,
N is the number of jets, and
w is the transverse-width projection of the jet.

A key parameter in mixing, therefore, is the jet-to-crossflow momentum flux ratio, J, defined as:

$$J = \frac{\rho_J u_j^2}{\rho_R u_R^2}$$

where the parameters with R subscript are defined as the flow in the quench zone immediately upstream of the quench-air jets, designated by parameters with the subscript J. It can be shown that:

$$J = \frac{\rho_R}{\rho_J}\left(\frac{\dot{m}_J}{\dot{m}_R}\right)^2\left(\frac{A_Q}{C_d A_J}\right)^2$$

where: ϱ_R = density of the rich gas,
ϱ_J = density of the jet gas,
$\dot{m}_J$ = mass flow of jet,
$\dot{m}_R$ = mass flow of crossflow (rich flow),
A_Q = crossflow area,
A_J = total area of jets, and
C_d = discharge coefficient of jets.

The ratio of the mass flow rates in the last equation may be replaced with $(1/s - 1)^2$, where s is the flow split between the rich zone and the quench zone. Once the design-point parameters for the combustor are chosen (in this particular case, supersonic cruise) — that is, the flow split and the desired fuel/air ratio overall — then the first factor, the density ratio, and the second factor, the mass flow ratio, are fixed; the only remaining free variables are the areas of the crossflow and jets.

While the effort to define, evolve, and optimize the quench vane involved numerous technical support efforts consistent with Item 6 of Section 4.3.2.3, an RQL combustor rig was essential to the final screening of candidate vane configurations. The single-module rig combustor configuration consisted of a fuel-injection device, a rich zone, a quench zone, and a lean zone as shown in Figure 87. An exploded 3D view of the combustor is shown in Figure 88. Rich-zone air flow was bled off of the inlet piping, upstream of an orifice plate, for delivery to the inlet of the quench zone spool piece. The flowpath details of the quench zone are shown in Figure 89. While this flowpath is not the most ideal configuration for fundamental testing, expedient use of existing hardware for rapid quench vane development testing was necessary. The rich-zone section consisted of a cylindrical length followed by a transition to the rectangular quench zone entrance. The cylindrical portion was 4.5-in long and had a 5-in ID. The transition had an axial length of 1.5 inches over which the combustor transitioned smoothly from a 5-in ID cylindrical cross section to a 4.06-in wide by 5.10-in high rectangular cross section to match the quench-zone entrance. A sampling-probe system at the exit of the combustor provided diagnostic emissions performance of the combustor.

A number of RSQ vane geometries were designed, fabricated, and tested to assess key quench-jet orifice parameters and effects on NOx emissions. The greatest number of configurations consisted of four vanes equally spaced in the quench zone: two in the center and two vanes buried half way into the wall. Configurations incorporating five vanes were also tested, in two quench zone channel heights. All RSQ vanes had the same dimension in the spanwise (quench zone channel length) direction: 4.06 in. Figure 90 shows the dimensional variations of quench channel/vane configurations evaluated.

Mixing studies are helpful for selection of relevant parameters and the initial design of the vanes. In this program the mixing study results were taken as a starting point about which perturbations were made to seek an optimum design. A number of vanes were made in the four-vane configuration in an effort to find the optimum mixing geometry as determined by emission measurements in the single-module rig combustor. The orifices for these vanes were rectangular, characterized by a width crosswise to the flow and a length. The web is the width between adjacent orifices. Figures 91 through 96 show representative quench vane geometries selected from those evaluated in the definition studies and the combustion rig tests.

Since the technology to make reacting-mixing measurements at pressures and temperatures is not available, water-tunnel flow visualization tests, chemical-kinetic-reactor-network calculations, CFD calculations, and a review of nonreacting mixing results for jets in crossflow were identified (in addition to the combustion testing) as program elements of this effort. All elements needed to be done concurrently, since there was limited time to gain this understanding.

Simultaneously, reacting 3D CFD calculations were made, using the commercially available code FLUENT, for these geometries. The objective of these calculations was to obtain detailed, spatially resolved, reacting, mixing information for the new designs. When coupled with the combustion tests, these calculations would improve understanding of the mixing and NOx formation process.

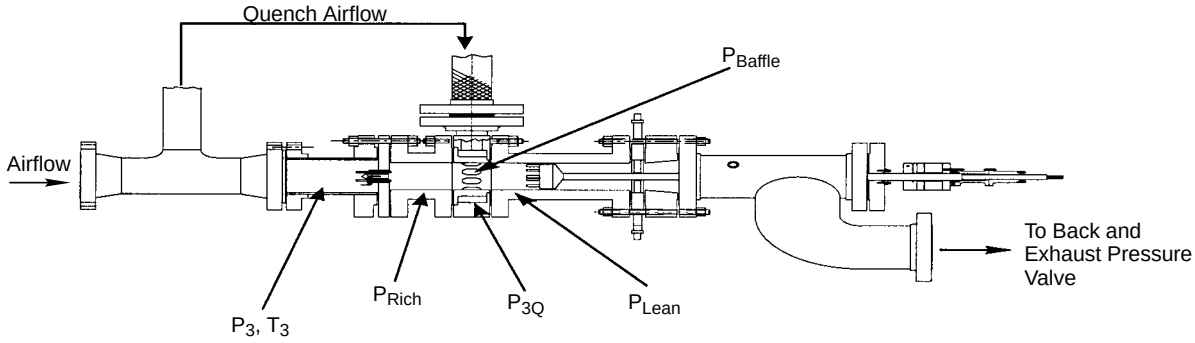

Figure 87. RQL Single-Module Rig Used for Investigating Quench Vane Parametrics

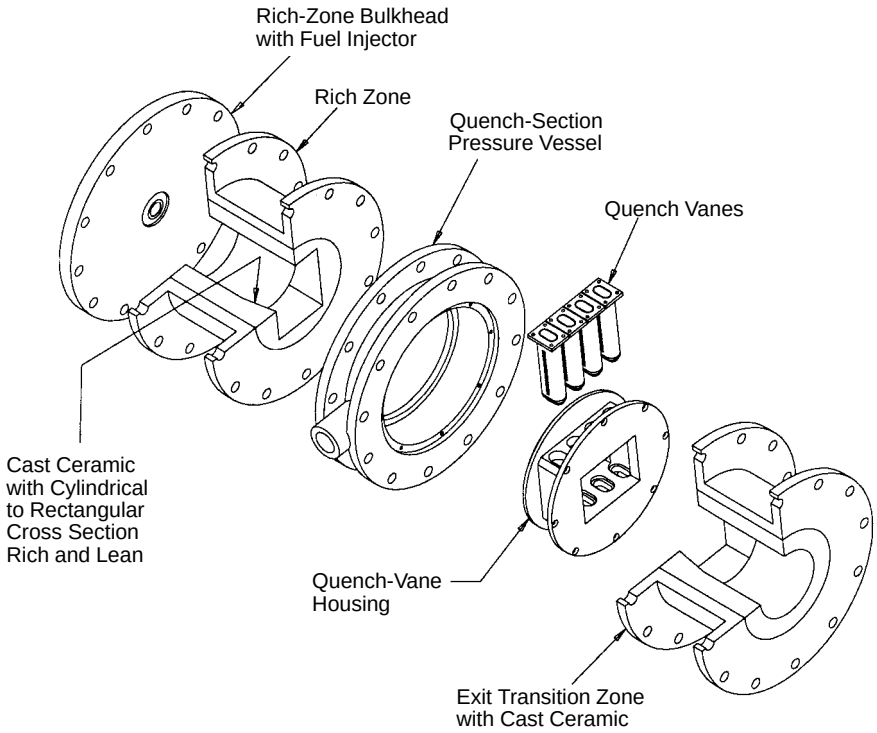

Figure 88. Exploded View of Single-Module Rig

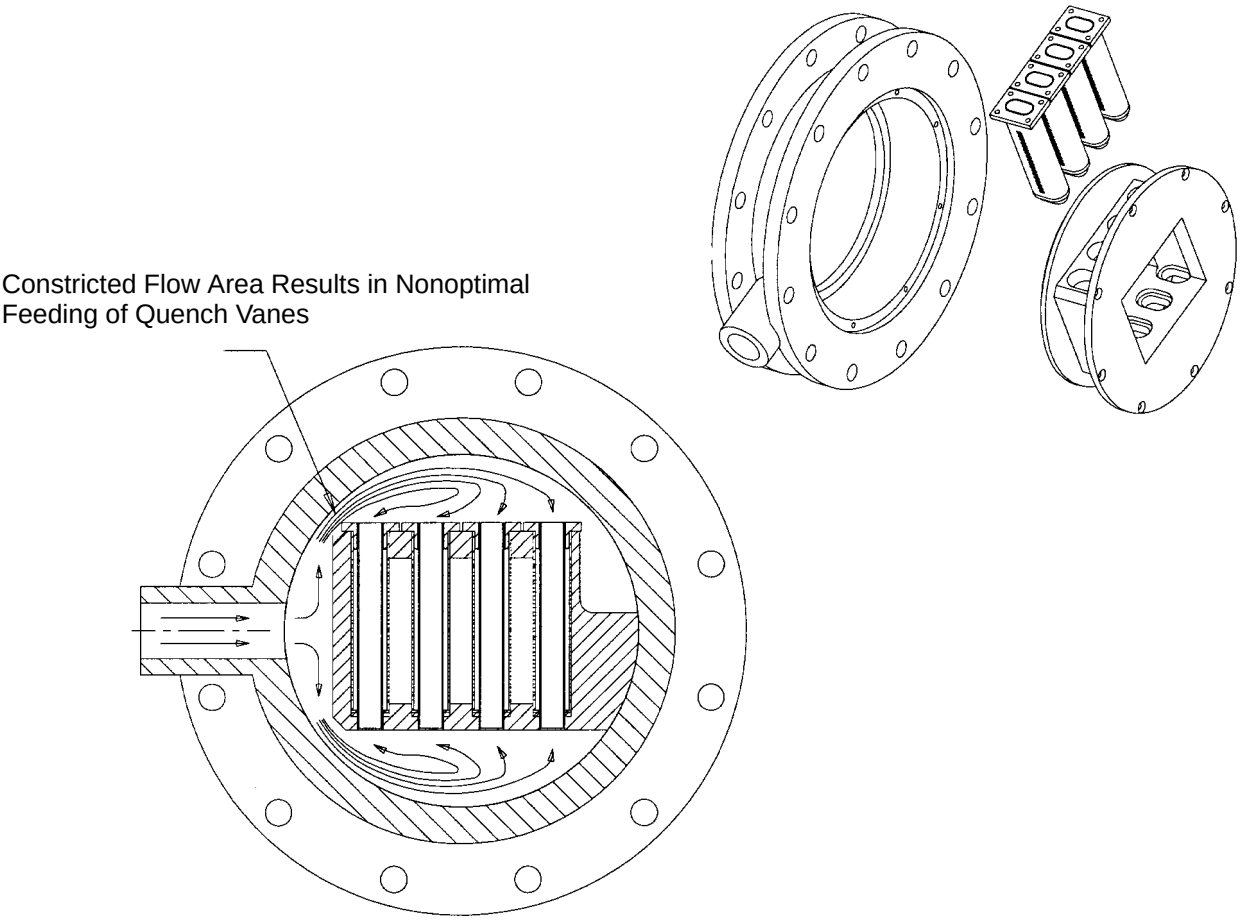

Figure 89. Flowpath Feeding Quench Vanes in Single-Module Rig Configuration

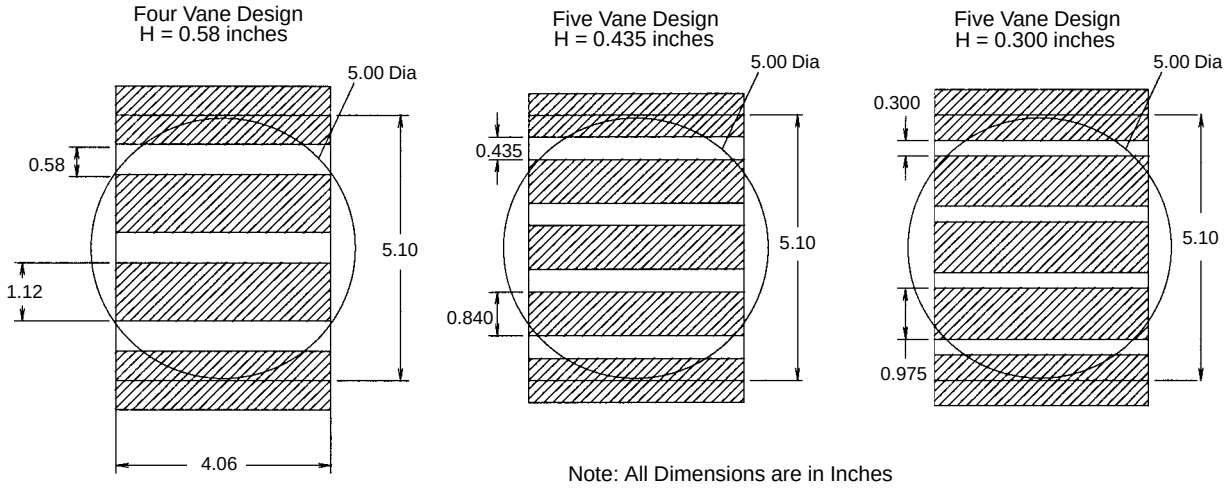

Figure 90. Relationship of Quench Channel Geometries to Quench and Lean-Zone Flow Areas – Single-Module Rig

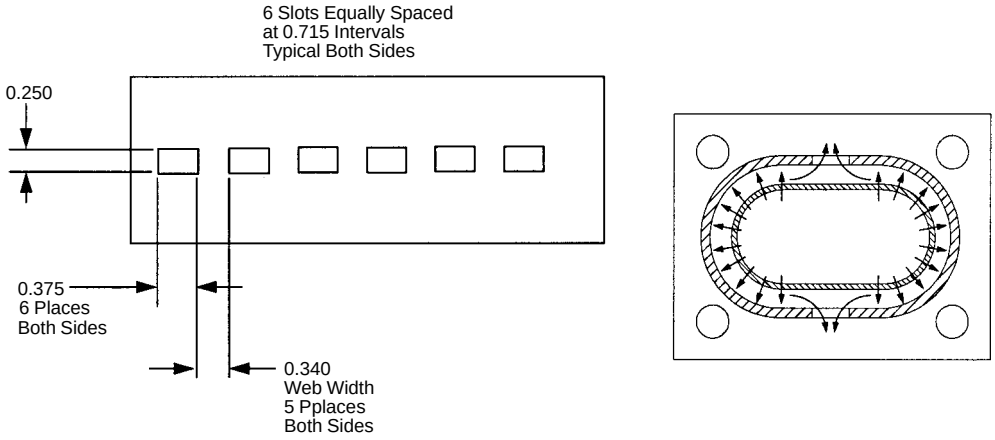

Figure 91. Vane Geometry No. 1

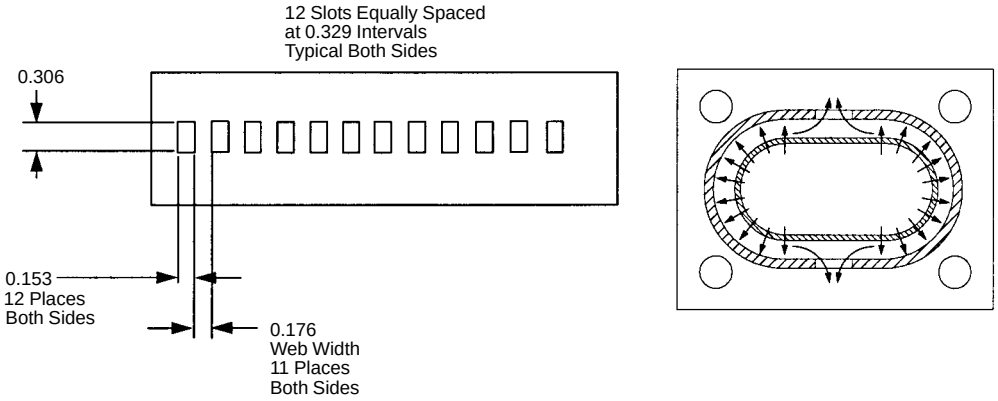

Figure 92. Vane Geometry No. 2

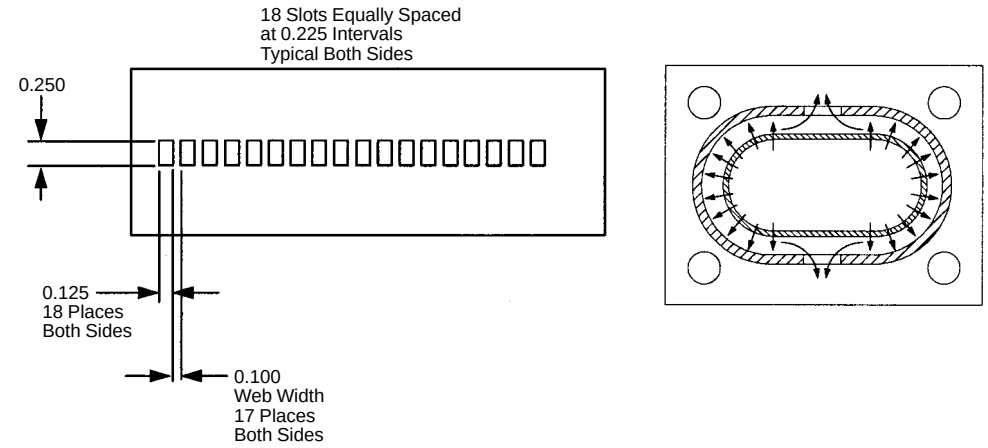

Figure 93. Vane Geometry No. 3

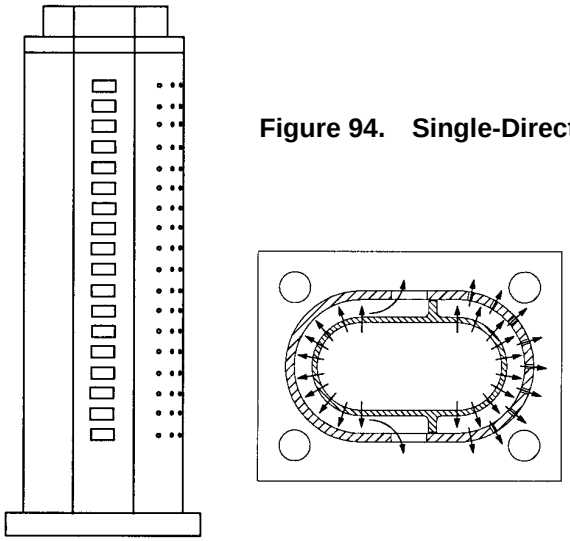

Figure 94. Single-Direction-Feed Quench Vane Geometry

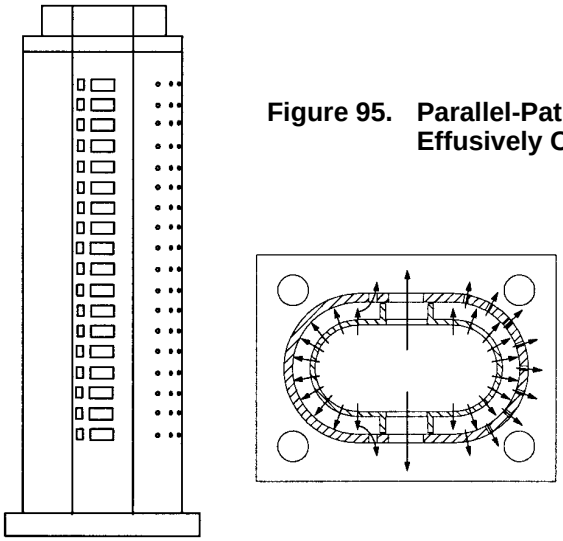

Figure 95. Parallel-Path Vane Geometry with Effusively Cooled Trailing Edge

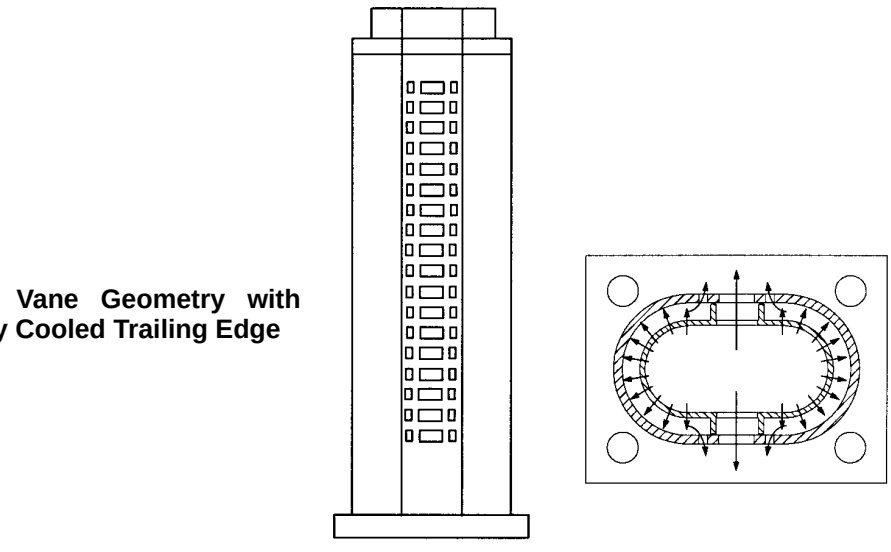

Figure 96. Parallel-Path Vane Geometry with Noneffusively Cooled Trailing Edge

CFD calculations were performed to determine the influence of geometric and flow boundary condition changes on the details of the flow field, thereby providing a basis for correlating measured NOx levels. Initial attempt to predict NOx levels directly ERE unsuccessful; the predicted levels were found to be extremely sensitive to such changes while the measured levels showed much smaller variations. An alternative means of correlating measured NOx levels with a relatively easy-to-compute flowfield parameter was developed.

CFD calculations were made for the RQL geometric family known as RSQ. Three-dimensional temperature and species distributions were assessed. EINOx levels were also calculated; however, for reasons presented in the following discussion, the predicted NOx values were not used in the final assessment of performance. For RSQ geometries, a single flow condition was used as the boundary condition. However, the effects of changes in strut number, slot length, slot width, number of slots, and slot orientation were modeled. Sensitivity of results to numerical issues was also examined.

CFD solutions were provided using the commercial code FLUENT, as it was the only code available to the program that was capable of providing two-phase, reacting, flow simulations (the fuel was modeled as a liquid injected into the airflow stream). Finally, the code includes a thermal NOx model that may also be run with a probability density function (PDF) model to incorporate the effects of fluctuating temperature and major species on EINOx. The fuel spray droplet size distribution was determined experimentally and fitted with a Rosin–Rammler distribution with a width parameter of 1.7 and characteristic size of 60 μm; these parameters correspond to 28-μm Sauter mean diameter.

The CFD calculations with the RSQ geometries took advantage of the upstream axisymmetric geometry to simplify the problem. An axisymmetric, two-phase flow case was first run upstream of the RSQ mixing section with flow conditions at the exit of the swirlers assigned. The axisymmetric profiles at the end of this section were then used as boundary conditions for the 3D flow through the RSQ mixing section. Note that the fuel was completely vaporized well upstream of the RSQ mixing section. The PDF model was used for the axisymmetric calculation; however, through the RSQ mixing section a two-step, mixed-is-burned model was used with the chemical reactions:

$$CO + \tfrac{1}{2}O_2 \rightarrow CO_2$$

$$H_2 + \tfrac{1}{2}O_2 \rightarrow H_2O$$

Thus, six chemical species were used for the RSQ mixing section: CO, CO_2, H_2, H_2O, O_2, and N_2.

It was necessary to limit the maximum number of grid points to about 200,000. As a consequence, it was not possible to resolve all of the important regions of the flowfield adequately. It was found that predicted NOx levels were very sensitive to grid resolution, and no satisfactory remedy was found. This limitation motivated the search for an alternative way of assessing performance. The active-volume parameter method described later shows much less sensitivity to grid resolution. For RSQ mixing geometries, a large number of slot length, width, and number combinations were modeled, together with different strut-to-strut spacing variations. For these calculations, three basic computational domains were modeled: full section, quarter section, and strut to strut.

Initial cases were run with the entire RSQ mixing section and lean zone simulated. A typical example is presented in Figure 97. Analyzing the entire geometry was motivated by the fact that the axisymmetric-flow calculations showed a large amount of residual swirl at the end of the rich zone. While it was anticipated that the struts removed essentially all of the swirl, there was no way to determine *a priori* what effect the residual swirl had on performance.

There was also concern that the maximum grid number did not provide adequate resolution of the flow in the spanwise direction, especially as the number of slots increased. Therefore, several additional cases were run using a quarter section, an example of which is shown in Figure 98. This approach obviously changed the nature of the swirling flow as it approached the struts, viewed in terms of the full domain.

Finally, to increase grid resolution even further, strut-to-strut domains were used; an example is presented in Figure 99. Here all effects of swirl were ignored, and the inlet boundary conditions were replaced by uniform, mass-averaged conditions from the axisymmetric case.

For an RSQ geometry calculation in which the grid was progressively refined in the strut-to-strut direction, the NOx levels increased proportionally. However, the flowfields showed little sensitivity to grid density, although it is known that NOx levels are very sensitive to local conditions. This sensitivity of results led to the examination of alternative means of assessing performance or correlating measured NOx levels with geometric changes — see the discussion of the active volume parameter, below.

The computed NOx levels for all of these calculations are shown in Figure 100. Note the extreme sensitivity to grid density. As the grid cell size was reduced, nonconvergent behavior of the predicted NOx is apparent. Recall that computed NOx levels are sensitive to changes in slot length, width, number, etc. as well as to changes in grid density or the geometry of the computational domain. The measured NOx values were much less sensitive to slot geometry in the active-geometry approach. An active-volume parameter (AVP) is defined:

$$AVP = \sum \Delta V_1 \qquad (F/A)_{\min} \le (F/A)_1 \le (F/A)_{\max}$$

Each control volume in a CFD solution can be viewed as a miniature chemical reactor that has the potential for producing NOx. For fixed inlet conditions, NOx production rates depend on the local fuel/air ratio or, equivalently, local temperature. In the simplest form (the manner in which it is used here), the active-volume parameter considers only those control volumes with a fuel/air ratio within a specified range. Based on knowledge of the NOx generation processes, attention was restricted to fuel/air ratios between 0.055 and 0.075, the latter being somewhat higher than the stoichiometric value. Specifically, the AVP is the total volume of gas within the specified fuel/air ratio range. In Figure 101, the range of variation for the AVP is shown for the baseline configuration using different modeling assumptions. In contrast to the variation of computed NOx levels for these cases (Figure 100), the AVP shows much less variation.

Figure 102 shows the volume represented by AVP for two different RSQ mixing geometries. One geometry has 6 quench-air injection orifices per side of the strut, and the other geometry has 18 quench-air injection orifices. The first geometry (6 orifices per side) has more volume at fuel/air ratios between 0.055 and 0.075 than the other (18 orifices per side); consequently, mixing was better and the NOx emissions would be expected to be lower.

The measured NOx versus AVP is plotted in Figure 103 for a number of RSQ geometries. It is observed that measured NOx decreases with decreasing AVP. It is also observed that the measured NOx trend with respect to AVP is independent of the calculation domain.

This task met the objectives to (1) design and fabricate various quench vane configurations that implement reduced-scale quench technology, (2) parametrically vary key geometric and flow vari-

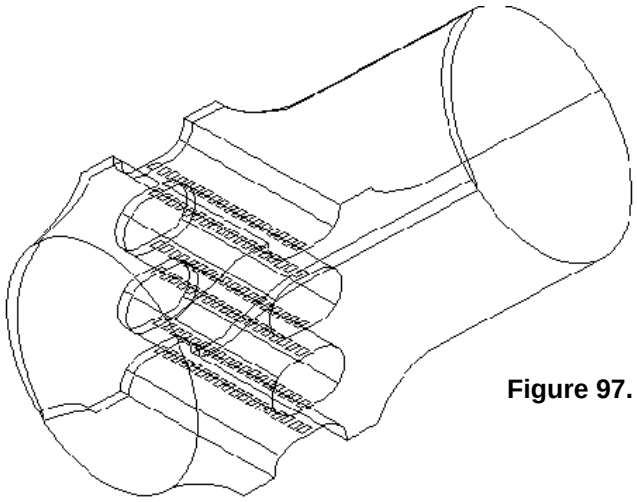

Figure 97. Full Domain for CFD Analyses of Quench Vane Geometries

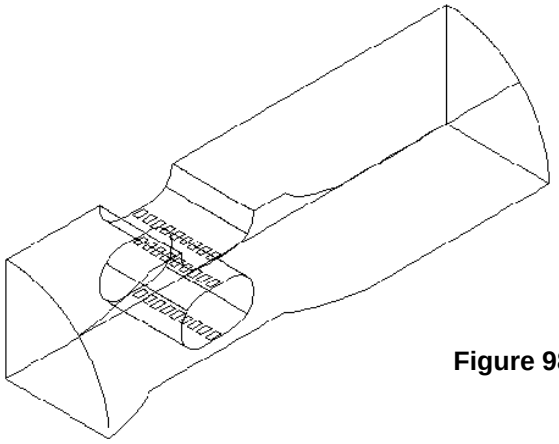

Figure 98. Quarter-Symmetry Domain for CFD Analyses of Quench Vane Geometries

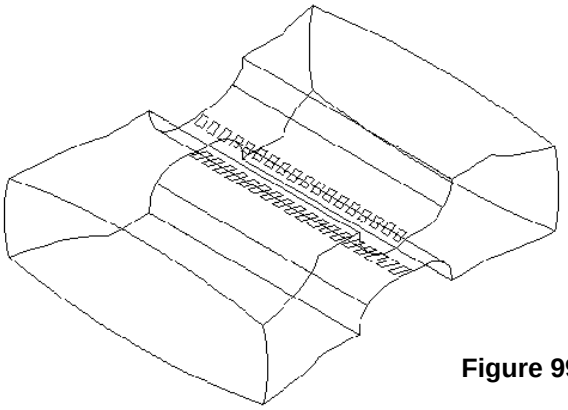

Figure 99. Strut-to-Strut Domain for CFD Analyses of Quench Vane Geometries

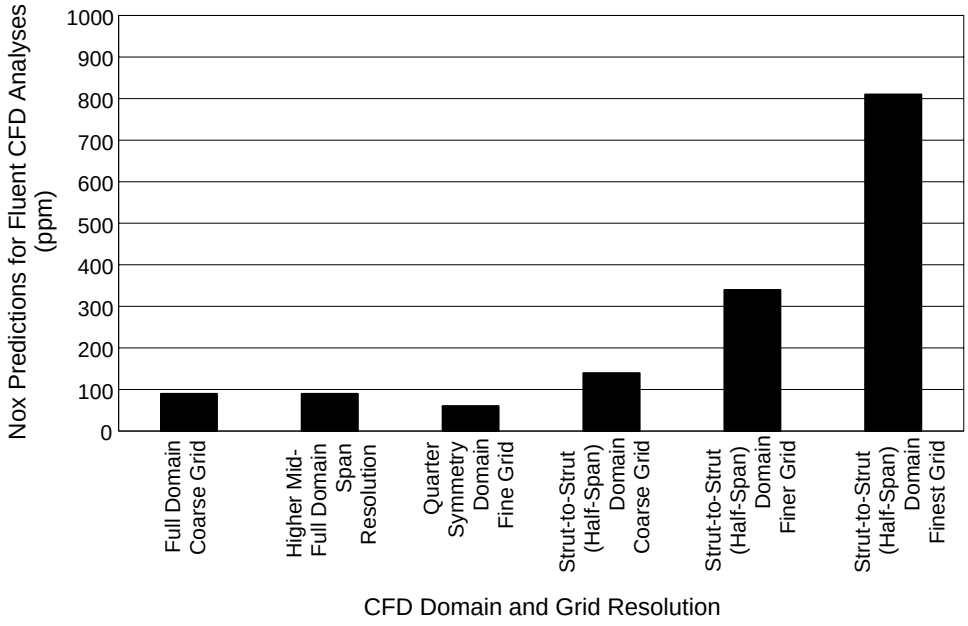

Figure 100. NOx Calculation Sensitivity to Grid Density

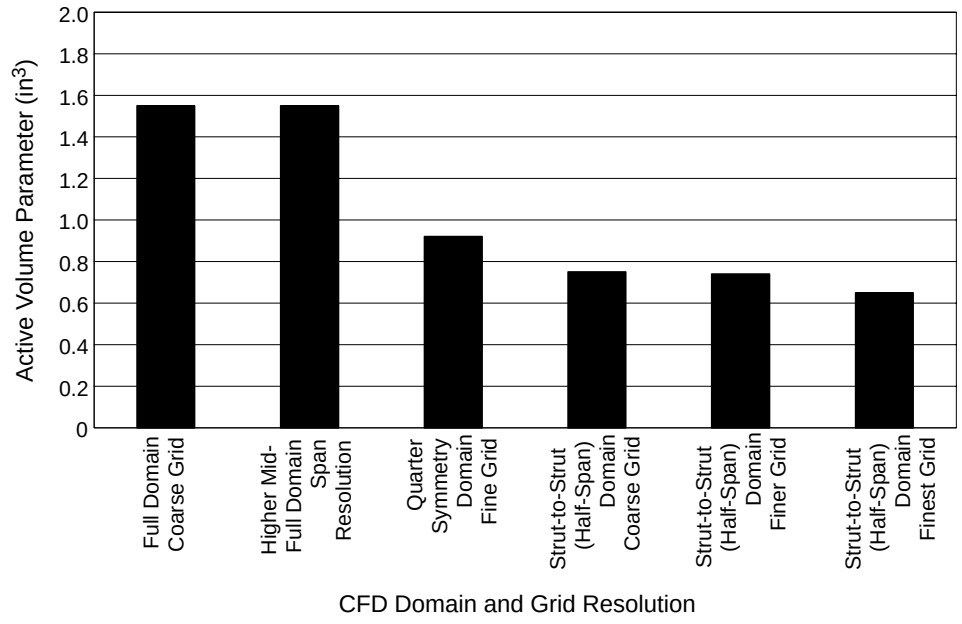

Figure 101. Active-Volume Parameter Insensitivity to Grid Density

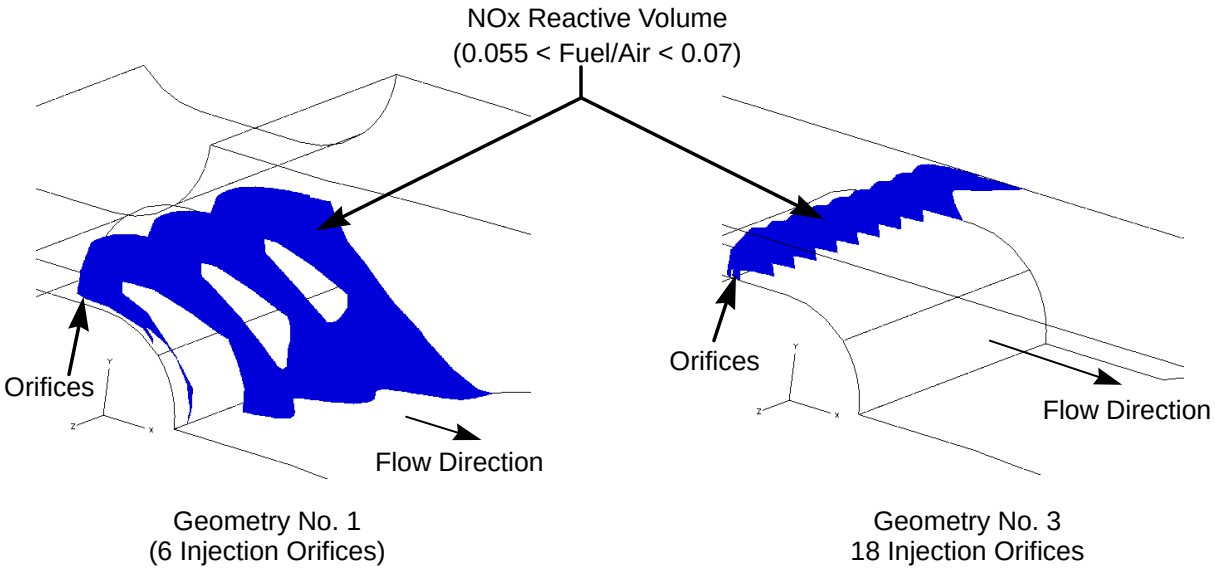

Figure 102. Active Volume Controlled by Quench Orifice Size and Spacing

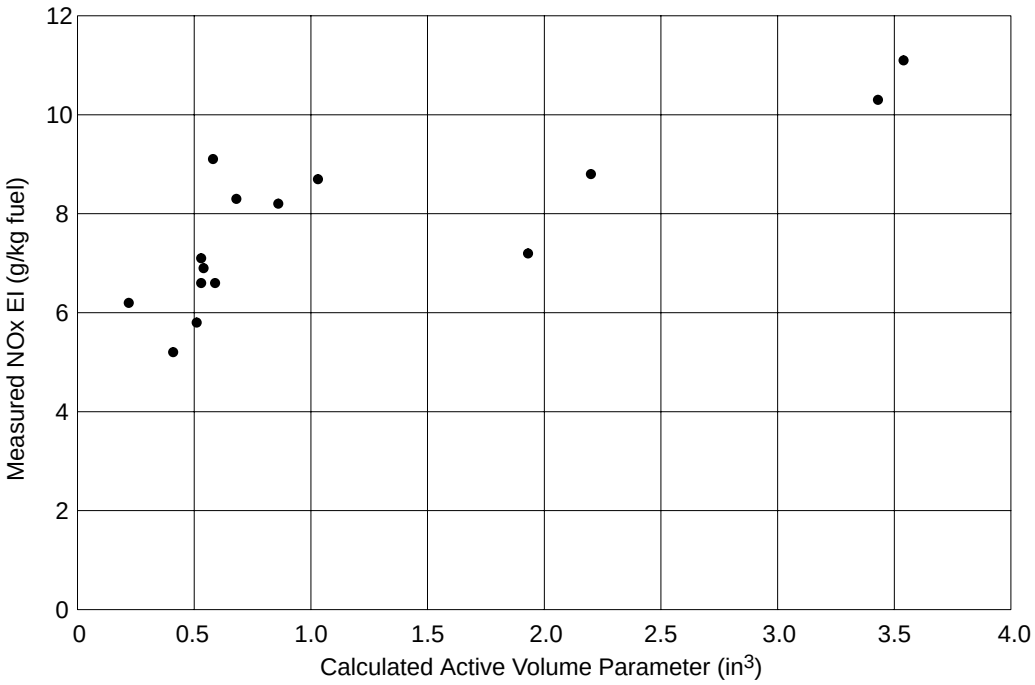

Figure 103. Calculated Active Volume Parameter Correlated Against Measured NOx Emissions

ables, and (3) evaluate performance in a single-module rig combustor in support of development of a product-like implementation of RSQ technology. It included CFD analyses and water-flow visualization of quench vane configurations to aid engineering comprehension of the flowfield impacts associated with various RSQ parameters.

4.4.2.5 RSQ Vanes for Product Module Rig

The RQL product module rig was designed to approximate one inner-bank module of the RQL 3770.54 product engine. The product engine design consisted of two banks radially with the inner bank flowing approximately 40% of the total combustor airflow. The inner bank was composed of 24 trapezoidal modules. The product module rig was therefore designed to fit within a 15° sector with an inner radius of 13.150 inches and an outer radius of 19.595 inches.

The Build 1/1A RQL configuration incorporates the RSQ concept by using quench vanes to break up the quench zone into three channels 0.500 inches wide by 4.797 inches long, as can be seen in Figure 104. These 0.500-in channels are created by two quench vanes and two sidewall turning strips. Figure 105 is a 3D solid-model exploded view of the combustor.

The rich-zone liner is a wire electrical-discharge machined (EDM), directionally solidified, nickel alloy (PWA 1422) in a basic trapezoidal sector. Two slots to accept the quench vanes are machined

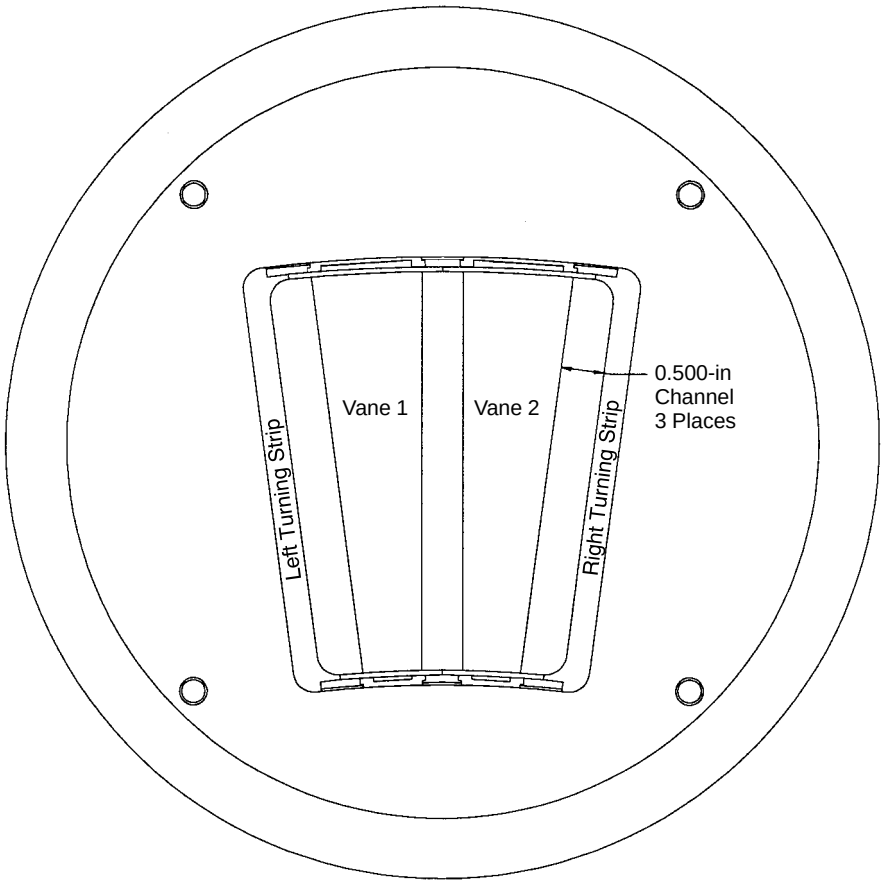

Figure 104. Aft-Looking-Forward View of Product Module Rig Build 1

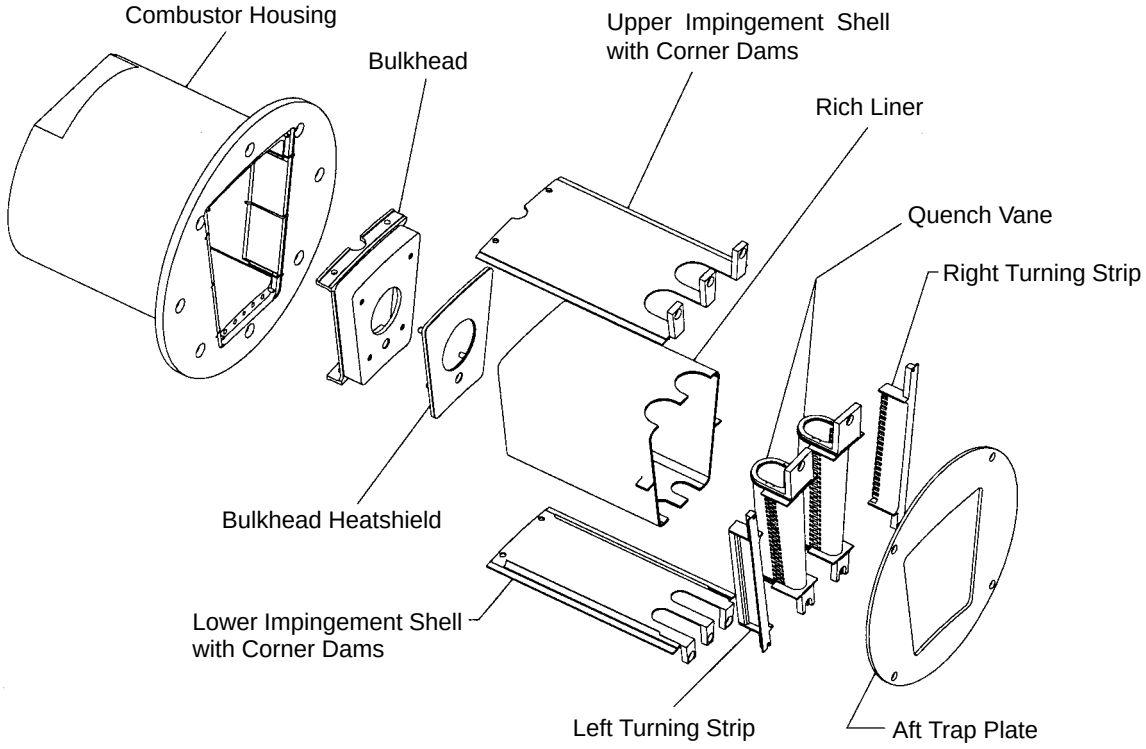

Figure 105. Exploded View of Product Module Rig Build 1

on the aft edge. The inner surface of the liner has TBC over the region exposed to flame. The upper and lower surfaces of the liner are impingement cooled. The spent impingement air is exhausted rearwards and convectively cools the area of the liner between the quench vanes before it is dumped into the exit transition zone. The side walls of the liner are convectively cooled. Figure 106 is an exploded view of the quench vane assembly. The platforms and supports are brazed to the outer vane shell with a gold/nickel braze. The vane impingement baffle is then electron beam (EB) welded to this assembly. The vane outer shell is wire-EDM cut from a single-crystal, nickel casting (PWA 1484). The shell profile is a tapered racetrack shape. The axial length is a constant 1.896 inches while the width of the vane tapers at a 7.5° angle from 1.284 inches at the OD to 0.644 inches at the ID. After the platforms and supports are brazed to it, the outer surface is TBC'ed and the quench orifices are laser cut. There are 22 main quench orifices on each side of the vane, each 0.123 inches wide by 0.250 inches axially. Upstream and downstream of the main orifices are exhaust slots for the spent impingement cooling air. These slots are 0.123 inches wide by 0.054 inches axially and are located in line with the main orifices thick structure wire cut from Inconel 625 bar stock. A staggered array of 299 impingement holes, 0.025 inches in diameter each, is laser cut into the leading and trailing edges of the shell (598 total holes per vane). The impingement baffle was welded at one end and allowed to move thermally at the other end.

The vane baffle is machined with rails that mate with a longitudinal pad on the inside of the vane outer shells to separate the impingement air from the main quench air as seen in Figure 107. A cruciform splitter is placed inside the impingement baffle. This cross-shaped piece separates the ID and OD sides of the vane after slot 17 out of 22 (with slot 1 toward the OD side of the vane). The

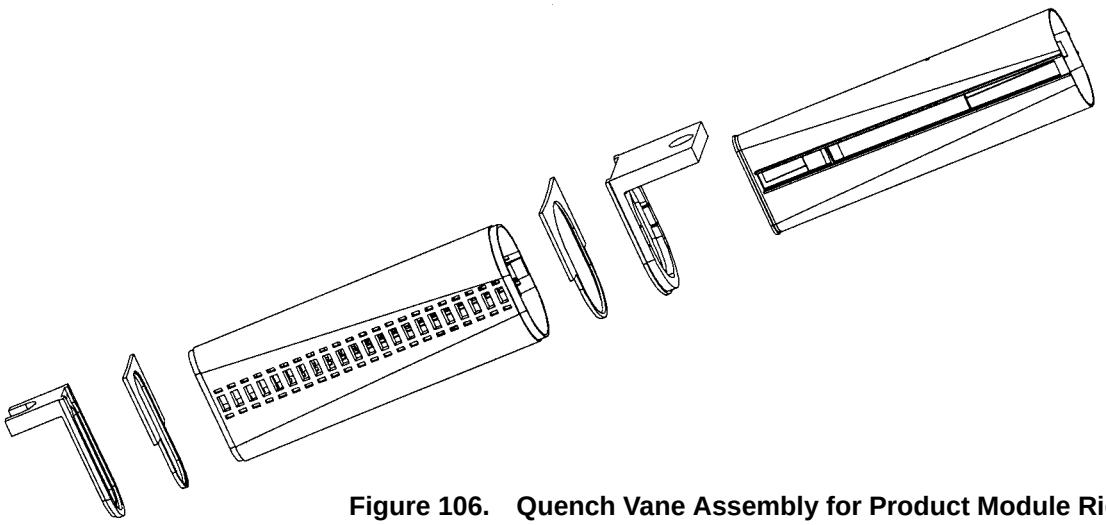

Figure 106. Quench Vane Assembly for Product Module Rig Build 1

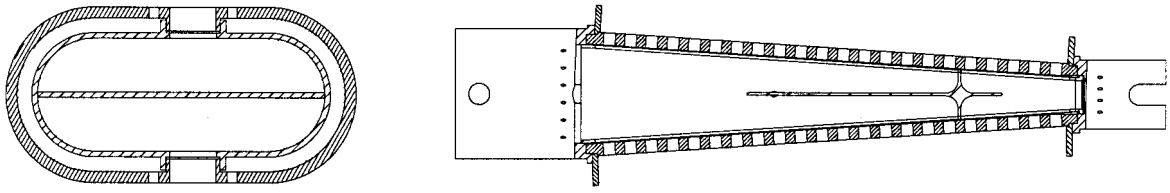

Figure 107. Product Module Rig Build 1 Quench Vane Flowpath Views

cruciform also separates the left and right sides of the baffle. Definition and optimization of these internal quench vane features were established by fluid dynamic experiments on an oversize model of the vane. A modification to the Build 1 design was intended to perturb the split within the combustor in an attempt to bring the split in line with design intent. The modification of Build 1 into Build 1A involved altering the airflow split between rich and quench flows by partial blockage of part of the fuel-injector swirlers.

Build 2 of the product module rig focused on the following major changes: smaller quench-zone channel height for improved emissions, simulation of an annular RQL configuration with improved feed of sidewall quench orifices, and improved rich-zone liner cooling control as shown on Figure 108. The design of Build 2 has four quench-zone channels, 0.3 inches wide relative to the Build 1 design that had three channels, 0.5 inches wide. The Build 2 design also incorporates “half vanes” instead of turning strips at the sidewalls to simulate an annular rich-zone design in this single fuel injector rig. The rich-zone liner was cooled on all four sides with impingement air. The spent impingement air was extracted from the rig, separately valved, and measured through a venturi.

Figure 109 is an exploded view of the quench vane assembly. The upper and lower supports are EB welded to the outer shell. The vane impingement baffle is then EB welded to this assembly. The vane outer shell is wire-EDM cut from Inconel 625 bar stock. The shell profile is a tapered racetrack shape. The axial length is a constant 1.896 inches while the width of the vane tapers from 0.854 inches at the OD to 0.540 inches at the ID. There are 37 main quench orifices on each side of the vane, each 0.073 inches wide by 0.150 inches axially. Upstream and downstream of the main orifices

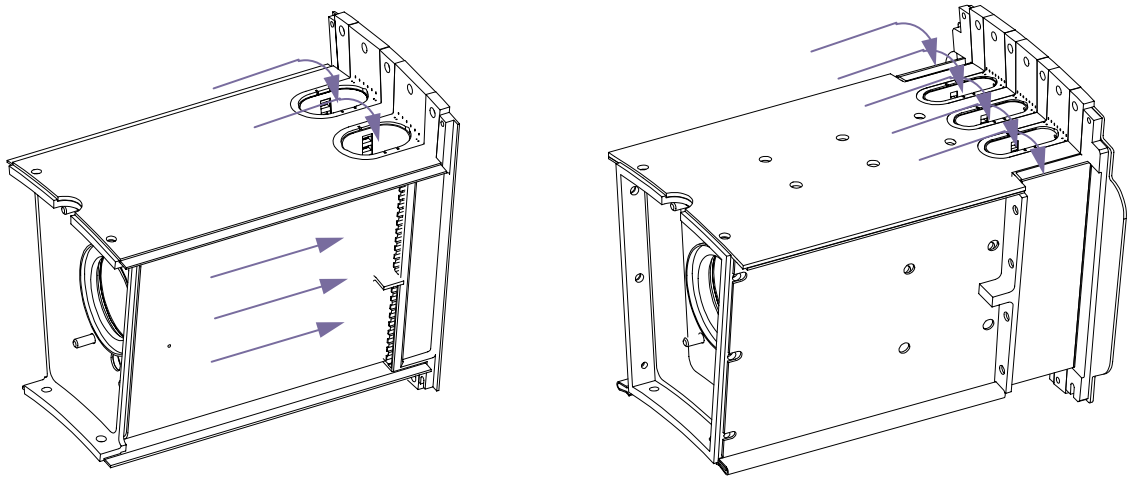

Build 1

- Air convectively cools liner side walls and is then turned into the combustor at the quench plane
- Liner ID and OD surfaces are impingement cooled

Build 2

- Sidewall vanes are fed from ID and OD shrouds (identical to center vanes)
- All liner surfaces are impingement cooled

Figure 108. Comparison of Airflow Paths for Product Module Rig Builds 1 and 2

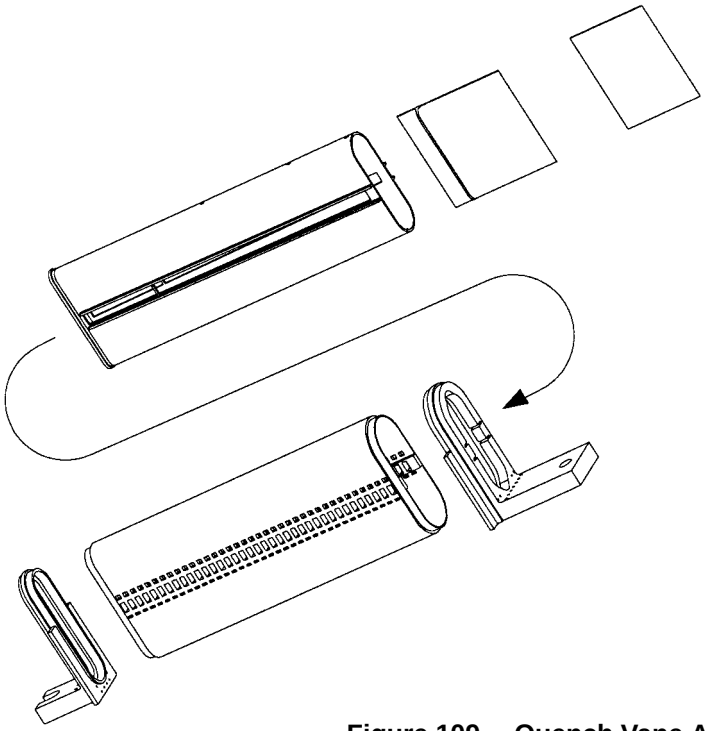

Figure 109. Quench Vane Assembly for Product Module Rig Build 2

are exhaust slots for the spent impingement cooling air. The upstream slots are 0.073 inches wide by 0.064 inches axially and the downstream slots are 0.073 inches wide by 0.032 inches axially. Both sets of exhaust slots are located in line with the main orifices.

Build 2A was a modification of Build 2. The 0.51 in^2 fuel injector swirler was removed and a 0.68 in^2 swirler was installed, changing the airflow split between the rich and quench zones. The objectives of this task was to design and fabricate a single-nozzle representation an inner bank of the full-scale, dual-annular, RSQ-vane RQL combustor design for testing in the product module rig. Subsection 4.6.3.3 will discuss the results of combustion tests at nominal supersonic cruise condition and at other critical conditions in the flight envelope, including airport vicinity and subsonic cruise conditions, to evaluate the performance, emissions, and operability of these concepts.

4.5 Subscale Sector Testing

Multiple subscale sector tests were run over the course of the program. Lean direct injection, lean premixed/prevaporized, and RQL systems were all tested. Subscale tests were used to better understand the interactions between various combustor components without incurring the significantly higher costs of full-scale tests. This allowed more design variations to be tested to maximize the chances of meeting the stringent emissions requirements of the contract. Additionally, early program plans called for the combustor to be tested in a demonstrator engine of current design. This determined the subscale size.

4.5.1 Lean Direct Injection System

It was desired that a LDI system be tested in a rectangular, stepped-dome sector environment to better understand the impact of interactions on emissions and stability. Five variations were tested at NASA–Glenn from June 1996, to May 1997. Each had a common three-dome setup, as shown in Figure 110. In all five tests, the inner and outer domes each contained 12 of the LDI injectors. In the first two tests, the center dome contained three cyclone pilots; in the other three cases, the pilots were replaced by another bank of 12 LDI injectors. Two tests were also run in which the center dome was flush with the inner and outer domes; in all other cases it was recessed.

As discussed in the subcomponent development section, the LDI injectors used simplex pressure atomizers to inject fuel at the throat of a venturi into swirling air flow. This forces rapid atomization and mixing with minimal chance for autoignition or flashback, both concerns in LPP systems.

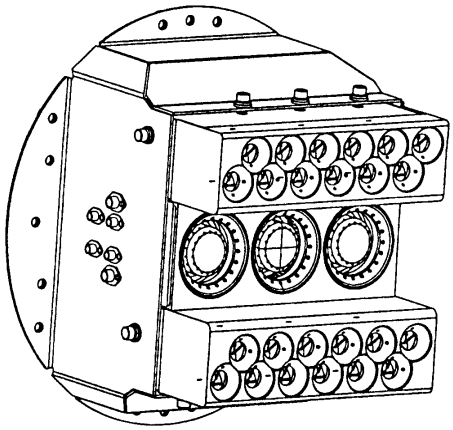

Figure 110. LDI Stepped-Dome: Multiventuri, Rectangular, Three-Cup Sector

A thick, ceramic casting was used to protect the sidewalls and liners. No combustor air was used for cooling these surfaces. Instead, for heat removal, water was forced through tubes brazed to the outside of the surfaces. Six gas-sampling probes were located at the exit plane (8.5×4.1-in rectangle), approximately 6.5 inches downstream of the inner and outer dome faces. A traversing probe was added for the fifth sector test. A range of inlet temperatures, pressures, pressure drops, and fuel/air ratios were tested to better understand their impact on emissions. This information was required for use in the LPP/LDI downselect process. The LDI concept was eventually eliminated in favor of continued LPP development.

4.5.1.1 LDI Sector Build 1

The first LDI sector tested was a rectangular, stepped-dome design with three cyclone pilots in the center dome. This was the primary LDI design expected to be used in an engine if emissions and operability targets could be met. The center dome was recessed 1.85 inches from the inner and outer domes to isolate the pilots. The cyclone pilots contained swirlers with 2.05-in inner diameters and sixty 70° vanes (1.0 swirl number). Each pilot contained six fuel-injection ports, on the centerbody, of the same design as those used in the LPP stepped-dome sectors and the highly mixed MRA sector (all described later). The inner and outer domes each contained 12 of the 45°, axially swirled LDI mixers described in the subcomponent development section. The swirlers were 0.85 inches in diameter with a 0.15-in diameter simplex fuel nozzle centerbody. The venturi throat was 0.54 inches in diameter, expanding to an exit diameter of 1.0 inches; 80° cone angle (40° half angle) converging and diverging sections formed the throat. Measured effective flow areas were 1.86, 1.61, and 1.82 in^2 for the outer, center, and inner domes, respectively (5.3 in^2 total). This corresponded to 35.1, 30.4, and 34.5% flow splits. Note that a cyclone flow split closer to 20% was to be used in an engine.

The test data are summarized in Table 14 and Figures 111 through 116. It was demonstrated that at 1070°F, 137 psia, 4.5% ΔP, and uniform 3490°R flame temperature, sector combustion efficiencies were 99.97% and NOx levels were approximately 8 EI. By comparison, the 45° axially swirled injector designs had demonstrated NOx values of 5.1 EI at 1050°F, 150 psia, 3.5% ΔP/P, and 3420°R flame temperature in subcomponent development (a 3×3 array with no pilots). Thus, as anticipated, the pilots were increasing system NOx at higher power conditions. Following the test, the NOx emissions data covering a wide range of operating conditions were correlated, as shown in Figure 112. The resulting empirical correlation was:

$$\text{NOx (EI)} = (8.1\times10^{-8})\,(T_3{}^{1.81})(e^{0.00176\text{Tfl}})(\Delta P/P)^{-0.602} - 2.18$$

where T_3 and Tfl are in °R and ΔP/P is in percent. The data collapsed onto this line quite well.

Based on the above information, it was projected that nominal supersonic cruise NOx would be 8 to 10 EI with all three domes operating at the same flame temperature. Because the pilot was primarily responsible for the elevated NOx at these conditions, the system was tested with a reduced pilot fuel/air ratio (while the fuel/air ratios of the inner and outer domes were increased to maintain the correct overall fuel/air ratio). The results are shown in Figure 113 (note that the nominal case was a 0.304 fuel fraction in the sector test). This test was quite successful. For example, at 1060°F, 150 psia, 5% ΔP/P, and 3460°R flame temperature, NOx declined from nearly 5.5 EI at a pilot fuel fraction of 0.304 to 4.1 EI at 0.23. This result was encouraging, since it showed that NOx could in fact be reduced by operating the pilot fuel/air ratio below that of the LDI injectors. This also simulated a pilot flow split closer to the 20% anticipated for use in an engine, although nonlinearities in NOx production make this an imperfect demonstration.

Table 14. LDI Stepped-Dome Sector Emissions Summary (Build 1)

T3	P3	Pressure Drop	Sample Dome	Flame Temperature	Sample NOx EI	Sample EI CO	Sample EI HC	Combustion Efficiency	Dome Equivalence Ratio Relative To Average		
(F)	(psia)	(%)	Equiv Ratio	(R)	(g/kg fuel)	(g/kg fuel)	(g/kg fuel)	(%)	Outer	Pilot	Inner
Fully Fired, 1062°F, 151 psia, 5.2% Pressure Drop											
1058	153.1	4.96%	0.453	3296	4.4	0.58	0.11	99.98%	100.4%	99.3%	100.4%
1064	150.5	5.12%	0.508	3481	7.1	0.70	0.09	99.97%	100.0%	100.3%	99.4%
1062	148.9	5.37%	0.540	3585	8.9	0.78	0.09	99.97%	100.0%	98.8%	101.5%
1063	151.7	5.47%	0.574	3695	11.1	0.87	0.09	99.97%	100.0%	100.8%	98.9%
Fully Fired, 1070°F, 134 psia, 4.5% Pressure Drop											
1075	136.6	4.54%	0.509	3492	7.8	0.74	0.17	99.97%	98.1%	101.6%	100.9%
1065	131.2	4.42%	0.553	3627	11.3	0.94	0.10	99.97%	100.3%	99.4%	100.3%
Fully Fired, 1070°F, 134 psia, 4.0% Pressure Drop											
1064	132.3	3.93%	0.448	3278	4.7	0.61	0.11	99.97%	101.1%	98.2%	100.0%
1063	132.1	4.01%	0.478	3380	8.3	0.68	0.10	99.97%	99.7%	101.3%	98.7%
1061	132.5	4.15%	0.522	3525	8.5	0.79	0.09	99.97%	100.9%	98.8%	100.6%
1052	134.2	4.02%	0.603	3777	12.6	1.15	0.11	99.96%	99.5%	99.2%	100.8%
1076	134.1	3.58%	0.602	3789	15.7	1.12	0.09	99.96%	99.7%	100.0%	100.0%
Reduced Pilot, 1069°F, 131 psia, 4.6% Pressure Drop											
1066	131.6	4.71%	0.512	3494	6.6	0.78	0.11	99.97%	106.6%	87.1%	104.7%
1072	131.2	4.57%	0.518	3518	7.5	0.82	0.11	99.97%	109.9%	81.1%	106.8%
Fully Fired, 886°F, 213 psia, 4.0% Pressure Drop											
884	213.8	4.12%	0.514	3379	4.2	0.55	0.05	99.98%	99.4%	101.3%	99.4%
887	212.0	3.63%	0.533	3446	5.4	0.64	0.06	99.98%	100.0%	100.3%	100.0%
884	213.4	4.03%	0.603	3676	8.5	0.65	0.05	99.98%	99.7%	99.7%	100.8%
887	211.3	4.07%	0.632	3770	10.9	0.68	0.05	99.98%	100.5%	99.7%	99.7%
Fully Fired, 592°F, 82 psia, 4.6% Pressure Drop											
596	83.3	4.08%	0.522	3187	0.8	28.35	16.47	97.69%	100.3%	100.3%	99.1%
592	82.2	4.26%	0.553	3290	1.0	11.68	4.46	99.28%	99.2%	100.8%	100.6%
595	82.9	4.95%	0.559	3312	1.1	6.05	0.51	99.81%	100.3%	100.8%	98.6%
588	80.2	5.24%	0.591	3415	1.5	1.35	0.07	99.96%	99.7%	100.8%	99.7%
587	83.0	4.82%	0.628	3534	2.4	1.40	0.02	99.96%	99.5%	99.0%	101.7%
595	82.9	4.46%	0.687	3720	4.2	2.19	0.02	99.95%	99.5%	100.7%	99.8%
Pilot Only, 865°F, 166 psia, 6.2% Pressure Drop											
863	166.7	5.88%	0.156	2049	7.1	8.81	1.55	99.64%	0.0%	330.9%	0.0%
866	165.1	6.48%	0.126	1918	3.5	37.82	13.40	97.77%	0.0%	330.8%	0.0%
Pilot Only, 574°F, 70 psia, 5.2% Pressure Drop											
574	68.9	5.22%	0.182	1900	1.0	40.19	20.82	96.97%	0.0%	332.1%	0.0%

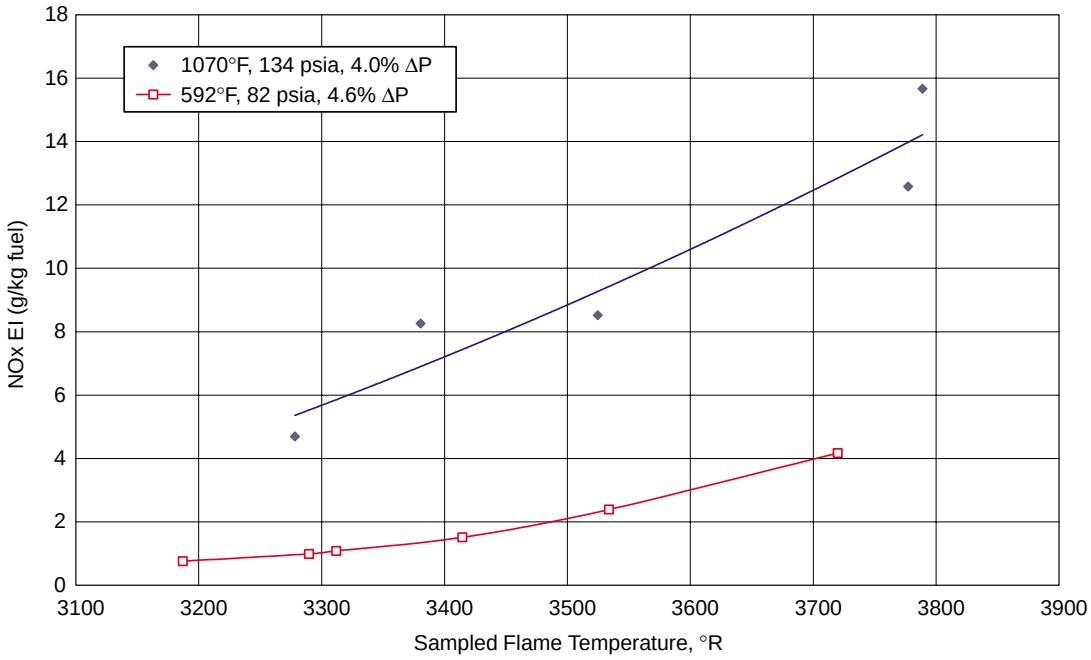

Figure 111. LDI Stepped-Dome Multiventuri Three-Cup Sector NOx Emissions (Build 1, Middle Dome Recessed with Cyclone Pilots)

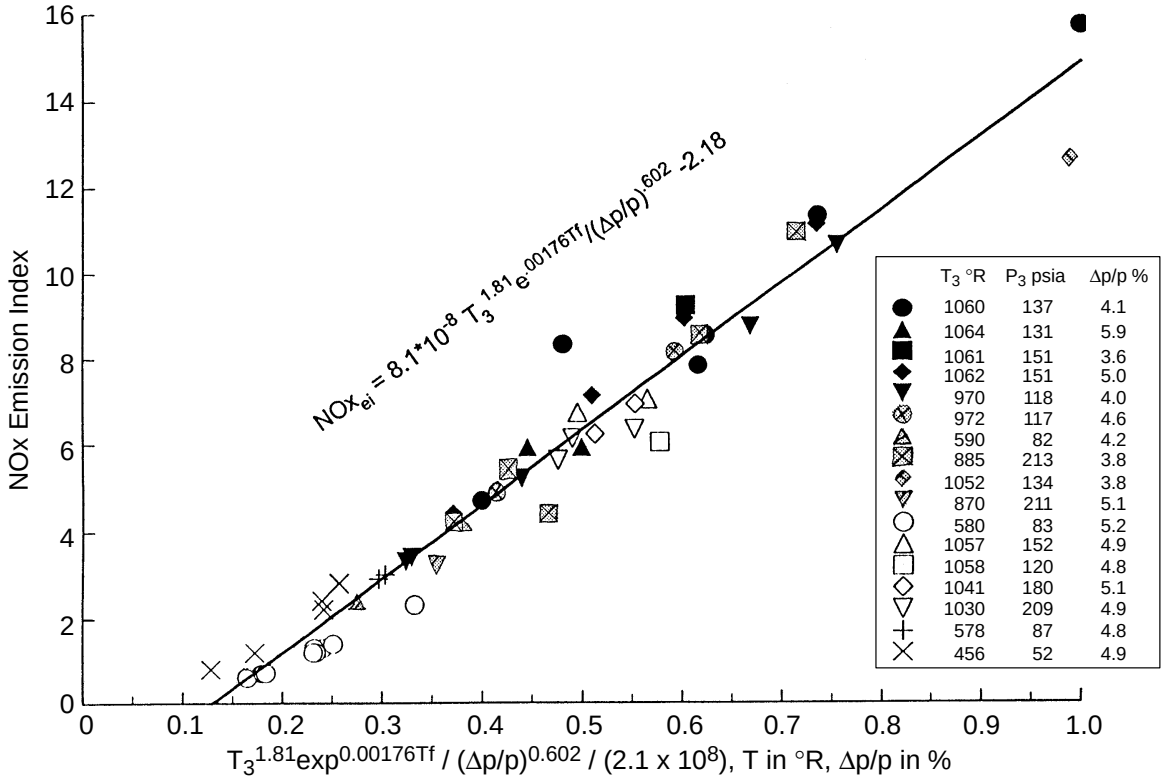

Figure 112. Multiventuri/Cyclone Sector, Stepped Dome NOx Correlation

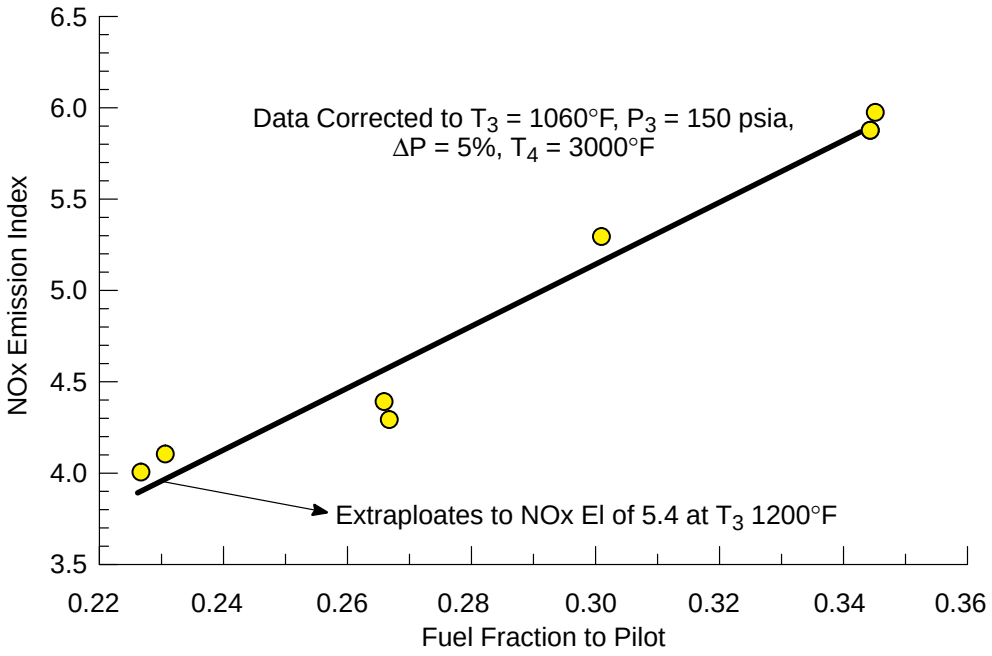

Figure 113. Multiventuri/Cyclone Sector, Stepped Effect of Pilot Fuel Flow

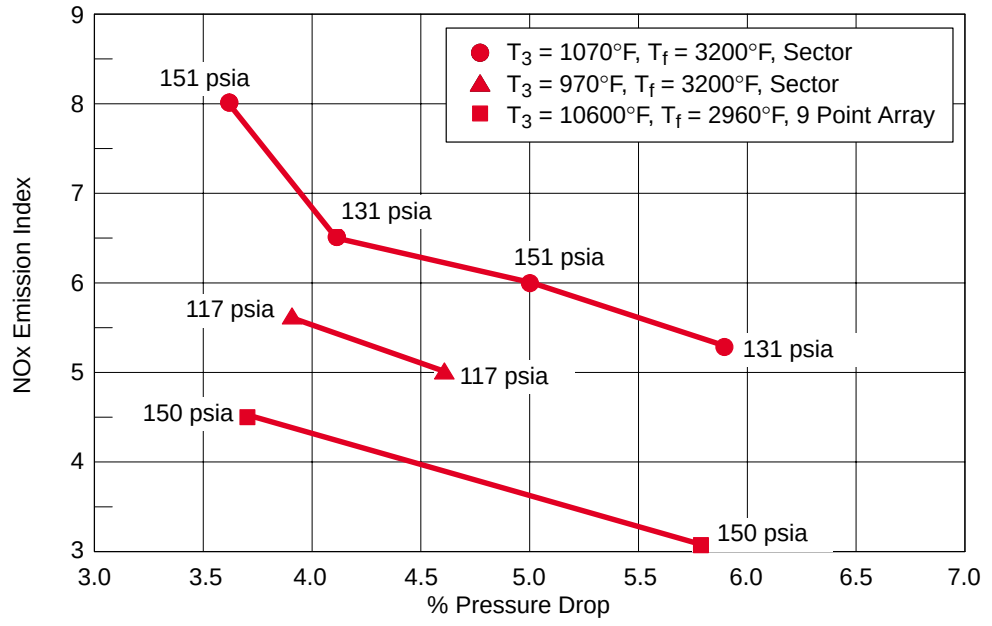

Figure 114. Effect of Pressure Drop on NOx: Multiple Venturi/Cyclone Sector and Nine-Point Multiple Venturi Array

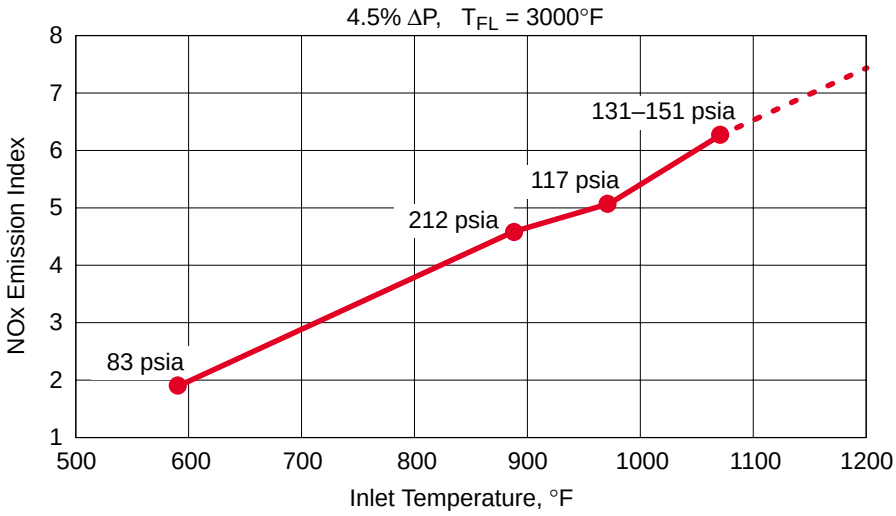

Figure 115. Effect of Inlet Temperature on NOx: Multiple Venturi/Cyclone Sector

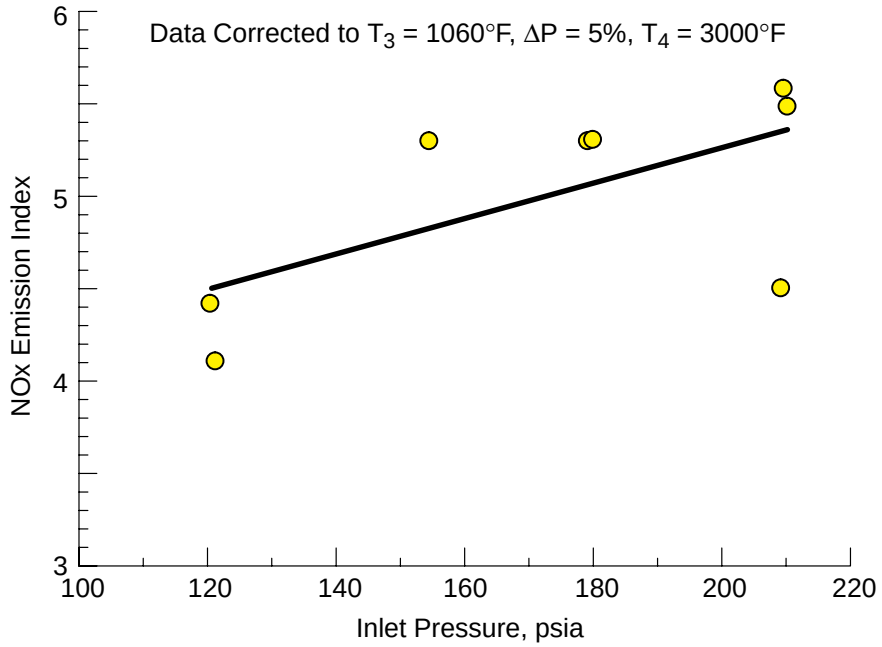

Figure 116. Multiventuri/Cyclone Sector: Stepped Effect of Inlet Pressure

Unfortunately, this method still resulted in a projected NOx of 5.4 EI at nominal supersonic cruise conditions (1200°F, 150 psia, 4% ΔP/P, 0.030 fuel/air ratio). This was getting very close to the target of 5 EI but was not quite sufficient. It was anticipated that with further design improvements in the pilot and/or LDI injectors that the targeted nominal supersonic cruise NOx emissions of 5 EI could be achieved. However, without such improvements, it is expected that the pilot would still have to be operated at a lower fuel/air ratio than the inner and outer domes to actually meet the requirement. From a practical standpoint, it is anticipated that such nonuniform operation would introduce undesirable combustor exit temperature profiles into the system. In fact, in terms of the turbine design it would be desirable to operate the center (pilot) dome hotter than the inner and outer domes, introducing something closer to a center-peaked profile. Thus, without significant improvements in the cyclone (primarily) and/or the LDI injector emissions, a tradeoff between exit profiles and emissions would have to be made.

Overall, the stepped-dome multiventuri/cyclone combustor concept worked well. Combustion efficiencies were acceptable at low and moderate power and quite good at higher power conditions. Nominal supersonic cruise NOx emissions were projected to be 8 to 10 EI, although operating the pilot at a lower flame temperature than the inner and outer (LDI) domes suggested that this could possibly be reduced to 5.4 EI. It is expected that additional cyclone pilot and LDI injector development would further improve emissions.

4.5.1.2 LDI Sector Build 2

In the second LDI sector build, the center dome was moved aft, reducing the recession to only 0.375 inches (the design did not quite allow for perfect alignment). Nothing else was changed for this test. The purpose was to find out if a flat dome could be used in the combustor, since this would certainly be easier to manufacture. The concern was that by eliminating the isolation of the center pilot dome, emissions would be adversely impacted, especially low-power CO and hydrocarbons.

The results are summarized in Table 15. Comparisons to the recessed dome data from Build 1 are presented in Figure 117. As anticipated, low-power combustion efficiency decreased significantly without the isolation offered by the recessed pilot dome. Although easier to cool and manufacture, the flush-dome design simply does not provide the isolation necessary to meet performance needs at low power.

Table 15. LDI Stepped-Dome Sector Emissions Summary (Build 2)

T_3 (°F)	P_3 (psia)	ΔP/P (%)	T_{flame} (°R)	Emissions Index (g/kg Fuel)			Combustion Efficiency (%)
				NOx	CO	HC	
1026	153.0	4.00	3735	12.8	1.01	0.02	99.97
1026	152.0	3.70	3585	8.8	0.82	0.02	99.98
1025	149.0	4.70	3302	3.7	0.61	0.02	99.98
1024	147.0	4.50	3236	2.7	0.60	0.03	99.98
1024	148.0	4.60	2999	0.9	4.20	0.16	99.89
Fully Fired, 1025°F, 150 psia, 4.5% Pressure Drop							

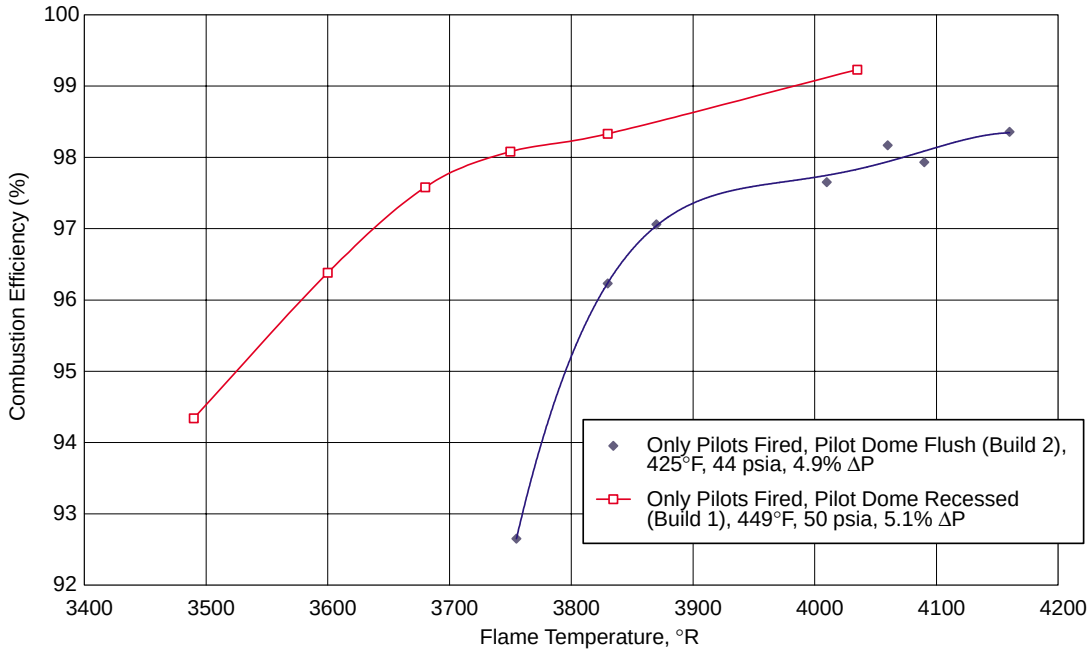

Figure 117. LDI Stepped-Dome Multiventuri Sector Combustion Efficiency (Build 2)

4.5.1.3 LDI Sector Build 3

In the third build of the LDI sector, the center dome cyclones would be replaced with another bank of 12 LDI injectors. Whereas the inner and outer domes had 45° axial swirlers, the center dome would contain 60° axial swirlers. The intent was for the 60° injectors to provide higher swirl and thus greater stability, somewhat simulating the cyclone pilots. Note that the center dome was recessed back to the original position, as tested in Build 1. Also note that the total effective flow area increased slightly, by about 0.1 in^2.

The results are summarized in Table 16. Comparisons to the Build 1 data are shown in Figures 118 and 119. NOx EI at near-cruise conditions was actually shown to be slightly better than Build 1 (by about 1.5). This made sense, since the 60° LDI injectors demonstrated NOx levels similar to the cyclone pilots at these conditions in single-cup tests. However, low-power combustion efficiency was significantly worse than the mulitventuri/cyclone combination used in Build 1. Thus, the Build 1 combination had the significant advantage in that it provided the best low-power efficiency with only slightly higher levels of high-power NOx.

4.5.1.4 LDI Sector Build 4

The fourth build of the LDI sector was identical to Build 3, except that the 60° center dome LDI injectors were replaced with 45° injectors identical to those in the inner and outer domes. Note that the total effective flow area increased by about 0.3 in^2 relative to the Build 1 configuration.

Table 16. LDI Stepped-Dome Sector Emissions Summary (Build 3)

T_3 (°F)	P_3 (psia)	ΔP/P (%)	T_{flame} (°R)	Emissions Index (g/kg Fuel)			Combustion Efficiency (%)
				NOx	CO	HC	
1052	153	4.3	3889	16.9	1.7	0.1	99.95
1052	152	4.8	3884	16.7	1.8	0.1	99.95
1052	153	4.9	3735	11.5	1.4	0.0	99.96
1054	149	4.9	3429	5.3	0.8	0.1	99.98
1055	150	4.8	3246	2.8	0.6	0.1	99.98
1055	152	3.0	3075	1.6	0.6	0.1	99.98
Fully Fired, 1053°F, 151 psia, 4.8% Pressure Drop							

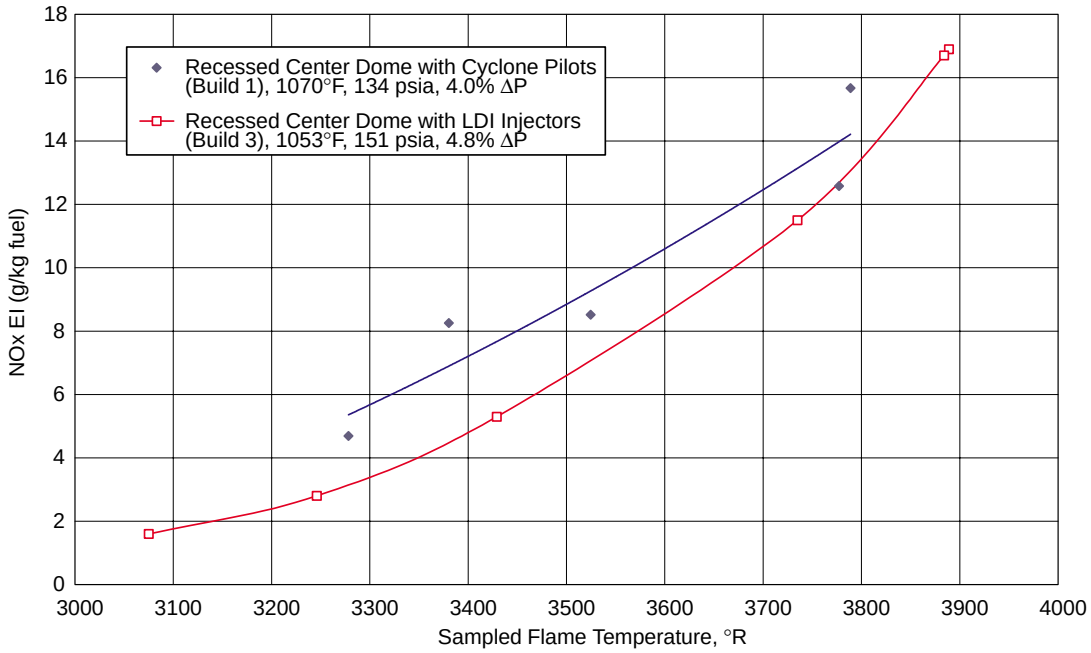

Figure 118. LDI Stepped-Dome Multiventuri Sector NOx Emissions (Build 3)

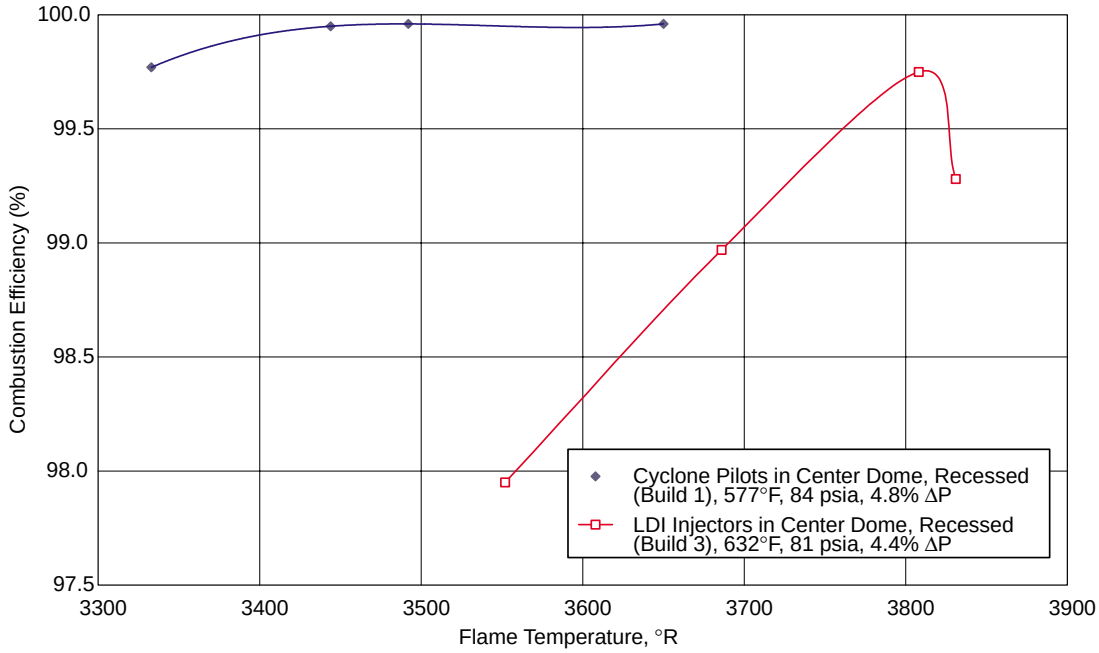

Figure 119. LDI Stepped-Dome Multiventuri Sector Combustion Efficiency (Build 3)

The results are summarized in Table 17. Comparisons to the Build 1 and Build 3 data are shown in Figures 120 and 121. NOx at near-cruise conditions was found to be 2-3 EI lower than the multiventuri/cyclone combination of Build 1. This was a significant step forward in getting closer to meeting the supersonic cruise NOx requirements of 5 EI (projected to be 5 to 7 EI at nominal supersonic cruise conditions). However, the low-power combustion efficiency was lower than the mulitventuri/cyclone combination used in Build 1, although it was much better than Build 3 with the 60° injectors. Although not shown in Figure 121, limited data at 450°F, 50 psia showed a much more significant reduction in combustion efficiency relative to Build 1. The differential is expected to be even greater at ground idle conditions (295°F, 45 psia). Thus, although this build had the lowest near-cruise NOx, the Build 1 combination had the best low-power efficiency. The stability problem of LDI injectors at low power was an inherent problem with the concept that would be difficult to overcome.

Table 17. LDI Stepped-Dome Sector Emissions Summary (Build 4)

T_3 (°F)	P_3 (psia)	ΔP/P (%)	T_{flame} (°R)	Emissions Index (g/kg Fuel)			Combustion Efficiency (%)
				NOx	CO	HC	
1023	150	4.4	2920	0.41	37.62	7.05	98.41
1026	151	4.6	3092	0.96	4.00	0.39	99.97
1026	149	4.8	3245	2.12	0.69	0.03	99.98
1026	154	4.2	3390	3.72	0.55	0.03	99.98
1025	150	5.2	3542	5.78	0.66	0.03	99.98
1025	151	4.2	3675	8.62	0.78	0.03	99.98
Fully Fired, 1025°F, 151 psia, 4.6% Pressure Drop							

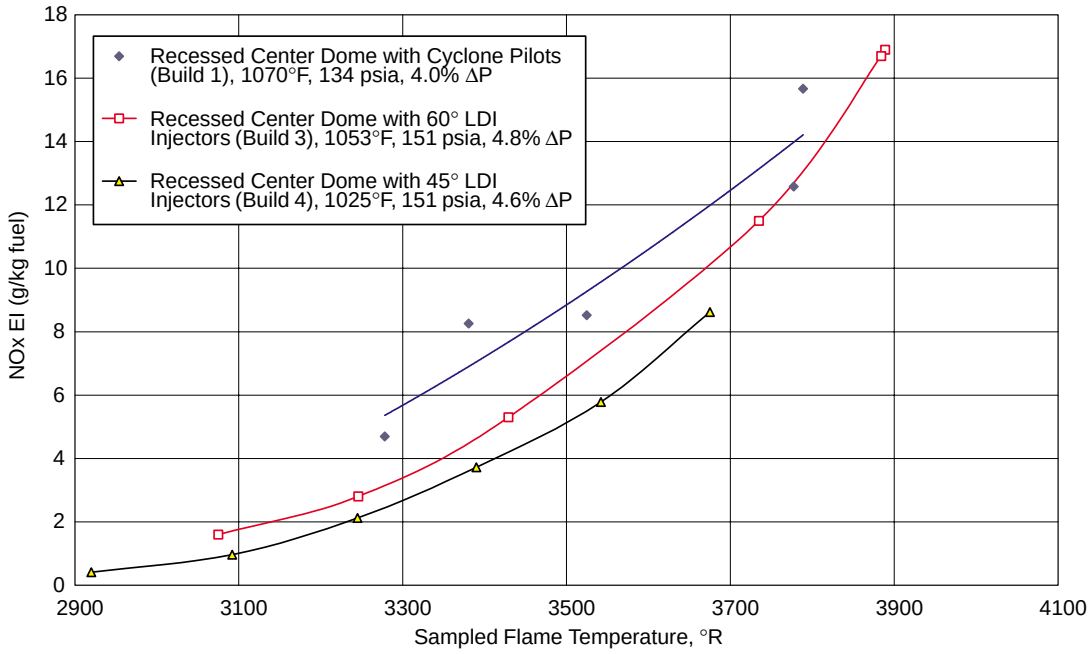

Figure 120. LDI Stepped-Dome Multiventuri Sector NOx Emissions (Build 4)

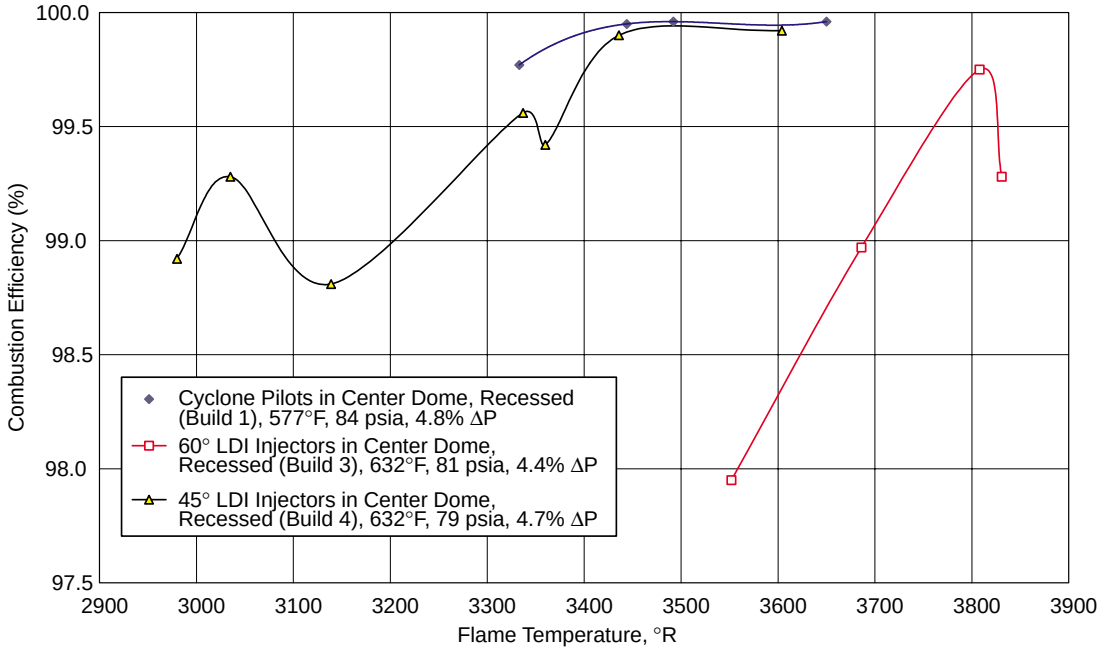

Figure 121. LDI Stepped-Dome Multiventuri Sector Combustion Efficiency (Build 4)

4.5.1.5 LDI Sector Build 5

The final LDI sector tested was identical to Build 4 except the center dome was moved aft to a flush position with the inner and outer domes (zero recession). The 45° LDI injectors were again used in all three domes.

The results are summarized in Table 18. Comparisons to the Builds 1, 3, and 4 data are shown in Figures 122 and 123. NOx EI at near-cruise conditions was found to be about 1 lower than the multiventuri/cyclone combination of Build 1. However, the low-power combustion efficiency again suffered relative to the mulitventuri/cyclone combination, although it was better than Build 3 with the 60° LDI injectors.

Table 18. LDI Stepped-Dome Sector Emissions Summary (Build 5)

T_3 (°F)	P_3 (psia)	ΔP/P (%)	T_{flame} (°R)	Emissions Index (g/kg Fuel)			Combustion Efficiency (%)
				NOx	CO	HC	
1047	150	4.7	2798	0.64	121.00	51.57	91.99
1047	148	4.9	2957	0.90	16.01	1.12	99.51
1048	150	4.5	3129	1.91	1.65	0.06	99.96
1047	151	4.7	3280	3.50	0.78	0.03	99.98
1050	149	4.8	3437	5.91	0.60	0.02	99.98
1046	150	4.2	3603	9.51	0.81	0.02	99.98
1048	150	4.5	3729	13.28	0.82	0.03	99.98
Fully Fired, 1047°F, 150 psia, 4.7% Pressure Drop							

Several key results came out of the five LDI sector tests. First, the recessed center dome appears to be extremely important in producing good low-power combustion efficiencies. When the domes were flush, low-power efficiencies dropped off significantly. Second, the use of cyclone pilots in the center dome consistently produced better low-power combustion efficiency than LDI injectors. The use of either 45° or 60° LDI injectors in the center dome was both found to be inferior to the cyclone at low power. Finally, none of the configurations were able to demonstrate the ability to comfortably meet 5 EI NOx at supersonic cruise conditions. Build 4 showed the most potential, with supersonic cruise NOx estimated to be in the 5 to 7 EI range. Unfortunately, the lack of low-power stability (that is, the poor combustion efficiency) of this concept discouraged continued development. This was a key driver in the selection of an LPP system at the time of the LPP/LDI downselect.

4.5.2 Lean Premixed Prevaporized Systems

Although NOx EI below 5 at supersonic cruise had been demonstrated in single-cup development tests of LPP subcomponent hardware, the impact of cyclone/IMFH interactions in a combustor system was still in question. Two fundamentally different LPP systems were tested: stepped-dome (SD) and multistage radial/axial (MRA). The stepped-dome is a triannular design in which the middle pilot stage is recessed from an inner and outer set of IMFH tube banks. The basic stepped-dome configurations used here were the same as those used in the LDI tests. The MRA design

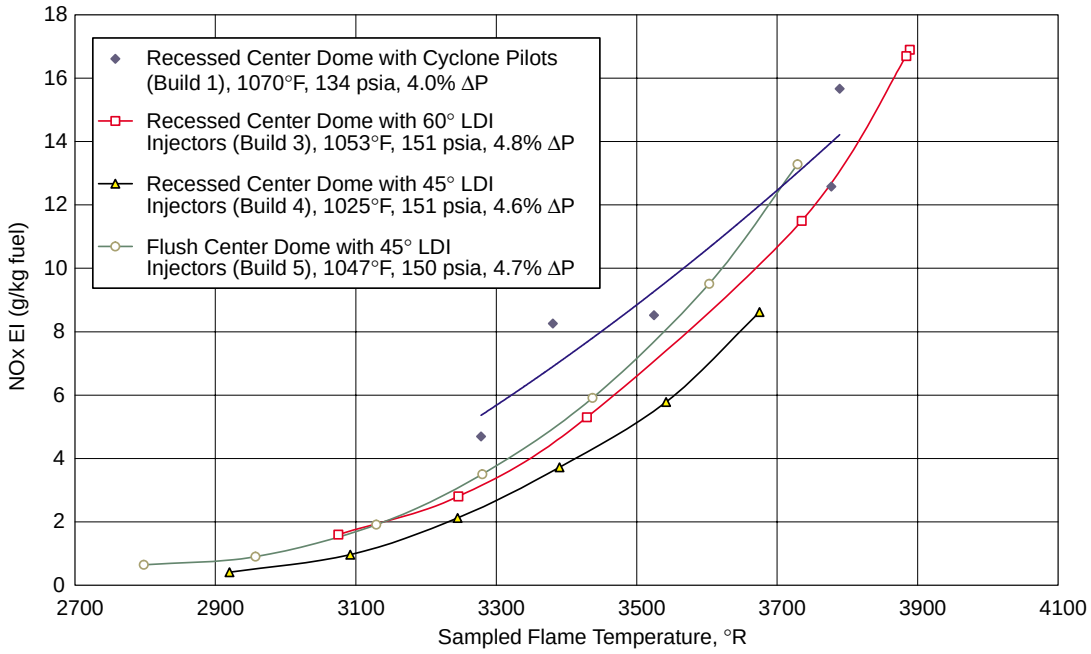

Figure 122. LDI Stepped-Dome Multiventuri Sector NOx Emissions (Build 5)

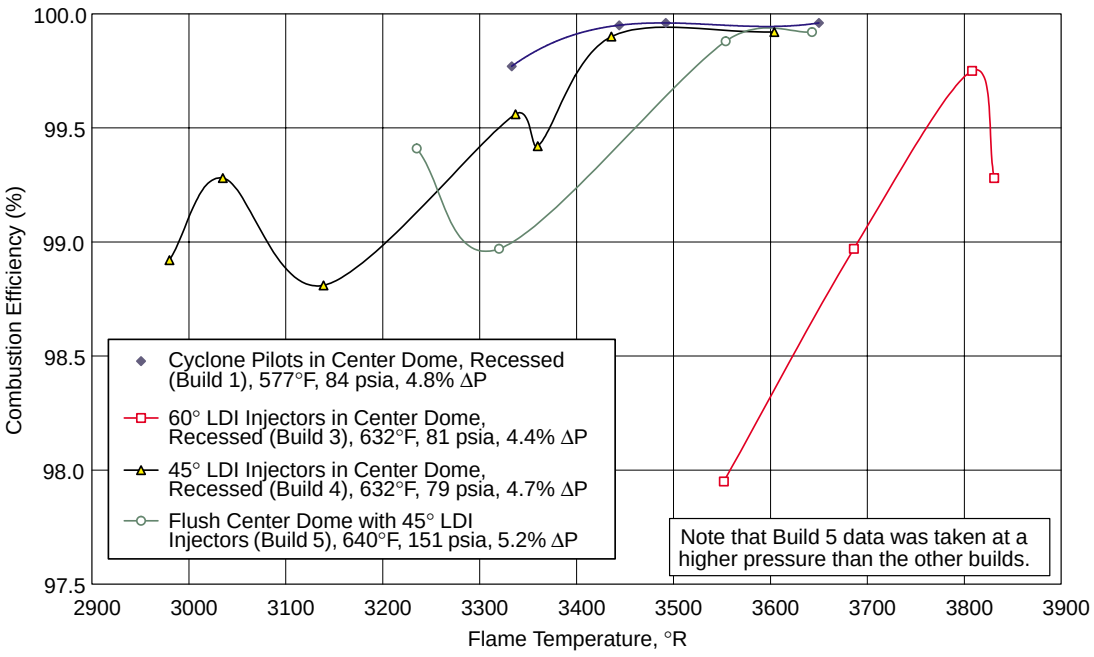

Figure 123. LDI Stepped-Dome Multiventuri Sector Combustion Efficiency (Build 5)

contains a main dome to which the IMFH tubes are attached, with a set of pilot cyclones on the outer portion of the combustor pointing radially inward. Multiple variations of each type were tested, as summarized in Table 19. The sector tests are described in chronological order. Some of these tests were run in parallel with the LDI tests described above; others were run after the LPP/LDI downselect. Note that the number of cups refers to the number of cyclone pilots in the sector (corresponding to the number of "sections" of an engine — typically there were to be 30 pilots per engine).

Table 19. LPP Sector Emissions Test Summary

Parameter		Sector Name						
		SD Impingement	**SD Lamilloy**	**HMMRA**	**SD Segmented**	**MMMRA Build 1**	**MMMRA Build 2**	**MMMRA Build 3**
Test Dates		4/94, 6/94	10/94	11/95, 7–8/96	12/96	2–3/97	9/97	1–4/98
Dome Style		Stepped	Stepped	MRA	Stepped	MRA	MRA	MRA
Fuel-Staging Mode		Radial	Radial	Radial	Radial	Radial	Circumferential	Circumferential
Liner Type		Impingement	Lamilloy	Impingement	Segmented	Impingement	Impingement	Impingement
Pilots in Sector		5	5	4	5	5	5	5
Fuel Stages Available		3	3	5	3	5	8	8
Cross Section		Rectangular 2D	Rectangular 2D	Rectangular 2D	Rectangular 2D	Curved 3D	Curved 3D	Curved 3D
Diffuser		None	None	None	None	Multipassage	Multipassage	Multipassage
IMFH Tube Diameter (in)		0.5	0.5	0.5	0.5	0.5	0.5	0.5
Fuel Injector Type		Hypo Tubes	Hypo Tubes	Hypo Tubes	Hypo Tubes	Stingers	Stingers	Stingers
Cycle Points and Emissions Data Points	Ground Idle		X	X		X	X	X
	15% LTO					X	X	X
	34% LTO					X	X	X
	65% LTO				X	X	X	X
	SLTO			X	X	X		
	Nominal Subsonic Cruise	X	X	X	X	X	X	X
	Start of Supersonic Cruise					X		
	Nominal Supersonic Cruise		X		X	X		X
	End of Supersonic Cruise					X		
	Start of Descent				X	X	X	
	Comparison Point	X	X	X	X	X		
Emissions Points Acquired		**26**	**123**	**35**	**34**	**111**	**116**	**319**

4.5.2.1 Highly Mixed MRA Sector

The first multistage radial/axial design tested was the so-called "highly mixed" MRA (HMMRA) sector. This was a rectangular (2D), four-cup sector with five fueling stages. Figures 124 through 126 show details of the design. The cyclone pilots contained swirlers with 2.05-in inner diameters and sixty 70° vanes (1.0 swirl number). Each pilot had six fuel-injection ports (plain jet air-blast atomizers) on the centerbody. They were of the same design as those used in the stepped-dome sectors (described later). For each pair of cyclone pilots, there were 28 associated IMFH tubes (each pilot was associated with 14 tubes, but adjacent sections were mirror images — not identical). The IMFH tubes were 5.5 inches in length with 0.56-in inner diameters. Hypo tubes were used for fuel injection. These were 0.042-in OD by 0.022-in ID tubes located 1 inch from the IMFH tube inlet. The main dome and 22 of the IMFH tubes were canted upward 45° from horizontal, with the bottom six IMFH tubes horizontal (parallel to the inner liner). The pilots and pilot dome were angled inward, 90° from the main dome face. It was this high degree of expected mixing and interaction that led to the "Highly Mixed" naming convention for this sector.

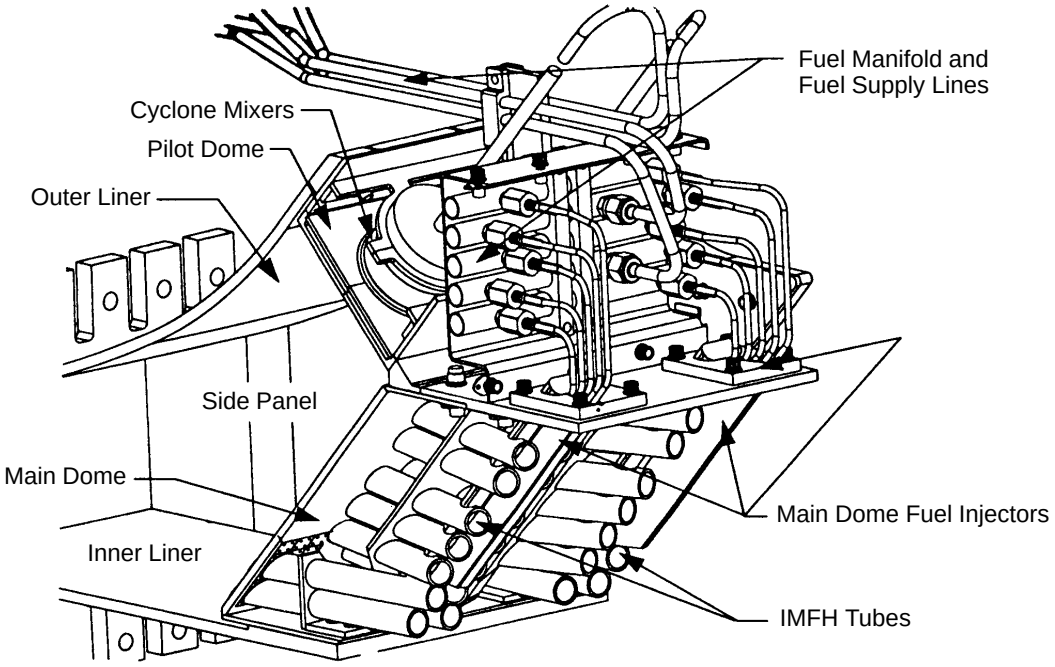

Figure 124. LPP Highly Mixed MRA Rectangular Sector

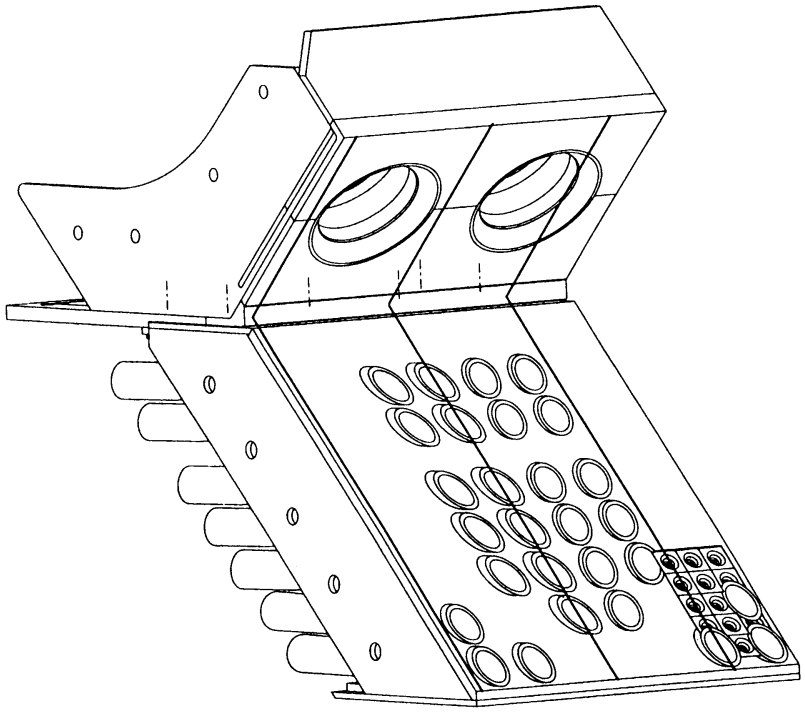

Figure 125. LPP Highly Mixed MRA Rectangular Sector Main Dome

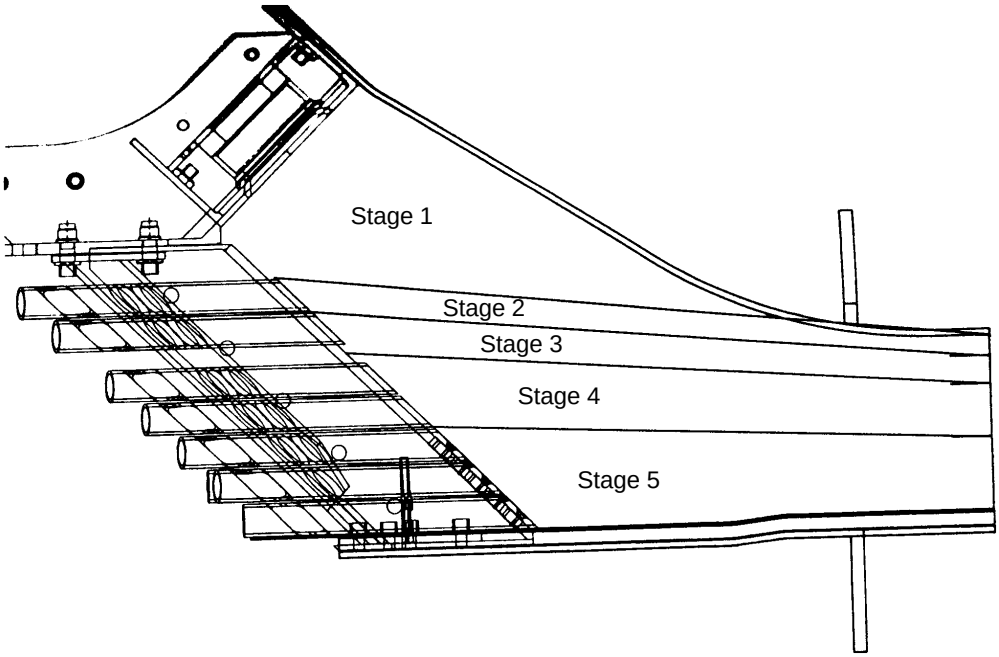

Figure 126. LPP Highly Mixed MRA Rectangular Sector Staging

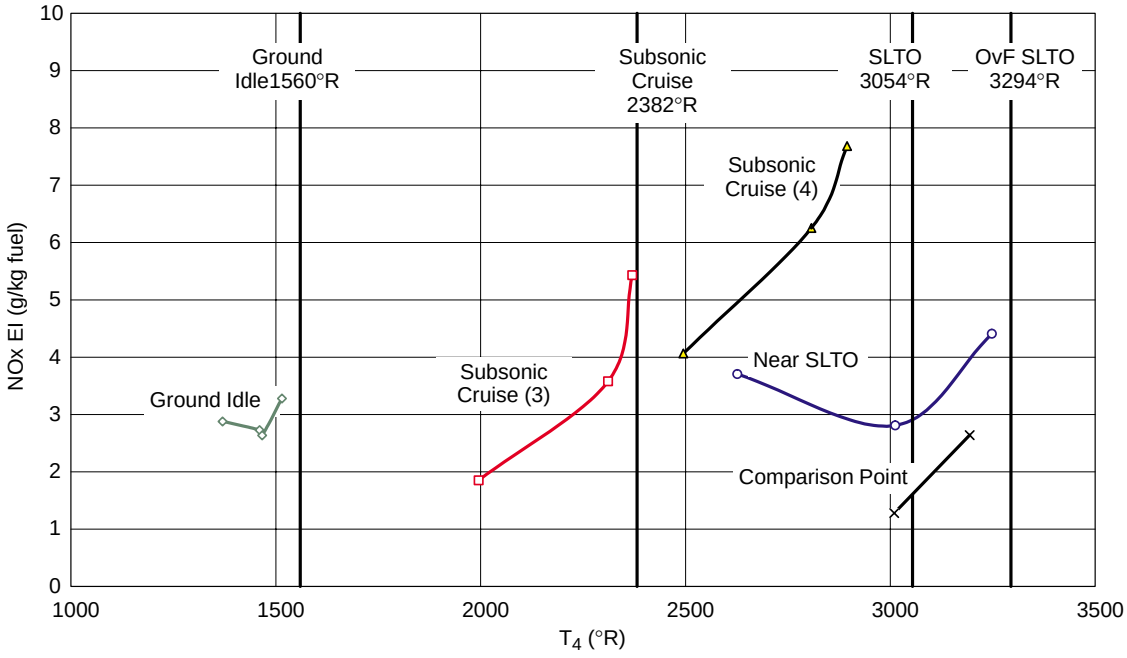

Figure 127. LPP Highly Mixed MRA Sector NOx Emissions

HMMRA Build 1

What turned out to be the first build of the HMMRA was tested at GEAE on November 2, 1995. The liners and sidewalls in this sector used ceramic tiles glued in place to protect the hot-side surfaces but relied on natural convection for back-side cooling. (The pilot liner was impingement cooled.) As it turned out, this was the downfall of the test. After less than an hour of fired testing, the outer liner burned through, ending the test before any emissions data were acquired. Several ceramic tiles had detached, causing damage to the inner liner and sidewalls as well, although much less severe than the outer liner damage. Fortunately the pilots, pilot dome, IMFH tubes, and main dome were not affected. This led to a rebuild of the sector, with new liners and sidewalls.

HMMRA Build 2

The second build was tested at GEAE from July 12 through August 7, 1996. Build 2 was conceptually identical to Build 1 but introduced back-side impingement cooling on the liners and sidewalls to mitigate the overheating problems previously encountered. In place of the ceramic tiles, a TBC was used to reduce the potential for losing the protective barrier. These changes proved successful in allowing the test to proceed. More than 40 data points were acquired, covering multiple staging configurations at four different inlet conditions: ground idle (GI), sea level takeoff (SLTO), subsonic cruise, and *comparison point 1* (950°F, 120 psia; a point at which data were available from other tests for comparison purposes). Regrettably, the sector was not run at supersonic cruise conditions.

Emissions were acquired using four 5-element gas-sampling rakes with the capability of sampling individually, ganged by rake, ganged by row, or as a total ganged sample. Not all combinations were measured at each point because of the significant amount of time required to do so. The data ganged by rake and by row were useful in understanding emissions and temperature profiles at the aft end of the combustor, while the ganged totals provided overall emissions information.

The results are summarized in Table 20 and Figures 127 through 129. Overall the emissions were good. GI combustion efficiency was low but seemed to be driven by higher than expected hydrocarbons (about 20 EI). The subsonic cruise operating point seemed to fall right between the three- and four-stage data tested. Four-stage operation required fuel/air ratios that were too low, but three stages was starting to get a bit too hot.

Table 20. LPP Highly Mixed MRA Sector Emissions Summary

Test Conditions Simulated	Stages Fired	T_3 (°F)	P_3 (psia)	ΔP/P (%)	Emissions Index (g/kg Fuel)			Combustion Efficiency (%)
					NOx	CO	HC	
Ground Idle	1 of 5	325	48	6.2	3.5	22	20	97.50
Subsonic Cruise	3 of 5	610	91	5.8	6	1.5	0.08	99.95
	4 of 5	610	91	5.8	3.3	25	25	97.00
Sea Level Takeoff (SLTO)	5 of 5	872	239	5.6	2.7	20	2.8	99.20
Overflow SLTO	5 of 5	872	239	5.6	4.8	21	0.27	99.92
Emissions index and combustion efficiency values are estimated								

Although three-stage subsonic cruise EINOx appeared to be about 6, the last data point is in question; it is quite possible that three-stage EINOx would actually be closer to 4. Exit temperature profiles

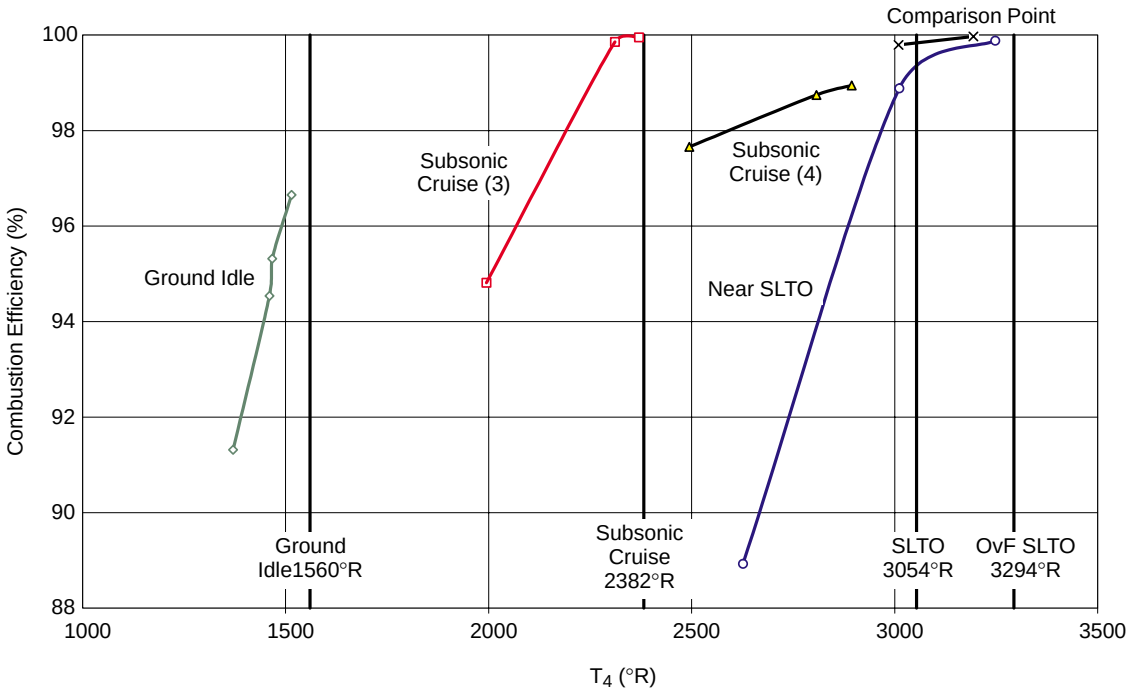

Figure 128. LPP Highly Mixed MRA Sector Combustion Efficiency

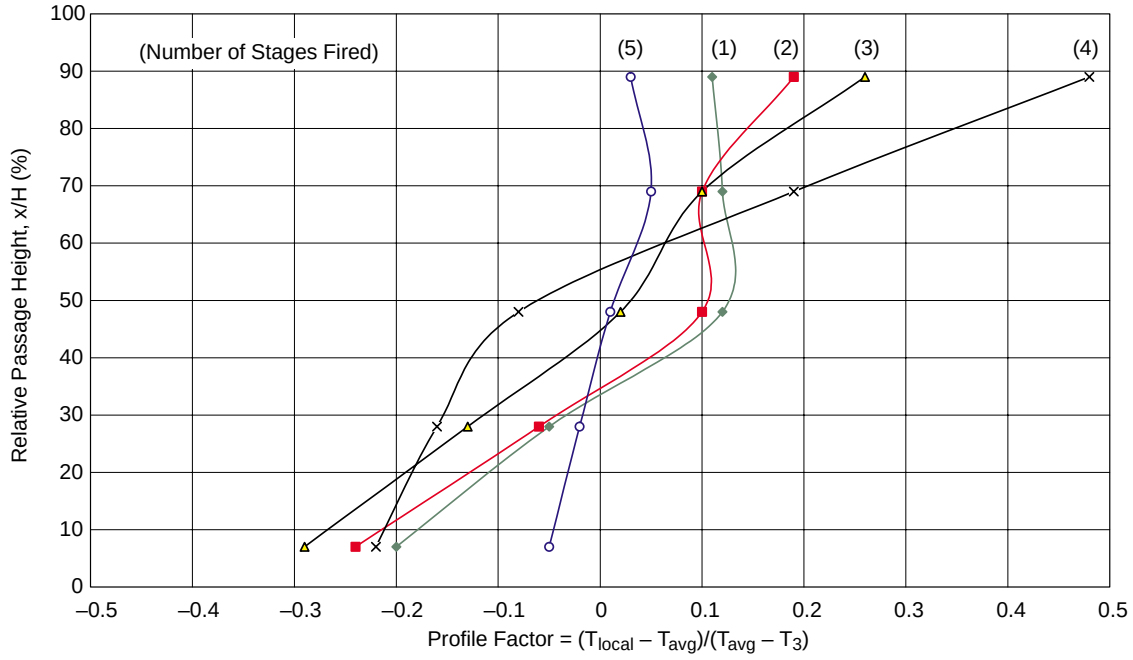

Figure 129. LPP Highly Mixed MRA Sector Exit Plane Profile Factors

where quite flat when fully fired (with all stages at the same fuel/air ratio) but became outer-peaked as inner tubes were shut off. Surprisingly, as more stages were turned off (starting at the bottom and moving upward), the profiles actually became *less* outer-peaked. The best explanation is that the pilot was penetrating to a point where it dominated the middle and upper portion of the exit plane. Thus, shutting off the innermost (bottom) stage shifted the profile outward, but turning off additional stages simply flattened the overall profile. In terms of stability, GI lean blowout was similar to levels observed in current engines, which typically have overall lean blowout fuel/air ratios on the order of 0.006 (Table 21). As expected, the lean blowout point decreased (that is, stability improved) as the combustor pressure drop was reduced. As a final note, the use of impingement cooling and the addition of the TBC on the liners and sidewalls were quite successful in protecting the hardware from overheating. No hardware damage was observed after completion of the test.

Table 21. LPP Highly Mixed MRA Sector Lean-Blowout Summary

Test Conditions Simulated	T_3 (ºF)	P_3 (psia)	ΔP/P (%)	FAR_{pilot} at LBO	FAR_{dome} at LBO
Ground Idle	324	47.0	6.25	0.0313	0.00700
	326	46.5	6.38	0.0314	0.00703
	327	47.2	3.90	0.0296	0.00663
	324	46.8	3.97	0.0291	0.00651
	322	48.1	2.17	0.0278	0.00622
	320	46.7	1.86	0.0280	0.00626
– – –	219	42.9	6.21	0.0316	0.00706
	218	42.6	6.18	0.0311	0.00696
	108	39.7	6.13	0.0322	0.00721
	111	39.8	6.26	0.0322	0.00720
	119	39.1	4.06	0.0284	0.00636
	121	38.8	4.04	0.0289	0.00647
	124	39.3	2.01	0.0267	0.00597
	124	38.2	2.08	0.0266	0.00595

4.5.2.2 Rectangular Stepped-Dome Sector

A rectangular, three-cup, stepped-dome sector identical to the one used for the LDI sector tests at NASA described above was tested next (Figure 130). The center dome was recessed 1.85 inches from the inner and outer domes to isolate the pilots. The cyclone pilots contained swirlers with 2.05-in inner diameters and sixty 70° vanes (1.0 swirl number). Each pilot contained six fuel-injection ports on the centerbody. They were of the same design as those used in previous stepped-dome sectors and the HMMRA sector. The 12 LDI injectors in each of the inner and outer domes were replaced with fourteen 0.56-in inner diameter IMFH tubes 5.5-in long. The IMFH premixers were fueled using 0.040-in OD by 0.022-in ID hypo tube injectors located 1 inch from the IMFH tube

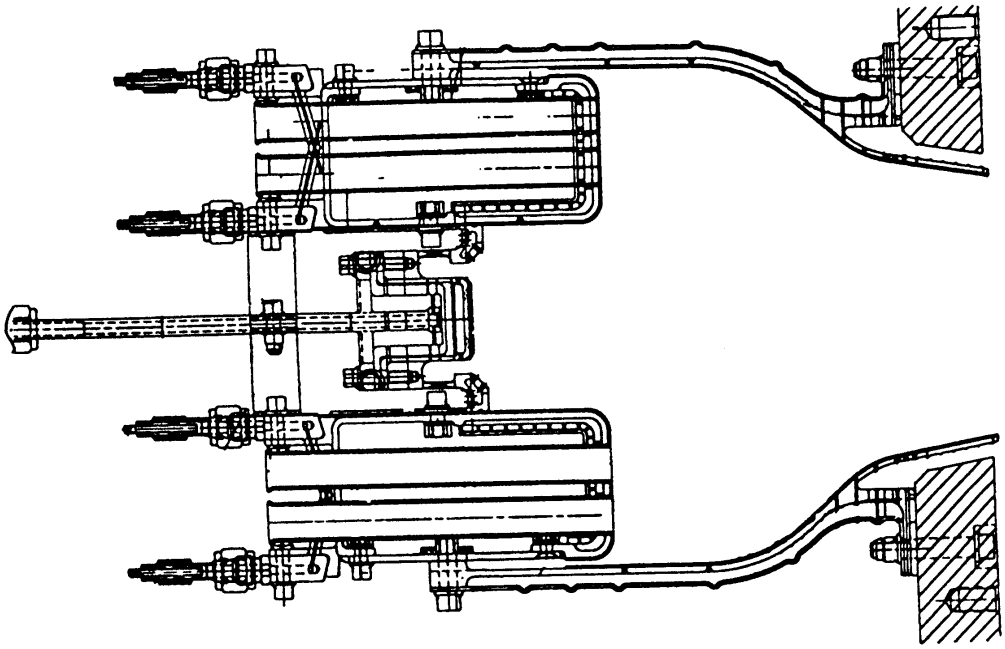

Figure 130. LPP Rectangular Stepped-Dome Sector

inlet. Note that by replacing the LDI injectors with IMFH tubes the total effective areas increased to 2.16 in^2 on each of the inner and outer domes (the pilot dome remained 1.61 in^2). Thus, the flow splits changed to 36.4, 27.1, and 36.4% for each of the outer, center, and inner domes.

The tests were run at NASA–Glenn in May 1996. The rig and gas-sampling system were identical to those used in the three-cup LDI tests at NASA. Two tests were actually run: one with the center dome recessed the other with it nearly flush with the inner and outer domes. Some of the results are shown in Figures 131 and 132. Pressures were 120 to 130 psia, and pressure drops were 4 to 5%. Dome recession had some impact on NOx, but no consistent trend was observed. At 950°F, the flush dome was quite a bit lower than the recessed dome. Dome recession had almost no impact on combustion efficiency at 950° or 1050°F; efficiencies were well above 99.9% at both of these conditions (because all three domes were fired, high efficiencies were expected).

4.5.2.3 IMFH FOD Blockage Test

A test was run at the Southwest Research Institute (Cliff Moses, Principle Investigator) from June 19 through July 16, 1996, to address concerns about the potential of foreign-object damage (FOD) to the IMFH tubes of an LPP combustor. This blockage test was set-up to monitor autoignition and flashback using thermocouples placed on the outside of the IMFH tubes, one near the entrance and the other about one inch upstream of the dome face on each tube. The hardware consisted of a bank of eight IMFH tubes (5.5 inches in length, 0.56-in ID, fueled by hypo tubes) cut from the dome of a previous stepped-dome sector test (Figure 133). A baseline test was run to measure temperatures throughout the system prior to running the test with blockage. The blockage test itself used short lengths (approximately 0.05 in) of 0.032-in diameter Hastalloy welding rod attached to the inlets of six of the eight IMFH tubes. On two of the tubes, the nodules were placed approximately one diameter apart; on two others they were placed two diameters apart; on the final two they were placed

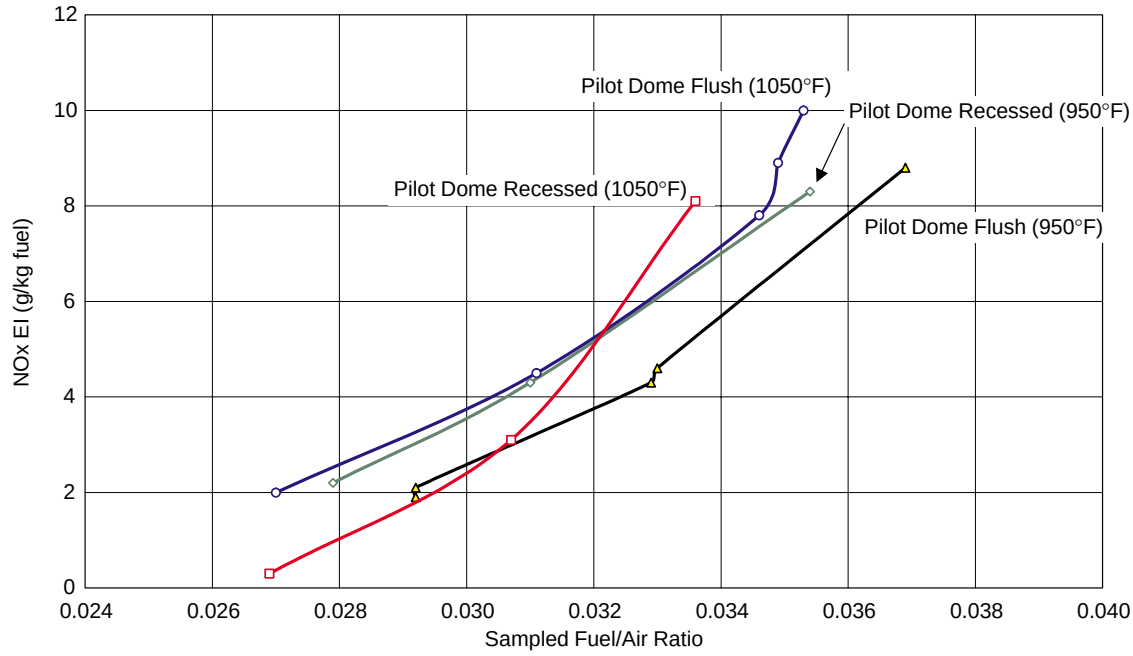

Figure 131. LPP Rectangular Stepped-Dome Sector NOx Emissions

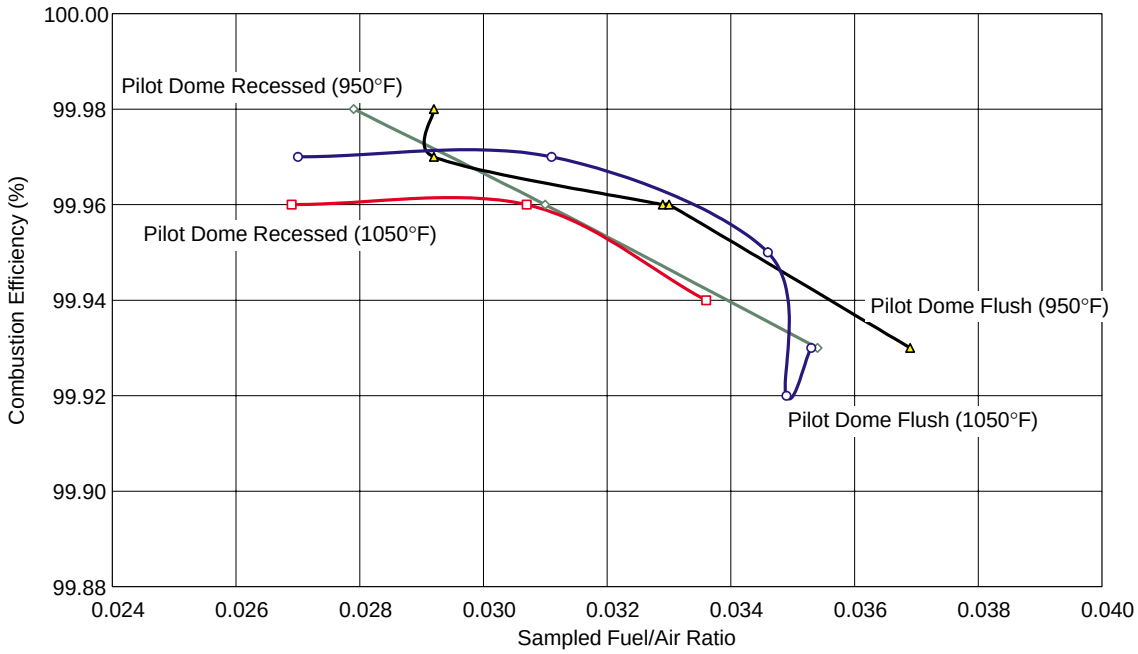

Figure 132. LPP Rectangular Stepped-Dome Sector Combustion Efficiency

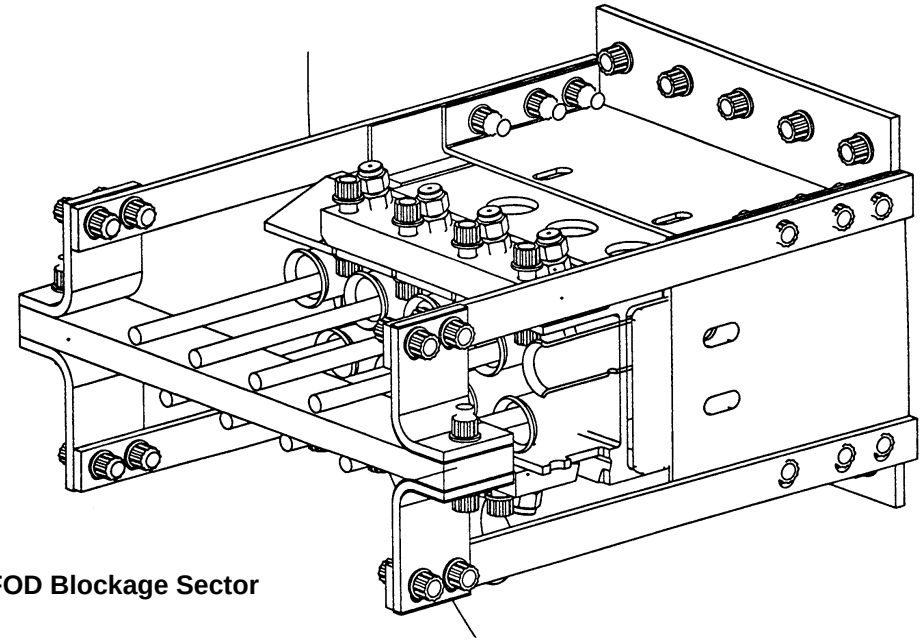

Figure 133. LPP IMFH FOD Blockage Sector

three diameters apart. The two with no blockage were considered to be the reference tubes. The blockages used were considered more severe than what would actually occur in an engine.

Conditions as high as 1200°F, 250 psia were tested — more severe than would ever be observed in an HSCT engine (see Table 22 and Figure 134). This provided margin over actual operating conditions. Thermocouple data showed no signs of autoignition or flashback in the IMFH tubes. Additionally, posttest inspections showed no signs of hardware damage, other than minor local loss of TBC in the hot section. Thus, the inherent resistance of the IMFH tubes to autoignition and flashback in a situation in which simulated FOD has occurred was successfully demonstrated. This was a significant demonstration of the feasibility of the IMFH design. Along with emissions results from other sectors, the success of the blockage test was a key factor in the eventual decision to continue LPP development instead of other LDI concepts.

Table 22. LPP IMFH Blockage Test Conditions

Parameter	Design		Blockage Test (Most Severe Case)
	SLTO	Supersonic Cruise	
Temperature (T_3), °F	870	1200	1200
Temperature (T_3), K	739	922	922
10,000/Temperature (1/K)	13.53	10.84	10.84
Pressure (P_3), psia	266	137	250
Pressure (P_3), atm	18.1	9.3	17
Mixer Residence Time (T_{res}), ms	0.9	0.8	1.0
$T_{res} \times P_3$, ms × atm	17	7.6	17.4
Autoignition Time × Pressure Estimate ($T_{auto} \times P_3$), ms × atm	94	20	20
Residence-Time Margin	82%	63%	14%

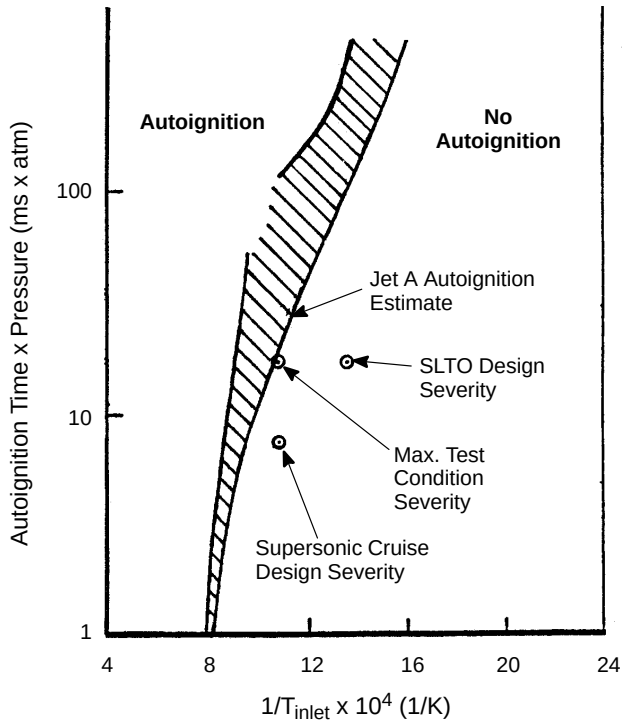

Figure 134. LPP IMFH FOD Blockage Autoignition Estimates

4.5.2.4 Stepped-Dome Segmented Liner Sector

The next sector tested was a rectangular (2D), stepped-dome, five-cup sector with segmented inner and outer liners (Figure 135). This testing took place at GEAE on December 12 and 13, 1996. This activity was primarily set up to be a heat transfer test to study the viability of segmented liners, although the impact on emissions was also of interest. The inner and outer domes each contained twenty-four ½-in diameter IMFH tubes (2 rows of 12 each) fueled by small hypo tubes. The middle dome was recessed relative to the inner and outer domes and contained five cyclone swirler pilots. The intent of the recession was to isolate the cyclone pilot stage from the IMFH tube banks in order to minimize interactions when the IMFH tubes were unfired. This was a concern, because interactions between hot combustion gases and cold unfired air have the potential to increase CO. Three fueling stages were available.

This was a follow-on test to the three-cup, stepped-dome sector described above and other stepped-dome designs tested under Contract NAS3-26617 (Large Engine Technology, Task 10) in which back-side-impingement-cooled liners were used. Back-side impingement has the advantage of not introducing air into the combustor, but it tends to require a fairly significant amount of air to keep the liners from overheating. Implementation of segmented liners was meant to reduce the amount of air needed for cooling the liners. The segmented liners allow some of the air to enter the combustor cavity. This cooling air creates a thin protective film over the liner surfaces and helps protect them from the intense heat. However, this has the potential to increase emissions beyond desirable levels because the “cold” film air can interact with the hot combustion gases. The concern is highest with regards to CO. Thus, the objectives of the test were: (1) to determine if the segmented liners could be kept sufficiently cool, even though the amount of air had been significantly reduced relative to the backside impingement cooling design, and (2) to measure the impact of the design on emissions.

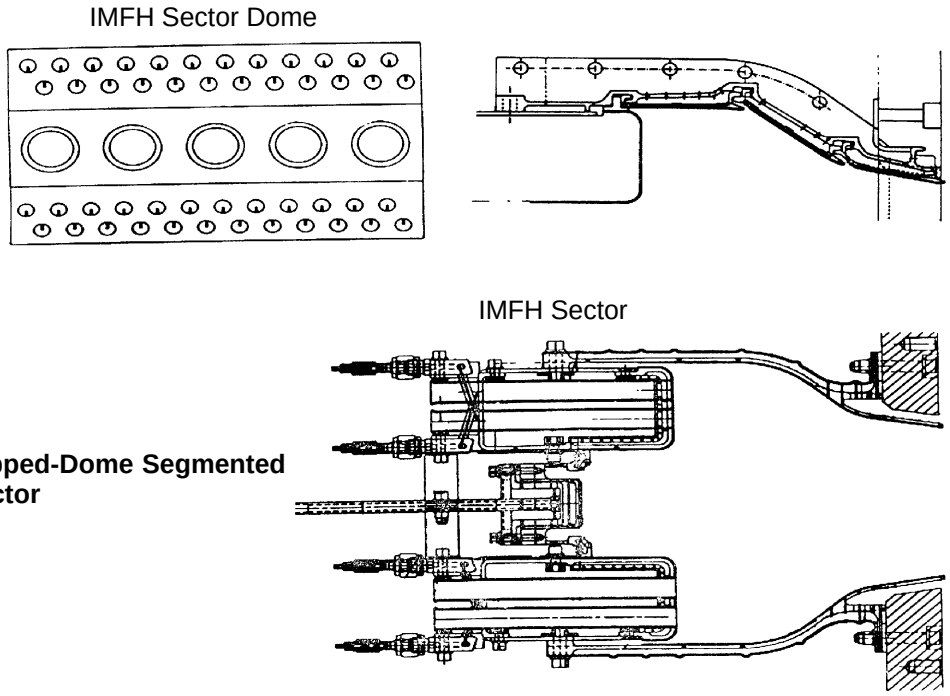

Figure 135. LPP Stepped-Dome Segmented Liner Sector

More than 35 data points were acquired over a range of operating conditions (T_3, P_3, ΔP, and FAR) and staging modes (number of domes fired). Operating conditions included SLTO, 65% LTO, start of descent, subsonic cruise, supersonic cruise, the comparison point, and several heat transfer points. This was the first sector test in which actual nominal supersonic cruise conditions were tested. Most of the data were acquired at higher power conditions, since this is where the cooling effectiveness is most important and most difficult to achieve (due to the already-high cooling air temperatures). Also, at low power the inner and outer dome IMFH tubes are unfired. Since they would shield the pilot stage from the liners anyway, it is unlikely that any emissions impact would be observed or could be directly attributable to liner film cooling.

Emissions data were acquired using four 5-element gas-sampling rakes with the capability of sampling individually, ganged by rake, ganged by row, or as a total ganged sample. Not all combinations were measured at each point because of the significant amount of time required to do so. The data ganged by rake and by row were useful in understanding emissions and temperature profiles at the aft end of the combustor, while the ganged totals provided overall emissions information.

The key results are presented in Figures 136 through 143. These test results were very encouraging. The most important was the demonstration of NOx EI right at 5 at true nominal supersonic cruise conditions, albeit with no margin. Low NOx had been extrapolated to these conditions from previous LPP stepped-dome designs, but this was the first test of a sector at true supersonic cruise inlet conditions. CO and unburned hydrocarbon (HC or UHC) levels were also very low (less than 1 EI CO and 0.1 EI UHC), leading to combustion efficiencies greater than 99.9% at supersonic cruise. Although not the main objective of the test, this was a significant event in the program progression.

As expected, exit profiles were strongly outer-peaked with two stages fired and very flat with all three fired (Figure 139).

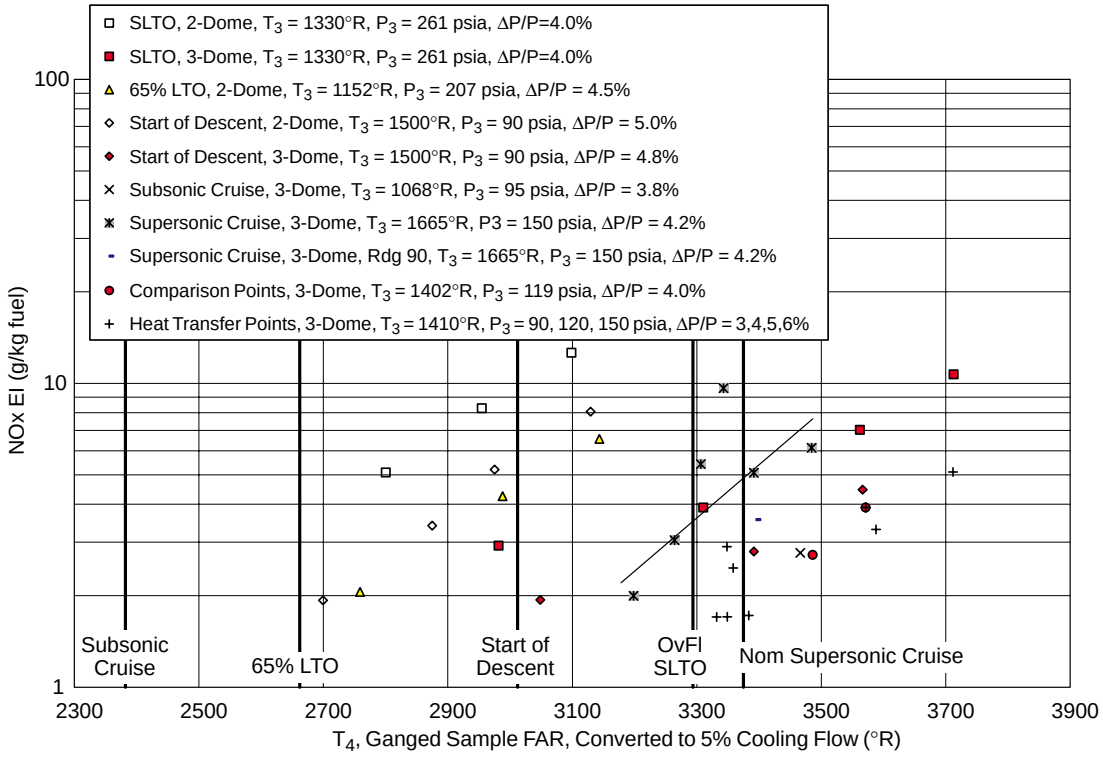

Figure 136. LPP Stepped-Dome Segmented Liner Sector NOx Emissions

See key in Figure 136 above.

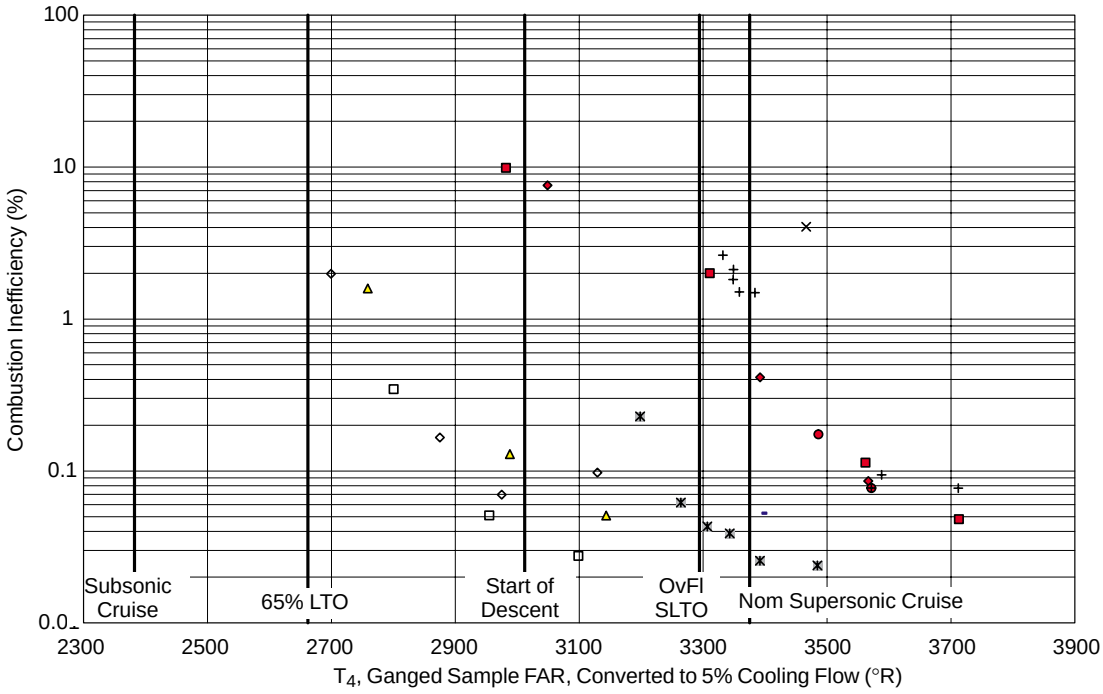

Figure 137. LPP Stepped-Dome Segmented Liner Sector Combustion Inefficiency

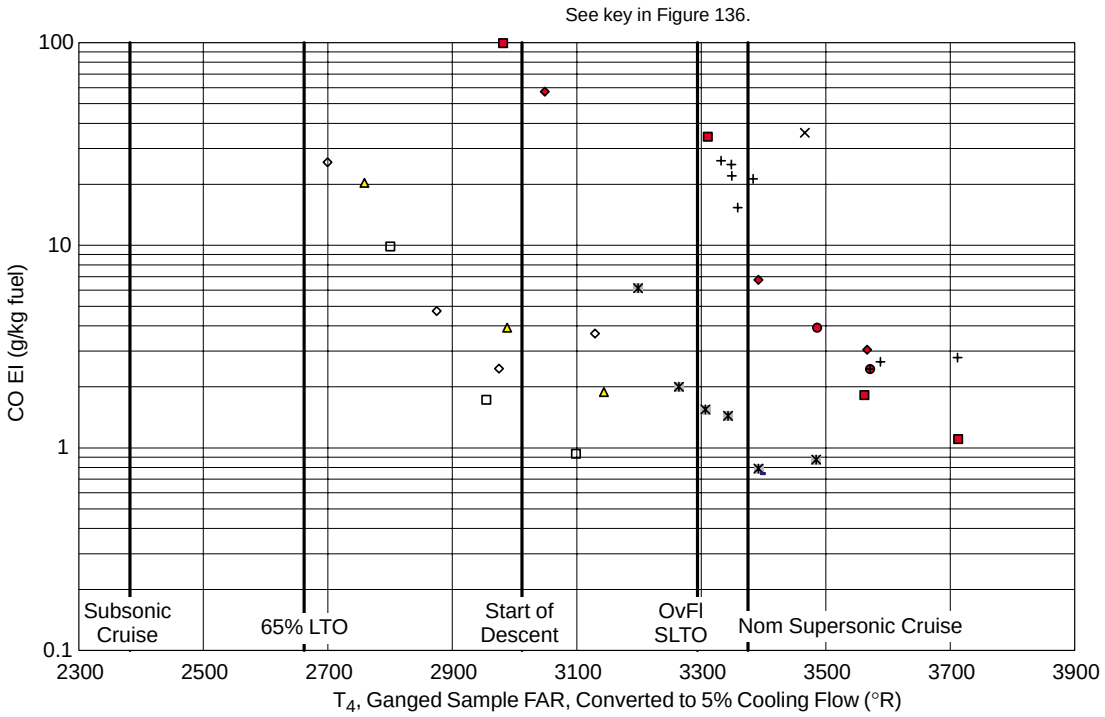

Figure 138. LPP Stepped-Dome Segmented Liner Sector CO Emissions

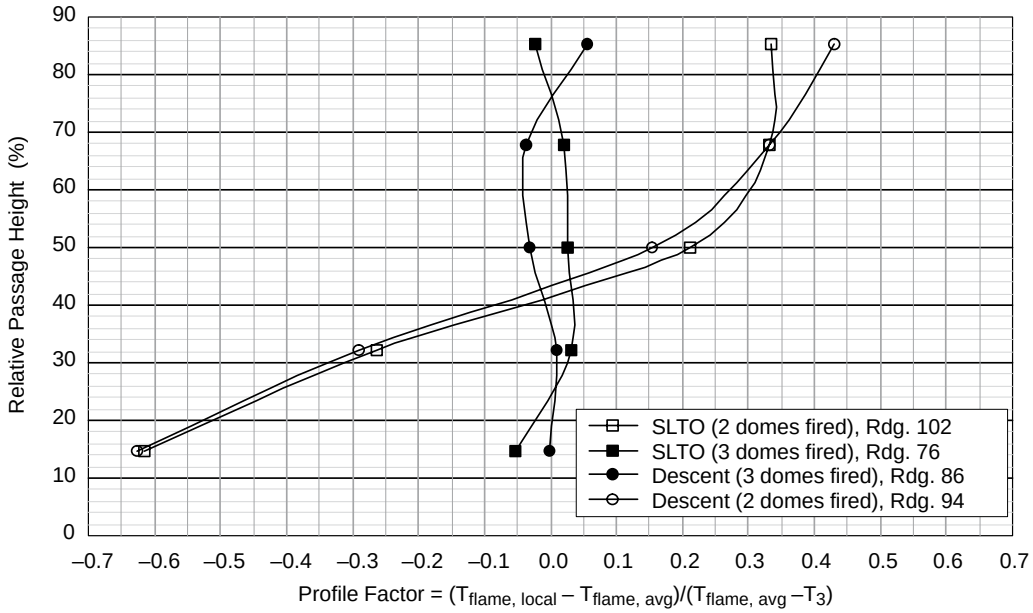

Figure 139. LPP Stepped-Dome Segmented Liner Sector Exit Profiles

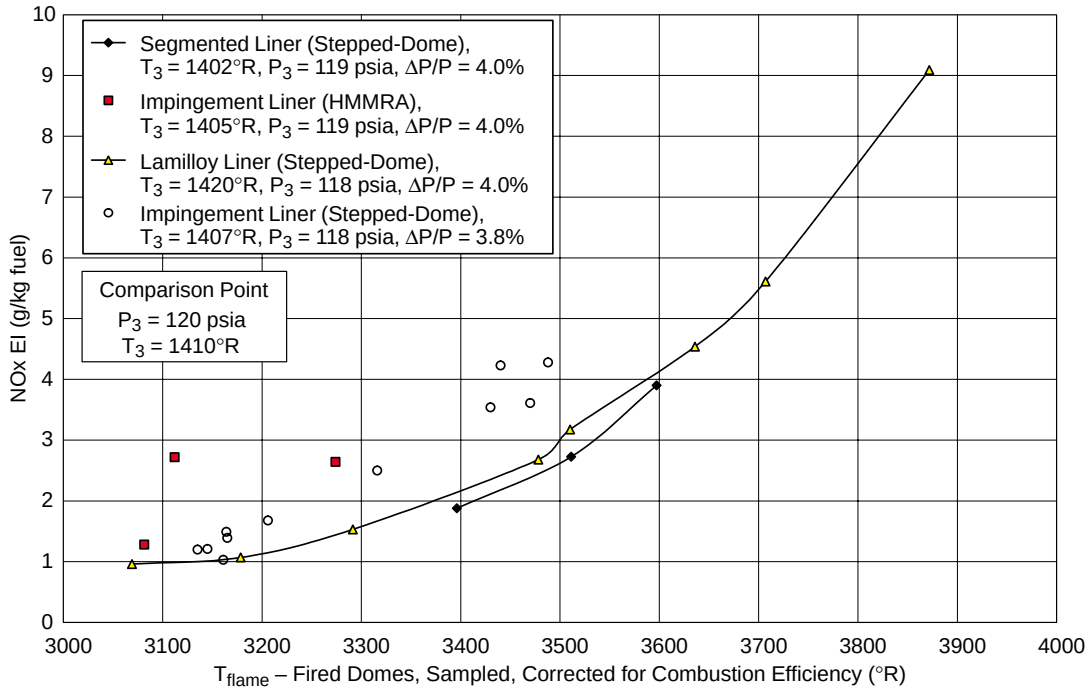

Figure 140. LPP Stepped-Dome Segmented Liner Sector NOx Comparisons

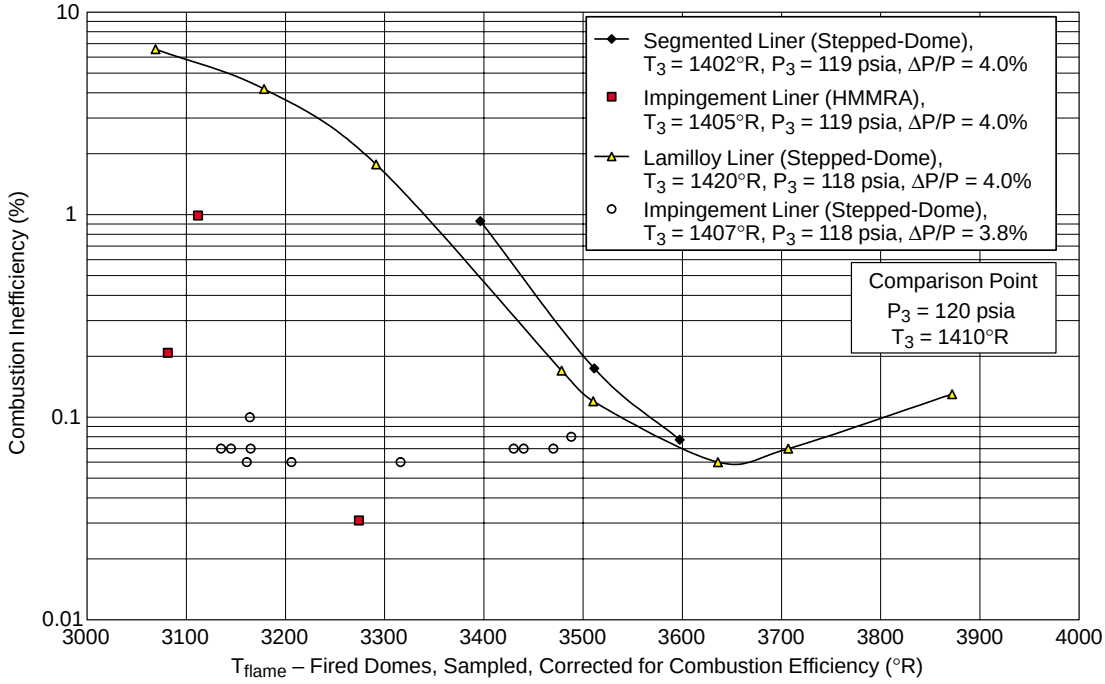

Figure 141. LPP Stepped-Dome Segmented Liner Sector Combustion Inefficiency Comparisons

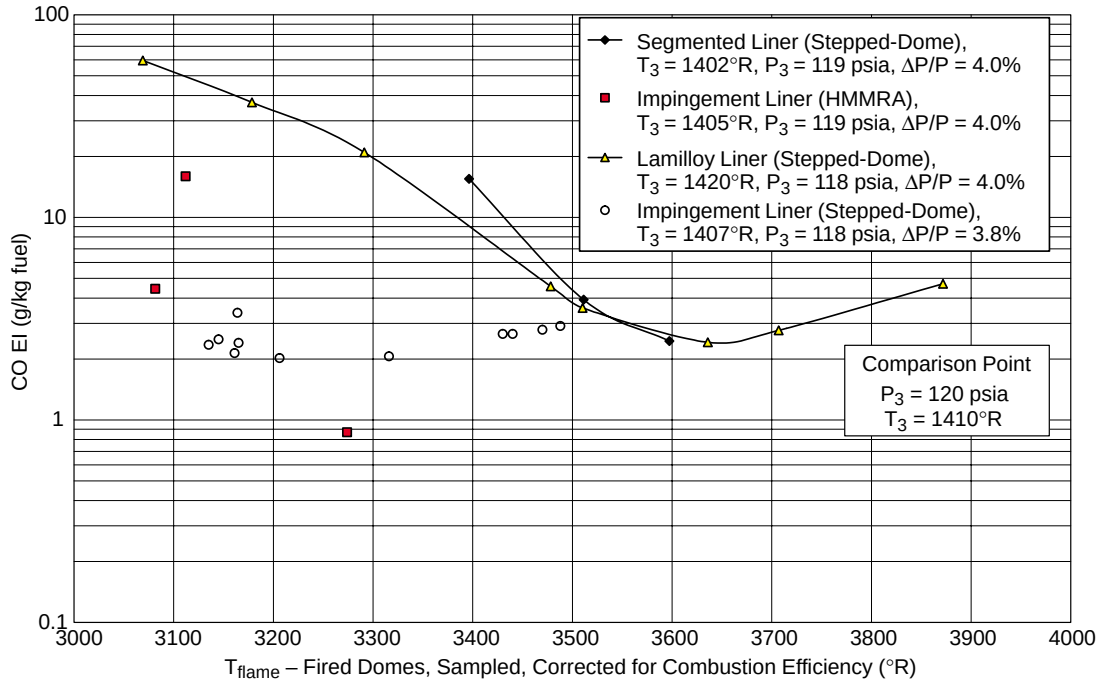

Figure 142. LPP Stepped-Dome Segmented Liner Sector CO Emissions Comparisons

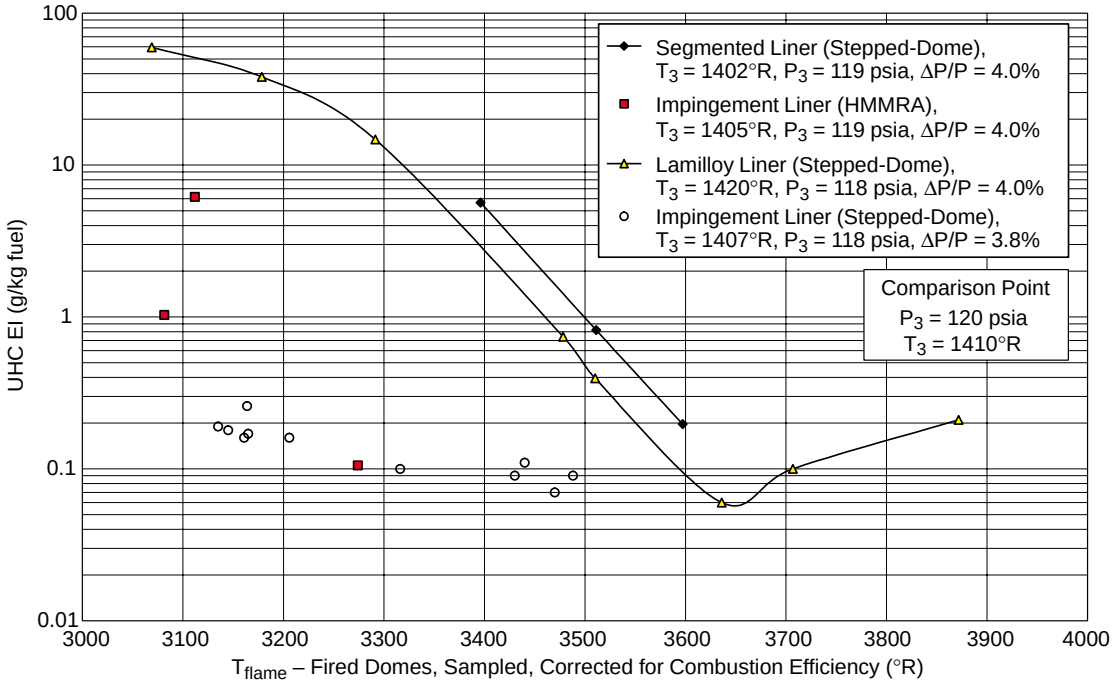

Figure 143. LPP Stepped-Dome Segmented Liner Sector UHC Emissions Comparisons

The segmented liner test data are compared to other sectors at the comparison point (950°F, 120 psia) in Figures 140 through 143. The stepped-dome Lamilloy liner and stepped-dome impingement liner data were acquired under Contract NAS3–26617 (Large Engine Technology, Task 10). Like the segmented liner, the Lamilloy liner allowed some cooling air to enter the combustion chamber. NOx was excellent for both the segmented and Lamilloy liner tests; however, CO, hydrocarbons, and combustion efficiency were not as good as designs without film cooling. In fact, the segmented and Lamilloy liner test data track each other very closely at these conditions.

CO and hydrocarbons were somewhat high at partially staged conditions, but the impact of the outer liners was inconclusive. In an engine, the combustor would most likely have been operated with five (or more) fueling stages. Thus, at partial power, the outermost and innermost IMFH tubes probably would have been unfired. Because only three stages were available, a complete bank of IMFH tubes had to be fired to simulate the aforementioned staging, resulting in fired tubes near the liner. Thus, the part-power, partially staged data must be discounted.

The thermal performance of the liners was excellent. Maximum temperatures observed were about 200°F below the design limits, suggesting the back-side impingement and small amount of film cooling were quite effective in protecting the hardware. These results suggest that the liners could either be operated at significantly higher flame temperatures than had originally been considered or liner cooling flows could be reduced even further from the levels tested here.

Overall, this was an extremely successful test, with over 35 data points taken. Heat transfer data were obtained, the cooling effectiveness of the design was excellent, and supersonic cruise emissions met contract requirements. The observance of NOx EI right at 5 at true nominal supersonic cruise was a significant step forward for the program. Further development would work to add margin to supersonic cruise NOx.

4.5.2.5 Transient Stepped-Dome Sector

The transient sector was a rectangular (2D) stepped-dome, five-cup sector with back-side impingement cooled inner and outer liners (see Figure 144). The inner and outer domes each contained 24 IMFH tubes fueled by hypo tube injection. The pilot dome was recessed and contained five cyclone pilots. The combustor overall was the same design as the stepped-dome segmented liner configuration discussed previously (all but the liners). The purpose of the test was to address potential autoignition and flashback concerns of the LPP system and address operability during “normal” and “abnormal” transients. Normal transients simulated aggressive engine accelerations and decelerations in which the combustor passed through different fueling stages. Abnormal transients were intended to represent the most severe dynamics that might occur during a compressor stall or an engine inlet unstart.

The sector was tested at the transient combustor test facility at the United Technologies Research Center in May and June 1997. Approximately 30 transients were run, as shown in Table 23. Combustor pressures and temperatures were monitored along with fuel and air flow rates.

A typical set of data is presented in Figures 145 through 147. These data were taken from the dynamic autoignition test in which air flow rate oscillations at 1 Hz were introduced into the combustor, causing periodic reverse flow through the dome. This assuredly sent flame back through the IMFH premixers and upstream of the dome. Average inlet conditions were set to simulate supersonic cruise (1200°F, although the pressure was slightly low at about 120 psia). This was one of the most severe tests the combustor was put through.

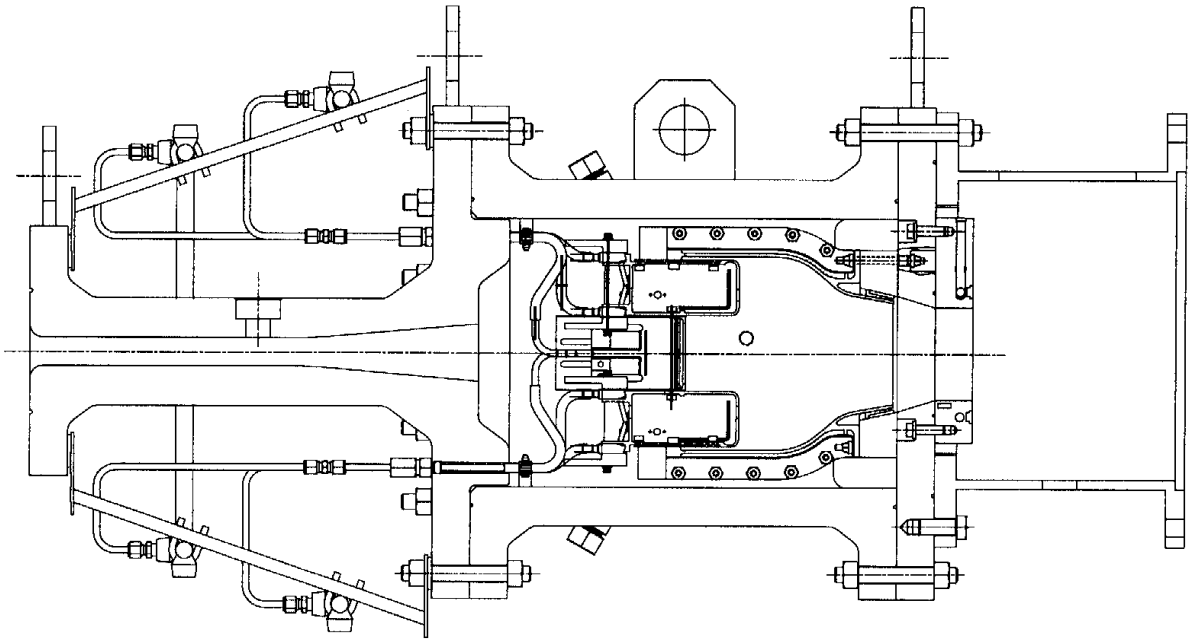

Figure 144. LPP Transient Stepped-Dome Sector

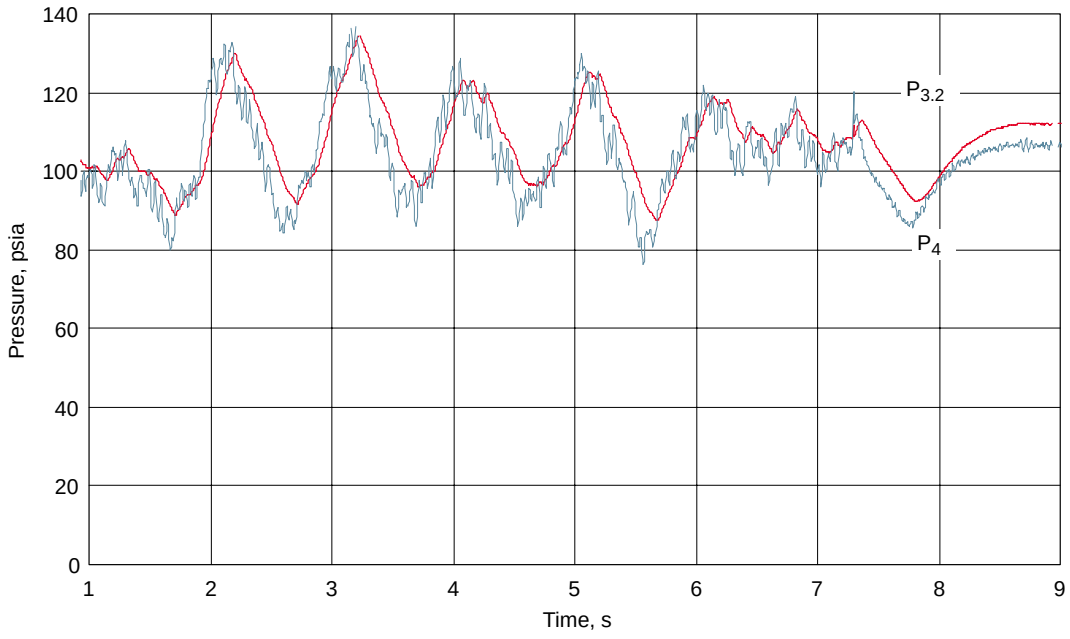

Figure 145. LPP Transient Stepped-Dome Sector Run 3207 Combustor Pressures

Table 23. LPP Transient Sector Test Point Summary

								AFTRAC Ctrl. Settings				
Run	Test Plan	Profile Name	Type	Fuel Cfg.	Duration (sec.)	WAC (lb/s)	T3 (F)	WFC1 (t=0) (pph)	WFC34 (t=0) (pph)	WFC5 (t=0) (pph)	Remarks	Date or (Time)
1512	4	LPP4	Decel	A	4	13.88	830	443	270	270	Transient; autoignition	
1707	4	LPP4	Decel	A	4	13.88	810	443	270	270	Transient; autoignition	
2407	3	LPP3FS	Accel	B	4	6.55	487	216	0	0	Transient	
2408	1	LPP1FSB	Accel	B	4	6.55	487	216	0	0	Init sys 3 one sec early. Init 35 pph flow 2 sec prior.	
2409	1	LPP1FSB	Accel	A	4	6.55	487	216	0	0	Transient	
2410	1	LPP1FSB	Accel	A	4	6.55	487	216	0	0	Repeat run	
2411	3	LPP3FS	Accel	A	4	5.97	456	180	0	0	Transient	
2412	1	LPP18FS	Accel	A	8	5.97	456	180	0	0	Transient	
2601,2		-	-	-	-	-	-	-	-	-	Calibrations, zeros	5/5/97
2603	1	LPP1FS	Accel	A	4	5.97	456	180	0	0	Transient	"
2604	3	LPP3FS	Accel	A	4	6.55	487	216	0	0	Transient	"
2605	1	LPP18FS	Accel	A	8	5.97	456	180	0	0	Transient	"
2606	1	LPP18FS	Accel	B	8	5.97	456	180	35	35	Transient	"
2607	3	LPP3FS	Accel	B	4	6.55	487	216	35	35	Transient	"
2608	1	LPP1FS	Accel	B	4	5.97	456	180	35	35	Transient	"
2801		Manual						0	0	0	Heater checkout to T3 = 1200 F with 13-hole baffle	
2901,2		-	-	-	-	-	-	-	-	-	Calibrations, zeros	5/27/97
2903	-	LPPLBO1	LBO	C	15	6.63	496	120 to 60	0	0	Transient fuel flow; no burning	"
2901											18-hole baffle placed upstream	"
2904	-	Manual	LBO	C	-	6.63	496	180	0	0	wf = 161 pph (JETDAS data)	"
2905	-	Manual	LBO	C	-	6.63	496	170	0	0	wf = 151 pph (JETDAS data)	"
2901		Manual	LBO	C	-	6.63	496	168	0	0	Lean Blow Out occurrence	"
3001,2		-	-	-	-	-	-	-	-	-	Calibrations, zeros	5/30/97
3003	2	LPP2FS	Accel	C	4	6.73	1039	207	170	35	Fuel sys 1, 2 interchanged in error	"
3004	2	LPP2FS	Decel	C	4	8.69	1200	261	214	261	Fuel sys 1, 2 interchanged in error	"
3101,2		-	-	-	-	-	-	-	-	-	Calibrations, zeros	6/2/97
3103	2	LPP2FS	Accel	C	4	6.73	1039	170	207	35		"
3104	2	LPP2	Decel	C	4	8.69	1200	214	261	261		"
3105	-	LPP10O	Osc.	C	2	8.63	1200	207	253	253	10 Hz	"
3106	-	LPP1O	Osc.	C	5	8.63	1200	207	253	253	1 Hz	"
3201,2		-	-	-	-	-	-	-	-	-	Calibrations, zeros	6/5/97
3203	2	LPP2FS	Accel	C	4	6.73	1039	170	207	35		"
3204	2	LPP2	Decel	C	4	8.69	1200	214	261	261	Curtailed data acquisition	"
3205	2	LPP2	Decel	C	4	8.69	1200	214	261	261	Repeat of Point 4	"
3206	-	LPP10O	Osc.	C	2	8.63	1200	207	253	253	10 Hz	"
3207	-	LPP1O	Osc.	C	5	8.63	1200	207	253	253	1 Hz	"
3301,2		-	-	-	-	-	-	-	-	-	Calibrations, zeros	6/11/97
3303	-	LPP10SB	Baseline	C	2	5.97	456	180.5	0	0	10 Hz	(0-0:42)
3304	-	LPP1SB	Baseline	C	2	5.97	456	180.5	0	0	1 Hz	(0:42-1:30)
3305	-	LPPSTP	-	C	2	10	R.T.	0	0	0	Single cycle check at room T	-
3306	-	LPP10SU	Unstart	C	2	9.17	1000	220	269	269	10 Hz	(1:30-2:11)
3307	-	LPP1SU	Unstart	C	2	9.17	1000	220	269	269	1 Hz	(2:11-2:51)
3308	-	LPP1SB	Baseline	C	2	5.97	456	180.5	0	0	Steady-state	-
3309	-	LPP1SB	Baseline	C	2	5.97	456	180.5	0	0	1 Hz	(2:51-3:28)

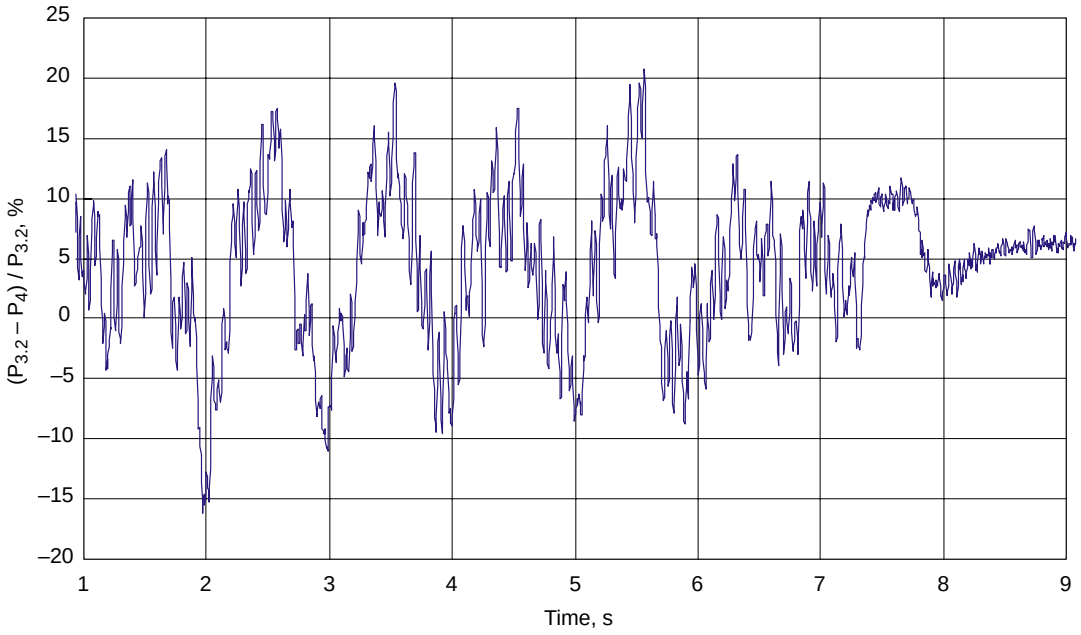

Figure 146. LPP Transient Stepped-Dome Sector Run 3207 Combustor Pressure Drop

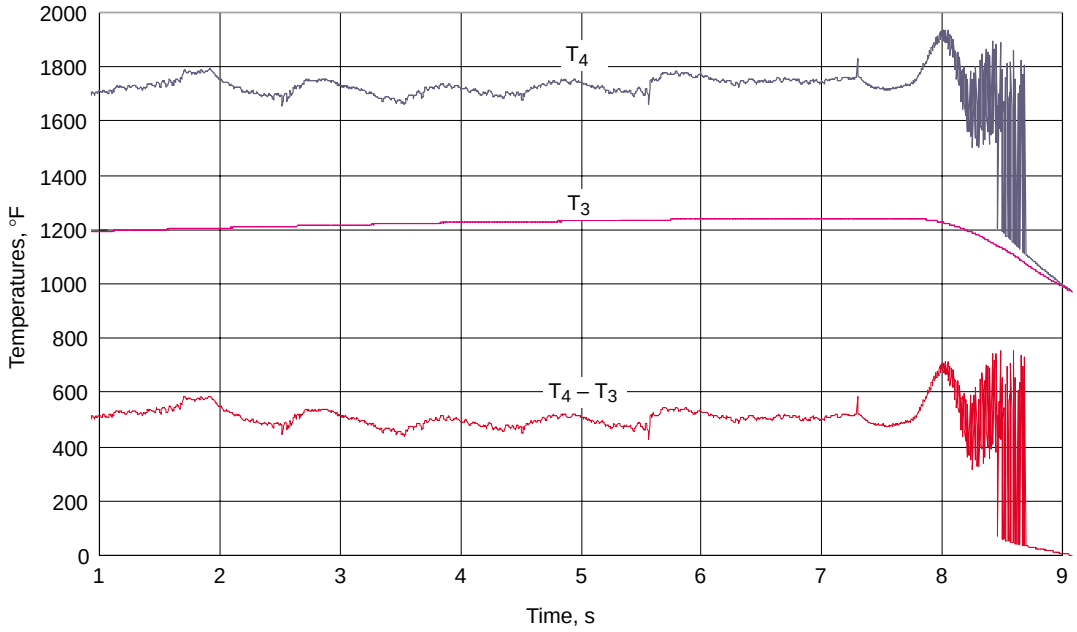

Figure 147. LPP Transient Stepped-Dome Sector Run 3207 Combustor Temperatures

Results of all the tests suggest that the design was quite resilient, showing strong resistance to autoignition, flashback, and flameholding. Reverse flow through the combustor dome certainly occurred during several of the transients, forcing flame upstream of the dome, but the fire appears to have quickly cleared with no resultant damage to the cyclone pilots or IMFH tubes. The only noticeable hardware damage was some sidewall and liner warpage and the associated loss of TBC that occurred because of the warpage. The TBC loss eventually led to small burn-throughs on the sidewalls, but without the TBC the life of the metal part obviously declines rapidly.

The combustor demonstrated excellent operability characteristics during the fast transients. The IMFH and cyclone premixers also both showed inherent robustness to the extremely severe abnormal transients. It was concluded that the LPP combustor suffers from no inherent disadvantages in operability or safety relative to a conventional diffusion flame combustor. This was a significant step forward in the substantiation of the LPP design. This information, along with emissions results, would lead to the selection of the LPP configuration over LDI concepts.

4.5.2.6 Moderately Mixed MRA Sector

The moderately mixed MRA (MMMRA) sector was set-up to simulate an engine-like flowpath as best as possible without having to go to a full-annular rig (which was to be tested later, after the basic technology had been developed and demonstrated). The rectangular cross section (2D) used in all previous sectors was replaced by one that was curved to simulate an engine-like (3D) flowpath (see Figures 148 and 149). A diffuser was located upstream of the combustor dome to provide more realistic entrance velocity profiles than those in the HMMRA sector, which was simply plenum-fed. The cross section was also extended tangentially to include five cups (63°) instead of four, as had been used in the HMMRA sector.

In principle, the combustor itself amounted to a simplified version of the HMMRA concept. In an attempt to improve the producibility of the combustor, the main dome was made to be vertical, with all of the IMFH tubes perpendicular to the dome face (making them parallel to the engine centerline). The pilot dome remained perpendicular to the main dome, with the cyclone pilots pointing radially inward. Half-inch diameter IMFH tubes were again used, but instead of using hypo tubes for fuel injection, separate fuel injectors using the recently developed “stinger” design (essentially Configuration 31 in the subcomponent development section of this report) were implemented (Figure 150). A new pilot was also added based on further advancements in the cyclone pilot development work (essentially Configuration 16 in the subcomponent development section of this report). The sector contained 5 cyclone pilots along with 60 IMFH tubes (5 banks of 12 tubes each). This design was referred to as the “moderately mixed” MRA because fewer interactions were expected between the various fueling stages than the “highly mixed” design. As it turned out, this design worked extremely well and would eventually become the configuration of choice for full-scale development.

Three builds of this configuration were tested. The first focused on emissions, lean blowout, exit profiles, and heat transfer. Fuel staging similar to that used in the HMMRA sector (five stages) was used. This tended to be more of a radial staging method, beginning with the pilot and moving radially inward as more stages are fired (Figure 149). Builds 2 and 3 looked at implementing circumferential staging (Figure 151), with significant interest in emissions and exit profiles. Lean blowout and heat transfer information was also obtained in these builds but was of less importance.

In all three builds, gas samples were collected using six 5-element rakes located one inch upstream of the combustor exit plane. Emissions could be sampled individually, ganged by rake, ganged by

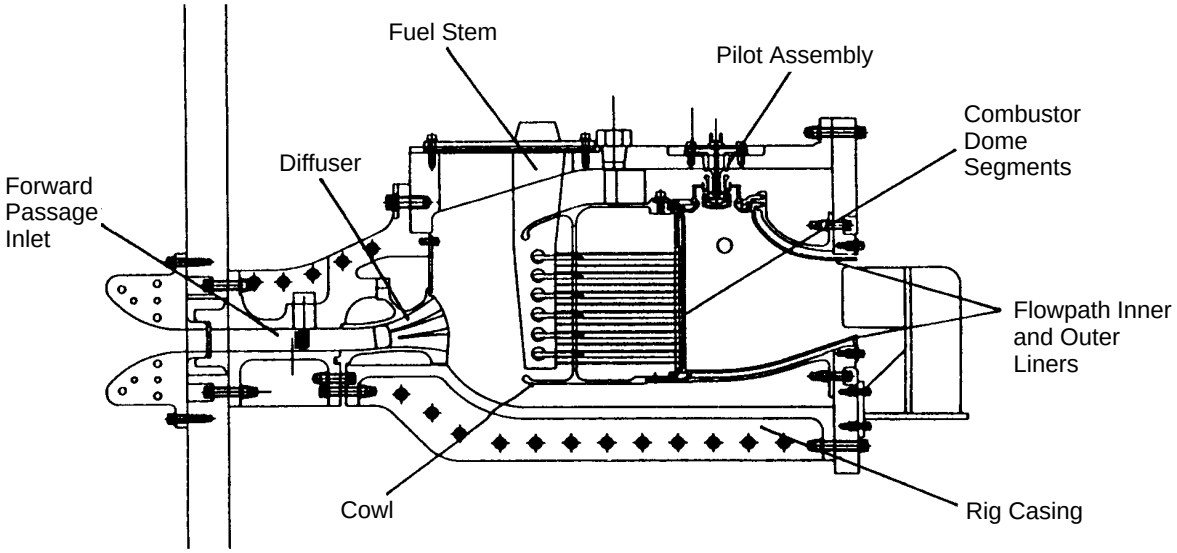

Figure 148. LPP Moderately Mixed MRA Curved Sector

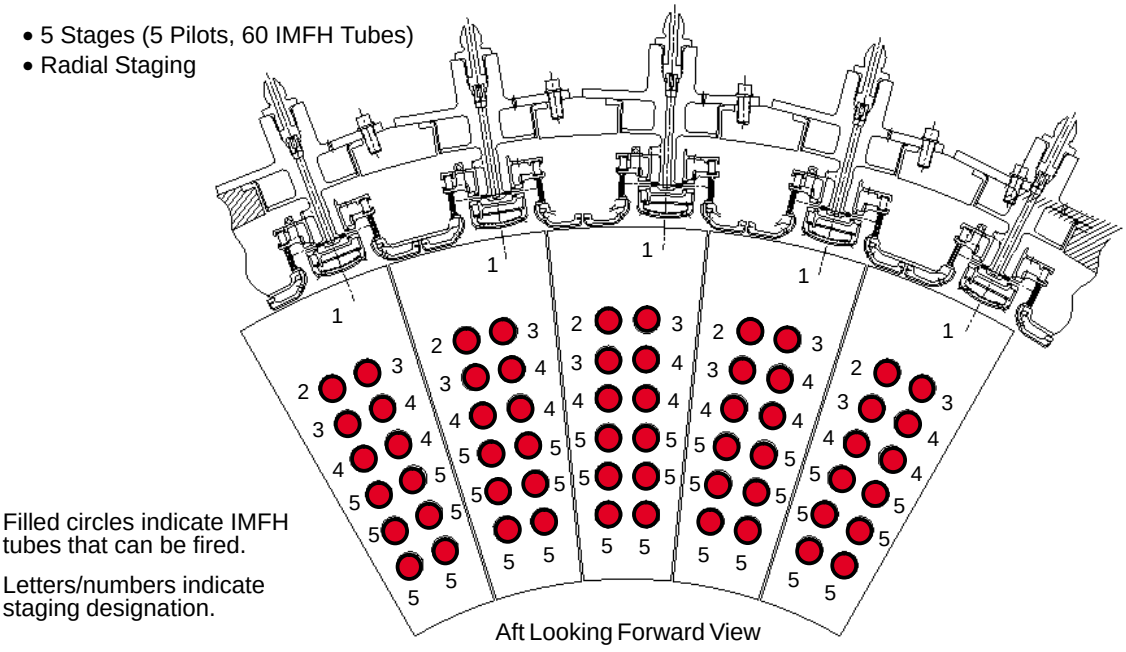

Figure 149. LPP Moderately Mixed MRA Curved Sector Build 1 Fuel Staging

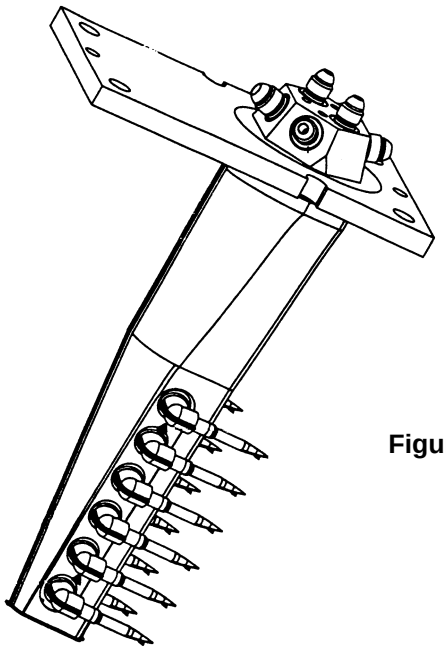

Figure 150. LPP MRA Curved Sector Build 2 Combustor Circumferential Exit Profiles

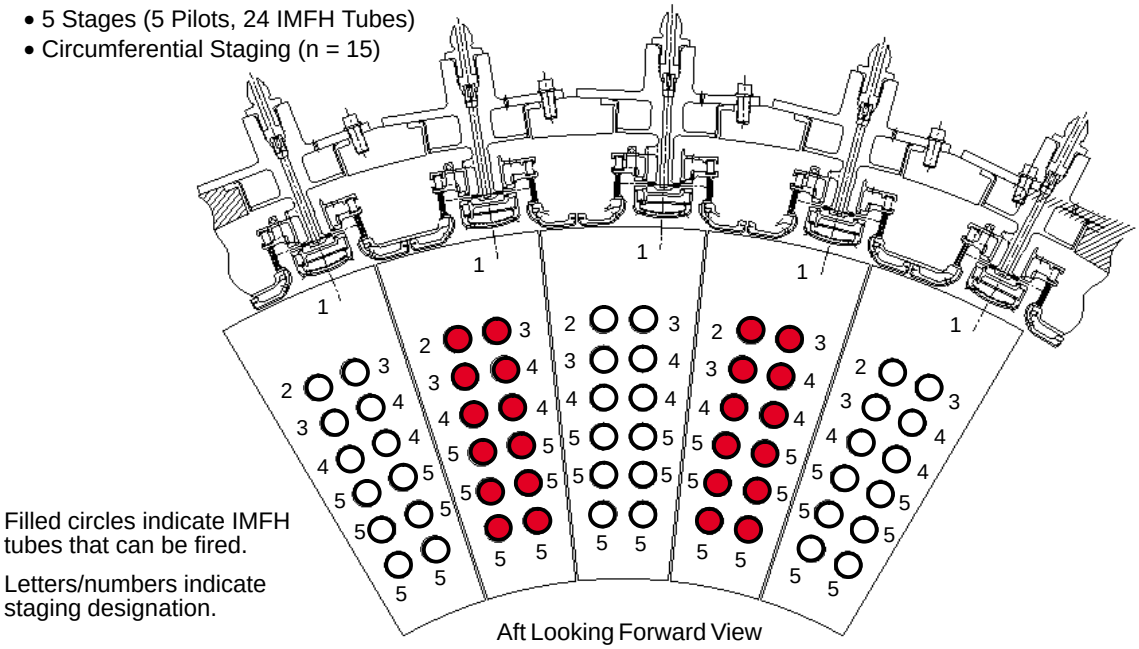

Figure 151. LPP Moderately Mixed MRA Curved Sector Build 2 Fuel Staging

row, or as a total ganged sample. Not all combinations were measured at each point because of the significant amount of time required to do so. The data ganged by rake and by row were useful in understanding emissions and temperature profiles at the aft end of the combustor, while the ganged totals provided overall emissions information.

This sector became a workhorse in development of the LPP sector concept. Nearly 550 data points were acquired during approximately 275 hours of fired testing of the three sector builds. Considering the hardware was designed for less than 100 hours of testing, it proved to be quite resilient.

Build 1

Build 1 of the MRA curved sector was the first look at the performance of the new design. The testing was performed at GEAE from February 21 through March 17, 1997. Five fueling stages were available, as was shown in Figure 149. The test was extremely comprehensive, assessing multiple staging configurations at each of 11 different inlet conditions, as shown in Table 24. This resulted in 111 emissions points being taken over the course of about 65 hours of fired testing. In addition, lightoff and lean blowout data were acquired at four different conditions.

Some of the key results are presented in Figures 152 through 159. Although a significant amount of information was learned from this test, the most important item was the demonstration of nominal supersonic cruise NOx and combustion efficiency that easily met the contract requirements. Nominal supersonic cruise NOx EI was only 3.8 (the requirement was 5), and the combustion efficiency was 99.98% (versus a contract requirement of 99.9%)! This was one of the most important and exciting events in the progress of the program since it was the first time that supersonic cruise requirements were met with significant margin.

In addition to the supersonic cruise data, emissions were acquired at every other key operating condition in the flight envelope. Emissions at each of these cycle points have been estimated and are shown in Table 25. As was observed in the HMMRA sector, the subsonic cruise point tended to fall right at a staging point. This resulted in high NOx with only three stages fired (because of the high flame temperature required to meet T_4) but was near blowout when a fourth stage was brought on line. Ground idle data were quite good overall, with NOx EI below 4 and combustion efficiency above 99%. CO EI was a bit high at 20 but was not out of line relative to current engines. Note that all of the estimates in the table are based on the limitations of a system with five fuel stages and the associated minimum step changes in fueling requirements. As will be shown in Build 3 — which used eight stages — other emissions levels can be achieved, many of which improve upon those shown here. The only limitations are obviously at low power (ground idle), which would typically be pilot-only operation, and at high power, in which all stages are fired.

Lightoff and lean blowout data for the sector are presented in Table 26. Note that each of these was a single test point; multiple tests undoubtedly would introduce variability around the numbers shown here. The results were encouraging, with both GI lightoff and windmill relights demonstrated using a commercial ignitor.

Combustor exit profiles are shown in Figure 159. All were strongly outer-peaked until the fifth stage was lit, at which time the profile became essentially flat. The profiles were of some concern, since the preference is to have nearly center-peaked profiles entering the turbine; outer-peaked profiles tend to reduce turbine efficiency. These concerns would be addressed in Builds 2 and 3 by introducing circumferential fuel staging into the combustor.

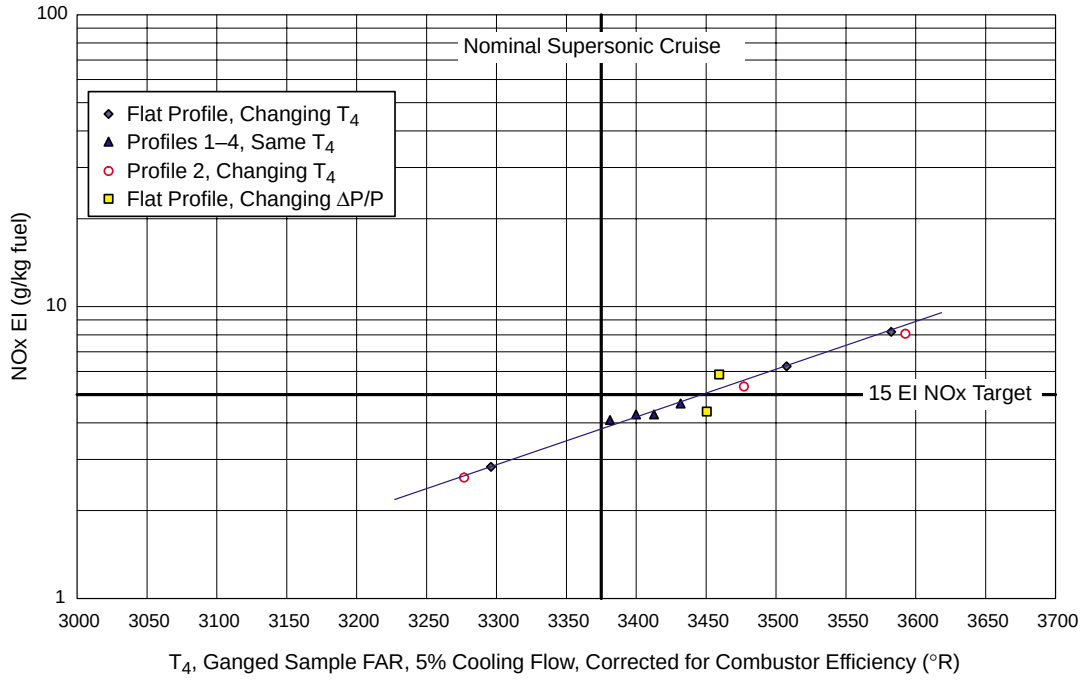

Figure 152. LPP MRA Curved Sector Build 1 Supersonic Cruise NOx Emissions

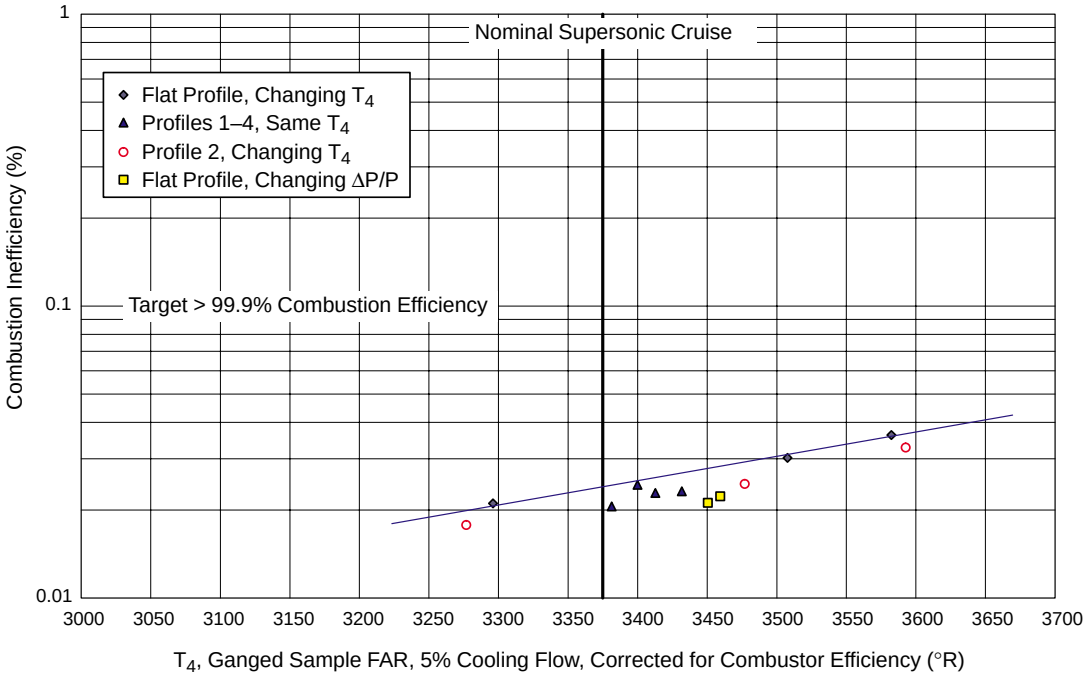

Figure 153. LPP MRA Curved Sector Build 1 Supersonic Cruise Combustion Inefficiency

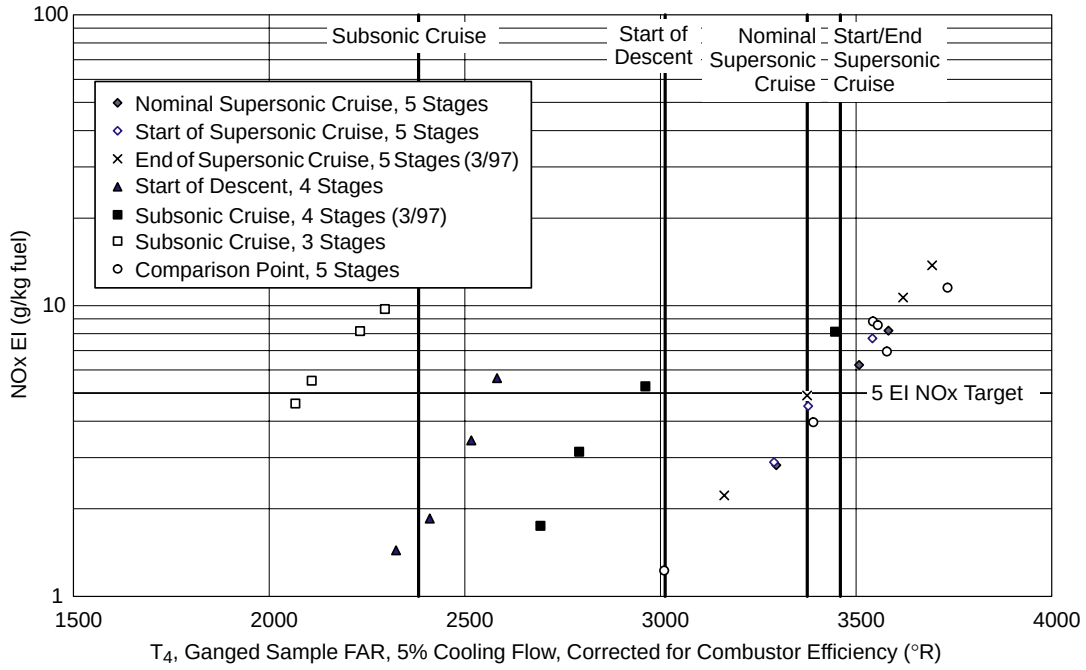

Figure 154. LPP MRA Curved Sector Build 1 Non-LTO NOx Emissions

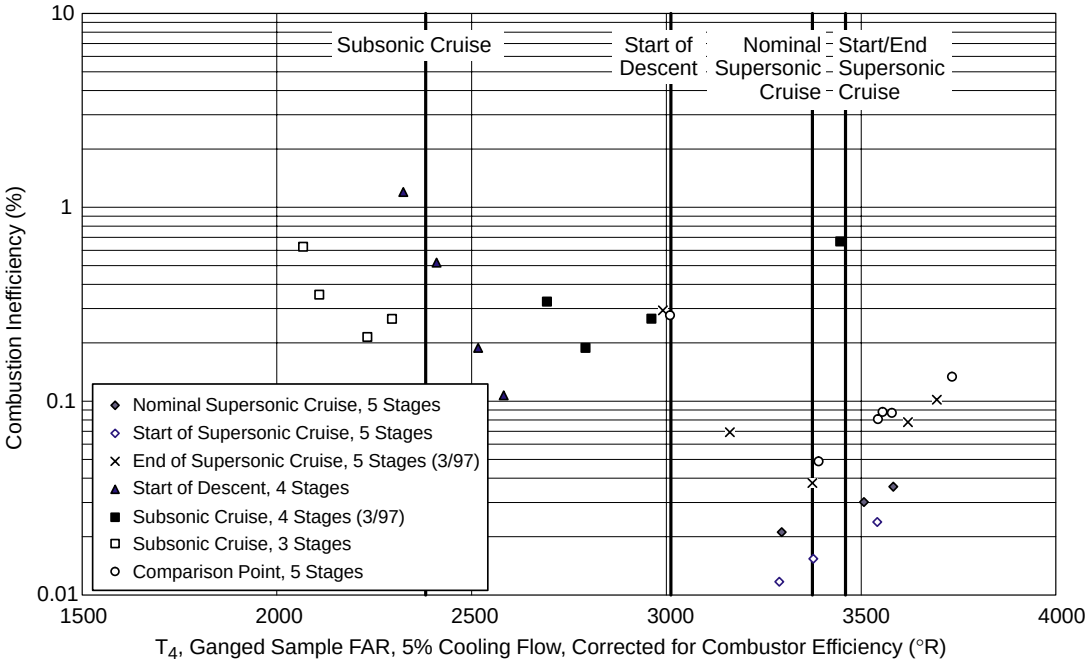

Figure 155. LPP MRA Curved Sector Build 1 Non-LTO Combustion Inefficiency

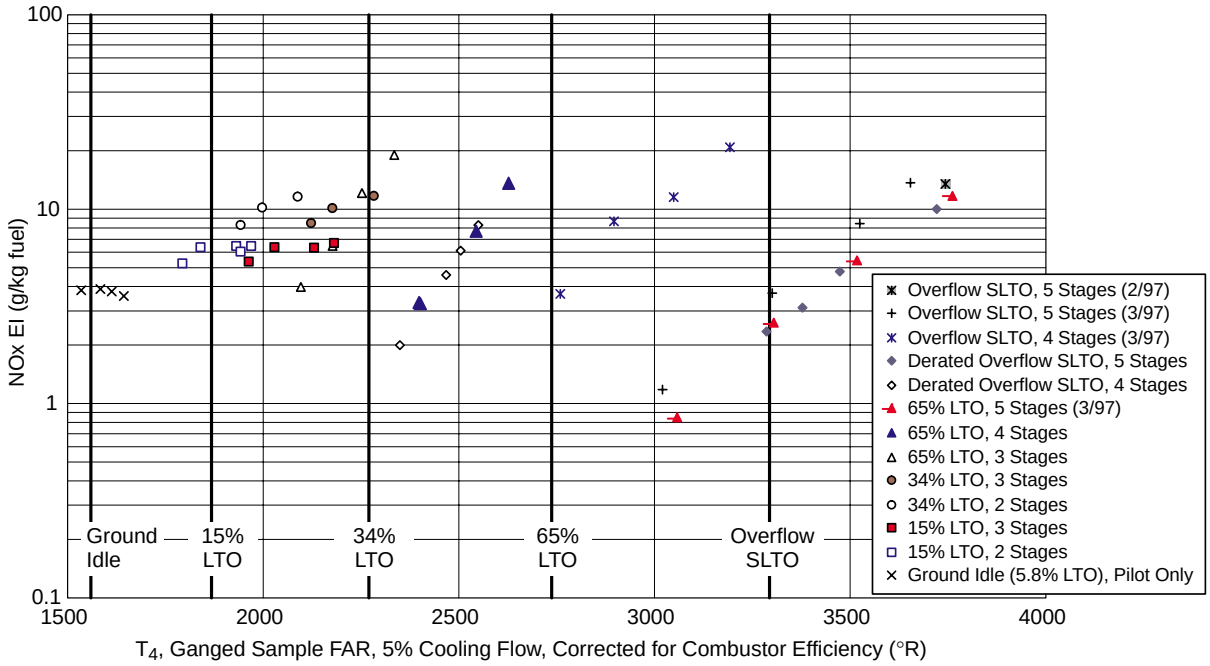

Figure 156. LPP MRA Curved Sector Build 1 LTO NOx Emissions

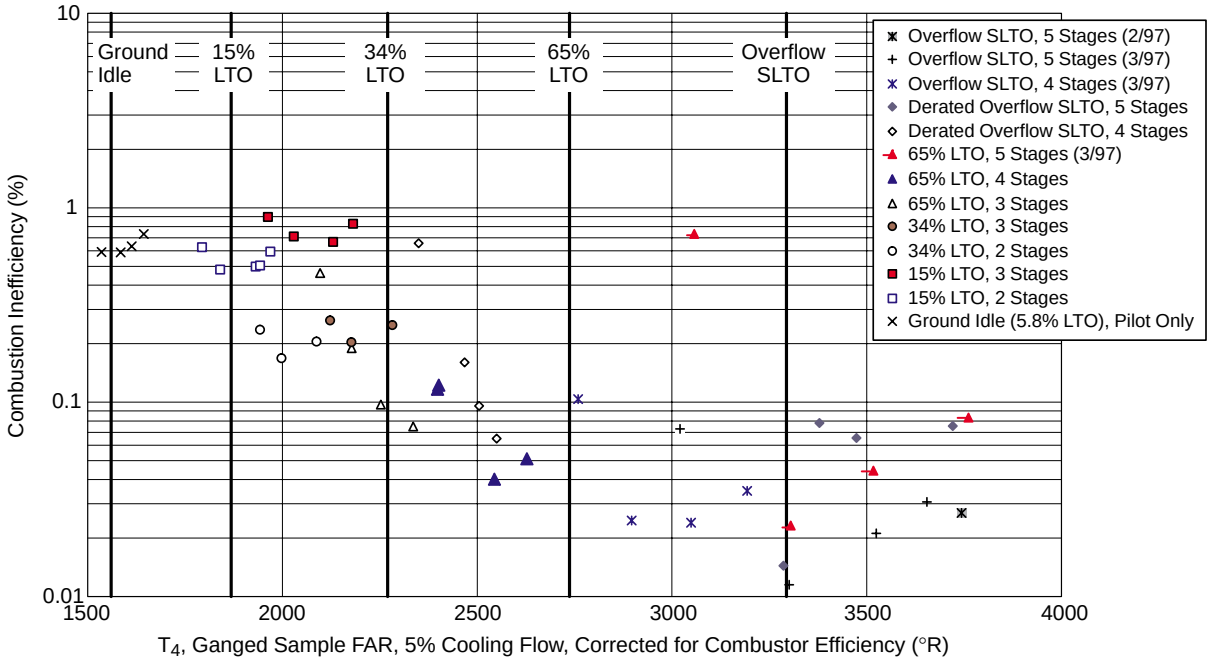

Figure 157. LPP MRA Curved Sector Build 1 LTO Combustion Inefficiency

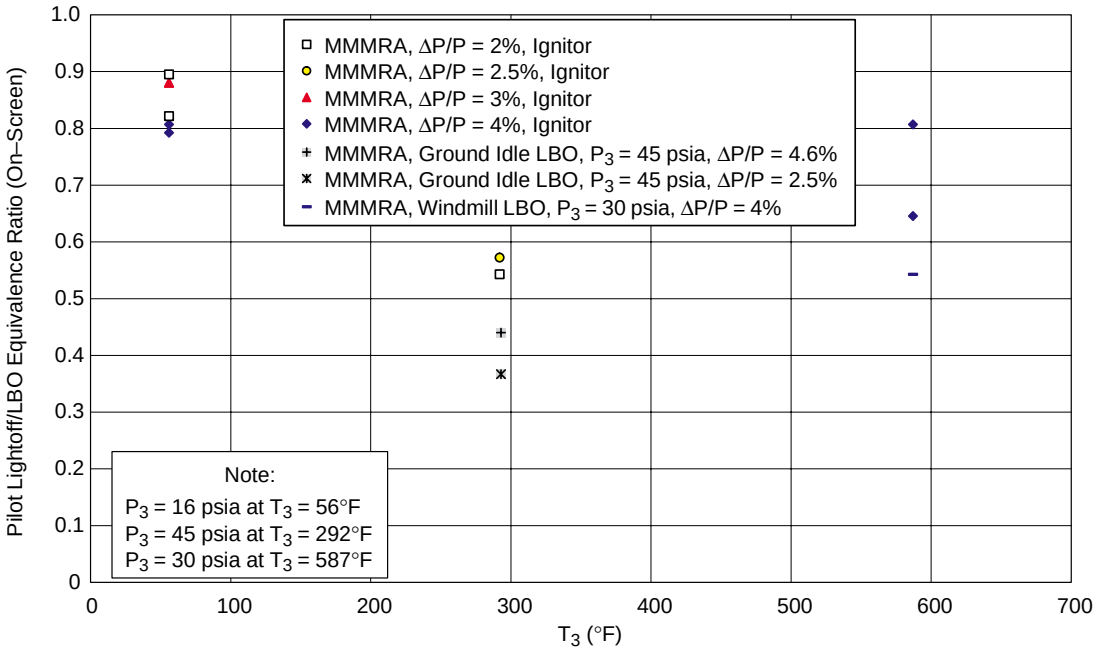

Figure 158. LPP MRA Curved Sector Build 1 Pilot Lightoff and Lean Blowout Results

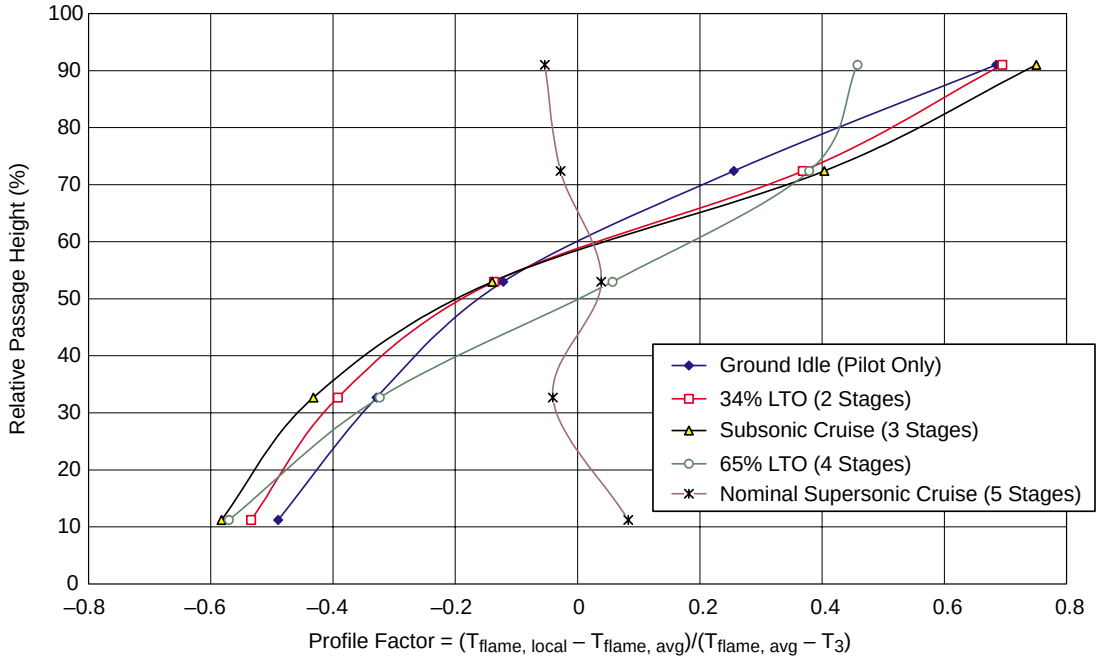

Figure 159. LPP MRA Curved Sector Build 1 Combustor Radial Exit Profiles

Table 24. LPP Moderately Mixed MRA Sector Build 1 – Summary of Conditions Tested

Test Conditions Simulated	T_3 (ºF)	T_3 (ºR)	P_3 (psia)	ΔP/P (%)	Stages Fired	Tflame (ºR)
Ground Idle	280	740	46	4.8	1 of 5	3563–3869
15% LTO	443	903	81	4.2–4.6	2 of 5 3 of 5	3498–3917 3181–3623
34% LTO	585	1045	135	4.1–4.3	2 of 5 3 of 5	3593–4001 3370–3692
65% LTO	737	1197	216	4.5	3 of 5 4 of 5 5 of 5	3148–3651 3088–3452 3141–3865
Overflow SLTO	920	1380	300	3.8–4.25	3 of 5 4 (Prof) 5 of 5	3605–4243 3777–4463 3095–3845
Derated Overflow SLTO	912	1372	204	4.2	4 of 5 5 of 5	2908–3149 3220–3821
Start of Descent	1035	1495	91	4.7–5.2	4 of 5	2802–3197
Subsonic Cruise	625	1085	80	4.3	3 of 5 4 of 5	3204–3673 3633–4357
Nominal Supersonic Cruise	1200	1660	153	4.25	4 (Plt Off) 5 (Rdc Plt) 5 (Prof) 5 of 5	3853–3822 3492–3557 3349–3680 3101–3669
Start of Supersonic Cruise	1200	1660	200	4.25	5 of 5	3363–3626
End of Supersonic Cruise	1200	1660	112	4.3	5 of 5	3049–3785
Comparison Point	945	1405	120	4.0–4.4	5 of 5	3080–3833
Ground Start	56	516	16	2.0–6.0	1 of 5	N/A
Ground Idle Lightoff/LBO	292	752	45	1.3–4.6	1 of 5	N/A
LBO/Relights at Windmill	587	1047	30	4.0	1 of 5	N/A

Table 25. LPP Moderately Mixed MRA Sector Build 1 – Emissions Summary

Cycle Point	Stages Fired	T_3 (ºF)	T_3 (ºR)	P_3 (psia)	T_4 (ºR)	Emissions Index (g/kg Fuel)			Combustion Inefficiency (%)	Combustion Efficiency (%)	Notes
						NOx	CO	HC			
Ground Idle	1 of 5	283	743	45	1546	3.9	20	1.3	0.6	99.4	Interpolated values
15% LTO	2 of 5 3 of 5	432	892	82.4	1832	6.35 5	12.4 18	1.9 10.5	0.48 1.6	99.52 98.4	Interpolated values Extrapolated values
34% LTO	2 of 5 3 of 5	568	1028	134	2216	16 11	16 8	0.06 0.35	0.28 0.22	99.72 99.78	Interpolated values Extrapolated values
65% LTO	3 of 5 4 of 5 5 of 5	714	1174	212	2662	[200] 18 [0.2]	[1.5] 2.2 [500]	[0.02] 0.05 [100]	[0.01] 0.057 [90]	[99.99] 99.943 [10]	Need 4 stages Extrapolated values Blowout anticipated
Overflow SLTO	4 of 5 5 of 5	919	1379	301.3	3294	30.2 3.7	1.8 0.31	0.05 0.04	0.047 0.011	99.953 99.989	Extrapolated values Interpolated values
Start of Descent	4 of 5	1039	1499	90	3012	[100]	[0.1]	[0.01]	[0.01]	[99.99]	Need 5 stages
Subsonic Cruise (SSC)	3 of 5 4 of 5	630	1090	80	2382	14 [1]	18 [24]	0.075 [100]	0.4 [10]	99.6 [90]	Extrapolated values Interpolated values
Nominal SSC	5 of 5	1200	1660	150	3375	3.8	0.83	0.045	0.023	99.977	Interpolated values
Start of SSC	5 of 5	1200	1660	200	3460	5.9	0.6	0.05	0.019	99.981	Interpolated values
End of SSC	5 of 5	1200	1660	110	3460	5.2	2	0.024	0.05	99.95	Interpolated values

Table 26. LPP Moderately Mixed MRA Sector Build 1 – Lean Blowout and Lightoff Summary, One Stage Fired

Cycle Point	T_3 (ºF)	T_3 (ºR)	P_3 (psia)	ΔP/P (%)	Lightoff FAR_{pilot}	LBO FAR_{pilot}
Ground Start	56	516	16	1.9	0.0585	–
	56	516	16	3	0.0600	–
	56	516	16	3.9	0.0545	–
	56	516	16	5.4	No Light	–
Ground Idle Lightoff	292	752	43	1.3	No Light	–
	292	752	45	2.1	0.037	–
	292	752	46	2.5	0.039	–
Ground Idle Lean Blowout	293	753	45	2.5	–	0.025
	293	753	45	4.6	–	0.030
Windmill Relight	587	1047	30	3.9	0.055	–
	587	1047	30	4	0.044	–
Windmill LBO	587	1047	30	4	–	0.037

Build 2

Build 2 of the MRA curved sector was tested at GEAE September 5 – 10, 1997. Over the course of more than 50 hours of fired testing, 116 emissions points were taken covering seven different inlet conditions, as shown in Table 19 (page 105). The purpose of the test was to look at the possibility of using circumferential fuel staging in the combustor. Build 1 data indicated the combustor exit profiles were strongly outer-peaked at low power (when partially staged). Circumferential staging offers the potential to reduce this effect by firing every other IMFH tube bank at low power (see Figure 160). As power increases, more tubes in a given bank are fired (essentially moving radially inward, as in Build 1) before moving to the adjacent bank. While this would help flatten the exit profile radially, it obviously brings up concerns about the resulting circumferential profiles. Also of concern was the impact on emissions, since more hot/cold interfaces exist with circumferential staging. This has the potential to increase CO at low power. Since all IMFH tubes would still be fired at high power, emissions would not change at these conditions. Therefore, they were not retested.

The results of the test are presented in Figures 161 through 165. Circumferential staging was very effective in flattening the radial exit temperature profiles, but it clearly introduced more circumferential variation. Emissions did not appear to be strongly impacted by the new staging modes, but it is difficult to compare these data directly to Build 1 because there are only a few cases in which the same number of IMFH tubes are fired for a given operating condition. Additionally, the odd number of IMFH tube banks (five) may bias the results since it includes a half cycle. This results in only two of five banks being fired, instead of two of every four. However, the fact that circumferential staging was so effective makes it a powerful tool for flattening the part-power radial profiles.

This test was inhibited by the staging limitations of the original sector (five stages). This made it difficult to operate the system at an optimized staging configuration for a given power setting.

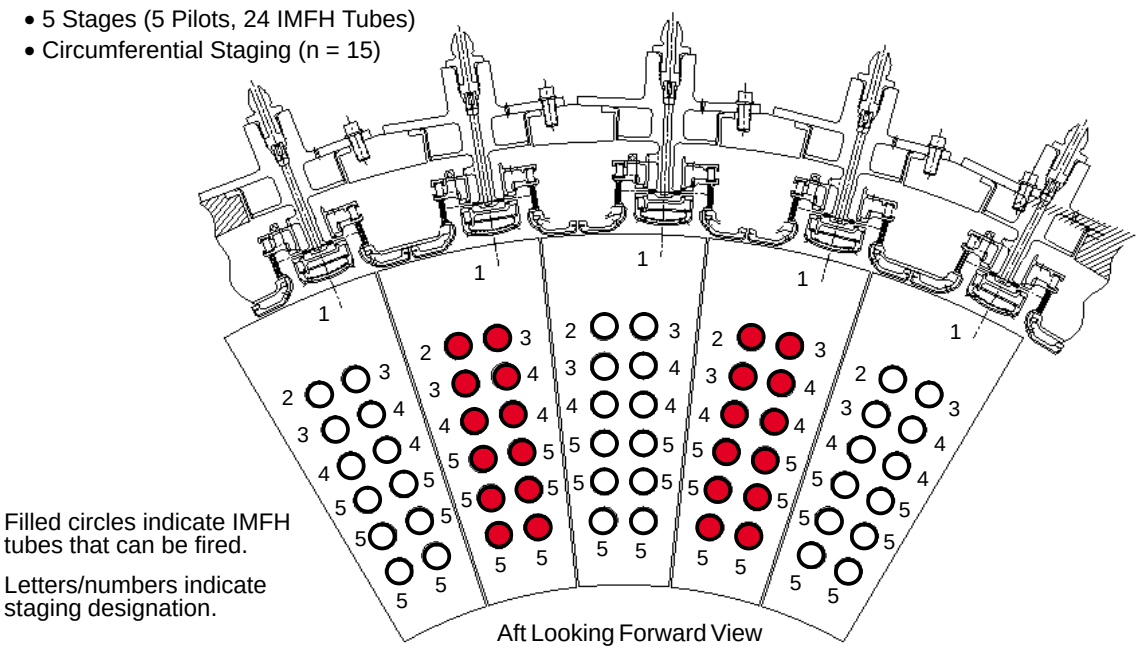

Figure 160. LPP MRA Curved Sector Build 2 Combustor Fuel Staging

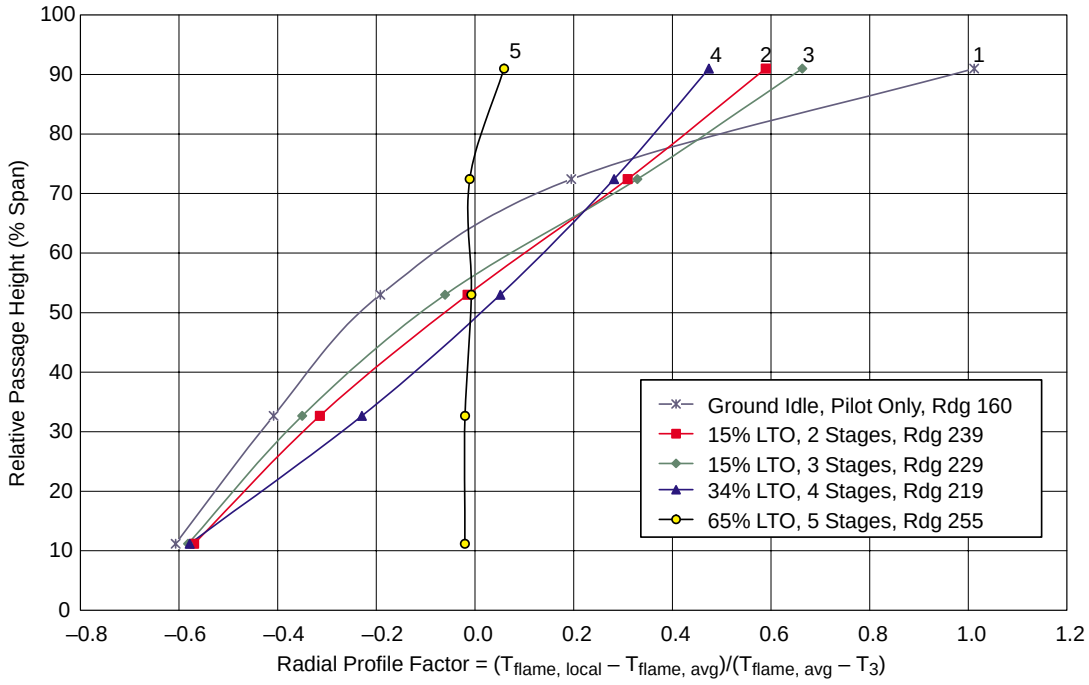

Figure 161. LPP MRA Curved Sector Build 2 Combustor Radial Exit Profiles

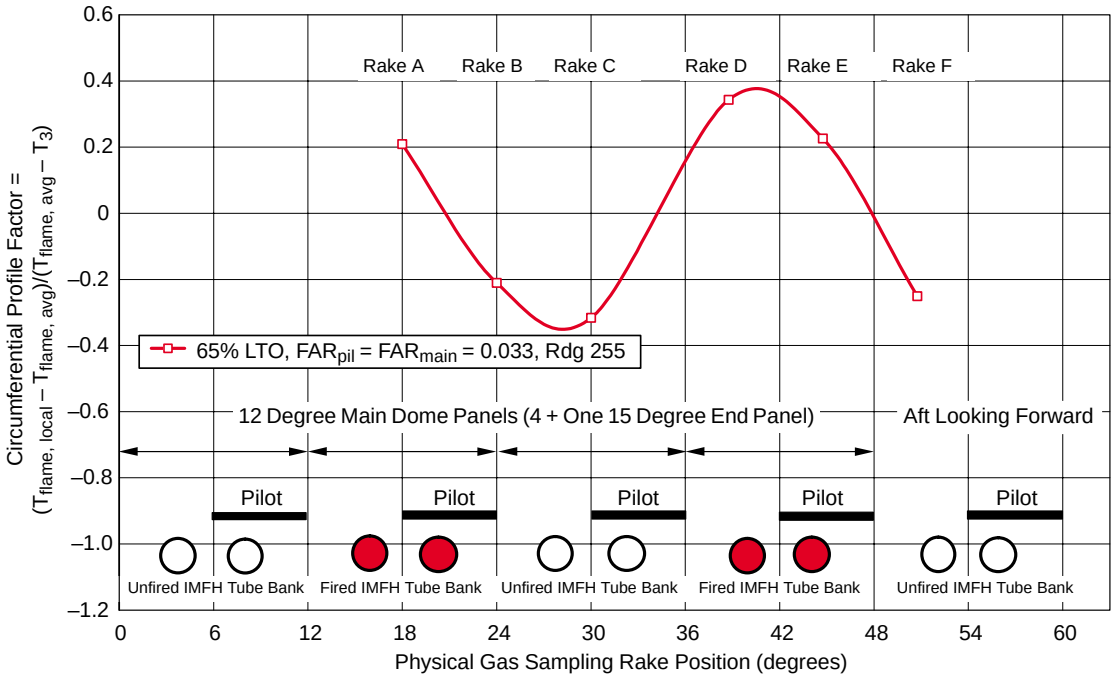

Figure 162. LPP MRA Curved Sector Build 2 Combustor Circumferential Exit Profiles

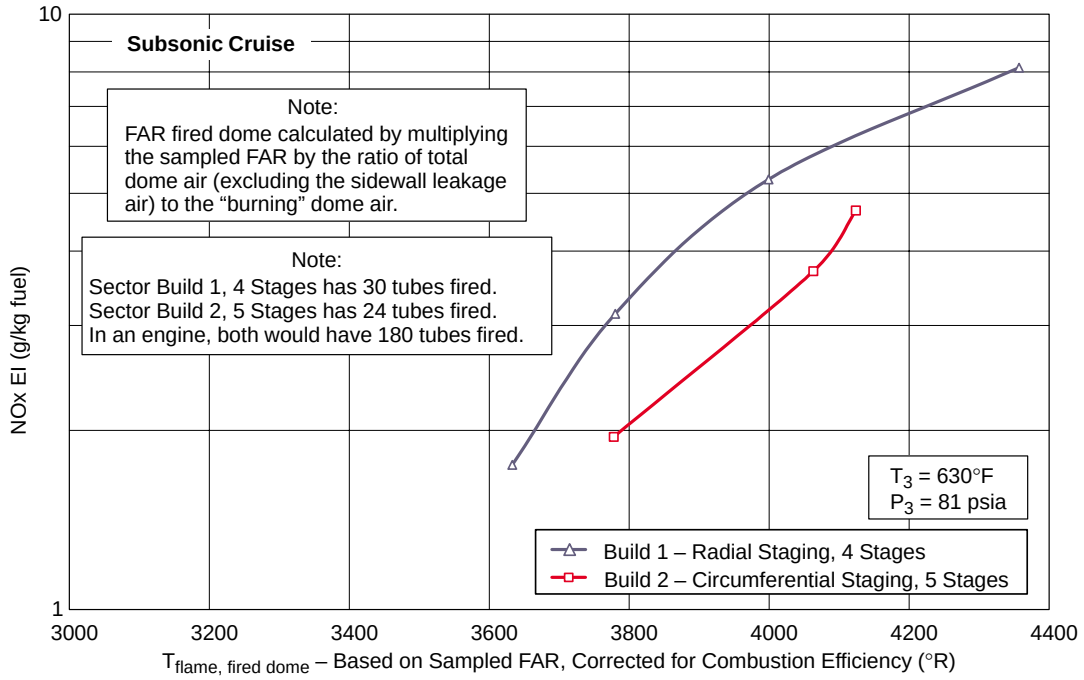

Figure 163. LPP MRA Curved Sector Radially and Circumferentially Staged Subsonic Cruise NOx Emissions

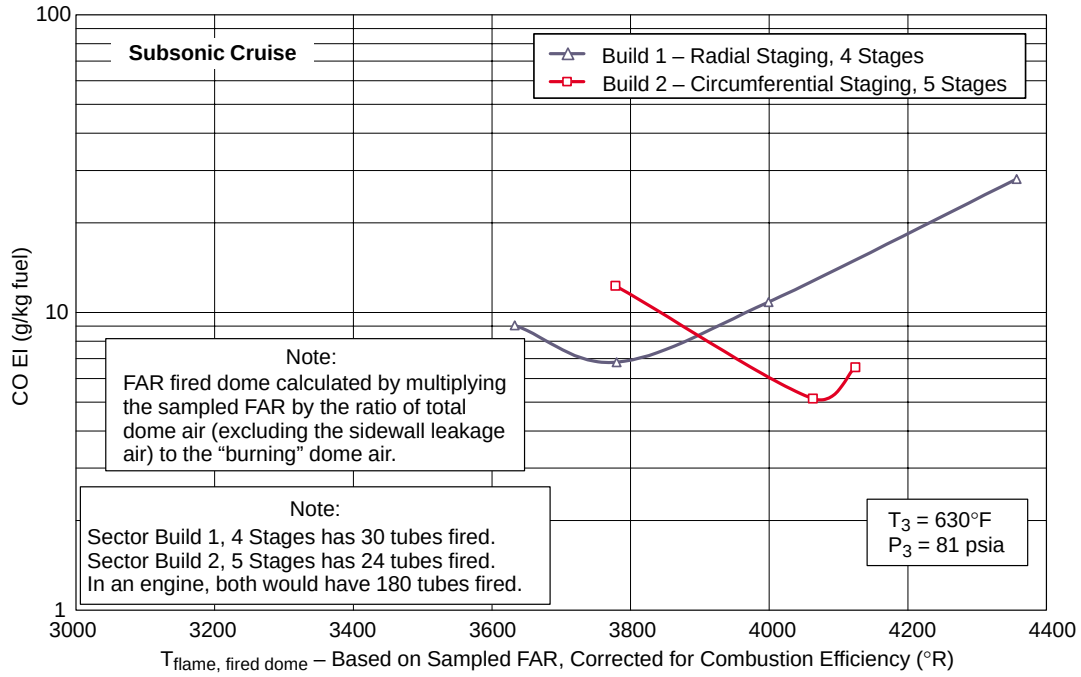

Figure 164. LPP MRA Curved Sector Radially and Circumferentially Staged Subsonic Cruise CO Emissions

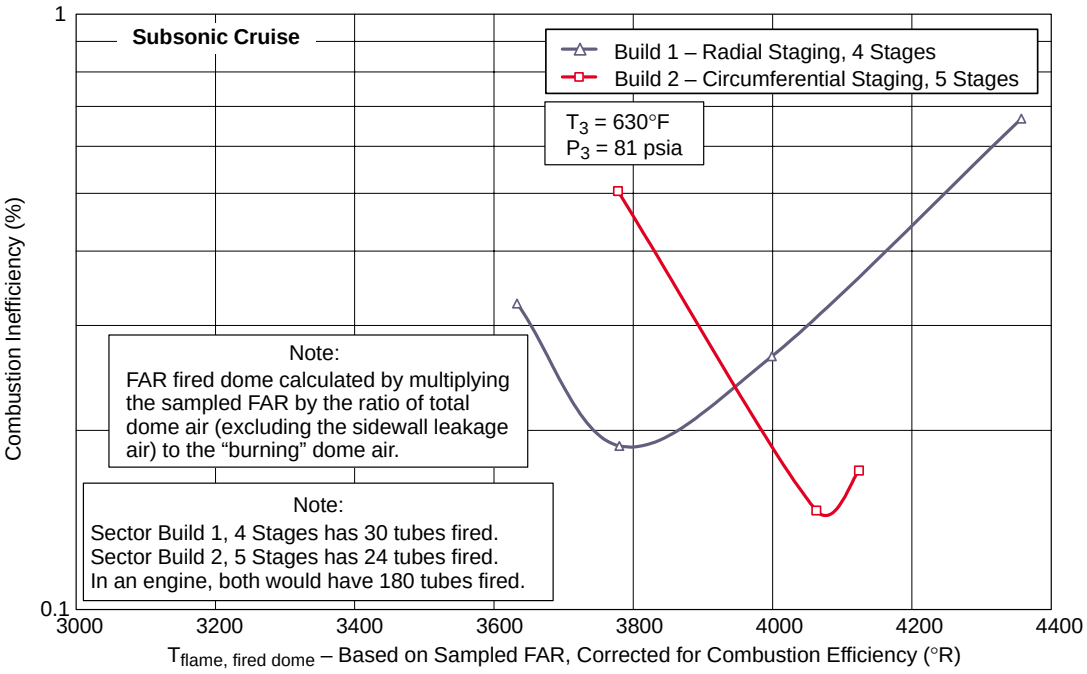

Figure 165. LPP MRA Curved Sector Radially and Circumferentially Staged Subsonic Cruise Combustion Inefficiency

Additionally, it was desired that a second type of circumferential staging be tested. The first type (tested here in Build 2) was called "n = 15" circumferential staging because 15 (of 30) of the IMFH tube banks are fired prior to firing tubes in the adjacent banks. Thus, the turbine sees 15 temperature cycles per revolution. The second type (to be tested in Build 3) was called "n = 30" circumferential staging. In this case, the left column of tubes in each bank of IMFH tubes (aft looking forward) is fired prior to moving to the adjacent column. Thus, the turbine sees 30 temperature cycles per revolution. This tends to produce a smoother exit profile (circumferentially) than the n = 15 mode, but it introduces more cold/hot interfaces. This has the potential to increase CO. Build 3 of the sector increased the number of available stages to eight and greatly increased the flexibility of the system by making each stage in a given IMFH tube bank independent from the adjacent bank.

Build 3

Build 3 of the MRA curved sector was tested at GEAE from January 22 through April 23, 1998. Over the course of about 150 hours of fired testing, 319 emissions points were taken covering seven different inlet conditions, as was shown in Table 19 (page 105). Build 3 comprised several subtests, Table 27. The purpose of this series of tests was to look at a variety of potential fuel-staging options and discover which provide the best balance of emissions and exit profiles for use in an engine. As stated above, the number of fuel stages was increased to eight for this test. In addition, flexibility was added so that any stage in any tube bank could be fired at any time. This allowed for the testing of both n = 15 and n = 30 circumferential staging modes, as shown in Figures 166 and 167. This refers to the number of temperature cycles per revolution that the turbine would see as a result of the circumferential staging. Note that each of the stages was independent of the others, and could be fired in any pattern (for example, stages B and F could be fired together, if desired).

Table 27. LPP Moderately Mixed MRA Sector Build 3 – Summary of Conditions Tested

Cycle Point	T_3 (°F)	T_3 (°R)	P_3 (psia)	T_4 (°R)	Build					
					3A1 (n = 15)	3A2 (n = 30)	3A3 (n = 15)	3A4 (n = 30)	3A5 (No Film Cooling)	3A6 (Film Cooling)
Ground Idle	295	755	45	1560		X	X	X	X	X
15% LTO	446	906	82	1868	X	X	X	X	X	X
34% LTO	588	1048	134	2270	X	X	X	X	X	X
65% LTO	740	1200	212	2737	X		X		X	
100% LTO	919	1379	301	3294						
Nominal Subsonic Cruise	630	1090	80	2382	X	X	X	X	X	X
Nominal Supersonic Cruise	1200	1660	150	3375		X		X		

Some of the key results are presented in Figures 168 through 173. The n = 15 and n = 30 circumferential modes were both successful in improving radial exit profiles. Circumferentially staged emissions show slightly higher CO and lower combustion efficiency than the radial staging but also appear to offer a bit lower NOx. In general, the "block" type of radial staging used in Build 1 provides lower part-power emissions than circumferential staging, but it produces less desirable exit temperature profiles. Circumferential staging appears to offer a reasonable balance between exit profiles and emissions.

The MMMRA sector proved extremely successful. It was tested over the entire range of cycle conditions in the flight envelope with excellent emissions results. Ground idle and subsonic cruise

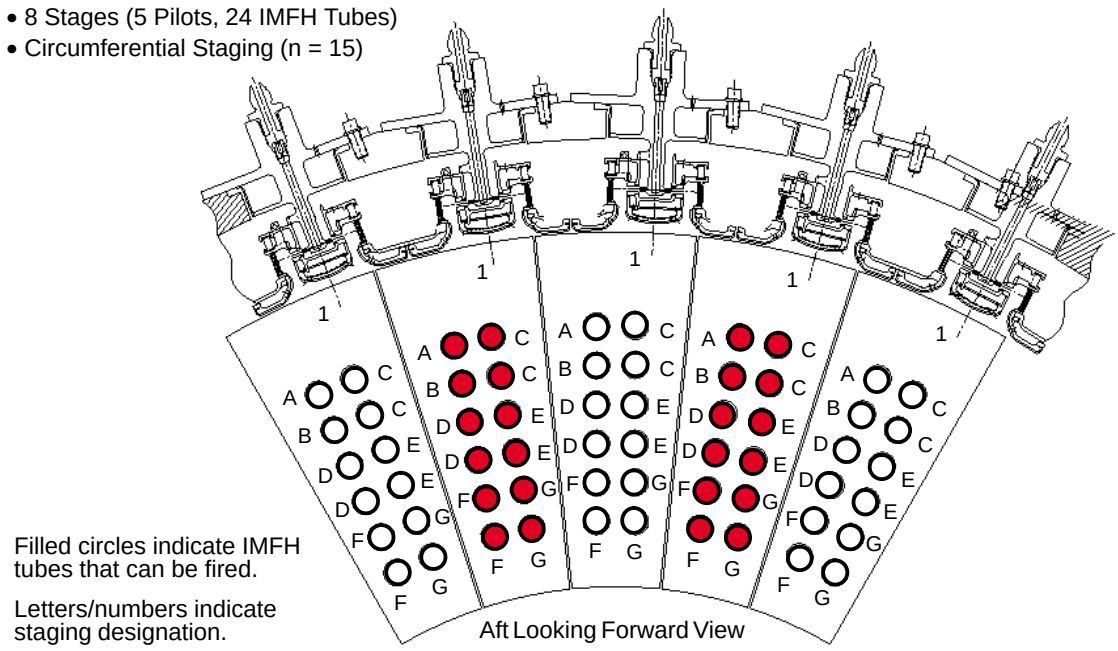

Figure 166. LPP MRA Curved Sector Build 3A1 Combustor Fuel Staging

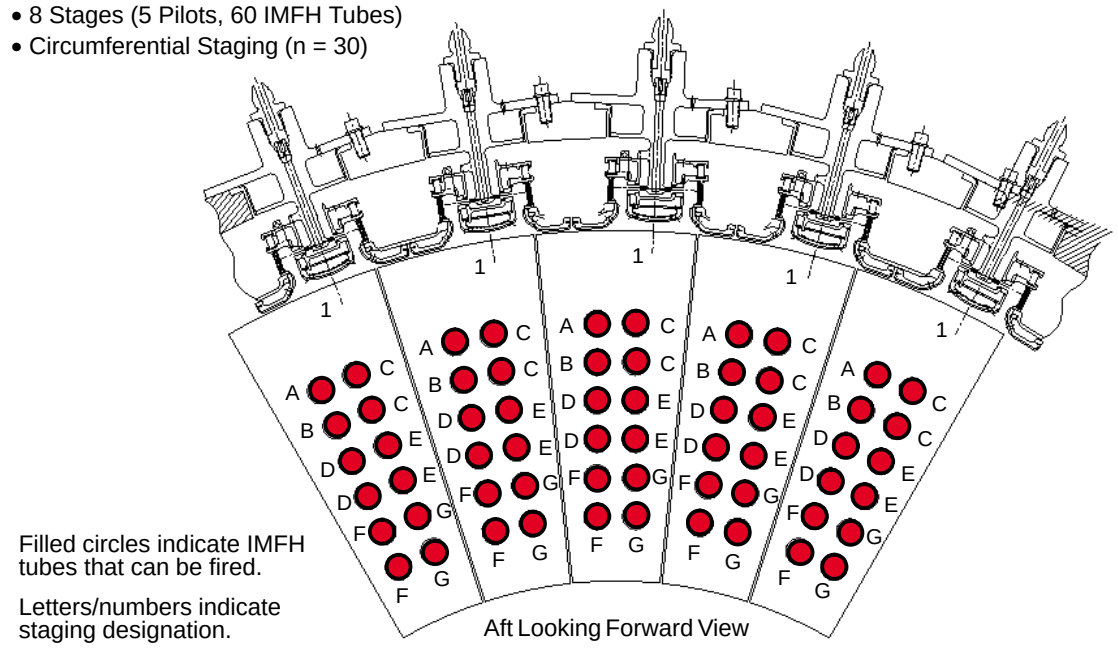

Figure 167. LPP MRA Curved Sector Build 3A2 Combustor Fuel Staging

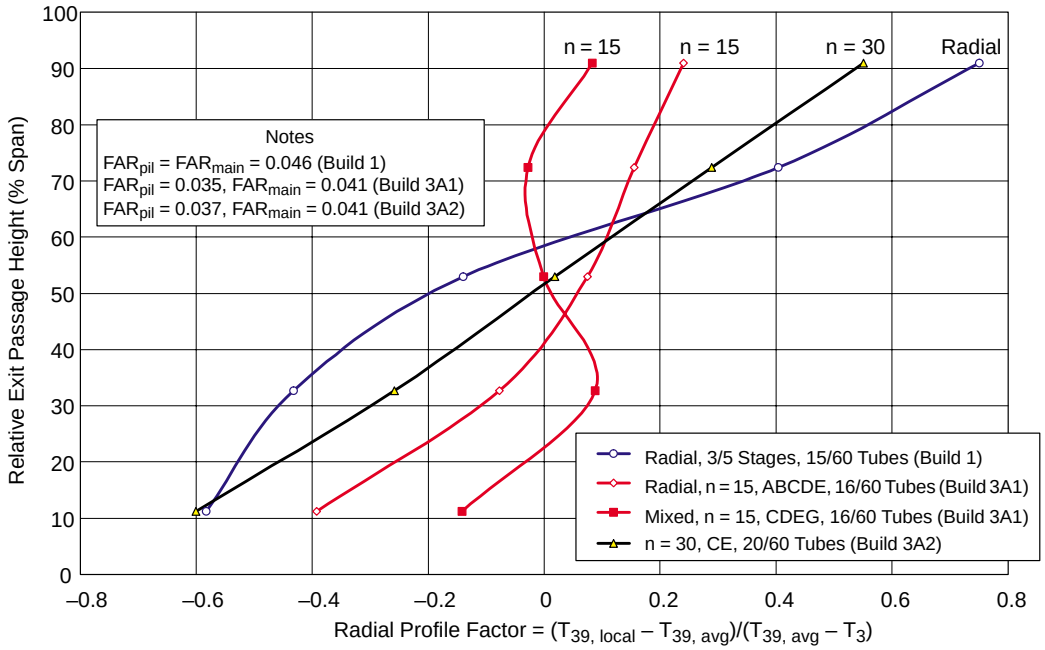

Figure 168. LPP MRA Curved Sector Radial Exit Profile Fuel Staging Mode Comparisons

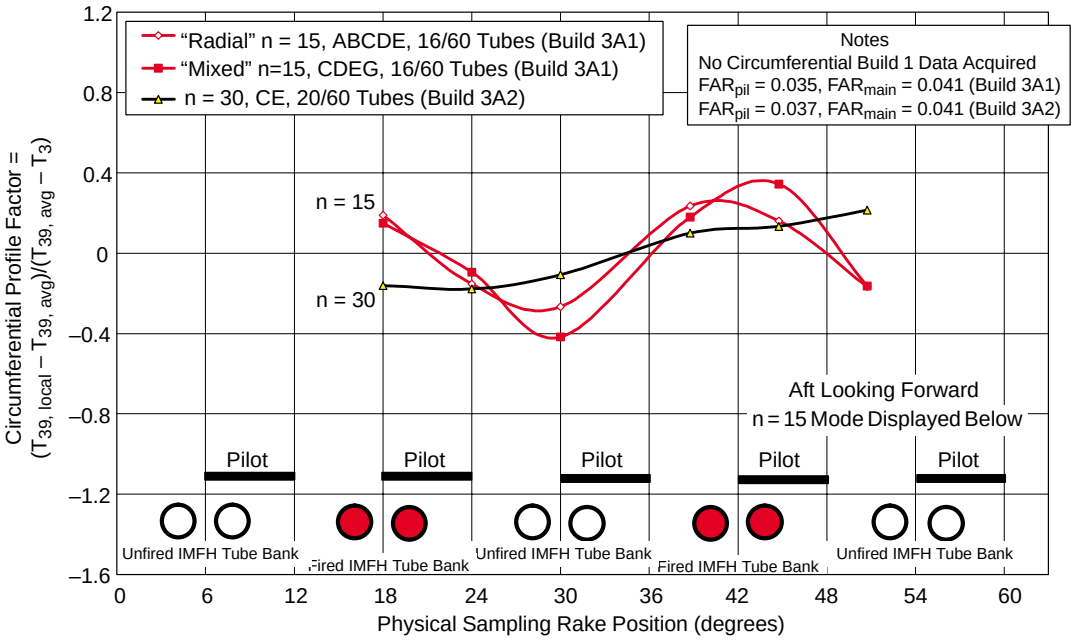

Figure 169. LPP MRA Curved Sector Circumferential Exit Profile Fuel Staging Mode Comparisons

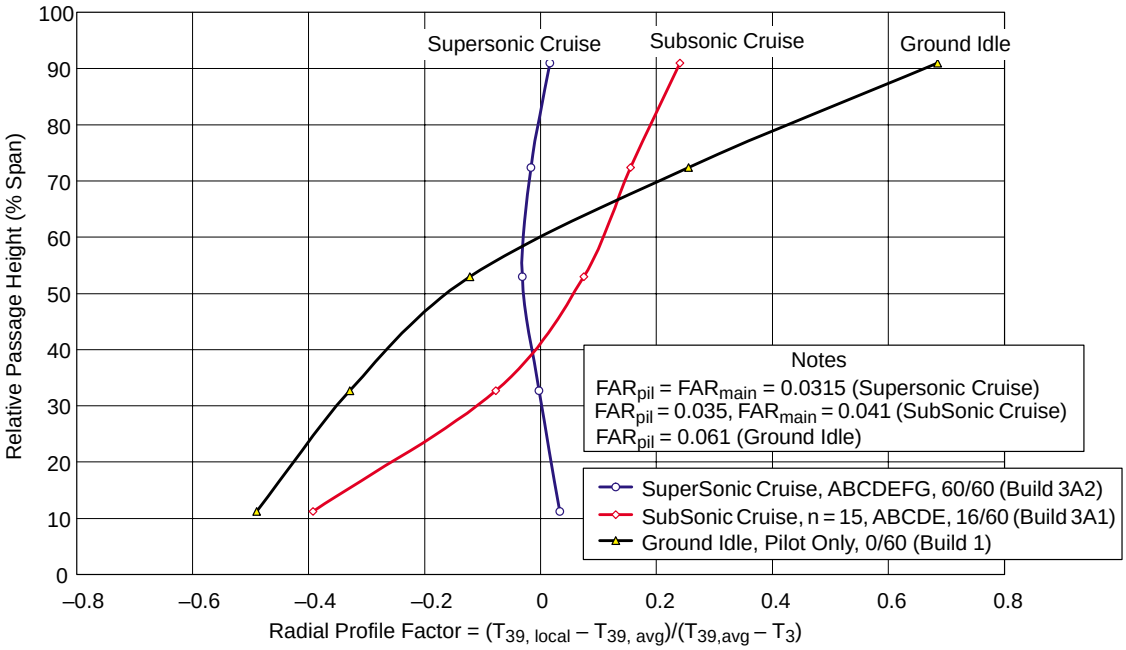

Figure 170. LPP MRA Curved Sector Radial Exit Profile Comparisons

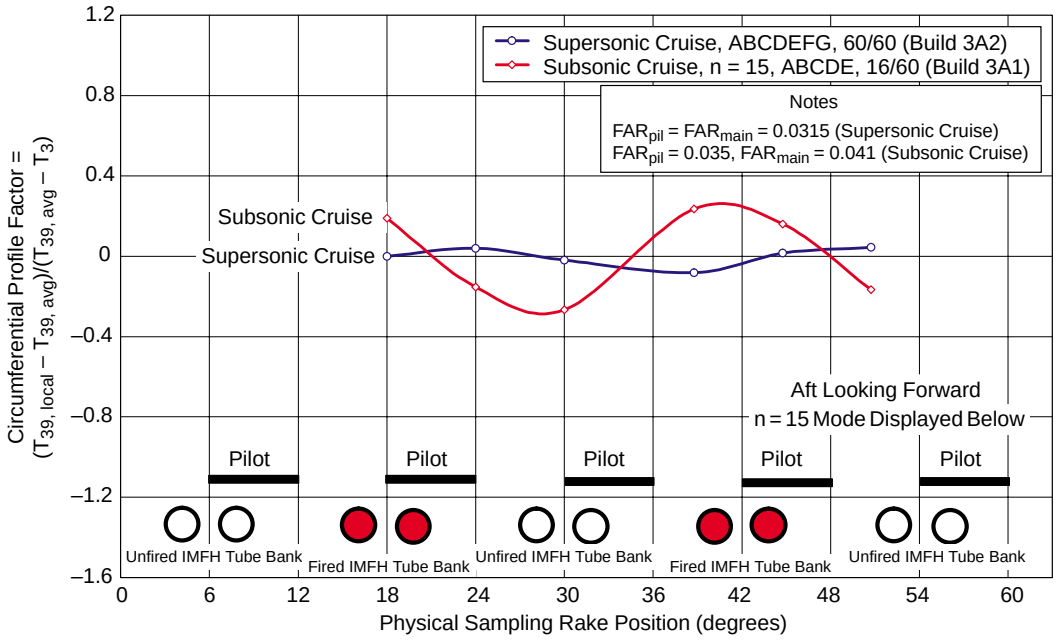

Figure 171. LPP MRA Curved Sector Circumferential Exit Profile Comparisons

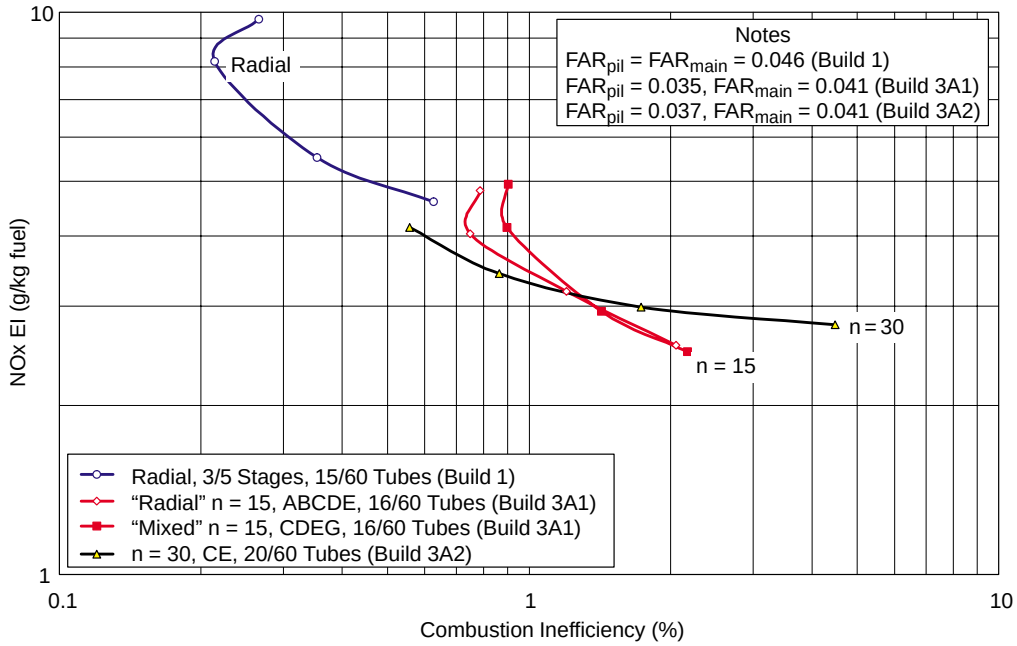

Figure 172. LPP MRA Curved Sector Subsonic Cruise NOx vs Combustion Inefficiency Fuel Staging Mode Comparisons

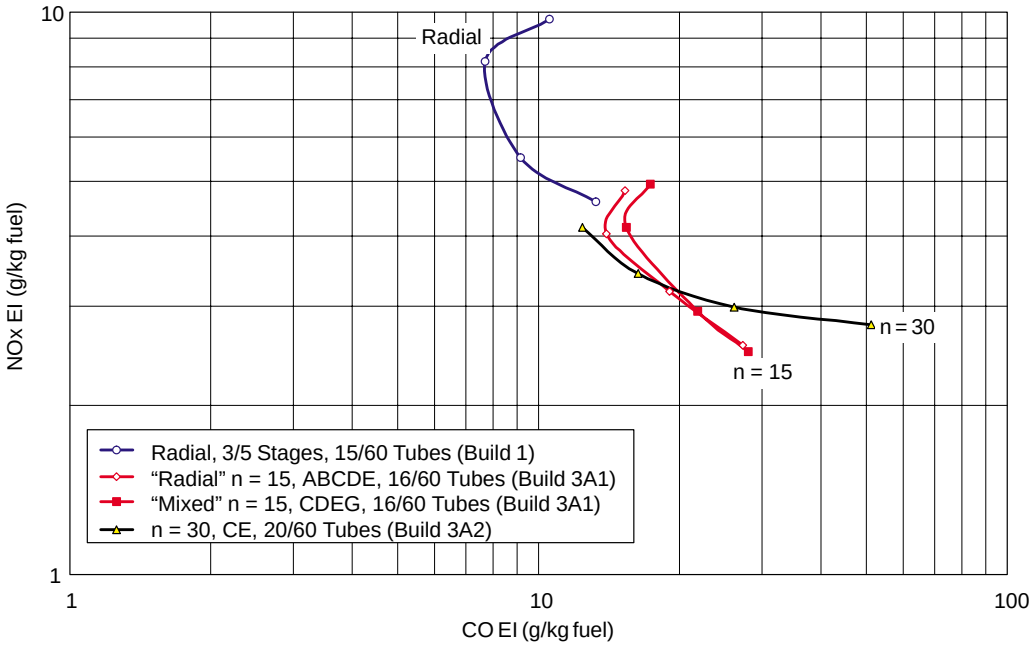

Figure 173. LPP MRA Curved Sector Subsonic Cruise NOx vs CO Fuel Staging Mode Comparisons

emissions were quite good, although GI CO emissions were a little higher than desired. Most importantly, the design demonstrated significant margin in meeting supersonic cruise NOx requirements. Finally, the introduction of circumferential staging appeared to offer exit profile improvement without detrimental impact to emissions. Success of the MMMRA sector eventually led to the selection of the LPP concept over RQL designs for continued full-scale development.

4.5.2.7 Cold-Flow Full-Annular Diffuser Rig

The cold-flow, full-annular, diffuser rig was tested at NASA–Glenn in November and December 1998. Although it was a full-annular test and not actually a sector, discussion is best placed along with the sector results. The test was set-up to quantify the effectiveness of the diffuser and determine the resulting air flow distribution in an MRA concept combustor. This particular rig was modeled after the "moderately mixed" MRA design described previously and is shown in Figure 174. It was made primarily of plastic (stereolithographic apparatus, SLA) and aluminum since it was to be operated at room temperature and low pressure. It was heavily instrumented with more than 200 pressure taps throughout the rig. A full-annular rig was used because end wall effects could have adversely impacted the operation of the diffuser.

Plane 3.0 and 3.1 velocity profiles are shown in Figures 175 and 176. Pressure recovery information is presented in Figures 177 through 179. Note how the velocity profiles changed as each of the three inlet profilers were used. The results indicate that the diffuser worked well, although some evidence suggests that the center passage of the diffuser may be separating (see Figure 176). This was demonstrated by the fact that changing the inlet profile changed the resultant velocity profile through the middle passage. However, because no large velocity defect or reverse flow was observed, it does not appear the middle passage had actually separated.

The full-annular diffuser rig completed the series of LPP sector tests.

4.5.3 Rich/Quench/Lean Systems

4.5.3.1 Integrated Module Rig – Wall Jet

An RQL combustor using the more conventional wall-jet technology was tested in an integrated module rig and demonstrated the capability of achieving EINOx of 13.6 at the supersonic flight condition (relative to the program EINOx goal of 5). This combustor also demonstrated capability of achieving the program goal of 99.9% efficiency at supersonic cruise. However, this wall-jet RQL combustor was operated at an elevated combustor pressure drop, approximately 8.5% (relative to a design target combustor pressure drop of 5%), to achieve this NOx and CO emissions performance. The quench throat diameter and quench extension length were found to be important geometric parameters for controlling the emissions performance of the wall-jet combustor configuration.

Combustion tests of the integrated-module rig were conducted in dedicated facilities in Cell 1E of the Jet Burner Test Stand (JBTS) at United Technologies Research Center. The series was initiated on January 11, 1996 and progressed through March 12, 1997. In this period, 44 tests were conducted.

The integrated module rig combustor contained a modular, 5-inch diameter RQL combustor that allowed evaluation of quench-section geometry components in a size scale consistent with the next major test vehicle anticipated in the program at the time: the subscale annular rig. The integrated module rig combustor was designed to accept either a wall-jet configuration or a convoluted liner/

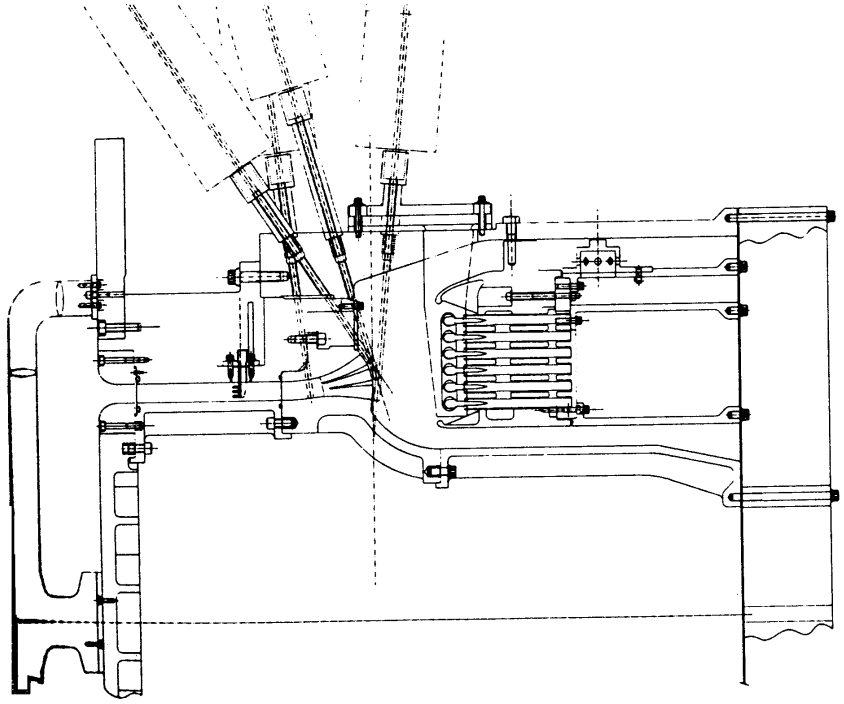

Figure 174. LPP Cold-Flow, Full-Annular Diffuser Rig

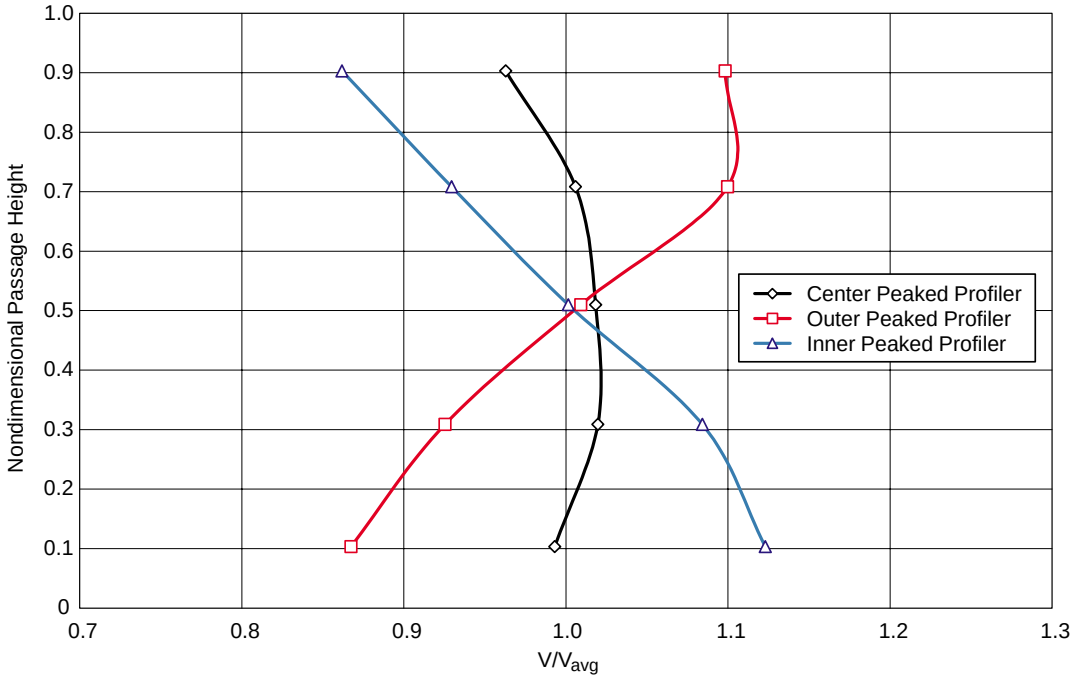

Figure 175. LPP Cold-Flow, Full-Annular Diffuser Test – Plane 3.0 Profiles

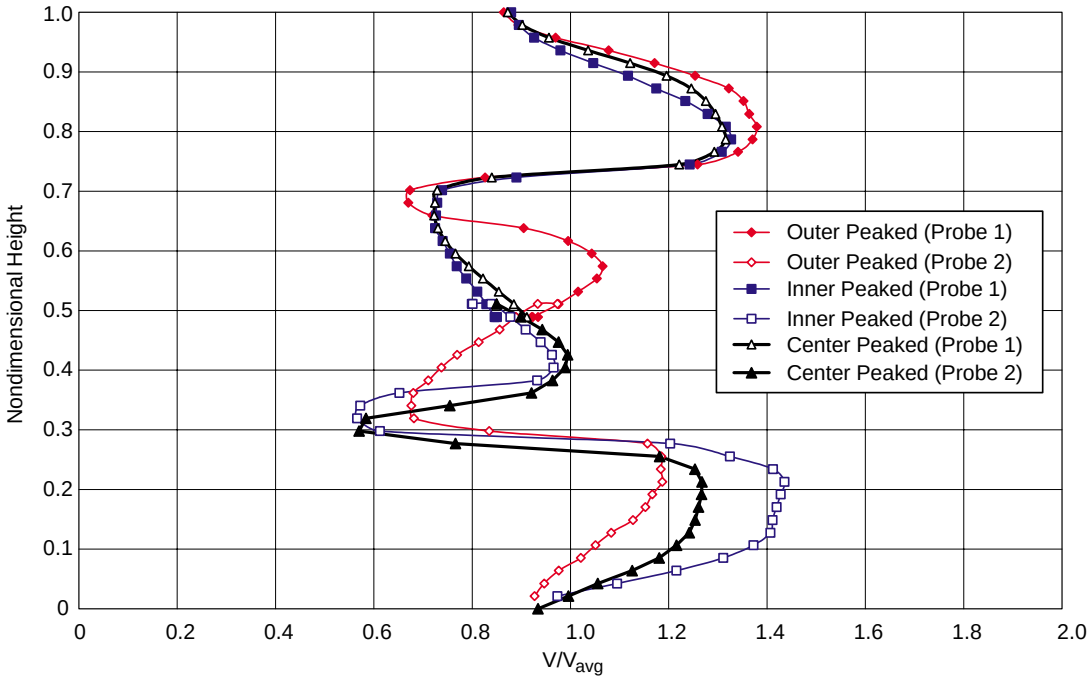

Figure 176. LPP Cold-Flow, Full-Annular Diffuser Test – Plane 3.1 Profiles

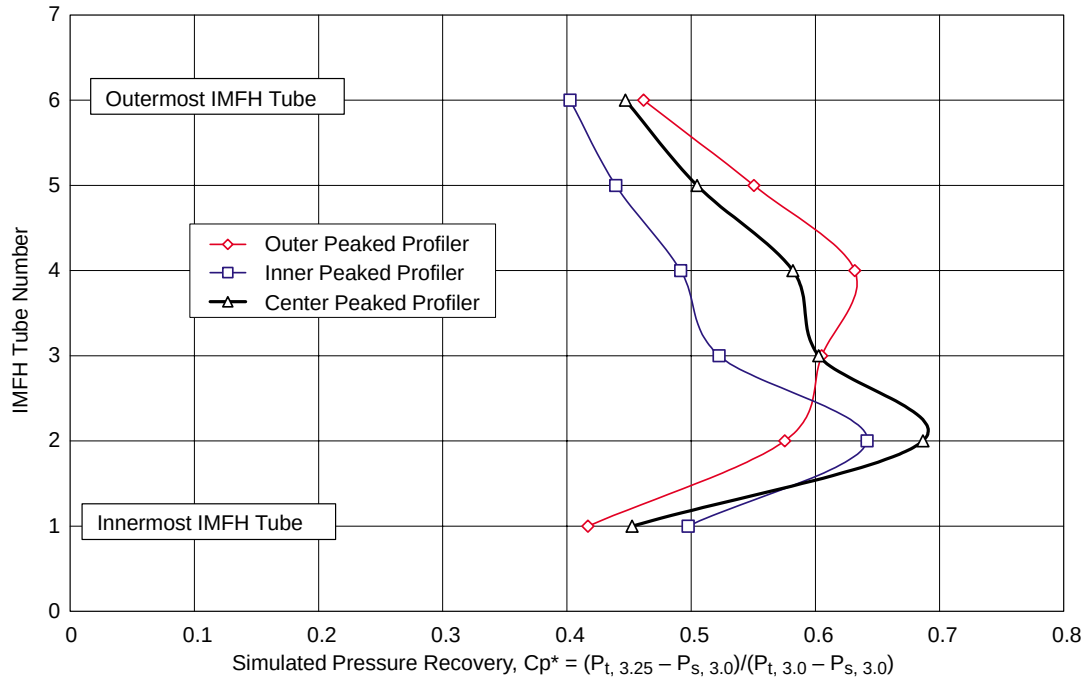

Figure 177. LPP Cold-Flow, Full-Annular Diffuser Test – IMFH Inlet Profiles

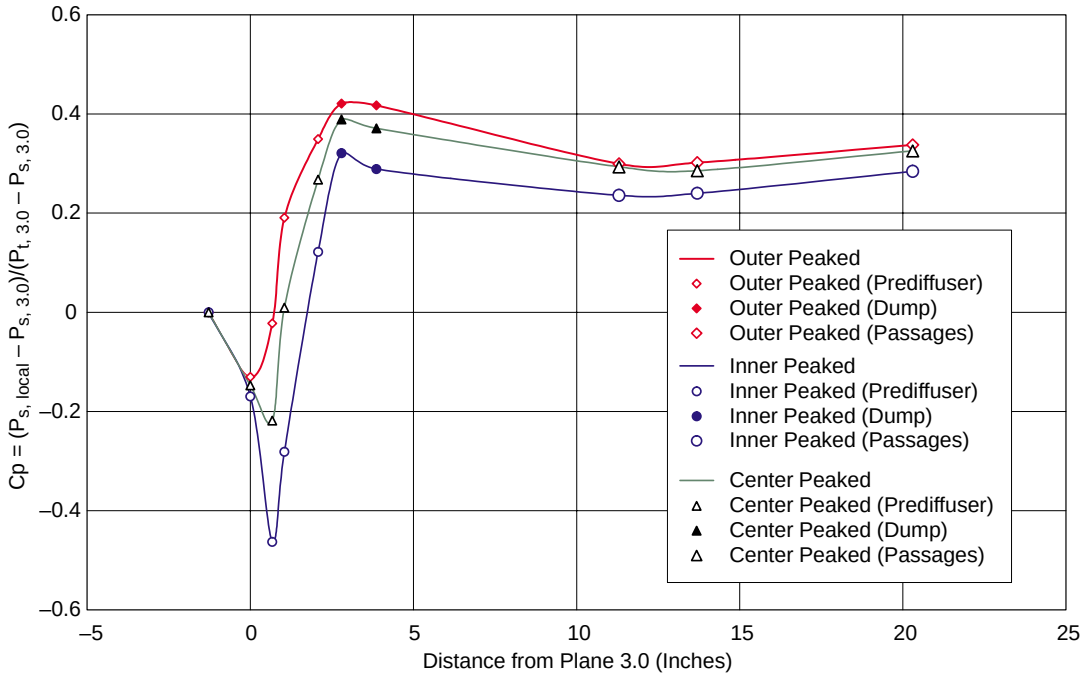

Figure 178. LPP Cold-Flow, Full-Annular Diffuser Test – Inner Passage Pressure Recoveries

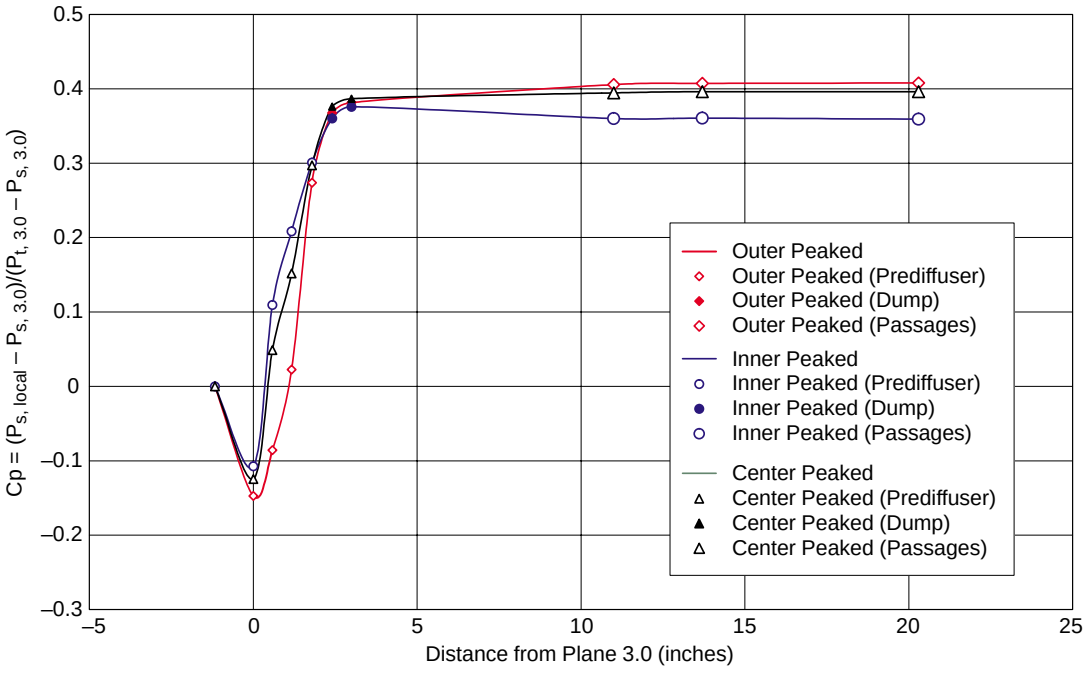

Figure 179. LPP Cold-Flow, Full-Annular Diffuser Test – Outer Passage Pressure Recoveries

quench plate configuration. Each of these configurations was designed using a modular construction technique to allow parametric changes to key combustor hardware. The rig and combustors were designed to provide easy access to the quench-section hardware in particular, since that region would be the focus of emissions-reduction technology. A diagnostic emissions probe system, capable of axial translation and rotational motion with individual port and ganged sampling, was developed to provide insight into the emissions characteristics of the RQL combustor.

The RQL combustor test facility included a high-temperature airflow distribution and control system, a variable-geometry fuel injector and control system, the RQL combustor, an emissions system, and an exhaust system as shown in Figures 180 and 181.

In the integrated module rig, the total combustor airflow traveled through a 6-inch pipe to the combustor. The rich-zone and quench-zone airflows were set by the combustor hardware and determined by the relative effective flow areas of the passages leading into each zone of the combustor. The variable-geometry fuel injector, as the name implies, provides a controllable, variable-effective-flow area for air introduced into the rich zone of the combustor; hence, the split of air into the rich zone or quench zone could be manipulated as a key parametric variable for exploration of emissions reduction potential as well as for operability and durability benefits.

The variable-geometry fuel injection system was designed to control airflow split by manipulating the effective area of the fuel injector/bulkhead assembly in combination with the fixed geometry of the rich-zone liner cooling/quench airflow passages. Design intent was to provide the desired rich-zone flow in the range of 10% to 40% of the total combustor airflow. The design is built on a baseline axial-flow swirler, aerating or air-blast injector geometry. Air was introduced through three passages, each equipped with independent vane swirlers (coswirled). Fuel was introduced in a thin annular film between the inner air stream and the intermediate air stream. In this concept, only the outer air passage flow area was modulated. When installed in a combustor with a nominal bulkhead height of five inches, it was evident the face of the air cap represented a substantial fraction of the cooled bulkhead surface. Figures 182 and 183 are photographs of the assembled triswirler injector including the nonflight-type actuation system and the combustor module hardware.

The fuel injector employed for some of the integrated module rig tests was an axial-flow swirler with an air-blast fuel nozzle that passed all of the rich-zone airflow. Air was introduced through two concentric annular passages, each equipped with independent vane swirlers. The two swirl passages induced corotating flow in the rich zone.

The effect of the fuel injector on emissions performance was assessed. Lean operation in the front end attempted to isolate the injector performance from the interactions with the other features of the RQL combustor. The fixed-geometry injector produced lower NOx than the variable-geometry injector, but CO emissions performance was similar for both injectors. Surprisingly, the unburned hydrocarbons were significantly worse for the fixed-geometry injector at these lean conditions.

The rich-zone liner was cylindrical. The leading edge of the liner necked down to accept the variable-geometry fuel injector or the bulkhead for the fixed-geometry injector. As the rich-zone flowfield progresses towards the quench plane, the liner shape is curved radially inward to create the quench throat diameter, a key parametric variable assessed during the combustion tests. Two quench throat diameters (and hence rich-zone liner exit diameters), 3.9 inches and 3.4 inches, were evaluated. The rich-zone liner was convectively cooled with the quench air flowing through an outer-shroud annulus. Use of convection-enhancement turbulators cast onto the outer surface of the

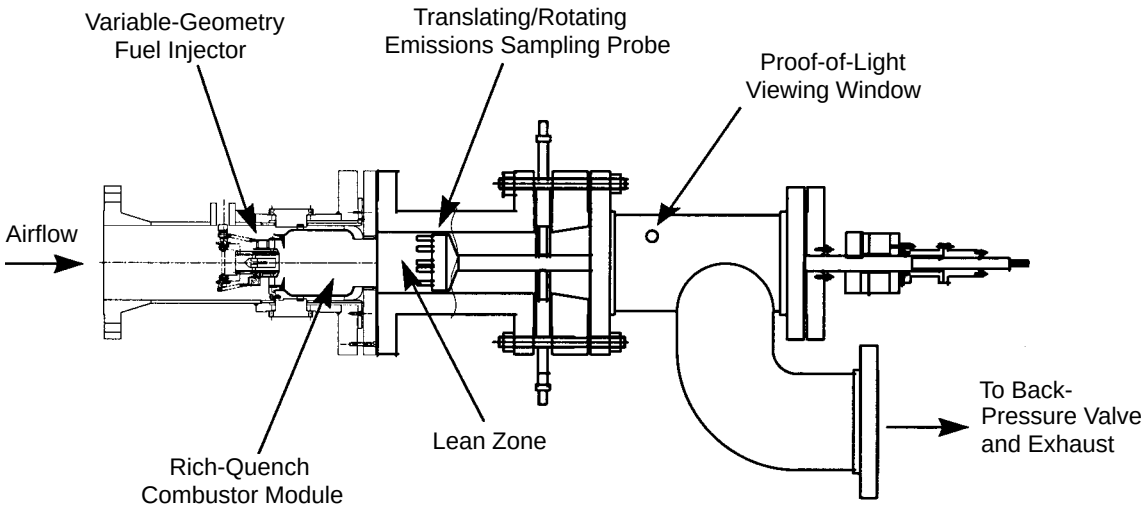

Figure 180. Integrated Module Rig Layout with Wall-Jet Combustor Configuration and Translating/Rotating Emission Probe System

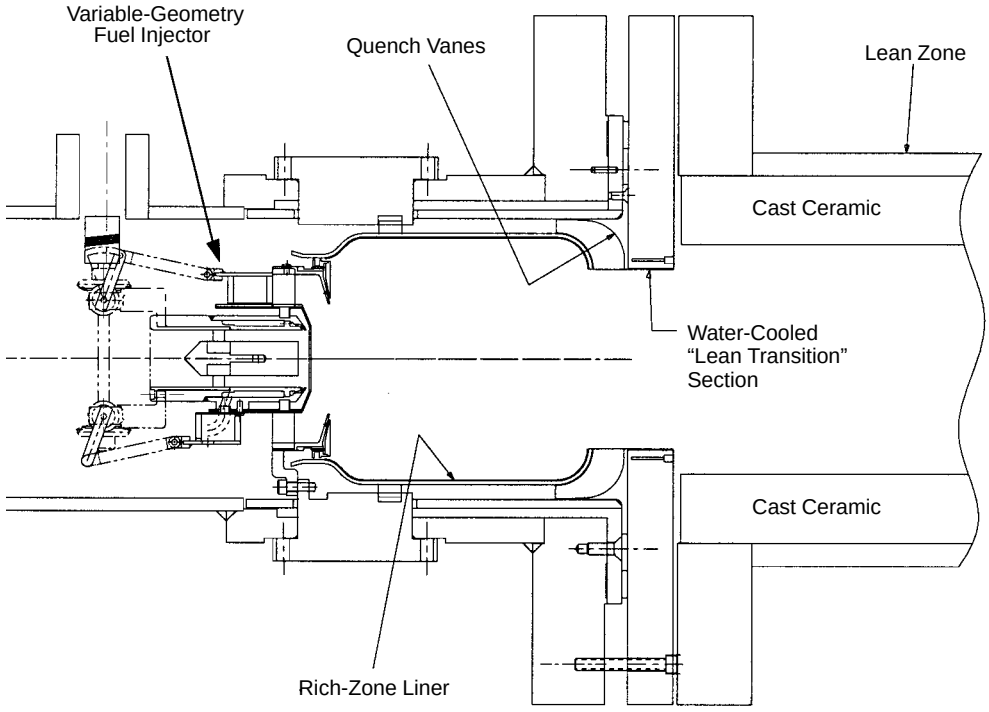

Figure 181. Integrated Module Rig Layout with Wall-Jet Combustor Configuration

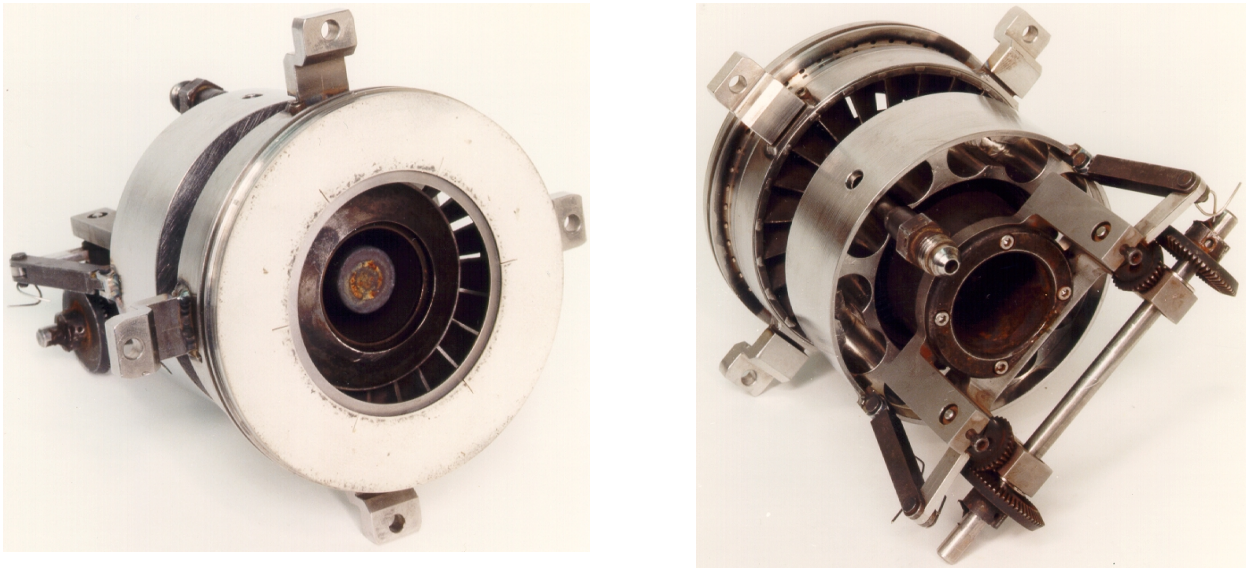

Figure 182. Variable-Geometry Fuel Injector for the Integrated Module Rig

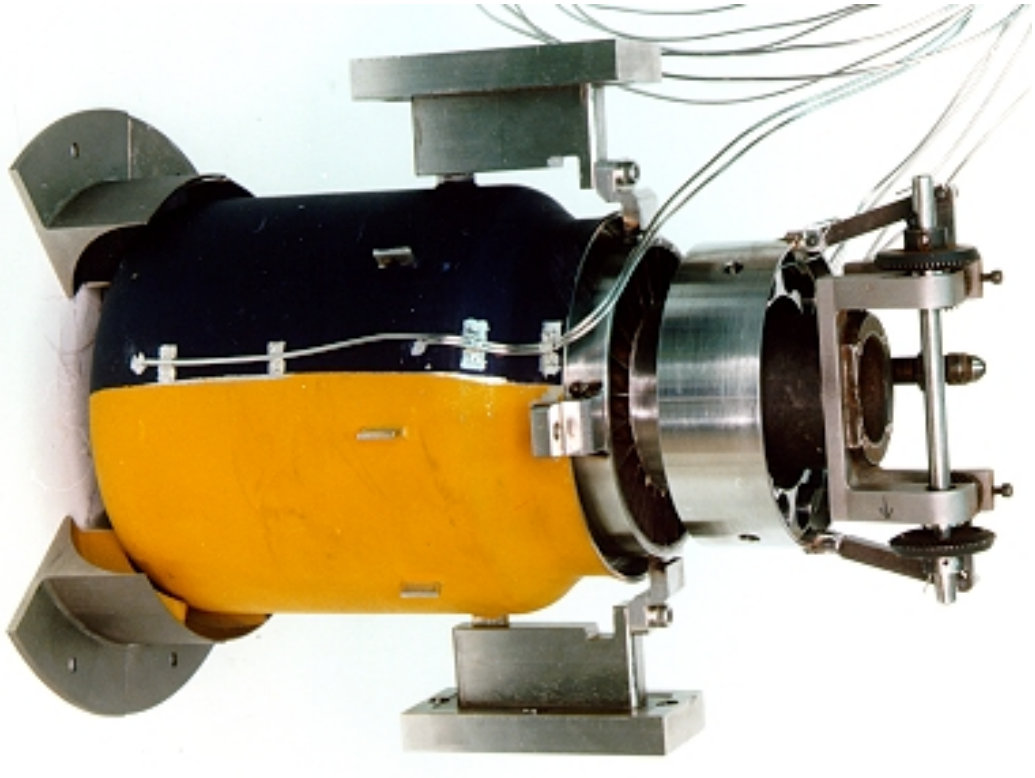

Figure 183. Rich-Zone Liner with Thermocouples, Quench Vanes, and Variable-Geometry Injector; Thermal Paint Applied for Heat Transfer Evaluation

rich-zone liner was evaluated as well. The convection-cooling annulus was created by the outer surface of the rich-zone liner and a tubular shroud. The tubular shroud also served as a mount flange for the quench vanes as well as providing the proper shroud annular height to maintain adequate convection cooling on the back side of the rich-zone liner. This shroud also served as a radiation shield to prevent the hot rich-zone combustor liner from radiating to the test section spool, and it provided a flame shield for safety in case of a rich-zone liner burn through.

The effect of this convection augmentation on emissions performance was assessed. While the main emphasis on convection augmentation is obviously impact on liner temperatures, the impact on emissions was also of interest. The emissions analyses showed that the augmentation adversely impacted CO emissions. It is hypothesized that the augmentation added significant turbulence to the liner convection cooling flow (hence improved heat transfer), causing the quench-jet penetration to decrease and, therefore, result in higher CO emissions.

The quench vanes were designed to take the rich-zone liner convective cooling air, turn it 90°, and divide it into discrete quench jets. To minimize pressure losses associated with this process, the air passage was designed to be continuously convergent as the vane transitions flow from the cooling annulus into the quench jet. Individual quench vanes were designed and fabricated to avoid the thermal stresses associated with a full-hoop structure. To allow the quench vanes to be thermally isolated from the rich-zone liner, a gap was implemented at the leading surface of the quench vane. The effect of the size of this gap was investigated in this program.

A number of quench vane geometries were designed, fabricated, and tested in this program to assess key quench jet orifice parameters and effects on NO_X emissions (Table 28).

Table 28. Summary of Quench Vane Geometries Investigated in Integrated Module Rig

Number of Vanes per Set	Quench-Zone Diameter (inches)	Quench Jet Orientation
8	3.9	Radial
8	3.9	10° Swirl
8	3.9	20° Swirl
12	3.9	Radial
16	3.9	Radial
24	3.9	Radial
8	3.4	Radial
12	3.4	Radial
24	3.4	Radial

The effect that the number of quench orifices had on emissions performance was assessed and is shown in Figures 184 and 185. The plots show behavior as a function of lean-zone residence time, as measured by axially traversing the emissions-probe system downstream during the combustion test. It appears that all configurations yielded similar behavior; these comparisons did not conclusively show a benefit of any particular number of quench jets.

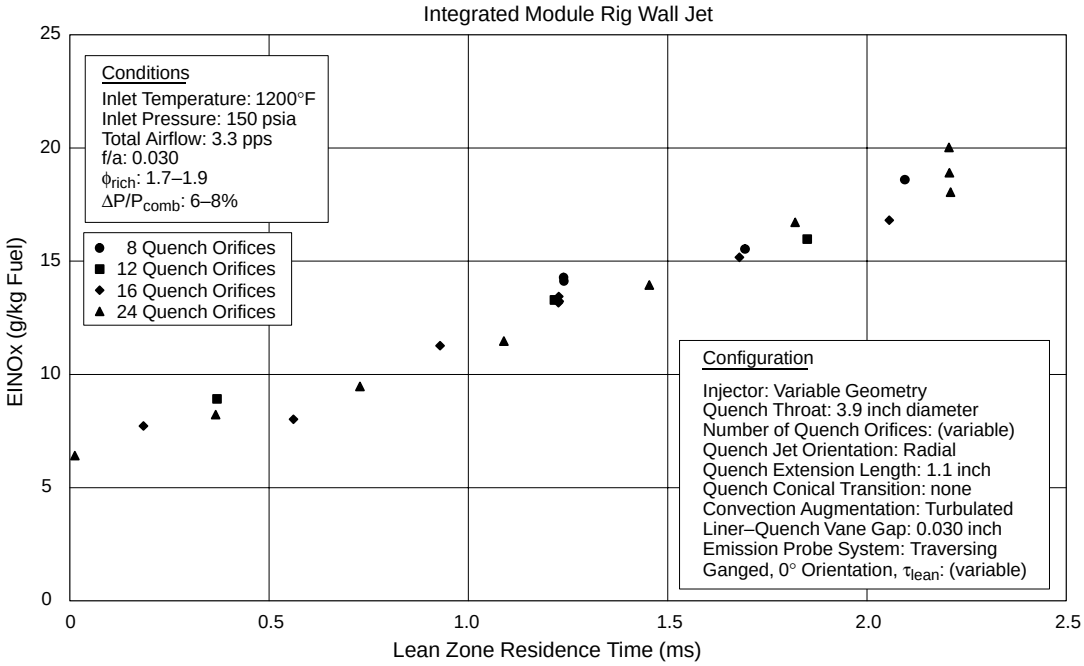

Figure 184. Effect of Number of Quench Vanes on NOx Emissions as a Function of Lean-Zone Residence Time

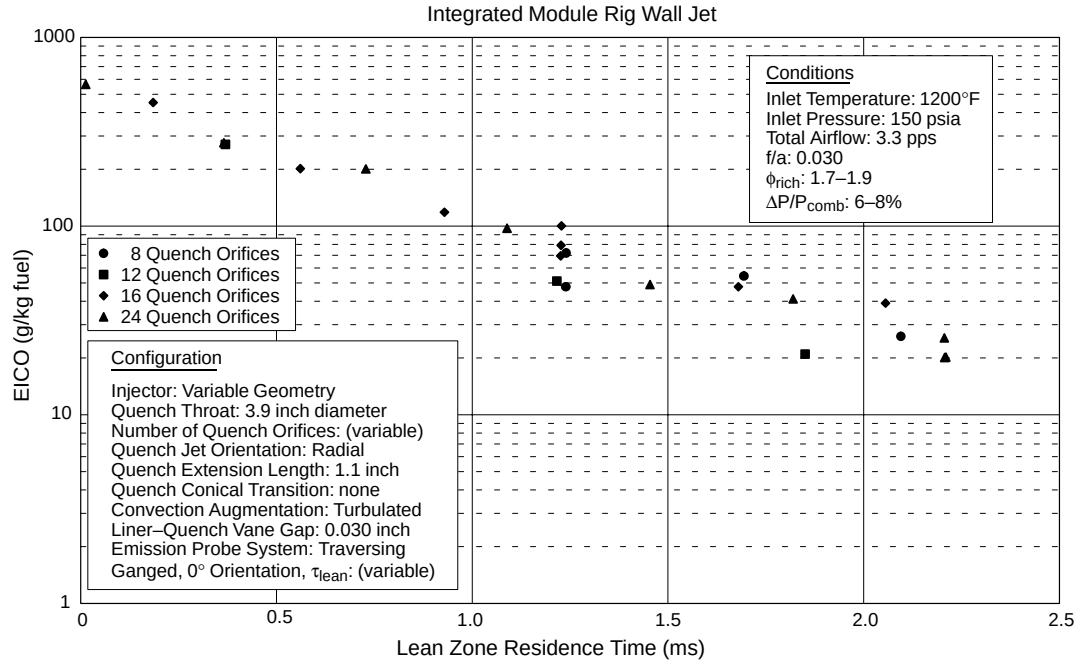

Figure 185. Effect of Number of Quench Vanes on CO Emissions as a Function of Lean-Zone Residence Time

The effect of the gap between the rich-zone liner and the quench vane had on emissions performance was assessed. Local diagnostic emissions sample measurements show that there is minimal impact on NOx and CO emissions from a change in this gap dimension. However, the unburned hydrocarbon emissions appeared to benefit from a smaller gap; therefore, the efficiency of the configuration with the larger gap was slightly lower.

The effect that swirling the quench jets had on emissions performance was assessed. The 10° swirl configuration did not significantly impact emissions. However, the 20° swirl configuration had a significant effect on the CO emissions performance. Detailed individual probe-sample emissions measurements show a very large CO peak in the center of the 20° swirl configuration. In addition, The emissions-based fuel/air ratio at the central region shows very high fuel/air ratios as the quench jets did not penetrate into the central region of the cylindrical flow field, as would be expected when the quench jet air is highly swirled. The lean-zone residence time excursion also shows the inability of this configuration to oxidize the CO from the rich combustion zone, as large EICO persists well downstream into the lean zone. Similar behavior occurs for unburned hydrocarbons with the 20° swirl configuration.

The geometrical shapes of the entrance and exit of the quench zone were assessed in the wall-jet combustor configuration to evaluate impact on emissions. Since the shapes of these inlet and exit regions had changed from previous single-module rig tests, particularly on the inlet side to enable incorporation of the quench vane geometry, an evaluation was performed in the integrated-module rig to find out if a conical shaped inlet or exit was essential to the low-emissions performance of the RQL combustor. A conical transition at the inlet to the quench region was formed by the use of the castable ceramic to create an insert at the aft end of the rich-zone liner. A conical transition exiting from the quench region, downstream from the quench extension region, was created by casting the desired shape into the lean-zone Plicast liners. The effect that the conical transition at the inlet to the quench region and at the exit from the quench region had on emissions performance was found to be insignificant to the emissions performance of this RQL combustor.

The quench extension section consisted of a water-cooled spool piece with a diameter that matched the quench throat diameter and extended for an axial distance to allow a confined region for the quench mixing process to occur prior to expansion or dump of the flow into the lean zone. Various quench extension lengths were evaluated in this program, including: 1.1, 1.6, 2.7, and 3.2 inches. The inner surface of the quench extension or lean transition section exposed to the combusting gases was either coated with a thermal barrier or protected with a castable ceramic liner insert to isolate the combusting gas from artificial cooling induced by water-cooling the spool section.

The effect that the length of the extended confined region immediately downstream of the quench air addition plane had on emissions performance was assessed. Figure 186 and Figure 187 describe the effect that the quench extension length had on emissions. CO and unburned hydrocarbon emissions benefited from an increase in the length of this quench extension region, hence the improvement in efficiency, while the NOx emissions remained relatively unaffected. The detailed individual emissions probe samples show a flatter NOx profile with the longer extension length, and no central CO peak as was observed with the shorter 1.1-inch quench extension.

The effect that the diameter of the quench throat at the quench air addition plane had on emissions performance was assessed. The emissions performance comparison from these runs investigating quench throat diameter is shown in Figures 188 and 189. The lean-zone residence time excursion shows lower NOx emissions for the smaller quench throat diameter, but the CO emission remained

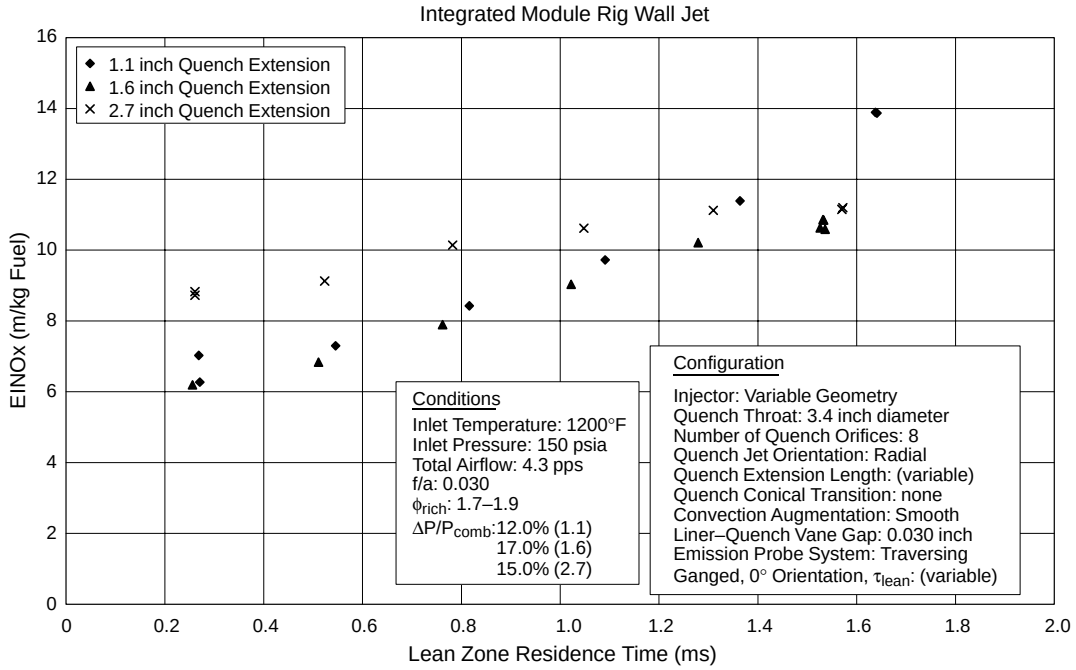

Figure 186. Effect of Quench Extension Length on NOx Emissions as a Function of Lean-Zone Residence Time

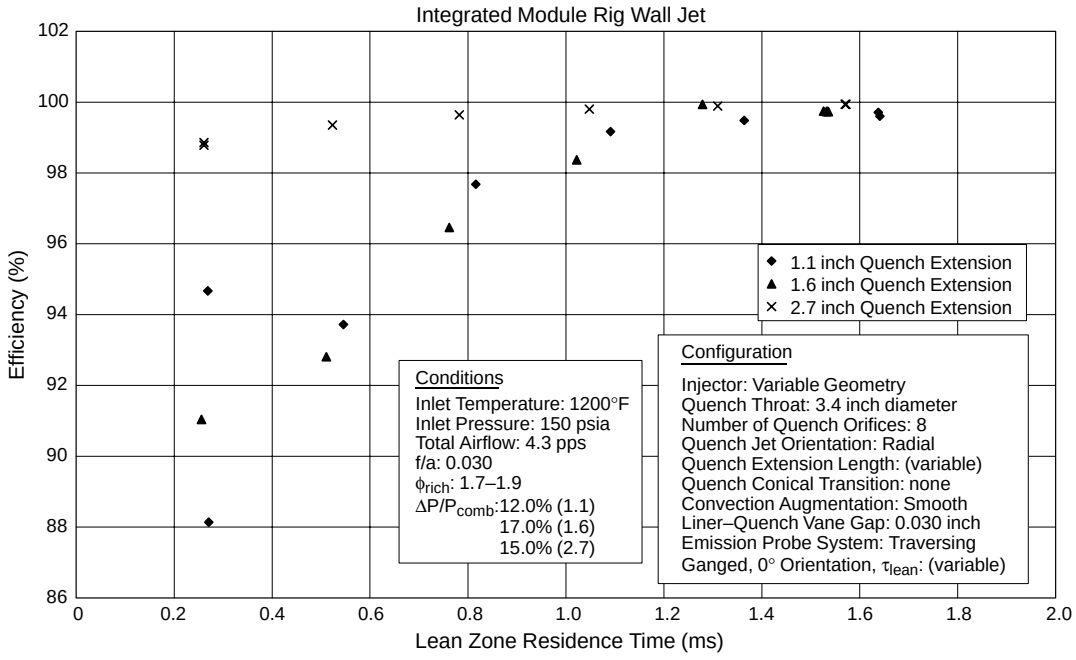

Figure 187. Effect of Quench Extension Length on Efficiency as a Function of Lean-Zone Residence Time

relatively unaffected by the change in quench throat diameter. These comparisons were for a constant airflow in the combustor. However, the smaller quench throat diameter resulted in the combustor operating at a higher overall pressure drop. It is not apparent whether the lower NOx emissions were a result of the improved mixing with the smaller quench throat diameter or a function of the increase in pressure drop. Unfortunately, a pressure drop excursion had not been conducted during these particular combustor configuration tests to provide insight into this phenomenon.

The lean-zone section was cylindrical and contained a castable ceramic liner to provide thermal insulation. For a majority of the tests an axially traversing, circumferentially rotating, emissions-sampling probe was mounted in the transition section along the combustor centerline. A fixed-location, emissions-sampling probe system was also used for some of the combustion tests. The exit plane for the combustor was defined by the location of the probe tips of the axially traversable emissions probe system. However, this could be shortened by traversing the probe system forward, making lean zone residence time a primary focus in the combustion test program.

Evaluation of all of the results obtained during the wall-jet combustor configuration tests indicated that the best emissions-performing configuration was the one in runs 32 and 33, which combined the long quench extension with the small quench throat diameter. Figures 190 through 195 summarize the results from this configuration.

A preliminary assessment was made of how a fuel-shifted wall-jet RQL combustor might perform throughout the flight envelope and especially in airport-vicinity emissions. Tests were conducted to simulate a variety of airport-vicinity conditions. Fuel/air ratio excursions were performed, and emissions were measured as a function of these conditions for both a module operating with a rich front end and a module operating with a lean front. These data were then combined using the method of superposition, accounting for an airflow distribution of approximately 60% for an OD bank of modules and 40% for an ID bank of modules, to estimate an integrated value of emissions at the exit of a fuel-shifted RQL combustor. The acquired data for both the lean and rich front-end conditions and the airport-vicinity emissions estimates are shown in Figures 196 through 199 and Table 29. A more comprehensive evaluation of fuel shifting for a reduced-scale-quench RQL combustor in a multiple module sector rig, including rich module/lean module interaction effects, was investigated using the fuel-shifting sector rig.

4.5.3.2 Integrated-Module Rig – RSQ/Convoluted Liner

An RQL combustor, using RSQ technology implemented in a convoluted-liner/quench-plate configuration, demonstrated the an EINOx of 9.2 fuel at the supersonic flight condition (relative to the program goal of 5). This rich/quench/lean combustor, with reduced-scale quench technology, also demonstrated exceptional efficiency: 99.98%, relative to the program goal of 99.9% at supersonic cruise conditions. During concept development, uniformity was discovered to play an important role in determining the emissions performance of the RSQ convoluted-liner/quench-plate combustor configuration.

The series of parametric tests in support of the RSQ convoluted-liner/quench-plate combustor design were conducted in the integrated module rig in Cell 1E of the JBTS at UTRC. The test series was initiated on November 5, 1996 and progressed through March 22, 1997. During this period, 18 tests were conducted.

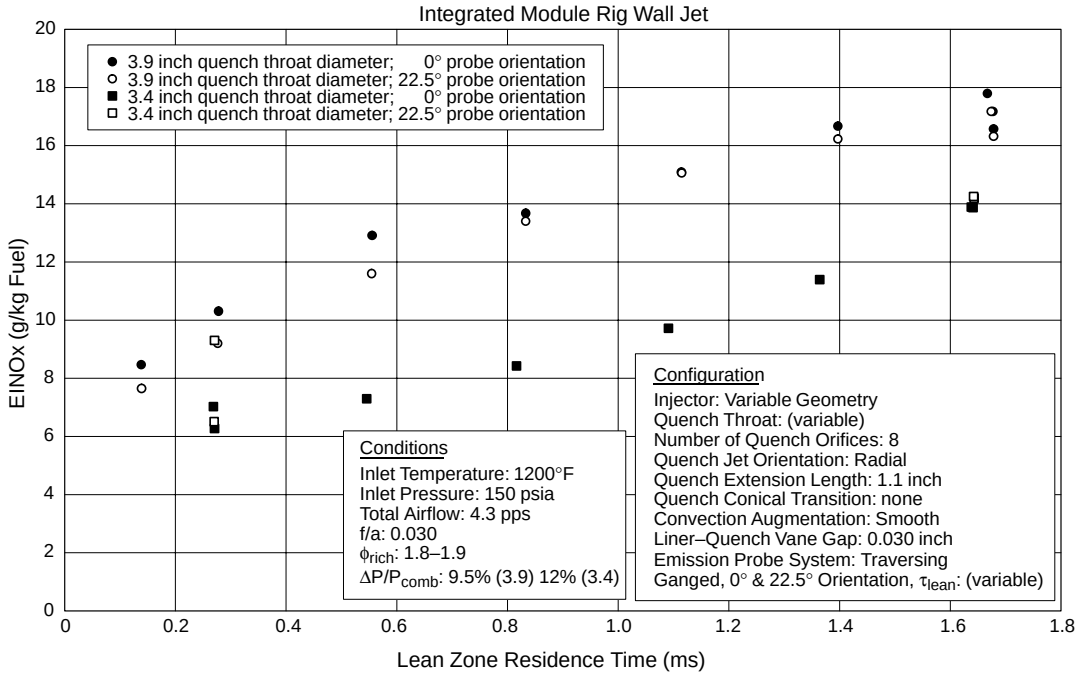

Figure 188. Effect of Quench Throat Diameter on NOx Emissions as a Function of Lean-Zone Residence Time

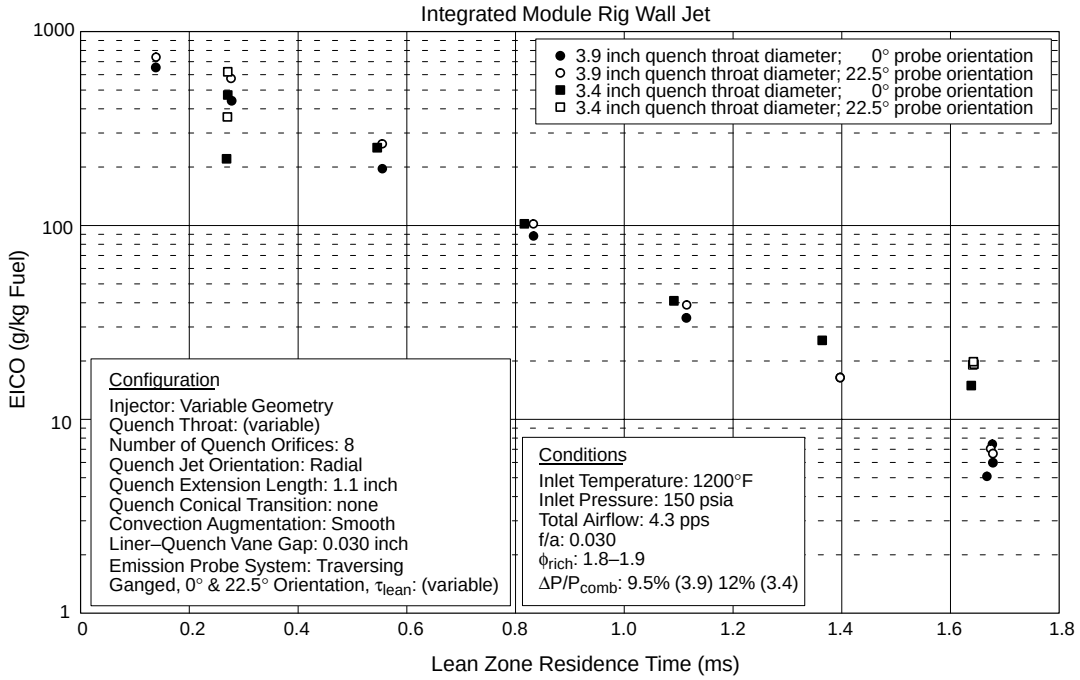

Figure 189. Effect of Quench Throat Diameter on CO Emissions as a Function of Lean Zone Residence Time

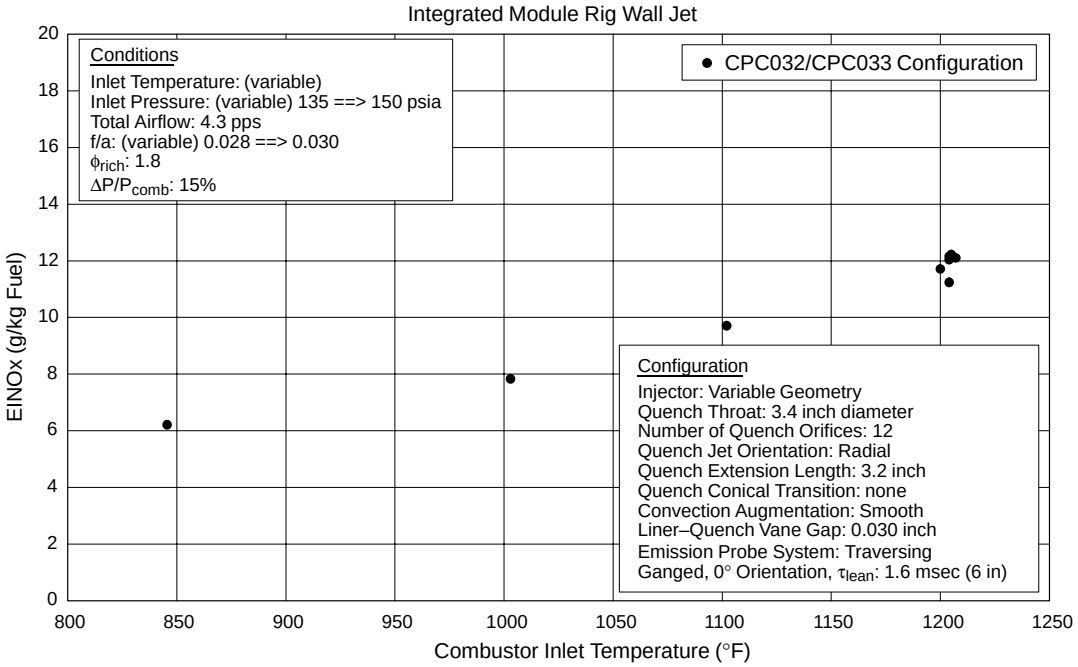

Figure 190. NOx Emissions as a Function of Inlet Temperature for Wall-Jet Configuration CPC032–CPC033

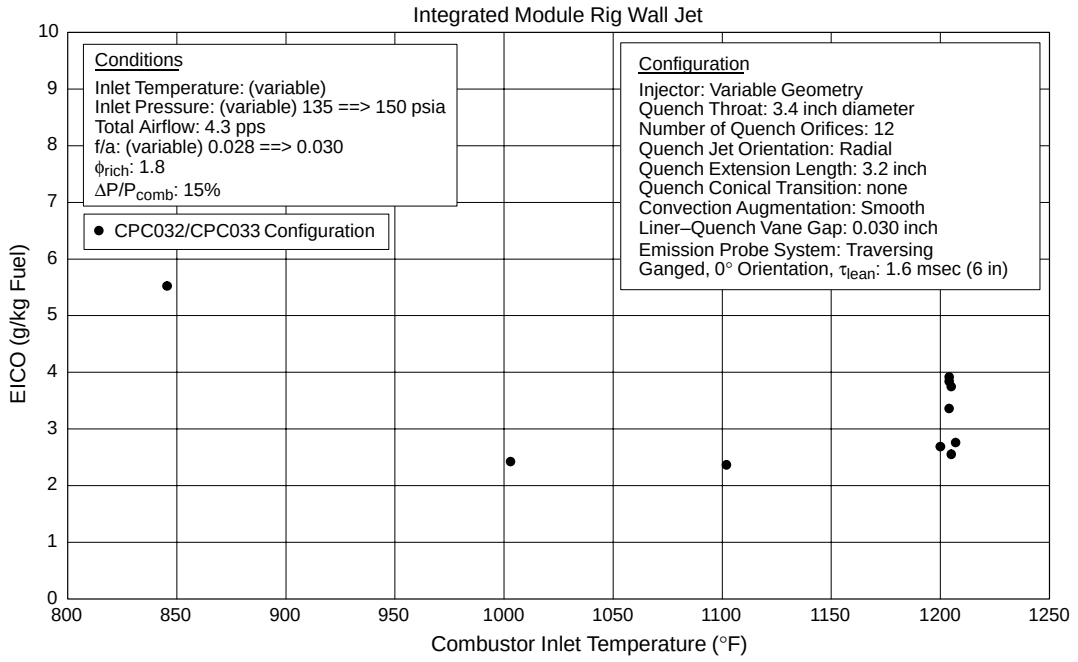

Figure 191. CO Emissions as a Function of Inlet Temperature for Wall-Jet Configuration CPC032–CPC03

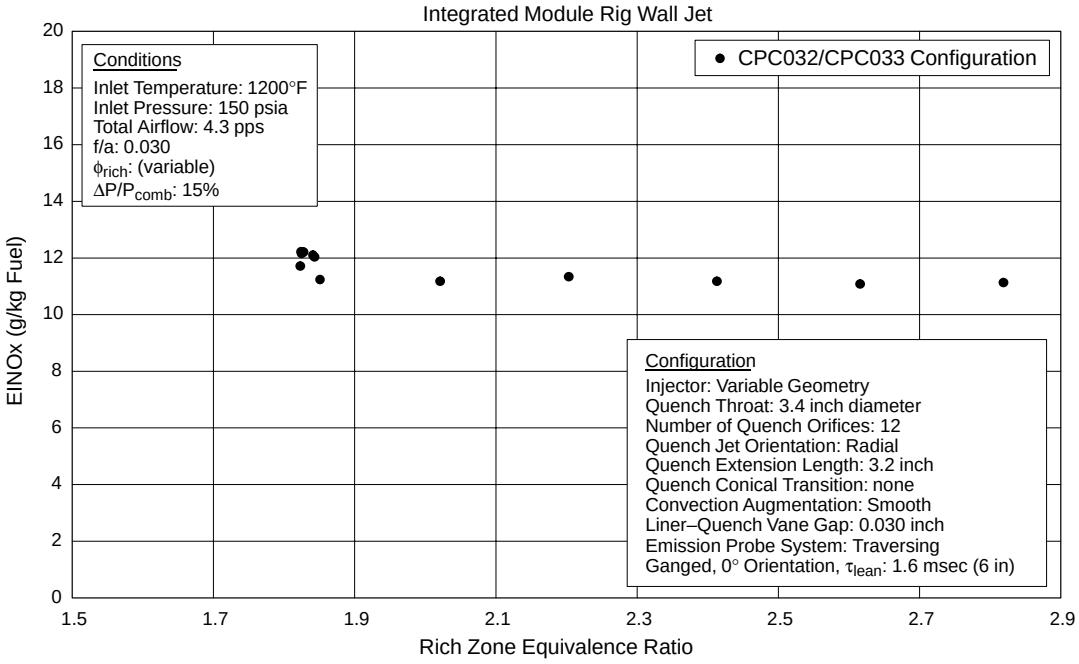

Figure 192. NOx Emissions as a Function of Rich-Zone Equivalence Ratio for Wall-Jet Configuration CPC032–CPC03

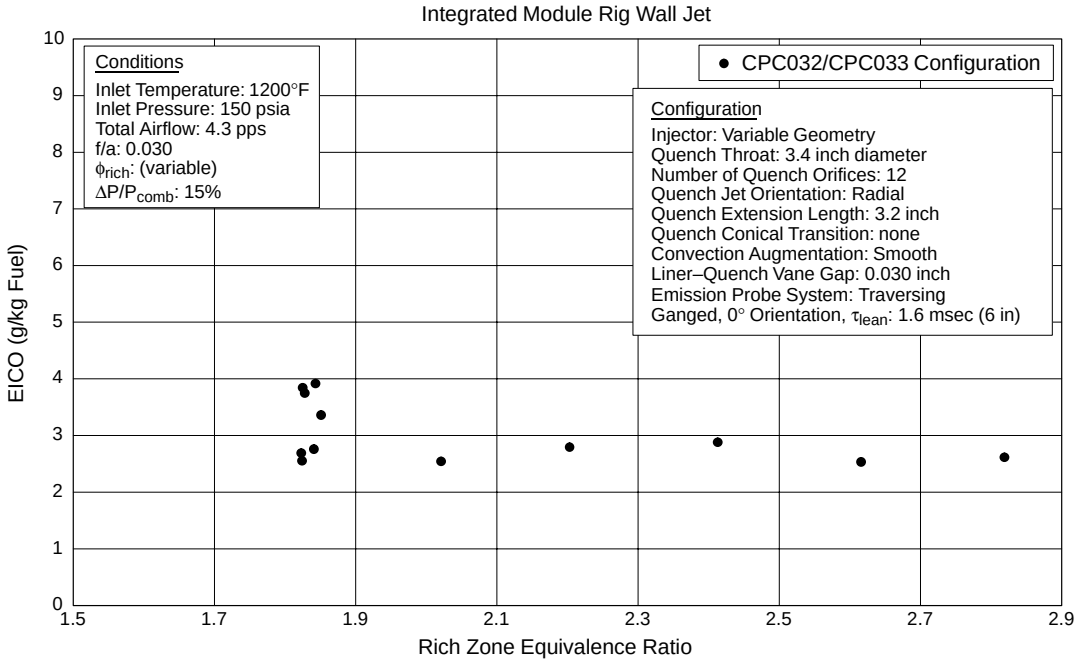

Figure 193. CO Emissions as a Function of Rich-Zone Equivalence Ratio for Wall-Jet Configuration CPC032–CPC033

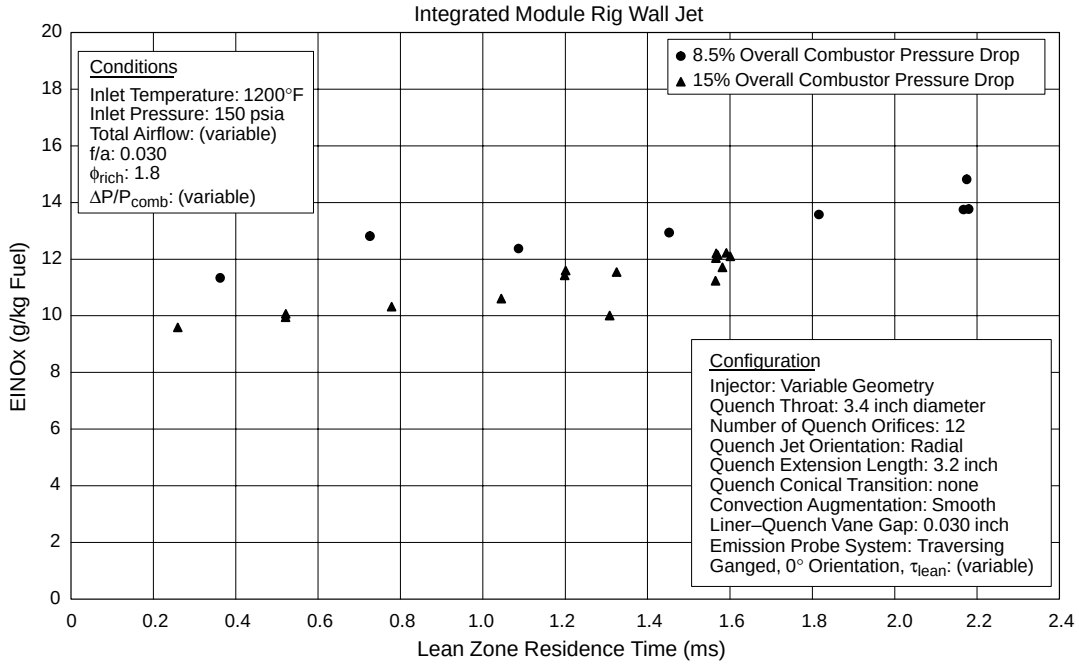

Figure 194. NOx Emissions as a Function of Lean-Zone Residence Time for Wall-Jet Configuration CPC032–CPC033

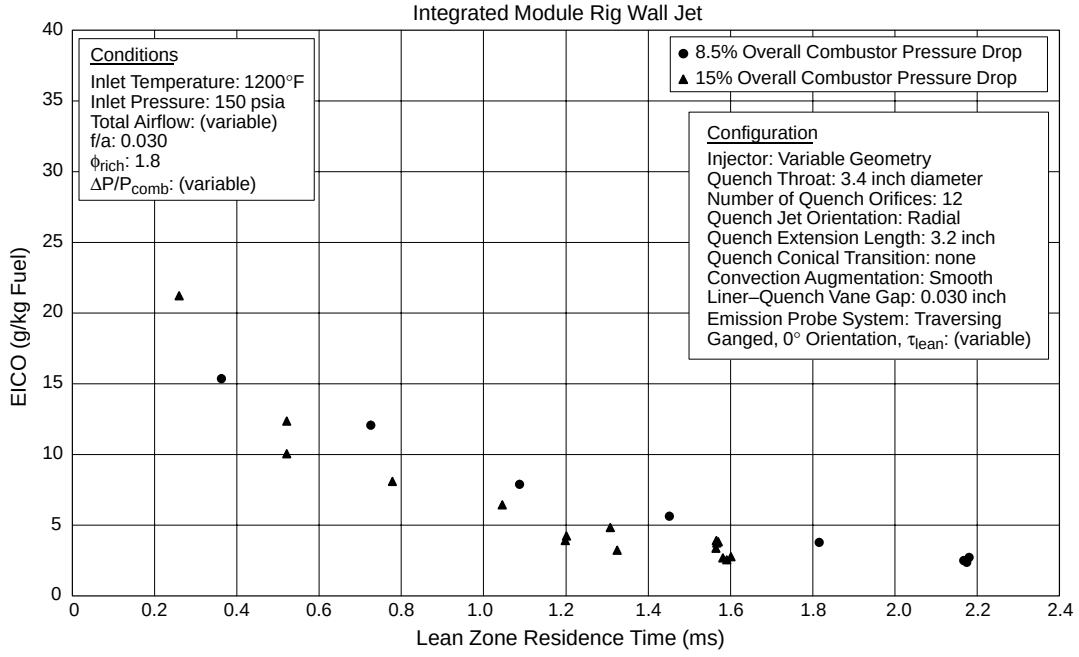

Figure 195. CO Emissions as a Function of Lean-Zone Residence Time for Wall-Jet Configuration CPC032–CPC033

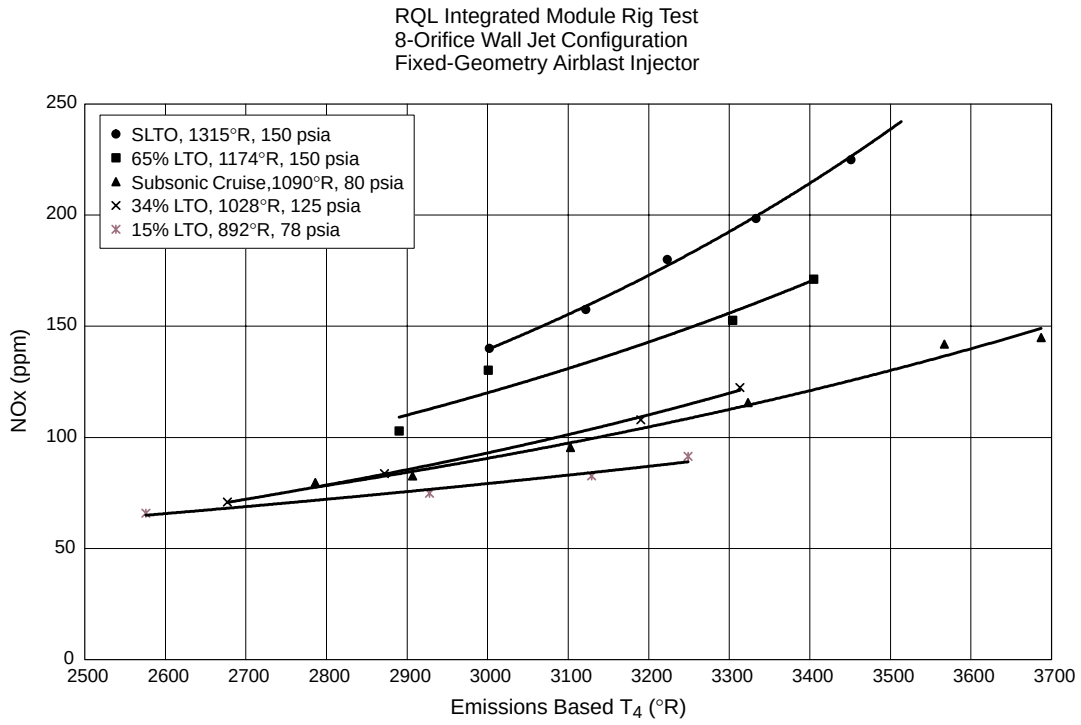

Figure 196. NOx Emissions of a Rich Module for Fuel-Shifting Assessment

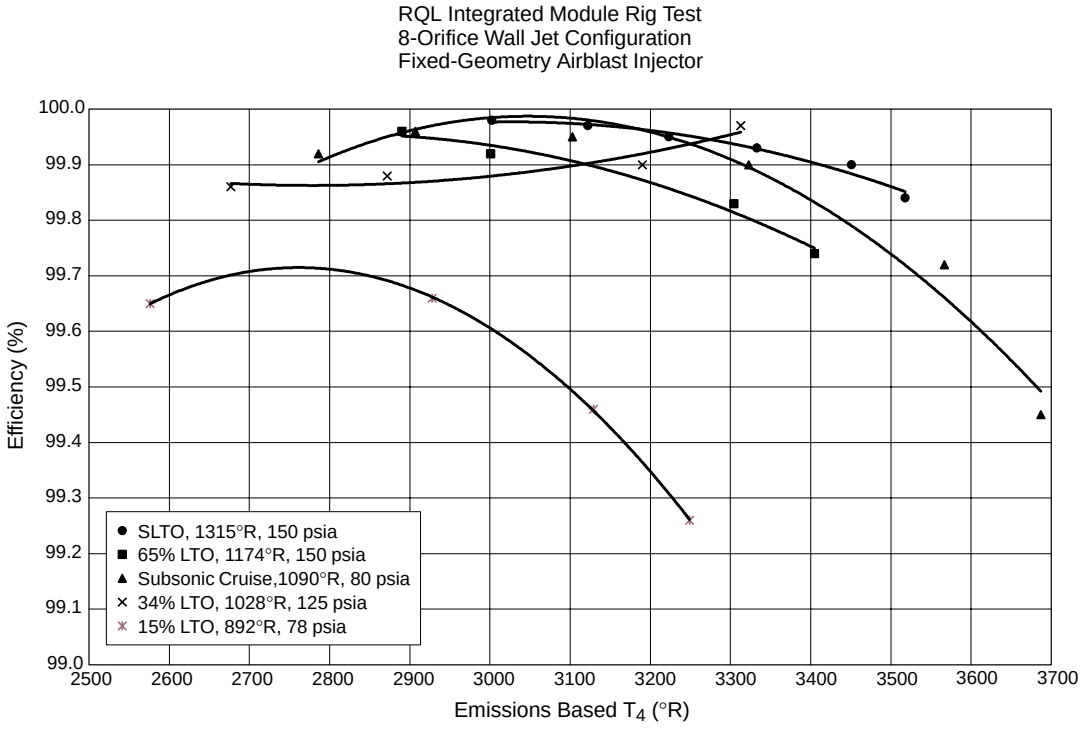

Figure 197. Efficiency of a Rich Module for Fuel-Shifting Assessment

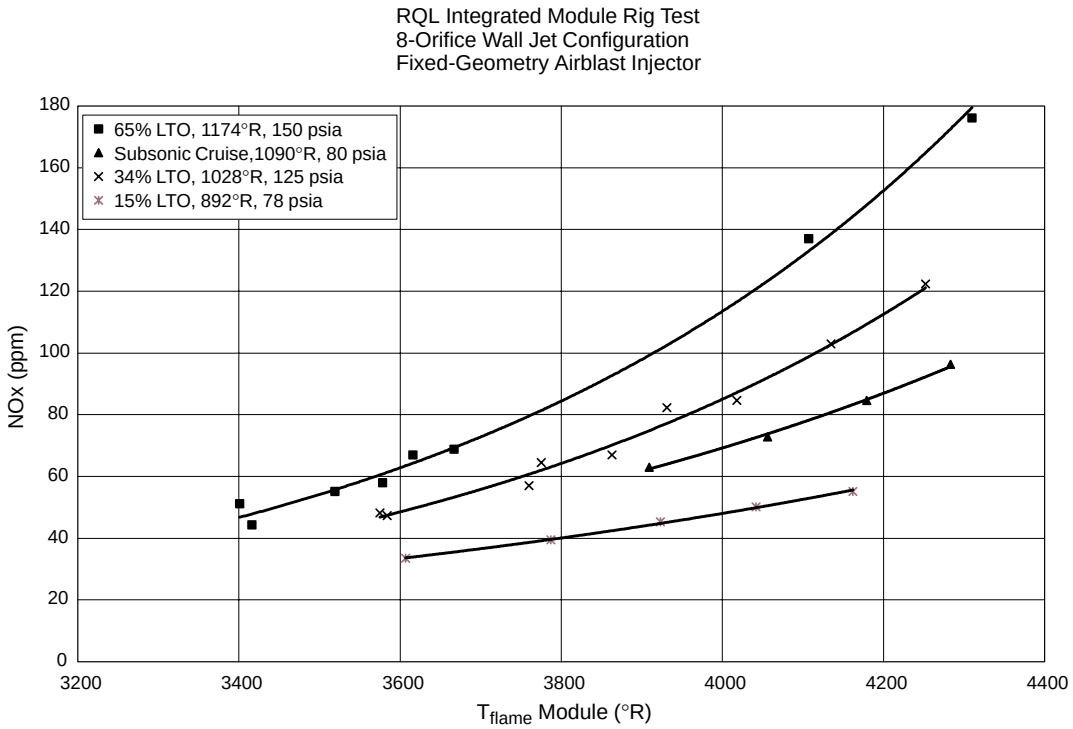

Figure 198. NOx Emissions of a Lean Module for Fuel-Shifting Assessment

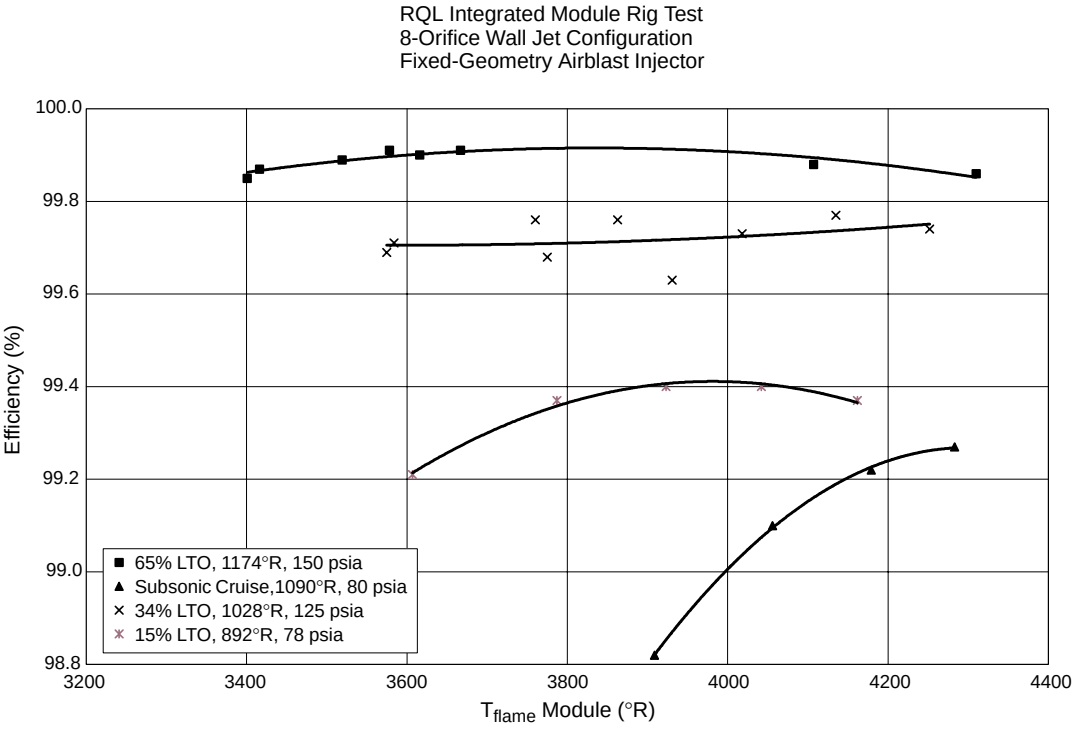

Figure 199. Efficiency of a Lean Module for Fuel-Shifting Assessment

Table 29. Airport Vicinity Emissions Assessment for a Fuel-Shifted, Wall-Jet, RQL Combustor

Thrust Settings and Time-In-Mode For Landing/Takeoff Cycle (Supersonic)

Index Number	Operating Condition	EINOx	EICO	EIHC
1	Idle	4.8	20.50	1.35
2	Descent	3.8	13.56	2.95
3	Approach	4.4	7.00	1.92
4	Climb	6.4	0.98	0.01
5	Takeoff	11.2	1.69	0.01
Integrated LTO Goal		5.2	7.9	0.7
Goal		< 5.0	< 7.8	< 1.0

The integrated-module rig RSQ convoluted-liner/quench-plate combustor configuration consisted of a fuel injection device (described previously for the integrated-module rig, wall-jet configuration), a convoluted rich-zone liner, an insert “nose piece” to guide the convective cooling air around the convoluted liner, a quench plate, and a lean zone as shown in Figure 200.

The rich-quench module consisted of a rich-zone liner, shown in Figure 201. The liner was cylindrical with a 5-in ID towards the front end of the rich zone. The leading edge of the liner necked down to accept the fuel injector/bulkhead. As the rich-zone flow field progresses towards the quench plane, the liner shape is convoluted to direct the rich-zone flow into four channels in preparation for injection of the quench air. All four channels are 0.5 inches in height. The rich-zone liner is convectively cooled with quench air. Towards the aft end of the rich zone section, the convective cooling air is guided, such that the air maintains contact with the rich-zone liner, through the use of an insert “nose piece” that acts as an aerodynamic guide so that the convective air maintains velocity and, hence, cooling effectiveness as it is channeled into the convoluted regions. The liner/nose piece assemblies were suspended inside a tubular shroud that forced the quench air across the upstream cylindrical surface of the rich liner for convective cooling of that region.

Beyond directing the cooling/quench air along the back-side surface of the convoluted liner, the insert “nose piece” also distributed quench air to the downstream edge of the liner. There it was injected into the rich-zone gas from small orifices in a toothed quench plate to produce the RSQ mixing. This quench plate was the main focus of the development and optimization efforts of this portion of the program.

A representative quench plate geometry designed, fabricated, and tested in this combustion rig is shown in Figure 202. The quench orifices were sized to control the pressure drop and, in combination with the rich-zone swirler effective flow area, provide the appropriate quantity of quench air to maintain the desired split of approximately 23% air into the front end of the combustor. The width of each slot varied throughout the channel lengths and was determined to provide optimum mixing for minimizing NOx emissions. The quench channels in the quench plate were designed to the same dimensions as the exhaust of the convoluted rich-zone liner. Additionally, a small fraction of the quench air (4% of total combustor air) was bled through small effusion holes on the downstream face of the plate as cooling air for the aft face of the quench plate.

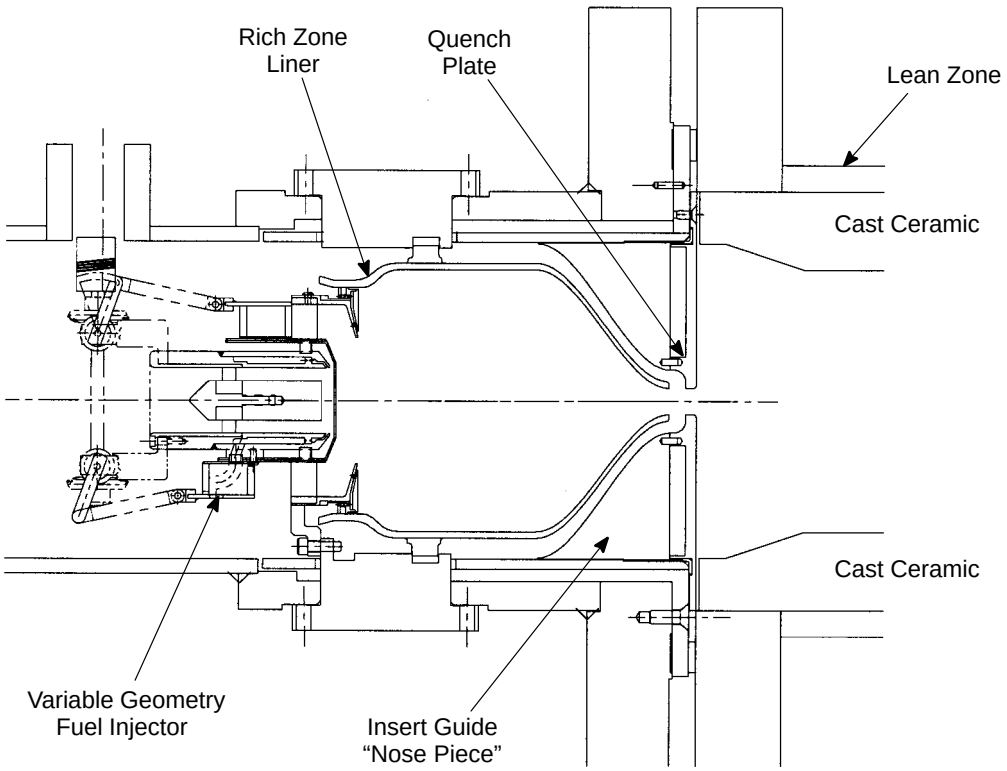

Figure 200. Integrated Module Rig Layout with RSQ Convoluted Liner/Quench Plate Combustor Configuration

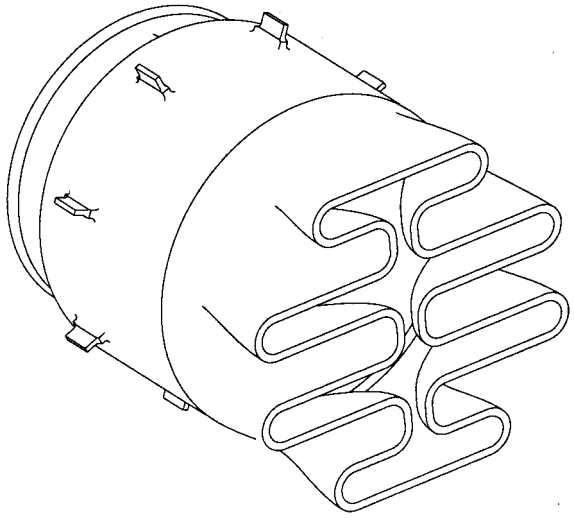

Figure 201. Rich-Zone Convoluted Liner

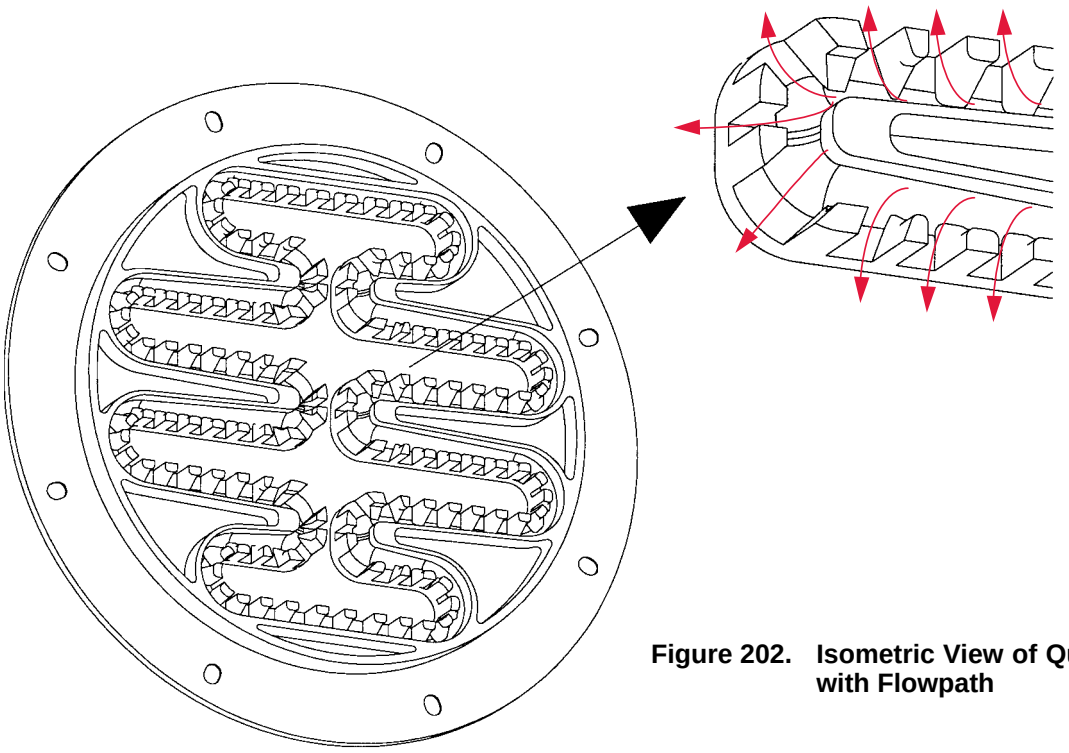

Figure 202. Isometric View of Quench Plate with Flowpath

The lean-zone section was cylindrical. The exit plane of the combustor was defined by the location of the probe tips of the axially traversable emissions-probe system. However, this length could be shortened by traversing the probe system forward, hence making lean-zone residence time a primary focus in the combustion test program.

A summary of performance for all RSQ convoluted-liner/quench-plate combustor configurations is shown in Figures 203 through 205. The figures show the behavior for a fuel/air ratio = 0.030 supersonic cruise condition. From the figures, especially the NOx vs CO plot, it is apparent that quench plate configuration No. 15 performed the best with the lowest NOx and CO emissions.

The effect that the gap between the convoluted rich zone liner and the quench plate had on emissions performance was assessed. Figures 206 and 207 show the impact of varying the gap between the convoluted rich zone liner and the quench plate. The NOx emissions appear unaffected by this geometric variation. However, The CO emissions were lower with the gap between the convoluted liner and the quench plate than without the gap.

The effect of an extended length of confined quench region immediately downstream of the quench air addition plane on emissions performance was assessed. Figure 208 and Figure 209 show the impact of this quench extension. NOx emissions are unaffected, but CO emissions are lower without the extended quench length for this lean-zone residence time excursion. Because of durability concerns with this region, subsequent testing beyond configuration No. 3 did not use any quench-extension hardware beyond the quench plate itself.

Optimization of the quench air addition and detailed diagnostic emissions measurements taken from the series of prior quench plate configurations (Nos. 1 through 14) resulted in the generation of quench-plate configuration No. 15, the best emissions performer for the integrated module rig tests.

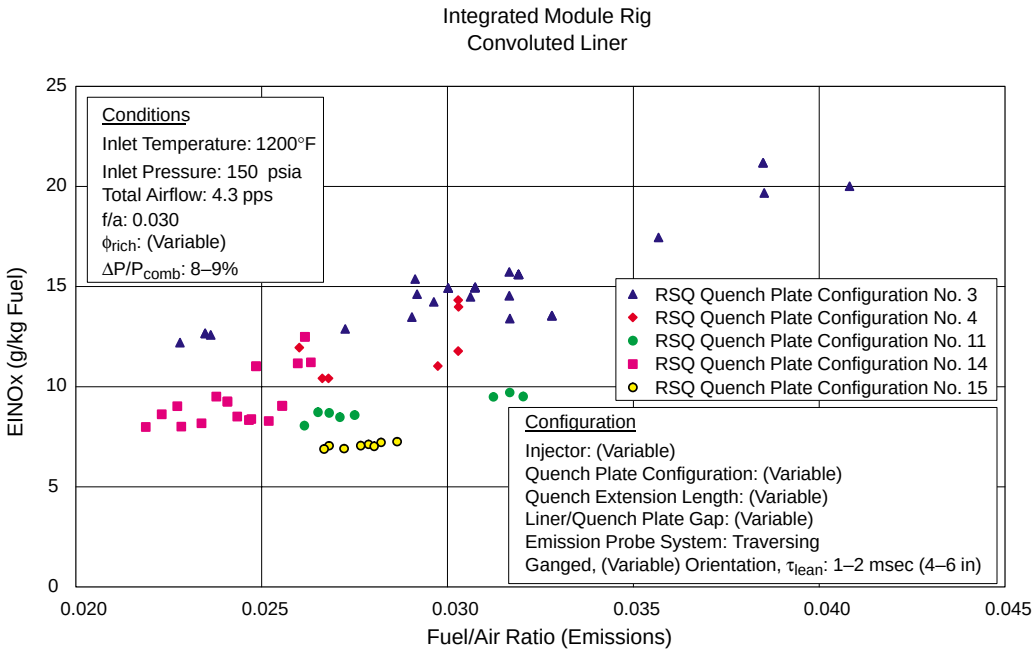

Figure 203. NOx Emissions as a Function of Emissions Fuel/Air Ratio for all RSQ Configurations

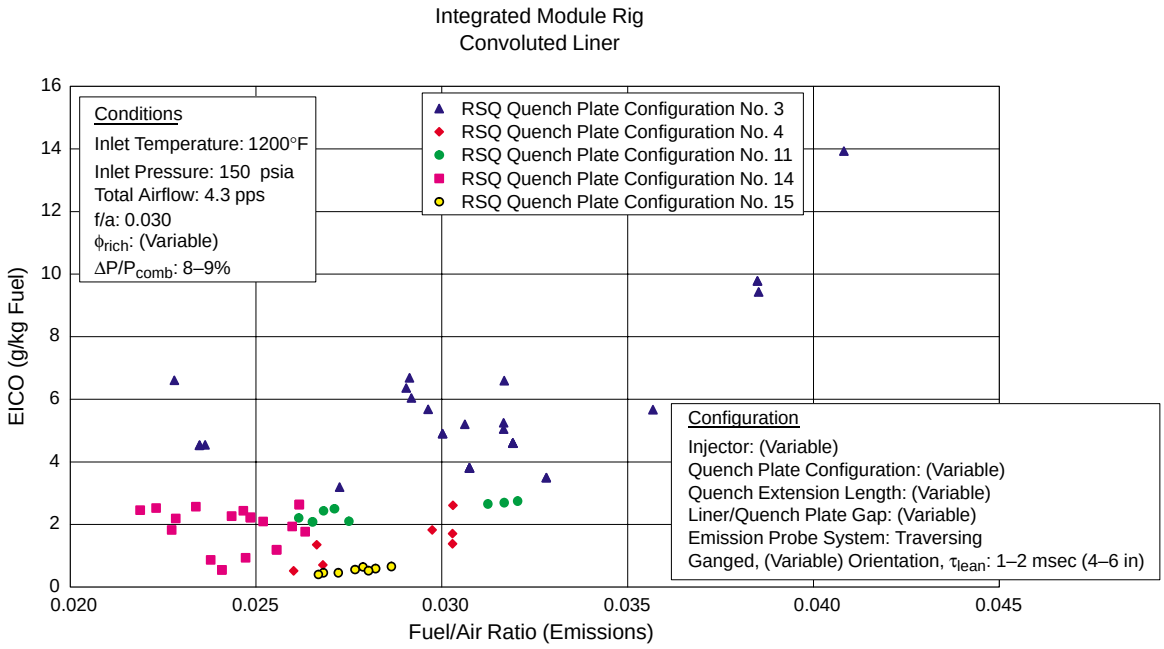

Figure 204. CO Emissions as a Function of Emissions Fuel/Air Ratio for all RSQ Configurations

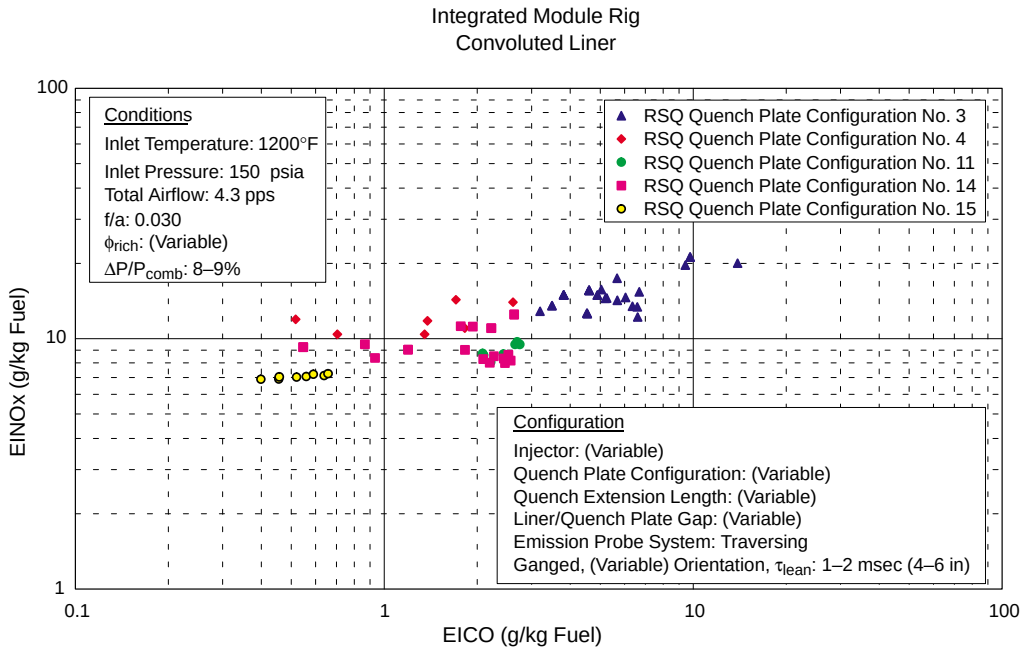

Figure 205. NOx Emissions as a Function of CO Emissions for all RSQ Configurations

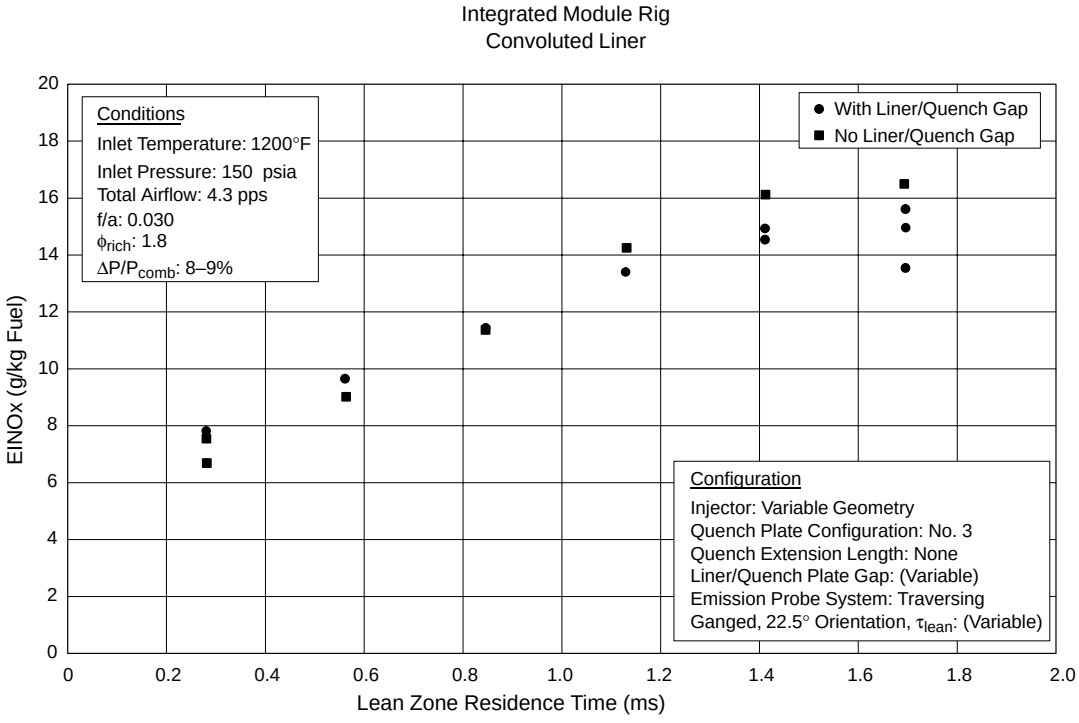

Figure 206. Effect of Gap Between Rich-Zone Convoluted Liner and Quench Plate on NOx Emissions as a Function of Lean-Zone Residence Time

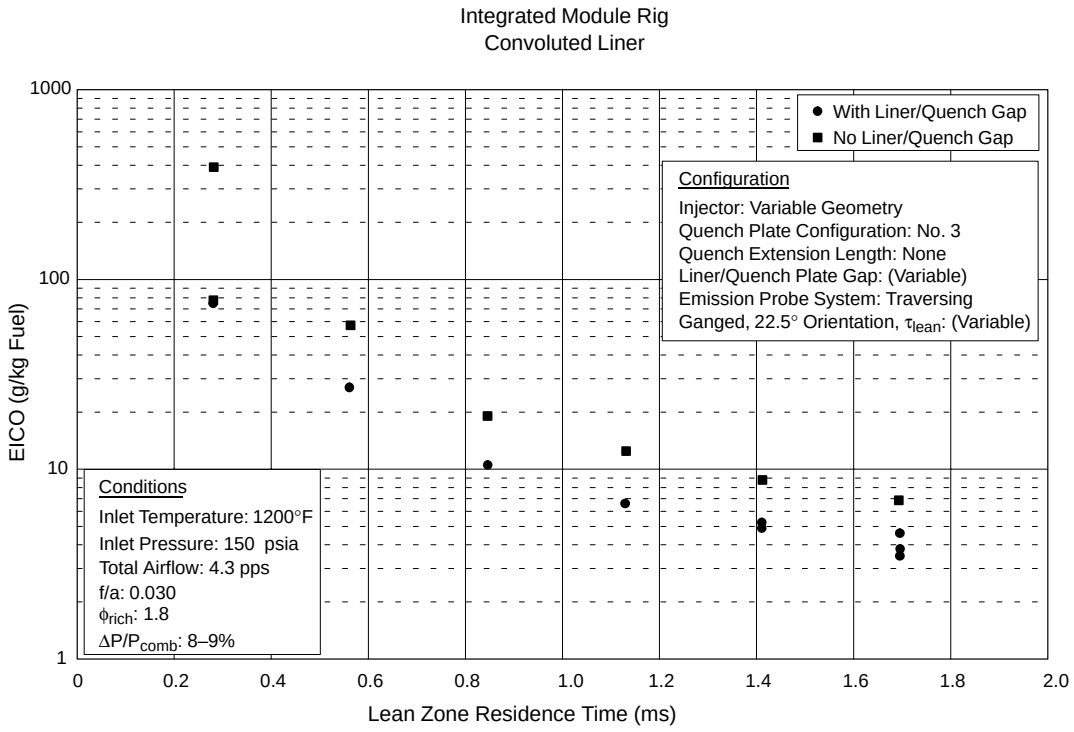

Figure 207. Effect of Gap Between Rich-Zone Convoluted Liner and Quench Plate on CO Emissions as a Function of Lean-Zone Residence Time

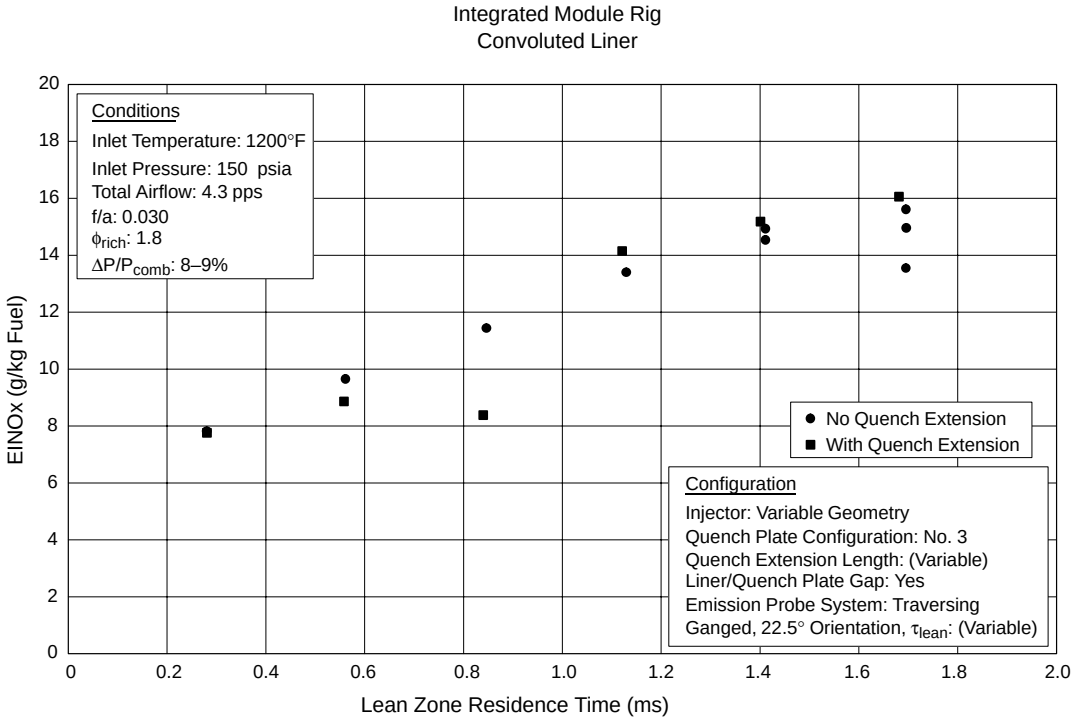

Figure 208. Effect of Quench Extension on NOx Emissions as a Function of Lean-Zone Residence Time

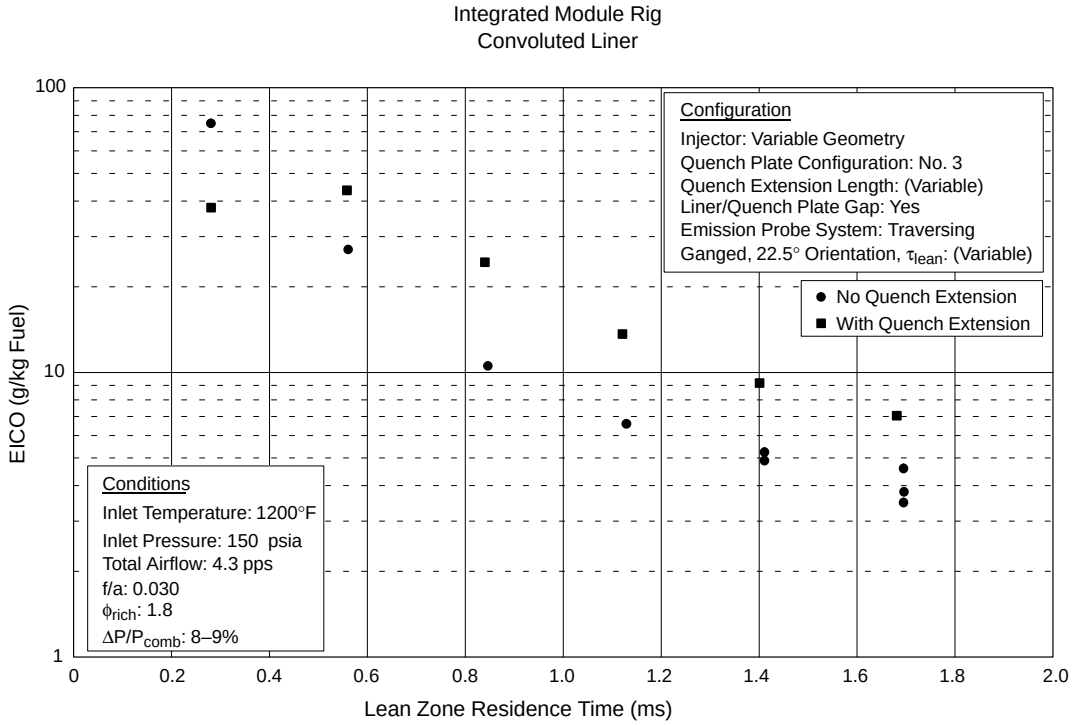

Figure 209. Effect of Quench Extension on CO Emissions as a Function of Lean-Zone Residence Time

Testing of quench plate configuration No. 15 focused on conditions taken from HSR/CPC Program Coordination Memo GE97–002–C, summarized in Table 30, with the primary intent of assessing supersonic cruise emissions in support of the combustor downselect. The emissions results for this configuration are summarized in Figures 210 through 215.

Table 30. Uniform Schedule of Test Points

Test Conditions	T_3 (°F)	P3 (psia)	Fuel/Air
Nominal Supersonic Cruise	1200	150	0.0300
Nominal Subsonic Cruise	630	80	0.0200
100% Thrust LTO (Takeoff)	919	301	0.0329
65% Thrust LTO (Climb)	740	212	0.0248
34% Thrust LTO (Approach)	588	134	0.0187
15% Thrust LTO (Descent)	446	82	0.0141
5.8% Thrust LTO (Idle)	295	45	0.0113

A preliminary assessment was made of how a fuel-shifted RSQ/convoluted-liner RQL combustor might perform throughout the flight envelope and especially in airport-vicinity emissions. Tests were conducted to simulate a variety of airport-vicinity conditions, focused on potentially fuel-shifted conditions of 15% thrust descent, 34% thrust approach, and subsonic cruise. Fuel/air ratio

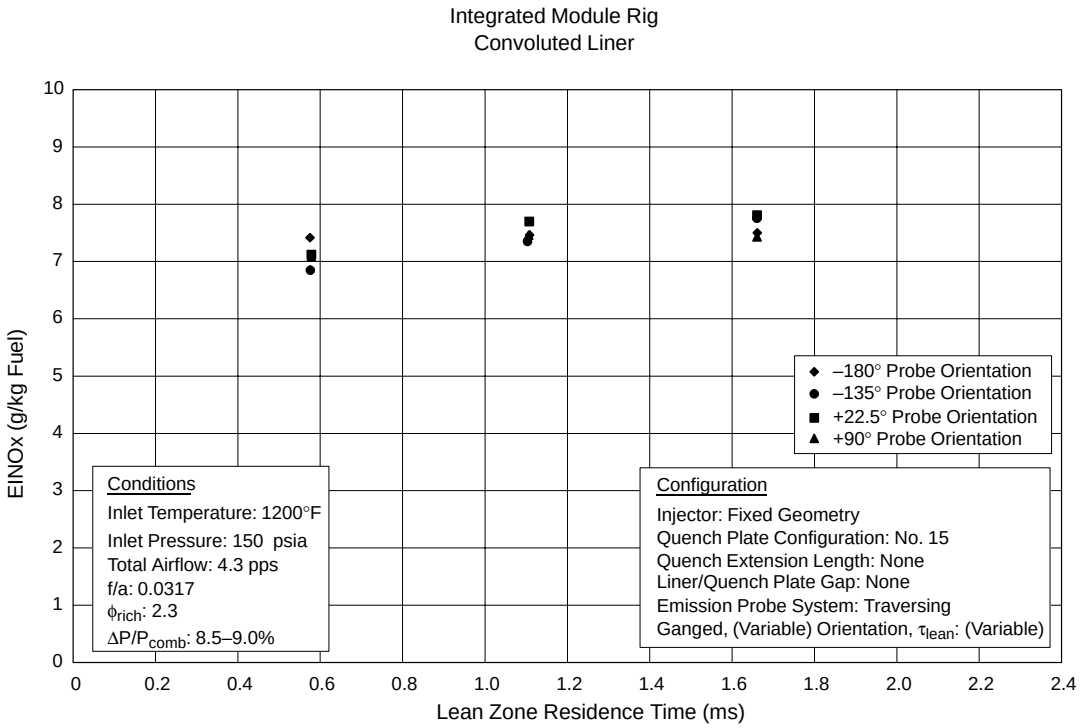

Figure 210. NOx Emissions as a Function of Lean-Zone Residence Time for Quench Plate Configuration No. 15

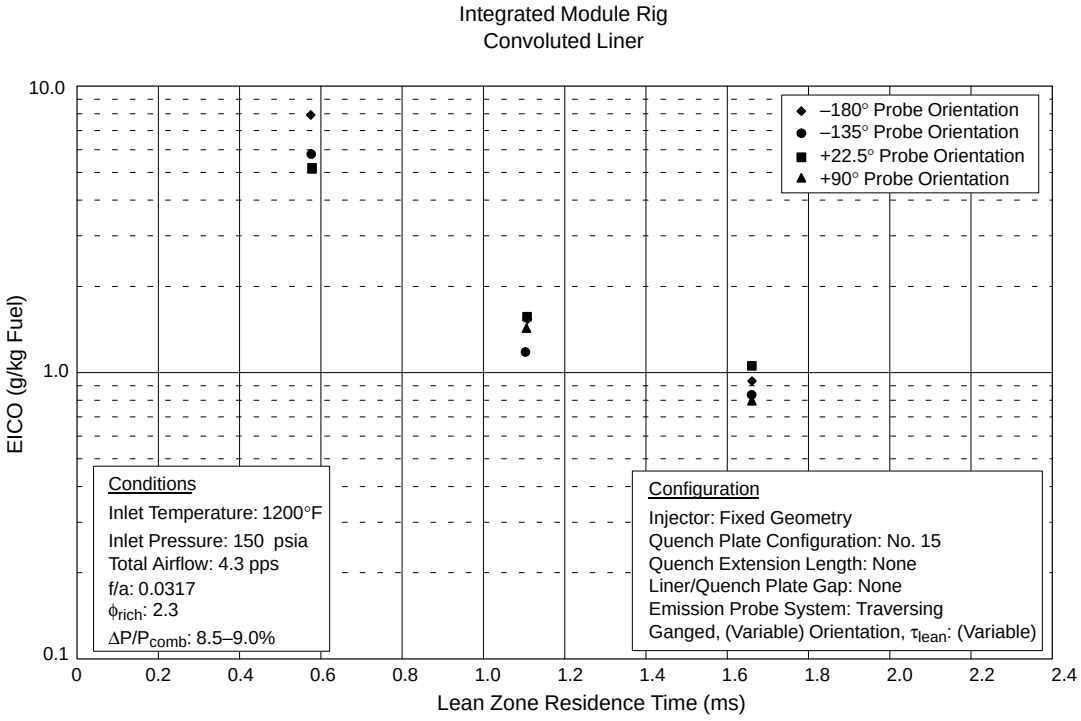

Figure 211. CO Emissions as a Function of Lean-Zone Residence Time for Quench Plate Configuration No. 15

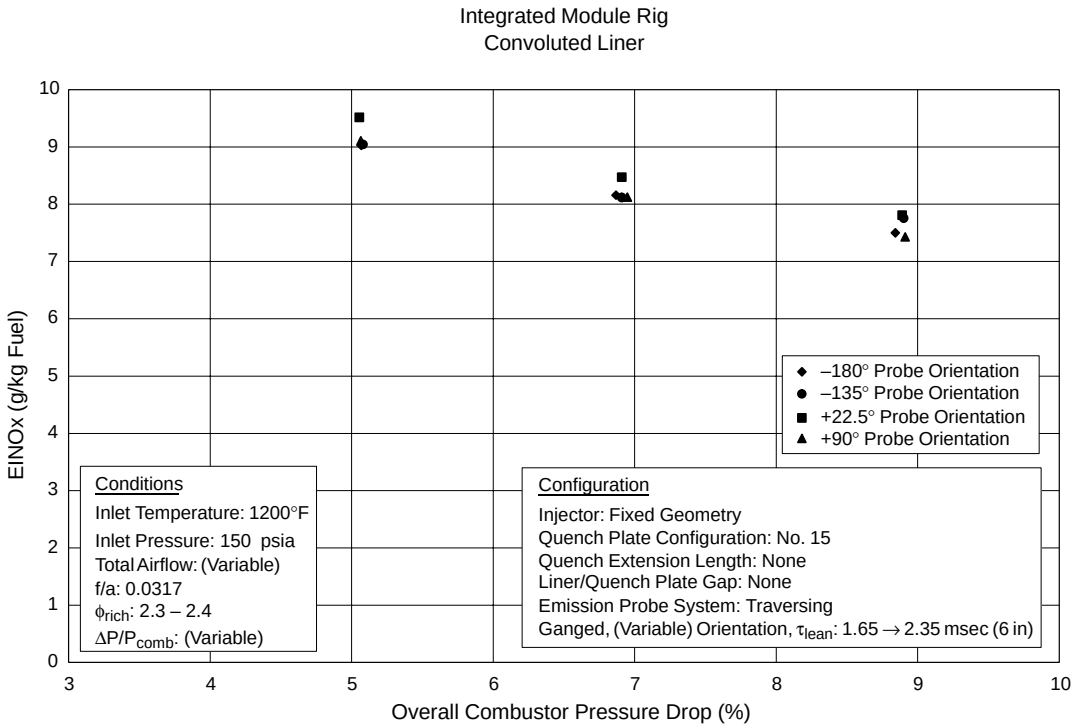

Figure 212. NOx Emissions as a Function of Combustor Pressure Drop for Quench Plate Configuration No. 15

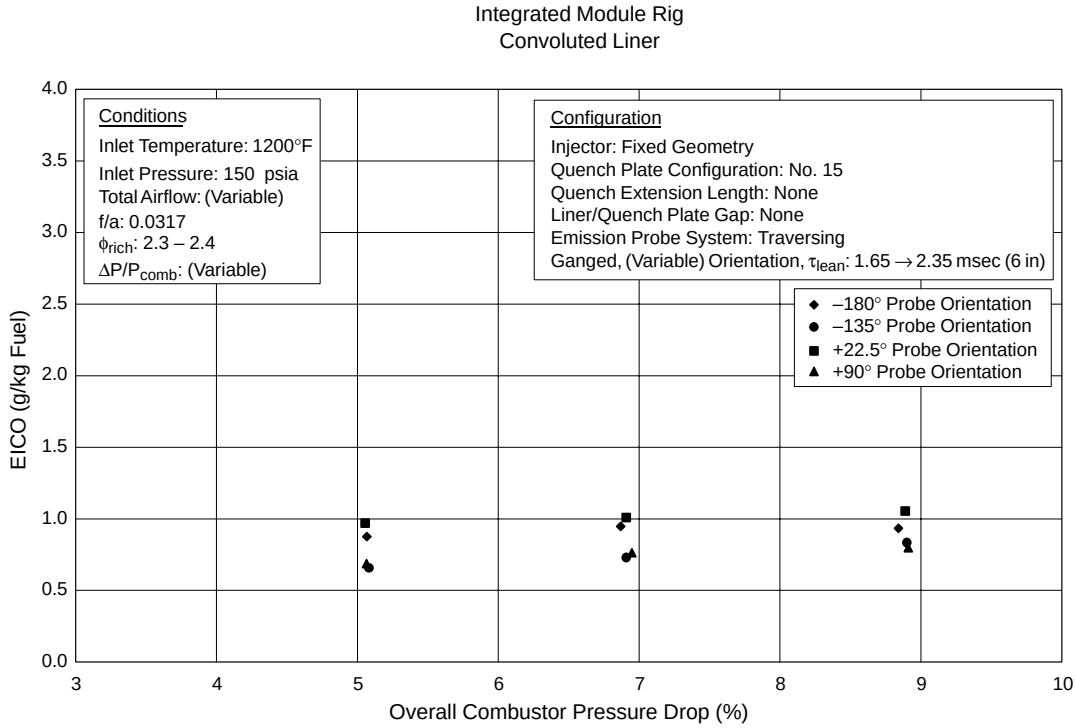

Figure 213. Emissions as a Function of Combustor Pressure Drop for Quench Plate Configuration No. 15

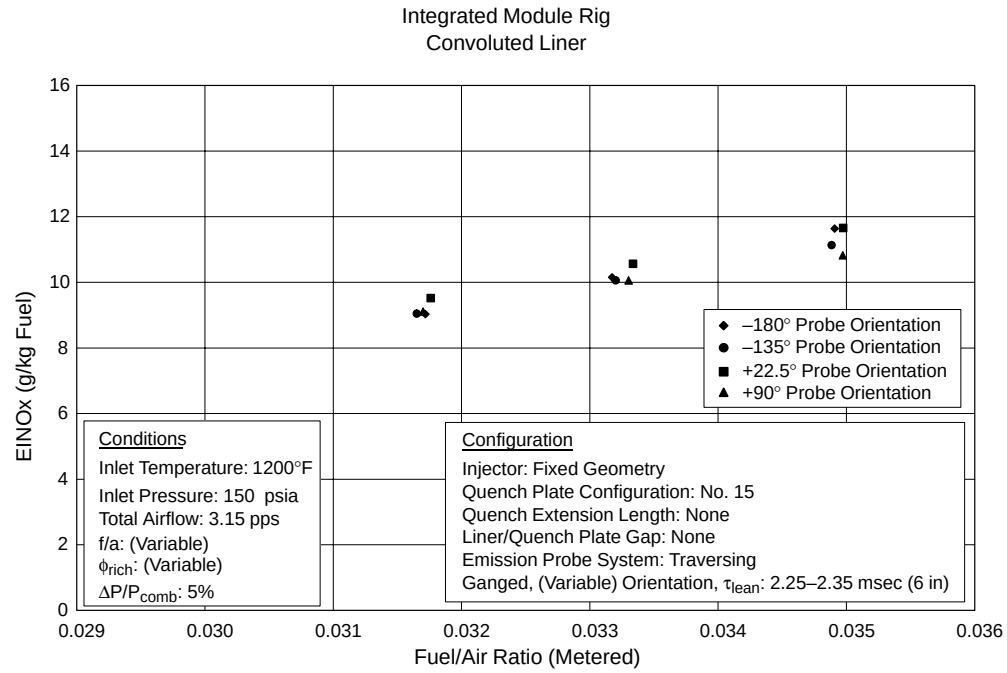

Figure 214. NOx Emissions as a Function of Fuel/Air Ratio for Quench Plate Configuration No. 15

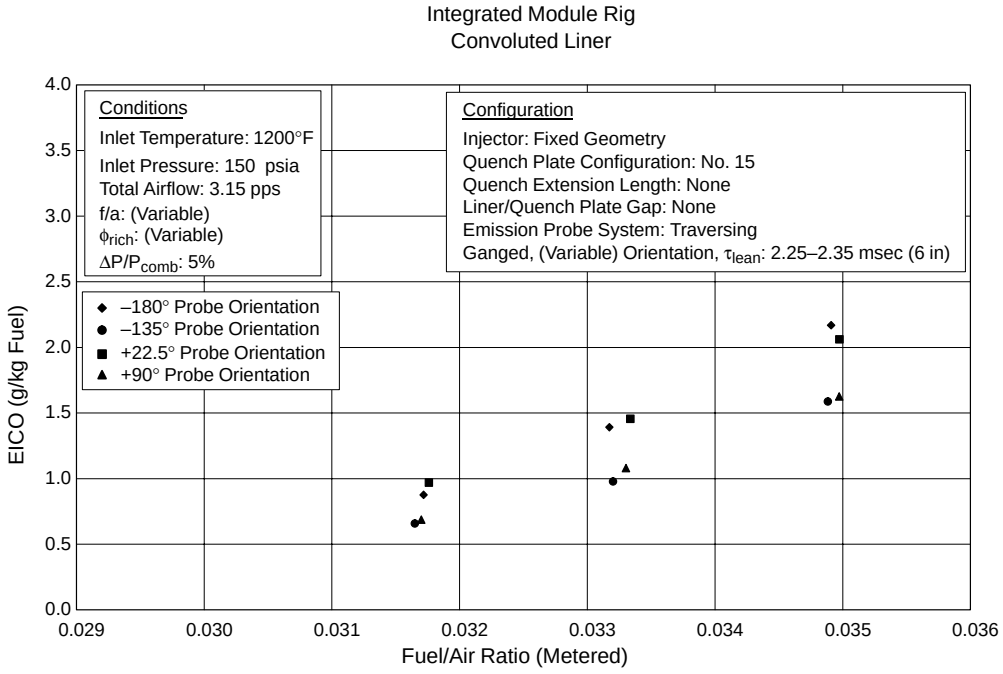

Figure 215. Emissions as a Function of Fuel/Air Ratio for Quench Plate Configuration No. 15

excursions were performed, and emissions were assessed as a function of these conditions for both a module operating with a rich front end and a module operating with a lean front. The results from those tests are summarized in Figures 216 through 221. The figures are marked with additional dotted lines signifying the fuel/air ratios that each of those modules would operate at in a fuel-shifted mode, assuming 5% of combustor air is reserved for cooling the lean-zone liners. It was found that satisfactory emissions and efficiency could be obtained at the subsonic cruise flight condition in a uniform, non-fuel-shifted condition. A more comprehensive evaluation of fuel shifting for an RSQ RQL combustor in a multiple-module sector rig, including rich-module/lean-module interaction effects, was investigated using the fuel-shifting sector rig.

4.5.3.3 Product Module Rig

The specific intent of this rig was to demonstrate a RQL combustor, using RSQ technology implemented in a quench-vane concept, capable of achieving the program goal of emissions of EINOx less than 5 fuel at the supersonic flight condition while maintaining combustion efficiencies in excess of 99.9%. Rig tests demonstrated the capability of achieving EINOx of 8.5 fuel at the supersonic flight condition. All configurations in the product module rig configuration demonstrated exceptional efficiencies, greater than 99.97%, at supersonic cruise conditions.

The design activities for the product-like implementation were conducted as a joint activity between Pratt & Whitney and United Technologies Research Center. Combustion tests of the product-module rig were conducted in Cell 1E of the JBTS at UTRC. The product-module rig combustors were designed and fabricated specifically for this task and targeted as a representative section of the full-scale RQL combustor concepts. The product-module rig combustor was designed as a drop-in replacement section for the single-module rig combustor — to make efficient use of the existing test facility and to support the rapid development process for the forthcoming combustor downselect.

In the product-module rig configuration, the total airflow traveled through a 6-inch pipe to the combustor, and the rich-zone and quench-zone airflows were set by the combustor hardware and determined by the relative effective flow areas of the passages leading into each zone of the combustor. The product-module rig configuration was designed to control airflow split via the effective areas of the fuel injector/bulkhead assembly and the rich-zone liner cooling/quench airflow passages. These flow passages were designed to provide the desired rich-zone flow of approximately 23% of the total combustor airflow.

The injector configuration consists of radial in-flow swirlers with air introduced through inner and outer passages. Each of these passages contained tangential slots through which air was admitted, imparting a swirl component to the flow. A centrally mounted fuel injector delivered fuel through radial jets, spaced at even azimuthal intervals. The radial in-flow swirler/fuel injector system was used in both builds of the product-module rig.

The RQL product-module rig was designed to approximate one inner-bank module of the RQL 3770.54 Product Engine, Figure 222. The product engine design consisted of two banks radially with the inner bank flowing approximately 40% of the total combustor airflow. The inner bank was composed of 24 trapezoidal modules. The product-module rig was therefore designed to fit within a 15° sector with an inner radius of 13.150 inches and an outer radius of 19.595 inches.

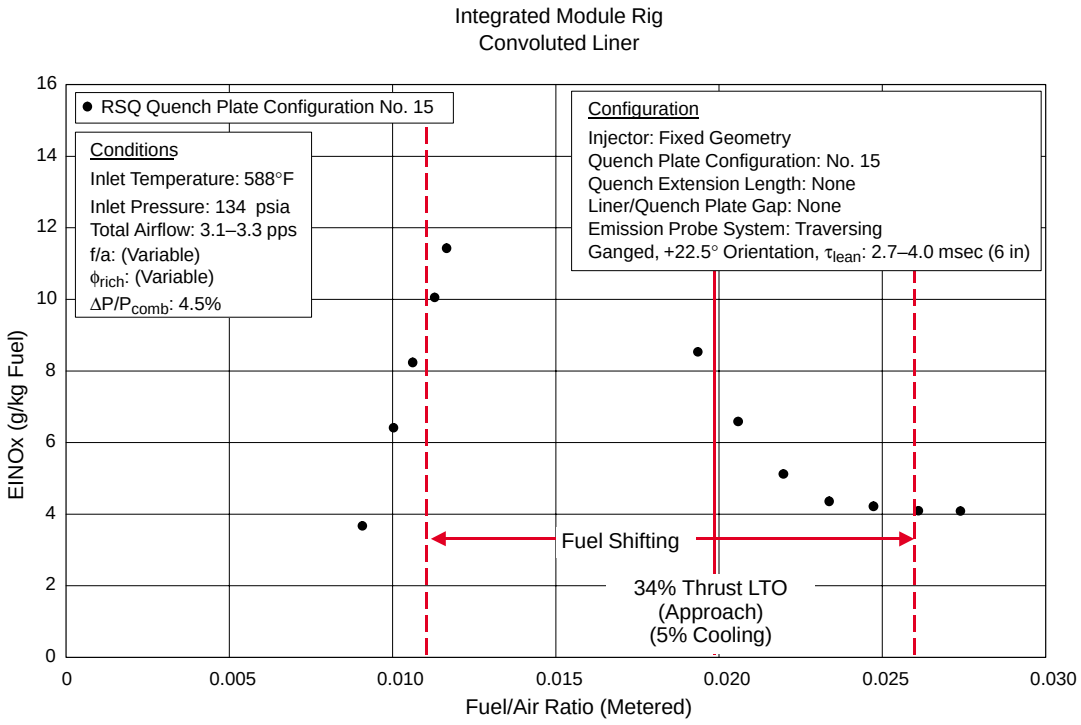

Figure 216. NOx Emissions at 34% Thrust LTO (Approach) for Quench Plate Configuration No. 15

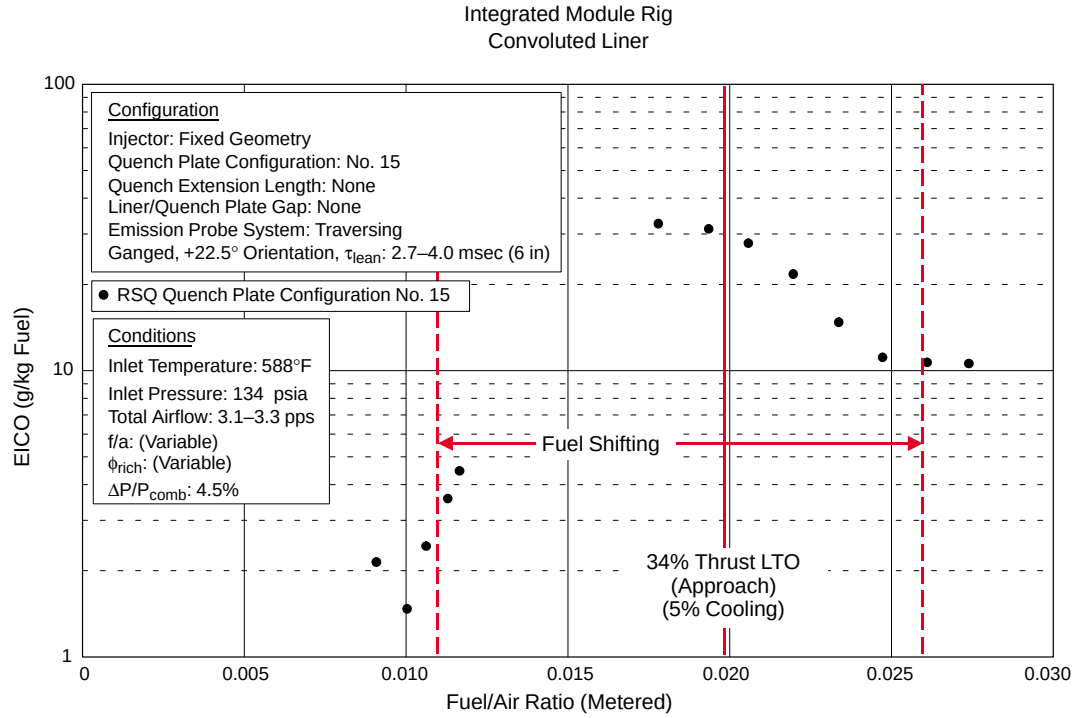

Figure 217. CO Emissions at 34% Thrust LTO (Approach) for Quench Plate Configuration No. 15

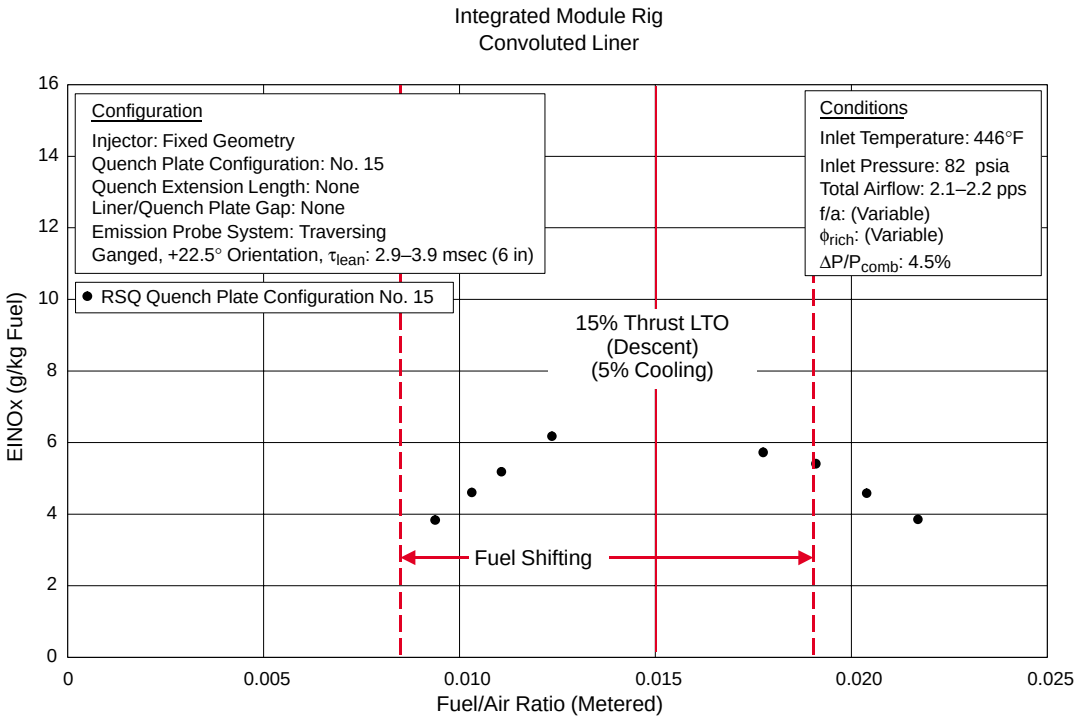

Figure 218. NOx Emissions at 15% Thrust LTO (Descent) for Quench Plate Configuration No. 15

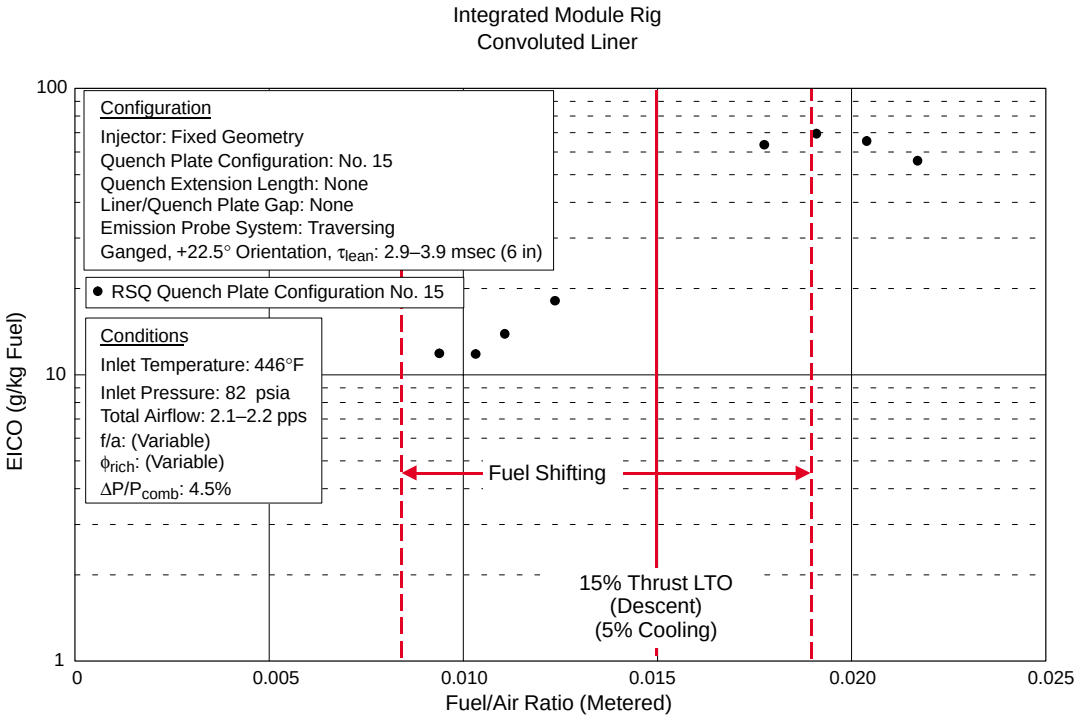

Figure 219. CO Emissions at 15% Thrust LTO (Descent) for Quench Plate Configuration No. 15

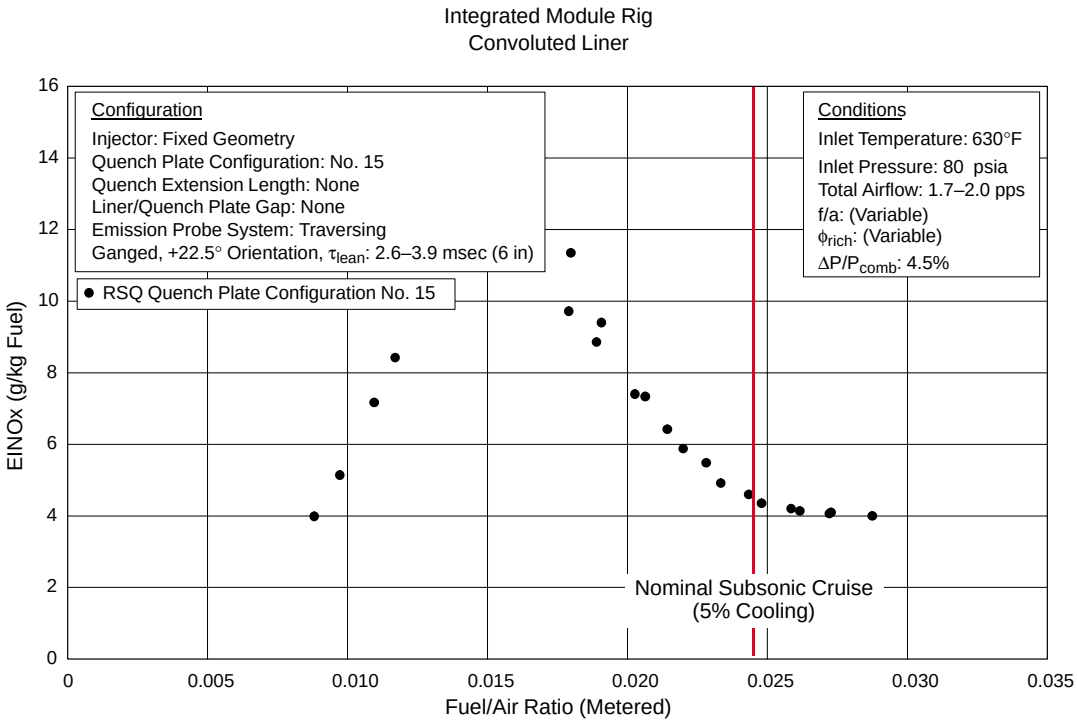

Figure 220. NOx Emissions at Nominal Subsonic Cruise for Quench Plate Configuration No. 15

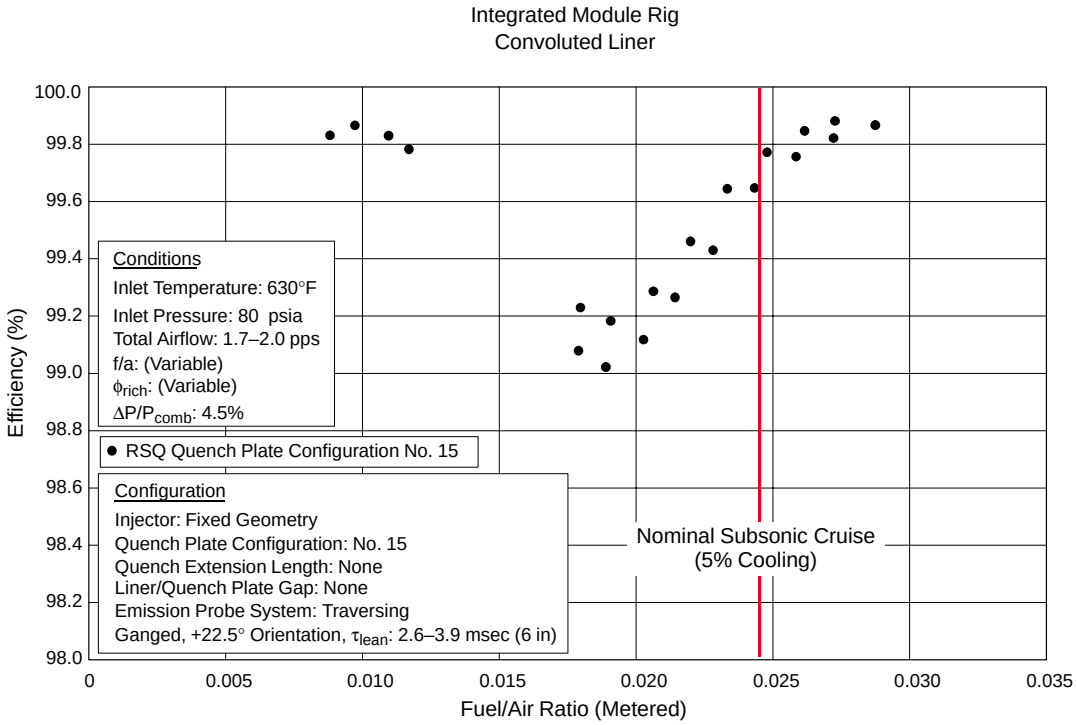

Figure 221. Efficiency at Nominal Subsonic Cruise for Quench Plate Configuration No. 15

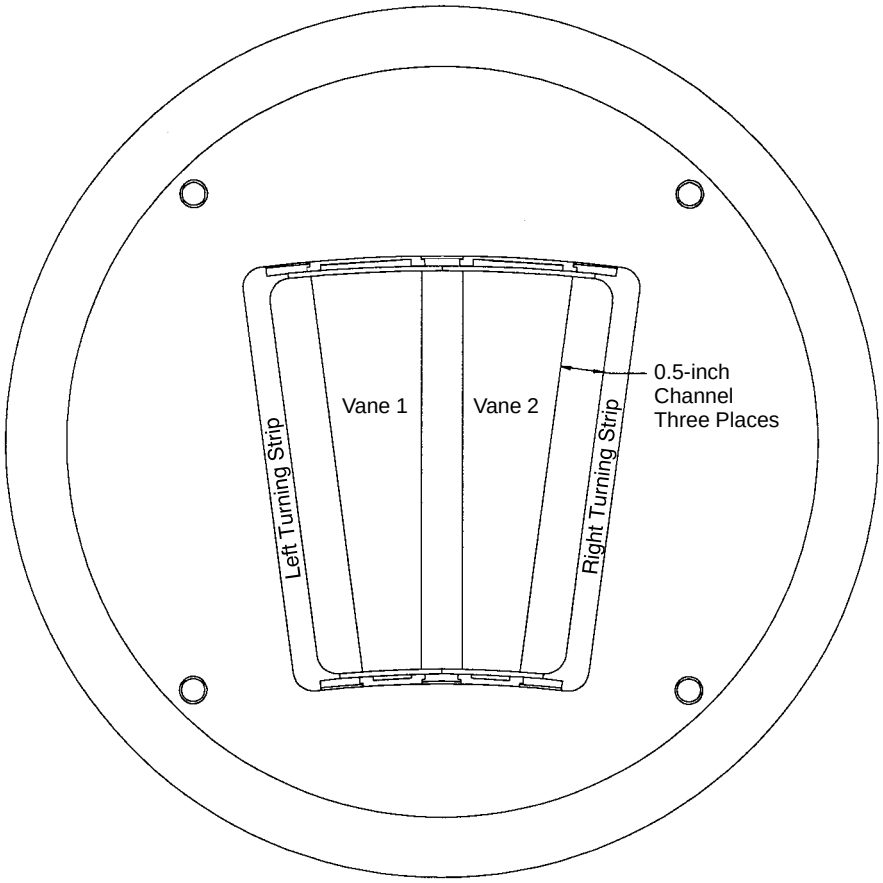

Figure 222. Product-Module Rig Build 1, Aft Looking Forward

Product Module Rig – Build 1

The product-module rig Build 1 and 1A RQL configurations incorporate the RSQ concept by using quench vanes to break up the quench zone into three channels, 0.5-in wide (see Figure 222). These 0.5-in channels are created by two quench vanes and by two sidewall turning strips. A cross section of the rig is shown in Figure 223, and a 3D solid-model exploded view of the combustor is shown in Figure 224.

Testing of build 1/1A of the Product Module Rig was conducted in Cell 1E of the JBTS at UTRC during the period of February 27, 1998 through March 2, 1998. Testing was focused on conditions taken from the HSR/CPC Program Coordination Memo GE97–002–C, summarized in Table 30 (page 166), with the primary intent of assessing supersonic cruise emissions in support of the combustor downselect.

The main test section houses the rich/quench module. The exit transition zone is water cooled and has a cast ceramic flowpath. The cast ceramic transitions the flowpath from a trapezoid to a cylindrical shape to facilitate emissions sampling. The rotating/translating emissions probe protrudes into the lean zone. The probe rotates about the pressure-vessel centerline and can be translated up to the trailing edge of the quench vanes. The trapezoidal flowpath for the 15° sector has been cut into the combustor housing.

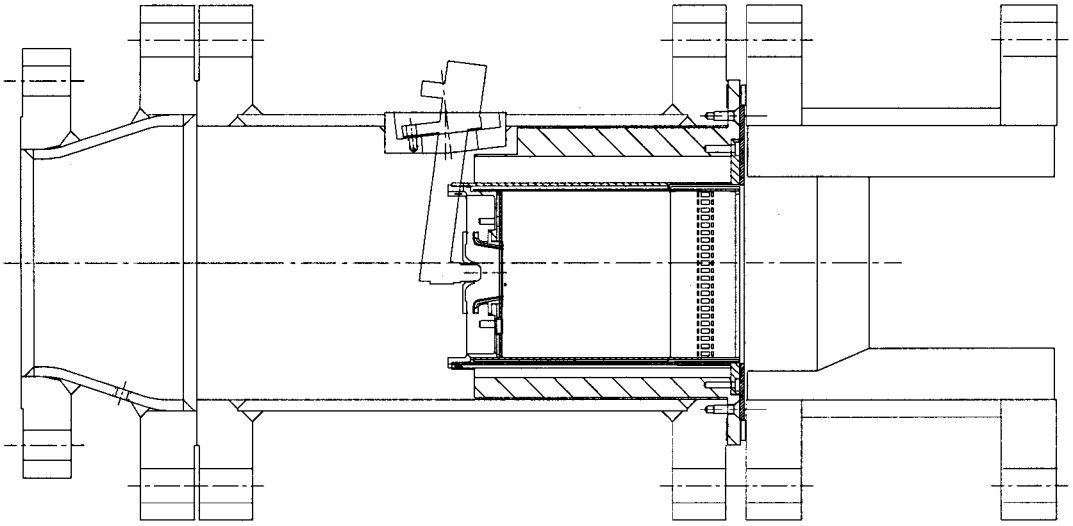

Figure 223. Cross Section of Product-Module Rig Build 1

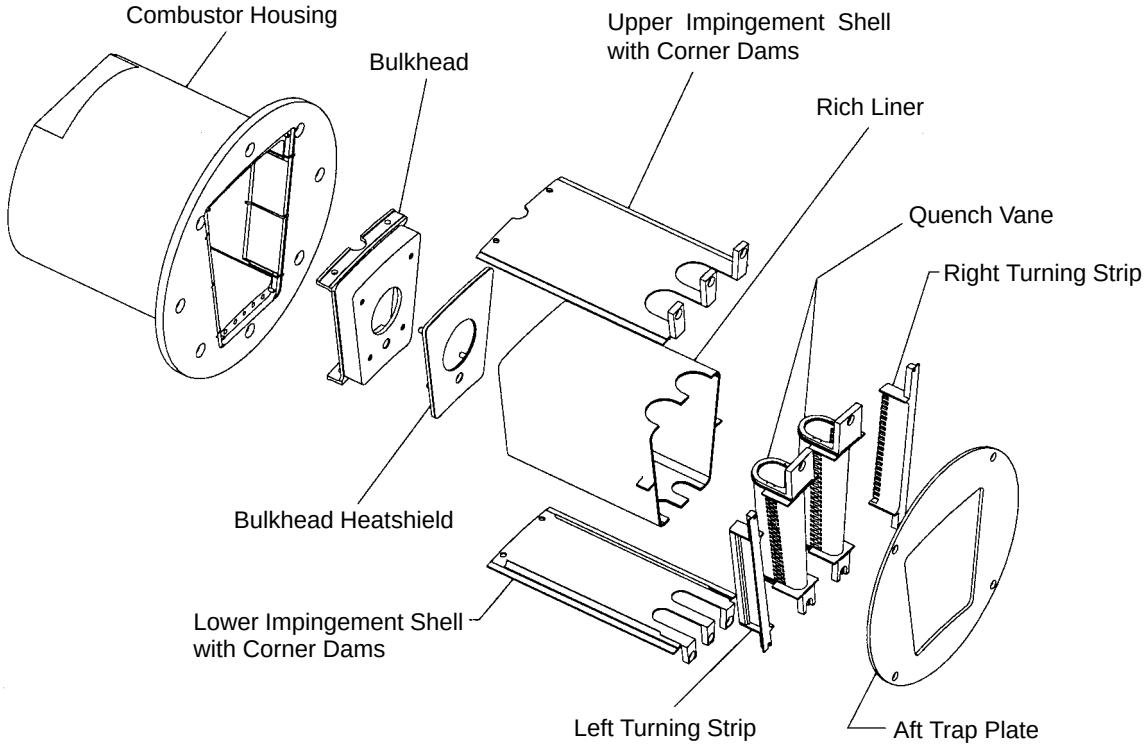

Figure 224. Exploded View of Product Module Rig Build 1

The bulkhead assembly consists of the bulkhead structure, the hea tshield, and the swirler. The bulkhead contains the mounting hole for the swirler and igniter and impingement cooling holes. The spent impingement air travels radially inward and mixes with the swirler air. Angled standoffs were placed on the bulkhead to add swirl to the spent impingement air, corotating with the outer swirler air. The swirler is a radial in-flow device. The fuel injector is a radial jet injector and sprays the fuel onto the filming surface of the radial in-flow swirler. The fuel injector used was an existing P&W engine fuel injector.

The rich-zone liner is a basic trapezoidal sector shape. The upper and lower surfaces of the liner are impingement cooled. Spent impingement air is exhausted rearwards and convectively cools the area of the liner between the quench vanes before it is dumped into the exit transition zone. The sidewalls of the liner are convectively cooled. Corner dams are tack welded to the upper and lower impingement shells. These dams are intended to separate the convection-cooled liner sidewalls from the impingement-cooled upper and lower surfaces of the liner.

The vane outer shell is a tapered racetrack shape. The axial length is constant while the width of the vane tapers from the OD to the ID. There are main quench orifices on each side of the vane. Upstream and downstream of the main orifices are exhaust slots for spent impingement cooling air, located in line with the main orifices.

The turning strips take air that was used to convectively cool the liner sidewalls and turns it 90° into the rich gas path. As the air is turned, it is also broken up into discreet jets. The aft end of the turning strip consists of an effusively cooled sidewall so that the turning strip ends at the same axial plane as the quench vanes.

A modification to the Build 1 design was intended to perturb the split within the combustor in an attempt to bring the split in line with design intent. Build 1 was modified into Build 1A by installing a blockage ring at the inlet to the radial in-flow swirler, a standard practice for parametric variations of flow split while conducting development combustor testing. This blockage ring was installed such that it reduced the airflow to only the inner swirler of the radial in-flow swirler. Installation of the blockage ring resulted in a net reduction in the overall bulkhead effective flow area (including inner swirler passage, outer swirler passage, and bulkhead cooling) from 1.11 in^2 for Build 1 to 0.90 in^2 for Build 1A.

Results from Builds 1 and 1A of the product module rig for the 15% thrust LTO descent condition are shown in Figures 225 through 227. Theoretically, for a fixed-geometry combustor, the stoichiometry of the rich zone must fall on a straight line that passes through the origin of the graph. Therefore, the curve fits shown on the graph have this behavior enforced. As expected, the NOx increases as the rich-zone approaches stoichiometric conditions and drops off significantly at higher fuel/air ratios, when the rich zone is well above stoichiometric conditions. There appears to be minimal impact on the NOx emissions by the change in split (that is, bulkhead effective flow area). The nominal set-point fuel/air ratio for the inlet condition specified is annotated on the graph. For this 15% thrust LTO descent condition, it is anticipated that the RQL would be operated in a fuel-shifted mode with approximately 40% of the burner operating like the lean front end of the graph and approximately 60% of the combustor operating like the rich portion of the graph. Superposition of the two behaviors, presuming minimal interaction effects, may be used to predict emissions at the LTO nominal fuel/air ratio condition. From the graph, it is apparent that approximately 4–5 EINOx would result from the superposition of these two behaviors. Excellent efficiency, greater than 99.5%, was obtained for most fuel/air ratios tested.

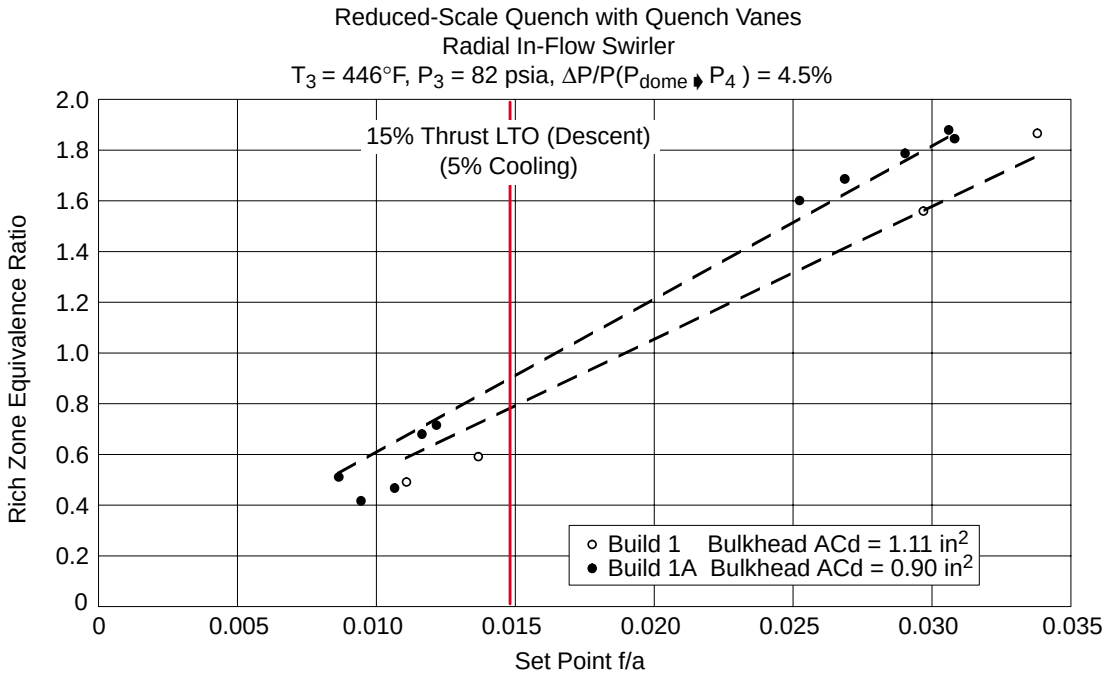

Figure 225. Rich-Zone Stoichiometry Comparison at 15% Thrust LTO (Descent) Condition for Product Module Rig Builds 1 and 1A

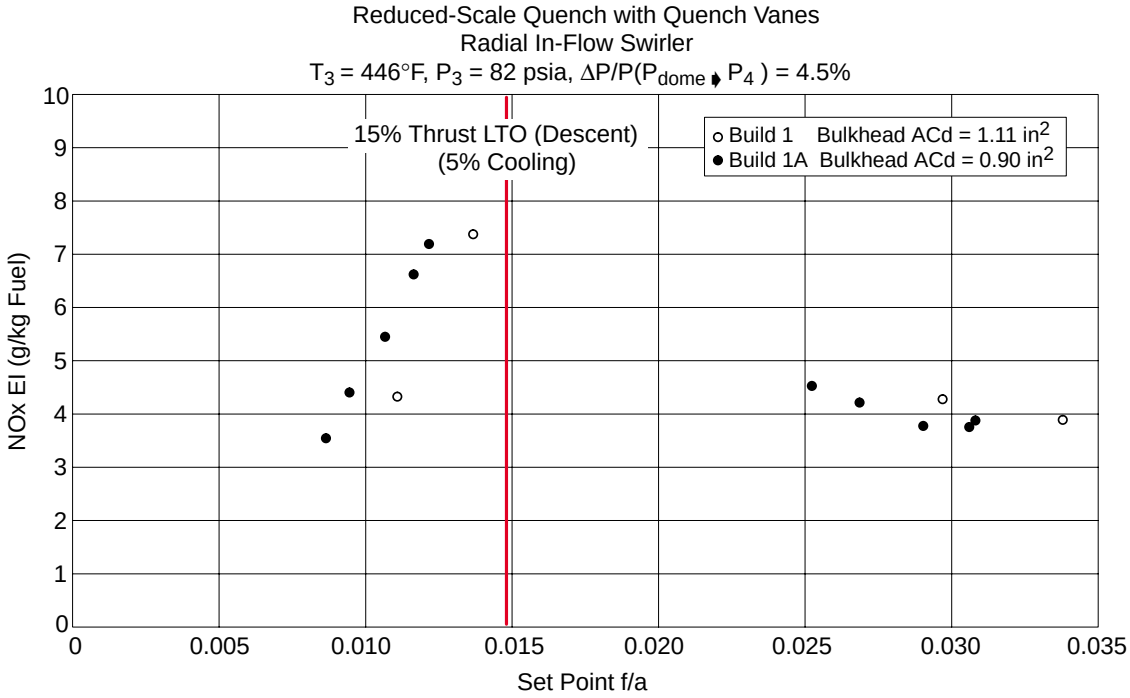

Figure 226. NOx Emissions at %15 Thrust LTO (Descent) Condition for Product Module Rig Builds 1 and 1A

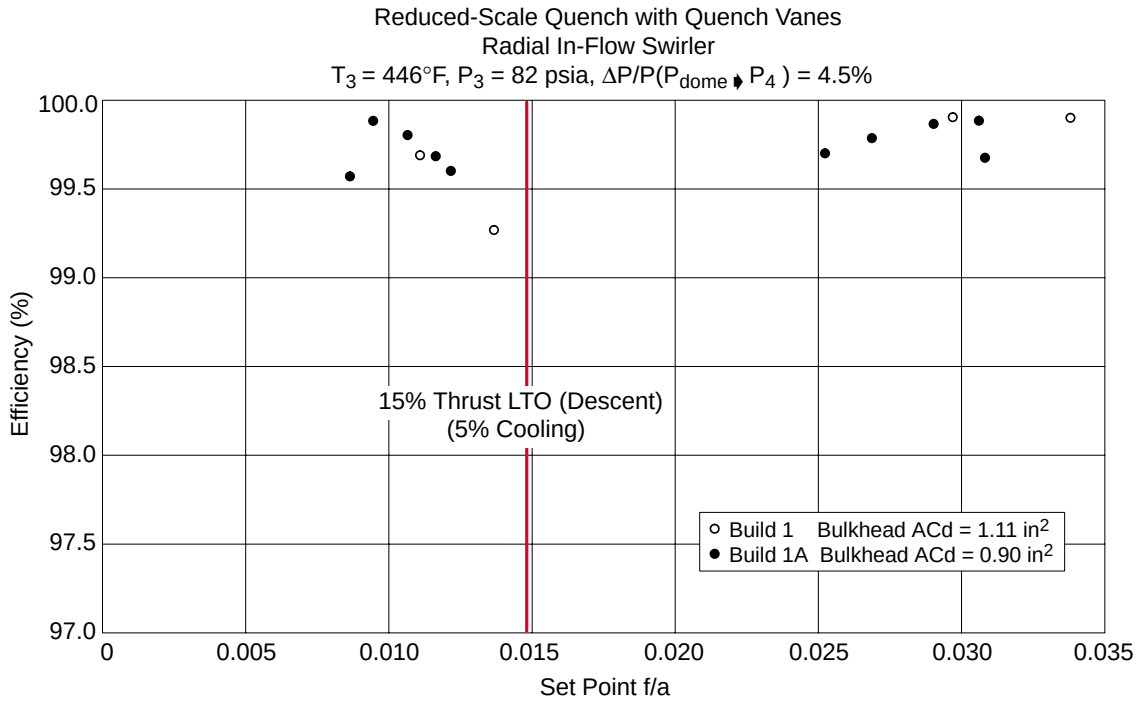

Figure 227. Efficiency at 15% Thrust LTO (Descent) Condition for Product Module Rig Builds 1 and 1A

A brief inspection of the combustor was conducted during the shutdown between Builds 1 and 1A. It was observed at this time that two of the four corner dams had apparently broken some welds and were out of position as shown in Figure 228. The two corner dams located on the ID of the rich zone were lifted up, partially blocking the sidewall/turning-strip airflow passage. These corner dams separate the sidewall/turning-strip flow from the spent top and bottom impingement cooling air. The corner dams were pushed back into place, and appeared to stay seated in the original position, so that combustion testing could continue.

Build 1A testing, with the blockage ring on the swirler, began on March 2, 1998. After testing at the descent condition, the combustor was blown-out so that the inlet conditions could be raised to the supersonic cruise condition. Immediately after light off at supersonic cruise, the airflow split was observed to have changed, and the rig was shut down. Inspection found significant distress to the rich-zone liner and quench vanes. All distress was limited to the heat-shield surfaces of the combustor; the major structural components showed no distress. The corner dams were again found lifted. A root-cause investigation identified the problem as fundamentally associated with these corner dams. The resultant position, after dislodging, significantly blocked sidewall flow, preventing adequate convective cooling of the sidewall. Without adequate cooling, the sidewall liner temperatures exceeded design limits, resulting in thermal distortion. Build 1/1A testing was terminated, and the lessons learned were applied to the next build of the product-module rig.

Product Module Rig – Build 2

Build 2 of the product module rig focused on the following major changes: smaller quench-zone channel height for improved emissions, simulation of an annular RQL configuration with improved feed of sidewall quench orifices, and improved rich-zone liner cooling control. The design of Build

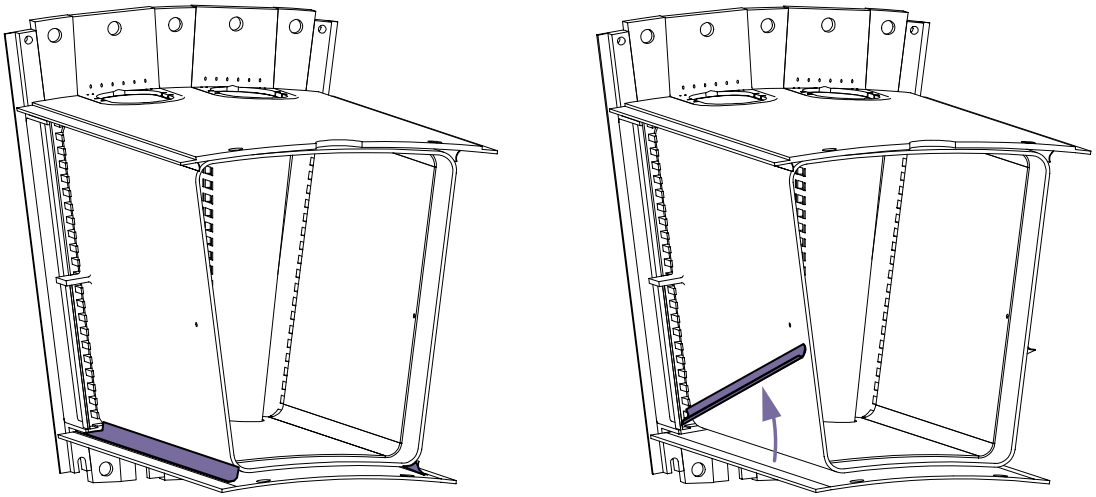

Figure 228. Forward-Looking-Aft View of Product Module Rig Build 1 Combusor Showing Corner Dam Weld Failure and Impact

2 has four quench zone channels, 0.3-in wide, as shown in Figure 229. Build 2 also incorporates "half vanes" instead of turning strips at the sidewalls to simulate a representation of an annular rich-zone design in this single fuel injector rig. The rich-zone liner was cooled on all four sides with impingement air. The spent impingement air was extracted from the rig and separately valved and measured through a venturi for improved liner durability. A cross section of the Build 2 design is shown in Figure 230. Figure 231 is an exploded 3D solid-model view of the components of the Build 2 combustor. A comparison of the flowpath between Build 1 and Build 2 is shown in Figure 232.

Build 2/2A of the product module rig demonstrated the capability of achieving a $EINO_X$ of 8.5 fuel at the supersonic cruise flight condition with exceptional efficiency, greater than 99.97%.

To facilitate a rapid redesign for this second build, many components were reused or designed with similar features to Build 1. The main test section, exit transition zone, and fuel injector were reused from Build 1. The combustor housing for Build 2 was similar to Build 1 except additional material was removed to provide room for the impingement exhaust tubes and to provide better flow of air to the liner impingement holes. The bulkhead assembly and aft trap plate were similar to Build 1.

The rich-zone liner for Build 2, while the ID and OD radius remained the same, incorporated tapered "half vanes" on the two sidewalls rather than straight turning strips. As a result, the sidewall angle for Build 2 is slightly different. In addition, three vane slots are required for Build 2. The sidewall shells also have provisions for extracting spent cooling air through an orifice for measuring airflow and a control valve before dumping into the rig exhaust stack.

The vane outer shell is a tapered racetrack shape. The axial length is constant while the width of the vane tapers at a angle from the OD to the ID. There are main quench orifices on each side of the vane. Upstream and downstream of the main orifices are exhaust slots for spent impingement cooling air. Both sets of exhaust slots are located in line with the main orifices. The supports include some effusion holes to cool the platform area.

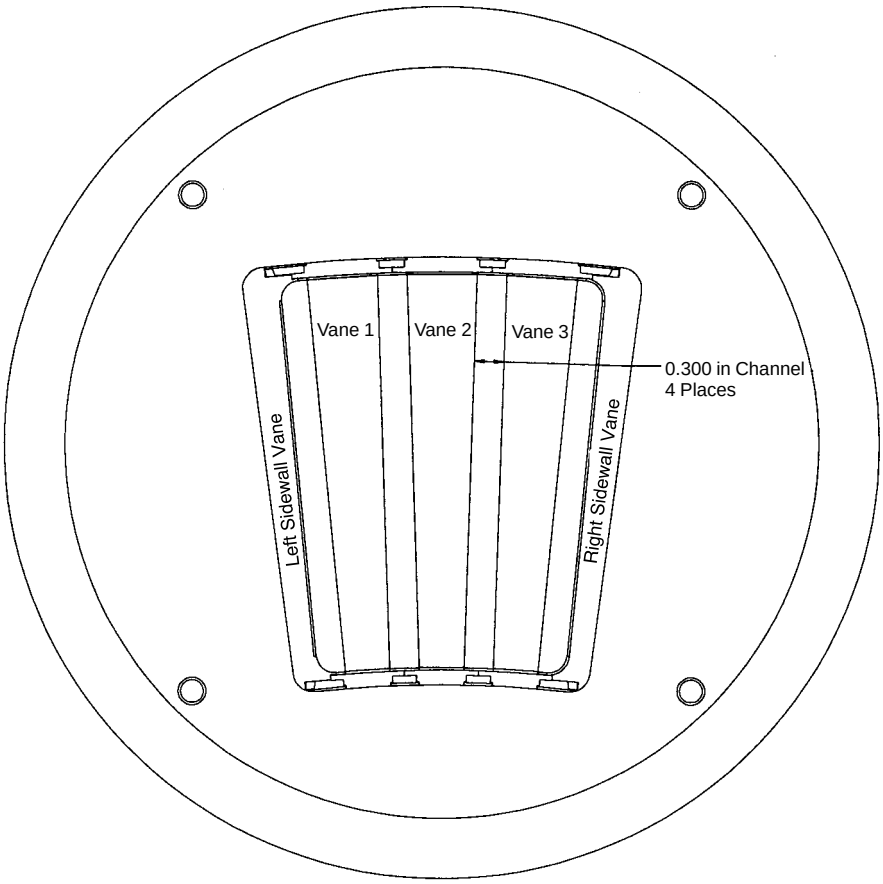

Figure 229. Product-Module Rig Build 2, Aft Looking Forward

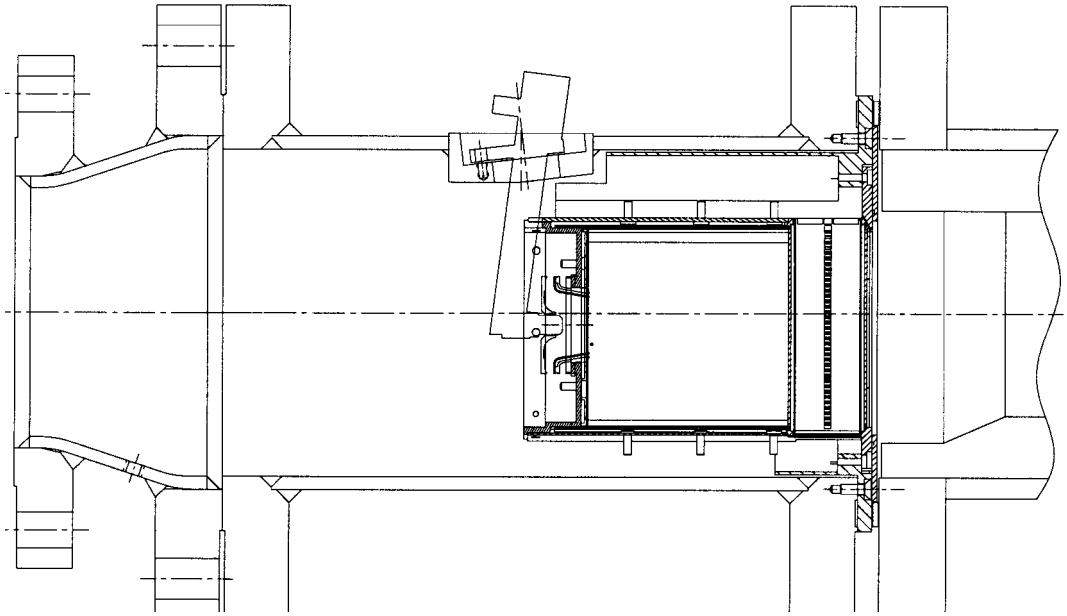

Figure 230. Cross Section of Product Module Rig Build 2

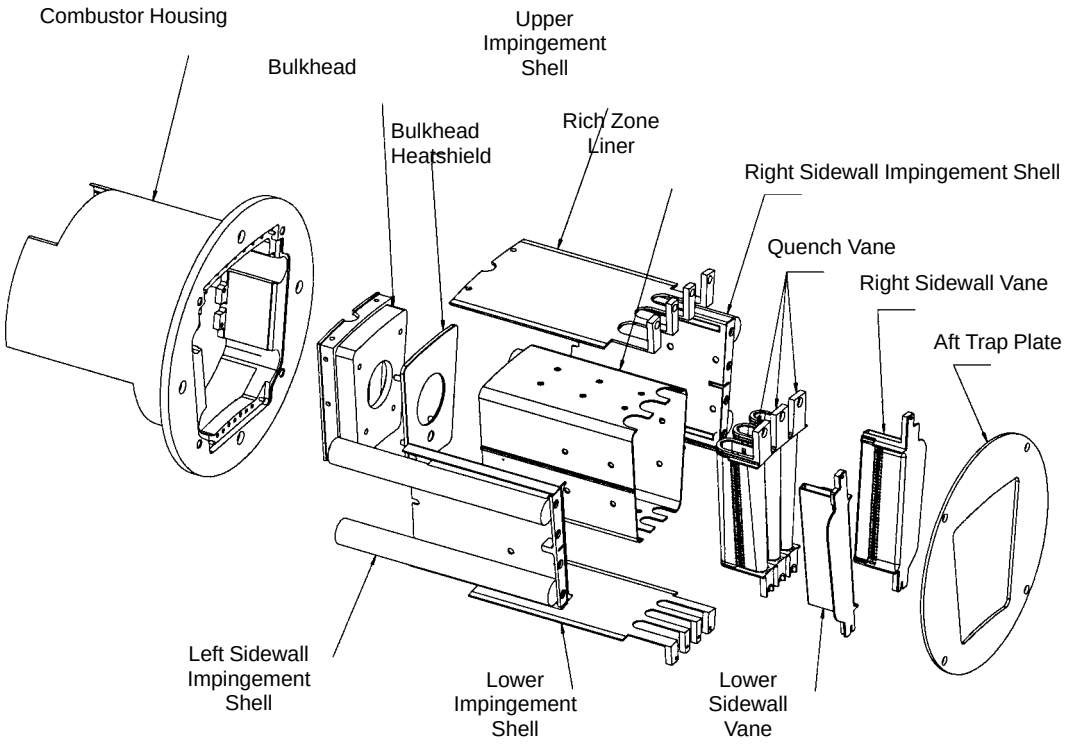

Figure 231. Exploded View of Product Module Rig Build

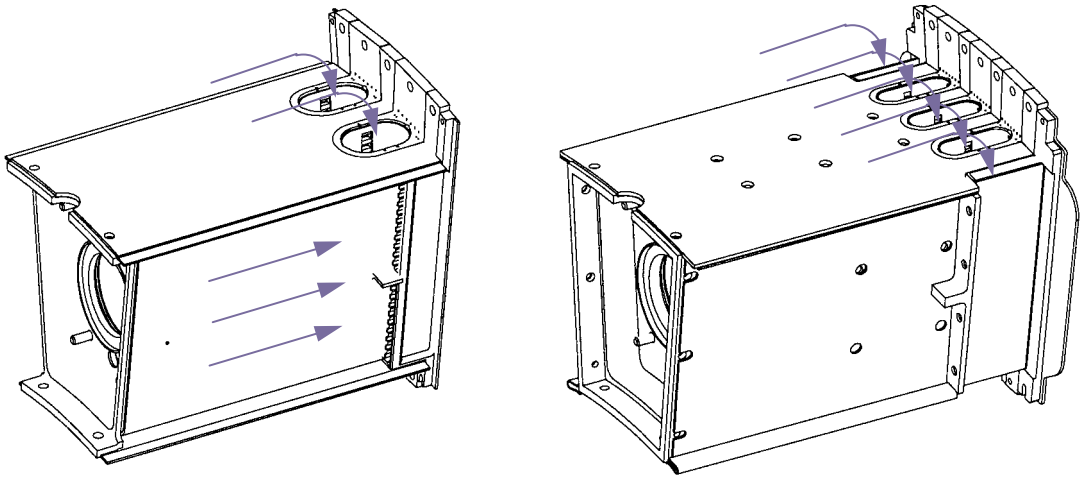

Build 1

- Air convectively cools liner side walls and is then turned into the combustor at the quench plane
- Liner ID and OD surfaces are impingement cooled

Build 2

- Sidewall vanes are fed from ID and OD shrouds (identical to center vanes)
- All liner surfaces are impingement cooled

Figure 232. Comparison of Airflow Paths for Product Module Rig Build 1 versus 2

The sidewall vanes are designed to simulate half of a normal quench vane. Because they are mounted flush with the sidewall of the rich-zone liner, they have a square leading edge, rather than a rounded front like the main quench vanes. In order to provide better feed of the quench air to the sidewall vanes, air is allowed to enter the sidewall vane baffle structure through holes machined in the outer face in addition to feed from the ID and OD sides.

When Build 2A was modified from Build 2 a larger effective flow area swirler was installed, changing the airflow split between the rich and quench zones. Data for Build 2A were acquired at the high-power conditions, focusing on the 100% thrust LTO takeoff and nominal supersonic cruise.

Results for the 5.8% thrust LTO idle condition for Build 2 are shown in Figures 233 through Figure 235. As shown in the stoichiometry graph, because of the lower than intended split associated with the Build 2 hardware, operation at nominal idle fuel/air ratio would result in rich-zone equivalence ratio of approximately 0.9, slightly higher than intended. As expected, NO_X emissions are very low at this low-inlet-temperature condition. CO emissions at idle appear much higher than intended, even for the lean-front-end conditions. The rather high UHC emissions at idle may be related to the particular flowfield characteristics of this swirler/injector combination at the fuel/air momentum ratios associated with these conditions. Poor idle efficiencies result from this CO and UHC behavior.

Results for the 15% thrust LTO descent conditions are shown in Figures 236 through 238 and are plotted along with the results from Build 1 and 1A. While NO_X emissions show similar behavior, the distinct differences in behavior that were observed in the CO and UHC emissions further support the presumption that the flowfield and fuel/air mixedness associated with the fuel injector/swirler used for Build 2 were not optimal for low-power performance.

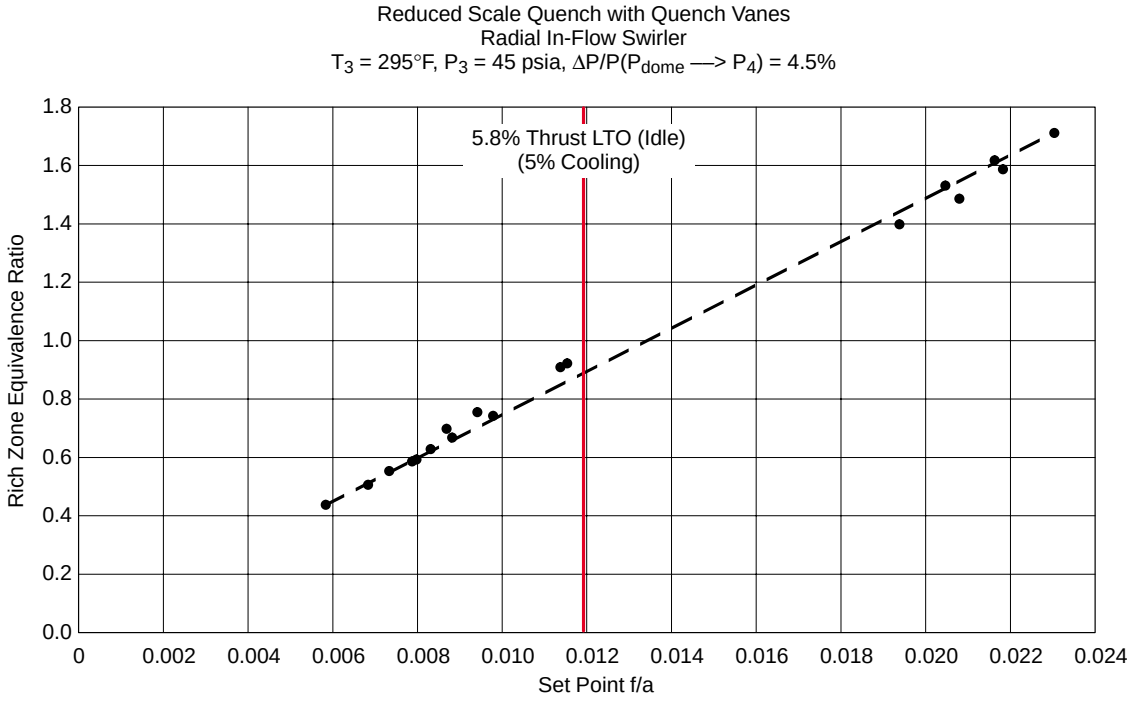

Figure 233. Rich-Zone Stoichiometry at 5.8% Thrust LTO (Idle) Condition for Product Module Rig Build 2

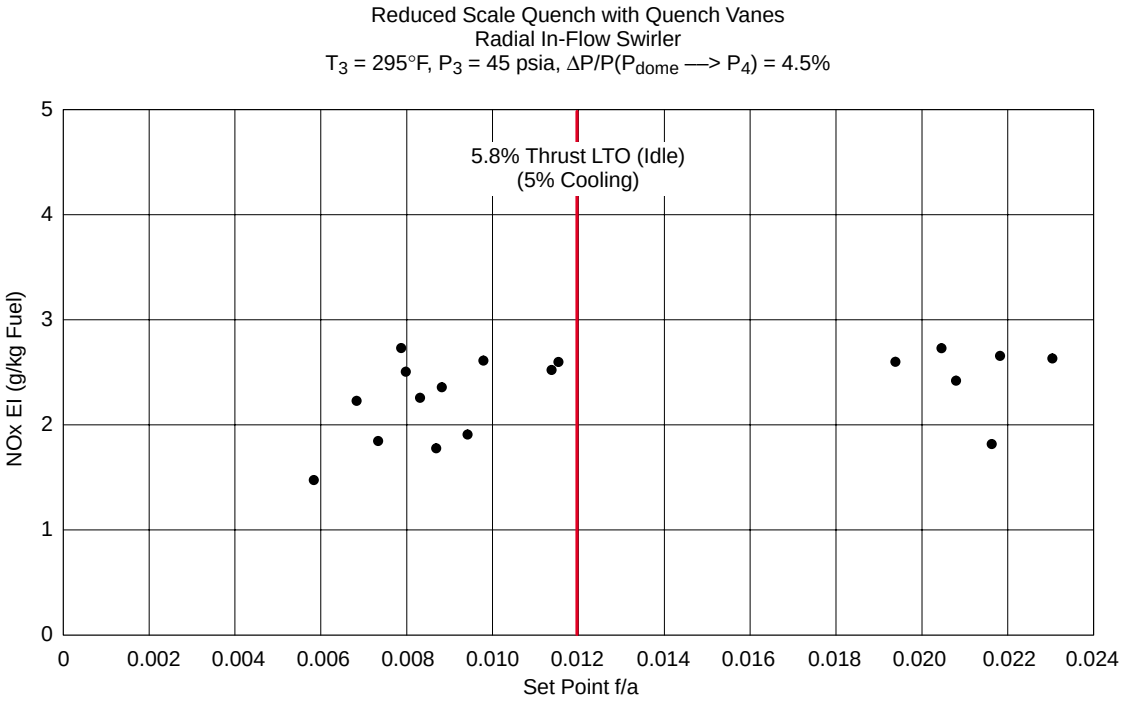

Figure 234. NOx Emissions at 5.8% Thrust LTO (Idle) Condition for Product Module Rig Build 2

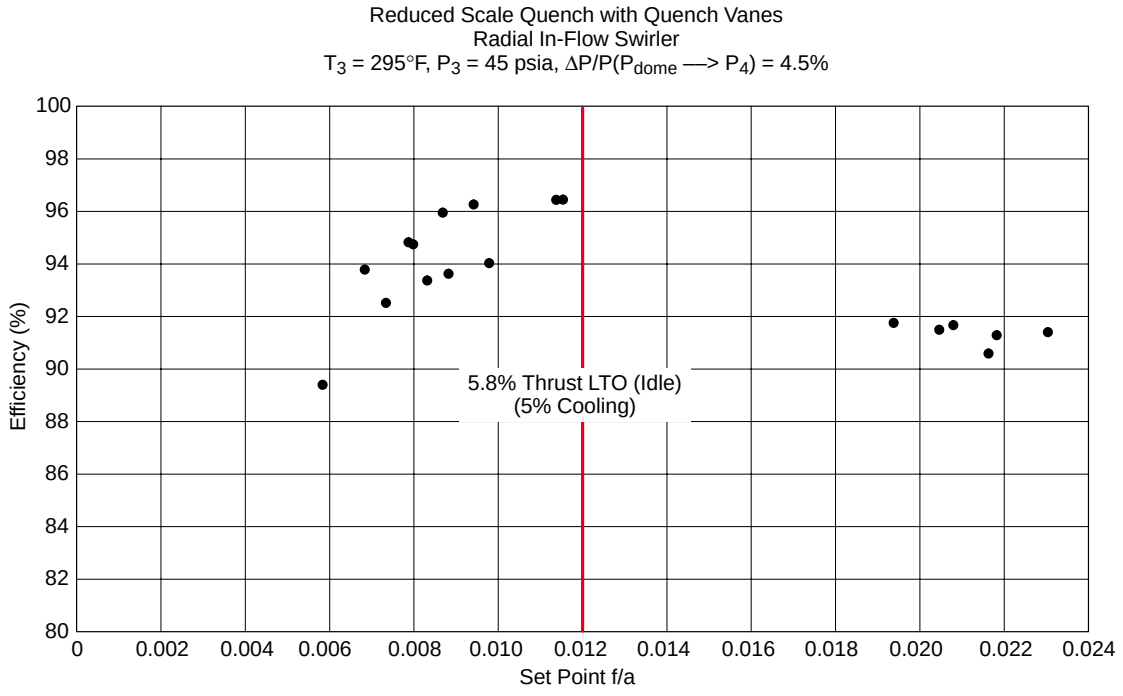

Figure 235. Efficiency at 5.8% Thrust LTO (Idle) Condition for Product Module Rig Build 2

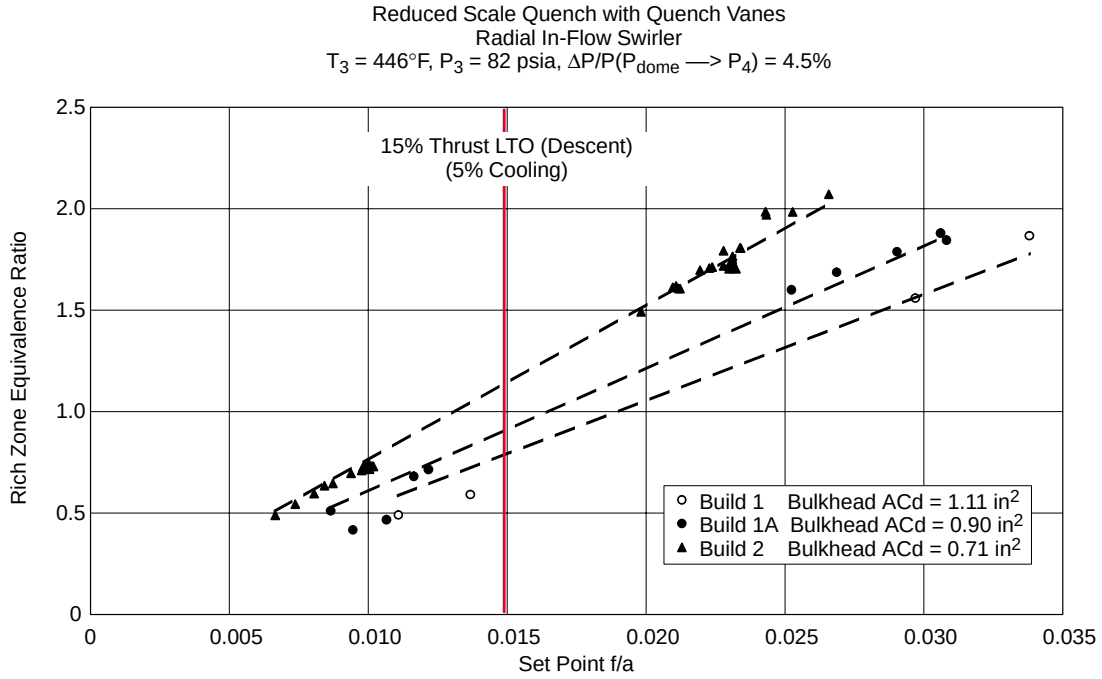

Figure 236. Rich-Zone Stoichiometry Comparison at 15% Thrust LTO (Descent) Condition for Product Module Rig Builds 1, 1A, and 2

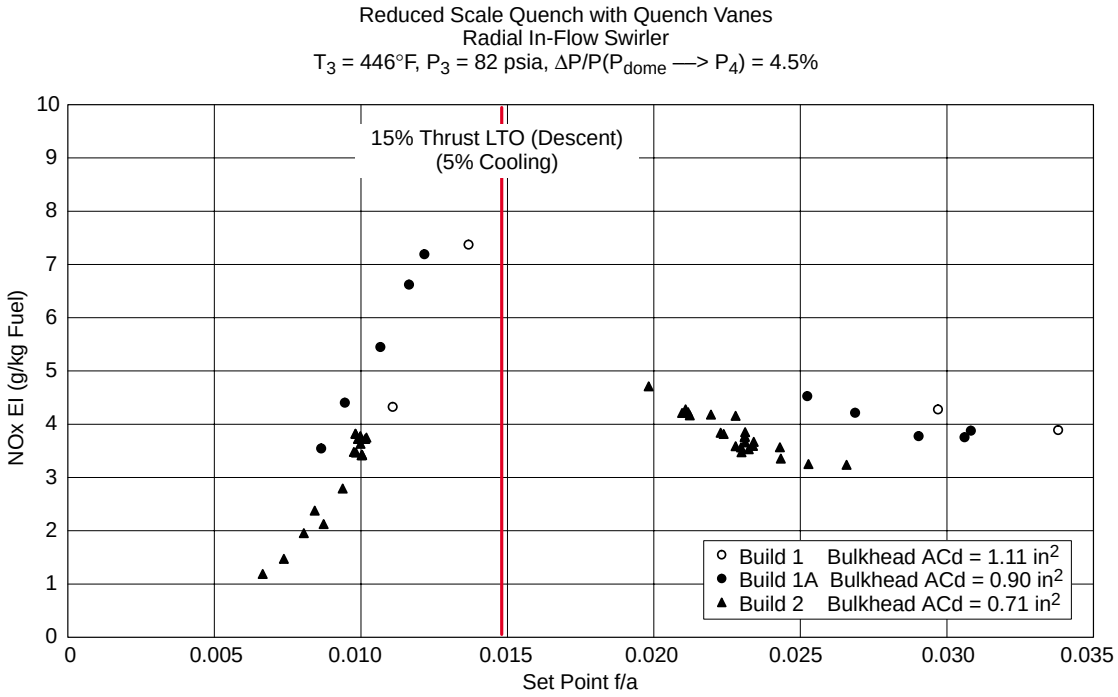

Figure 237. NO_X Emissions at 15% Thrust LTO (Descent) Condition for Product Module Rig Builds 1, 1A, and 2

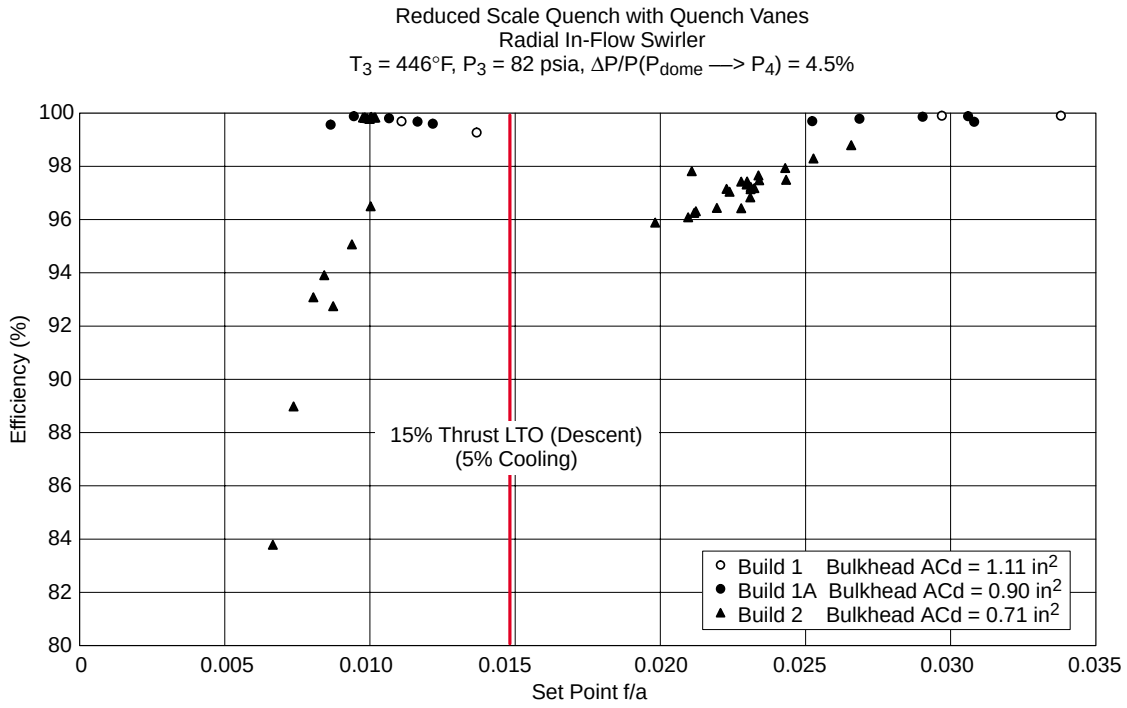

Figure 238. Efficiency at 15% Thrust LTO (Descent) Condition for Product Module Rig Builds 1, 1A, and 2

Nominal subsonic cruise results are shown in Figures 239 through 241. As shown in the stoichiometry graph, at the nominal subsonic cruise fuel/air ratio, for the split associated with the Build 2 fuel injector/swirler, the rich-zone equivalence ratio would be 1.6. However, data were taken at richer conditions and much leaner conditions initially, for the purposes of estimating the emissions performance without subjecting the liner to the potential of high temperatures prior to acquiring emissions at the supersonic cruise condition, the prime goal of this series of tests. It was anticipated that with additional time available after testing at the supersonic cruise condition, additional data could have been acquired at the exact nominal subsonic cruise fuel/air ratio. As anticipated, the NO_X behavior when the rich zone operates above stoichiometric conditions is fairly insensitive to fuel/air ratio where as the lean portion of the curve shows a much steeper dependency of NO_X as a function of fuel/air ratio. Combining the CO and UHC emissions behavior, the resultant combustor efficiency at the nominal subsonic cruise condition would be expected to be greater than the goal value of 99% required for cycle and economic performance of the HSCT aircraft.

Takeoff performance was assessed at a derated, reduced-pressure-condition, based on limitations of the facility that prevented operation of the combustor at inlet pressures above 150 psia. Time did not permit acquiring emissions as a function of inlet pressure at this condition. These data are usually acquired to determine the pressure dependency by which the data could be scaled to true combustor inlet pressure. However, experience with RQL combustors indicates that NO_X emissions typically scale as a function of the square root of the pressure ratio scale factor. Data acquired on other RSQ combustors in this program have shown pressure dependencies with scale factors as low as the pressure ratio raised to the 0.3 power.

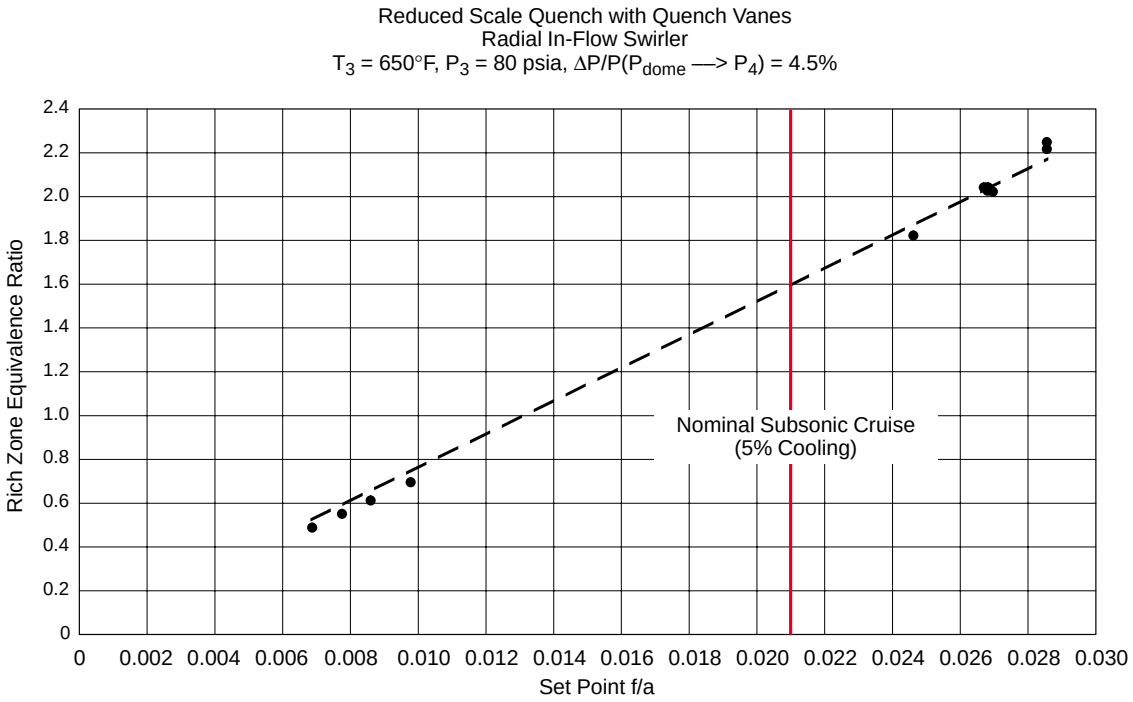

Figure 239. Rich-Zone Stoichiometry at Nominal Subsonic Cruise Condition for Product Module Rig Build 2

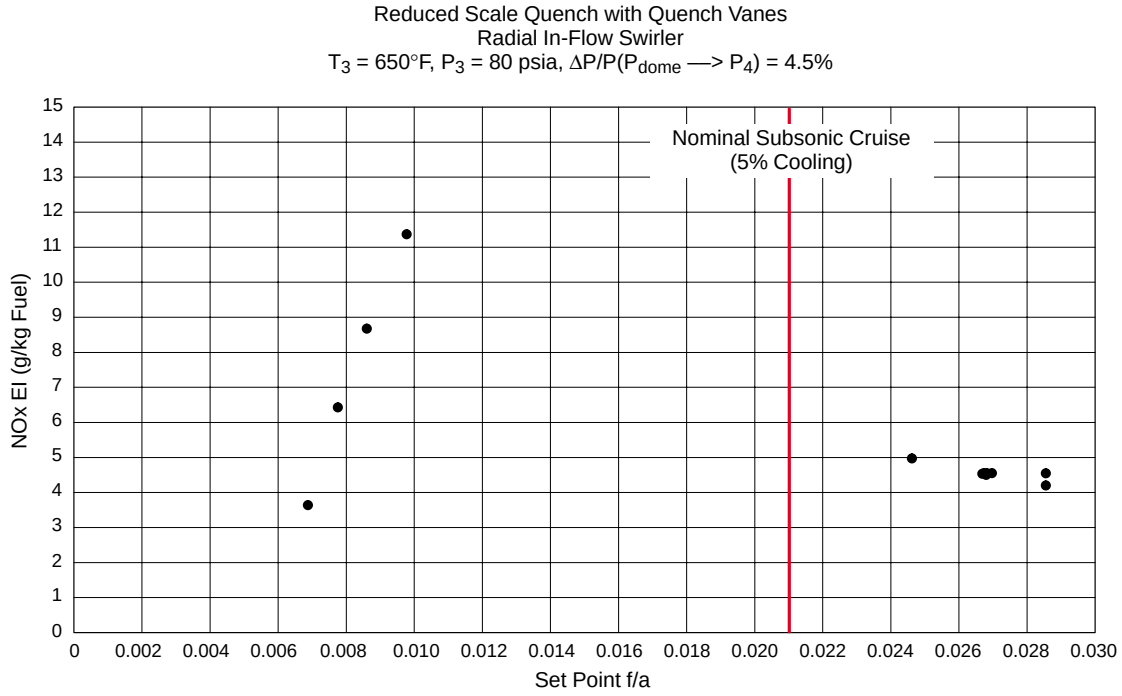

Figure 240. NO_X Emissions at Nominal Subsonic Cruise Condition for Product Module Rig Build 2

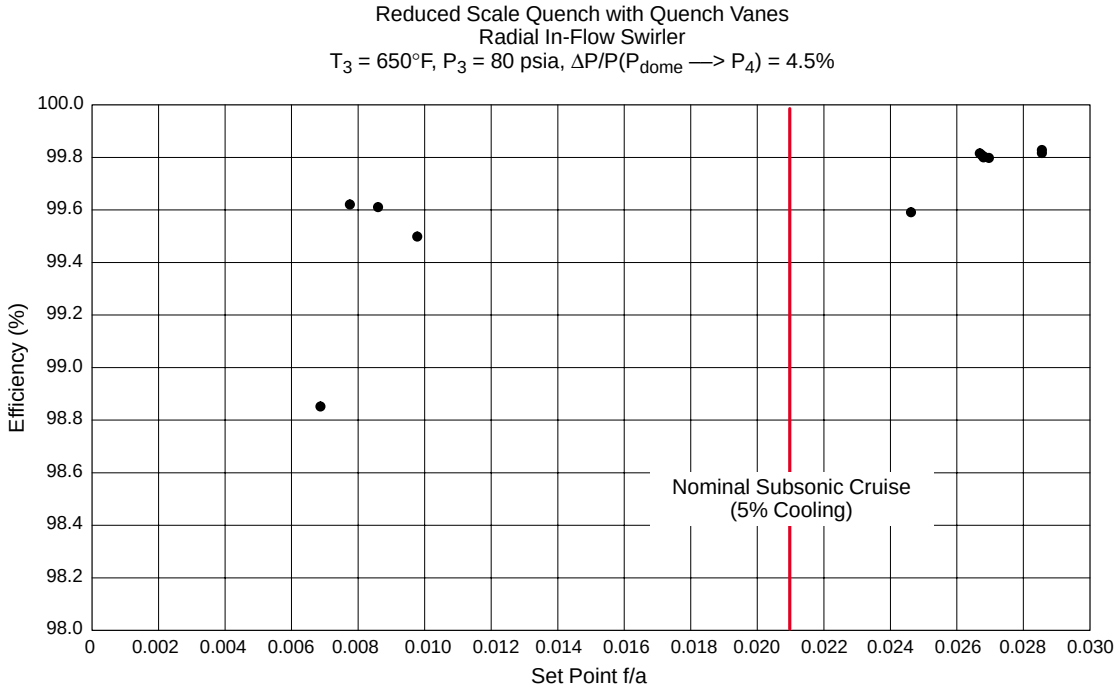

Figure 241. Efficiency at Nominal Subsonic Cruise Condition for Product Module Rig Build 2

As shown in the stoichiometry curve of Figure 242, because of the lower than intended split for Build 2, the rich-zone equivalence ratio would have been excessive at the nominal 100% thrust LTO takeoff condition fuel/air ratio. Data are shown for both Build 2 and Build 2A. The fuel/air excursion was curtailed to a maximum fuel/air ratio of 0.032, slightly below the nominal fuel/air ratio for this LTO condition, due to time constraints and the desire to proceed to the supersonic cruise condition. However, the emissions behavior can be extrapolated from the data acquired. NO_X emissions shown in Figure 243 highlight the behavior of an RQL combustor where NO_X is fairly insensitive to changes in fuel/air ratio because most of the emissions are formed in the quench zone and are not impacted significantly by the combustor exit flame temperature. CO emissions are very low, and UHC emissions are negligible as would be expected for these conditions, resulting in efficiencies greater than 99.9% (Figure 244). The NO_X and efficiency performance of the Build 2A combustor showed behavior similar to that observed in Build 2. The only difference observed is a slightly reduced sensitivity of NO_X emissions at the higher end of the fuel/air ratios tested.

Supersonic cruise performance is shown on Figure 245 through Figure 247. Again, the stoichiometry curve shows the higher than desired rich-zone equivalence ratio, 2.6 vs 2.0, at the nominal supersonic cruise fuel/air ratio, for the Build 2 configuration. Build 2A reduced the front-end equivalence ratio of 2.1. NO_X emissions at supersonic cruise show a slightly increasing dependency as a function to fuel/air ratio as the inlet temperature and fuel/air ratio combine to result in a combustor exit flame temperature that is just on the border of inducing additional NO_X production in the aft end of the combustor. However, this contribution is minimal compared the NO_X produced in the quench region of the combustor. $EINO_X$ of 8.5 was determined from the NO_X data. The change in split for Build 2A did not appear to impact the NO_X emissions performance. At this condition

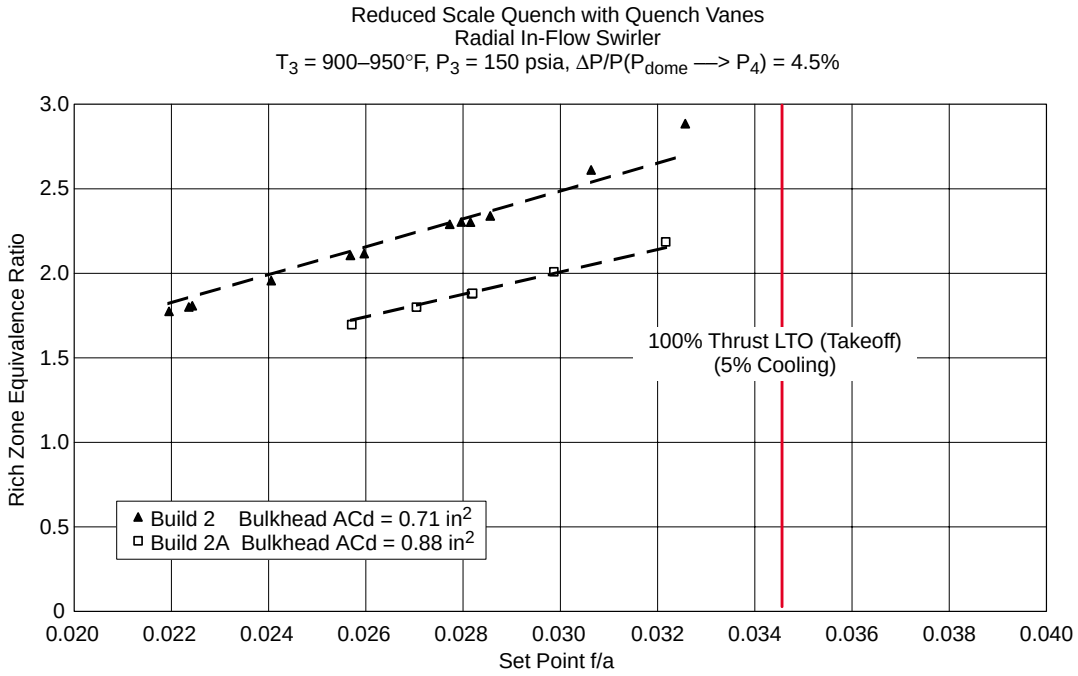

Figure 242. Rich-Zone Stoichiometry Comparison at Derated, Reduced Pressure 100% Thrust LTO (Takeoff) Condition for Product Module Rig Builds 2 and 2A

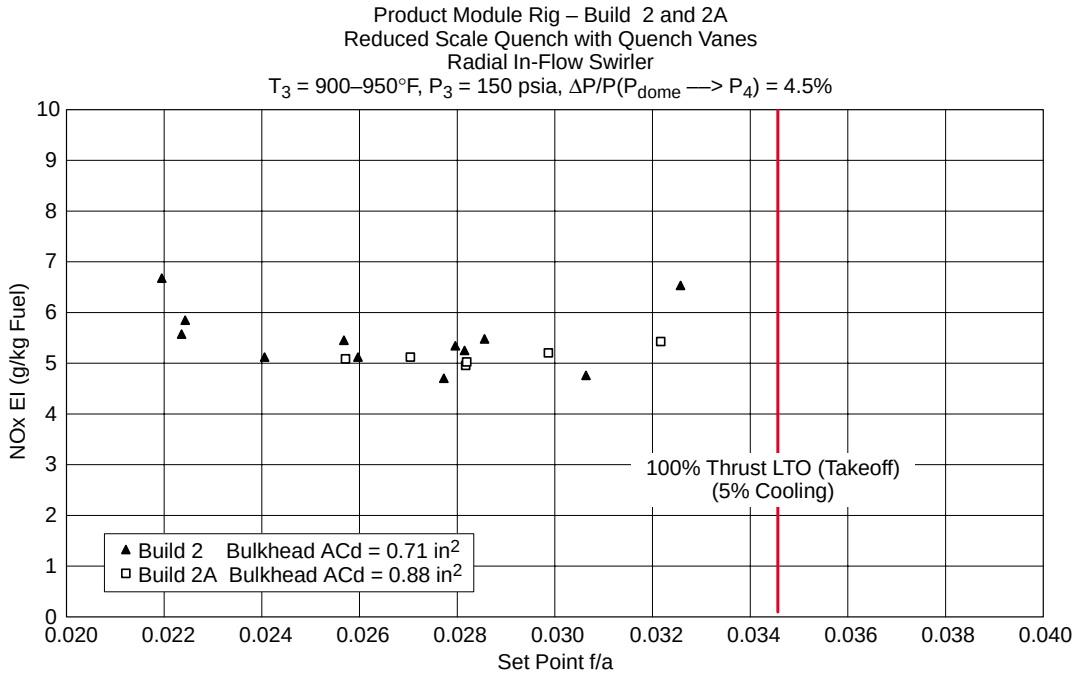

Figure 243. NO_X Emissions at Derated, Reduced Pressure 100% Thrust LTO (Takeoff) Condition for Product Module Rig Builds 2 and 2A

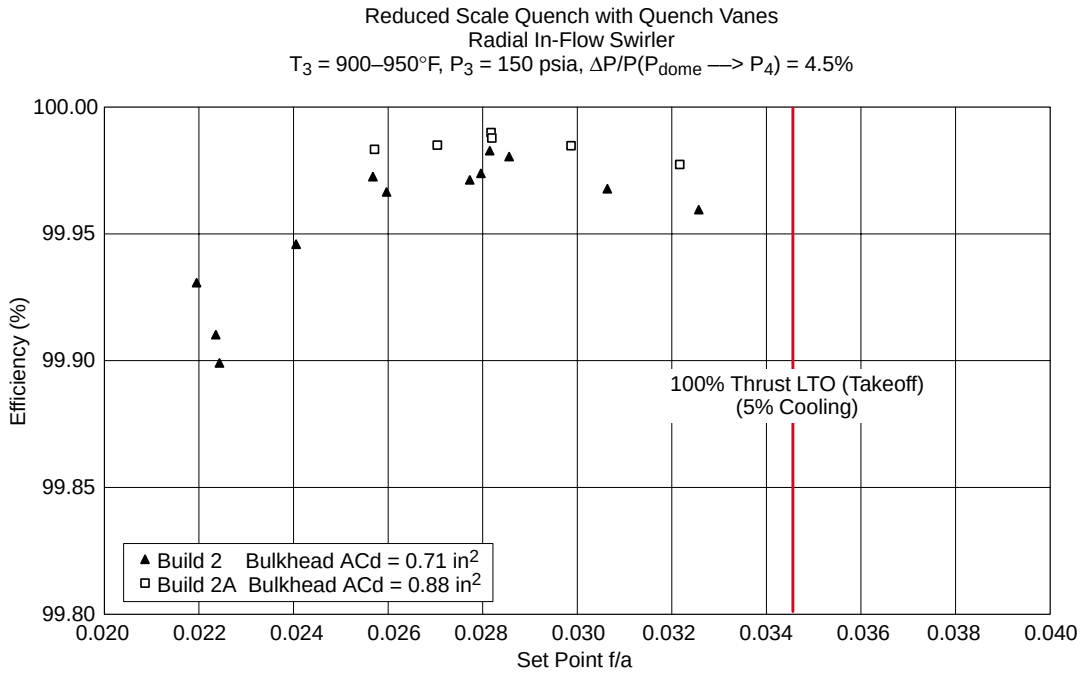

Figure 244. Efficiency at Derated, Reduced Pressure 100% Thrust LTO (Takeoff) Condition for Product Module Rig Builds 2 and 2A

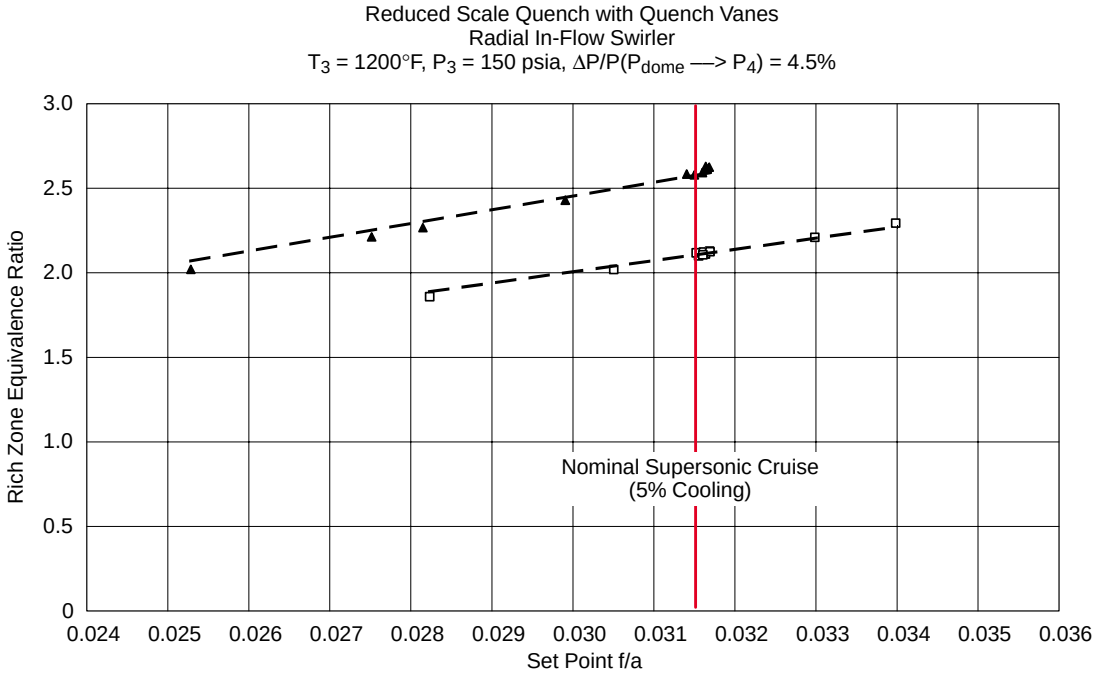

Figure 245. Rich-Zone Stoichiometry Comparison at Nominal Supersonic Cruise Condition for Product Module Rig Builds 2 and 2A

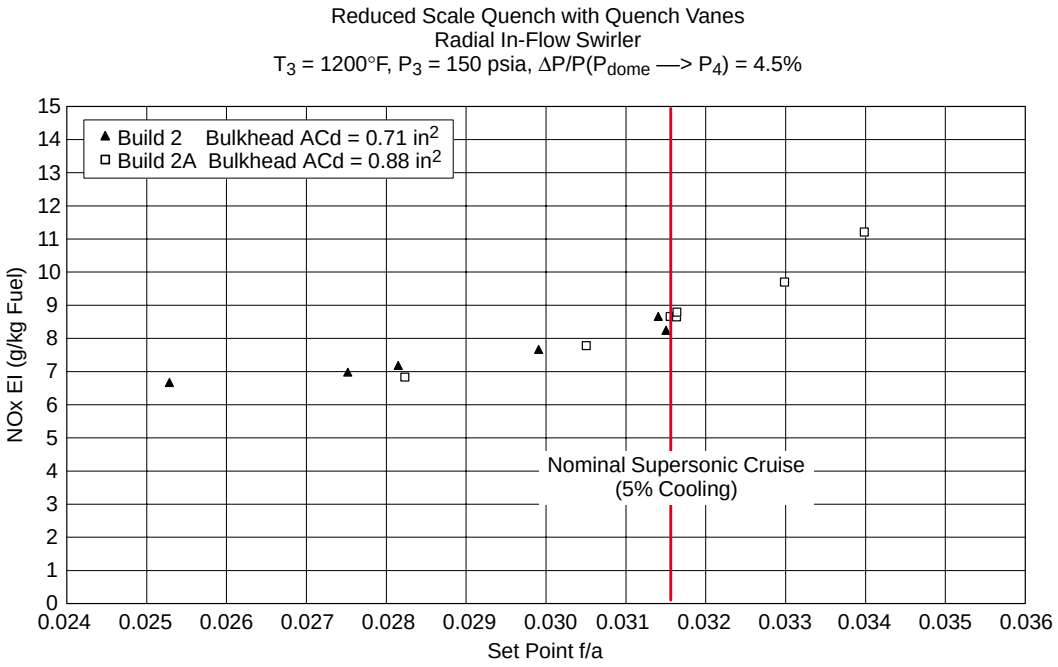

Figure 246. NO_X Emission Comparison at Nominal Supersonic Cruise Condition for Product Module Rig Builds 2 and 2A

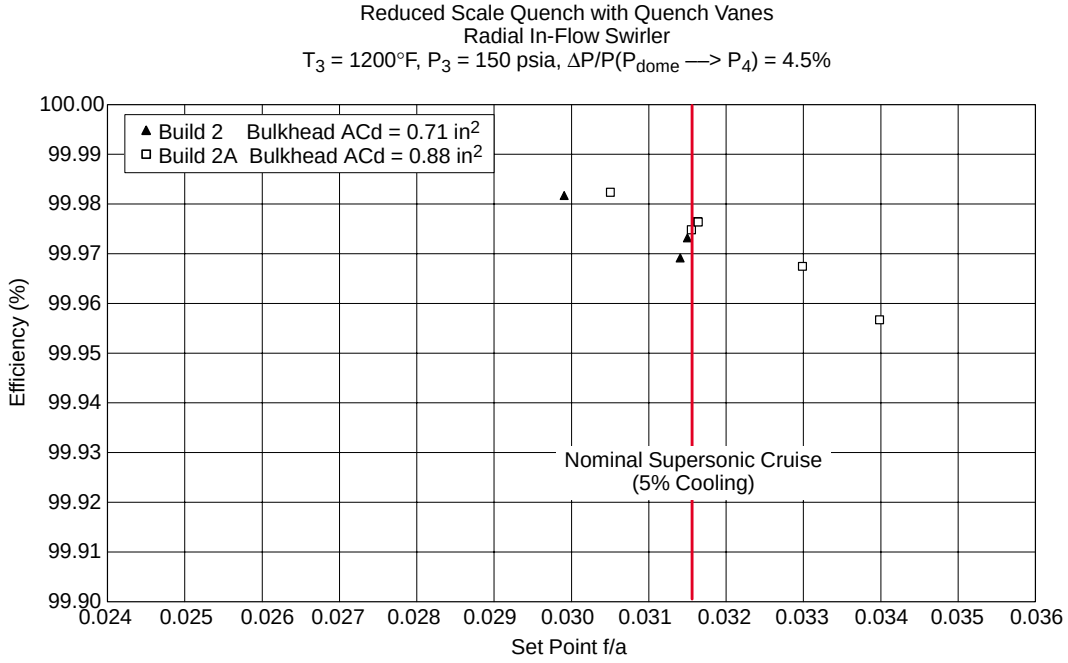

Figure 247. Efficiency Comparison at Nominal Supersonic Cruise Condition for Product Module Rig Builds 2 and 2A

COEI of 1.2 was recorded. Again, UHC emissions are negligible at this high inlet temperature condition, resulting in combustor efficiencies of 99.97%.

4.5.3.4 Fuel Shifting Sector Rig

The specific intent of this sector rig was to evaluate fuel shifting as a combustor control methodology for a multiple-bank RQL combustor, using RSQ technology implemented in a convoluted-liner-with-quench plate concept. Use of this control technique significantly reduces the risk associated with RQL combustors by eliminating the need for a variable-geometry mechanism to control combustor airflow while still maintaining low emissions, good performance, and operability throughout the flight envelope. Results are summarized as follows.

EINOx 3.5 and combustion efficiency of 99.6% at subsonic cruise were demonstrated in a non-fuel-shifted mode of operation, satisfying the HSCT combustor requirements of less than 10 EINOx and greater than 99% efficiency. NOx emissions throughout the airport-vicinity conditions tested were low in fuel-shifted as well as uniformly fueled modes. CO emissions benefited from fuel shifting at descent and approach conditions with minimal, acceptable increases in NOx emissions at those conditions relative to a uniformly fueled mode. Radial profiles observed from fuel shifting were moderate and anticipated to occur primarily at moderate to low engine power levels. In a fuel-shifted mode, NOx and CO emissions for the rich-operating module were insensitive to fuel/air ratio perturbations. At low inlet temperatures, the higher fuel/air ratios aided the oxidation of the CO produced in the rich zone by raising the exit transition zone temperature locally in the region downstream of this module. In a fuel-shifted mode, NOx and CO emissions for the lean operating module increased as the equivalence ratio approached stoichiometric; increases were observed for equivalence ratios greater than or equal to 0.6. Excellent operability was observed with LBO at front-end equivalence ratios of 0.3 or below.

Through the combustion tests conducted, information on emissions and performance (NOx, CO, UHC, and combustion efficiency) was obtained at various key operating points including the airport-vicinity conditions (5.8% thrust idle, 15% thrust descent, 34% thrust approach, 65% thrust climb) as well as subsonic cruise. Emissions behavior was assessed as a function of the degree of fuel shifting applied to the combustor to evaluate the overall emissions characteristics as well as radial-profile characteristics associated with fuel-shifting technology. Data acquired provided insight into the tradeoffs among emissions, performance, and the combustor exit profile.

The design activities for the fuel-shifting sector rig were conducted as a joint activity between P&W and UTRC. Combustion tests were conducted in dedicated facilities in Cell 3 of the JBTS at UTRC. The facility contained a fuel delivery and control system capable of providing independent fuel control and metering to each fuel injector of the RQL test combustor. The combustor rig contained two modules positioned vertically to simulate the ID and OD banks of the product-design concept. This configuration allowed evaluation of fuel-shifting control technology in a size scale consistent with a product implementation of RSQ technology for an RQL combustor under development in the HSR program

The fuel-shifting sector rig combustor configuration was designed to control the airflow split between the rich and quench zone sections via the effective areas of the fuel injector/swirler/bulkhead assembly and the rich-zone liner cooling/quench airflow passages. These passages were designed to provide the desired rich-zone flow of approximately 23% of the total combustor airflow.

The RQL fuel-shifting sector rig was designed to approximate a small, narrow sector of the RQL 3770.54 product engine. The product engine design consisted of two banks radially with the inner bank flowing approximately 40% of the total combustor airflow and the outer bank sized to flow approximately 60% of the total combustor flow. The inner bank was composed of 24 modules. The fuel-shifting sector rig was therefore designed to fit approximately within a 15° sector. However, for expediency of hardware design and fabrication, both modules in the fuel-shifting sector rig were designed and fabricated to be the same size module with the same effective flow area. The representation of behavior associated with a 60/40 OD/ID split of airflow between banks as envisioned for the product combustor concept was simulated through weighting of sampling ports in the emissions-sampling system.

The fuel shifting sector rig combustor configuration, shown in Figure 248, consisted of rich-zone spool piece that housed two rich-quench modules oriented in a vertical configuration. Each rich-quench module contained a fuel injector device, igniter, and convoluted rich-zone liner with quench plate that formed the rich combustor and the rapid-quench process of the RSQ technology. Both modules were aft mounted on a water-cooled bulkhead, and exhaust gases were dumped into a common exit transition zone with cast ceramic combustor liners contained within the lean-zone spool piece.

The rich-quench modules were mounted in parallel in an over-and-under, vertical configuration similar to the engine concept. The upper module was designated as Module 1, or the outer-diameter (OD) combustor. The lower module was designated as Module 2 or ID combustor. Each combustor module, as shown in Figures 249 and 250, consisted of a water-cooled, rich zone bulkhead with a fuel-injection device mounted to the bulkhead to allow the appropriate quantity of air, approximately 23% of total combustor air, to enter the rich zone. This fuel-injection device is described in further detail in the following paragraphs. An igniter was also positioned to protrude slightly through the rich-zone bulkhead to deliver a spark to the rich zone of the combustor. The rich-quench module also consisted of a convoluted rich-zone liner, nose piece, and quench plate, also discussed in the following paragraphs. The module assemblies were suspended inside a tubular shroud.

The fuel injector employed for the fuel-shifting sector rig combustion tests with the RSQ convoluted-liner/quench-plate configuration was a radial in-flow swirler that passed all of the rich-zone airflow. Fuel was injected through a radial jet injector. The configuration consists of radial in-flow swirlers with air introduced through inner and outer passages. Each of these passages contained tangential slots through which air was admitted, imparting a corotating swirl to the flow. A centrally mounted fuel injector delivered fuel through radial jets.

The rich-quench module also consisted of a rich-zone liner. The liner was cylindrical with a 5-in ID towards the front end of the rich zone. The leading edge of the liner necked down to accept the rich-zone bulkhead. As the rich-zone flow field progresses towards the quench plane, the liner shape is convoluted to divide the rich-zone flow into four channels in preparation for injection of the quench air. All four channels are 0.5 inches in height. The rich-zone liner was convectively cooled with quench air. Towards the aft end of the rich-zone section, the convective cooling air was guided, such that the air maintained contact with the rich-zone liner, through the use of a “nose piece” that acts as an aerodynamic guide so that the convective air maintains velocity and, hence, cooling effectiveness as it is channeled into the convoluted regions. The liner/nose-piece assemblies were suspended inside a tubular shroud that forced the quench air across the upstream cylindrical surface of the rich liner for convective cooling of that region.

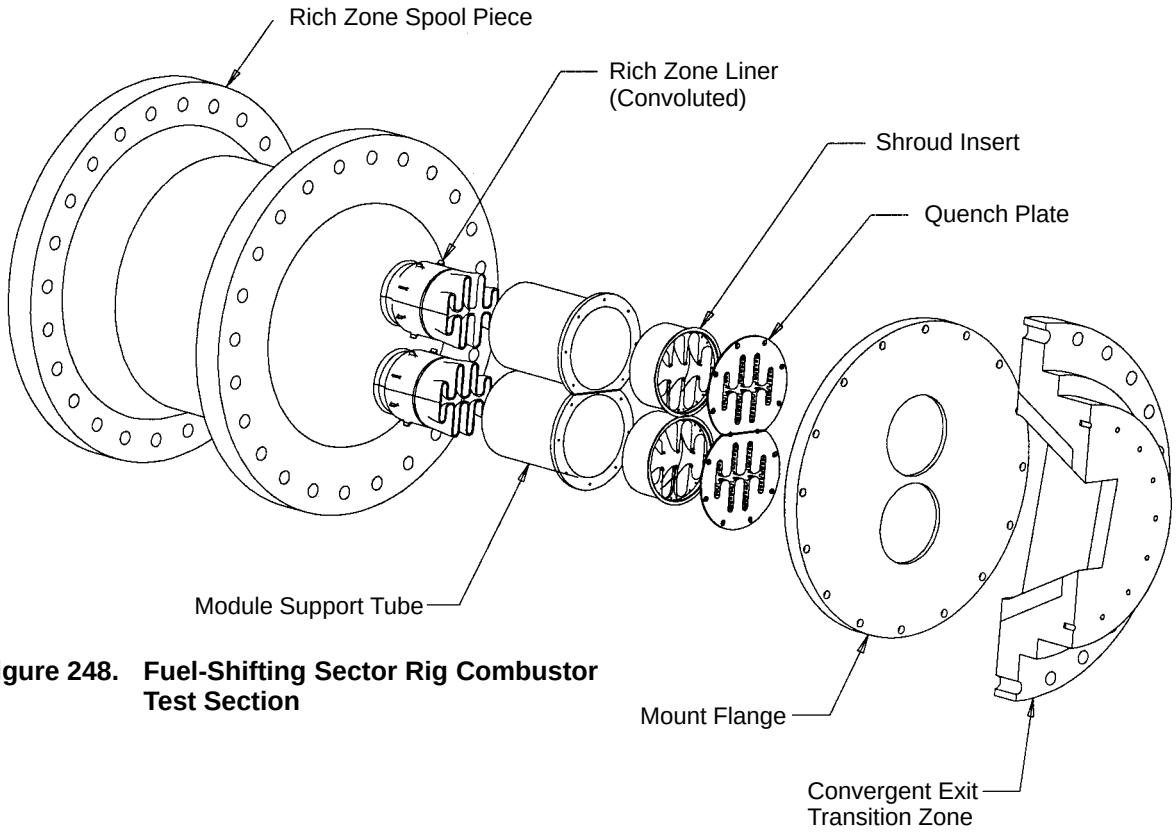

Figure 248. Fuel-Shifting Sector Rig Combustor Test Section

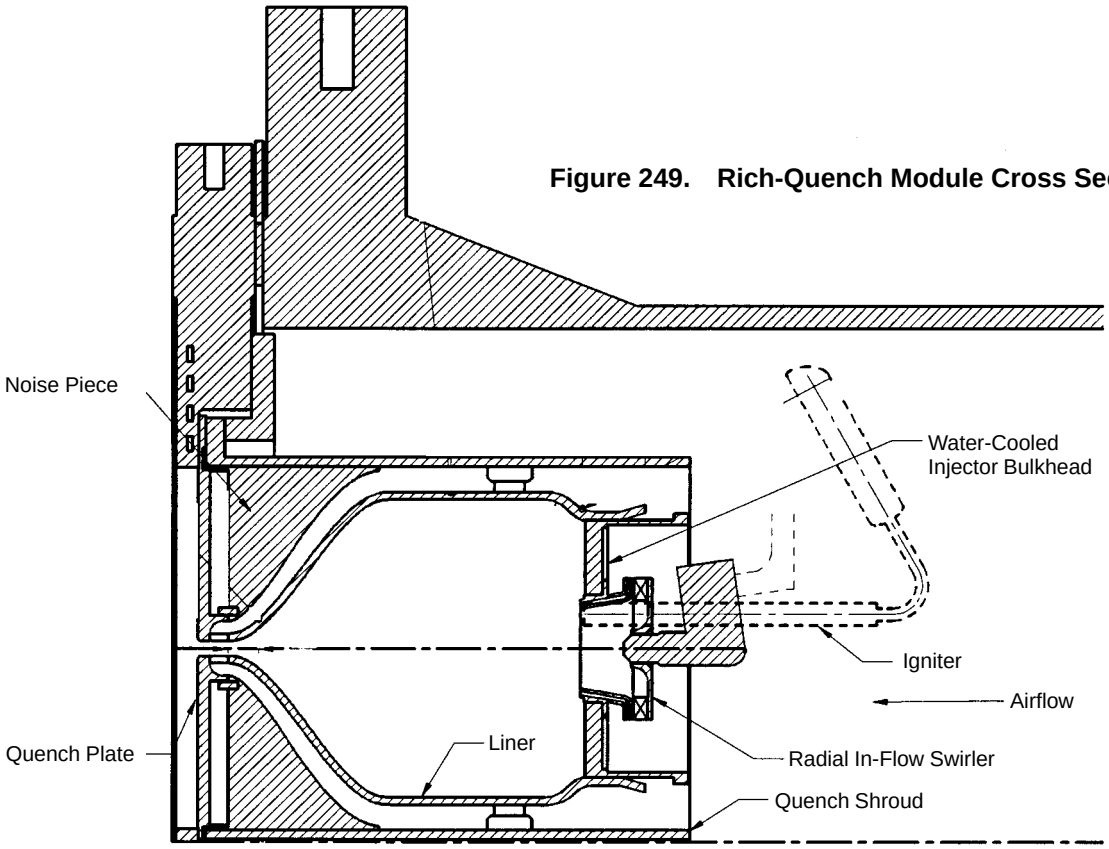

Figure 249. Rich-Quench Module Cross Section

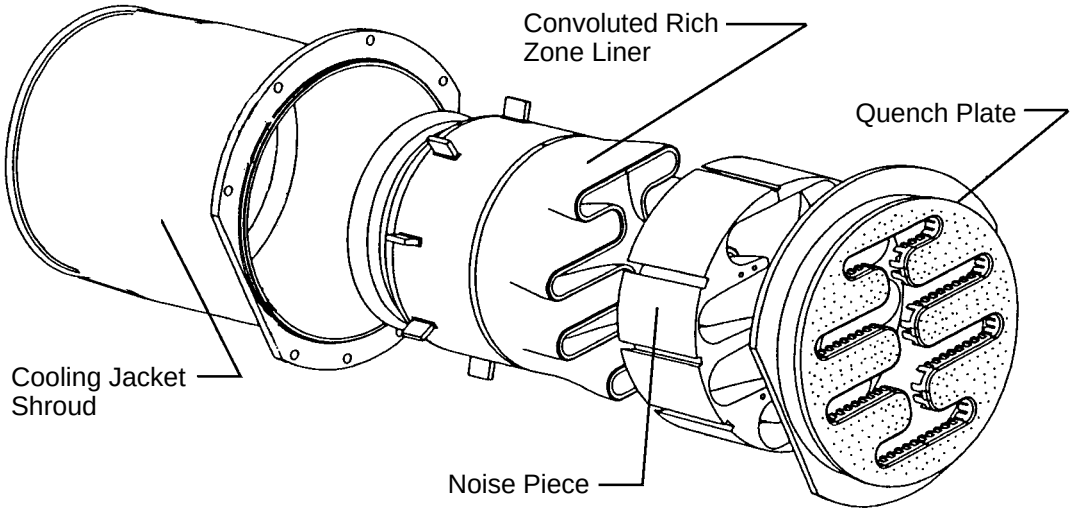

Figure 250. Exploded View of Rich-Quench Module Assembly (Bulkhead Subassembly Not Shown)

Beyond directing the cooling/quench air along the back-side surface of the convoluted liner, the "nose piece" also distributed the quench air to the downstream edge of the liner. There it was injected into the rich-zone gas from small orifices in a toothed quench plate to produce the RSQ mixing. This quench plate had been developed and optimized under a related task. The resultant, optimized geometry, known as quench plate No. 15, was used in this combustion rig. The quench orifices were sized to control the pressure drop and, in combination with the rich-zone swirler effective flow area, provide the appropriate quantity of quench air to maintain the desired split of approximately 23% air into the front end of the combustor. The width of each slot varied throughout the channel lengths and was determined by the previous effort to provide optimum mixing for minimizing NOx emissions. The quench channels in the quench plate were designed to the same dimensions as the exhaust of the convoluted rich-zone liner. Additionally, a small fraction of the quench air (4% of total combustor air) was bled through small effusion holes, on the downstream face of the plate, as cooling air for the aft face of the quench plate.

The reacting gas entered a lean combustion zone after passing through the modules. For the fuel-shifting sector rig, this zone represented a sector portion of this annular-exit transition zone. A castable liner of a commercially available ceramic was molded inside this piece to provide the flowpath surfaces. The exit transition zone was sized to accept the effluent from the modules entering this exit transition zone. From there, the flowfield was contracted on both the inner and outer (top and bottom) surfaces of this exit transition zone, progressing towards the combustor exit plane. The sidewalls of the exit transition zone were nonconvergent as the flow progressed axially, representing a sector of the annular exit transition zone.

Emissions testing for the RSQ convoluted-liner/quench-plate combustor was focused on conditions taken from the HSR/CPC Program Coordination Memo GE97–002–C, summarized in Table 30 (page 166), with the primary intent of assessing airport-vicinity emissions in support of the combustor downselect and for evaluation of fuel-shifting benefits.

A series of tests with the RSQ convoluted-liner/quench-plate combustor as a plenum-fed configuration began as Build 2 on January 16, 1998 with lean-blowout tests and continued with emissions tests through February 10, 1998. A series of tests with the RSQ convoluted-liner/quench-plate combustor in a diffuser-fed configuration began as Build 2a on March 10, 1998 and completed testing on April 7, 1998.

The subsonic cruise operating condition was tested at the specified inlet pressure and temperature and various fuel/air ratios for the plenum-fed configuration (Build 2). Tests were conducted in the uniform and fuel-shifted modes. All the emissions and performance goals were satisfied at this condition. The NOx data for both the uniform and fuel–shifted modes are plotted in Figure 251. Both modes produced NOx emissions below the 10 EINOx goal. The uniform mode produced the lowest NOx at about 3 EI. In the fuel-shifted mode, NOx decreased as the amount of fuel shifting increased. Figure 252 shows that the combustor efficiency at subsonic cruise was above the goal of 99.0% in uniform and fuel shifted modes.

The 34% thrust LTO (approach) condition was tested at the specified inlet temperature, inlet pressure, and a range of fuel/air ratios in uniform, nonshifted as well as fuel-shifted modes including both ID-rich and OD-rich modes for the plenum-fed configuration, Build 2. Emissions and efficiency data at the 34% thrust LTO condition are shown in Figures 253 and 254. A uniform equivalence ratio between the ID and OD banks produced lower NOx emissions than fuel-shifted cases at fuel/air ratios above 0.020. This is similar behavior to that observed for the subsonic cruise conditions and is expected since both conditions are fairly close in inlet temperature, pressure, and fuel/air ratio.

Combustor efficiency also improved with fuel shifting.

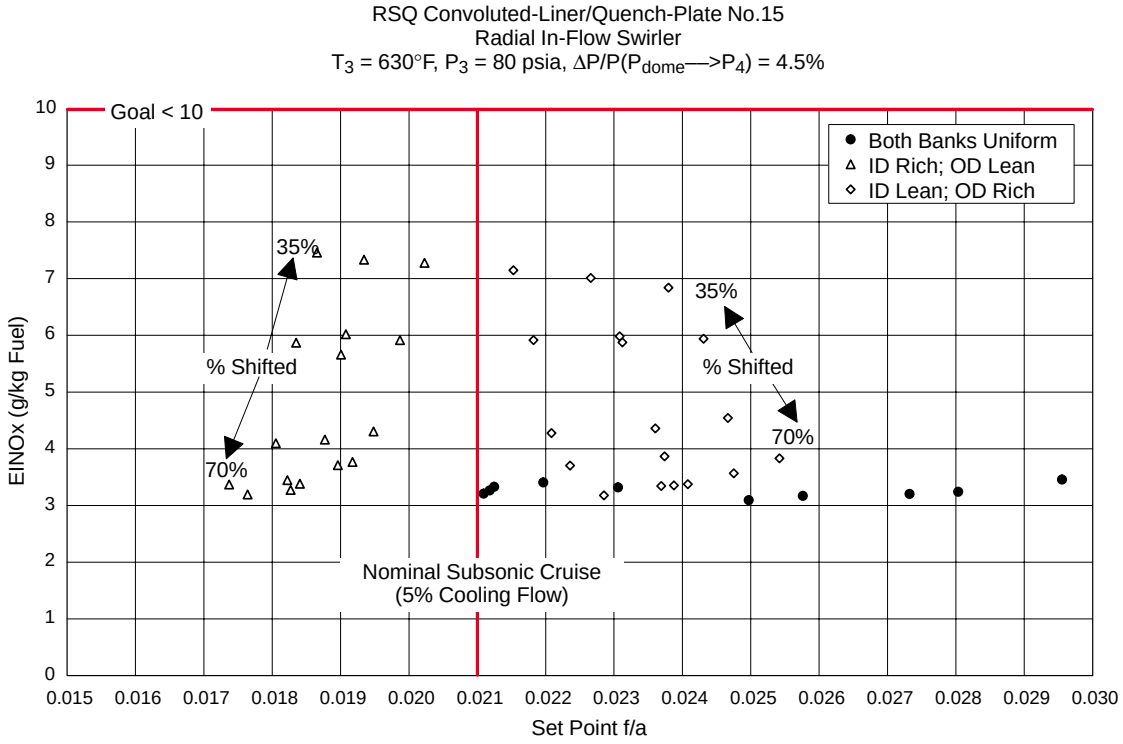

Figure 251. NOx Emissions at Nominal Subsonic Cruise for Fuel-Shifting Rig Build 2

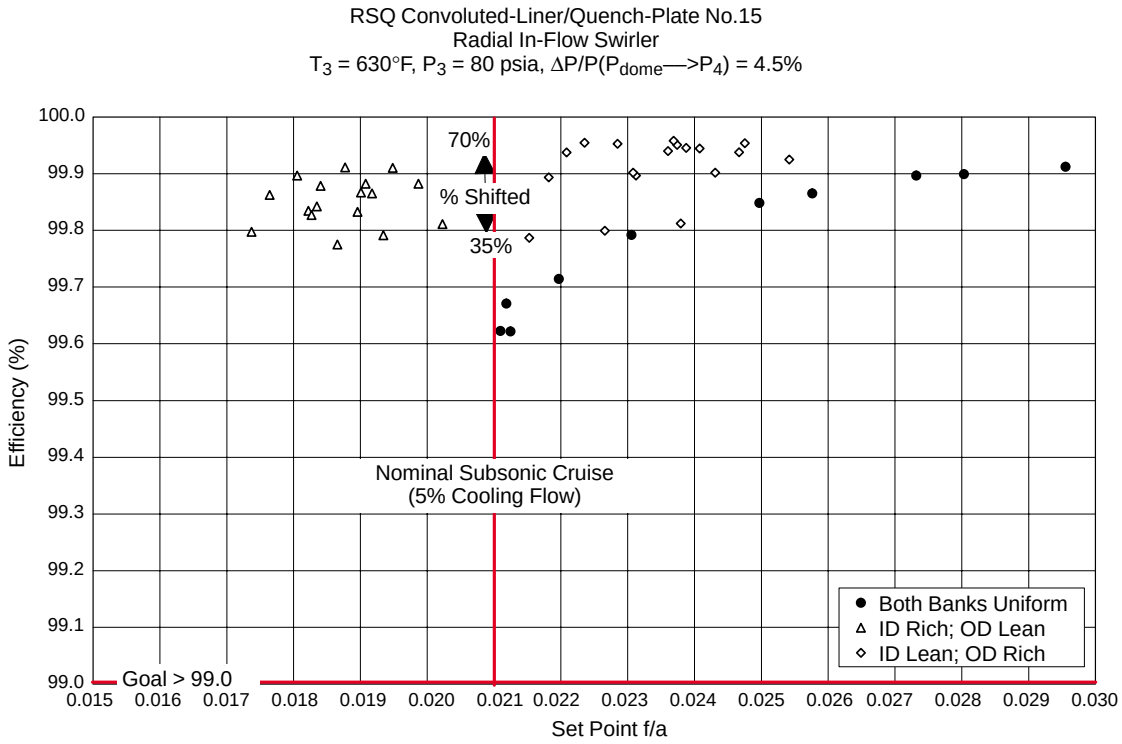

Figure 252. Efficiency at Nominal Subsonic Cruise for Fuel-Shifting Rig Build 2

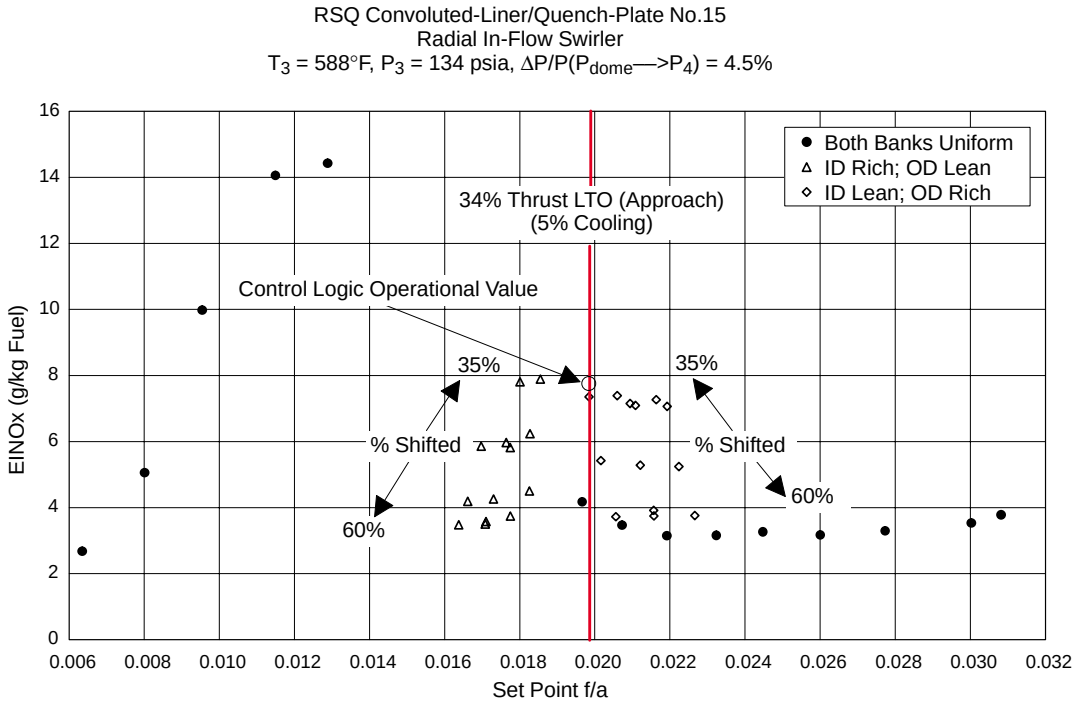

Figure 253. NOx Emissions at 34% Thrust LTO Condition for Fuel-Shifting Rig Build 2

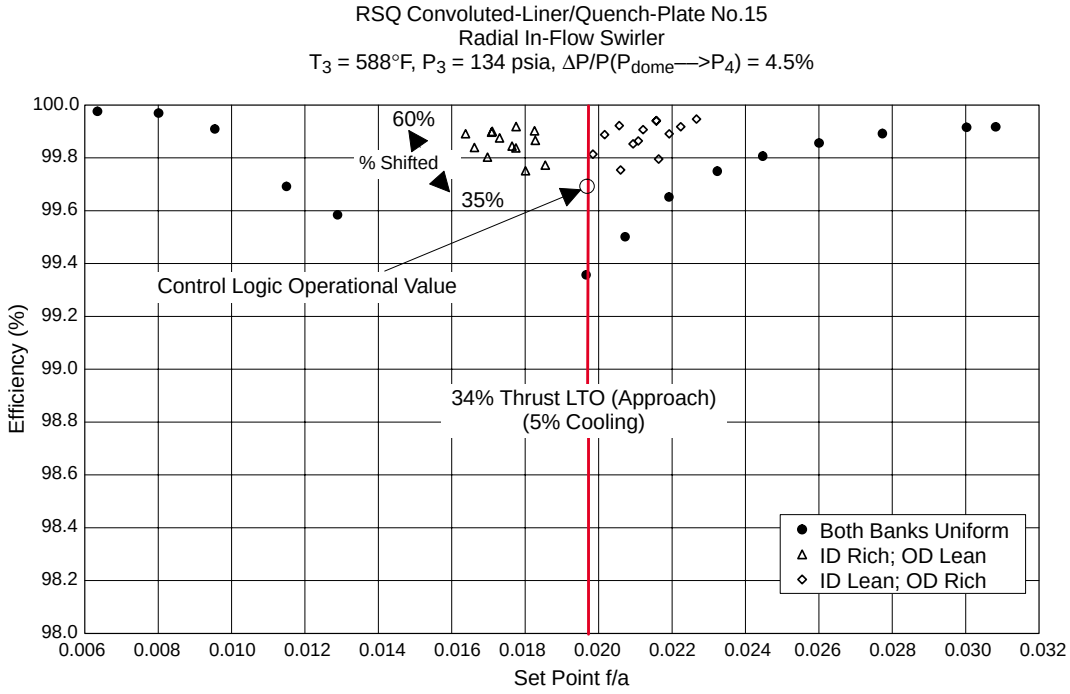

Figure 254. Efficiency at 34% Thrust LTO Condition for Fuel-Shifting Rig Build 2

Engine control logic would dictate that, at this power level (inlet temperature and fuel/air ratio), the combustor should be operated in a mode 30% fuel shifted with a rich OD module. Interpolating/ extrapolating the acquired data for this fuel-shifting scenario led to NOx and CO emissions of 8 and 12 EI, respectively, and efficiency of about 99.7%.

The turbine inlet temperature profile factor was assessed with fuel-shifting operation. The maximum radial profile factor is plotted as a function of percent fuel shifted in Figure 255. The profile factor would be ID or OD peaked commensurate with shifting towards ID-rich or OD-rich configurations, respectively. A profile factor of less than 0.2 was predicted at the operating point determined by the engine control logic for this condition. Figure 256 shows the profile factor as a function of percent radial span for the OD-rich cases and the estimated cycle operating condition for this combustor. The profile curves decreased in magnitude with decreased fuel shifting, as expected.

The 15% thrust LTO (descent) condition was tested at the specified inlet pressure and temperature and a range of overall fuel/air ratios for the plenum-fed configuration. Data were acquired for uniform and fuel-shifted modes. The emissions and efficiency data at this condition are shown Figures 257 and 258. NOx emissions levels were highest in the uniform mode and decreased with increased fuel shifting, as would be expected since at the overall fuel/air ratio of 0.015 the module front ends are operating near stoichiometric equivalence ratios and would produce significant quantities of NOx given the relatively long residence times associated with the front end “rich” zones of an RQL combustor.

Fuel shifting improved efficiency, but there was no obvious trend as a function of percent fuel shifting. The maximum radial temperature profile factor is plotted in Figure 259 as a function of percent shifted. The profile factor became more severe with increased fuel shifting, as expected. The

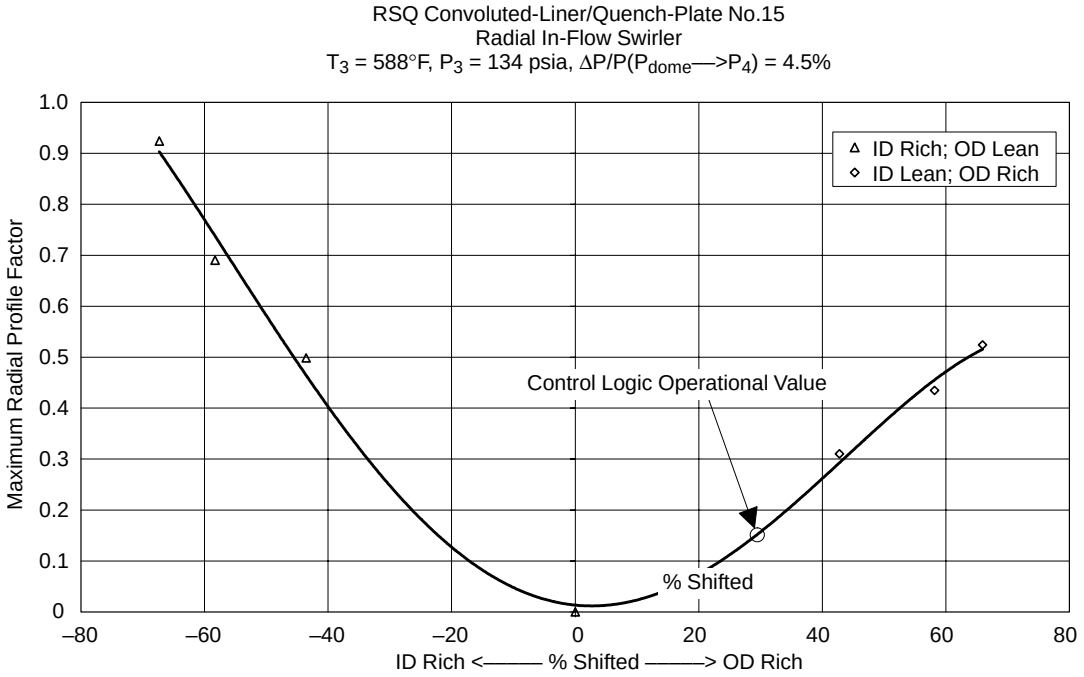

Figure 255. Maximum Temperature Profile Factor at 34% Thrust LTO Condition for Fuel-Shifting Sector Rig Build 2

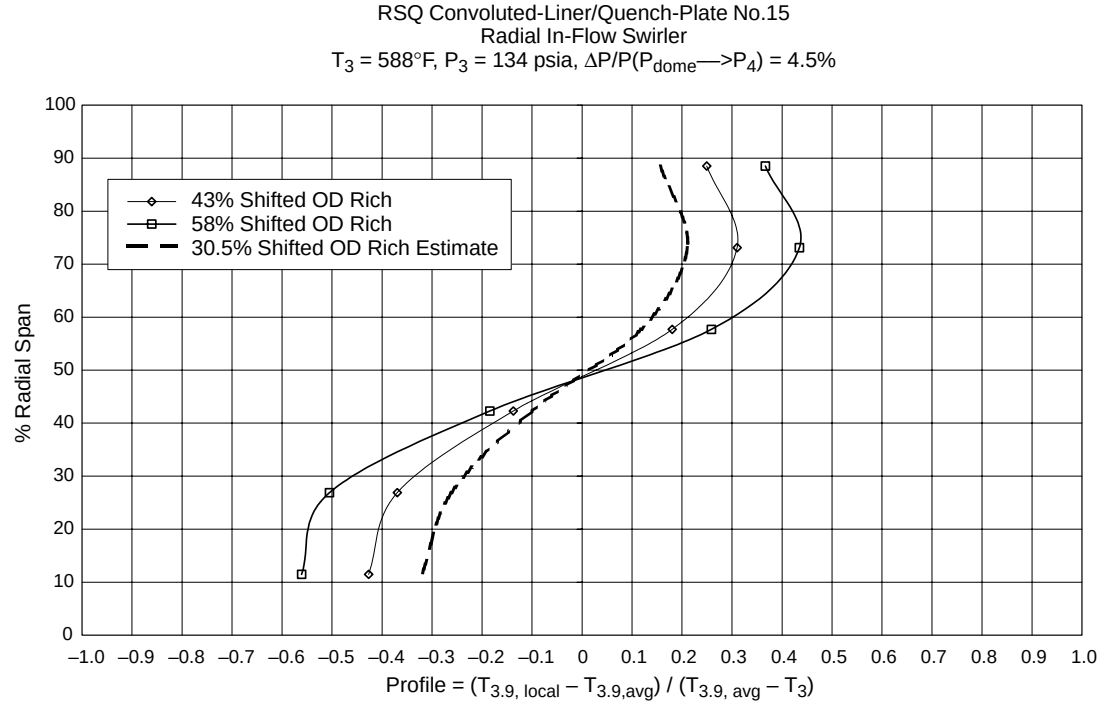

Figure 256. Temperature Profile Factor Over Radial Span at 34% Thrust LTO Condition for Fuel-Shifting Rig

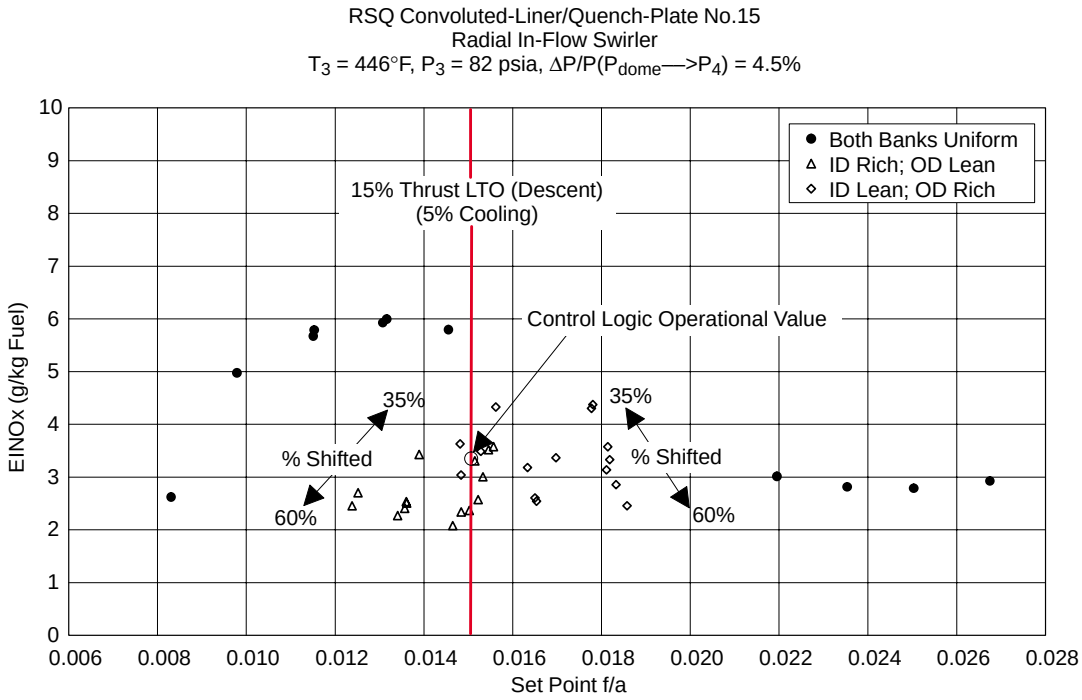

Figure 257. NOx Emissions at 15% Thrust LTO Condition for Fuel-Shifting Rig Build 2

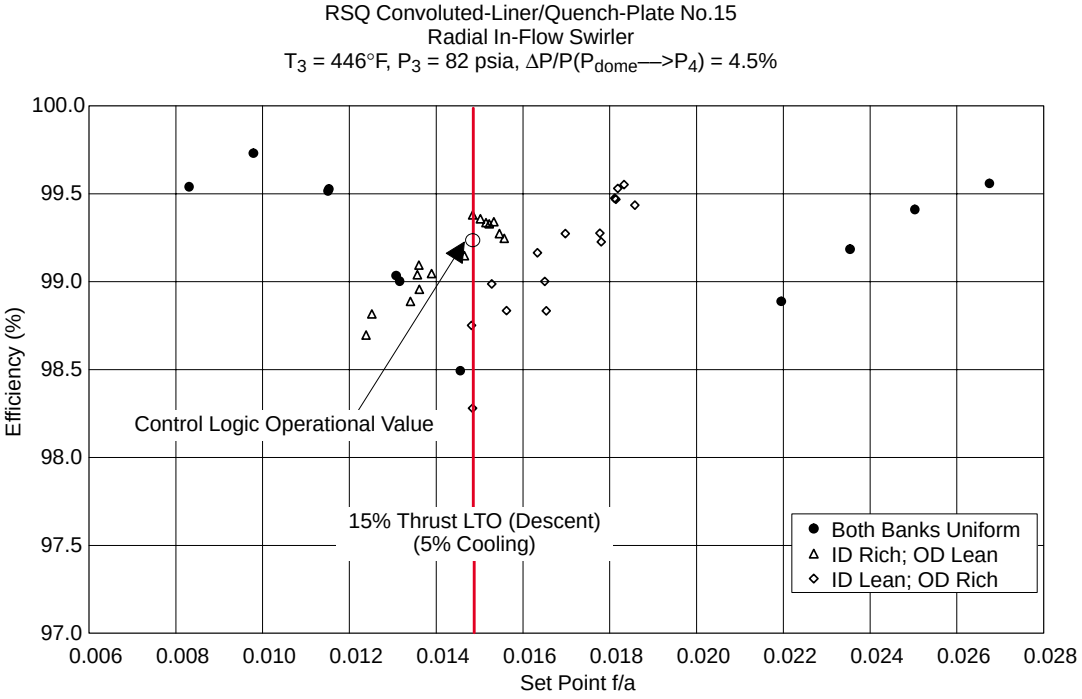

Figure 258. Efficiency at 15% Thrust LTO Condition for Fuel-Shifting Rig Build 2

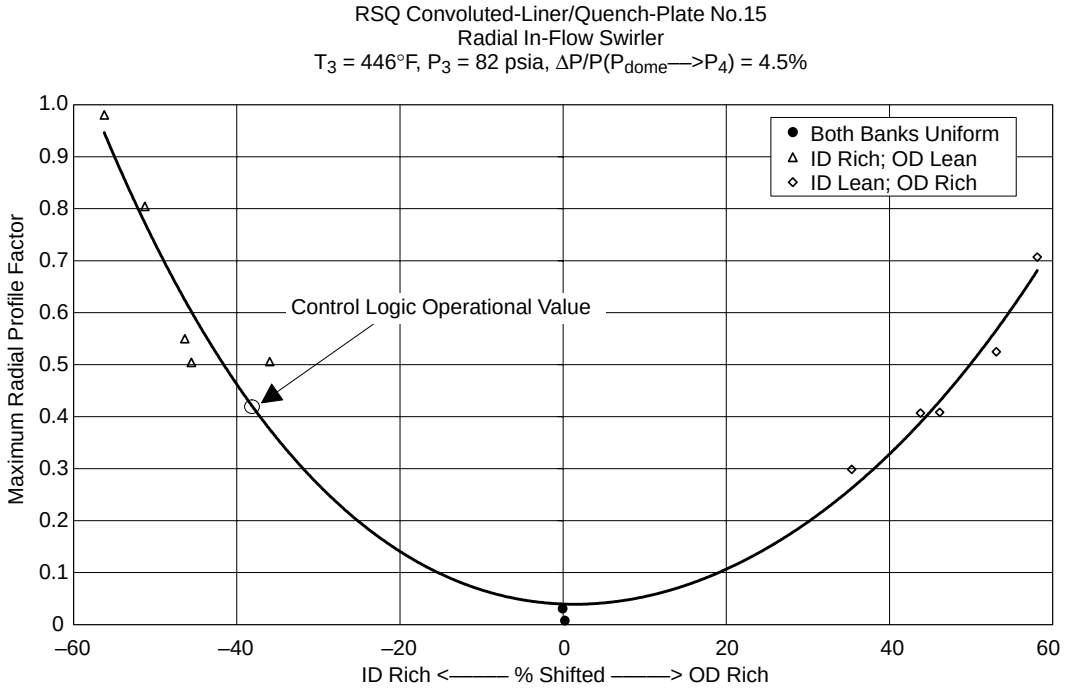

Figure 259. Maximum Temperature Profile Factor at 15% Thrust LTO Condition for Fuel-Shifting Rig Build 2

operating value of the maximum radial profile factor determined using engine control logic was just over 0.4, ID peaked. Figure 260 shows the profile factor as a function of percent radial span for various fuel shifting configurations at this condition including a uniform configuration that highlights the different behavior between a uniform and fuel shifted configuration. The profile factor was peaked at the ID and steadily decreased to the OD.

A single-passage, shallow-angle diffuser was installed in the fuel-shifting rig to provide a representative full-scale flowfield and evaluate effects on emissions. This rig build was designated as Build 2a. No attempt was made to induce any inlet profiling since the purpose of these test was to investigate the impact of a diffuser flowfield on an RQL with reduced-scale quench, and proper flow expansion from the prediffuser through the dump region was modeled with this flat profile diffuser. The tests of the 34% thrust LTO (approach) condition were repeated to determine diffuser effects on emissions and performance. Similar fuel/air ratio excursions and some fuel shifting conditions were repeated to assess the effects of a diffuser-fed flowfield on emissions behavior. This condition was chosen because it is expected that it would be fuel shifted in engine operation. The diffuser did not have a strong impact on the emissions, efficiency, or exit profiles of the combustor. The NOx emissions for the diffuser-fed combustor are plotted along with the plenum fed configuration in Figure 261. The efficiency is shown in Figure 262, and the temperature profile factors are shown in Figure 263. Data comparisons from all these figures shows that the diffuser-fed flow field had minimal impact on emissions and performance for this combustor configuration.

Based on all of the data acquired during this test program, airport-vicinity emissions were estimated for this RSQ convoluted-liner/quench-plate combustor configuration with fuel-shifting control technology. Since the facility was limited in inlet temperature and pressure, data for the climb

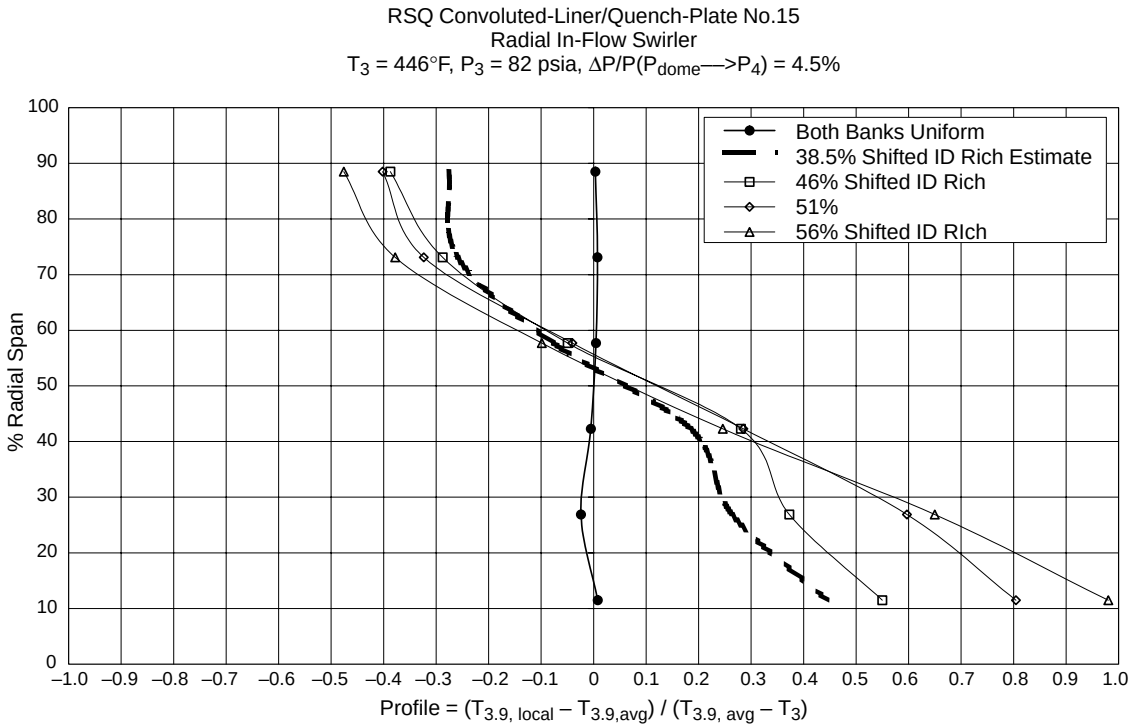

Figure 260. Temperature Profile Factor Over Radial Span at 15% Thrust LTO Condition for Fuel-Shifting Rig Build 2

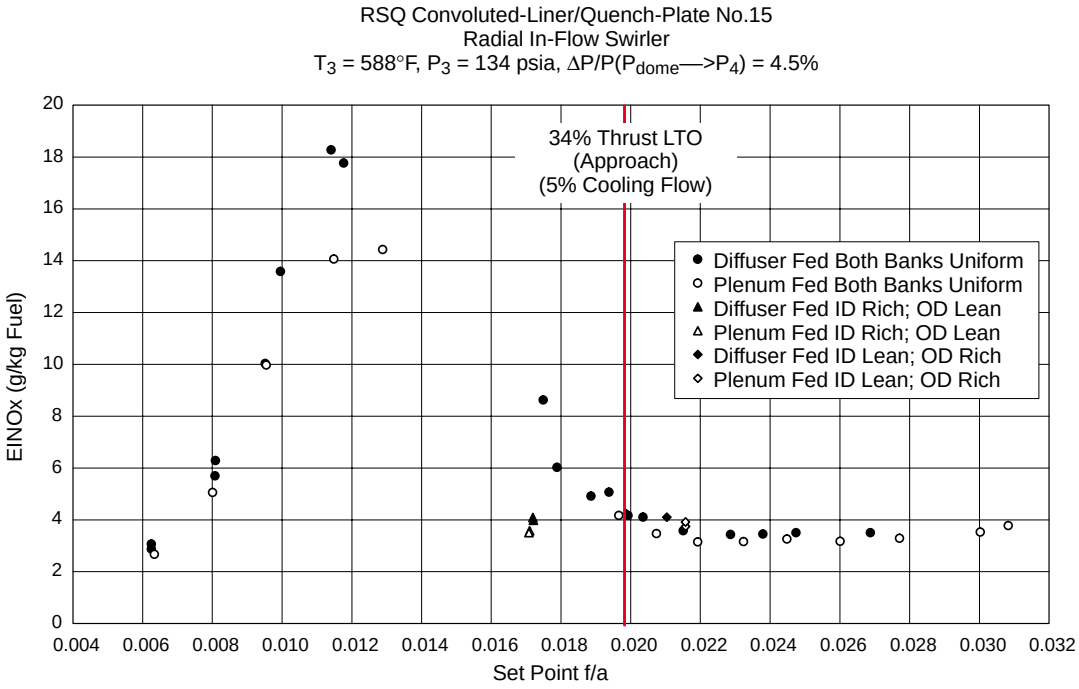

Figure 261. NOx Emissions at 34% Thrust LTO Condition for Fuel-Shifting Rig Build 2a

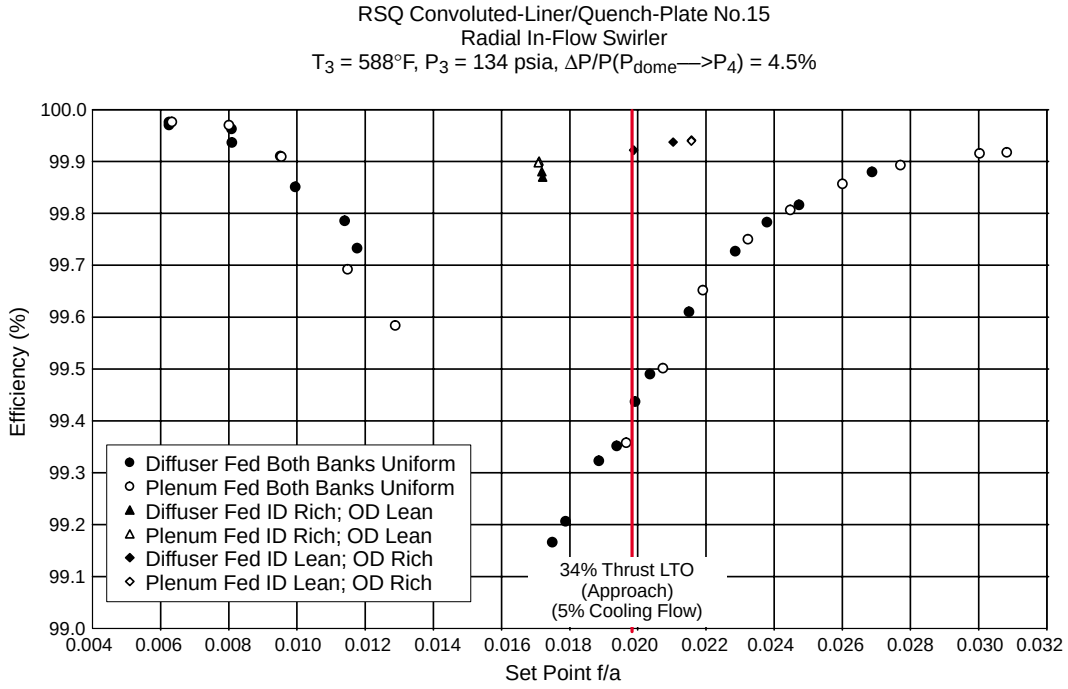

Figure 262. Efficiency at 34% Thrust LTO Condition for Fuel-Shifting Rig Build 2a

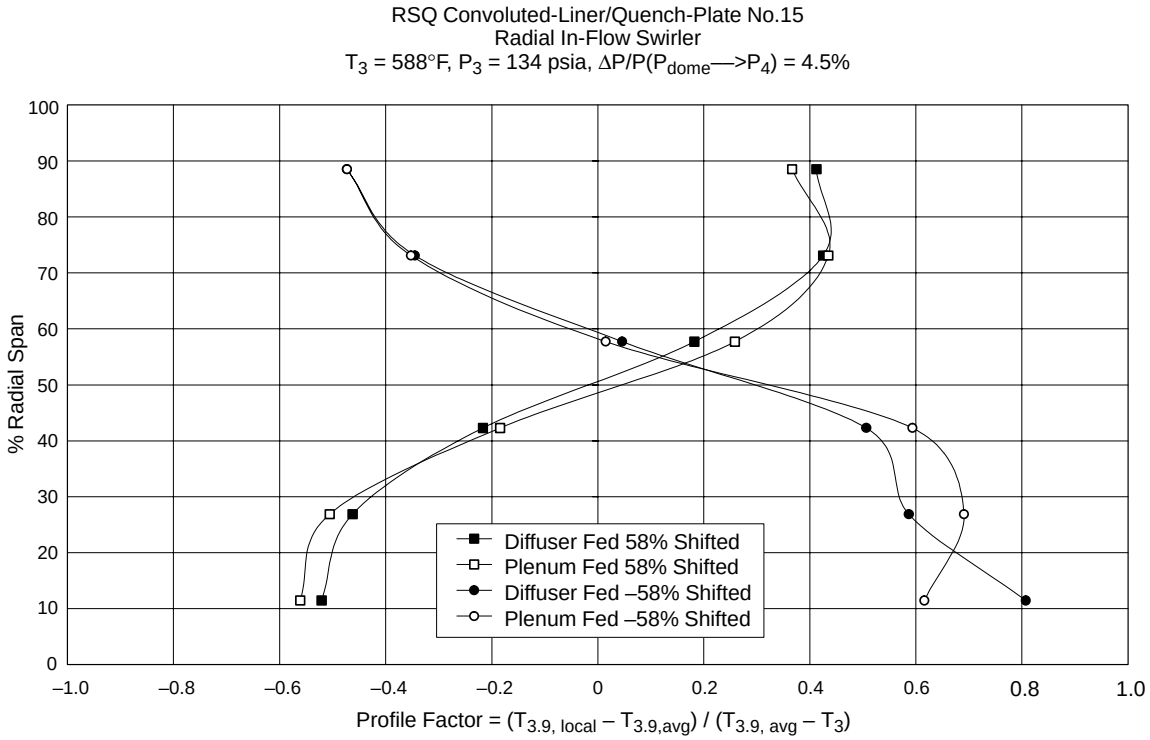

Figure 263. Temperature Profile Factor Over Radial Span at 34% Thrust LTO Condition for Fuel-Shifting Rig Build 2a

condition were based on extrapolating results from 150 psia to 212 psia. Takeoff data were acquired at derated, reduced pressure of 150 psia from the integrated module rig testing of a single module of identical configuration and scaled accordingly to the cycle operating pressure. The results of estimates for integrated landing/takeoff cycle airport vicinity emissions are listed in Table 31.

Table 31. Integrated LTO Airport-Vicinity Emission

Operating Condition	Weighting Factor	EINOx	EICO	EIHC	Efficiency	Max. Profile Factor
Idle	0.305	3.5	49.5	0.80	98.76%	–
Descent	0.029	3.3	31.0	0.10	99.26%	0.45
Approach	0.109	7.5	12.1	0.01	99.71%	0.15
Climb	0.179	3.8	1.5	0.01	99.96%	–
Takeoff	0.183	12.3	6.2	0.10	99.84%	–
Integrated LTO		4.9	18.7	0.3		
Goal		<5.0	<7.8	<1.0		

Lean-blowout (LBO) test data from the RSQ RQL combustor, are shown in Figure 264. The inlet temperature was varied from 300°F to 800°F while the inlet pressure was varied along a simulated sea level operating line. At the 800°F condition, inlet pressures were limited by the facility to 150

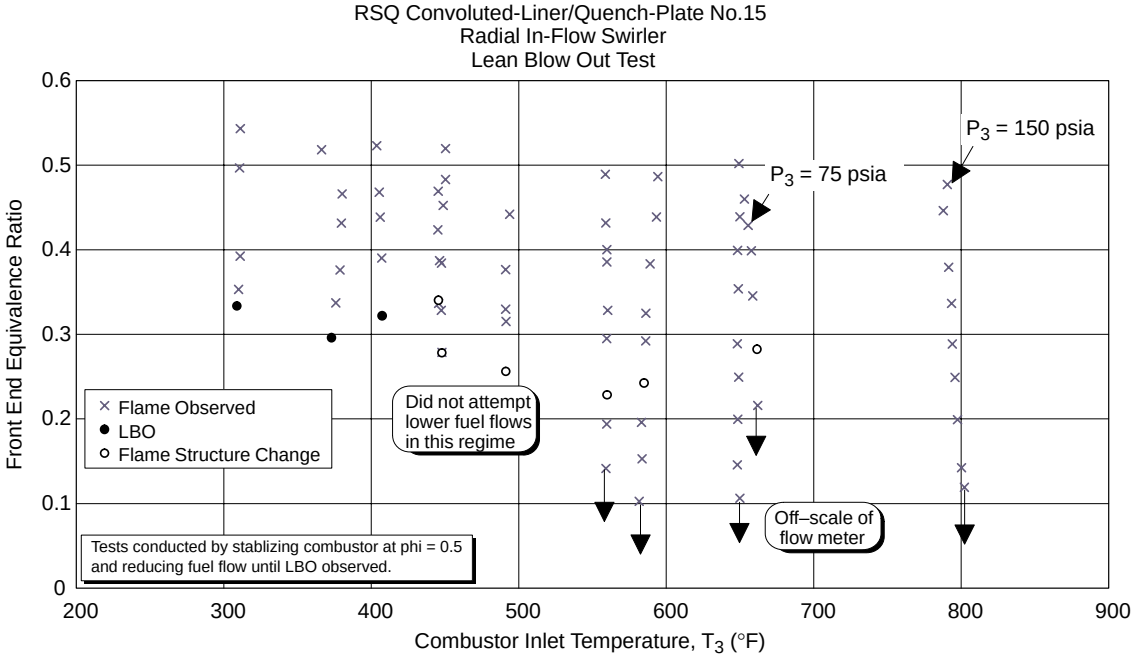

Note: Unless otherwise specified, Combustor Inlet Pressure, P_3 [psia] = 0.3135*T_3[°F] – 56, a sea level operating line simulation ΔP/P across nozzle was nominally 2.5%

Figure 264. Lean-Blowout Equivalence Ratio as a Function of Temperature and Pressure for Fuel-Shifting Rig Build 2

psia. In addition LBO was assessed at 75 psia at the 650°F condition to evaluate operability at the subsonic cruise condition. In each case, the front-end equivalence ratio was stabilized at $\phi = 0.5$ and then reduced until LBO was observed.

From about 400°F and below, LBO occurred around $\phi = 0.3$. Above this temperature, LBO was not observed within the range that the fuel control was able to adequately control the fuel flow or the fuel flow meters could reliable measure. Instead, a distinct change in the flame structure was observed. This occurred, in most cases, between $\phi = 0.2$ and 0.3. At $T_3 = 800°F$ and $P_3 = 150$ psia, there was no change in flame structure observed over the entire range of ϕ tested.

4.5.4 Ceramic-Matrix Composite Sector

4.5.4.1 Summary

The objective of this work was to test ceramic-matrix composite (CMC) liner materials in an HSCT combustor. The combustor requirements included subjecting the CMC liners to at least three diverse inlet temperatures, inlet pressures, and flame temperatures as well as a fuel-flow transient in a supersonic cruise condition for at least 50 hours. An RQL combustor operated in a nominal HSCT flight cycle was selected for this task. The combustor met and exceeded all of the requirements. CMC liners throughout the combustor were exposed to more than three different operating conditions and fuel flow transients for at least 60 hours. Some parts saw well over 100 hours.

During the tests, CMC liner failures included the primary-zone module liners and lean-transition-zone Miller fasteners. Also, deterioration of the heat shield became substantial after 100 hours of operation. These problems were corrected as they occurred or were under investigation at this writing.

4.5.4.2 Combustor Design

The CMC RQL combustor sector was designed and developed by Pratt & Whitney. Figure 265 shows a cross section of the combustor. The combustor comprised four main elements: a variable-geometry fuel nozzle, a primary combustion module, a quench/transition zone, and a lean zone. The elements will be briefly discussed here. Subsections 4.2.2 through 4.3.2 contain more detailed discussions of RQL combustion.

The CMC rig was a 60° sector with two primary zone combustion modules. Pictures of the rig are shown in Figures 266 and 267. A variable-geometry triswirler aerating fuel nozzle controlled the airflow into the cylindrical/conical primary zone modules. A stable equivalence ratio that minimized NOx emissions and maximized efficiency was maintained in this zone. The module liner was fixed on the downstream end and held in place on the upstream end by a spring. The spring compensated for differences in thermal growth between the cooler metal and hotter CMC materials. Wall jets in the quench zone mixed air with the gasses exiting the primary zone. The quenched gasses then passed through a cylindrical transition zone and entered the lean zone where combustion was completed.

The lean zone was an annular sector that incorporated various cooling techniques to test the CMC materials in a variety of applications. The lean-zone shell was made entirely of metal. Three impingement-cooled panels were mounted on the bulkhead, and six convection-cooled floatwall panels covered the inner diameter. The outer diameter had three offset impingement baffles and two

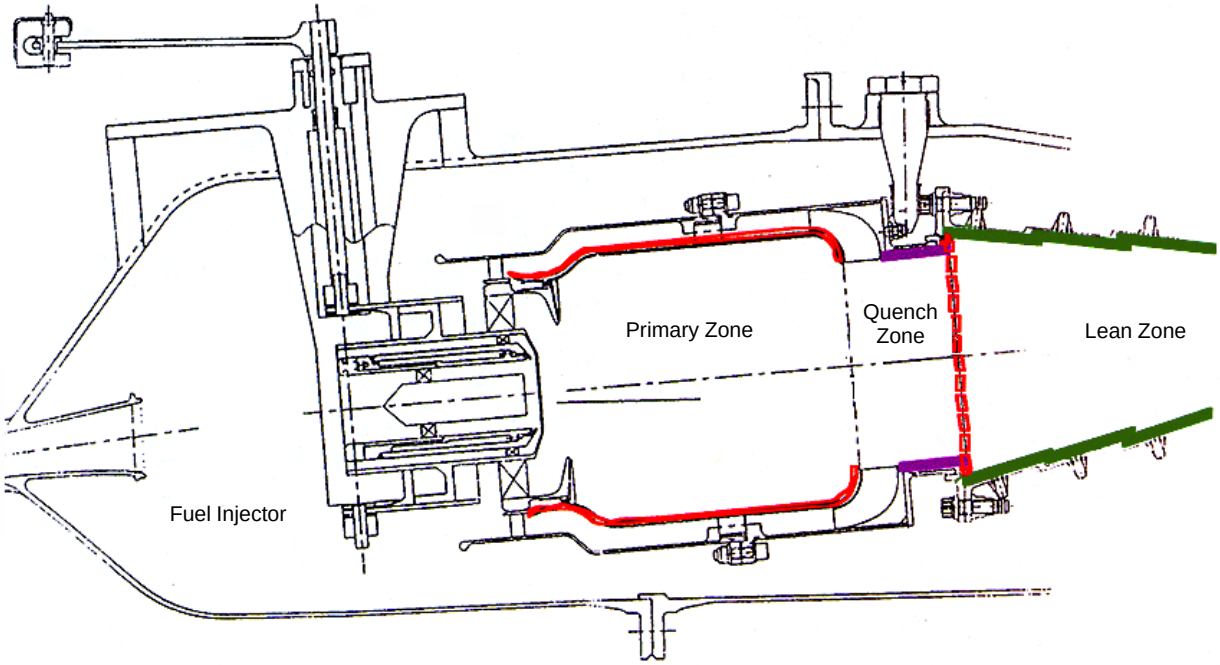

Figure 265. CMC Sector Cross Section

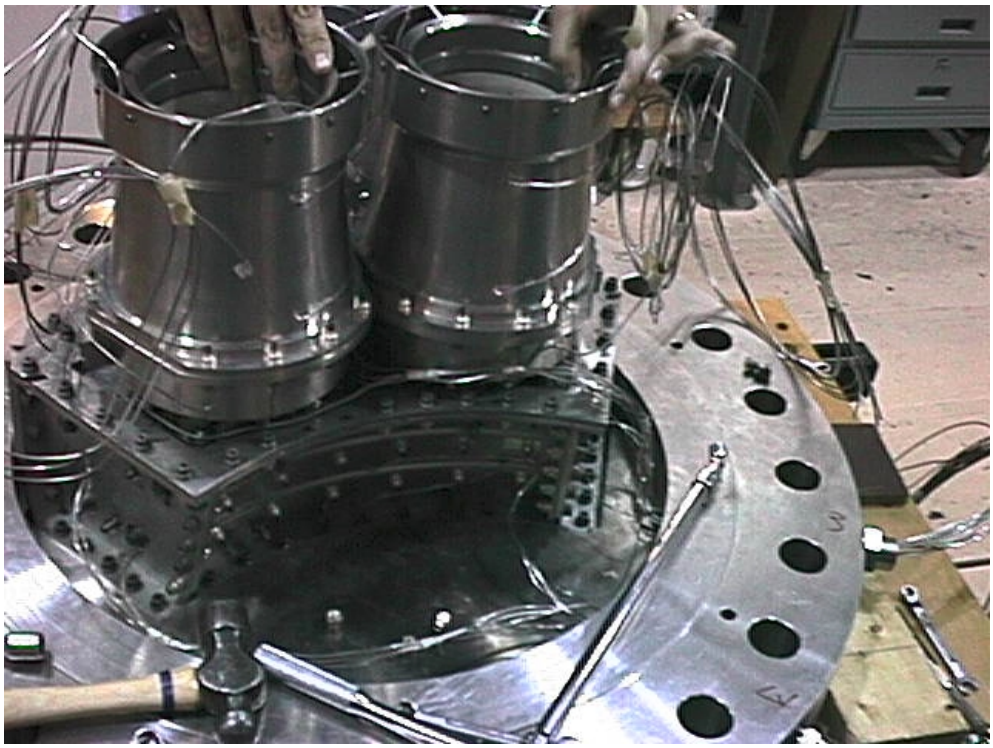

Figure 266. CMC Sector Hardware Mounted on Instrumentation Flange (Variable-Geometry Fuel Nozzle Not Installed)

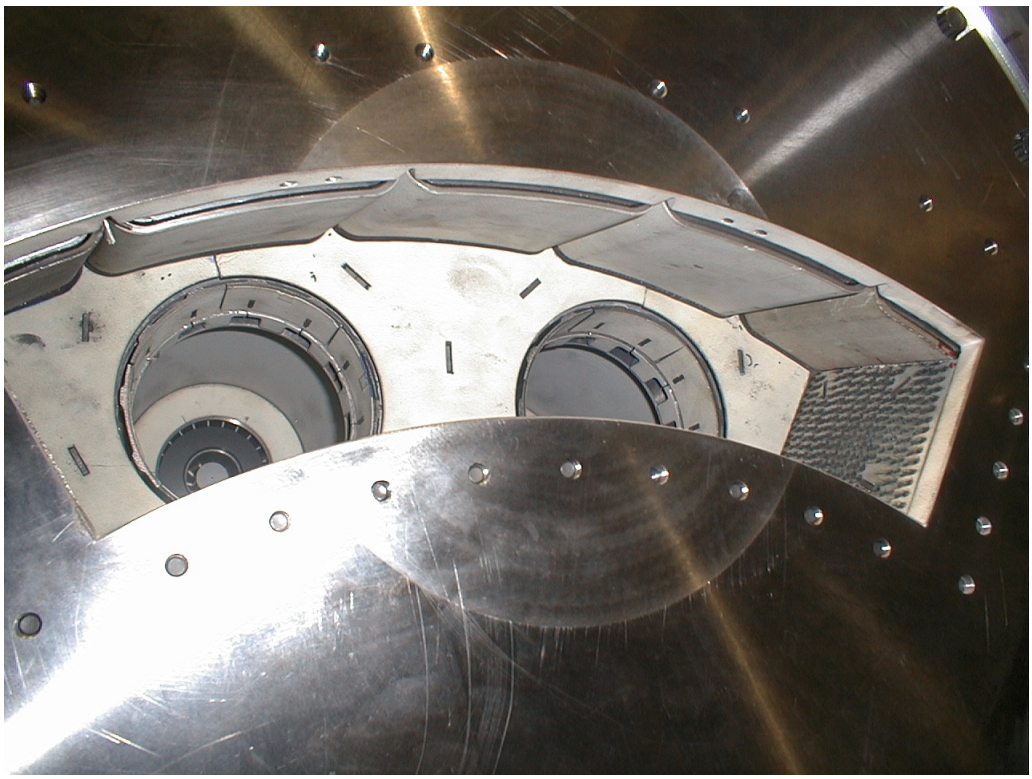

Figure 267. CMC Sector Hardware – View of Lean Zone

half-baffles on either side of the sector with heat shields. The sector sidewalls had single impingement/effusion-cooled panels. Pictures of the various types of CMC liners and their locations in the combustor are shown in Figure 268.

4.5.4.3 Combustor Operation

In general, the CMC combustor sector maintains a constant rich equivalence ratio in the primary zone over the entire HSCT power cycle. This equivalence ratio was established during preliminary tests to minimize emissions and maximize efficiency. Primary zone liner temperatures were also considered.

At some low-power conditions (subsonic cruise and descent), the equivalence ratio inside the primary combustion zone was lean. Maintaining rich equivalence ratios well above stoichiometric would not be practical at the corresponding low fuel flows. Nevertheless, the fuel nozzle maintained a stable flame under lean conditions, and stoichiometric combustion was avoided.

4.5.4.4 Test Plan

The cycle was a modified version of the HSCT operating cycle. Initial tests used metal liners to allow shakedown tests to be completed without risk of damage to the CMC liners. Adjustments were made during these tests to meet the specific task requirements. The test plan is shown in Table 32.

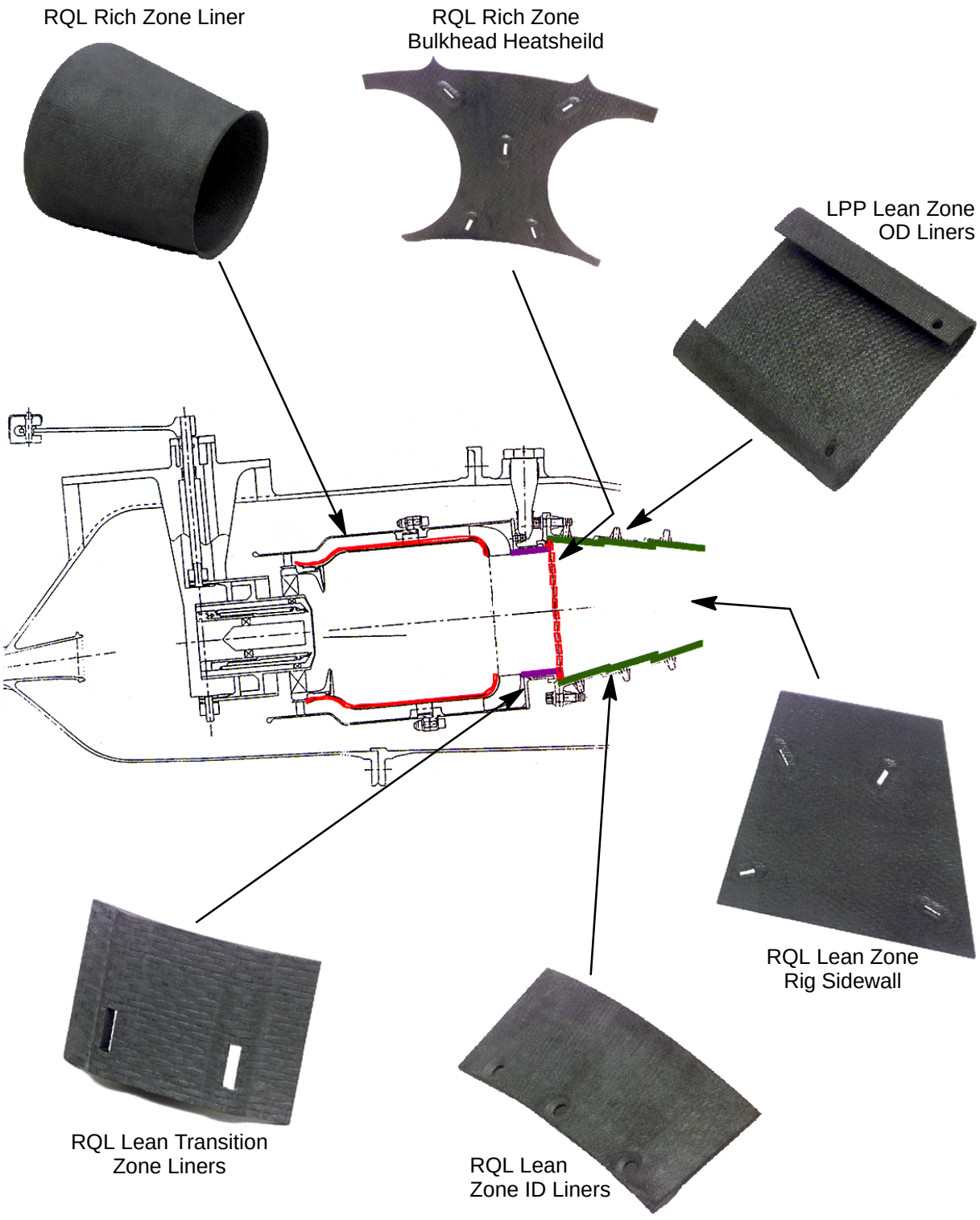

Figure 268. CMC Liners and Locations in Sector

Table 32. Nominal CMC Sector Operating Points

Pt	Condition		T_3 (°F)	T_3 (°R)	P_3 (psia)	$\Delta P/P_{comb}$ (%)	W (lbm/s)	f/a (Overall)	VG Pos. (% Open)	Φ (Primary)	Duration
1	Ignition	Begin	400	860	57.3	4.0	3.6	0.0140	0	1.40	–
2	Ignition	End	490	950	57.3	4.0	3.4	0.0140	0	1.40	–
3	Subsonic Cruise	Begin	490	950	57.3	6.0	4.2	0.0140	0.579	0.80	30 min
4	Subsonic Cruise	Nominal	490	950	57.3	6.0	4.2	0.0140	0.579	0.80	ramp
5	Subsonic Cruise	End	690	1150	57.3	5.0	3.8	0.0140	0.579	0.80	–
6	Takeoff	Begin	690	1150	200	6.0	13.2	0.0266	0.193	1.80	25 min
7	Takeoff	Nominal	851	1311	200	6.0	12.4	0.0266	0.193	1.80	ramp
8	Takeoff	End	870	1330	200	6.0	12.3	0.0266	0.193	1.80	–
9	Supersonic Climb	Begin	870	1330	200	6.0	12.3	0.0303	0.271	1.80	30 min
10	Supersonic Climb	Nominal	993	1453	200	6.0	11.8	0.0303	0.271	1.80	ramp
11	Supersonic Climb	End	1050	1510	200	6.0	11.6	0.0303	0.271	1.80	–
12	Top of Supersonic Climb	Begin	1050	1510	200	6.0	11.6	0.0312	0.271	1.80	5 min
13	Top of Supersonic Climb	Nominal	1050	1510	200	6.0	11.6	0.0312	0.271	1.80	–
14	Top of Supersonic Climb	End	1050	1510	200	6.0	11.6	0.0312	0.271	1.80	–
15	Supersonic Cruise	Begin	1050	1510	108.9	6.0	6.3	0.0315	0.271	1.80	100 min
16	Supersonic Cruise	Nominal	1050	1510	108.9	6.0	6.3	0.0315	0.271	1.80	
17	Supersonic Cruise	End	1050	1510	108.9	6.0	6.3	0.0315	0.271	1.80	–
18	Supersonic Transient	Begin	1050	1510	108.9	6.0	6.3	0.0315	0.271	1.80	5 min
19	Supersonic Transient	Nominal	1050	1510	108.9	6.0	6.3	0.0230	0.000	1.80	transient
20	Supersonic Transient	End	1050	1510	108.9	6.0	6.3	0.0315	0.271	1.80	–
21	Subsonic Climb	Begin	1050	1510	108.9	6.0	6.3	0.0266	0.246	1.80	20 min
22	Subsonic Climb	Nominal	890	1350	108.9	6.0	6.7	0.0266	0.246	1.80	ramp
23	Subsonic Climb	End	800	1260	108.9	6.0	6.9	0.0266	0.246	1.80	–
24	Descent	Begin	800	1260	75.3	6.0	4.8	0.0141	0.014	0.80	25 min
25	Descent	Nominal	700	1160	75.3	6.0	5.0	0.0141	0.014	0.80	ramp
26	Descent	End	600	1060	75.3	6.0	5.2	0.0141	0.014	0.80	–

4.5.4.5 Results

CMC Sector Performance

The metal liners were replaced with CMC liners upon completion of the shakedown tests. The combustor was operated over the entire HSCT flight cycle repeatedly, until the desired number of hours was achieved. To maximize use of available facility time, the supersonic cruise and transient conditions were repeated within the cycle. A typical cycle is shown in Figure 269.

Primary-Zone Module Liner Cracking

The primary-zone module CMC liners failed after eight hours of testing. Pictures of the two liners are shown in Figures 270 and 271. The failure was observed during a borescope inspection between tests. Analysis of the data did not reveal the moment of failure. Possible causes for the cracks were proposed, and tests were conducted on the liners. It was determined that the upstream spring that holds the liner in place was compressed beyond the intended range. The resulting high circumferential stresses in the liner caused the CMC material to separate along the splice joints.

During the investigation period, metal module liners were used to allow testing to continue on the other CMC liners. At the conclusion of the investigation, the springs were modified and installed into the combustor, along with new CMC module liners, and testing continued.

After over 60 hours of operation on the new module liners, cracks were observed during a routine inspection. Pictures of the second set of failed liners are shown in Figures 272 and 273. The cause for the cracks was being investigated at the time of this writing. During the investigation, a third set of CMC liners was installed into the combustor sector to allow testing to continue.

Miller Fastener Failure

A transition-zone liner was found liberated after 106 hours of operation. It was observed that both Miller fasteners holding the panel in had failed. These parts are pictured in Figure 274. Upon closer inspection, other Miller fasteners in the lean transition zone were found cracked. It was suspected that these fasteners were installed improperly. The broken fasteners were replaced, and no other Miller fastener failures occurred during the tests.

Fuel Nozzle Heat Shield Deterioration

At the time the second set of primary-zone module liners were found cracked, significant deterioration of fuel nozzle heat shields was observed. A picture of a heat shield after 100 hours of operation is shown in Figure 275. Two fuel nozzles were modified to increase heat shield cooling airflow and extend the life. These were installed in the rig to begin testing on the third set of module liners.

4.5.4.6 Discussion

The CMC combustor sector provides the necessary environment to test CMC liner materials. It subjects materials to both rich and lean conditions over a wide range of inlet temperatures, inlet pressures, and flame temperatures. The variable-geometry capability gives the investigator the power to select the environment the materials are exposed to. The sector has also been proven rugged enough to test materials over a long period of time despite liner failures. The exception to this was

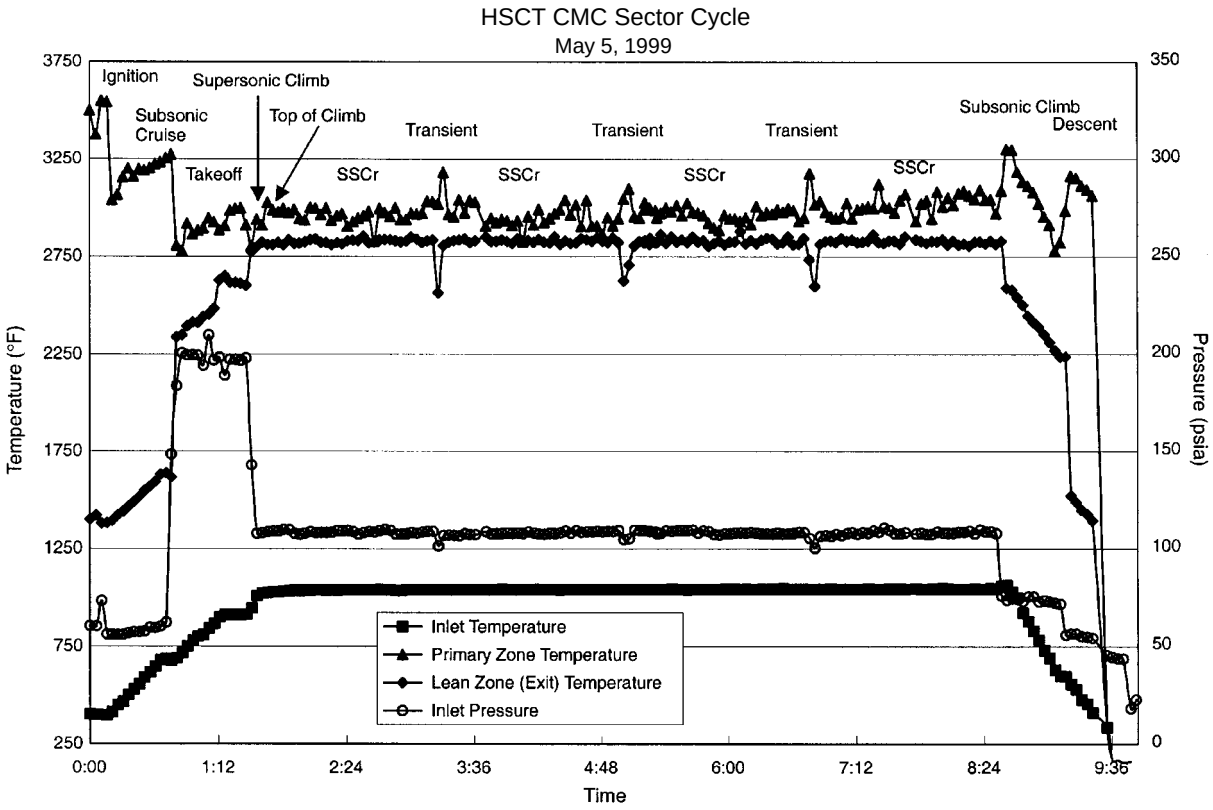

Figure 269. Typical HSCT CMC Sector Cycle

Figure 270. First Primary-Zone Module Liner Failure (Control Room Side)

Figure 271. First Primary-Zone Liner Failure (Parking Lot Side)

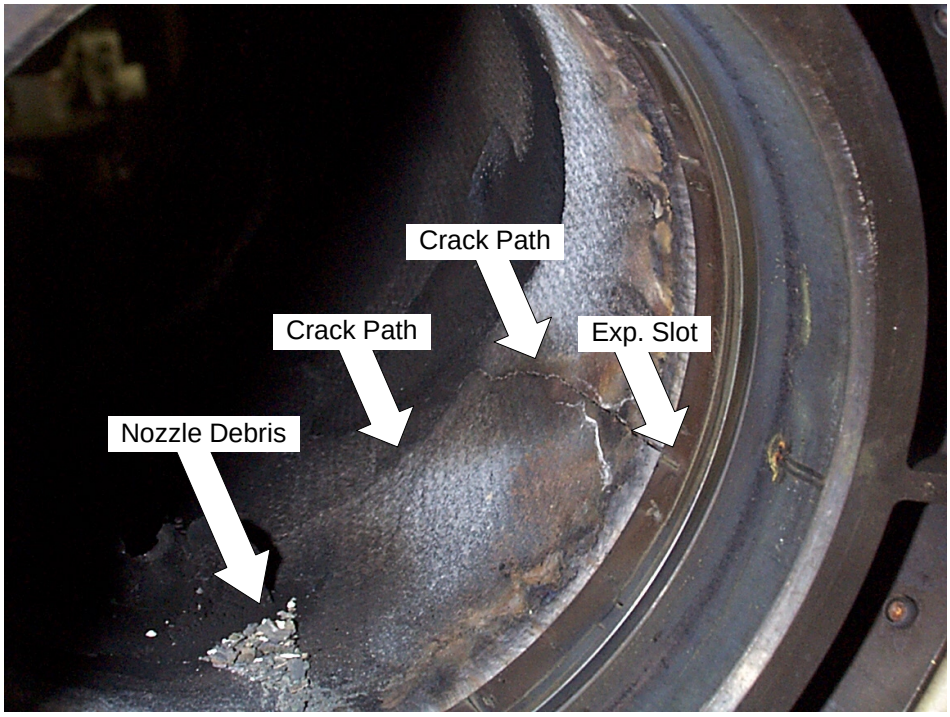

Figure 272. Second Primary-Zone Liner Failure (Conrol Room Side)

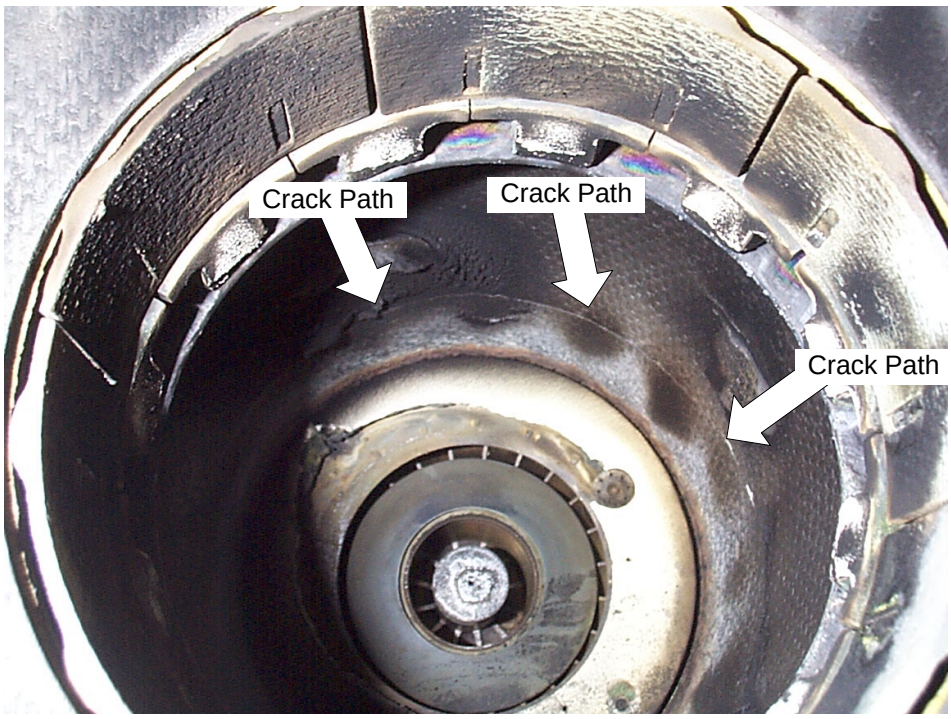

Figure 273. Second Primary-Zone Liner Failure (Parking Lot Side)

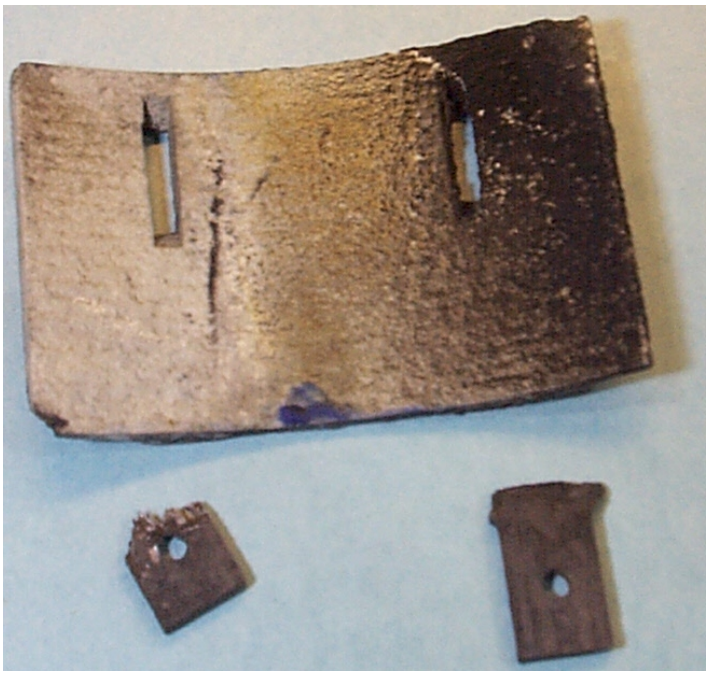

Figure 274. Liberated Lean Transition Zone Heat Shield and Miller Fasteners

Parking Lot Side, Old Nozzle

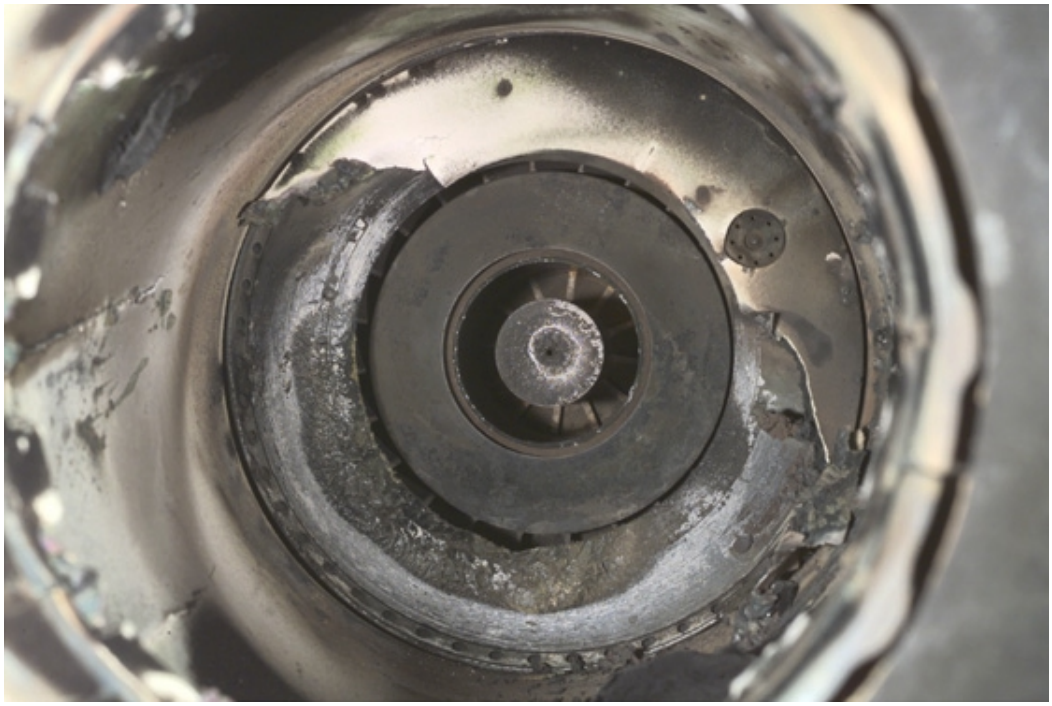

Figure 275. Deterioration of Variable-Geometry Fuel Nozzle Heat Shield

the heat shields of the variable-geometry nozzles. It is expected that this flaw can be corrected with only minor changes to the hardware.

4.6 Lean Downselects

Two primary downselects were required to reduce the three fundamental concepts down to one. The first was to decide between the use of a lean direct-injection system or a lean premixed/prevaporized system. Once the LPP system was chosen, a choice had to be made between a stepped-dome and a multistage radial/axial layout. The MRA concept was eventually chosen for full-scale development.

4.6.1 LDI/LPP Downselect

The primary criteria used in the LDI/LPP downselect were supersonic cruise NOx and autoignition/flashback. Although considered, low-power emissions were given less weight since the primary function of the main dome fuel/air mixers was to provide low emissions at moderate and high power; the cyclone pilot emissions tend to dominate at low power. Supersonic cruise NOx was the primary driver of most development early in the program. The advances necessary to meet the stringent 5 EI target at such severe conditions were considered to be huge hurdles to clear before an engine could ever be commercialized. Thus, significant emphasis was placed on this requirement, not only for the LDI/LPP downselect, but for all others as well.

The lowest supersonic cruise EINOx in an LDI system was projected to be in the 5 to 7 range (Build 4 of the LDI rectangular sector). There were two concerns with this projection. First, since testing

was not performed at actual supersonic cruise operating conditions, the 5–7 EI estimate was not at all certain (and still may not meet the requirement). Second, because the dome contained only LDI mixers (no cyclone pilots were used), the low-power efficiency was relatively poor. Although not the primary consideration, it was felt that improvements to low-power operation without a cyclone pilot would have been extremely difficult. The multiventuri/cyclone combination provided better low-power operation but was expected to produce supersonic cruise EINOx in the 8 to 10 range, which was unacceptably high.

In contrast, the lowest supersonic cruise EINOx from an LPP system was right at 5, in the stepped-dome, segmented-liner sector. (At the time of this particular downselect, the moderately mixed MRA had not been tested; it eventually demonstrated 3.8 EI.) Although no margin was available, the data had at least been acquired at the nominal conditions, unlike the LDI numbers — which were extrapolated. This provided significantly more confidence that the 5 EINOx requirements at supersonic cruise could actually be met using an LPP system.

Table is an additional point of comparison used in the downselect. It directly compares NOx emissions over a range of operating conditions for two nearly identical sectors: the three-cup multiventuri/cyclone LDI sector (Build 1) and the three-cup IMFH/cyclone LPP Sector. The LPP sector consistently demonstrated lower NOx, further support for the selection of an LPP system.

Table 33. LDI/LPP Downselect Emissions Comparison (Three-Cup Rectangular Sectors)

Test Conditions			EI NOx (g/kg Fuel)	
T_3 (°F)	P_3 (psia)	T_{flame} (°R)	LDI Multiventuri/Cyclone	IMFH/Cyclone
590	82	3500	2	1
879	211	3500	6	5
962	119	3500	7	3.5
1050	132	3500	8	2

Autoignition and flashback were of primary concern in the LPP designs. Although considered, the LDI systems tend to have short enough residence times that autoignition does not come into play. One advantage of the LPP IMFH designs is that they provide longer residence times, allowing more time for prevaporization and premixing but pushing up against the autoignition limits. Additionally, the lack of small, flame-arresting features in the IMFH tubes made flashback a concern. The IMFH blockage test and stepped–dome transient sector test successfully demonstrated that the IMFH designs were highly resistant to both autoignition and flashback events. The transient sector in fact induced reverse flow of combusting gases through the IMFH tubes, which quickly cleared without damaging the hardware as the flow returned to normal. Additionally, of the hundreds of hours of IMFH testing that had been done, both in single–cup flametube tests and sector tests, not a single autoignition or flashback event had been recorded.

In addition to emissions and autoignition considerations, mechanical concerns had to be addressed. The primary concern was how to package the LDI mixers into the main dome. This was especially true for an LDI system using radial swirlers, although space limitations were even making those with an axial swirler difficult to locate. On the other hand, the IMFH tubes could effectively be smaller in diameter and still provide the same flow area as a larger diameter LDI mixer. This mitigated some of the packaging concerns and was additional impetus for an LPP system.

The significant resistance to autoignition and flashback, low supersonic cruise NOx, superior packaging feasibility, and the fact that more development had been done on the LPP system subcomponents (corresponding to a higher overall confidence level) led to the selection of LPP over LDI for further development.

4.6.2 LPP Stepped-Dome/MRA Downselect

Emissions, exit profiles, and manufacturability were the key inputs to the LPP stepped-dome/MRA downselect. Because both concepts used the same basic components (cyclone pilots and IMFH tubes), the trick was to determine which arrangement was best.

The downselect criteria described in Section 4.1 were used as guides in making the selection. Both designs clearly had great potential, as shown in Table 34. The primary concern with the stepped-dome design was ability to meet LTO cycle emissions requirements. In both designs, some concern existed over exit profiles.

Table 34. LPP Stepped-Dome/MRA Downselect Status Summary

Combustor Downselect Criteria			LPP SD	LPP MRA
Emissions and Performance	Supersonic Cruise	NOx	Y	Y
		Combustion Efficiency	Y	Y
	Subsonic Cruise	NOx	Y	(N)
		Combustion Efficiency	(N)	Y
	Airport Vicinity LTO Emissions		N	Y
	Particulates		?	Y
	Transient Stability (Autoignition, Flashbacks)		Y	Y
	Combustor Blowout Margin		Y	Y
	Altitude Relight		?	?
	Profile and Pattern Factor		(N)	(N)
	Combustor Overall Pressure Loss		Y	Y
	Fuel System Coking		?	?
	Compressor Distortion		?	?
Product Viability	Safety		X	X
	Complexity		X	X
	Combustor Dynamics		?	?
	Controls Stability		X	X
	Maintainability		X	X
	Component Life		Y	Y
	Reliability		X	X
	Initial Cost and Producibility		Y	Y
	Size and Weight		Y	Y
	Repairability		X	X

Y (Yes) = Criteria Met, N (No) = Criteria Have Not Been Met, ? = Unknown/No Data,
X = Not Addressed or Expected to be the Same for Both Designs
(N) = Criteria Not Demonstrated But Should be Able to Overcome (Such as by Different Fuel Staging)

Emissions at all power levels were considered. Ground idle CO and combustion efficiency, subsonic cruise NOx and combustion efficiency, and supersonic cruise NOx and combustion efficiency were the focal points. Subsonic cruise data were given less weight because changes to the fuel staging (the number of fuel stages and staging points) could be made to improve emissions at this intermediate point. Emissions are summarized in Table 35. Note that the subsonic cruise data are strongly impacted by the fuel-staging mode selected and must be discounted. Although emissions from the stepped-dome designs were quite good at high power, low-power emissions and combustion efficiencies suffered. The MRA concept consistently produced much lower emissions and higher combustion efficiencies than the stepped-dome configurations.

Table 35. LPP Stepped-Dome/MRA Downselect Emissions Comparison

Comparison Parameter		Stepped Dome		Moderately Mixed MRA
		Lamilloy Liners	Segmented Liners	
Ground Idle	EICO (g/kg Fuel)	50	36	20
	Combustion Efficiency	89.50%	94.23%	99.40%
Subsonic Cruise*	EINOx (g/kg Fuel)	32	1.5	14
	Combustion Efficiency	99.40%	90.59%	99.60%
Supersonic Cruise	EINOx (g/kg Fuel)	4.5	4.7	3.8
	Combustion Efficiency	99.97%	99.97%	99.98%
* Subsonic cruise values are dependent on fuel staging; alternate staging could alter these values.				

Exit profiles were of primary concern in the MRA configuration. The pilots in the stepped-dome concepts were located in the center dome. Thus, at low power, exit profiles were generally center-peaked. As fuel was introduced into the IMFH tubes in the inner and outer domes, the profiles would become slightly inner- or outer-peaked, depending on the staging preference. The profiles would become flat when all the stages were fired.

In contrast, the pilots in the MRA concept were located at the top edge of the main dome. Although they were directed radially inward, exit profiles at low power were outer-peaked. To increase power, the IMFH tubes were fueled beginning with the outer tubes and moving radially inward. Thus, the exit profiles remained outer-peaked until all the tubes were fired, at which time the profile was flat.

The outer-peaked profiles were a concern because they generally result in reduced turbine efficiency. Circumferential staging considered as a way of flattening the outer-peaked profiles. It was successfully tested in the MRA curved sector and shown to have minimal impact on emissions. Circumferential staging had no impact on ground idle profiles, which remained strongly outer-peaked because only the cyclone pilot were fired. Similarly, fully fired profiles were unchanged (sea level takeoff, supersonic cruise). Circumferential staging appeared to be a viable method of improving combustor exit profiles without significantly impacting emissions.

Manufacturability was a concern with both concepts. The stepped dome was fairly complex and would have been difficult to manufacture. More importantly, cooling was a primary concern, as the step used to isolate the pilot and improve low-power emissions produced a very high heat load on the inner and outer surfaces of the outer and inner domes, respectively. Although a flat “stepped dome” sector was tested, low-power emissions suffered significantly, and the concept was not

pursued. Finally, the development of a removable fuel nozzle for such a concept was highly complex. Because the nozzle would have to contain injectors for the IMFH tubes as well as a cyclone injector/centerbody combination, it would have been expensive and excessively large and heavy. Because the IMFH domes were aft relative to the pilots, the IMFH fuel injectors would have to have been long appendages attached to the nozzle. Thus, the case hole required to remove the nozzle would have to have been tremendously long, adding length (and therefore weight) to the overall engine and potentially weakening the case itself. The MRA concept had the advantage of a flat main dome and a separate pilot. This allowed each to have a fuel nozzle, each of which was a simpler design than required for the stepped dome. The flat dome was also less costly to produce and much easier to cool.

Although both were relatively complex systems, the MRA design had several inherent advantages over the stepped dome. It was somewhat easier to produce and effectively cool, providing advantages in manufacturability, reliability, cost, and weight. The reduction in supersonic cruise EINOx from 5 for the stepped dome to 3.8 for the MRA was a significant driver in the selection of the MRA. Although a concern, it was felt that the MRA exit profiles could be improved through various combinations of circumferential staging. Based on this information, the MRA concept was selected for further development.

4.7 LPP/RQL Combustor Downselect

For the final LPP/RQL downselect, each team was to propose a combustor design for use in an HSCT engine. The designs had to demonstrate the ability to meet a prespecified set of criteria using test data, analyses, assessments, and current product experience. Up to this point, the two primary concepts remaining under development were the lean premixed/prevaporized MRA and the rich/quench/lean, dual-annular, reduced-scale, quench vane designs. After a period of comprehensive design, development, and testing efforts, it was time to reduce the options down to one primary concept.

4.7.1 Criteria

An extensive list of criteria was used in making the downselect decision. These were presented in Section 4.1, but are repeated here in Table 36 for convenience. The criteria had been created very early in the program and had been the drivers of the development efforts for all of the concepts considered along the way. Emissions were clearly given significant consideration, with supersonic cruise NOx being the focal point of much of the development effort.

4.7.2 Process

Both concepts were to be evaluated against the criteria in Table 36. Industry participants presented detailed information regarding the position of the designs relative to the criteria. Test data, analytical predictions and comparisons, thermal and stress evaluations of the component designs, potential risks, and final recommendations were presented. Members of NASA, industry participants, and other experts in the field were represented at the review. Final selection was then made based on the recommendations of this panel.

Table 36. Combustor Downselect Criteria

Combustor Downselect Criteria			Requirement
Emissions and Performance	Supersonic Cruise	NOx	< 5 EI (g/kg Fuel)
		Combustion Efficiency	> 99.9%
	Subsonic Cruise	NOx	< 10 EI (Typical Subsonic Aircraft)
		Combustion Efficiency	> 99% (Typical Subsonic Aircraft)
	Airport Vicinity Landing/Takeoff (LTO) Emissions	NOx (Supersonic*)	< 5 lbm/klbm–°F–hr
		CO (Supersonic*)	< 7.8 lbm/klbm–°F–hr
		UHC (Supersonic*)	< 1 lbm/klbm–°F–hr
		NOx (Subsonic**)	< 64.3 g/kN
		CO (Subsonic**)	< 118 g/kN
		UHC (Subsonic**)	< 19.6 g/kN
	Particulates per cm^3 of Exhaust Gas		< 10^7 (Typical Subsonic Aircraft)
	Transient Stability (Autoignition, Flashbacks)		
	Combustor Blowout Margin		> 0.1 Equivalence Ratio Units
	Altitude Relight		
	Profile and Pattern Factor		< 5%
	Combustor Overall Pressure Loss		
	Fuel System Coking		
	Compressor Distortion		
Product Viability	Safety		
	Complexity		
	Combustor Dynamics		
	Controls Stability		
	Maintainability		
	Component Life		
	Reliability		
	Initial Cost and Producibility		
	Size and Weight		
	Repairability		

4.7.3 Results

The results were presented at NASA–Glenn in April and May 1998. Unfortunately, although the RQL concept was anticipated to meet all product viability requirements, at the time of the downselect the RQL combustor was still struggling to meet emissions targets. This effectively limited participation in the downselect to the LPP design. Management teams decided that the MRA concept would be selected, barring any technological “show stoppers” (items that could halt the eventual development of a commercially viable product), as determined by the reviewing team members.)

Cross sections of the proposed MRA design are presented in Figures 276 through 280. Essentially, it is a full-scale version of the moderately mixed MRA concept described previously, modified to

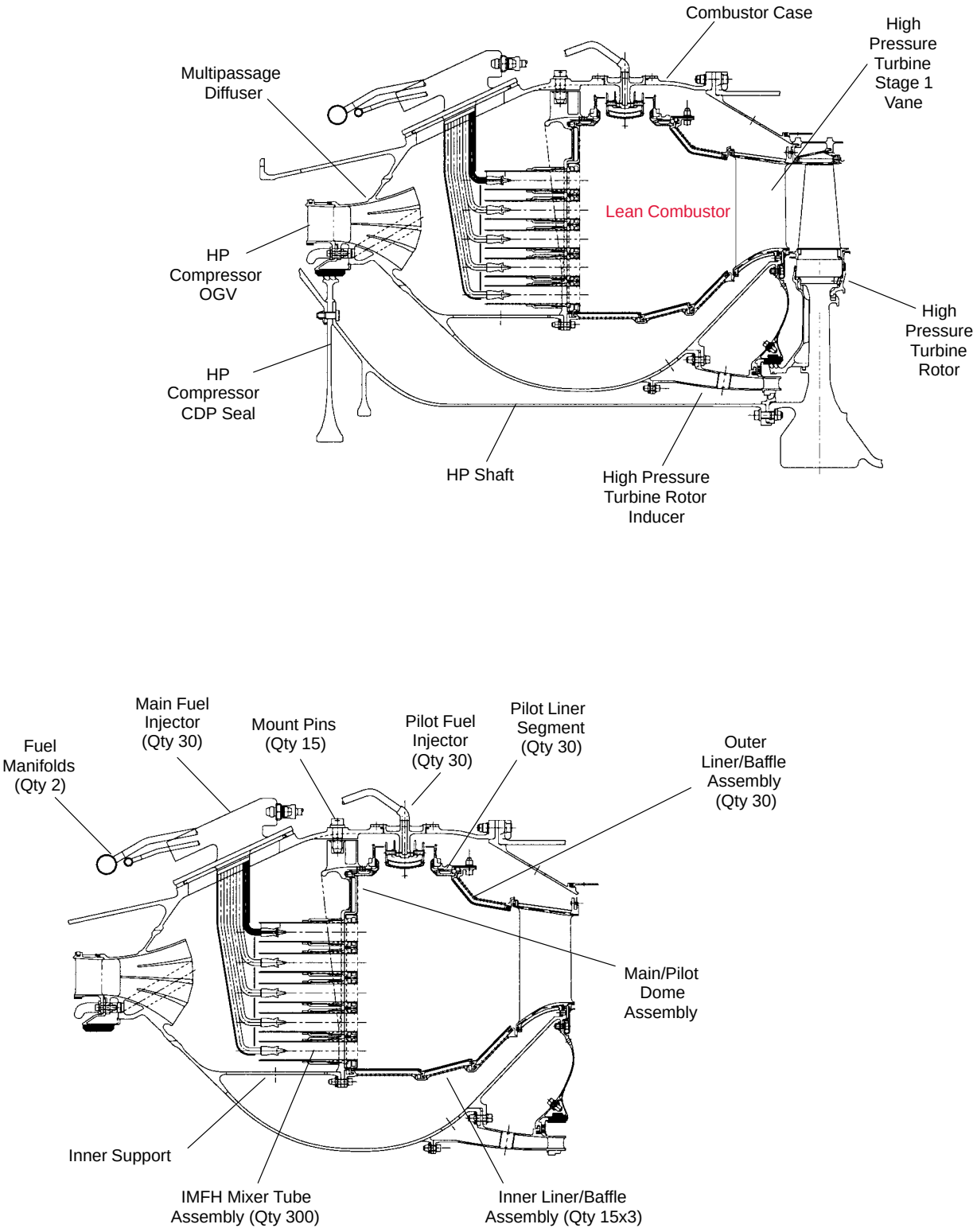

Figure 276. Full-Scale LPP MRA Combustor Preliminary Design – Side Views

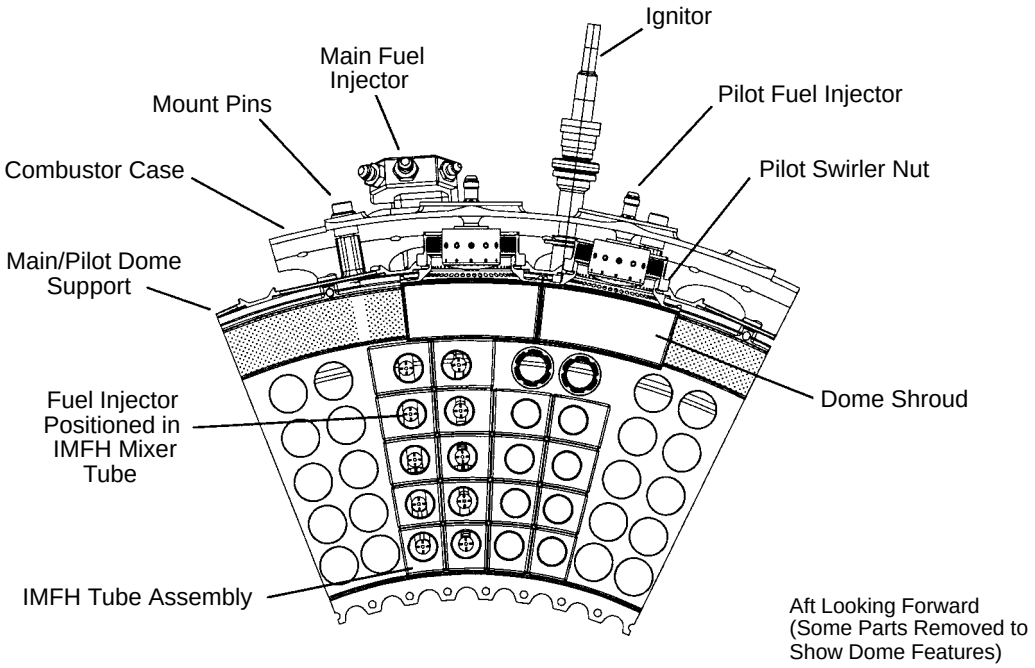

Figure 277. Full-Scale LPP MRA Combustor Preliminary Design – End View Aft Looking Forward

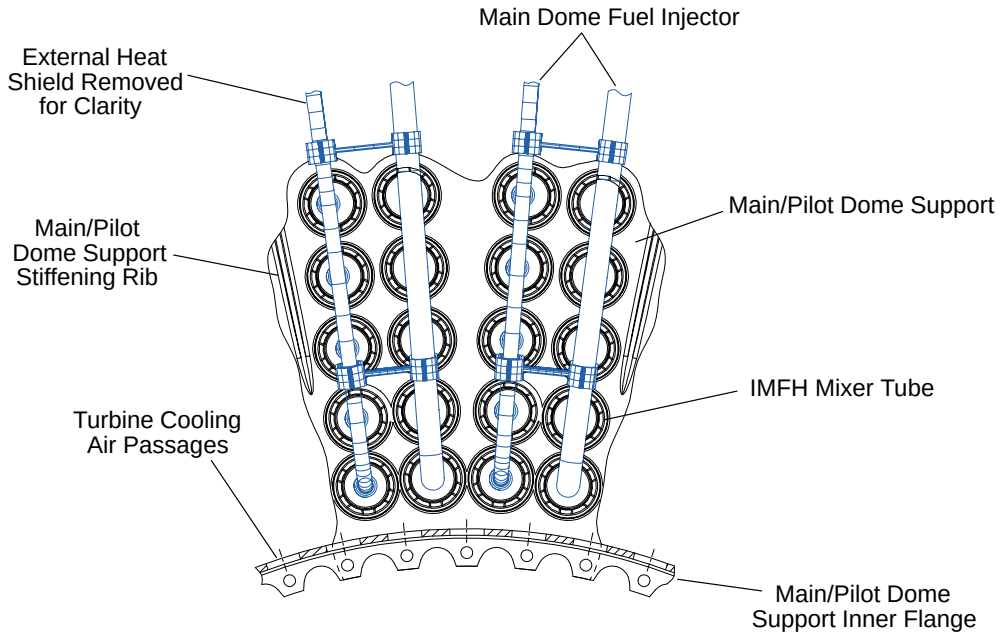

Figure 278. Full-Scale LPP MRA Combustor Preliminary Design – End View Forward Looking Aft

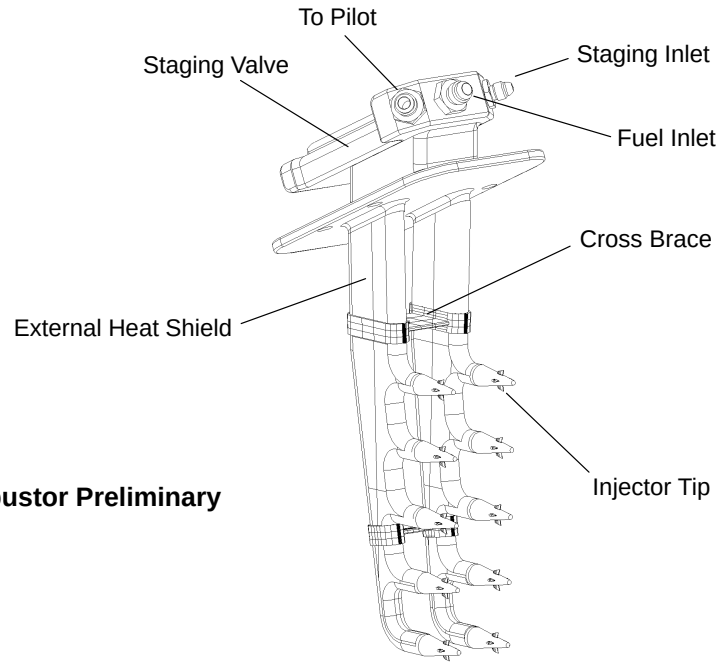

Figure 279. Full-Scale LPP MRA Combustor Preliminary Design – Fuel Nozzle

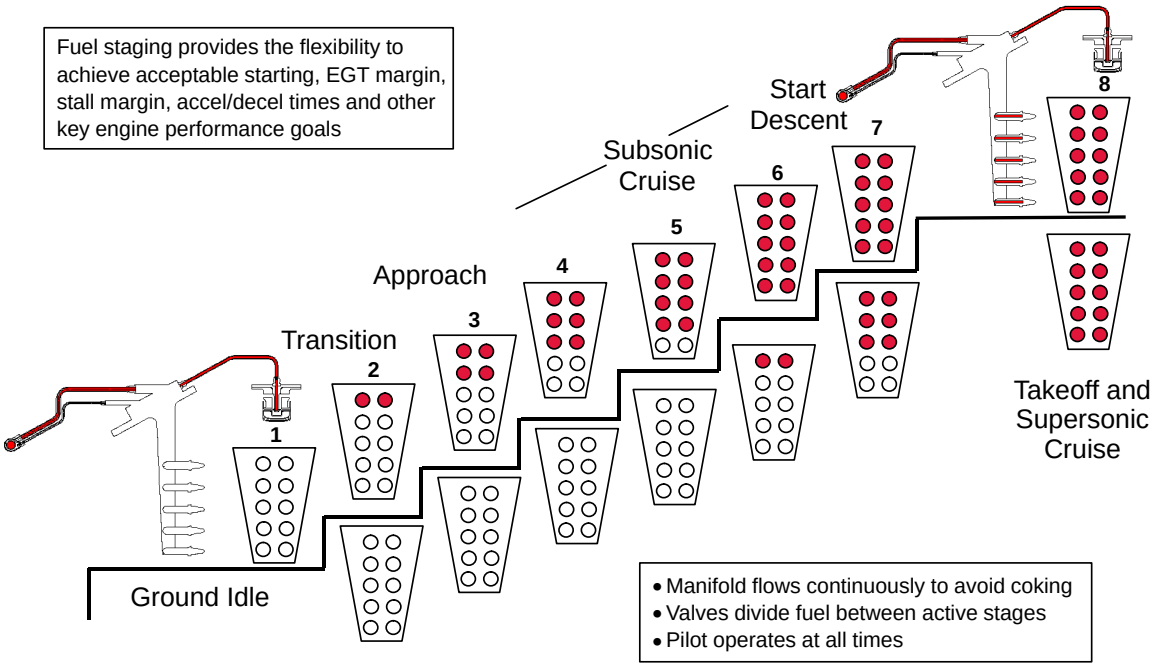

Figure 280. Full-Scale LPP MRA Combustor Preliminary Design – Fuel Staging Schematic

meet geometric size requirements and reflect advances made during full-scale subcomponent development. A new diffuser design and lighter, simpler fuel nozzles are evident.

Modifications were made to convert from ½-in IMFH tubes with a single-port stinger fuel injector to 1-in tubes with four-port stingers. This was significant, since 1200 ½-in IMFH tubes would have been required in the full-scale engine. One-inch tubes reduced this number to a more manageable 300. Thirty cyclone pilots were used, the chosen design being based on full-scale subcomponent results.

To meet mechanical needs, and because of the improved cooling effectiveness, segmented inner liners were used. The outer liner was segmented circumferentially (for mechanical reasons) but not axially because of concerns over the potential impact on low-power emissions (the impact of the inner liners on low power emissions was not a concern since the inner IMFH tubes were already unfired at these conditions.

Table 37 is a summary of the criteria and the associated results for the MRA concept. It was clearly quite successful in meeting the requirements set forth in the contract. Most of the emissions and performance categories had been demonstrated using actual sector results, while those in the product-viability group relied more on assessments and analytical results. Several categories ("Blue") have not been specifically demonstrated but were not anticipated to present any significant obstacles to eventual completion. It is expected that these could be met with relatively straightforward design and development efforts. No categories were classified as having the potential to end the program ("Red"), and only one — Combustor Dynamics — was classified as needing significant additional work ("Yellow").

In the end, the LPP MRA concept was selected as the primary configuration for the HSCT engine. Although all criteria were considered, three primary factors led to selection of the MRA.

- First, supersonic cruise NOx emissions were well below contract requirements for the MRA combustor (3.8 EI versus a 5 EI target). Although additional development had the potential for improvements, the RQL concept was unable to demonstrate target levels at that time. This was of great significance, since high supersonic cruise EINOx levels were considered a threat to the continuation of the program.

- Second, no "show stoppers" were identified with the MRA design. Thus, although certain criteria had not specifically been physically demonstrated in subcomponent or sector evaluations, it was determined that these items did not involve significant advances beyond current capabilities and could be implemented in the future without undue additional cost and time. The only area that needed additional work of any significance was combustor dynamics.

- Finally, because the LPP design appeared to be in more advanced stages of development, it was considered to be somewhat lower risk. The RQL design was to be retained as a backup should significant problems appear during development of the full-scale MRA combustor. Overall, reviewers seemed to be pleased with the progression of the concept and considered the combustor development to that point to be quite successful.

Table 37. Combustor Downselect Criteria

LPP Combustor Downselect Criteria			Status	Method
Emissions and Performance	Supersonic Cruise	NOx	G	Flametube and Sector Test Data, Analysis
		Combustion Efficiency	G	
	Subsonic Cruise*	NOx	B	
		Combustion Efficiency	B	
	Airport Vicinity LTO Emissions		B	
	Particulates		G	Sector Test Data
	Transient Stability (Autoignition, Flashbacks)		G	Transient Sector Test Data
	Combustor Blowout Margin		G	Flametube and Sector Test Data
	Altitude Relight		B	Sector Test Data, Analysis
	Profile and Pattern Factor		G	
	Combustor Overall Pressure Loss		G	Analysis
	Fuel System Coking		B	
	Compressor Distortion		B	
Product Viability	Safety		G	
	Complexity		B	Assessment
	Combustor Dynamics		Y	Product Experience
	Controls Stability		G	Test Data, Analysis, Experience
	Maintainability		G	Assessment
	Component Life		G	Analysis
	Reliability		G	
	Initial Cost and Producibility		B	
	Size and Weight		G	
	Repairability		B	Assessment

* Subsonic cruise NOx and combustion-efficiency status were **Blue** at the downselect of the MRA sector; additional sector data later showed these criteria to be **Green**.

Green: Has met criteria.
Blue: Has not met criteria, but no significant obstacles envisioned.
Yellow: Has not met criteria, and more development is needed to state confidently it could do so.
Red: Is not expected to meet criteria without appreciable unidentified additional work.

For reference, the basics of the proposed backup dual-annular, reduced-scale quench vane RQL design are illustrated in Figures 281 through 283. It consists of 22 fuel nozzles feeding the inner and outer rich zones. The quench zones contain 110 quench vanes in the outer annulus and 88 on the inner. The inner and outer quench zones feed into the transition (lean) zone before exiting the combustor. This design was to be pursued if the LPP concept were to hit any significant roadblocks during final development.

Following downselect, full-scale subcomponent development continued on the IMFH premixer and cyclone pilot designs. Detailed design and fabrication of a full-scale MRA sector was also initiated. The remainder of this report focuses on these final tasks and outlines remaining program challenges.

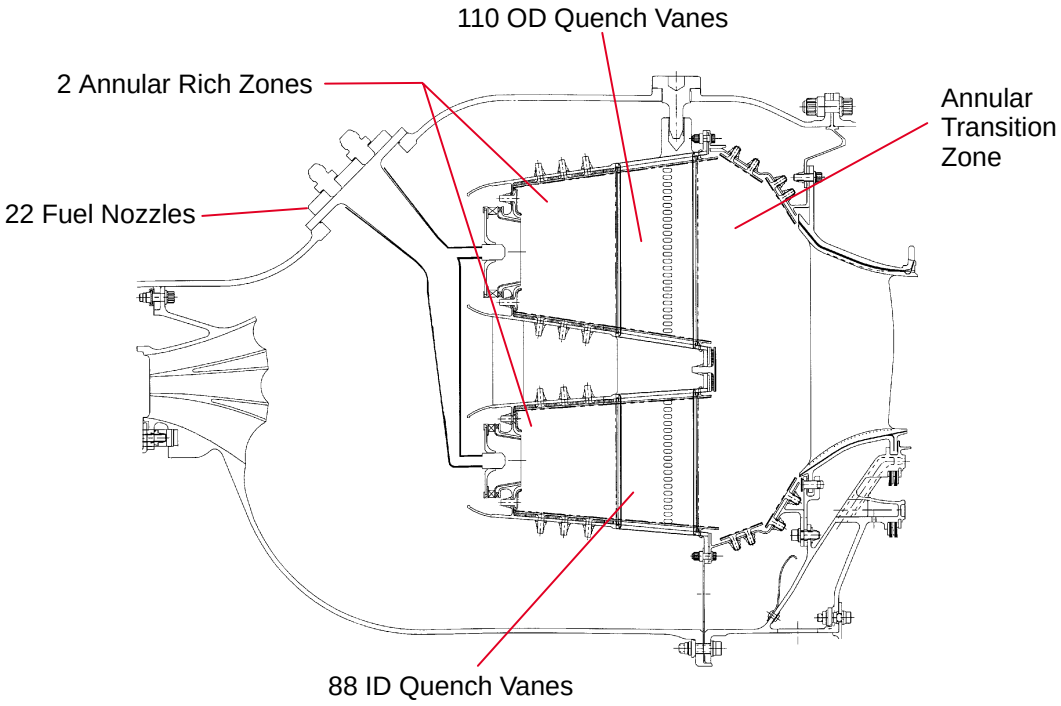

Figure 281. Full-Scale RQL Reduced-Scale Quench Vane Preliminary Design – Side View

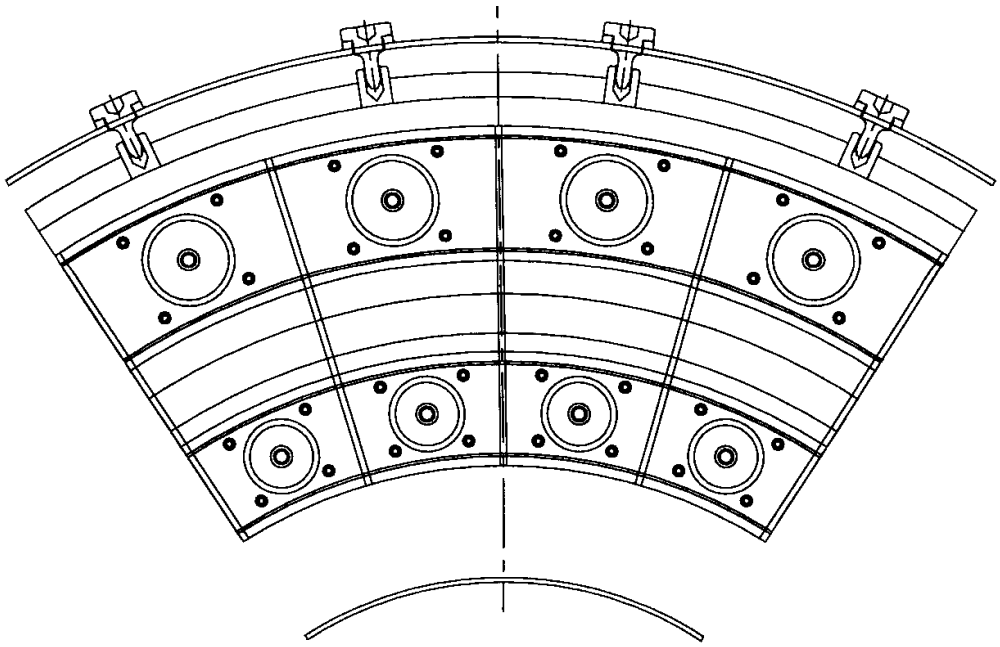

Figure 282. Full-Scale RQL Reduced Scale Quench Vane Preliminary Design – Rich Zone Bulkhead (End View, Aft Looking Forward)

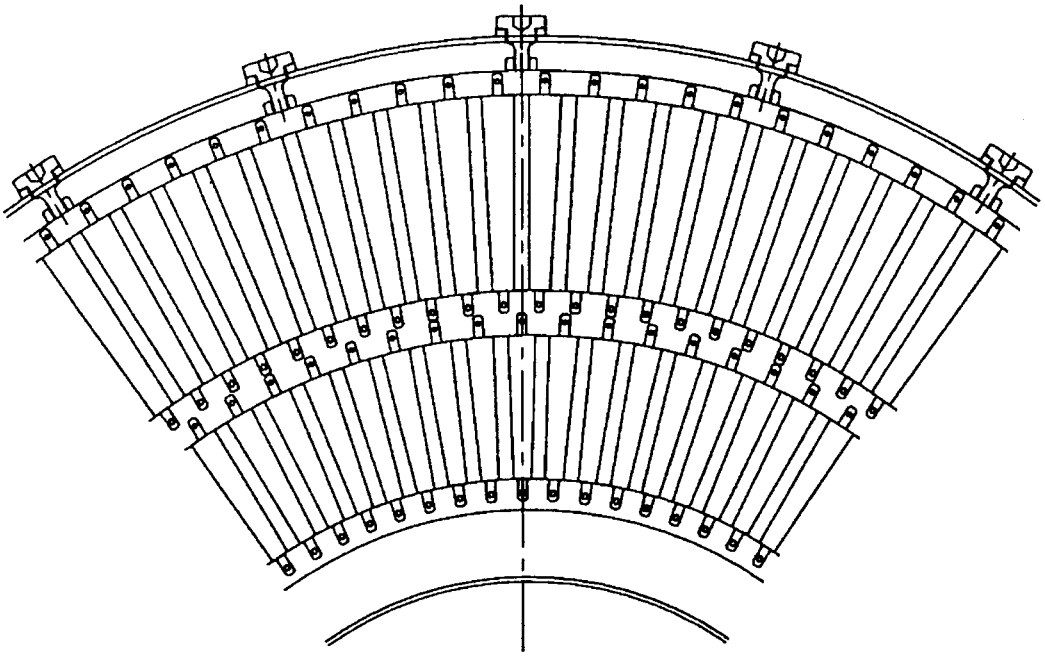

Figure 283. Full-Scale RQL Reduced-Scale Quench Vane Preliminary Design – Quench Vanes (End View, Aft Looking Forward)

4.8 Postselection Subcomponent Development

4.8.1 IMFH Premixer Flametube Tests

The purpose of this work was to continue the development of the IMFH subcomponent started by GEAE. Many areas were identified where improvements in the length, mixing, and flame-stabilization characteristics of the combustor could be made. These areas included the fuel injection, dome cooling air injection, injector aerodynamics, IMFH tube inlet aerodynamics, and IMFH tube spacing. Investigations began in each of these areas; however, only variations in the dome cooling air injection reached the test phase. The effects of changing the percent of dome cooling air to total IMFH tube flow, momentum ratio, and number and angle of cooling injectors was investigated. Cold-flow tests were conducted on a stereolythography model of the full-scale, one-inch IMFH tube assembly to determine cooling flow aerodynamics. Emissions tests were conducted with the IMFH assembly used in the earlier GEAE tests. The overall emissions from the baseline case matched well with those measured previously. Tests on a second configuration were being conducted at the time of this writing. Additional tests were needed to obtain conclusive results on cooling-flow injection.

4.8.1.1 Combustor Integrated Mixer/Flameholder

The full-scale, one-inch IMFH tube assembly used in the tests was designed and fabricated by GEAE (Figure 284). In brief, the most combustion air entered the upstream end of the tube and passed around the fuel injectors. On the downstream end of the fuel injectors, fuel was injected crosswise into the air stream and mixed with the air as it passed through the tube. A portion of the air was diverted around the IMFH tube and impinged on the dome for cooling. The spent cooling air was

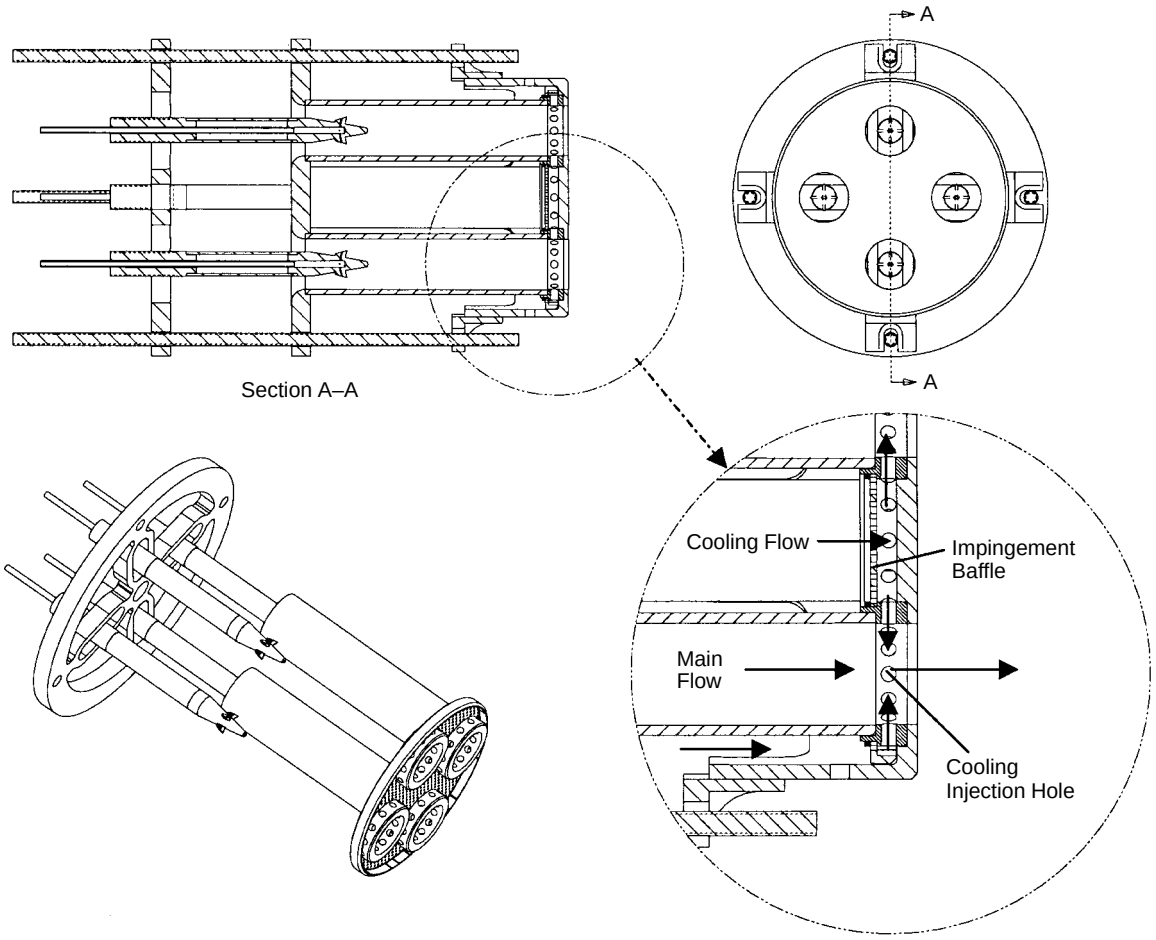

Figure 284. Full-Scale, One-Inch IMFH Tube Assembly Cross Section

then injected into the mainstream at the downstream end of the tube. The fuel/air mixture was then dumped into the combustion chamber where it was ignited and burned. Figure 285 is a picture of the assembly.

The work discussed here focused on cooling-air injection. The effects of the cooling air on emissions and flame stabilization were not completely understood. Theory suggested that the mass and momentum ratios between the injected cooling air and the mainstream air and the diameter of the injection holes would have strong influences on the mixing characteristics of the IMFH tubes. Theory and experience also indicated that the addition of swirl to the flow would promote mixing as well as increase flame stability. With these in mind, modifications were made to the full-scale assembly cooling injector holes and impingement baffle to study these effects.

4.8.1.2 Test Plan

Hardware Matrix – The hardware matrix contained a ½ full-factorial-level eight array to allow a Taguchi analysis to be conducted. Other hardware configurations included in this matrix isolated the effects of the different factors (mass ratio, momentum ratio, number of holes, and swirl) or were previously identified as possible candidates. The test matrix was built off a baseline configuration

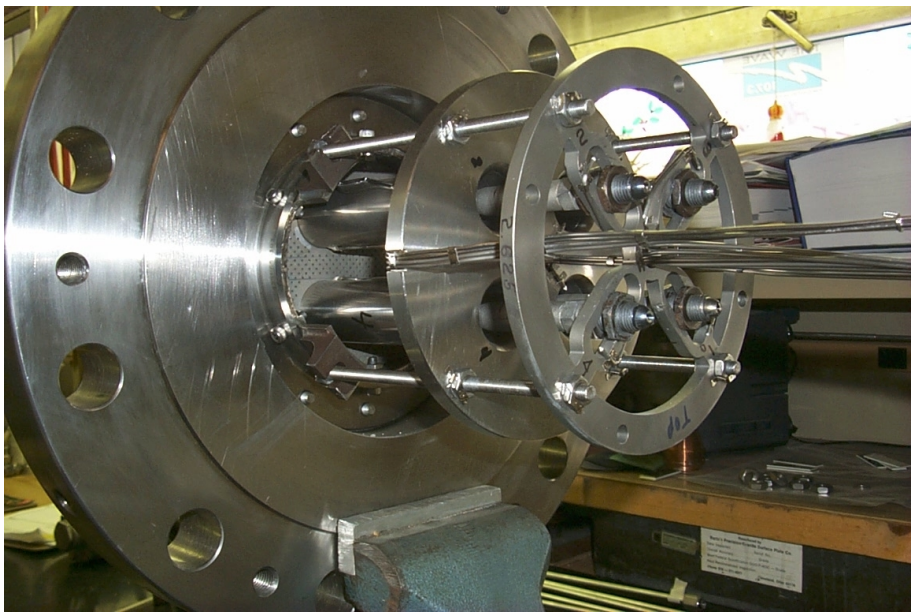

Figure 285. Full-Scale, One-Inch IMFH Tube Assembly Hardware

that was tested by GEAE and was found to have good characteristics. This configuration would provide continuity between tests. Previously existing hardware and geometric constraints determined the magnitudes (levels) of the parameters for each of the other configurations. A computer model was developed to help determine the geometry necessary to provide the desired aerodynamics. Table 38 is the final hardware matrix.

Test Matrix – The same test matrix was used for each of the configurations in the hardware matrix. The test matrix attempted to recreate the range of operating conditions that would occur in a typical HSCT cycle. Each of the nominal HSCT operating points would be tested. In addition, fuel/air ratio excursions would be conducted at subsonic cruise, 100% LTO, and supersonic cruise. Unfortunately, the facility and the absence of the pilot that would exist in an operating combustor limited the range of the tests. The final test matrix is shown in Table 39.

4.8.1.3 Results

Cold-Flow Tests – Cold-flow tests were conducted at Pratt & Whitney Florida's Aerothermal Design Lab to verify the computer model. Parts were first formed by stereolithography and flow tested. Figure 286 compares the results of these tests with the computer model. The test results were close to predicted at low momentum ratio; however, at higher ratios, the predictions were inaccurate. Corrections were made to the model before fabricating the parts out of metal. The expected characteristics of the parts used in the emissions tests are also shown in Figure 286.

It was suspected that the overall effective area of the IMFH tube assembly would be affected by the amount of air diverted for cooling. Although a change in overall effective area would not negatively affect emissions results, it would make design changes difficult in the LPP combustor. Figure 287 shows the percent baseline effective area as a function of percent cooling flow. The percent cooling flow did not have a significant effect on total effective area.

Table 38. Hardware Matrix

Configuration No.	Cooling Characteristics				
	J	% Split	N	a	
1	0.6	17%	12	0	GE Reproduction
2	0.6	17%	12	30	Factor Isolation
3	0.6	17%	18	0	
4	0.6	12%	12	0	
5	0.8	17%	12	0	
6	0.2	12%	8	0	GE PDR
7	0.6	17%	18	30	1/2 FF Level 8 Array
8	0.6	12%	12	30	
9	0.6	12%	18	0	
10	0.8	17%	12	30	
11	0.8	17%	18	0	
12	0.8	12%	12	0	
13	0.8	12%	18	30	
14	0.8	12%	8	0	Variation of GE PDR, Constant J

Table 39. Test Matrix

Test Point	Condition	T_3 (°F)	$P_{3.2}$ (psia)	$\Delta P/P$	f/a (IMFH)	Comment
1	15% LTO	446	78	4.40%	0.0475	Nominal
2	34% LTO	588	131	4.40%	0.0425	Nominal
3	SubCr.	630	80	4.40%	0.0430	Nominal
4	SubCr.	630	80	4.40%	0.0400	f/a Excursion
5	SubCr.	630	80	4.40%	0.0450	f/a Excursion
6	65% LTO	740	207	4.40%	0.0375	Nominal
7	100% LTO	919	293	4.40%	0.0350	Nominal
8	100% LTO	919	293	4.40%	0.0320	f/a Excursion
9	100% LTO	919	293	4.40%	0.0380	f/a Excursion
10	SSCr.	1200	146	4.40%	0.0329	Nominal
11	SSCr.	1200	146	4.40%	0.0300	f/a Excursion
12	SSCr.	1200	146	4.40%	0.0360	f/a Excursion

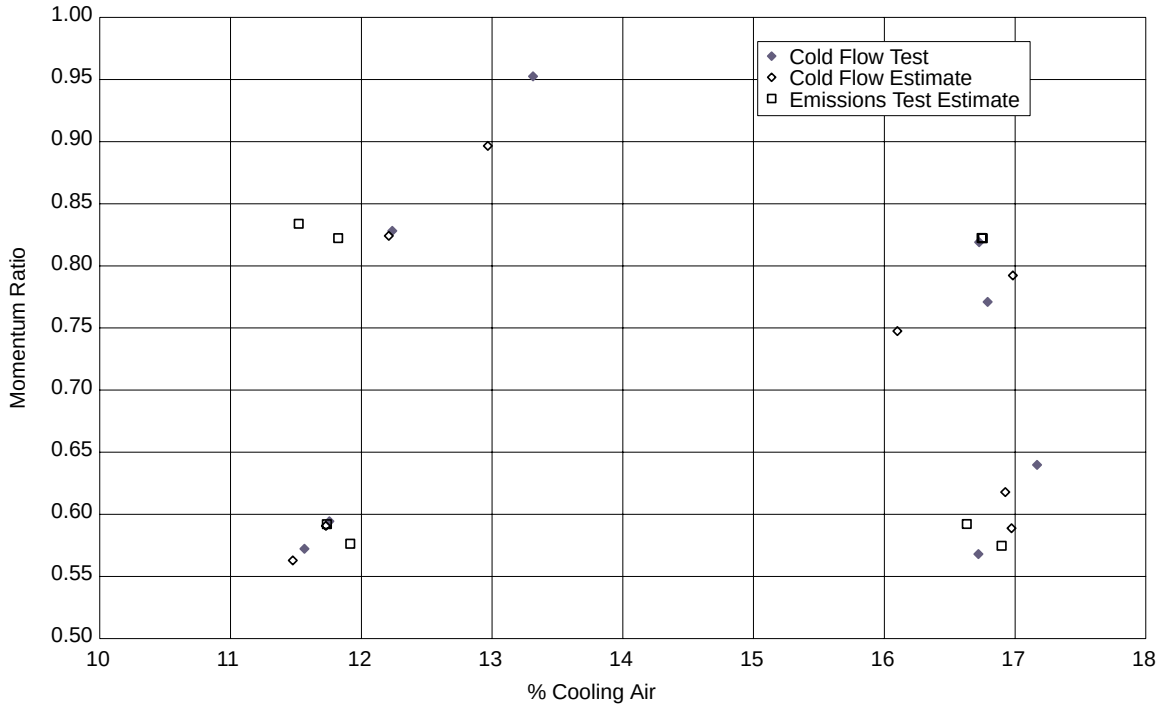

Figure 286. IMFH Tube Momentum Ratio vs Percent Cooling Air

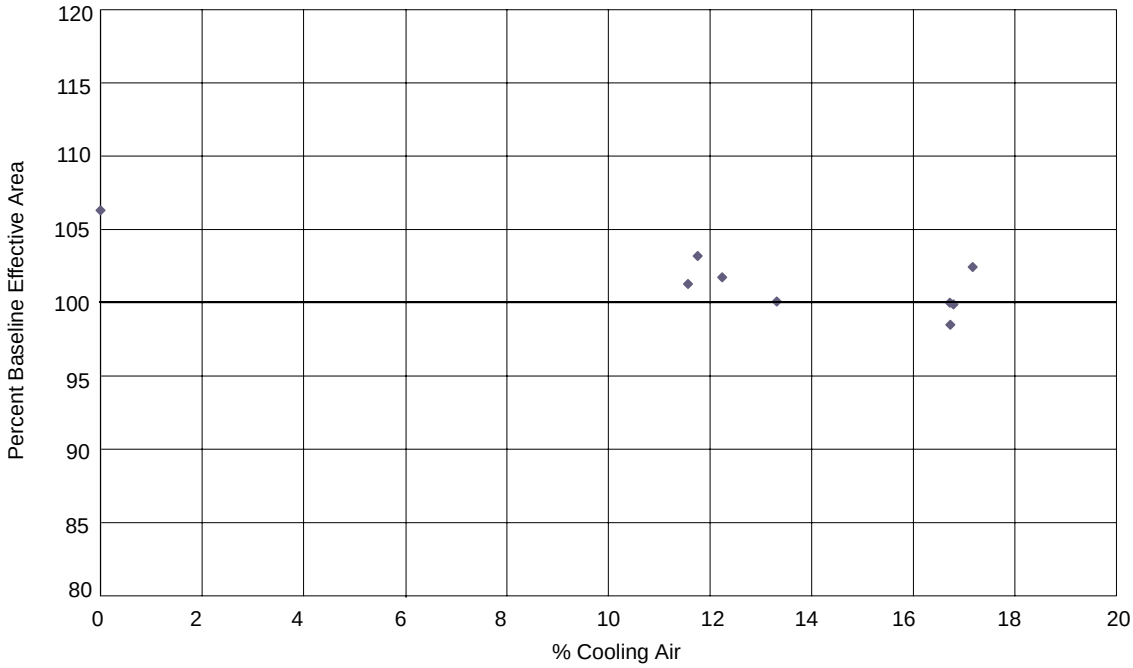

Figure 287. IMFH Tube Effective Area vs Percent Cooling Air

Emissions Tests – Emissions tests were conducted in test cell RL–23 at the NASA Glenn Research Center. Figures 288 through 291 compare the overall emissions data for Configuration 1 to the GEAE data. The magnitude and trends in the NOx, CO, UHC, and combustion efficiency are similar. In both tests the configuration met the supersonic cruise emissions goal of less than 5 EINOx and the efficiency goal of greater than 99.9%.

Figures 292 through 296 compare the local emissions data as a function of radial position for Configuration 1 from the two data sets. The probe used at NASA only traversed over half the diameter of the cylindrical chamber downstream of the IMFH assembly, but the GEAE probe was able to traverse the entire diameter. The profiles shown from both tests are between IMFH tubes. There are clear discrepancies between the profiles measured at the two facilities. Both sets of results show peaks in the data; however, the peaks are not always at the same locations and operating points.

4.8.1.4 Discussion

Overall, NASA tests of the full-scale, one-inch IMFH tube assembly reproduced the results from earlier tests by GEAE. However, profiles across the combustor were not reproduced. The discrepancies may be a result of changes in the alignment of the emissions probes with respect to the combustor, specifically the fuel injectors. Each of the injectors may produce a unique fuel spray and profile. Variations in the facilities and emissions systems may also contribute to differences.

Discrepancies between NASA and GEAE emissions tests should not discredit future results. The overall emissions are the critical values. However, discrepancies between fuel injectors should not be overlooked.

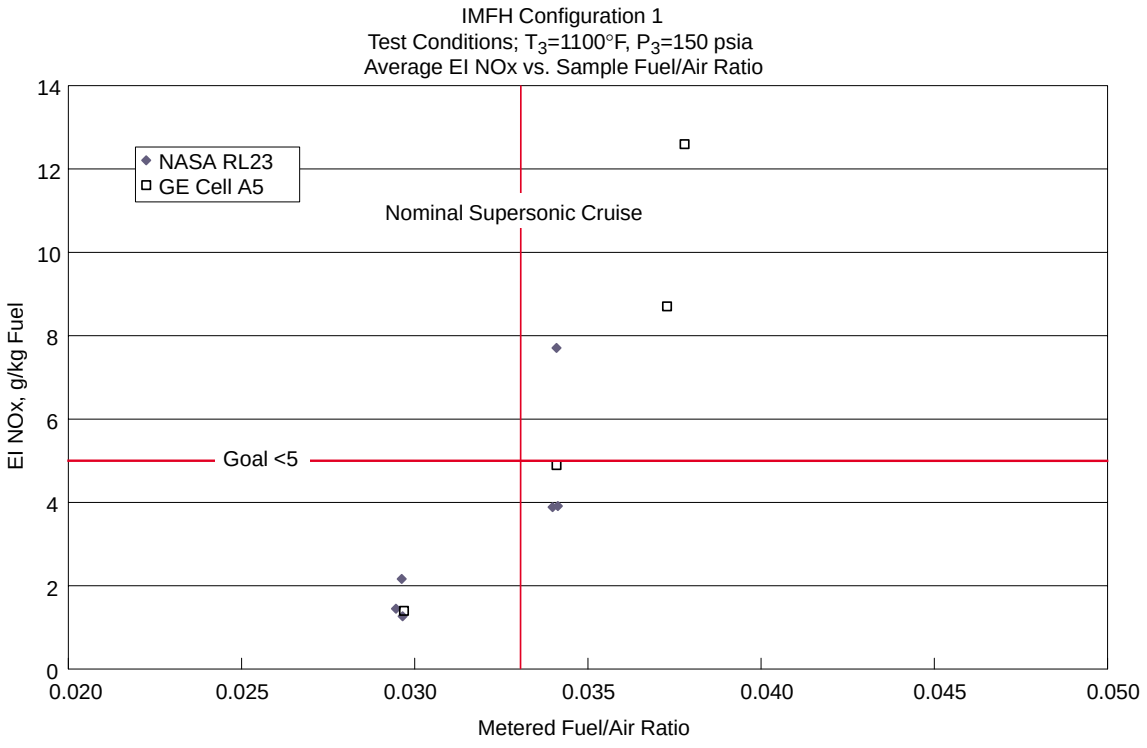

Figure 288. IMFH Tube NOx vs Fuel/Air Ratio

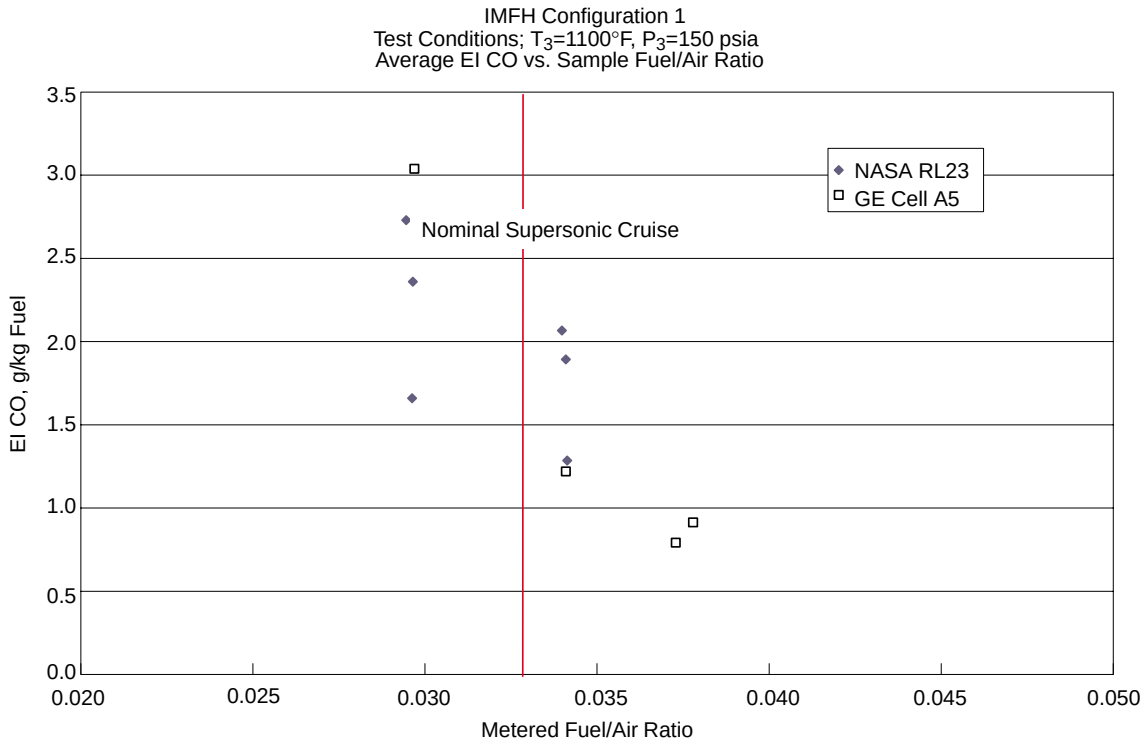

Figure 289. IMFH Tube CO vs Fuel/Air Ratio

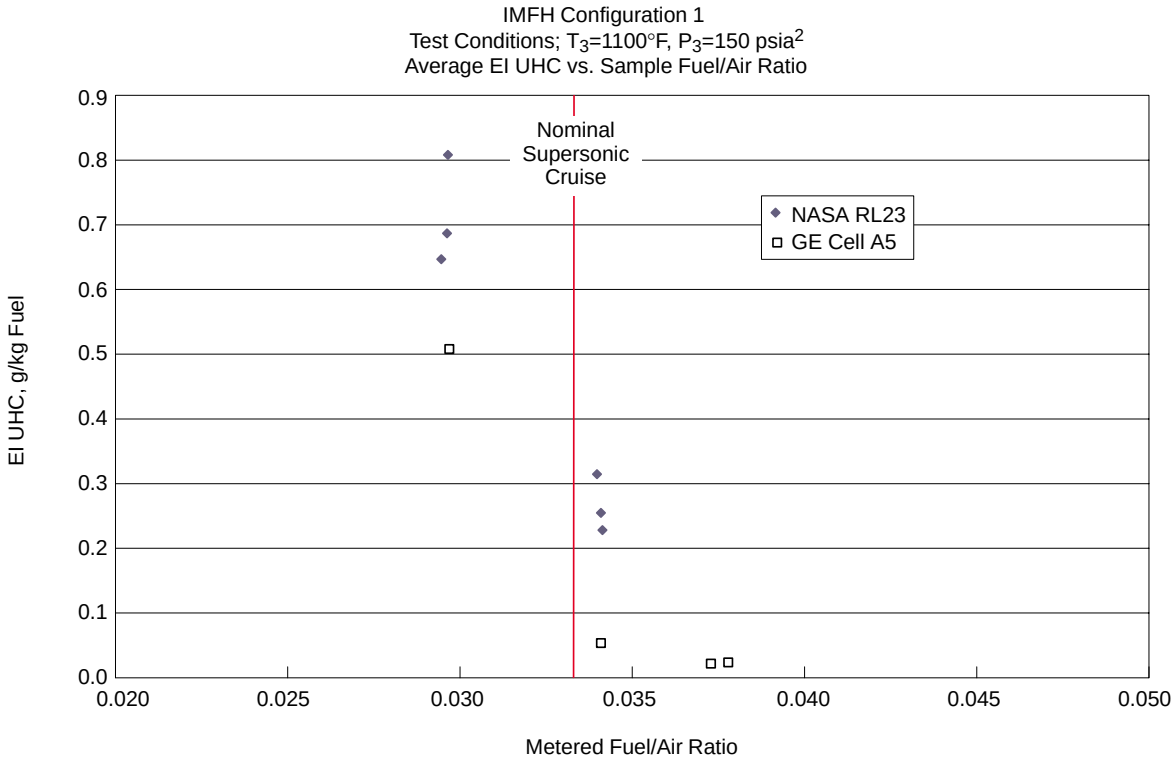

Figure 290. IMFH Tube UHC vs Fuel/Air Ratio

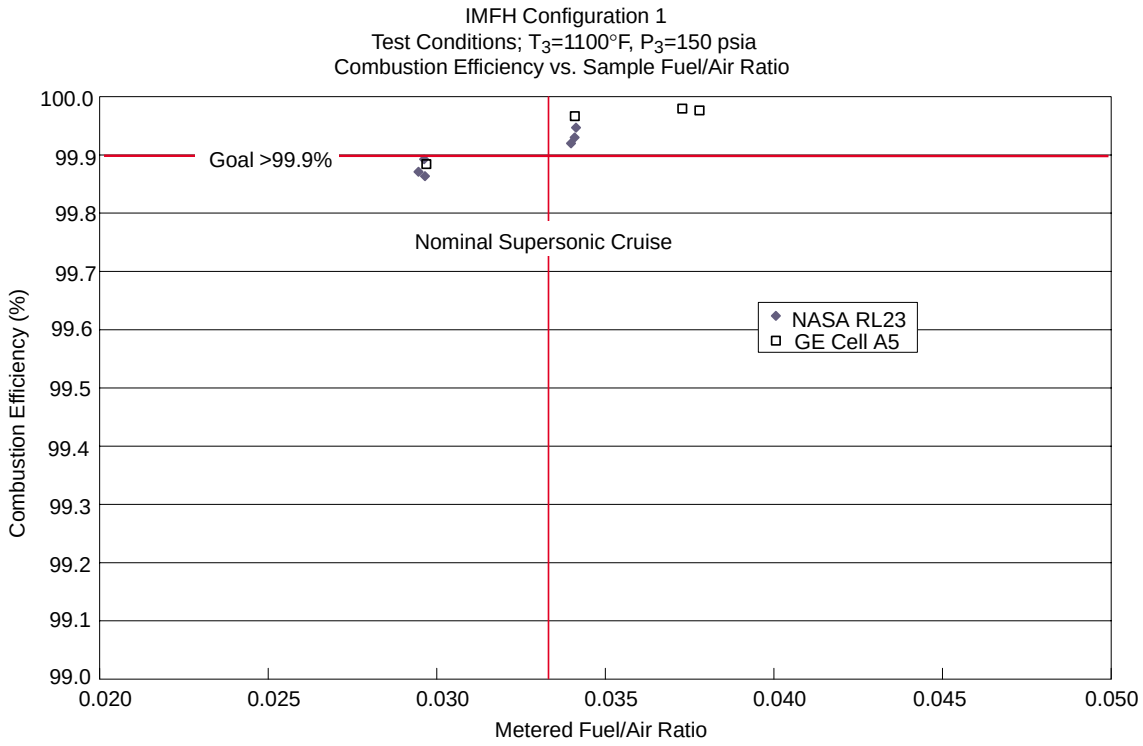

Figure 291. IMFH Tube Combustion Efficiency vs Fuel/Air Ratio

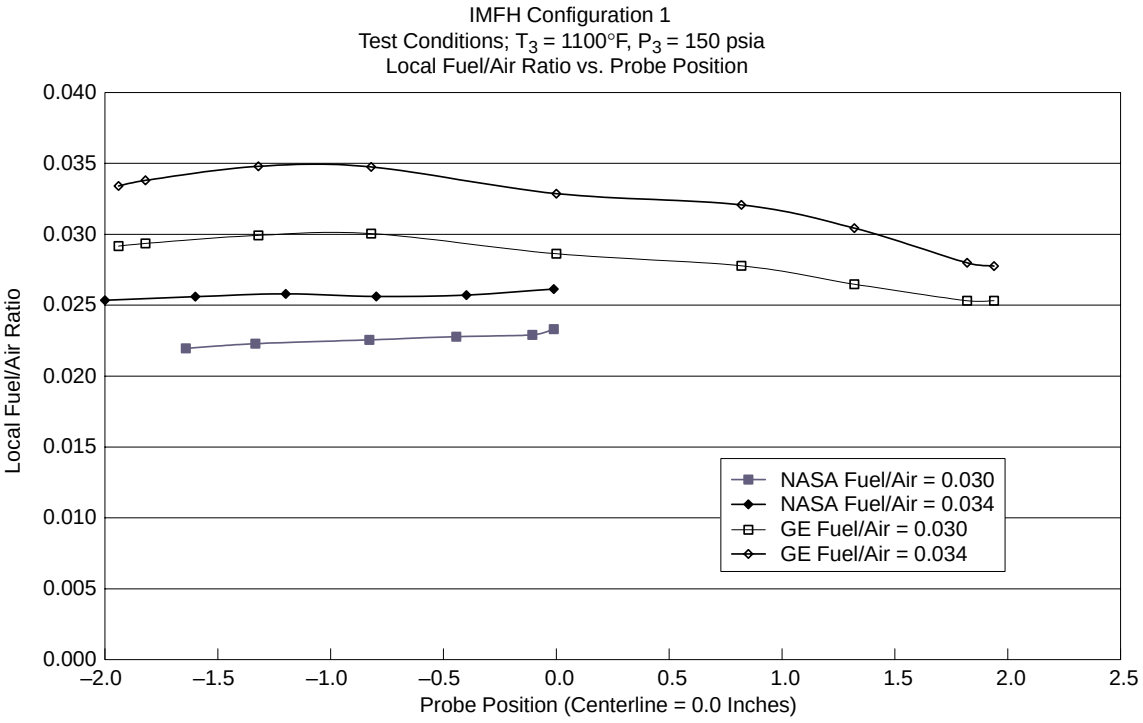

Figure 292. IMFH Tube Local Fuel/Air Ratio vs Radial Position

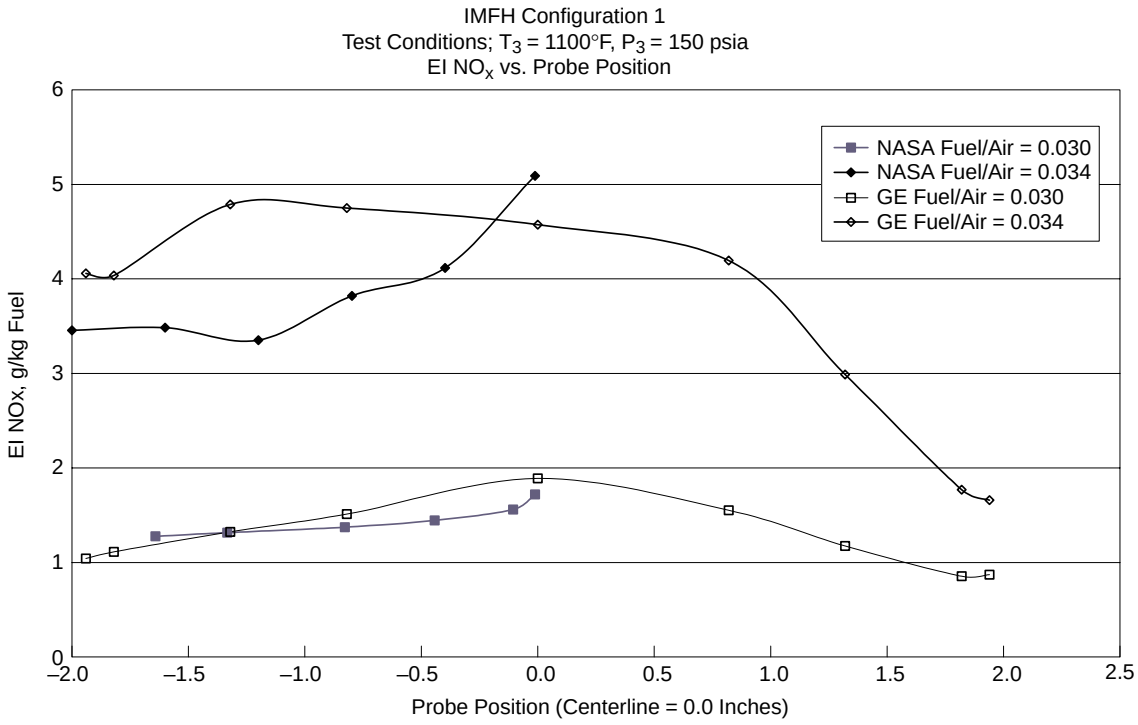

Figure 293. IMFH Tube NOx vs Radial Position

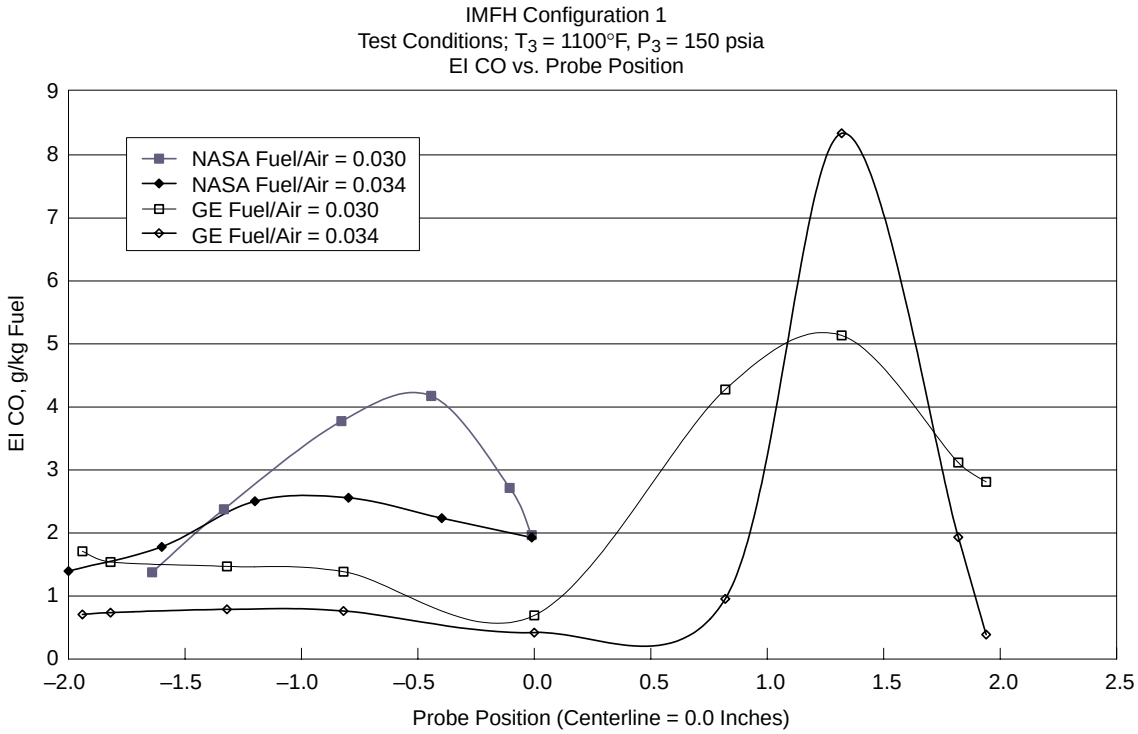

Figure 294. IMFH Tube CO vs Radial Position

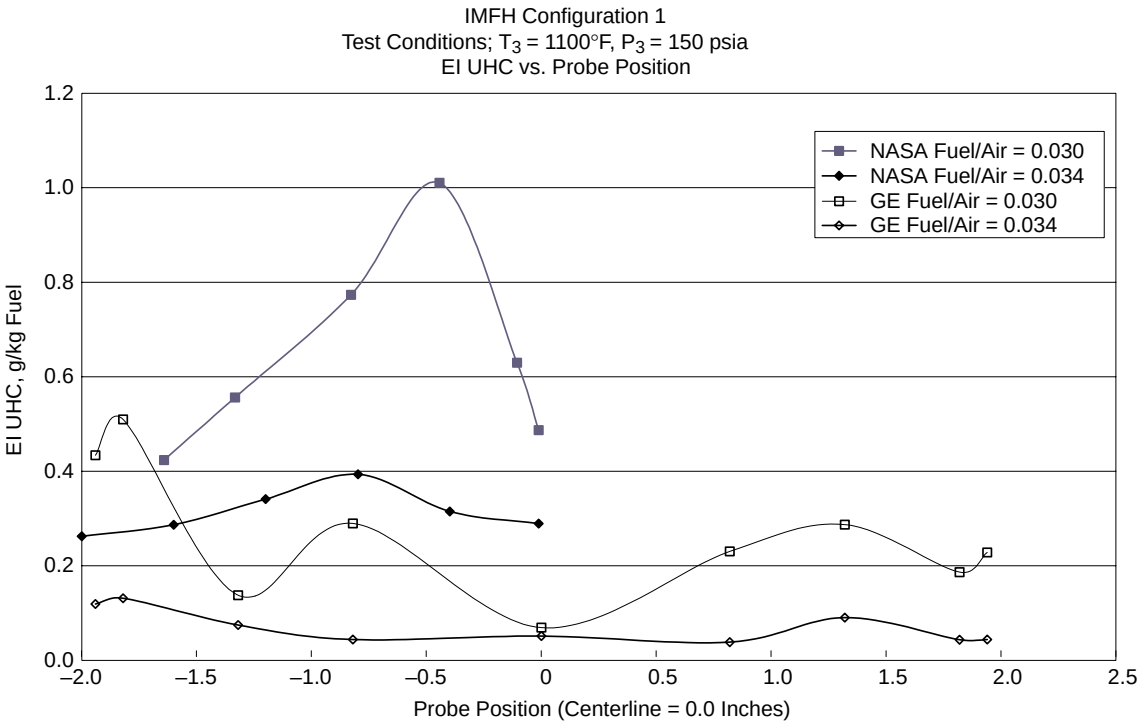

Figure 295. IMFH Tube UHC vs Radial Position

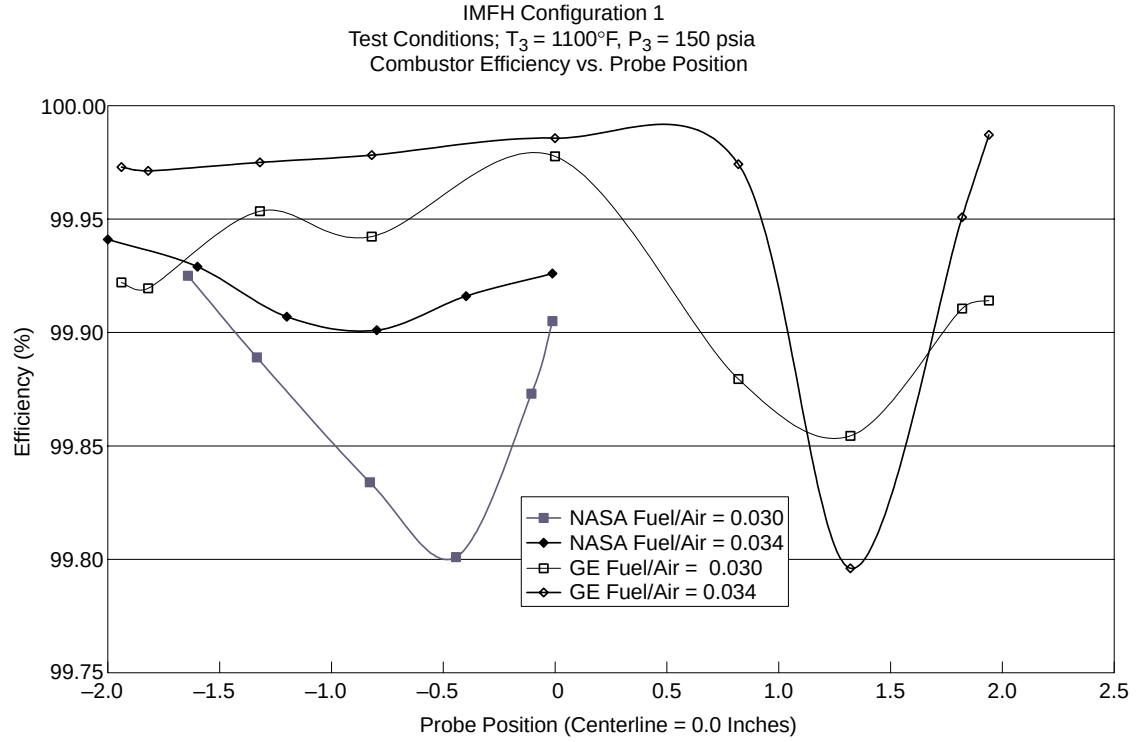

Figure 296. IMFH Tube Combustor Efficiency vs Radial Position

4.8.2 Main Fuel Injector Development

The purpose of this work was to continue to investigate and develop IMFH technology, specifically the mixing mechanisms in the full-scale, one-inch IMFH tube. The work focused on fuel injection and dome cooling-air injection. Other areas considered important in IMFH development included fuel injector aerodynamics, inlet aerodynamics, and tube spacing. Results presented here include comparisons of different cooling injection configurations using CFD as well as initial combustion diagnostics tests on the full-scale IMFH tube assembly. Combustion diagnostic tests were being conducted at the time of this writing and are not included.

4.8.2.1 CFD Modeling

Various cooling-flow injection configurations were investigated with CFD at NASA–Glenn. A quarter sector of each IMFH tube was modeled. Figures 297 and 298 show the mass fraction of injected cooling air at the injection point and tube exit, respectively, over a tube sector for four different configurations. The variations in circumferential and radial distribution of air with changes in the size and number of holes and percent cooling flow are shown in each figure. The penetration of the cooling jet is evident in Figure 298.

4.8.2.2 Combustion Diagnostics

Combustion diagnostics tests were conducted at NASA–Glenn. Tests included planar laser-induced fluoresence (PLIF) imaging and phase Doppler particle analyzer (PDPA) measurements. PLIF imaging shows a quantitative representation of the spatial distribution of the fuel exiting the IMFH mixing tubes downstream of the air injection holes. PDPA measurements provide droplet diameters and velocities at the tube exit. These tests were being conducted at the time of this writing.

4.8.2.3 Discussion

The effects of percent cooling air, momentum ratio, and number of holes can be seen in CFD. However, at the time of this writing, no data were available to indicate effects on emissions.

4.8.3 Cyclone Pilot Flametube Tests

Following the LPP/RQL downselect, six additional full-scale cyclones were tested. The six configurations are summarized in Table 40, along with Configurations 16 and 20.3 tested prior to downselect (for reference). A cyclone cross section with feature definitions was shown in Figure 58 (page 54) and coincides with the information in the table. Note that these designs have flow areas approximately the same as Configuration 20.3, but they are somewhat smaller overall. This change was made because of circumferential space limitations on the pilot dome. Note that this was not done without penalty, as the swirl number was reduced from 1.16 to 0.91. This was a bit of a concern because it generally follows that as the swirl number increases, cyclone stability improves.

Configurations 21.1, 21.2, and 21.3 were identical except the number of fuel injection ports changed. This was an attempt to determine the impact of the number of fuel injection ports on emissions and stability. Configurations 21.12, 21.22, and 21.32 were identical to each of the first three configurations tested, except that a 0.040-in annular air gap was added around the centerbody.

Labels indicate injector hole diameter in mils and percent cooling air.

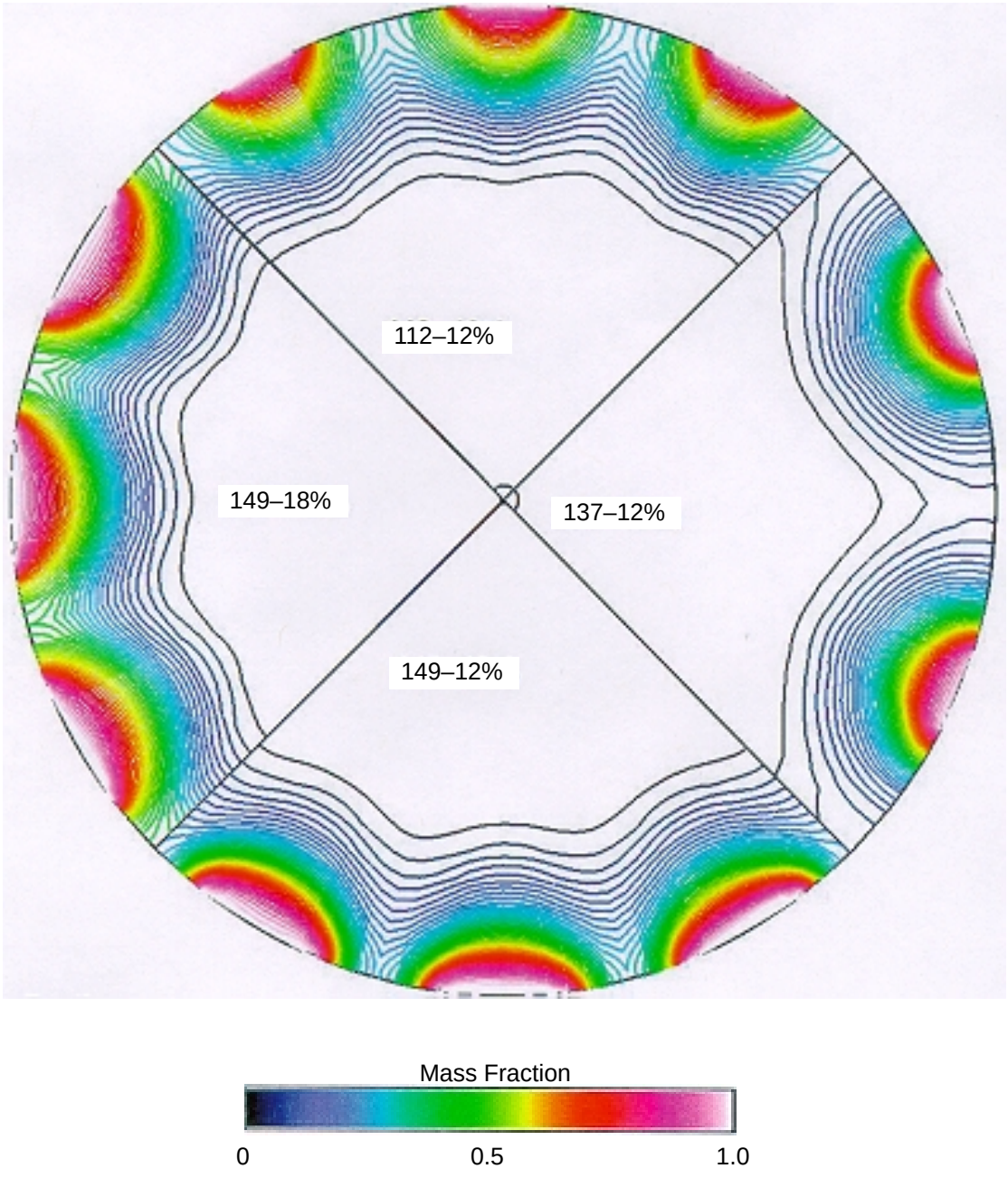

Figure 297. Mass Fraction of Cooling Air at Injector Inlet

Labels indicate injector hole diameter in mils and percent cooling air.

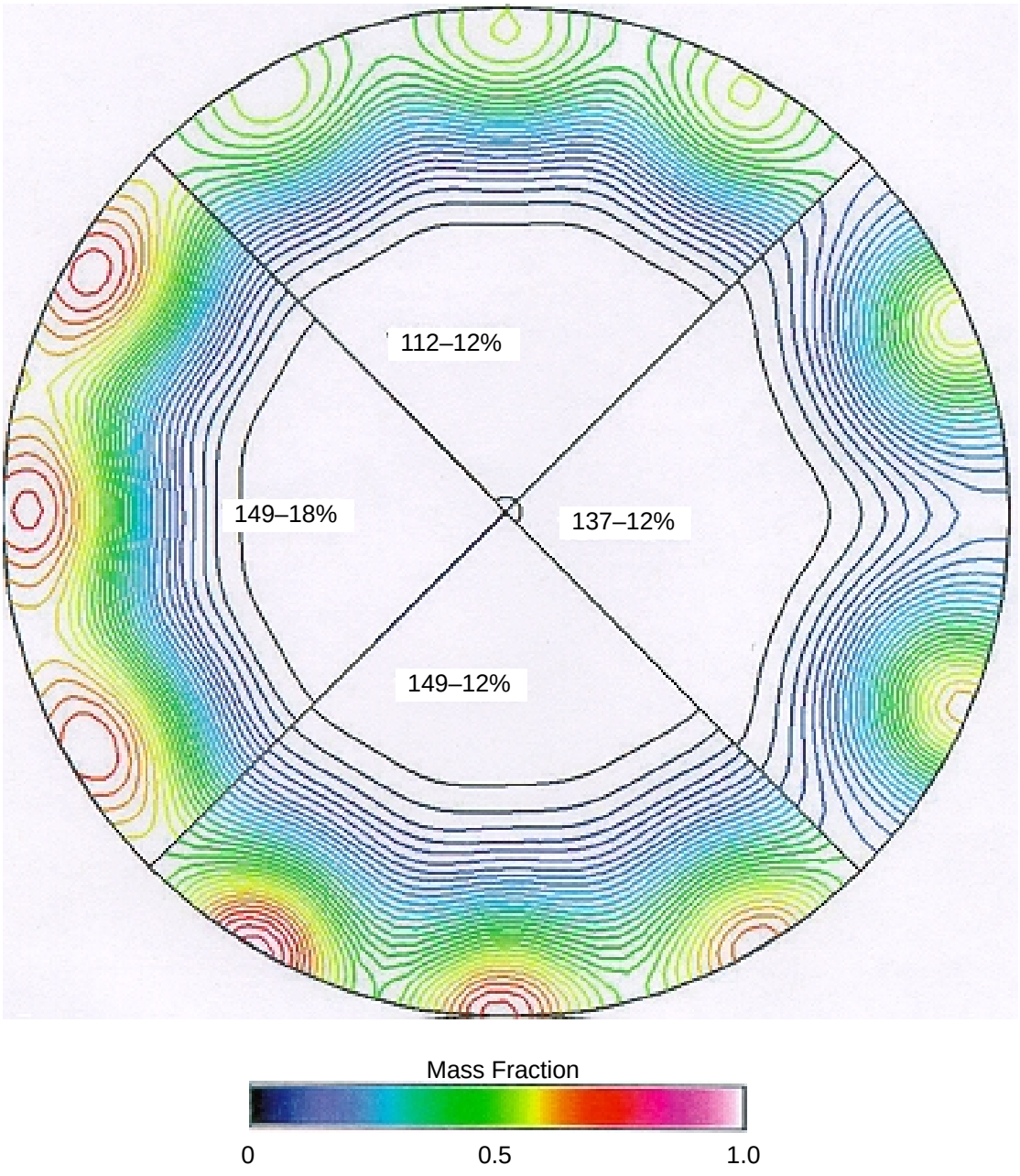

Figure 298. Mass Fraction of Cooling Air at IMFH Tube Exit

Table 40. Cyclone Design Summary Table

Parameter		Subscale Config 16	Full Scale Config 20.3	Full Scale Config 21.1	Full Scale Config 21.2	Full Scale Config 21.3	Full Scale Conf 21.12	Full Scale Conf 21.22	Full Scale Conf 21.32
General	Overall Effective Flow Area, in^2	0.6	1.70	1.73	1.75	1.75	1.94	1.95	1.96
	Swirl Number	0.85	1.16	0.91	0.91	0.91	0.91	0.91	0.91
	Air Gap Around Centerbody, in	0.15	None	None	None	None	0.040	0.040	0.040
Swirler	Inner Diameter, in	1.736	3.800	3.250	3.250	3.250	3.250	3.250	3.250
	Outer Diameter, in	1.975	4.050	3.500	3.500	3.500	3.500	3.500	3.500
	Number of Slots	48	80	72	72	72	72	72	72
	Slot Angle, °	45	50	43	43	43	43	43	43
	Slot Height, in	0.504	0.450	0.525	0.525	0.525	0.525	0.525	0.525
	Slot Width, in	0.025	0.050	0.050	0.050	0.050	0.050	0.050	0.050
Centerbody	Outer Diameter, in	1.181	2.750	2.125	2.125	2.125	2.125	2.125	2.125
	Fuel Injection Air-Assist Hole Dia, in	0.110	0.130	0.140	0.165	0.120	0.140	0.165	0.120
	Number of Holes	6	15	12	8	16	12	8	16
Throat	Diameter, in	1.592	3.400	2.850	2.850	2.850	2.850	2.850	2.850
	Side Cooling Hole Diameter, in	0.145	0.135	0.126	0.126	0.0126	0.126	0.126	0.126
	Number of Holes	20	30	48	48	48	48	48	48
Fuel Injector	Number of Injection Ports	6	15	12	8	16	12	8	16
	Tube OD, in	0.065	0.0625	0.0625	0.0625	0.0625	0.0625	0.0625	0.0625
	Tube ID, in	0.020	0.020	0.020	0.020	0.020	0.020	0.020	0.020

This increased the effective flow area by about 10%, to nearly 1.95 in^2. Note that this is more than three times the flow area of the Configuration 16 designed used in the MMMRA sector. The air gap was added to simulate a feature that was anticipated for the full-scale sector (described later). It was necessary to verify that emissions and stability were not impacted and that no autoignition or flashback resulted from the gap.

Five of the configurations (all except 21.2) were tested by Dr. Cliff Moses at the Southwest Research Institute. Configurations 21.1 and 21.3 were tested in May and June 1998. The latter three were tested from February to May 1999. As with the precursor (prior to downselect) cyclone tests, five gas-sampling probes were located seven inches downstream of the dome face, positioned to sample approximately equal-area regions of the exit plane. A schematic of the test rig was shown in Figure 59 (page 55). Configurations 21.1, 21.2, and 21.3 were also tested at NASA–Glenn in July and August 1998. Here, six gas-sampling probes were located seven inches downstream of the dome face, also positioned to sample approximately equiarea regions of the exit plane. A schematic of the NASA test section is shown in Figure 299; it is very similar to the rig used at SwRI.

Comparison plots are shown in Figures 300 through 308, and the test results are summarized in Tables 41 through 44. Several significant observations can be made. First, all of the Configuration 21 variations showed significant improvement (by nearly a factor of 2 at low power) in lean blowout characteristics over the subscale design (Configuration 16). This is very important, because the lean blowout point directly impacts the location of fuel-staging points. This provides the flexibility to either operate with greater stability margin with the same number of fuel stages or to simply operate at lower fuel/air ratios, reducing the number of stages required. It was interesting that the variations with the centerbody air gap showed additional improvement over the no-gap designs (by 0.05 to 0.1, based on equivalence ratio) and were much flatter in the low-power region in which they were tested. The tremendous improvement in stability over the subscale designs was very positive in making the full scale system viable.

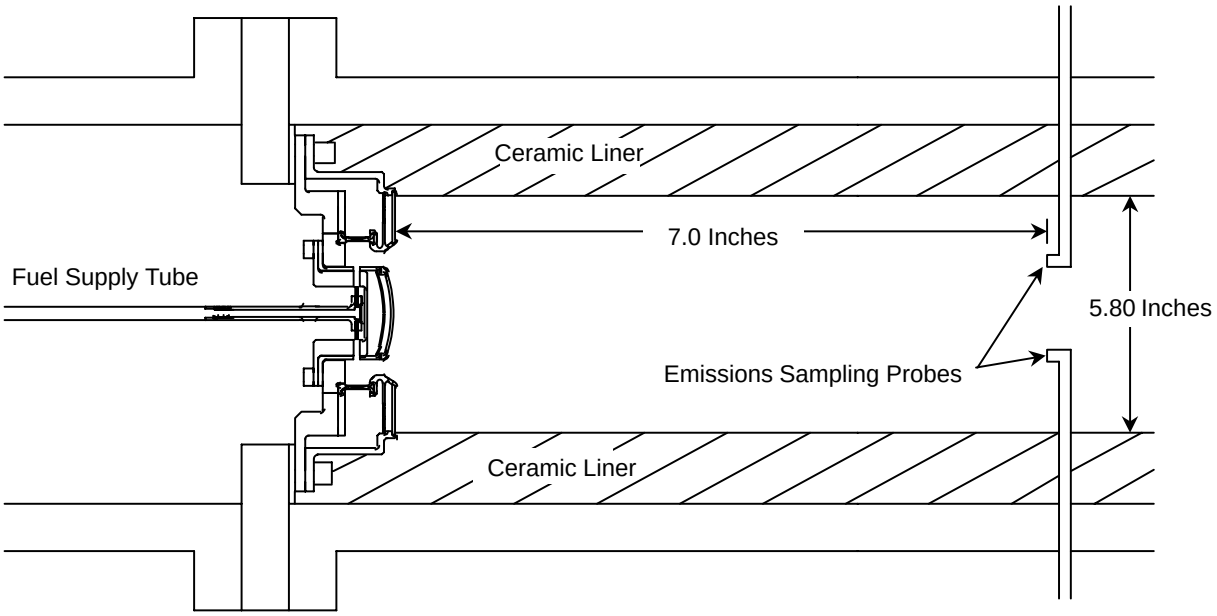

Figure 299. NASA Test Rig Schematic

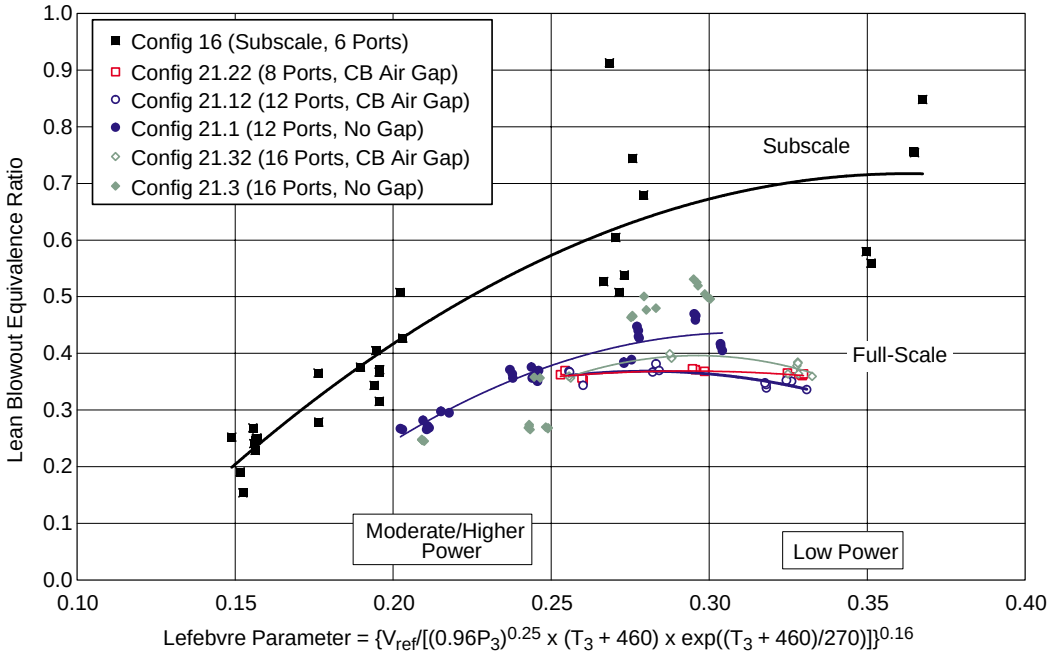

Figure 300. Subscale and Full-Scale Cyclone Lean Blowout Data

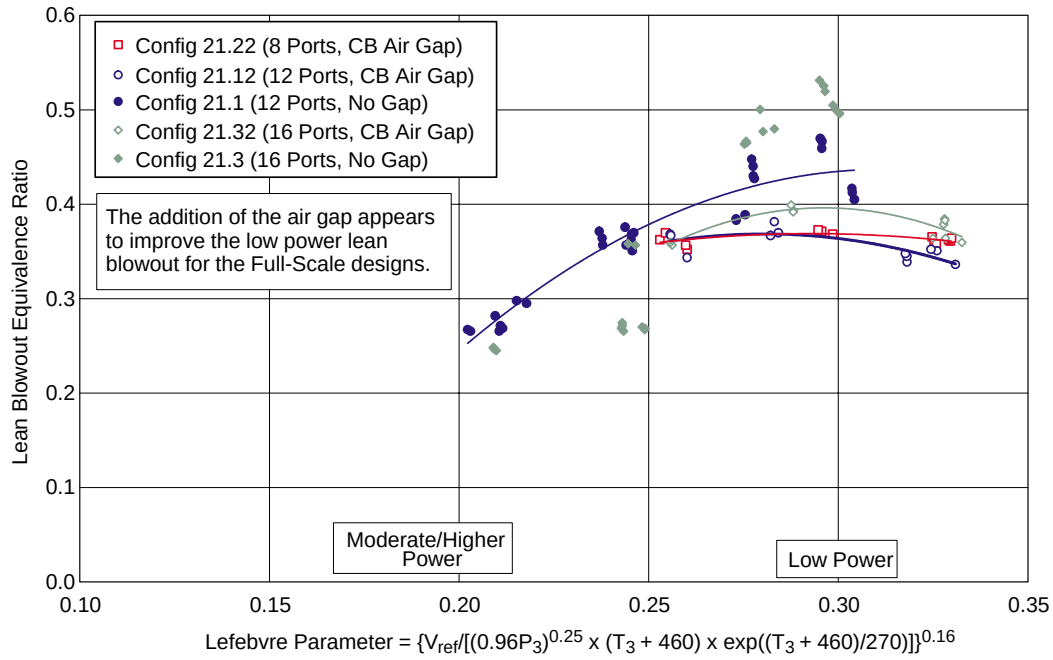

Figure 301. Full-Scale Cyclone Lean Blowout Data, With and Without Air Gap

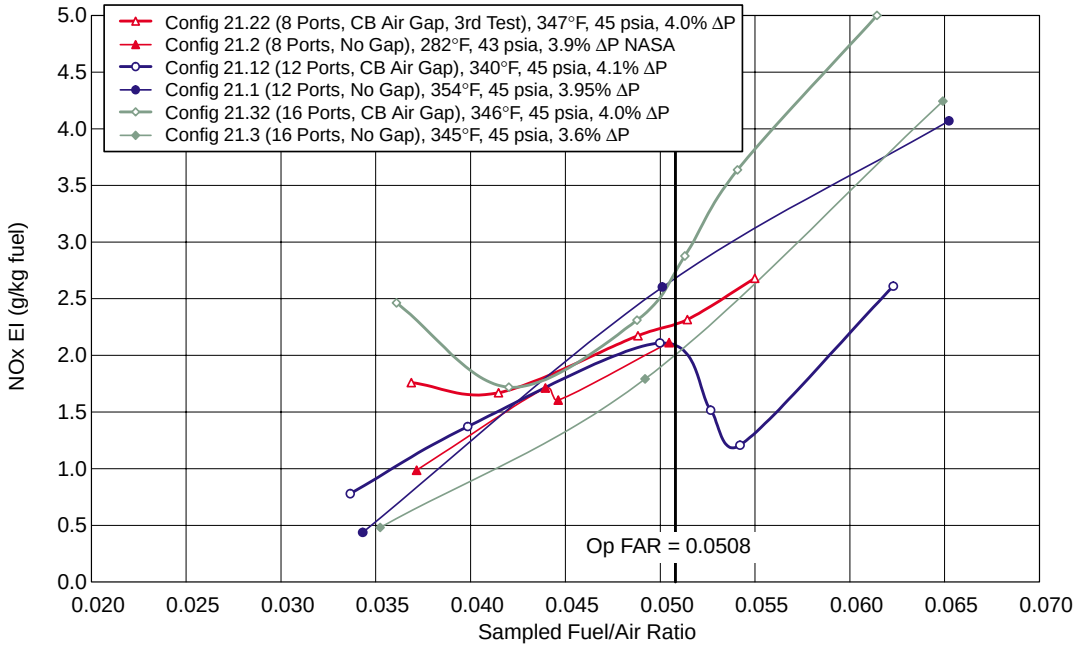

Figure 302. Full-Scale Cyclone Ground Idle NOx

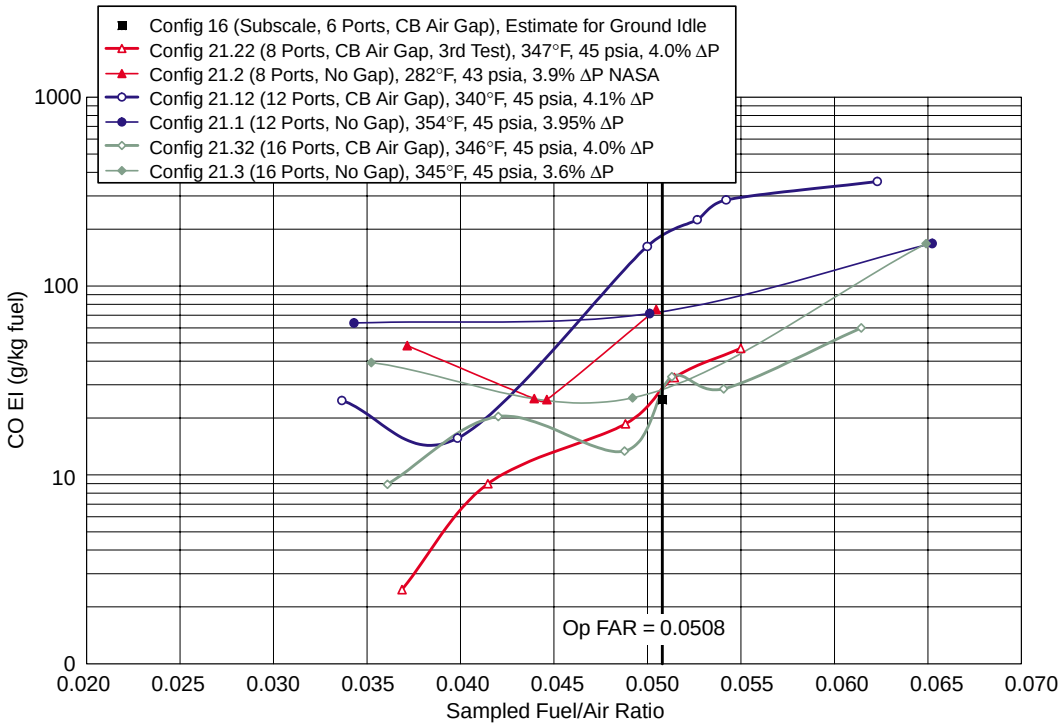

Figure 303. Full-Scale Cyclone Ground Idle CO

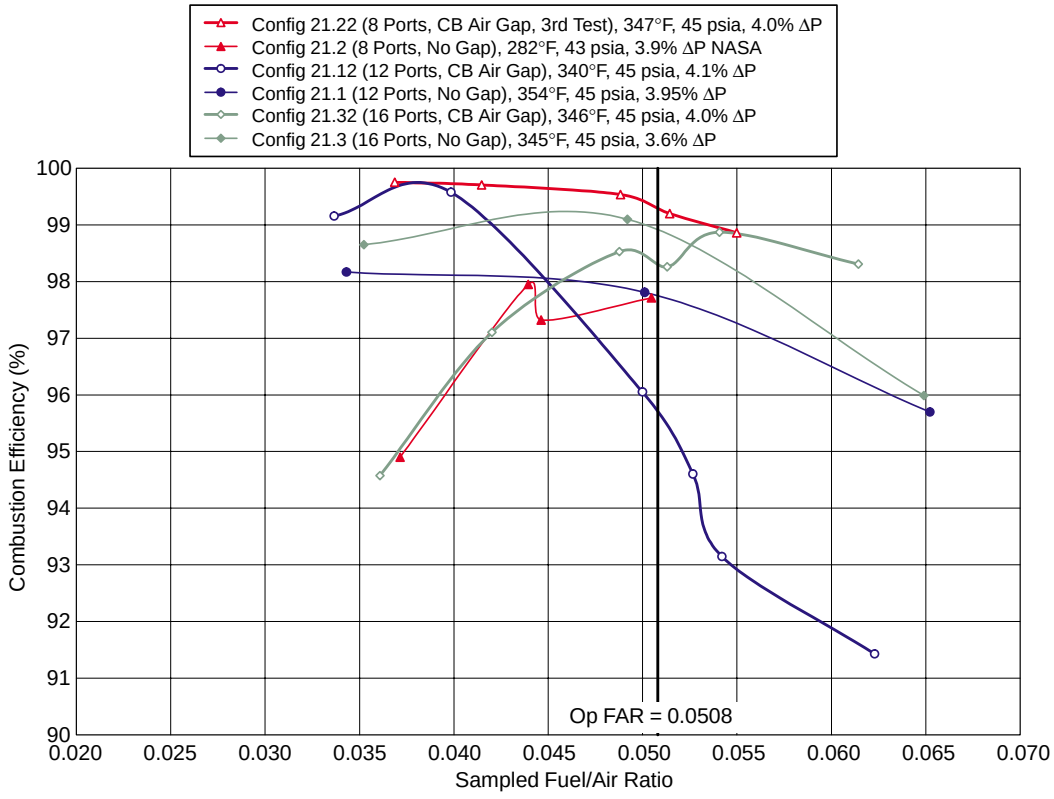

Figure 304. Full-Scale Cyclone Ground Idle Combustion Efficiency

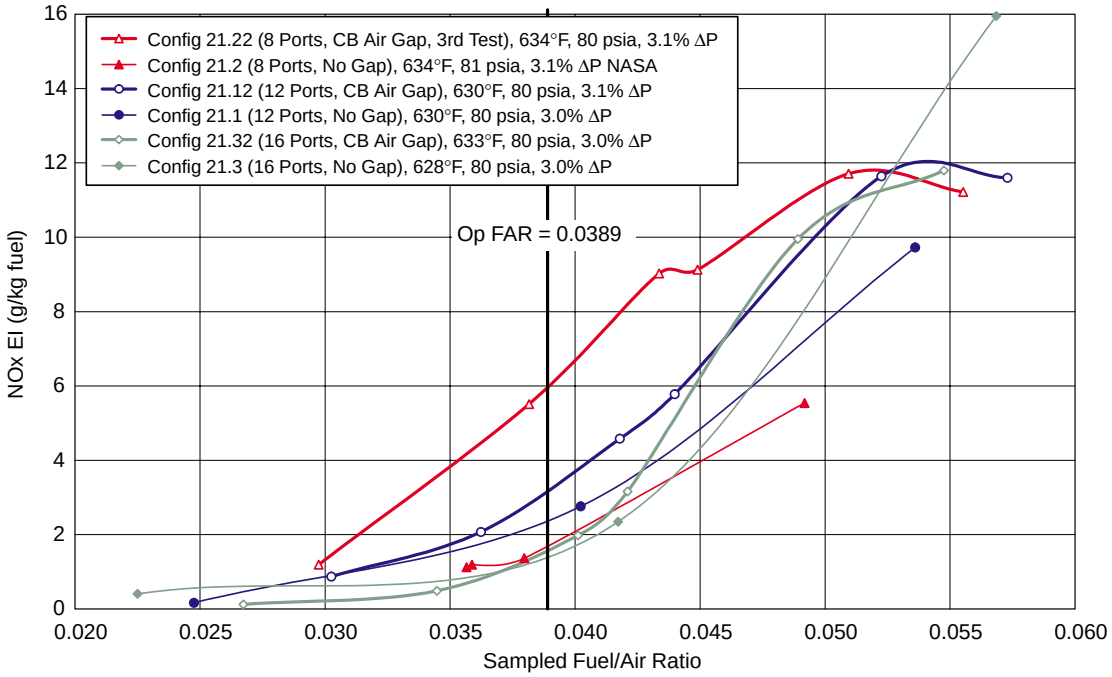

Figure 305. Full-Scale Cyclone Subsonic Cruise NOx

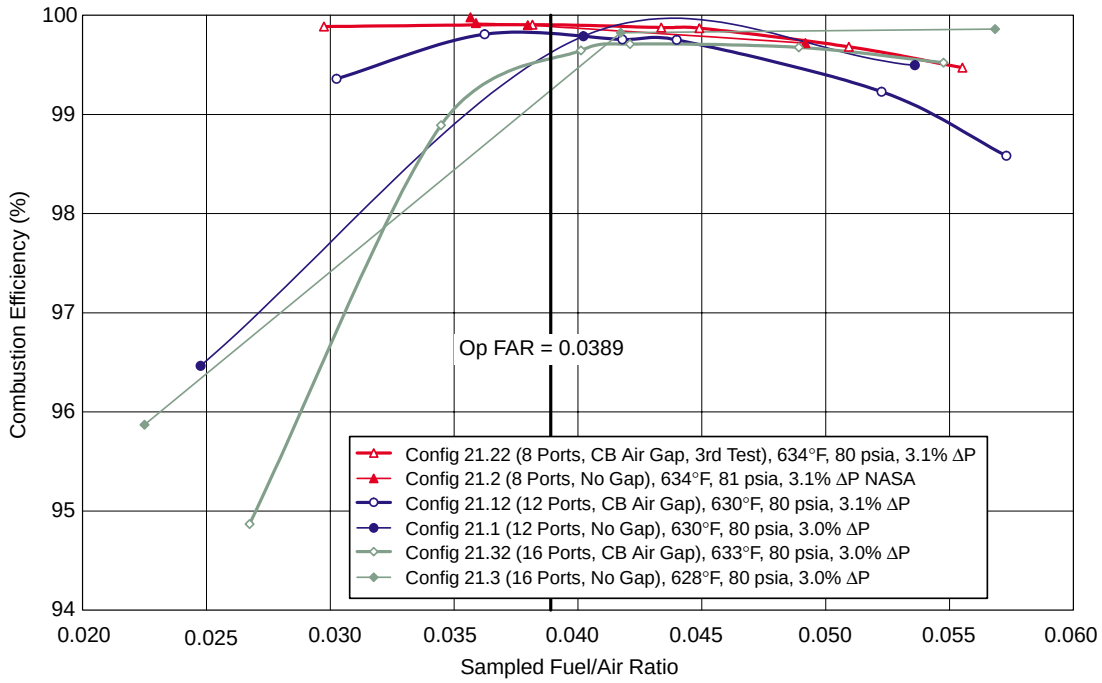

Figure 306. Full-Scale Cyclone Subsonic Cruise Combustion Efficiency

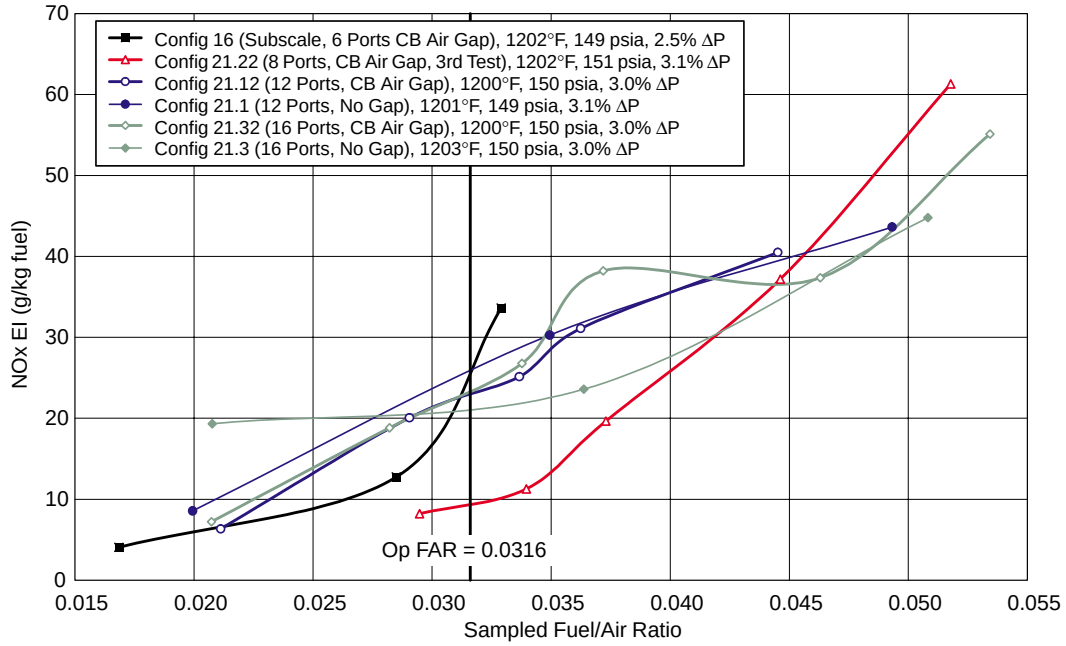

Figure 307. Full-Scale Cyclone Supersonic Cruise NOx

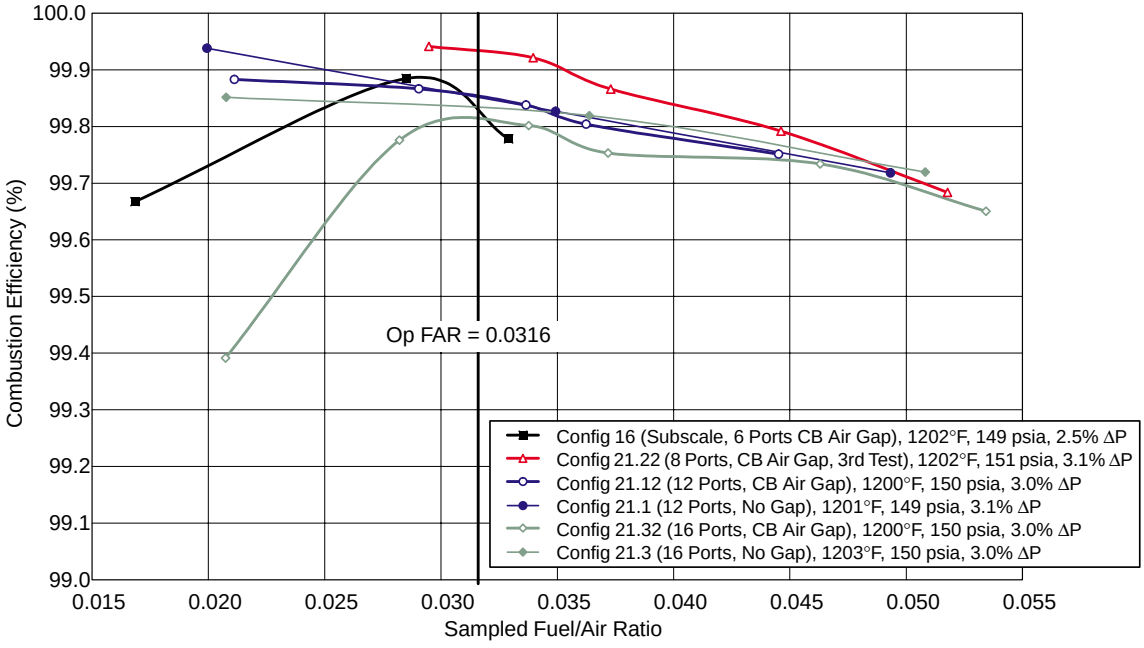

Figure 308. Full-Scale Cyclone Supersonic Cruise Combustion Efficiency

Table 41. Full-Scale Cyclone Ground Idle Emissions Estimates

Parameter		Configuration						
		16*	**21.1**	**21.2**	**21.3**	**21.12**	**21.22****	**21.32**
Test Location		SwRI	SwRI	NASA	SwRI	SwRI	SwRI	SwRI
Emissions Index	NOx	–	2.7	2.1	2.0	2.1	2.8, 2.3	2.8
	CO	est. 25	74	80	28	180	35, 29	29
	HC	–	4.9	5	2.5	1.1	0.37, 0.13	10
Combustion Efficiency, %		–	97.8	97.7	99.01	95.7	99.3, 99.3	98.4
No. of Fuel-Injection Ports		6	12	8	16	12	8	16
T_3, °F		–	354	282	345	340	333, 347	346
P_3, psia		–	45	43	45	45	45, 45	45
ΔP, %		–	3.95	3.9	3.6	4.1	4.0, 4.0	4.0

* Configuration 16 was the subscale design (reference point).

** Configuration 21.22 was tested twice at these conditions.

Table 42. Full-Scale Cyclone 15% LTO Emissions Estimates

Parameter		Configuration						
		16*	**21.1**	**21.2**	**21.3**	**21.12**	**21.22****	**21.32**
Test Location		SwRI	SwRI	NASA	SwRI	SwRI	SwRI	SwRI
Emissions Index	NOx	–	5.6	–	3.0	5.4	6.2, 5.9	5.2
	CO	–	18	–	14	4	13, 7	11
	HC	–	0.57	–	1.6	0.16	0.4, 0.18	3.2
Combustion Efficiency, %		–	99.34	–	99.46	99.9	99.5, 99.7	99.4
No. of Fuel-Injection Ports		6	12	8	16	12	446, 450	16
T_3, °F		–	446	–	446	450	8	446
P_3, psia		–	82	–	83	81	82, 83	82
ΔP, %		–	3.85	–	3.75	4.1	3.9, 3.9	3.8

* Configuration 16 was the subscale design (reference point).

** Configuration 21.22 was tested twice at these conditions.

Table 43. Full-Scale Cyclone Subsonic Cruise Emissions Estimates

Parameter		Configuration						
		16*	21.1	21.2	21.3	21.12	21.22	21.32
Test Location		SwRI	SwRI	NASA	SwRI	SwRI	SwRI	SwRI
Emissions Index	NOx	–	2.3	1.6	1.8	3.1	5.9	1.4
	CO	–	1.7	2.3	6.1	2.6	1.1	2
	HC	–	1.9	0.53	0.91	1.2	0.45	4
Combustion Efficiency, %		–	99.75	99.9	99.76	99.8	99.9	99.6
No. of Fuel-Injection Ports		6	12	8	16	12	8	16
T_3, °F		–	631	634	628	630	634	633
P_3, psia		–	80	81	80	80	80	80
ΔP, %		–	3.0	3.1	3.0	3.1	3.1	3.0
* Configuration 16 was the subscale design (reference point).								

Table 44. Full-Scale Cyclone Supersonic Cruise Emissions Estimates

Parameter		Configuration						
		16*	21.1	21.2	21.3	21.12	21.22	21.32
Test Location		SwRI	SwRI	NASA	SwRI	SwRI	SwRI	SwRI
Emissions Index	NOx	24	24	–	22	23	9	23
	CO	0.74	1.4	–	1.5	0.78	0.28	0.72
	HC	0.37	0.027	–	0.34	0.27	0.17	0.74
Combustion Efficiency, %		99.83	99.845	–	99.925	99.85	99.95	99.8
No. of Fuel-Injection Ports		6	12	8	16	12	8	16
T_3, °F		1202	1200	–	1203	1200	1202	1200
P_3, psia		149	150	–	150	150	151	150
ΔP, %		2.45	3.1	–	3.0	3.0	3.1	3.0
* Configuration 16 was the subscale design (reference point).								

Second, all of the full-scale designs demonstrated supersonic cruise NOx EI at least as good as the subscale design, generally in the 20 to 24 range. In fact, Configuration 21.22 (eight fuel ports) actually demonstrated significant improvement, dropping to only about 9 EI — less than half of previous values. It was felt that in order for the full-scale sector to meet the 5 EI NOx requirement as the MMMRA sector had, the pilot had to produce supersonic cruise NOx at least as good as the subscale design. Configuration 21.22 was chosen as the baseline for the full-scale sector. Because of the significant improvement observed, it is expected that the full-scale system will meet NOx requirements and may even be lower than observed in the MMMRA sector.

Third, ground idle CO was slightly higher than desired. It was estimated that Configuration 16 produced approximately 25 EI CO at GI (although it was never tested at actual GI conditions). Several of the full-scale designs produced EI's in the 28 to 35 range, but others were well above 75. The Configuration 21.22 design chosen for the full-scale sector demonstrated 29 and 35 EI in two separate tests. It is expected that GI CO in the sector will be similar to, or slightly higher than, it was in the MMMRA. As stated above, the final emissions results will be impacted by the interactions between the pilots and IMFH premixers in the sector.

Fourth, subsonic cruise NOx was quite low in all of the designs. Most were in the 1.5 to 3 EI range, although Configuration 21.22 was nearly 6 EI. This was of no real concern, since the targeted value for the cyclone was 10 EI. Regrettably, Configuration 16 was never tested at these conditions, making it impossible to compare it directly to the full-scale designs. It is expected that subsonic cruise NOx in the full-scale sector will remain quite low.

Finally, the addition of the air gap around the centerbody did not show any signs of autoignition or flashback. In fact, the gap allayed some fears about the potential for autoignition in the recirculation region formed by the no-gap design (even though none had ever been observed in the no-gap design in several hundred hours of testing).

This information was used to select a design for use in the full-scale sector. The sector configuration chosen was not quite identical to any shown here but was essentially the same as Configuration 21.22 (eight fuel ports) with a slightly longer throat (it will be described in more detail later in this report). The increased throat length resulted from mechanical design needs in assembling the pilot dome and swirler. It is not anticipated that this will materially impact pilot performance.

4.9 Full-Scale MRA Sector Detailed Design

Following the LPP/RQL downselect, detailed design of the full-scale MRA sector was initiated. Enhancements were made to the preliminary design presented at the downselect to mitigate the risks and concerns raised by the reviewers. Additional information from the subsequent subcomponent development described in the previous section was also used to develop the final sector design.

4.9.1 Combustor Enhancements/Risk Mitigation

The LPP risk assessment chart from the LPP/RQL downselect is presented in Table 45. It contains the 10 items considered highest risk to the program. Clearly, combustor dynamics were of primary concern, with all other items considered low or moderate risk. Table 46 summarizes the mitigation plans for each of the top 10 risks identified in Table 45. Testing and analytical methods both were to be used to address the program risks and ensure successful development of the full-scale combustor. The full-scale MRA sector was to be one of the primary vehicles for obtaining test data.

4.9.1.1 Combustor Dynamics and Stability

Combustor dynamics was the item of highest concern from the risk assessment. Analytical models anchored in rig testing were to be used address this risk with the full-scale MRA sector as the primary source of test data.

The five-year modeling activity was structured as a joint effort. GEAE was responsible for the basic acoustic models; NASA was responsible for the heat-release models, and P&W was responsible for

Table 45. LPP MRA Risk Assessment

Impact to the Program if Risk Occurs

Probability that Risk Will Occur	0.1 Low	0.3	0.5 Medium	0.7	High 0.9
High 0.9				1. Combustor Dynamics	
0.7	Low	Moderate	2. Fuel-System Coking	High	Very High
0.5 Medium			4. SC Combus. Efficiency 9. Sensitivity to Leakage		
0.3		7. Profile and Pattern Factor 10. Structural Vibration	3. Blowout Margin 6. Inlet Airflow Nonuniformity	5. Autoignition, Flashback	
0.1 Low					8. Combustor Burn Through

Table 46. LPP MRA Risk-Mitigation Plans

Risk	Plan
1. Combustor Dynamics	Anchor analytical models to existing data and predict engine combustor characteristics.
2. Fuel-System Coking	Conduct 3D heat transfer analysis; perform fundamental and component coking tests.
3. Combustor Blowout Margin	Generate and analyze steady-state and fuel-transient data in full-scale sector test.
4. Subsonic Cruise Combustion Efficiency	Additional cyclone and IMFH development and CFD analyses planned; verification in full-scale sector test.
5. Autoignition and Flashback	Advanced autoignition and flow-visualization testing planned; CFD analyses planned.
6. Inlet Airflow Nonuniformity	CFD analysis planned, anchored to subscale and cold-flow diffuser test.
7. Profile and Pattern Factor	CFD analysis anchored to subscale sector test planned; verification in full-scale sector test.
8. Combustor Burn Through	Investigate certification issues.
9. Combustor Sensitivity to Leakage	Full-scale combustor leakage to be included in full-scale sector test.
10. Combustor Structural Vibration	Perform 3D vibration analysis.

modeling the acoustic boundary conditions. Because the HSR program was limited to FY1999 effort, only the IMFH tube impedance modeling activity could be completed. The objective of the P&W FY1999 modeling effort was to provide an impedance model for the IMFH tube section of the MRA sector rig to be employed by GEAE in their acoustic model. The existing GEAE acoustic model considered the combustor only with the upstream boundary condition assumed to be acoustically closed. The frequency prediction was slightly higher than the test data for the MRA sector rig. Incorporating a more complex boundary condition for the IMFH tubes and the upstream domain may improve the frequency predictions for the MRA sector.

The impedance model for the IMFH tube section was based on one-dimensional linear acoustic theory. First, a system transfer function was determined. With a specified boundary condition on one side, the impedance on the other side can be determined thereafter. For the MRA test rig, a large plenum existed upstream of the profiler. The rest of the domain is split into nine sections as illustrated in Figure 309. The discontinuities for the adjacent two sections are also modeled as interfacial boundary conditions. Eight additional elements are considered to accommodate the discontinuities. A total of 18 elements define the system transmission matrix.

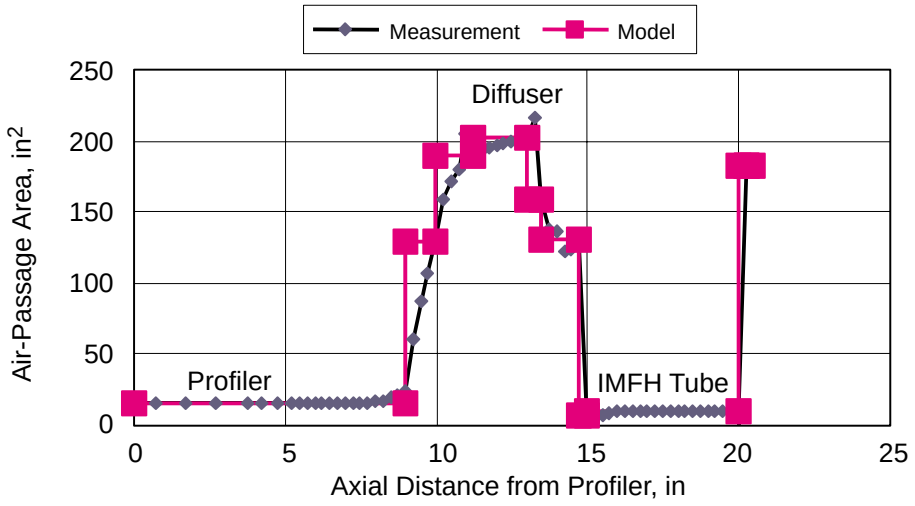

Figure 309. HSCT Curved-Sector Air Passage Area Distribution

Six conditions were studied: ground idle, 15% LTO, 34% LTO, 65% LTO, subsonic cruise, and supersonic cruise. Since the upstream is justified as an acoustic open–end, T_{12}/T_{22} will be the output parameter in this study representing the impedance of the entire upstream section ahead of the combustor. In this study, the location of interest is the exit of the IMFH tube (x = 20 in). In the spectrum of the impedance magnitude, the maximum peak represents the frequency with the highest impedance, approaching a closed end. The results (Figure 310) indicate that the upstream domain has a relatively high impedance (like an acoustic closed end) in the frequency range between 400 to 700 Hz. Therefore, the original assumption of a perfectly closed end is a reasonable approximation in that narrow frequency range.

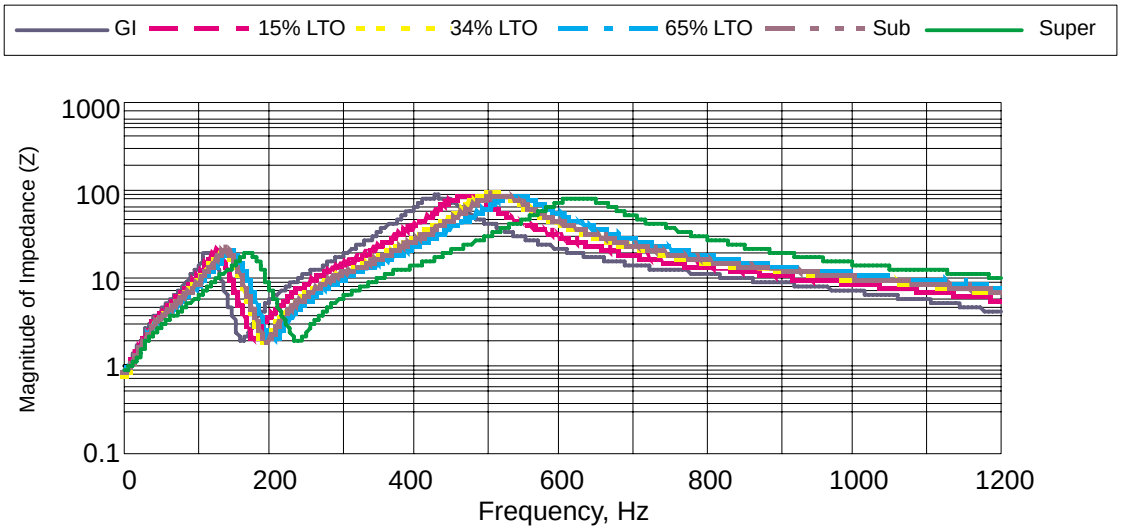

Figure 310. IMFH Impedance Magnitude Spectrum

4.9.1.2 Fuel Coking

The risk of coke formation in the fuel system was given a moderate probability of occurring with a medium impact on the program if it were to occur. Coke is capable of forming in both flowing and nonflowing fuel passages, and both types must be addressed.

Coke formation rate is a function of time and temperature. Thus, one of the primary methods of mitigating the risk is to ensure that fuel temperatures are kept low. This is accomplished by various cooling methodologies, such as heat shielding, active cooling circuits, and the avoidance of dead zones in the fuel circuits. Such stagnation regions allow heat to build up and coke to form. Similarly, because fuel staging is needed to meet emissions requirements, fuel can stagnate in stages as the fuel flow is turned off. This allows fuel temperatures to rise and coke formation to occur over a period of time. While purge systems can be used in ground-based systems and test facilities with relative ease, it tends to add more weight, cost, and complexity than can be tolerated on an aircraft. Thus, it becomes critically important to use cooling methods that keep the fuel temperatures low throughout the flight envelope, whether in a flowing or nonflowing circuit.

Both the cyclone pilot fuel injectors and the main fuel nozzles had to be cooled appropriately to reduce the coking risk. Coking was less of a concern in the pilots because fuel was always flowing through the circuits throughout the flight envelope, making them relatively easy to keep cool. In the main fuel nozzles, a combination of heat shielding and active cooling was used. The heat shields were simple metal barriers used to isolate the internal fuel tubes from the convective heating of the high-temperature air. In addition, fuel flow to the pilots was first diverted through the main fuel nozzles to help keep them cool. Calculations were made to estimate the heat pick up of the cooling flow to ensure that bulk temperatures remained within desirable levels prior to entering the pilots.

Prior to implementation in a flightworthy engine, it is recommended that additional fuel coking tests be performed. This should include both flowing and nonflowing tests of long duration on actual fuel system parts at the most severe operating conditions, as well as a series of tests that cycle the parts through the flight envelope. Similar tests have already been run on subscale development parts with very promising results. These tests were described earlier in this report.

4.9.1.3 Autoignition and Flashback

Autoignition and flashback were considered in the risk assessment to be relatively high impact to the program but to have a relatively low probability of occurring. A plan was put into place to model autoignition and to anchor the model with data from a four-tube rig.

The modeling effort examined three methods for modeling flameholding and flashback within the IMFH tube assembly: (1) a modified Magnussen–Hjertager combustion model with a flame eddy-dissipation-concept extinction mode, (2) monitoring of ignition delay times within the premixing/prevaporizing tube with conjugate heat transfer to and from the tube, and (3) a recently UTRC-developed coupled mixing/kinetics model. A computational grid representing a quarter section of the IMFH autoignition rig at UTRC, including a complete flame tube, was generated as a numerical test-bed of the three approaches. Appropriate modifications to the CFD code were made to use the above submodels under conditions appropriate to HSR, and CFD runs were initiated.

The UTRC-located autoignition and flashback test facility was designed, fabricated, and installed. A three-dimensional, solid model of this facility is shown in Figure 311. Air at temperatures up to 1200°F approaches the test facility. A bypass leg is in place to keep the flow rate through the electric heater at the required levels. For autoignition testing, a pressure drop of nominally 6% is set across the fuel injectors and flow diverted to the bypass leg. Pressure drop is then reduced until the pressure drop is approximately 2% or autoignition is detected.

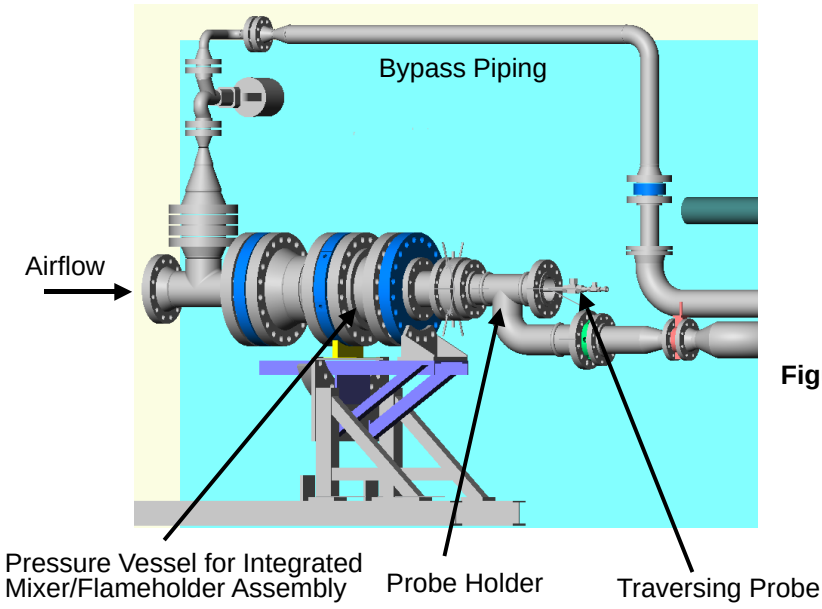

Figure 311. Autoignition and Flashback Test Facility

Figure 312 is a photograph of the assembled IMFH assembly from the upstream side. Each IMFH tube was instrumented with three surface thermocouples and three static pressure taps along the length of the tube. In addition, each tube had two optical probes. The optical probes and the surface thermocouples are used to determine whether autoignition or flashback has occurred.

During the initial shakedown runs, severe acoustics were encountered. The supporting threaded rods sheared, but no damage to the IMFH tubes was observed. No additional tests were conducted due to termination of the overall program.

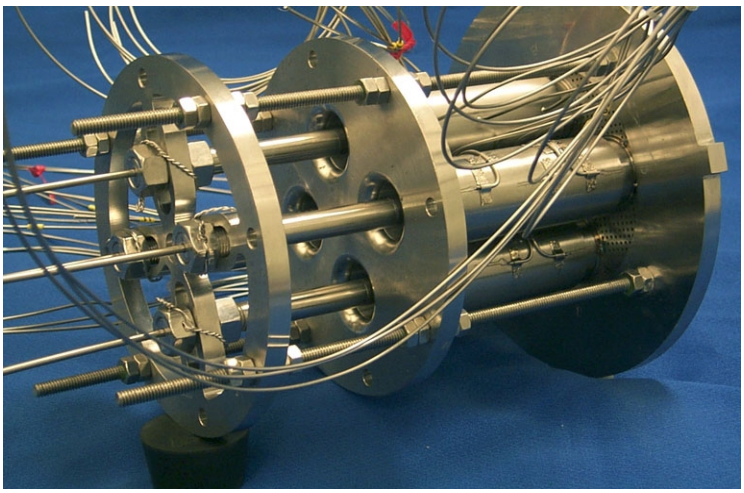

Figure 312. Photograph of IMFH Assembly from the Upstream Side

4.9.2 Sector Design

The detailed design of the full-scale MRA sector is described below. The design is principally the same as the one presented at the LPP/RQL downselect, with additional detail and modifications to reflect ongoing development. Figure 313 is a general cross section. Because circumferential staging was to be tested, the sector was expanded to six cups (pilots) covering a 75° section. This was based on lessons learned from the MMMRA Sector, which had five cups (pilots) and covered 63°. The five cups and IMFH tube banks were asymmetric in terms of circumferential staging and led to many uncertainties in analyzing and interpreting the data. Thus, although the larger sector would be more costly, the added symmetry was necessary to provide quality data that could be properly interpreted.

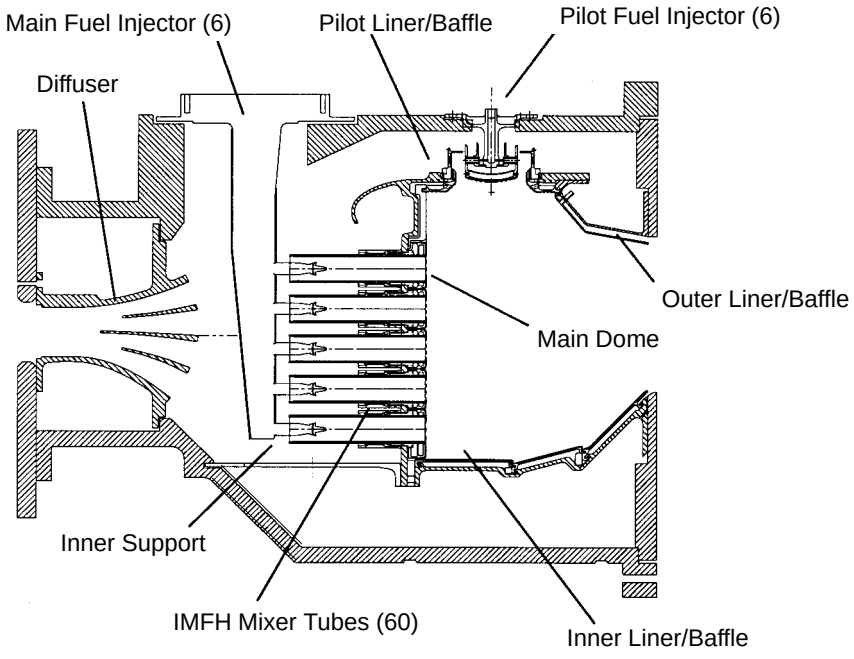

Figure 313. Full-Scale MRA Sector Cross Section

4.9.2.1 Aerodynamic Considerations and Fuel Staging

From an aerodynamic standpoint, the intent of the full-scale design was to mimic the subscale MMMRA sector as best as possible. This included the internal flow splits between the various flowpaths in the sector as well as knowledge gained about the fuel staging necessary to meet emissions targets.

The final design airflow distribution is illustrated in Figure 314, and fuel-staging patterns are presented in Figures 315 through 320. The small dots in the fuel staging figures represent the locations of the gas-sampling probes at the combustor exit plane relative to the main dome. The circumferential fuel staging selected is similar to the "n = 15" staging used in Builds 2, 3a1, and 3a3 of the subscale MMMRA sector (described previously). This mode demonstrated improved intermediate-power exit profiles over radial staging without materially impacting emissions. Ground idle (pilot only), takeoff (fully fired), and supersonic cruise (fully fired) are not impacted by the fuel staging selected because either none or all of the IMFH tubes are fired at these operating conditions. Note that the sector has been designed with enough flexibility to test both radial and circumferential staging, should there be a need to do so.

4.9.2.2 Diffuser

The Diffuser shown in Figure 321 is cast as a single 75.35° sector. The material is Inconel 718. The diffuser design contains four independent axial air passages developed within the inner and outer radii. The radial structural struts, located along the whole length of these passages, were cast as an integral part. These struts support and integrate the system as one unit. The four independent flowpaths expand to larger sections as they transition further aft towards the exit, reducing the air velocity prior to entering the combustor.

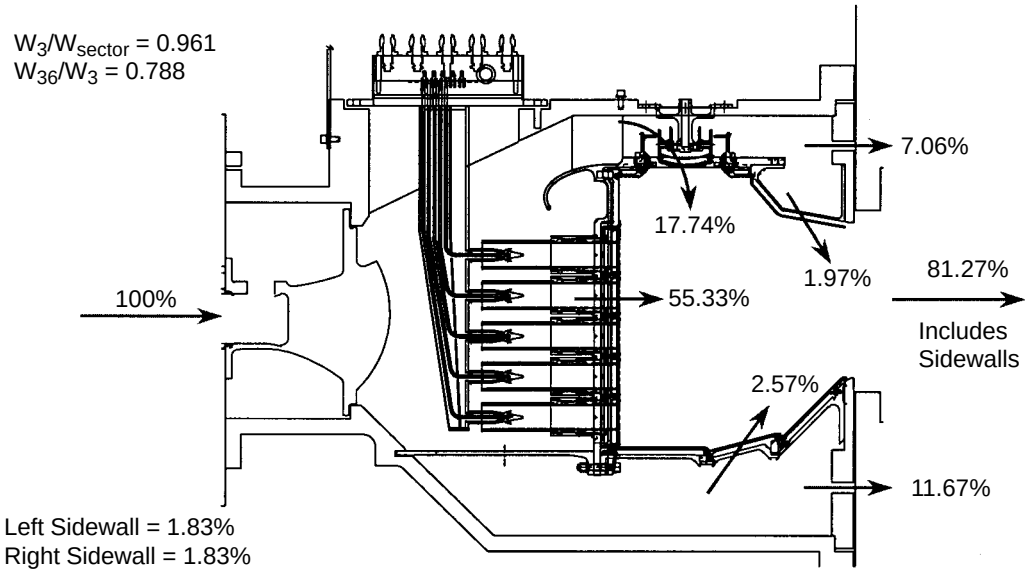

Figure 314. Full-Scale MRA Sector Internal Airflow Distribution

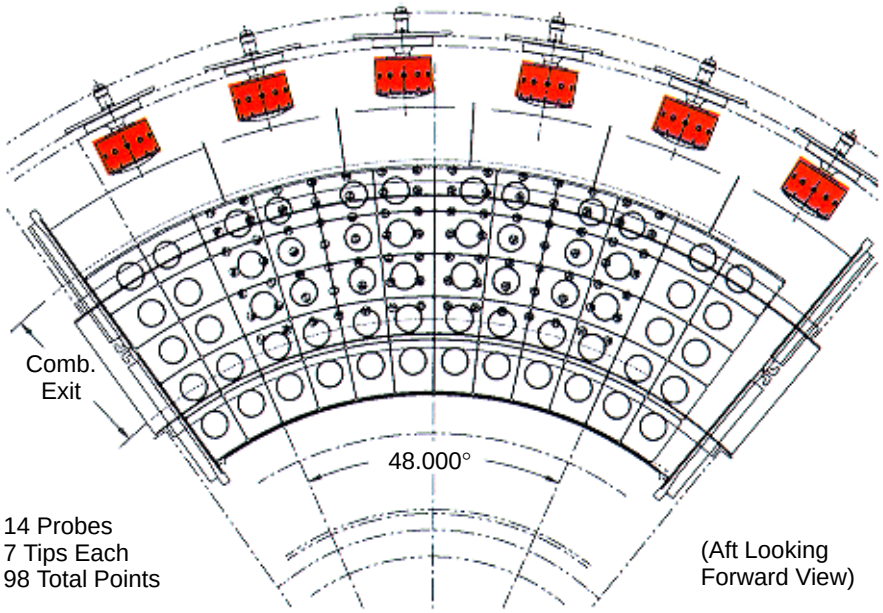

Figure 315. Full-Scale MRA Sector Ground Idle Fuel Staging

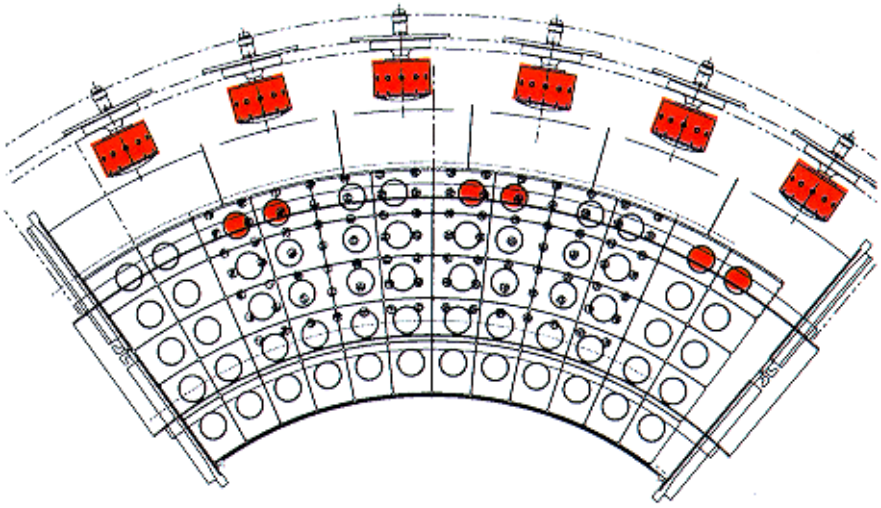

Figure 316. Full-Scale MRA Sector 15% LTO Fuel Staging

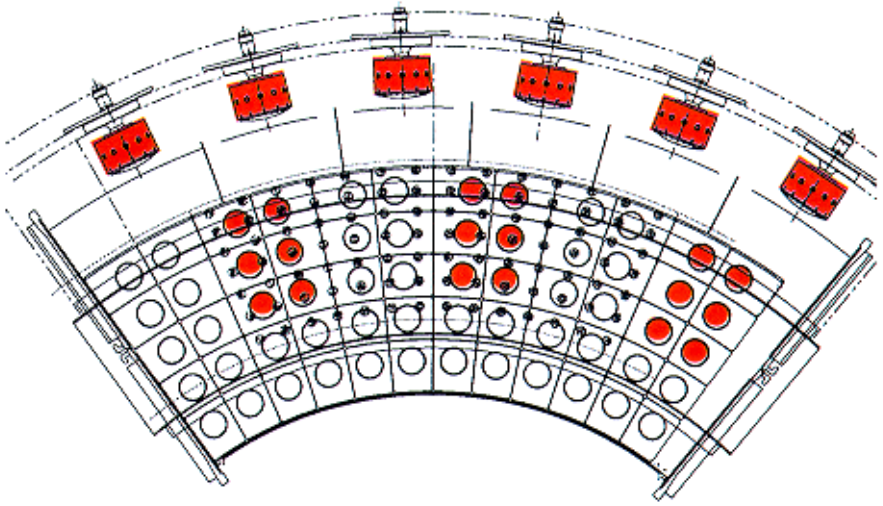

Figure 317. Full-Scale MRA Sector 34% LTO Fuel Staging

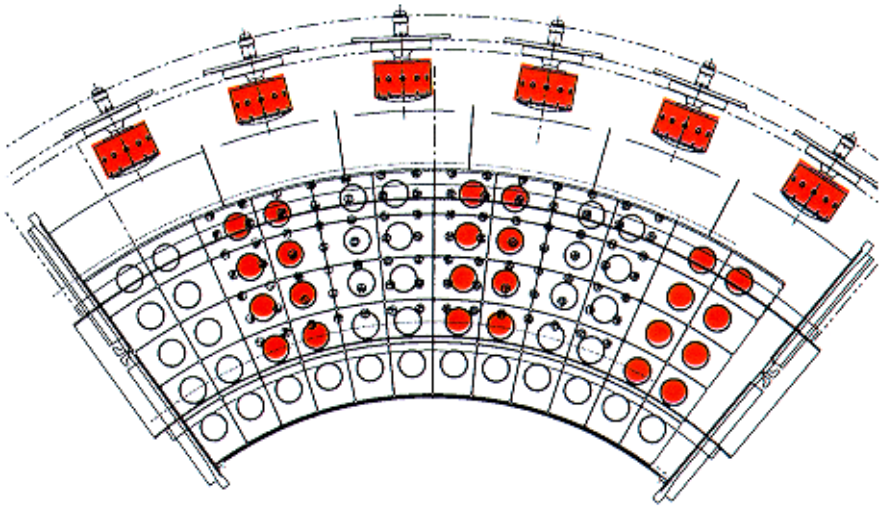

Figure 318. Full-Scale MRA Sector Nominal Subsonic Cruise Fuel Staging

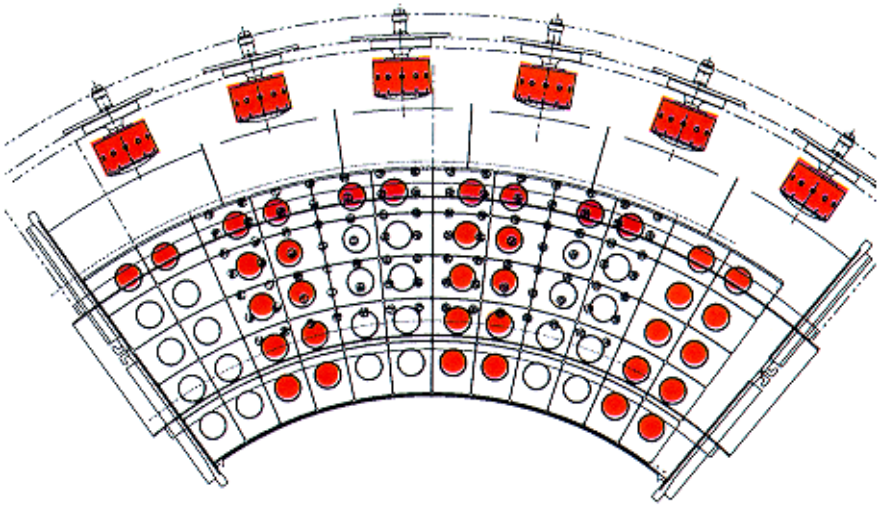

Figure 319. Full-Scale MRA Sector 65% LTO Fuel Staging

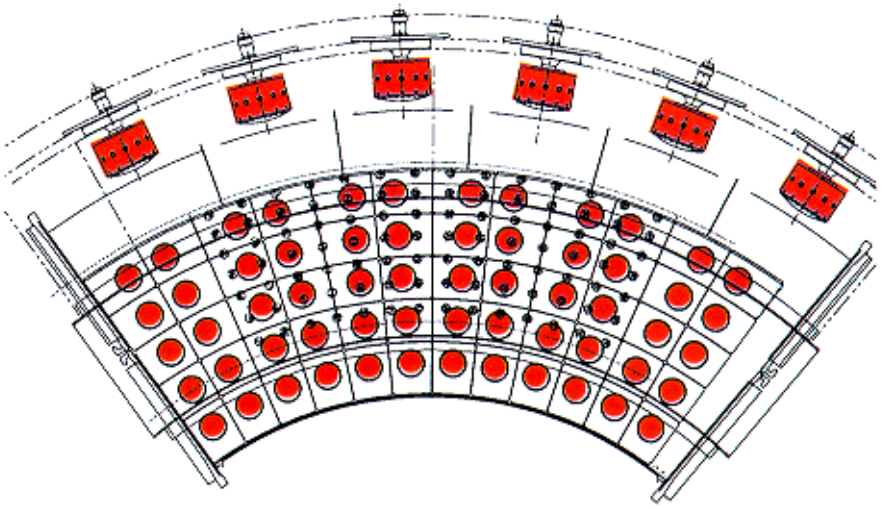

Figure 320. Full-Scale MRA Sector Nominal Supersonic Cruise and 100% LTO Fuel Staging

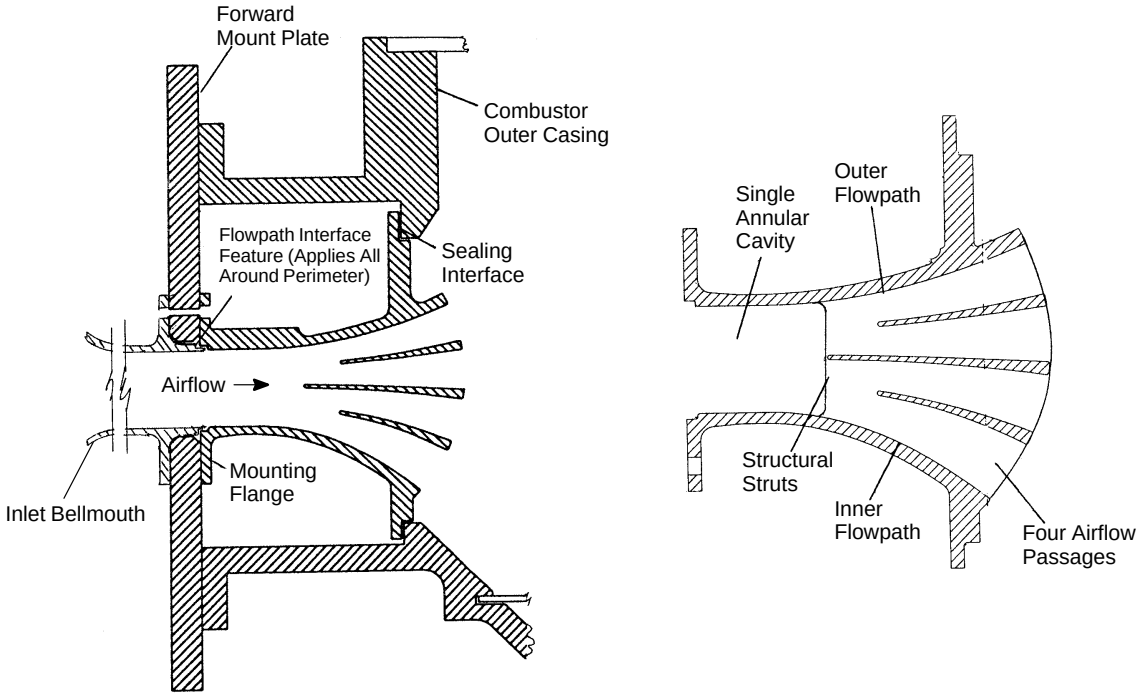

Figure 321. Full-Scale MRA Sector Diffuser Design Features

Forward of the integral struts/passages, the flowpath transitions to a single annular passage. In an engine system (with a compressor), this annular cavity would contain the compressor outlet guide vanes (OGV). These airfoil-shaped vanes redirect the compressor exit air flow angle to an axial direction. For these tests, heated shop air flowing axially is used.

In a full-annular design, 15 struts would be equally spaced every 24°. Three struts are present in the sector (plus sidewalls). The circumferential orientation is aligned with every other main dome fuel injector. Figure 322 is an aft-looking-forward view. Note that the sidewalls at the circumferential ends are an integral part of the diffuser. This provides full containment of the air within each passage.

The diffuser forward flange is bolted to the forward plate. The inlet bell mouth, with an axial aft-length extension, also fastens to the forward face of this plate. Note that an interface feature between the aft bell mouth extension and the forward surface of the diffuser must blend smoothly. This feature is also shown in Figure 322. This transition allows a smooth passage for the high-speed air crossing between these two mating parts, thereby minimizing air pressure losses and boundary layer trips.

4.9.2.3 Main Dome and IMFH Premixers

The main dome shown in Figure 323 is the main structure for the combustor module. The dome structure is cast from Inconel 625 and machined to final configuration. The structure consists of a vertical wall, with the upper end forming a 90° bend, and continues aft. The vertical face contain the diameter openings to mount and support all the IMFH/heat Shields and dome shrouds. Its outer circumferential end (90° bend) supports the mounting for the pilot liners, pilot swirlers, and outer

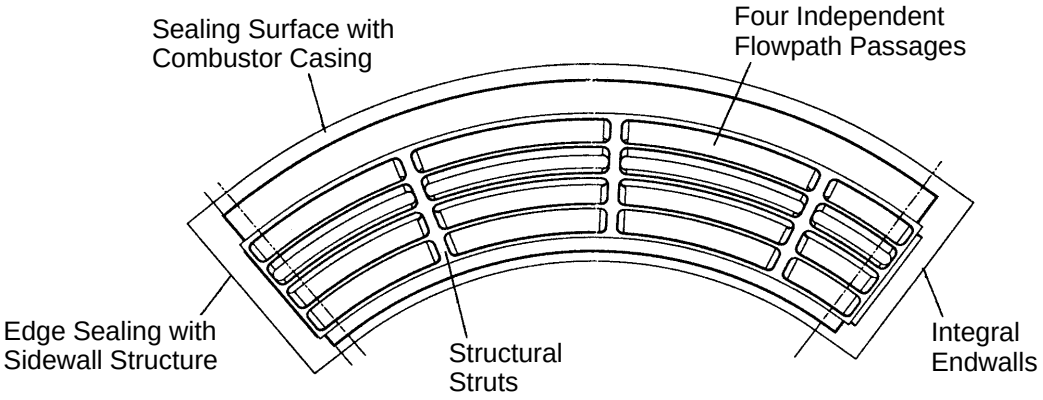

Figure 322. Full-Scale MRA Sector Diffuser End View (Aft Looking Forward)

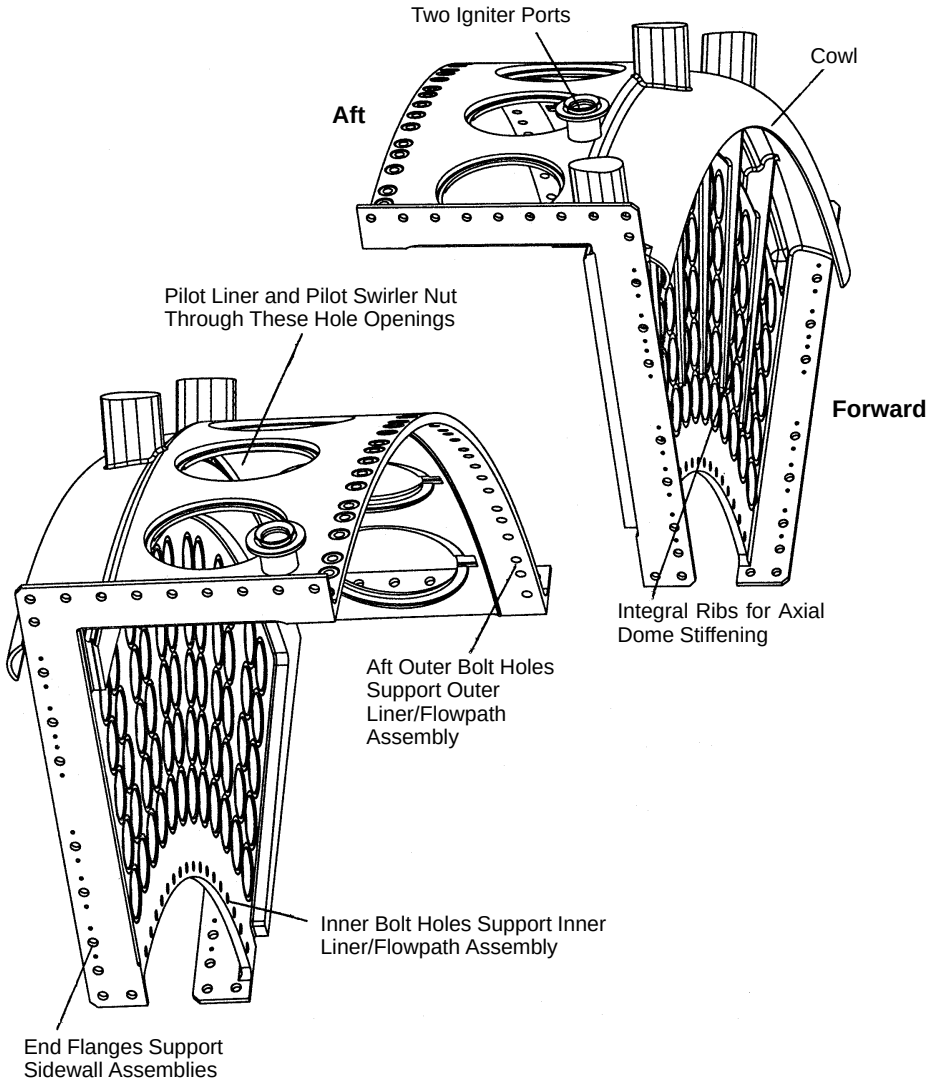

Figure 323. Full-Scale MRA Sector Main Dome Design

liner/baffle as shown in Figure 324. The lower end of the Dome structure contains bolt holes for mounting the Inner Liner flow path module and the Forward Inner Support.

The IMFH/heat shield assembly shown in Figure 325 is manufactured from an Inconel 625 bar for the IMFH tube and machined down to 1-in diameter. It is then brazed to a René 125 cast heat shield. The heat shields contain enhancement features to reduce the amount of cooling air, while maintaining the objective surface temperatures. The heat shield surface exposed to the combustion gases is thermal-barrier coated.

The total length of the IMFH tube is 5.5 inches (from air inlet to exit into the combustion cavity). The IMFH/heat shield is assembled to the dome using the diameter openings in the dome wall (for each IMFH tube to penetrate through). Once the tube is inserted through the wall, the IMFH nut fastens the part within the dome structure, as shown in Figure 326. The IMFH tube and fuel injector design chosen for the sector is an adaptation of Configuration 46 discussed in the single-cup development section of this report.

4.9.2.4 Main Fuel Injector

The main fuel injector design was based on work done by GEAE for the full-scale engine PDR. Options for cooling the main fuel injector were investigated. Preliminary prints of a triple-walled tube design and a design with a cast stem were produced, and competitive quotes were received from a number of vendors. Based on vendor information and risks associated with both approaches, the cast stem approach was chosen. The aerodynamic features of the tip and the fuel injection orifice size and location were kept consistent with the GEAE design. The cooling scheme is shown in Figure 327.

In order to eliminate cicumferential vibration, a series of cross braces connect the two towers of the main fuel injector. The resulting vibration analysis is illustrated in Figure 328.

4.9.2.5 Cyclone Pilot and Pilot Liner

The cyclone pilot shown in Figure 329 is machined from Inconel 718 bar stock. The two main features are (1) the 43° angle, vertical slotted swirler vanes on the upper part of the cyclone, resulting in a swirling rotational movement of the air, and (2) the machined threads on the lower portion of the cyclone. These threads function as a nut, fastening each of the pilot liner segments to the dome structure as shown in Figure 330. The general design is an adaptation of Configuration 21.3 discussed in the single-cup development section of this report.

The Pilot Liner shown in Figure 331 forms the forward part of the outer flowpath. The material is cast René 125 segments, machined to final dimensional features. The flowpath surface is thermal-barrier coated, and the liners are back-side impingement cooled. Enhancement features are cast in the “cold” side of the liner surface, which reduce the amount of cooling air requirements while meeting the objective temperatures on the “hot” liner surface. The postimpingement air exits through forty-eight 0.126-in diameter holes and then mixes with the fuel/air mixture exiting into the combustion chamber. The large center opening has a 45° conical transition and is aerodynamically formed to provide the passage of the fuel/air into the flowpath. Axial spline seals extending along the length of the liners are provided to minimize air leakage between the segments. The torque applied by the cyclone pilot to the pilot liner results in assembly to the dome structure as shown in Figure 332.

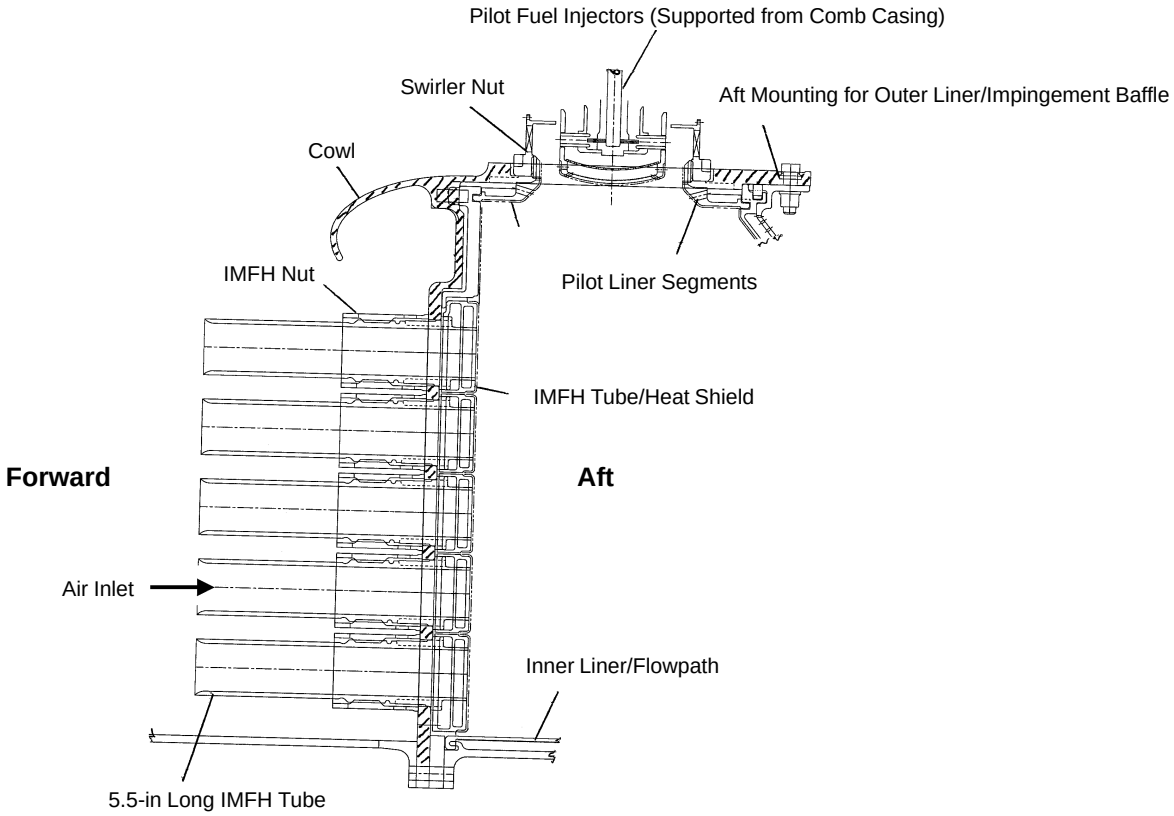

Figure 324. Full-Scale MRA Sector Main Dome Component Assembly

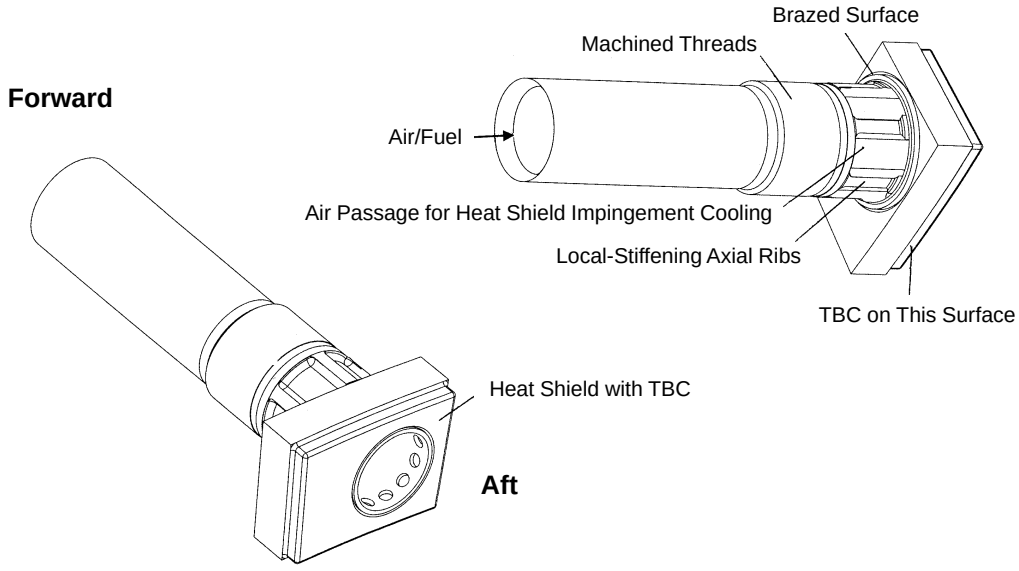

Figure 325. Full-Scale MRA Sector IMFH/Heat Shield Design

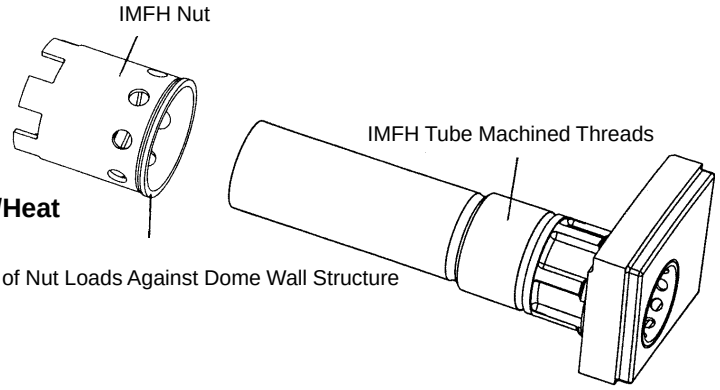

Figure 326. Full-Scale MRA Sector IMFH/Heat Shield Nut Assembly

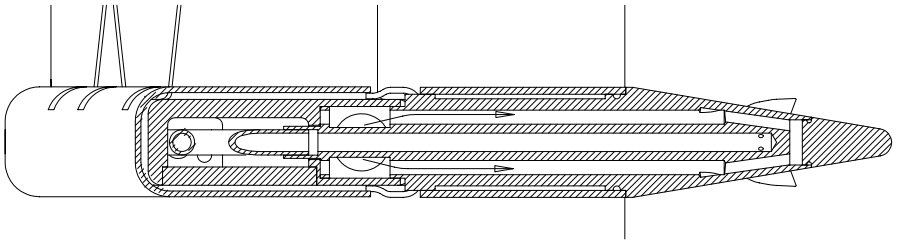

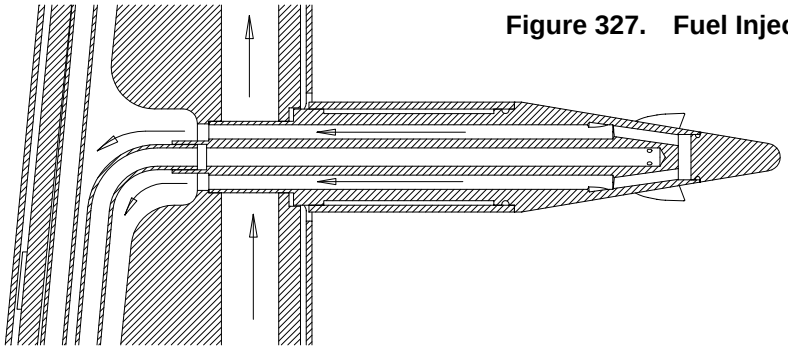

Figure 327. Fuel Injector Tip-Cooling Circuit

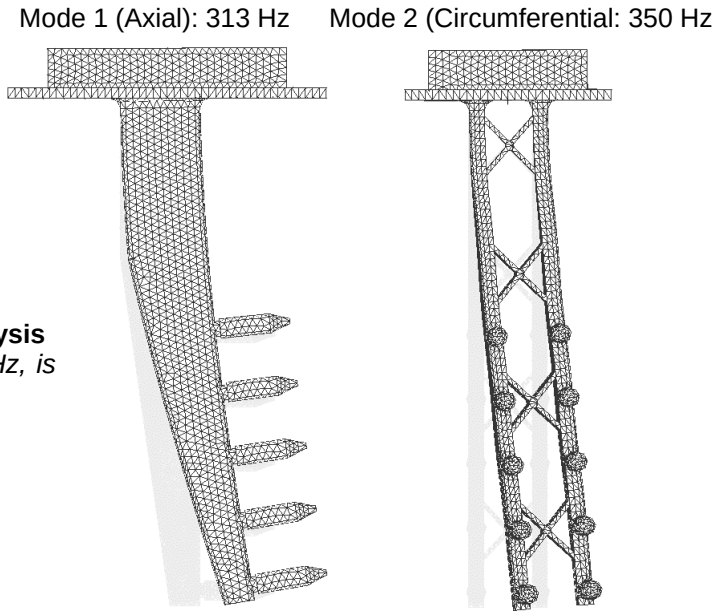

Figure 328. Fuel Injector Vibration Analysis
First natural frequency, 313 Hz, is acceptable for rig operation.

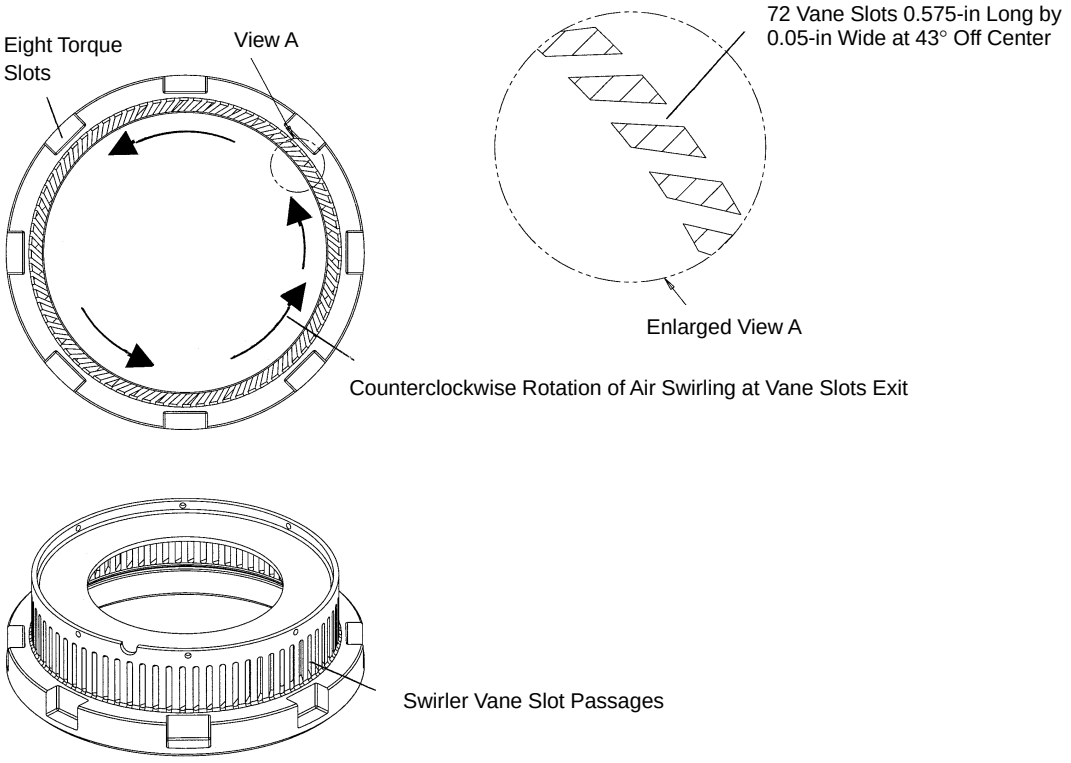

Figure 329. Full-Scale MRA Sector Cyclone Pilot Design Features

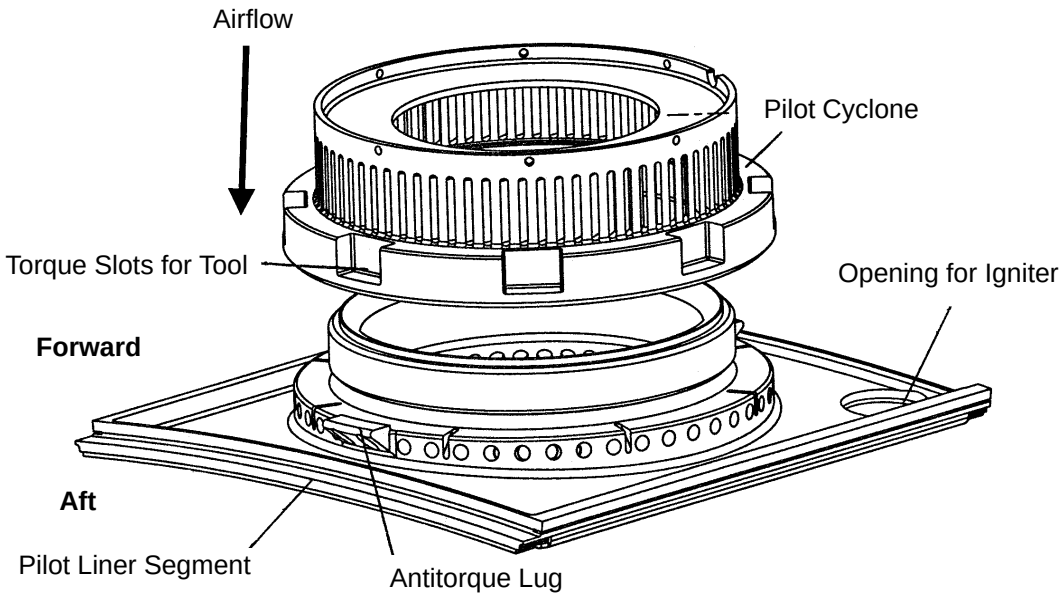

Figure 330. Full-Scale MRA Sector Cyclone Pilot/Pilot Liner Assembly

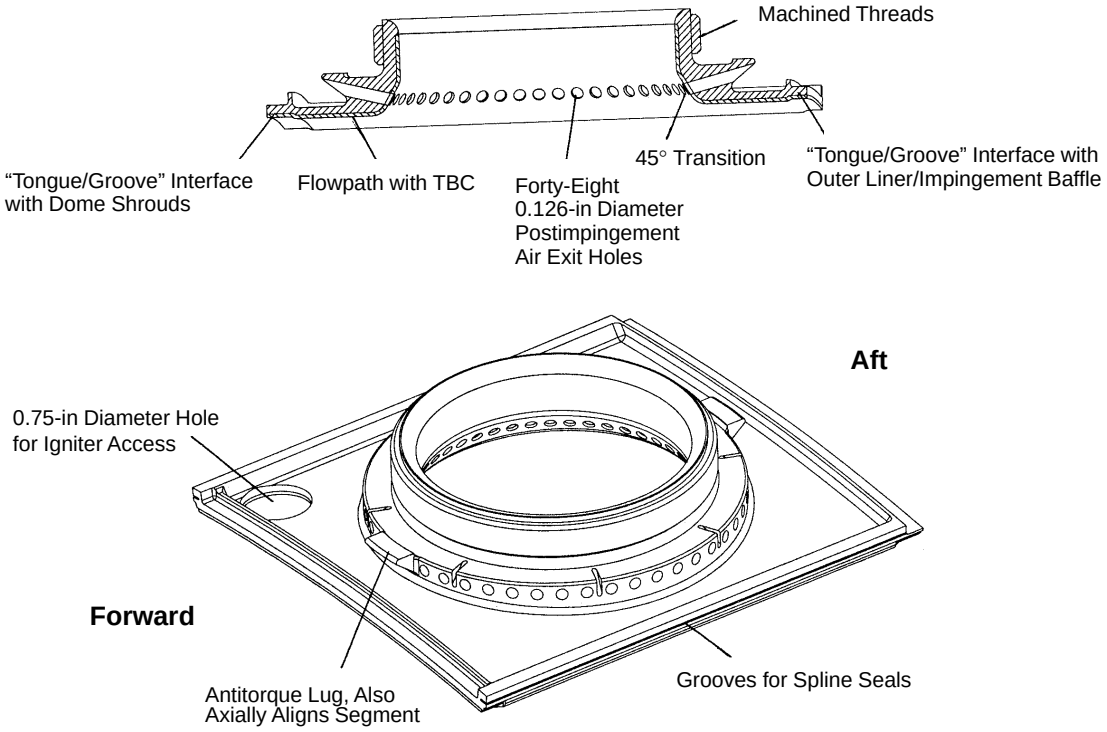

Figure 331. Full-Scale MRA Sector Pilot Liner Segment Design Features

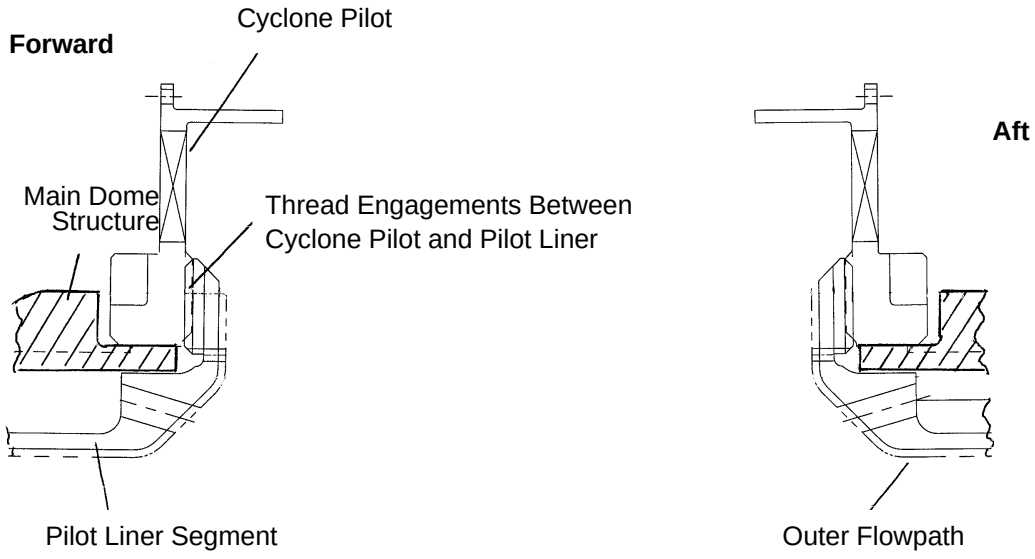

Figure 332. Full-Scale MRA Sector Cyclone Pilot and Pilot Liner Assembly

4.9.2.6 Outer Liner and Impingement Baffle Assembly

Outer Liner Panel – The six outer liner panels were sized in the circumferential and axial directions based on a conservative operating temperature of 2000°F. Each panel is bolted to the impingement baffle by seven edge-positioned studs (Figure 333). The stud attachment scheme alleviates discharge flow-area restrictions inherent in a hook attachment, resulting in improved impingement cooling effectiveness. The edge-positioned studs also provide positive panel retention, minimizing leakage and desensitizing the design to thermal distortions. The panel cooling array consists of 0.030 by 0.030 by 0.030-in pyramids and results in a maximum surface area enhancement of 118% (goal: 60% area enhancement). The array of 0.030-in pyramids also results in a relatively small percentage of flow blockage (8.85%), see Figure 333. The 0.030-in pyramids were selected based on manufacturability and the results of a parametric study that rated several schemes based on overall surface enhancement and flow blockage. The cooling features and panel studs are to be cast into liner panels using an ACTUA ™ wax rapid prototyping process. This process minimizes hardware lead time and reduces machining cost. After the liners are cast, only machining of the perimeter rails and chasing of the stud threads will be required. Machining of the perimeter rails is required to ensure proper fit with the impingement baffle resulting in minimized leakage around the liner.

Impingement Baffle – The impingement baffle is a single-piece 75.35° sector machined from a one-piece Inco 625 forging. The 6 outer liner panels bolt to the baffle through 24 clearance holes, 12 clearance slots, and 6 close-tolerance slots. The slots allow the liner design to follow the flowpath bend. The close-tolerance slots act as piloting slots for positioning the liner segments during installation. Based on heat transfer analysis, the design incorporates approximately 7055 impingement holes (0.019 to 0.021-in diameter each).

Supporting Analysis – A finite-element analysis of the HSCT sector rig outer combustor liner was commissioned to assess performance under anticipated operating loads. Temperature and stress results for the liner are summarized in Figures 334 and 335.

4.9.2.7 Inner Liner

The inner flowpath liner segments are cast from MAR–M–509 material, and each is machined to the final configurations. Figure 336 shows the three axial segmented features, supported by a single impingement baffle. There are three equal-arc-length segments for the forward, middle, and aft liners.

The radial support for the liners consists of integral hooks located in the forward and aft ends. The hooks are segmented (scalloped) to reduce the thermal stress between these cooler hooks and the hot liner surface above them. The scalloping also allows postimpingement air to exit through the scalloped passages.

These hooks engage a similar feature on the impingement baffle, shown in Figure 337. Tangential support is provided for each liner by a slot in the middle of each arc (located at the forward section) and by engaging a lug located on the impingement baffle. Each of the liners is axially supported on the forward set of hooks while allowing free axial growth on the second set of hooks located at the aft end.

Surface-enhancement features are machined into the “cold” side of the liner thickness, reducing the amount of air required to cool the “hot” surface to within the temperature objectives. The postimpingement air traverses axially and exits through passages provided between scalloped hooks and

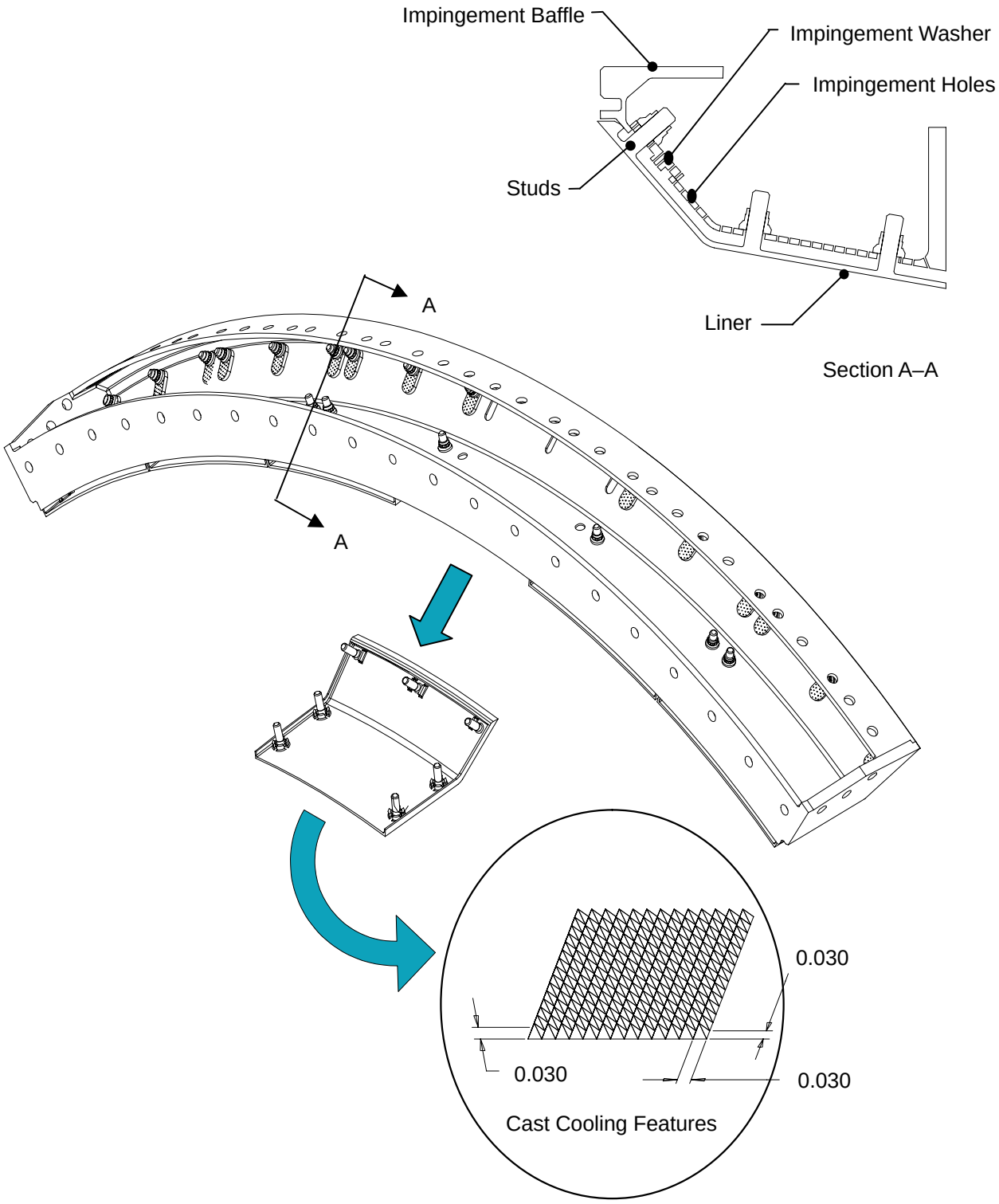

Figure 333. Outer Liner and Impingement Baffle Assembly

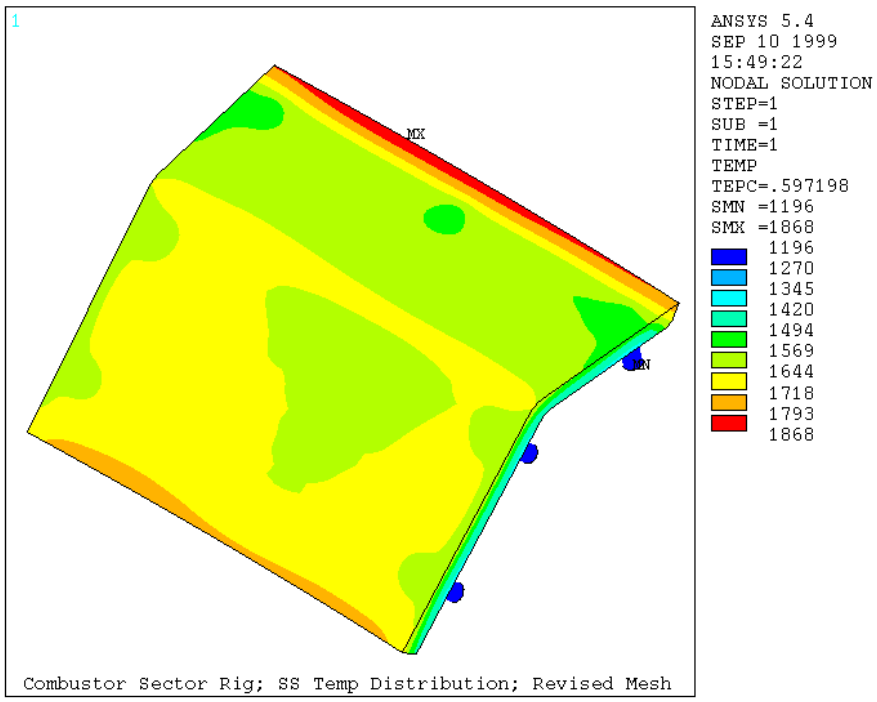

Figure 334. Steady-State Temperature Distribution – Final Geometry and Heat Transfer Coefficients

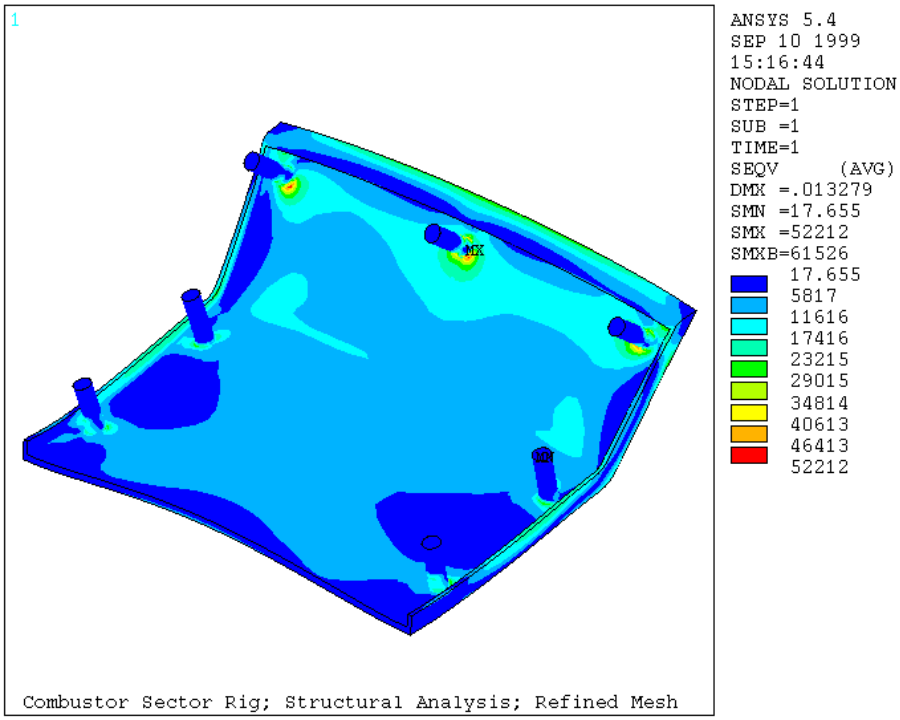

Figure 335. VonMises Stress Distribution – Final Geometry and Boundary Conditions, Full Model

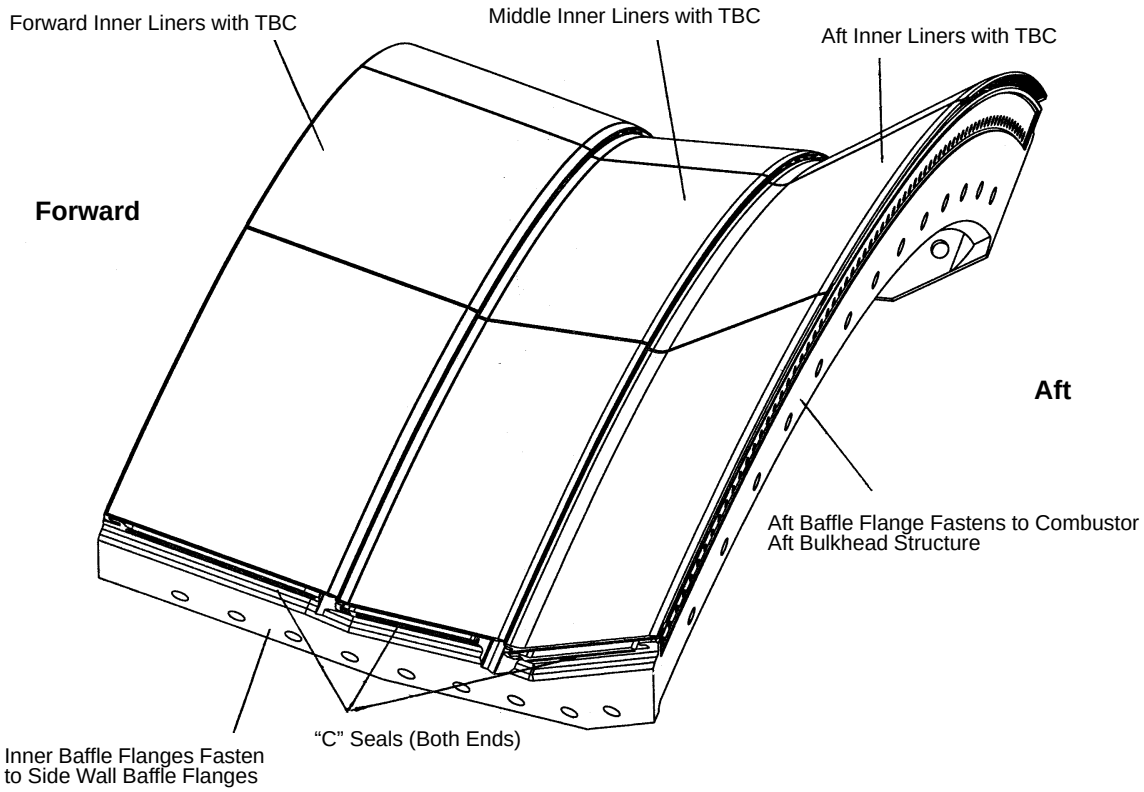

Figure 336. Full-Scale MRA Sector Inner Liner Segment/Impingement Baffle Assembly

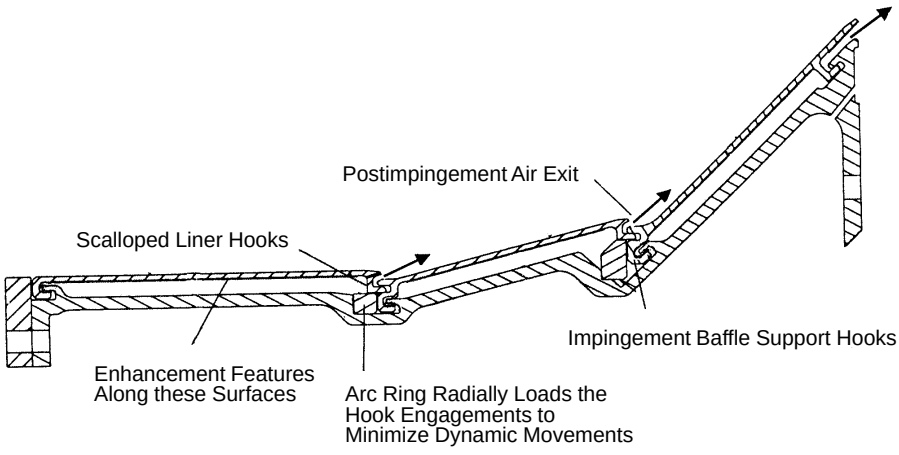

Figure 337. Full-Scale MRA Sector Inner Flowpath Liner Assembly

into the flowpath. The forward liner also has ninety-five 0.020-in diameter holes drilled on the aft end of the liner thickness. The air through these holes provides added convection cooling and also adds film cooling to the first portion of the mid liner.

The design also uses two separate arc rings that are preloaded at two axial stations when assembled. These rings provide a radial load to the hook engagement and thus minimize the effects of radial stack-up by eliminating dynamic movement while also providing damping. To minimize air leakage between the segments, spline seals are engage two adjacent ends and axially extend the length of each liner.

4.9.2.8 Exit Vane Pack/Gas-Sampling System

Vane Pack Probe Design – The vane pack assembly (Figure 338) consists of 14 emissions-sampling vanes, 7 dummy vanes, one left-hand end-wall vane and one right-hand end-wall vane. The emissions-sampling vanes consist or an inner and outer platform, body, seven emissions-sampling tips, a cooling water supply tube, and seven emissions-sampling tubes. The emissions-sampling array is a centralized 48° segment consisting of 98 points. This density was chosen to provide adequate resolution for all staging modes. All of the vanes are water cooled to withstand the high temperatures associated with combustor emissions sampling. The cooling water is supplied to the vanes by the vane pack cooling water manifold at 2.5 gpm per probe. The stresses in the vanes are well within the maximum allowable for Inco 625. Further, the probe natural frequency of 461 Hz is acceptable for rig operation.

Vane Pack Cooling Water Manifold – The vane pack cooling-water manifold provides coolant to the vane pack. Each vane is fed by a ½-in AN fitting with a constraining orifice (Figure 339). The orifice provides back pressure so that if a vane is lost or damaged the rest of the vanes will not loose the required flow.

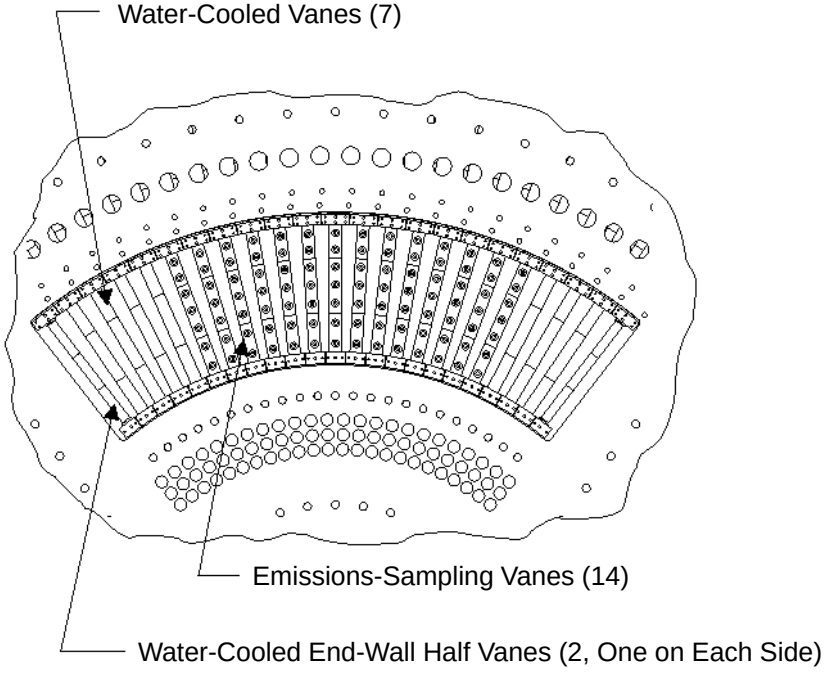

Figure 338. Vane Pack Gas-Sampling System

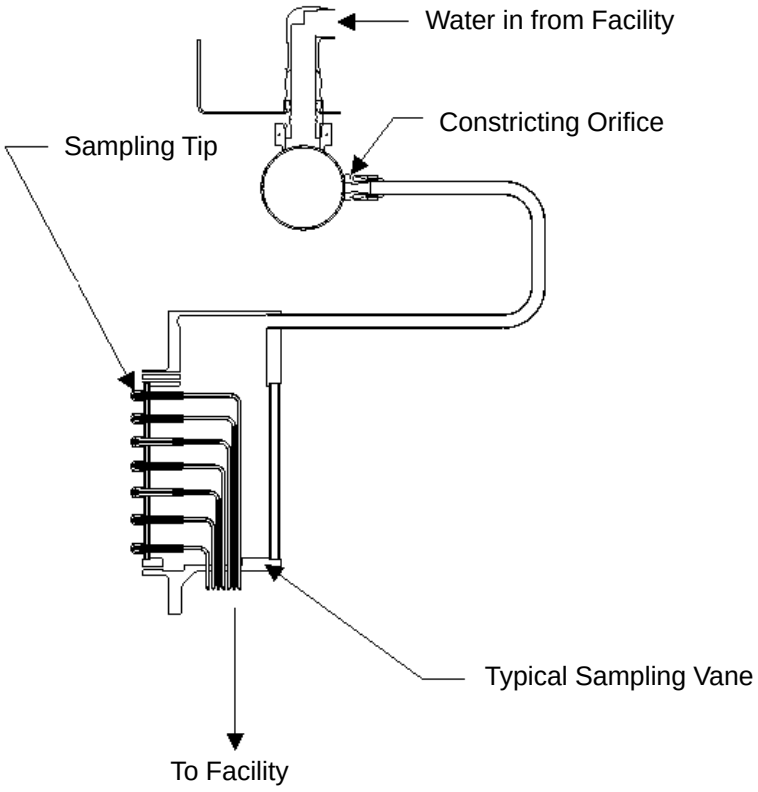

Figure 339. Emissions-Sampling Vane Section

4.9.3 Manufacturing and Assembly of the Combustor Large-Scale Sector Rig

Figure 340 is a cutaway view of the rig; detailed assembly information is available in P&W layout drawing L98WL013.

Emissions System Assembly (Figure 341) – The emissions systems assembly consists of the large aft plate with the emissions probe vane pack attached by two ¼-in double hex bolts at the OD and one 5/16-in double hex bolt at the ID. This Assembly is bolted between the combustor housing assembly and exhaust duct extension assembly. The large aft rig plate is 45.7 inches in diameter and 2.0 inches thick and is manufactured from Inconel 718 (AMS 5596 Ni Alloy). The emissions probe vane pack consists of 23 gas sampling probes mounted to the aft rig plate in a circular pattern of 75.350° at a mean radius of 20 in. The probes are water cooled with a 3-in stainless steel manifold supplying the cooling water. Water is supplied to the manifold by the facility.

Combustor Assembly (Figure 342) – The combustor assembly consists of an inner liner impingement baffle and inner flowpath liner segments, an outer liner impingement shell with inner flowpath liner segments, pilot liner segments retained by a pilot liner swirler nut, a dome support, a dome shroud with IMFH heatshield assemblies, and an inner fairing support bolted to the inner impingement baffle. This assembly is bolted to the small aft plate that bolts to the large aft plate.

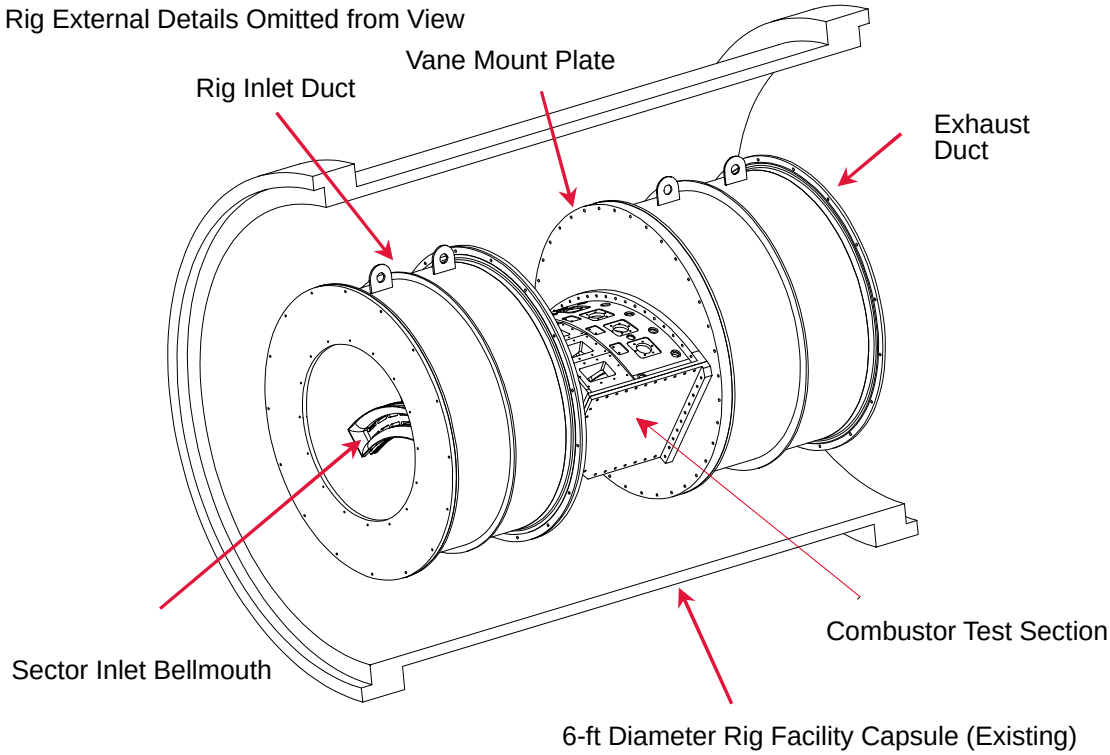

Figure 340. Overall Combustor Large Scale Sector Rig

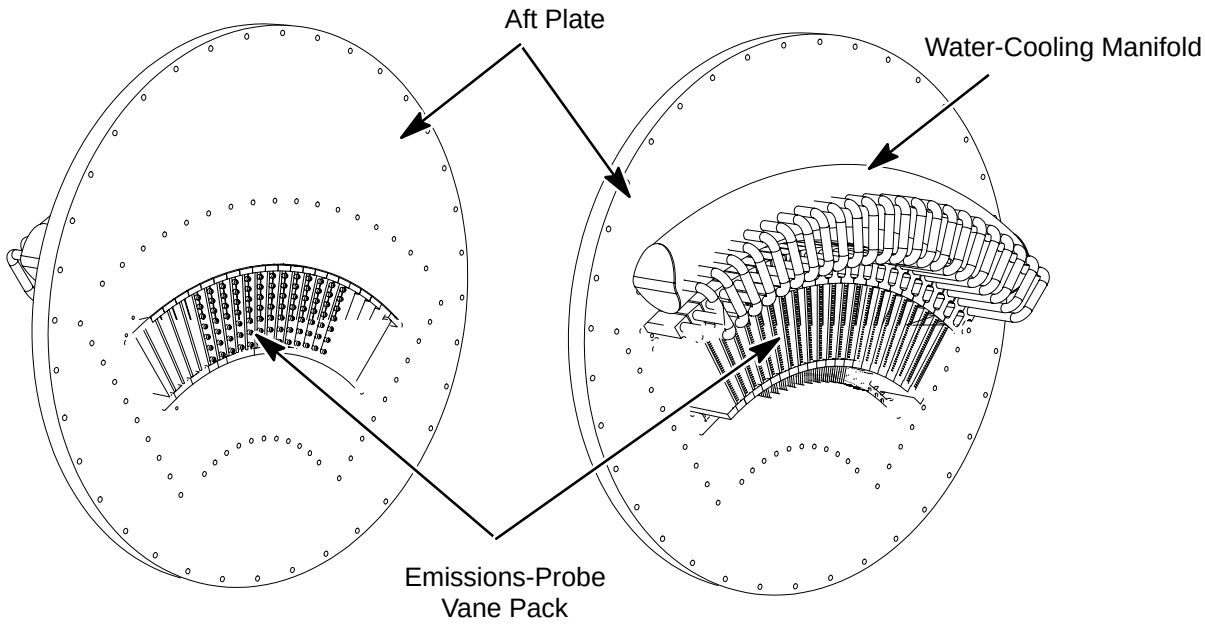

Figure 341. Emissions System Assembly

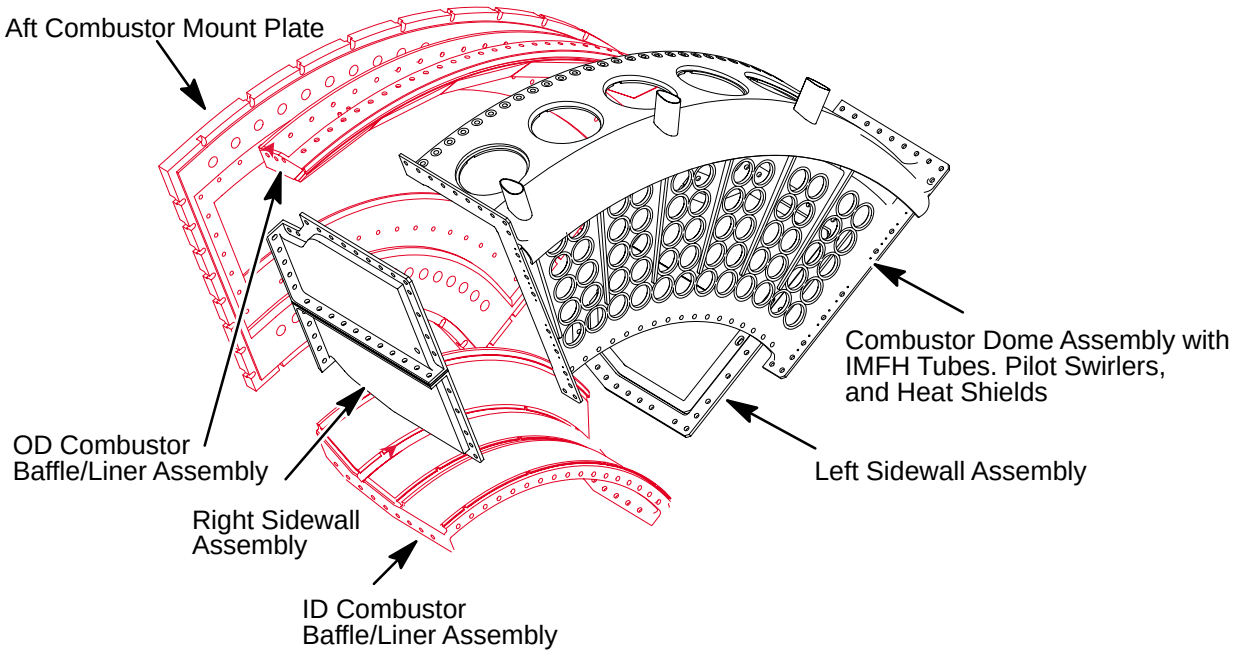

Figure 342. Combustor Assembly

Combustor Housing Assembly (Figure 343) – The combustor housing assembly is a sector made of 321 or 347 stainless steel. This assembly consists of a front mount plate, an aft mount plate, an inner and outer housing and a left and right sidewall. This housing encloses the combustor assembly and is mounted to the large aft plate by bolts. Six water-cooled fuel nozzles are bolted to the outer housing and extend into the combustor housing. Six pilot fuel injectors and mounted to the OD housing. A diffuser housing is bolted at the front, inside of the combustor housing.

Prediffuser Inlet Assembly (Figure 344) – This is a bolted assembly consisting of a bellmouth sector, an inlet profile plate, and a prediffuser inlet channel. All parts are manufactured from 316, 321 or 347 stainless steel. This assembly is bolted to the small forward plate that is then bolted to the front flanges of the combustor housing.

Rig Inlet Duct Assembly (Figure 340) – The rig inlet duct assembly is 24 inches long and made of 321/347 stainless steel. It is a rolled cylinder of 5/16-in plate with circumferential flanges butt-welded to each end. A circular ring is welded to the OD of the duct at the center for added hoop strength. Two lugs are welded to the top of the duct for lifting the duct assembly.

Exhaust Duct Assembly – The exhaust duct (SKR5806) is 33.172-in long and made of 321/347 stainless steel. The duct is a cylinder rolled and welded of 0.5-in plate with a 41.95-in OD. Circumferential flanges are butt-welded on each end of the duct. For added hoop strength, a circular ring is fillet-welded to the cylinder OD at the center of the duct. Two lugs are fillet welded to the top with 1.5-in diameter holes in each lug for lifting the duct assembly. Thirty-six 0.375-in diameter bolts equally spaced attach the forward flange to the aft rig plate (SKR5817). Sixteen 0.375-in diameter bolts equally spaced attach the aft flange to the support cone (XR–561830).

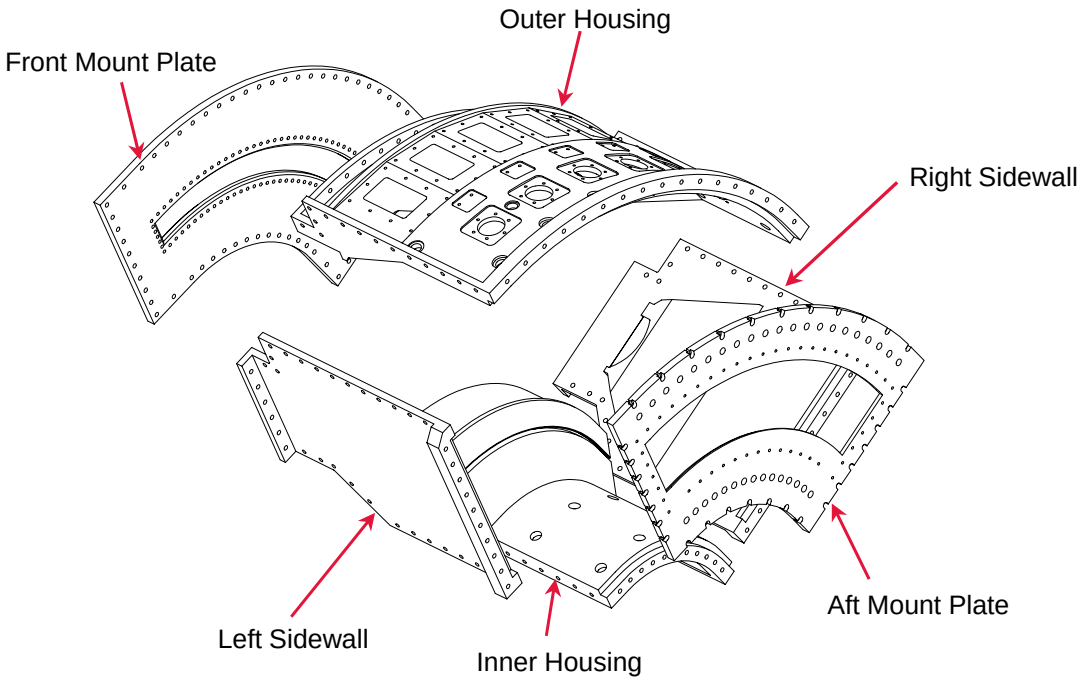

Bolted Assembly of Six Stainless Steel Components

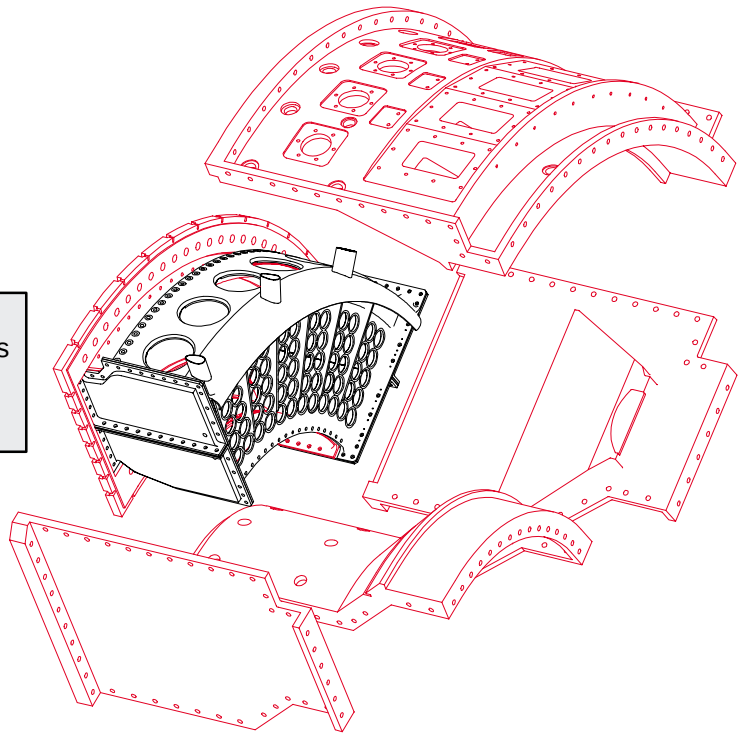

1. Attach housing OD and ID structures, routing instrumentation through egress holes.
2. Attach sidewall structures

Figure 343. Combustor Housing Assembly

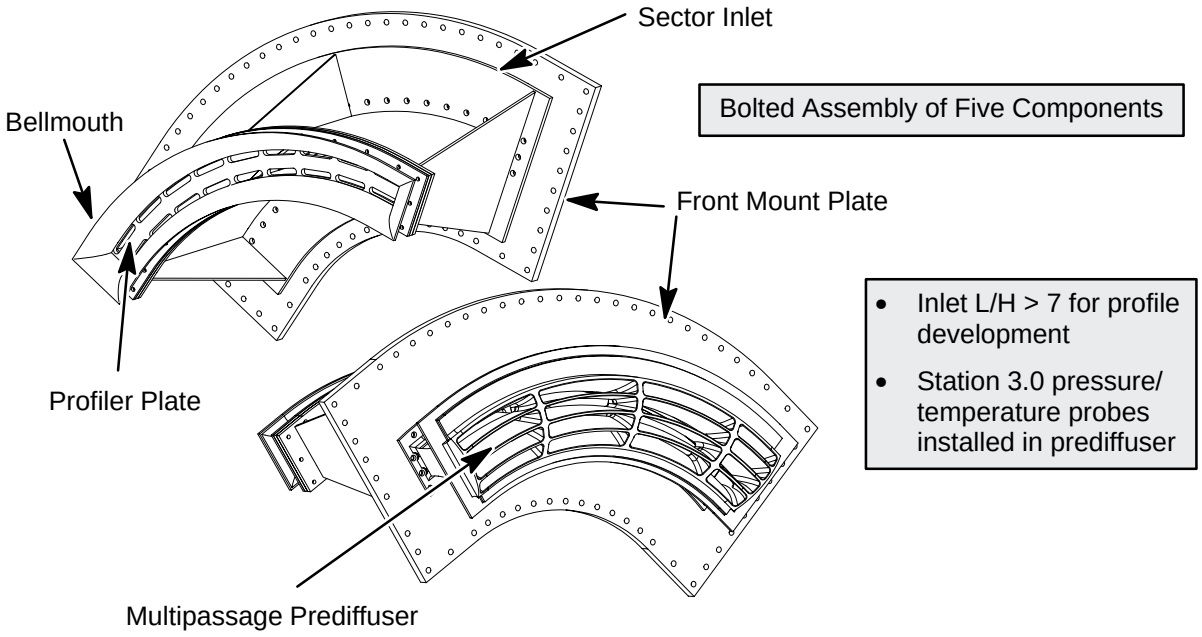

Figure 344. Prediffuser Inlet Assembly

Forward Duct Assembly (Figure 345) – The forward duct assembly is a cylindrical duct 31.213 inches long and 27.75 inches in diameter. Circumferential flanges are butt-welded to each end of the duct. The forward flange has sixteen 0.5-in diameter bolts equally spaced, and the aft flange has sixty 0.25-in diameter bolts for mounting the assembly. At the center of the duct, a 360° ring is weld into the center of the duct for added hoop strength. A lift lug is welded to the top of the stiffening ring for lifting the assembly. All parts are made from Inconel 625.

Rig Externals (Figure 346) – Six main fuel injectors are mounted to the OD housing using shims for positioning. Ten main fuel manifolds are connected to the injectors by jumper tubes supply the main fuel injectors. The jumper tubes and manifolds are 0.028-in wall AMS 5557 stainless steel brazed tube assemblies with 37° type cone seat fittings. The main injectors are cooled by two 0.75-in diameter manifolds providing supply and return water to and from the main injectors through 0.375-in diameter jumper tubes. The cooling manifolds and jumper tubes are 0.028-in wall AMS 5557 stainless steel brazed tube assemblies with 37° type cone seat fittings. Six pilot fuel injectors mounted directly to the combustor assembly outer housing are supplied by one 0.75-in diameter fuel manifold. The pilot injectors are connected to the pilot fuel manifold by 0.375-in diameter jumper tubes. The pilot fuel manifold and jumper tubes are 0.028-in wall AMS 5557 stainless steel brazed tube assemblies with 37° type cone seat fittings. Five sheet metal brackets mounted to the combustor assembly outer housing support the pilot fuel manifold, cooling water manifolds, and main fuel manifolds. The brackets are constructed of 0.125-in thick Inconel 625 (AMS 5599) with welded gussets. All fuel manifolds include a port for N_2 purge. The end fittings on the pilot fuel manifold and cooling water manifolds are configured differently to fool-proof assembly. A 3-in diameter manifold provides cooling water to the emissions probe vane pack through 23 orifice fittings.

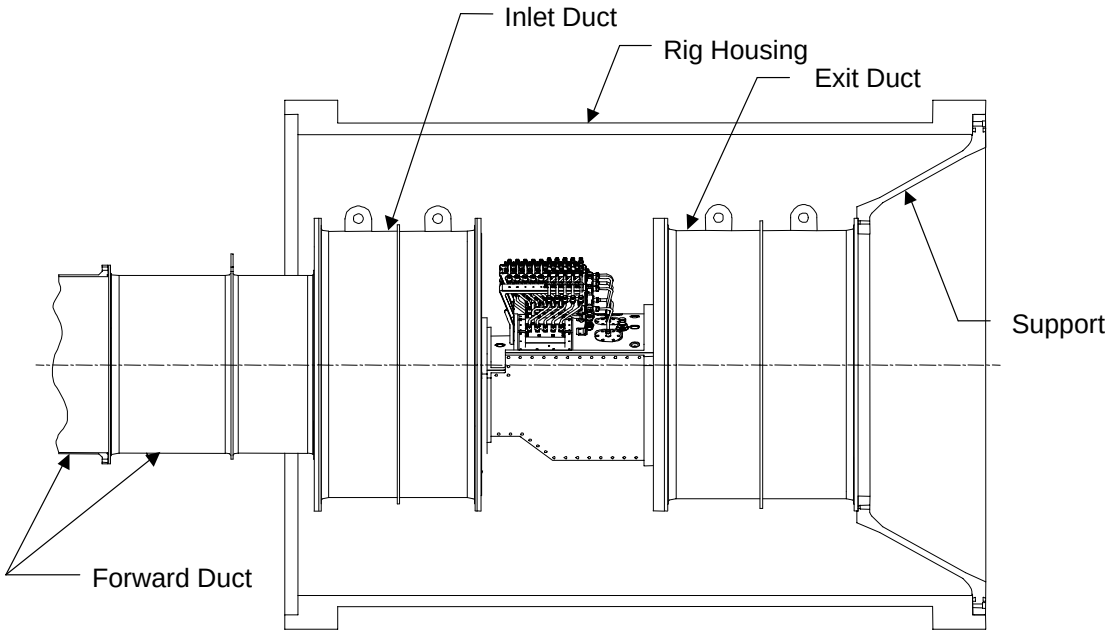

Figure 345. HSCT Large-Scale Combustor Sector Rig Hardware

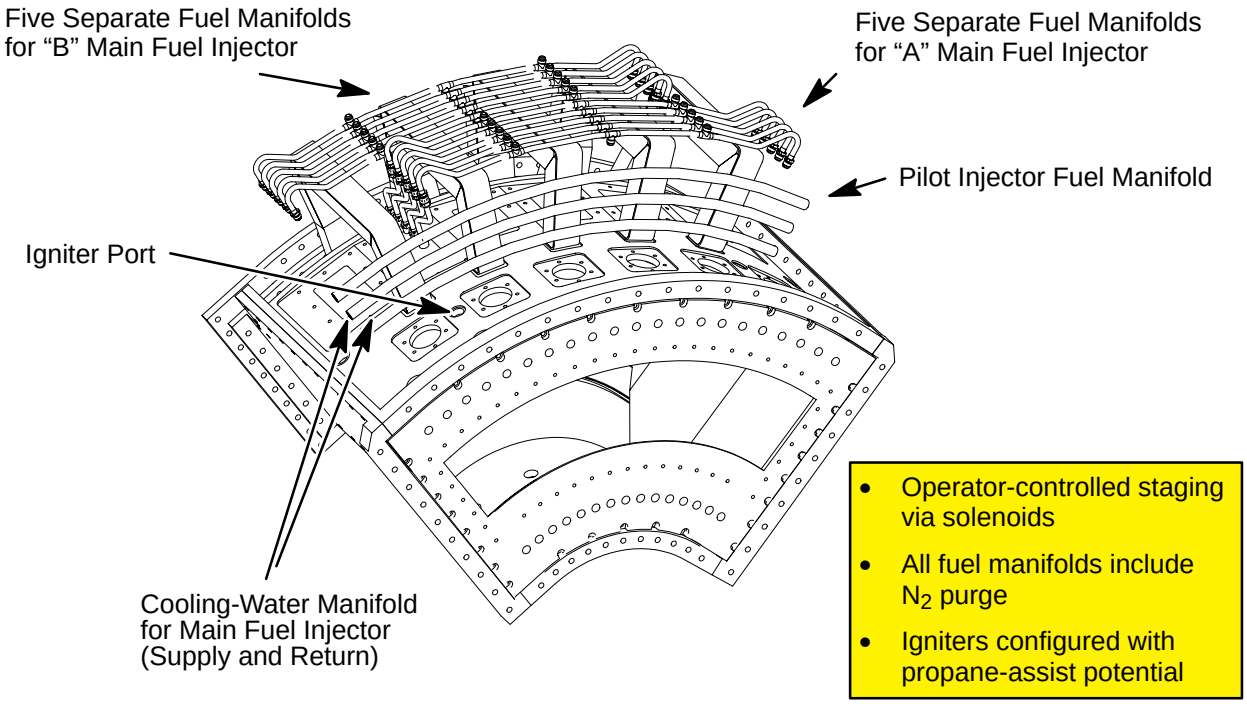

Figure 346. Combustor Rig Externals

Orifices are conservatively sized at 0.22-in diameter and may be reamed to a larger diameter as required. Inlets to the manifold consist of five 1-in diameter fittings. The manifold is a welded tube assembly constructed of 0.065-in wall, AMS 5557 stainless steel with 37° type cone seat fittings. The manifold is mounted to the vane pack aft plate by three 0.078-in thick, Inco 625 (AMS 5599) sheet metal brackets with welded gussets.

4.9.4 Sector Instrumentation

The planned instrumentation for the full-scale MRA sector is principally the same as that presented at the LPP/RQL downselect. The purpose of the instrumentation is to determine the inlet and exit boundary conditions, evaluate sector rig performance, determine flowpath pressure drop, monitor rig component temperatures and performance, and provide acoustic and structural information.

Instrumentation consists of an inlet pressure rake and an exit emissions rake. The exit emissions probes are integrated in a combustor vane pack that extends the width of the combustor exit, providing uniform back pressure and better simulating the first row of turbine vanes. Emissions measurements will be used to calculate flame temperature (T_4).

Static pressure taps will be placed at critical points in the flowpath to determine diffuser performance and flow uniformity (Figure 347). Further, additional static pressures will be measured in the cooling passages of the liners. This information will be used to help determine the accuracy of the heat transfer parameters used to design rig cooling.

Thermocouples will be placed in the flowpath at several locations to help monitor the rig performance. Ten platinum-platinum/rhodium thermocouples are to be placed in the combustor flowpath to assure that the combustor is lit as required by the facility safety guidelines. Thermocouples will also be placed on the liners and bulkheads to monitor durability and measure cooling performance (Figure 348).

Dynamic pressure measurements will be taken to observe combustor dynamic performance. Measurements will be made in the cavity upstream and the cavity downstream to give boundary conditions, after the prediffuser, in the combustor and at the combustor exit. In addition, strain gages will be installed on the fuel struts, the pilot stem, and between the IMFH tubes (Figure 349).

4.9.5 Test Rig and Facility

Design Requirements – This rig is designed to be assembled and tested at the Middletown X960 facility. The rig sits inside a 6-ft diameter pressurized housing provided by the facility called the rig "capsule." The capsule is pressurized with 100° to 300°F air maintained at 10 psi above the combustor inlet pressure. This eliminates the need to design the combustor and diffuser cases to handle the high-pressure loads seen in actual engine parts.

The air feeding the combustor is transitioned to the 75.35° sector with a bellmouth inlet followed by a constant-area inlet channel. Profile control plates to achieve a flat, OD-peaked, or other profile can be placed between the bellmouth and the inlet channel.

Rig Assembly – The rig can be seen in Figure 345 (page 273) as assembled in the facility. The rig attaches to the facility housing and is supported by the rear support cone.

Facility Hook-Ups – The facility will provide thirty 3/8-in AN connections to provide fuel to the main fuel injectors and six 3/8-in connections to provide fuel to the pilot fuel injectors. Further there

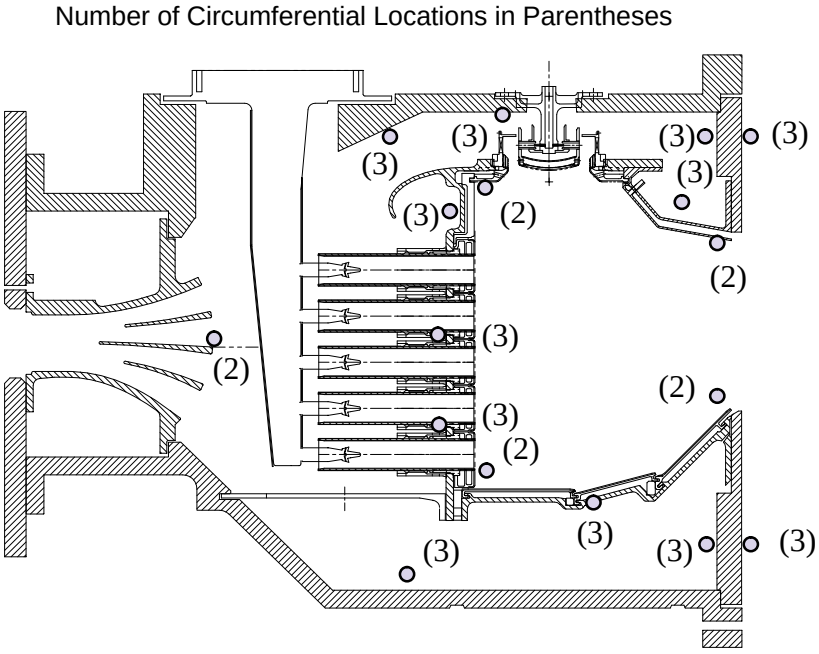

Figure 347. Location of Rig Flowpath Static Pressures

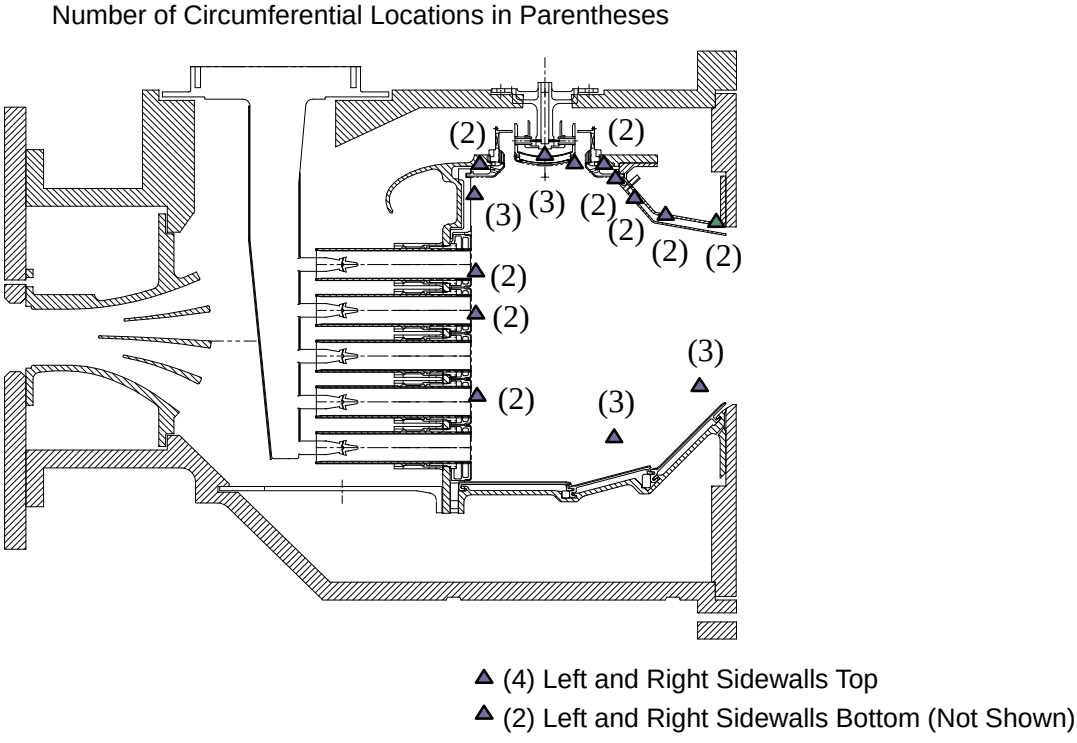

Figure 348. Location of Liner/Heat Shield Thermocouples

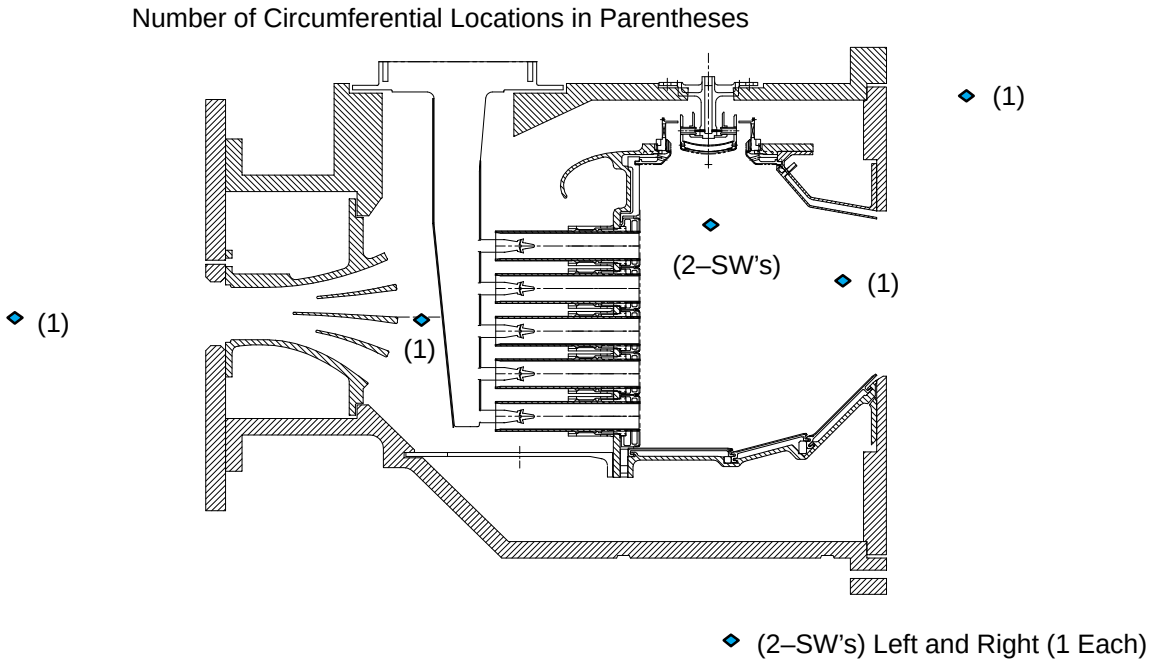

Figure 349. Location of Dynamic Pressure Measurements

are six supply and six return 3/8-in AN connections to be made to provide adequate cooling to the main manifold. The supply and return fittings will be of opposite type to ensure proper installation.

Exhaust Cooling – A series of spray rings to cool the exhaust prior to reaching the back-pressure control valve are included in the X960 facility. Since the emission-probe cooling water will be sprayed into the exhaust stream, some or most of these spray rings may not be required. The exhast temperature will be monitored and controlled by the test facility group.

Fuel Control – Eleven independent fuel controls are required for running the full-scale sector rig. The flow requirements and control method have been communicated with the X960 facility engineers. Currently the new valves and control system required has not been specified or ordered.

Emissions System – Due to the highly staged nature of the LPP combustor, a high-density emissions measuring vane pack has been designed. The test facility will need to be able to measure 98 sample points individually or ganged in radial or circumferential combinations. This ability will require 98 new solenoid valves, a mixing chamber, a draw-down pump, and control system.

4.9.6 Sector Test Plans

A plan for the full-scale sector testing was presented at the detailed design review. The goals of the test plan are to evaluate and verify the performance, emissions, operability, and structural integrity of the concept. The data from the test plan will be used as a database for optimizing control schedules and will be used to scale the full-annular combustor.

That plan is still considered acceptable for future tests. Over 1200 test points were proposed — which would require considerable time and expense to obtain. The plan will be modified to meet testing and budgetary constraints using best engineering judgement as additional information and experience with the rig become available.

The plan objectives are outlined in Table 47. All the flight points are tested at nominal conditions, with excursions in fuel/air ratios and accompanying staging taking place for all the LTO conditions, nominal subsonic cruise, and nominal supersonic cruise. Additionally, excursions in T_3, P_3, and $\Delta P/P$ will be performed at the 5.8% thrust LTO, 100% thrust LTO, and nominal supersonic cruise. Radial and circumferential profiles will be measured for all the fuel/air excursions. Particulates will be measured for 5.8% thrust LTO, 100% thrust LTO, nominal subsonic cruise, and nominal supersonic cruise.

Exit radial profiles will be taken by ganging the probes by row. Circumferential profiles will gang the probes together by rake. Probe by probe maps will be made for the 5.8% thrust LTO, 100% thrust LTO, nominal subsonic cruise, and nominal supersonic cruise conditions as well as the 15% thrust LTO and the 34% thrust LTO conditions.

Table 47. Summary of Planned Test Points

Condition	Nominal	Excursions				Staging	Profiles		Particulates
		f/a	T_3	P_3	$\Delta P/P$		Radial	Circumferential	
5.8% Thrust LTO	X	X	X	X	X	X	X	X	X
15% Thrust LTO	X	X				X	X	X	
34% Thrust LTO	X	X				X	X	X	
65% Thrust LTO	X	X				X	X	X	
100% Thrust LTO	X	X	X	X	X	X	X	X	X
Nominal Subsonic Cruise	X	X				X	X	X	X
Start Subsonic Cruise	X								
End Subsonic Cruise	X								
Nominal Supersonic Cruise	X	X	X	X	X	X	X	X	X
Start Supersonic Cruise	X								
End Supersonic Cruise	X								

4.10 Remaining Challenges

Several challenges remain in the development of a viable combustor for an HSCT engine. Testing of the full-scale MRA sector described in the previous subsection will clearly provide important information regarding emissions and operability. Every effort has been made to ensure that the design will be successful. Although it is fully expected that the design will meet all criteria set forth in the program guidelines, the scale-up has the potential to impact the combustor performance and make it fall short of requirements. In addition to the scale-up concerns, potential problems with a full-annular design may be encountered when it is placed in an engine, and the future impact of any changes to the engine operating requirements must also be considered. These concerns are addressed in the following subsections.

4.10.1 Performance Impact of Hardware Scale-Up

The LPP MRA concept was successfully demonstrated in a sector using a subscale design. Scale-up of such a design, although seemingly straightforward, does pose certain difficulties and raise certain concerns. A simple example of how direct scale-up can cause problems comes in comparing some-

thing as simple as diameters and lengths: doubling a diameter causes area to quadruple; whereas doubling a length only causes area to double. This can pose problems in scaling hardware features.

The primary concern with scale-up is impact on emissions. Because the entire combustion chamber is significantly larger, interaction effects between the cyclone pilots and the IMFH tubes are less well understood. Depending on how well the cyclone vortex and the main IMFH air flows interact, the potential for ground idle CO and supersonic cruise NOx to increase are very real. Additionally, significant concerns exist over the emissions from the scaled-up IMFH's and the pilots themselves. During development, it was not clear if the appropriate levels of premixing and prevaporization could be achieved in the larger hardware versions. Subcomponent development and testing indicated that not only could emissions levels be maintained, they could actually be reduced at some operating conditions, relative to subscale counterparts, through additional design improvements. An additional concern that impacts emissions is fuel staging. If the scale-up were to impact the number of fuel stages available and/or the points at which staging were to occur, emissions would have the potential to increase. However, the staging scheme implemented in the full-scale design mimicked the subscale design very well. Thus, based on subcomponent evaluations and the overall experience gained in developing the concept, it is fully expected that emissions requirements will be met.

In terms of combustor stability, hardware scale-up may actually be an improvement. It was demonstrated in subcomponent tests that the full-scale cyclone lean blowout improved significantly relative to the subscale design. On the other hand, the larger diameter IMFH tubes have the potential to be less stable. However, it is anticipated that the hot gases from the pilots should be able to offset this situation. Lightoff and crossfiring are not expected to be any great concern, since the pilots are tightly packed and the rotational flowfields tend to promote crossfiring to adjacent pilots.

The impact of scale-up on exit profiles is expected to be minimal. The primary concern is really ground idle operation, since the penetration depth of the larger cyclone pilot is uncertain (mainly due to uncertainty in the level of interaction with the IMFH crossflow). Should this pilot flow be unable to penetrate sufficiently inward, it would result in significantly outer-peaked exit profiles. Knowledge about the exit profiles will be obtained in the full-scale sector test.

Autoignition and flashback concerns had to be dealt with in scaling up the cyclone pilots. If the subscale cyclone design had simply been scaled up, autoignition most certainly would have resulted, since the bulk residence time of the fuel/air mixture would have risen nonlinearly. The full-scale design was modified to eliminate this problem. The IMFH tubes were not of concern, since the bulk residence time of the fuel/air mixture was unchanged (the tube length and flow velocity were unchanged).

Coking in the fuel supply lines and fuel injectors is another concern with the scale-up. Because larger fuel nozzles lead to longer fuel tubes and passages, the risk of the fuel reaching undesirable temperatures increases. High fuel temperatures lead to coke formation, which has the potential to block passages. Thus, the fuel nozzle was redesigned to improve thermal protection of the fuel. Additionally, the scale-up actually helped improve the effectiveness of the cooling in the stinger tip, since active fuel cooling could be implemented. The subscale stingers had been too small to add such a feature. Thus, although coking remains a general concern, scale-up of the fuel system is not expected to cause problems worse than the subscale design, and scale-up actually reduces risk in the fuel injector tip design.

Acoustics remain one of the primary concerns with the MRA system. Because acoustics are impacted by chamber size (in addition to a multitude of other parameters), it is expected that the

frequencies and amplitudes of the full-scale design will be different from the subscale. These must be monitored closely to ensure that hardware is not damaged during the sector test. In addition, improved tools to predict acoustics ought to be developed. Available tools are very limited and often do not perform well. Typically, they are capable of predicting frequencies fairly accurately, but amplitudes remain a significant problem.

Most of these concerns will be addressed when the full-scale MRA sector is tested. Note that further changes to the overall engine size would require additional development in each of the aforementioned areas prior to implementation in an engine.

4.10.2 Mechanical Impact of Hardware Scale-Up

In addition to performance considerations, scaling up hardware introduces mechanical concerns. The first is obviously packaging all the subcomponents given specific combustor and engine case diameter and length limitations. This often arises because of nonlinear scaling but can also result from increased minimum metal thicknesses as part sizes increase.

Larger pieces of hardware also introduce mechanical and thermal stress concerns. Vibration modes are altered; sufficient cooling becomes more difficult; tolerances, clearances, and positioning become more challenging; and increased stress loads must be dissipated. The best example of this is the combustor liners. Ideally, a single piece could be used, but tremendous stress loads have the potential to induce cracking. This was one reason for using segmented liners in the full-scale sector.

One often overlooked concern is that simple fabrication of scaled-up hardware becomes significantly more difficult and costly. Raw material suppliers are more limited, and customized parts, fixtures, and other equipment become necessary. Parts rapidly grow beyond current casting capabilities. Machining requires larger, specialized equipment. And larger parts often distort, leading to clearance and positioning problems during assembly and repair. Each of these must be considered in designing such a large device.

4.10.3 Operability and Acoustic Control in a Full-Annular System

As indicated above, scale-up of the MRA design introduces multiple concerns for the sector. In addition, implementation in a full-annular system must be considered. The primary concern in transitioning from a sector to a full-annular combustor is acoustics. A full-annular system is expected to demonstrate acoustic amplitudes and frequencies somewhat different from those in a sector because some of the sector acoustic modes result from the presence of sidewalls, which are obviously not present in a full-annular system. In addition, features upstream and downstream of the combustor itself are different in a sector and an engine. Such features can impact the acoustic boundary conditions and frequencies observed in the combustor.

Acoustic control in the sector tests relied mostly on introducing nonuniformities into the flowfield. This was usually accomplished by changing the pilot fuel/air ratio relative to the main stages. Unfortunately, this has the potential to impact emissions, although the magnitude tended to be relatively small and was dependent on the operating conditions and the staging configuration at the time. A possible alternative would be the addition of acoustic baffles, which are often used in rockets to help mitigate dynamics. However, these are rarely used in aircraft engine applications because of the weight penalty. Additionally, unlike rockets, aircraft engines operate over a wide range of cycle conditions with each flight. This leads to changes in the acoustic frequencies and amplitudes

as cycle conditions change, limiting the effectiveness of the baffles to only certain operating conditions in the flight envelope. This would be unacceptable for practical applications.

4.10.4 Design Robustness in Engine Dynamic Environment

In addition to the problems that may arise in transitioning from a sector to a full-annular system, other concerns are added when that full-annular system is placed into an actual engine. These result from the transients required for an aircraft to take-off and land. Additionally, the accelerations and decelerations occur at different rates as well as at different operating conditions in the flight envelope. This introduces additional dynamic stress loads and vibrations that are not typically encountered in a static sector test. The hardware must be designed to withstand this severe environment.

Reverse flows resulting from acoustics or a compressor stall can lead to hardware damage. Not only can hot combustor gases flow backwards through the IMFH tubes (and potentially the pilots), but cooling flows can reverse, causing metal temperatures to rise rapidly. Fortunately, the LPP transient sector tests demonstrated that the IMFH and cyclone mixers were able to rapidly clear themselves without damaging the hardware in the presence of such a reverse flow event. Thus, the overall robustness of the design in this scenario has already been demonstrated at a subscale level. The full-scale designs are expected to provide similar robustness, although additional transient testing is recommended prior to implementation in an engine.

4.10.5 Changes to the Operating Cycle

Prior discussions focused on the impact of scaling the combustor and the transition from a sector to a full-annular system capable of being used in an engine. This final subsection will address the impact of changes to the engine operating cycle, should they be made at some point in the future.

Changes to the engine operating cycle would clearly impact the pressure (P_3, P_4), temperature (T_3, T_4), air flow (W_{a3}, W_{a36}), and fuel flow (W_{f36}) entering and exiting the combustor. The impact is dependent on the conditions that actually change, the direction they are changed (higher or lower), and the magnitude of the change. Additionally, operation would be impacted differently at each of the different engine operating conditions.

At low power, increasing pressure and/or inlet temperature would tend to improve lean-blowout margin, reduce CO and hydrocarbon emissions, and improve combustion efficiency. On the contrary, since ground idle EICO is already moving along the equilibrium line, increasing T_4 at the current inlet pressure and temperature (that is, increasing the flame temperature) would actually increase EICO, reducing combustion efficiency. Autoignition, fuel coking, and hardware cooling effectiveness are of limited concern at low-power conditions. Proper design of these features at higher power conditions ensures adequate operation at low power.

It is difficult to determine how intermediate power emissions would be impacted by changes to the operating cycle, since the number of fuel stages available and the fuel-staging points selected for the combustor greatly impact the resulting emissions. It is expected that intermediate-power emissions would not be significantly altered, assuming fuel staging could be adjusted appropriately. As was the case at low power, autoignition is of limited concern at these operating conditions. Fuel coking becomes more of a concern but (like emissions) is a function of the fuel staging selected. In general as temperatures, pressures, and air velocities increase, it becomes more difficult to protect the fuel from the resulting heat load, increasing the risk of coking. Hardware cooling effectiveness also

becomes a concern at high-temperature, low-pressure conditions (such as deceleration from supersonic cruise). Similarly, if the cycle is changed such that temperatures rise and pressures fall, cooling becomes more difficult. Thus, as these parameters are changed the percentage of the total air flow required for cooling must be altered accordingly to prevent hardware damage. This air must be taken from the primary combustor (reducing W_{36} for a given W_3), which is undesirable.

At high power, increases to T_4 (via higher flame temperatures) would certainly result in higher NOx emissions. In general, NOx would also be expected to increase as pressure increased, although subcomponent IMFH and cyclone pilot development seemed to suggest otherwise. Autoignition becomes a primary concern at these conditions, and subcomponents would have to be redesigned if pressures and temperatures were to rise. Fuel coking remains a concern as temperatures, pressures, and air velocities increase, increasing the heat load. One advantage, however, is that at high power all stages are flowing fuel, reducing the risk of coking in nonflowing passages. Unfortunately, reducing power (by turning off stages) at these elevated-temperature conditions poses the greatest coking risk in the flight envelope and must be addressed. As was the case at intermediate power, hardware cooling effectiveness remains a concern as temperatures rise and pressures fall. Thus, as these parameters change, the percentage of the total air flow required for cooling must be altered accordingly. Again this air must be taken from the primary combustor (reducing W_{36} for a given W_3), which is undesirable.

In general, changing the operating cycle can have far-reaching impact. Changes to the size of the overall combustor could be required. Changes to the size, and potentially quantity, of the IMFH premixers and cyclone pilots could be necessary. Modifications to the number of fuel stages and to the points at which fuel staging occurs are also likely. Acoustic frequencies and amplitudes would likely change as well but could either get better or worse at any particular operating point. Fuel coking and hardware cooling effectiveness would have to be addressed at intermediate- and full-power conditions. Autoignition would be of primary concern only at high power, and subcomponents would have to be designed to these conditions. Thus, changes to the engine operating cycle clearly have the potential to require a significant amount of combustor redesign before one could be placed in an engine. Additional subcomponent development and sector or full-annular tests would likely be necessary to verify that the modified design meets operational requirements and is still commercially viable.

REPORT DOCUMENTATION PAGE

Form Approved
OMB No. 0704-0188

1. AGENCY USE ONLY (*Leave blank*)	2. REPORT DATE	3. REPORT TYPE AND DATES COVERED
	May 2005	Final Contractor Report

4. TITLE AND SUBTITLE

Critical Propulsion Components
Volume 2: Combustor

5. FUNDING NUMBERS

WBS–22–714–09–447
NAS3–27235

6. AUTHOR(S)

Pratt and Whitney and General Electric Aircraft Engines

7. PERFORMING ORGANIZATION NAME(S) AND ADDRESS(ES)

Pratt & Whitney
Advanced Engineering Operations
P.O. Box 109600
West Palm Beach, Florida 33410

8. PERFORMING ORGANIZATION REPORT NUMBER

E–15051–2

9. SPONSORING/MONITORING AGENCY NAME(S) AND ADDRESS(ES)

National Aeronautics and Space Administration
Washington, DC 20546–0001

10. SPONSORING/MONITORING AGENCY REPORT NUMBER

NASA CR—2005-213584-VOL2

11. SUPPLEMENTARY NOTES

This research was originally published internally in September 2000. Pratt & Whitney, Advanced Engineering Operations, P.O. Box 109600, West Palm Beach, Florida 33410; and General Electric Aircraft Engines, Advanced Engineering Programs Department, One Neumann Way, Cincinnati, Ohio 45215–6301. Responsible person, Diane Chapman, Ultra-Efficient Engine Technology Program Office, NASA Glenn Research Center, organization code PA, 216–433–2309.

12a. DISTRIBUTION/AVAILABILITY STATEMENT

Unclassified - Unlimited
Subject Categories: 01, 05, 07

Available electronically at http://gltrs.grc.nasa.gov

This publication is available from the NASA Center for AeroSpace Information, 301–621–0390.

12b. DISTRIBUTION CODE

13. ABSTRACT ***(Maximum 200 words)***

Several studies have concluded that a supersonic aircraft, if environmentally acceptable and economically viable, could successfully compete in the 21st century marketplace. However, before industry can commit to what is estimated as a 15 to 20 billion dollar investment, several barrier issues must be resolved. In an effort to address these barrier issues, NASA and Industry teamed to form the High-Speed Research (HSR) program. As part of this program, the Critical Propulsion Components (CPC) element was created and assigned the task of developing those propulsion component technologies necessary to: (1) reduce cruise emissions by a factor of 10 and (2) meet the ever-increasing airport noise restrictions with an economically viable propulsion system. The CPC-identified critical components were ultra-low emission combustors, low-noise/high-performance exhaust nozzles, low-noise fans, and stable/high-performance inlets. Propulsion cycle studies (coordinated with NASA Langley Research Center sponsored airplane studies) were conducted throughout this CPC program to help evaluate candidate components and select the best concepts for the more complex and larger scale research efforts. The propulsion cycle and components ultimately selected were a mixed-flow turbofan (MFTF) engine employing a lean, premixed, prevaporized (LPP) combustor coupled to a two-dimensional mixed compression inlet and a two-dimensional mixer/ejector nozzle. Due to the large amount of material presented in this report, it was prepared in four volumes; Volume 1: Summary, Introduction, and Team. Propulsion System Studies, Volume 2: Combustor, Volume 3: Exhaust Nozzle, and Volume 4: Inlet and Fan/Inlet Acoustic Team.

14. SUBJECT TERMS

High speed civil transport; High speed research; Mixed-flow turbofan; NO_x emissions; Lean direct injection; Lean premixed prevaporized; Rich-quench-lean

15. NUMBER OF PAGES

314

16. PRICE CODE

17. SECURITY CLASSIFICATION OF REPORT	18. SECURITY CLASSIFICATION OF THIS PAGE	19. SECURITY CLASSIFICATION OF ABSTRACT	20. LIMITATION OF ABSTRACT
Unclassified	Unclassified	Unclassified	